NASA CONTRACTOR REPORT

NASA CR-66665-2

NASA CR-66665-2

N68-34051
(ACCESSION NUMBER) (THRU)
(PAGES) (CODE)
(NASA CR OR TMX OR AD NUMBER) (CATEGORY)
FACILITY FORM 602

GPO PRICE $
CSFTI PRICE(S) $
Hard copy (HC)
Microfiche (MF)
ff 653 July 65

SOFT LANDER PART II

Mars Soft Lander Capsule Study (Entry From Orbit) - Introduction And Parametric Studies

Prepared by

MCDONNELL DOUGLAS ASTRONAUTICS COMPANY
EASTERN DIVISION
Saint Louis, Missouri 63166 (314) 232-0232

for Langley Research Center

NATIONAL AERONAUTICS AND SPACE ADMINISTRATION • WASHINGTON, D.C. • SEPTEMBER 1968

NASA CR-66665-2

SOFT LANDER PART II

Mars Soft Lander Capsule Study (Entry From Orbit) -
Introduction And Parametric Studies

Distribution of this report is provided in the interest of information exchange. Responsibility for the contents resides in the author or organization that prepared it.

Issued by Originator as McDonnell Douglas Astronautics Report G346

Prepared under Contract No. NAS 1-7977 by

MCDONNELL DOUGLAS ASTRONAUTICS COMPANY
EASTERN DIVISION
Saint Louis, Missouri

for Langley Research Center

NATIONAL AERONAUTICS AND SPACE ADMINISTRATION

TABLE OF CONTENTS

Page

2. INTRODUCTION. 2-1
   2.1 STUDY OBJECTIVES 2-1
   2.2 STUDY APPROACH 2-2
   2.3 CONSTRAINTS. 2-4
   2.4 SCOPE OF THE STUDY 2-6
   2.5 STUDY RESULTS. 2-8
   2.6 SYMBOLS AND ABBREVIATIONS 2-8
3. PARAMETRIC STUDIES. 3-1
   3.1 MISSION PARAMETRIC STUDIES 3.1-1
      3.1.1 Launch, Arrival, and Orbit. 3.1-1
         3.1.1.1 Launch opportunities 3.1-1
         3.1.1.2 Arrival conditions 3.1-9
         3.1.1.3 Orbit and landing location selection . . . 3.1-9
      3.1.2 Deorbit And Descent 3.1-34
         3.1.2.1 Deorbit velocity increment and geometry . 3.1-35
         3.1.2.2 Capsule descent time 3.1-40
         3.1.2.3 Capsule lead angle 3.1-44
         3.1.2.4 Landing geometry 3.1-49
         3.1.2.5 Post-landed view time. 3.1-53
         3.1.2.6 Entry angle of attack. 3.1-56
         3.1.2.7 Entry and landing dispersions. 3.1-58
         3.1.2.8 Deorbit and descenttselection. 3.1-70
      3.1.3 Entry 3.1-74
         3.1.3.1 Trajectory parameters. 3.1-74
         3.1.3.2 Reduced corridor effects 3.1-81
         3.1.3.3 Rotating planet effects. 3.1-81
      3.1.4 Terminal Deceleration 3.1-95
         3.1.4.1 Deployment altitude. 3.1-97
         3.1.4.2 Aeroshell/lander separation. 3.1-97
         3.1.4.3 Terminal velocity. 3.1-102
         3.1.4.4 Entry corridor and atmosphere variations . 3.1-102
         3.1.4.5 Rotating planet effects. 3.1-111

TABLE OF CONTENTS (CONTINUED)

		Page
3.2	SYSTEM PARAMETRIC STUDIES	3.2-1
3.2.1	Science	3.2.1-1
3.2.1.1	Landed science payload	3.2.1-2
3.2.1.2	Entry science payload	3.2.1-6
3.2.1.3	Lander facsimile camera	3.2.1-9
3.2.1.4	Lander atmospheric pressure transducer	3.2.1-34
3.2.1.5	Lander atmospheric temperature transducer	3.2.1-51
3.2.1.6	Lander wind sensor	3.2.1-56
3.2.1.7	Lander atmospheric humidity sensor	3.2.1-58
3.2.1.8	Landed mass spectrometer operation	3.2.1-66
3.2.1.9	Lander alpha spectrometer	3.2.1-67
3.2.1.10	Entry pressure, temperature, and acceleration sensors	3.2.1-72
3.2.1.11	Entry humidity sensor	3.2.1-80
3.2.1.12	Entry mass spectrometer	3.2.1-93
3.2.2	Communications	3.2.2-1
3.2.2.1	Entry communications	3.2.2-1
3.2.2.2	Landed communications	3.2.2-24
3.2.2.3	Total data return analysis	3.2.2-58
3.2.3	Power	3.2.3-1
3.2.3.1	Requirements	3.2.3-1
3.2.3.2	Candidate subsystems	3.2.3-6
3.2.3.3	Performance	3.2.3-11
3.2.4	Guidance And Control System	3.2.4-1
3.2.4.1	Attitude/deorbit velocity control electronics	3.2.4-1
3.2.4.2	Landing radar systems	3.2.4-10
3.2.4.3	Radar altimeter	3.2.4-20
3.2.5	Sequencer System	3.2.5-1
3.2.5.1	Memory type	3.2.5-1
3.2.5.2	System configuration comparison	3.2.5-4

List of Pages

i through iii
2-1 through 2-14
3-1
3.1-1 through 3.1-117
3.2-1
3.2.1-1 through 3.2.1-105
3.2.2-1 through 3.2.2-63
3.2.3-1 through 3.2.3-57
3.2.4-1 through 3.2.4-27
3.2.5-1 through 3.2.5-5

2. INTRODUCTION

Exploration of Mars in the 1970's requires planning based on understanding of the science requirements, selection of system designs within the achievable state-of-the-art, and determination of suitable mission profiles for fulfilling the exploration objectives. These must be balanced in an integrated plan to assure efficient mission accomplishment. Such a plan requires parametric study of science goals, missions, system design characteristics, and resource requirements in order to determine specific goals which can be economically attained. The various elements needed for the exploration of Mars, principally the launch vehicle, the Mars orbit insertion propulsion stage, the Mars orbiter, and the entry and landing capsule must each be examined. Differing, and often competing, requirements and capabilities for each element must be analyzed and the results integrated. In studying each element, it is important to retain sufficient options to allow optimization of the total program rather than of the individual elements. On the other hand, retention of too many options would dilute the effort which can otherwise be devoted to approaches showing most promise. The Mars Soft Lander Capsule Study (Entry from Orbit), conducted under contract NAS1-7977, is one of several studies performed for the Langley Research Center to support planning for the exploration of Mars.

2.1 Study Objectives

The principal objective of the study was to define the spectrum of entry and landing capsules suitable for Mars exploration using the 1973, 1975, and 1977 launch periods. It will aid in the mission and capsule concept selection leading to procurement and operation of the equipment for planetary exploration. Parameter studies were conducted to promote understanding of the effects of mission and capsule design variables as well as to provide a basis for total capsule description. In order to identify the effects of the assumed environment description, a parametric environment sensitivity analysis was performed. In addition, cost trends were analyzed and various designs were ranked to identify minimum cost concepts.

Discrete conceptual designs were prepared for representative points in the capsule spectrum. These served to confirm the parametric analysis and permit better comprehension of specific design and capsule integration problems. Descriptions of capsule systems and an estimate of capsule performance were made for each conceptual design.

2.2 Study Approach

The results of this study incorporate those of previous McDonnell Studies of Mars exploration; the most important is the VOYAGER Capsule Phase B study conducted for the Jet Propulsion Laboratory under contract 952000. Extensive use has been made of both the data and methodology created during these earlier activities. Parallel study of interdependent systems was facilitated because of the availability of this background. The range of design parameters to be studied was extended beyond that which was expected to be necessary and ranges of sequential operating parameters were overlapped to facilitate this parallel study and to compress the study into the scheduled three months. This background also contributed to the efficiency of the study by permitting concentration on those mission aspects and system design features that were critical to this study, while utilizing previously generated data for the remaining items. This technique was particularly useful in minimizing the amount of new work required on the launch, interplanetary cruise, and orbit portions of the mission, although these are important to capsule detail design.

The discrete points chosen for conceptual design were chosen to exhibit a range of performance and also to exhibit alternate selections of support system design. Concept I has the lowest cost of these systems. It will perform the minimum mission; weight and cost efficiency is achieved by modifying some constraints and by providing less operational flexibility than nominal. Concept II provides for the minimum science, minimum lifetime mission in the presence of the full range of specified environments, with support systems being based on conventional concepts, and with substantial flexibility being retained for operational planning. Concept II provides the minimum lifetime under the worst landed operational environment (continuous cold, cloudy day) and for extended lifetime in the presence of an environment deemed likely for

low latitude landing sites. Concept IV provides for maximum capability within the constraints of the study. Work on Concept IV was halted during the study to allow greater emphasis on the smaller capsules. Concept V provides for extended lifetime (like III) within the same environment/flexibility constraints as for Concept I. Within these five cases, there are three power system concepts, two aerodecelerator types, two communication modes, two terminal propulsion concepts, and two deorbit propulsion concepts in addition to various lifetimes and science payloads. Confirmation of the parametric studies was achieved by identifying those points in the parametric study results which represent the conceptual designs.

To facilitate comparisons and minimize the uncertainty caused by arbitrary decision making, neither the capsule parametrics nor the conceptual designs include specific allowances for unit redundancy or unallocated weight margins. Design on the basis of no-unit-redundancies allows a redundancy requirements analysis to be conducted on an unbiased basis and results in assignment of weight for redundancy in the most effective manner. This approach was used in McDonnell's VOYAGER Phase B study and resulted in the addition of 73 pounds, slightly less than 2 percent of the total to provide a reliability for performing all capsule functions of .71.

The uncertainty of the Martian environment causes substantial inefficiencies in the design and operation of an entry and landing capsule. Although the actual value of some environment parameters, e.g., the surface level atmospheric density, has imposed some rigorous constraints, more serious problems are caused by inefficiencies related to the wide range of parameters which must be accommodated. Low density scale height atmospheres, for instance, cause maximum dynamic pressure and heating rates but high scale height atmospheres present the most difficult situation for the descent UHF relay communications. A single "worst case" environment is therefore impossible to define. Parametric study was done to determine which of the environment specifications was most demanding of the capsule design. This study, it is hoped, will direct attention to certain of these parameters with the intent of determining probability of occurrence and possible relaxation of some constraints.

Capsule design and development planning are now sufficiently advanced to permit cost trend analysis to enter into design decision making. For this study, cost trends were most useful in comparing discrete system candidates. For example, it is appropriate to make cost comparisons of systems using monopropellant terminal propulsion systems with those using bipropellants. It was also feasible to cost-optimize some continuous design variables, such as the terminal vertical velocity to be provided by the aerodynamic decelerator. Finally, the relative cost of providing extra capability can be determined. Selection of the velocity increment capability of the deorbit motor is a particularly good example of this.

Throughout the study, our approach has been to emphasize the items which will critically affect the feasibility of using a soft lander within the resources available for early Mars exploration. More detail is therefore provided on such items as terminal propulsion, science, communications, and power than on systems for which feasibility is clear. Identification of the various systems and parts of the capsule is illustrated in Figure 2.2-1.

2.3 Constraints

Constraints assumed for the study were generally consistent with those for various Mars exploration studies during the past several years. In addition some specific study constraints were applied throughout the study period; others were imposed during the course of the study. Except as separately noted, the following documents were used as references.

a) Description of the Deep Space Network Operational Capabilities as of January 1, 1966, Technical Memorandum No. 33-255, July 1, 1966.

b) Planned Capabilities of the DSN for VOYAGER 1973, JPL EPD-283 (Revision 2) January 1, 1967.

c) 1973 VOYAGER Capsule Constraints and Requirements Document, (SE002BB002-2A21) January 1, 1967; Revision 2, 12 June 1967

d) Planetary Quarantine Plan, VOYAGER Project, (PQ001BB001-1B51), March 15, 1966; Revision 1, 15 October 1966; Revision 2, 1 January 1967.

CAPSULE TERMINOLOGY

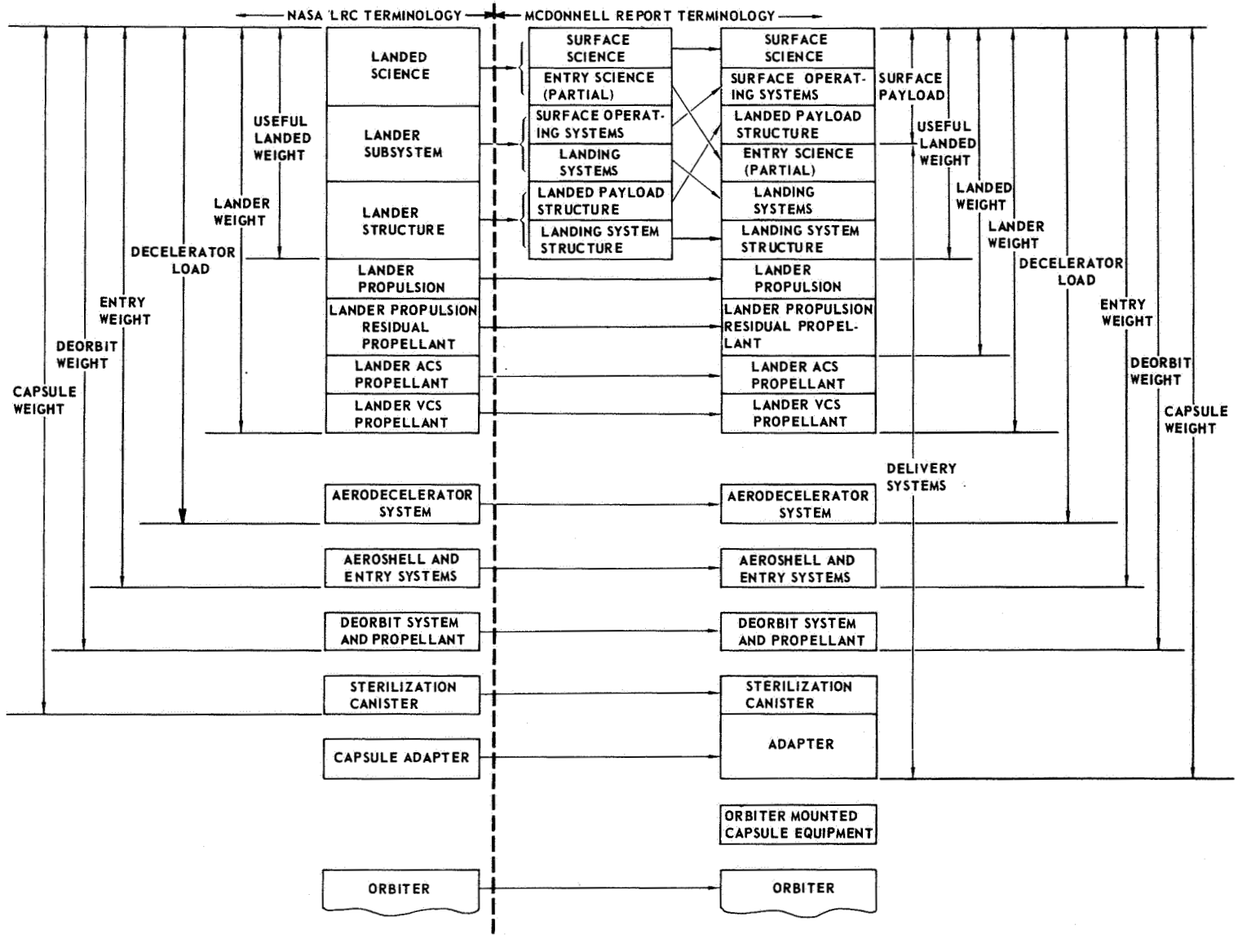

FIGURE 2.2-1

f) Performance and Design Requirements for the 1973 VOYAGER Mission, General Specification for, (SE002BB001-1B21), January 1, 1967.

g) Standard Procedures for the Microbiological Examination of Space Hardware, NASA Document NHB 5340.1, August 1967.

Constraints initially applied to limit the study to particular areas of interest are listed in Table 2.3-1. Some of these were changed during the study and the modifications are also shown in Table 2.3-1. The sensitivity to several of these constraints has been examined as a part of the parametric study which it affected. Sensitivity to environmental constraints received special attention as provided in the contract.

2.4 Scope of the Study

The spectrum of capsules ranged from austere, small science payload, short surface lifetime vehicles for 1973 missions to more ambitious capsules generally associated with the later missions. For parametric studies the surface science extremes were an atmospheric data package weighing only 10 pounds and a 118 pound package which included facsimile cameras, a subsurface probe, and life detection equipment. For conceptual design purposes, a more ambitious minimum science payload was established. It contained facsimile cameras, an alpha spectrometer for surface composition measurements and an atmospheric data package.

Lifetime targets were originally established as a few days to a few months, but subsequent consideration established one day (one diurnal cycle) as the minimum allowable lifetime. For extended lifetime, a nominal value of ninety days was used. Lifetime considerations are closely related to the selection of power source; nominal lifetimes longer than a few days are feasible only if a regenerative power system is used.

The original size limitation to 16 foot diameter aeroshell was subsequently changed to allow sizes with a 16 foot outside shroud diameter. The original weight range of 1000 to 5000 pounds was reduced slightly to be consistent with the other constraints.

TABLE 2.3-1

SPECIFIC DESIGN AND OPERATIONAL CONSTRAINTS AND ASSUMPTIONS

	INITIAL	MODIFICATIONS
DESIGN		
CAPSULE		
SHAPE:	SPHERE CONE	
WEIGHT:	1000 TO 5000 POUNDS	
AEROSHELL DIAMETER:	16 FT MAXIMUM	
STERILE CANISTER DYNAMIC ENVELOPE:		15 FT 4 IN. MAXIMUM
OPERATIONAL		
LAUNCH, INTERPLANETARY CRUISE, & MARS ORBIT		
OPPORTUNITIES:	1973, 1975, 1977	EMPHASIS ON 1973
TRAJECTORY TYPE:	TYPE I AND TYPE II	
LAUNCH WINDOW	30 DAY MINIMUM BASED ON C_3 (PREFERRED)	COMPATIBLE WITH LANDING AT $\phi = 10°N$, $i = 60°$, $\Gamma_s = 60°$
FIRING WINDOW:	1 HR MINIMUM DAILY (PREFERRED)	
DECLINATION, OUTGOING:	5° TO 36° (PREFERRED)	5° TO 50°
INCLINATION TO ECLIPTIC:	> 0.1 DEG	
HYPERBOLIC EXCESS SPEED AT MARS:	3 KM/SEC MAXIMUM (PREFERRED)	
MARS ORBIT SIZE:	SYNCHRONOUS, NOMINAL 25 HR PERIOD SEMI-SYNCHRONOUS, NOMINAL 12.5 HR	SYNCHRONOUS ONLY
MARS ORBIT INCLINATION		INCLUDE $i = 60°$
SEPARATION, DESCENT, AND LANDING		
ENTRY ALTITUDE:	800000 FT	
ENTRY VELOCITY:	13000 TO 15200 FPS (INERTIAL)	
ENTRY FLIGHT PATH ANGLE:	GRAZE TO −20 DEG	
ATMOSPHERES:	VM-1 THROUGH VM-10	
AERODYNAMIC DECELERATOR DEPLOYMENT:	PARACHUTE AT MACH 2. ATTACHED INFLATABLE DECELERATOR AT MACH 6	
SURFACE SLOPE:	UP TO 34° ABOVE LOCAL HORIZONTAL	
LANDING SITE		NEAR EQUATORIAL, 60° SOLAR ANGLE
POST-LANDING		
EXPERIMENTS:	TO BE DEFINED BY MCDONNELL & APPROVED BY NASA	
EARTH COMMUNICATIONS:	COMPATIBLE WITH DEEP SPACE NETWORK 10^7 BITS MIN; 10^8 BITS DESIRED	

2.5 Study Results

The study results are presented in this four volume report. Section 1 is a summary of the study. Parametric analysis to provide quantitative understanding of the feasible Mars exploration capsules has been emphasized in the study; they are reported in Section 3. The conceptual designs are described in Section 4. In addition, key capsule systems and important conclusions have been described in three oral briefings during the study.

Parametric study results relate capsule system design parameters to performance. Accomplishment of mission objectives by capsules composed of the most likely combinations of systems is reported, using "surface payload" weight as an intermediate performance measure. The "surface payload" is defined as that portion of the capsule which is needed only to perform the post-landed mission. The primary function of the remainder of the capsule, then, is the delivery of the useful payload to the Martian surface. The sensitivity of design and performance is presented in a form which highlights the environmental parameters that have the greatest effects and thus require more detailed study. A non-dimensional form is used for presentation of the cost trends; this is sufficient to identify the low cost designs, indicate which capsule systems are most expensive, and aid in focusing future cost reduction efforts.

Each of the conceptual designs is described in a separate subsection of the report. Some repetition is caused by this technique, but the advantage of completeness of each description outweighs this disadvantage. The conceptual designs were prepared in parallel with the last parts of the parametric studies and may not reflect the final results of these studies. These inconsistencies are not so large as to affect the primary conclusions of the study.

2.6 Symbols and Abbreviations

The list of symbols and abbreviations used in this report are presented in Table 2.6-1.

TABLE 2.6-1

LIST OF SYMBOLS AND ABBREVIATIONS

A = Total Area

ACVM = Alternating Current Volt Meter

AGC = Automatic Gain Control

AMO = Air Mass Zero

AID = Attached Inflatable Decelerator

A_p = Projected Area To Sun

A_t = Throat Area

AU = Astronomical Unit

a_s = Solar Absorptance

B = Battery Section of Lander (As Subscript)

BCH = Bose Chaudhuri Hocquenghem (Coding)

B_{LO} = One Sided Noise Bandwidth

BPD = Bits Per Day

BPS = Bits Per Second

BT = Bandwidth Pulsewidth Product

BW = Bandwidth

C* = Characteristic Velocity

C_3 = Vis-Viva Energy

C_A = Axial Force Coefficient

CC&S = Central Computer And Sequencer

C_D = Drag Coefficient

C_{D_o} = Nominal Drag Coefficient

C_f = Thrust Coefficient

C_h = Channel

C_M = Pitching Moment Coefficient

C_{M_∞} = Pitching Moment Coefficient Slope

C_{m_q} = Pitch Damping Coefficient

C_N = Normal Force Coefficient

C_{N_∞} = Normal Force Coefficient Slope

cg = Center Of Gravity

cp = Specific Heat At Constant Pressure

cw = Continuous Wave

D = Deployment

TABLE 2.6-1 CONTINUED

$D_{A/S}$ = Aeroshell Diameter

DCVM = Direct Current Volt Meter

DGB = Disk Gap-Band Parachute

D/J = Direct Signal Over Indirect Signal Ratio

DO = Deorbit

D_o = Nominal Parachute Diameter

DRO = Destructive Readout

d = Distance

dB = Decibel

dBM = Decibel Referenced To A Meter

dBm = Decibel Relative To A Milliwatt

E = Energy

$E_{♂}$ = Elongation Angle Of Mars

ERP = Effective Radiative Power

e = Emittance, <u>or</u> Electron Charge, <u>or</u> Entry

F = Gray Body Radiation Shape Factor

FM = Frequency Modulation

f = Frequency (CPS or HZ)

fps = Feet Per Second

2FSK = Two Tone Frequency Shift Keying

g or g_E = Earth Gravity

g_M = Martian Gravity

Hz = Hertz

H_ρ = Density Scale Height

h = Height

h_a = Apoapse Altitude

h_c = Convection Heat Transfer Coefficient

h_D = Deployment Height

h_i = Altitude At Terminal Propulsion Ignition

h_p = Periapse Altitude

I = Moment Of Inertias <u>or</u> Current <u>or</u> Mass Spectrometer Analyzer Current

ID = Identification Ward In The Format

If = Intermediate Frequency

IMU = Inertial Measurement Unit

TABLE 2.6-1 CONTINUED

I_{sp} = Specific Impulse

I_t = Total Impulse

i = Inclination

in = Inch

KBPD = Kilo Bits Per Day

k = Thermal Conductivity

L = Landing

lb = Pound

LM = Lunar Module

M = Mach Number

M_D = Mach Number At Deployment

MFSK = Multiple Frequency Shift Keying

m = Mass

m/C_DA = Ballistic Parameter

mCp = Heat Capacity

mw = Milliwatt

NDRO = Nondestructive Readout

No = Noise Density

n = Relative Acceleration

o = Outside Environment Condition (As Subscript)

P = Power

PCM = Phase Change Material

PEPP = Planetary Entry Parachute Program

P_e = Probability Of Error

P_f = Orbit Then Passing Over Outgoing Approach Asymptote, Prime France Synchronization Ward

PN = Posigrade Approach From North

P_o = Power Output <u>or</u> Atmospheric Pressure At Surface

PS = Posigrade Approach From South

PSD = Phase Sensitive Detector

PSK = Phase Shift Keying

p = Body Rates About Roll Axes <u>or</u> Prototype (As Subscript)

Q = Total Heat Transfer Per Unit Area

Q_c = Total Convective Heat Transfer Per Unit Area

TABLE 2.6-1 CONTINUED

Q_R = Total Radiative Heat Transfer Per Unit Area

q = Heat Transfer Rate Per Unit Area <u>or</u> Body Rates About Pitch Axes

q_c = Convective Heat Transfer Rate

q_D = Deployment Dynamic Pressure

q_R = Radiative Heat Transfer Rate

R = Range <u>or</u> Resistance <u>or</u> Data Rate

RAG = Recovering Antenna Gain

R_f = Radio Frequency

RIU = Remote Interface Unit

R_N = Aeroshell Nose Radius

r = Radius <u>or</u> Burning Rate <u>or</u> Body Rates About Yaw Axes

S = Signal

SNR = Signal Noise Ratio

S_o = Parachute Reference Area (Essential Cloth Area)

s = Laplace Operation

$\bar{s}$ = Location Of Outgoing Vector Parallel Approach Asymptote But Passing Through Planet Center

sps = Sample Per Second

T = Thrust <u>or</u> Temperature

T_A = Time Of Arrival

T_{BL} = Maximum Bond Line Temperature Of Heat Protection Material

T_e = Initial Temperature

T_F = Flight Time

T_L = Landing Time

TM = Telemetry

t = Time

t_{SH} = Shadow Time

UHF = Ultrahigh Frequency

V = Potential <u>or</u> Volume

V_e = Entry Velocity

V_H = Horizontal Velocity Component

V_{HP} = Hyperbolic Excess Velocity

V_T or V_E = Terminal Vertical Velocity

V_V = Vertical Velocity Component

V_1 = Velocity After Deorbit ΔV

TABLE 2.6-1 CONTINUED

W/A = Unit Weight Of Entry Heat Protection

W_C = Capsule Weight

W_D = Decelerator System Weight

$W_{D.L.}$ = Deceleration Load Weight

W_E = Entry Weight

W_L = Lander Weight

WPMaF = Words Per Major Frame

WPMiF = Words Per Minor Frame

WPS = Words Per Second

W_{SP} = Surface Payload Weight

w = Watts

X = Reactance

XAG = Transmitting Antenna Gain

x = Insulation Thickness

Y = Admittance

Y(s) = Transfer Function

Z = Impedance

α = Thermal Diffusivity <u>or</u> Angle Of Attack on Mars Longitude

α_E = Entry Angle Of Attack

β = Sideslip Angle <u>or</u> Deorbit Velocity Pointing Angle, Measured From Local Horizontal

Γ_S = Solar Angle

γ = Isentropic Exponent <u>or</u> Flight Path Angle

γ_e = Entry Flight Path Angle

γ_g = Ground Referenced Flight Path Angle

γ_1 = Flight Path Angle After Deorbit ΔV

$\Delta\beta$ = Apsidal Precession Rate

$\Delta\theta_e$ = Entry Capsule Lead Angle At Entry

Δf = Bandwidth Of Amplifier <u>or</u> Frequency Shift

ΔV = Velocity Increment

δ = Deflection Angle <u>or</u> Latitude

TABLE 2.6-1 CONTINUED

ε = Expansion Ratio

ζ = Damping Ratio <u>or</u> Asymptote Half Angle

η = Efficiency

θ,ψ,ϕ = Euler Angles (Pitch, Yaw, Roll)

θ = Duration Of Entry Heat Pulse

θ_{DO} = Deorbit True Anomaly

θ_e = Entry True Anomaly

θ_L = Landing True Anomaly

λ = Wavelength

μ = Micron

ν = Volumetric Loading <u>or</u> Prandtl Meyer Angle

ρ = Periapse Rotation Angle <u>or</u> Density

σ = Heading Angle <u>or</u> Dispersion

σ_e = Entry Azimuth

σ_o = Effective Radar Cross Section Per Unit Area

τ = Time Constants

Φ_s = Declination Of The Outgoing Asumptote

Ω = Ascending Node

$\dot{\Omega}$ = Nodal Regression Rate

ω = Agrument of Periapse <u>or</u> Angular Frequency (RAD/SEC)

$\dot{\omega}$ = Apsidal Precession Rate

ALL ENGINEERING DRAWING UNITS ARE IN INCHES UNLESS OTHERWISE SPECIFIED.

3. PARAMETRIC STUDIES

The design of a Mars capsule which will accomplish the desired science objectives must be capable of following a planned mission profile and satisfy all the design and operational constraints. The mission profile must be selected to enhance the value of the scientific data accumulated; system and operational constraints must be questioned when they do not serve the program objectives; and system selections must be based on total flight capsule performance.

In addition, the resources required to attain specific scientific objectives must be determined and methods to reduce these resource requirements identified.

The following pages present the results of the study in five major subsections: missions, systems, flight capsule, environmental effects, and cost trends.

3.1 Mission Parametric Studies

Mission analyses and the definition of capsule system requirements require trajectory data to be generated over a wide range of values for numerous parameters. This data is summarized in the four major mission phases shown in Figure 3.1-1: (1) launch, arrival, and orbit; (2) deorbit and descent; (3) entry and atmospheric flight; and (4) terminal deceleration.

3.1.1 LAUNCH, ARRIVAL, AND ORBIT - The mission, as defined by this study, begins with delivery of the capsule from orbit. However, the time of launch, arrival conditions, and the orbit location and orientation, do affect several capsule systems. Consequently, a brief examination of the probable range of these parameters has been made for the 1973, 1975, and 1977 launch opportunities.

3.1.1.1 Launch opportunities - Basic assumptions for the launch opportunity are defined in Table 3.1.1-1. Each of these major constraints could be modified if necessary; the values given are preferred for mission flexibility or minimum change to the support operations. The launch opportunities for both Type I and Type II trajectories are presented in Figures 3.1.1-1 through -3, with shaded areas indicating constraints of the previous table. Table 3.1.1-2 lists the dimensions of these opportunties, given a 30 day launch window constraint. For the 1973 opportunity, considering this size of window with minimum vis viva energy, C_3, the Type I trajectory is preferred, Table 3.1.1-3. For high values of C_3 (> 25 km^2/sec^2) the Type II trajectory has only slightly longer flight times and is considered suitable for use. In the 1975 and 1977 launch opportunities, Type II trajectories are generally preferred, because the Type I trajectories have higher hyperbolic approach velocities, V_{HP}, and higher declinations of the outgoing asymptote, Φ_S. Declinations compatible with the normal range safety and boost tracking azimuths (60° - 120°) of the Eastern Test Range are in the 5° to 36° range. Higher declinations (up to 50°) will require range safety deviations and ships for boost tracking. However, final selection of trajectory types for the later opportunities will depend on mission requirements.

TYPICAL MISSION PROFILE

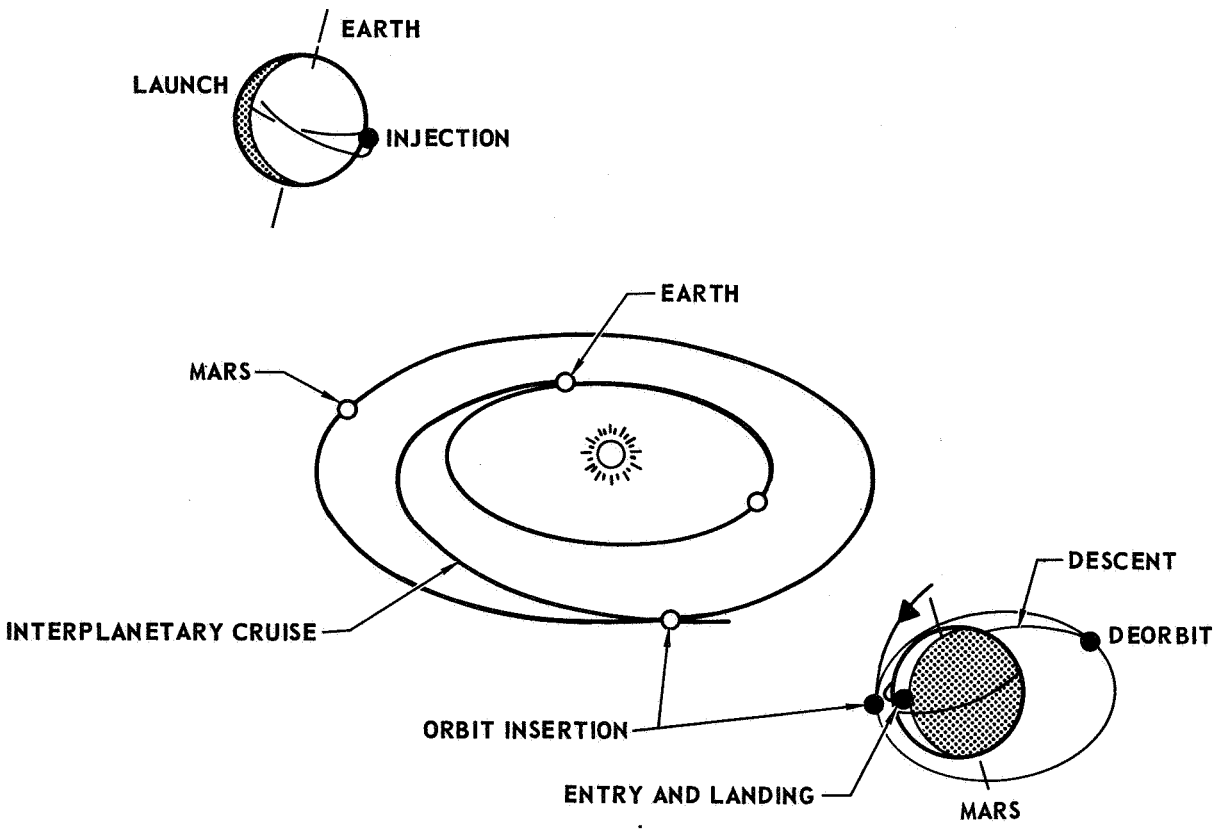

FIGURE 3.1–1

TABLE 3.1.1–1

LAUNCH OPPORTUNITY CONSTRAINTS

CONSTRAINT	PREFERRED LIMIT	COMMENT
LAUNCH WINDOW	30 DAY MINIMUM	WINDOW SHOULD BE SUFFICIENTLY LONG TO PERMIT RECYCLING AND LAUNCH OF BOOSTER
FIRING WINDOW	1 HR DAILY MIN	DAILY FIRING WINDOW SHOULD PROVIDE SOME FLEXIBILITY IN FIRING TIME
LAUNCH SITE	EASTERN TEST RANGE	PROVIDES EASTWARD LAUNCH
DECLINATION OF OUTGOING ASYMPTOTE	$5^\circ \leq \lvert \Phi_S \rvert \leq 36^\circ$	TO LIMIT LAUNCH AZIMUTH TO NORMAL RANGE SAFETY LIMITS AND BOOST PHASE TRACKING OPERATIONS
	$5^\circ \leq \lvert \Phi_S \rvert \leq 50^\circ$	TO PERMIT LOWER LAUNCH AZIMUTHS
INCLINATION TO ECLIPTIC	$i \geq 0^\circ.1$	TO PROVIDE INTERPLANETARY TRACKING ACCURACY SUFFICIENT FOR GOOD ORBIT DETERMINATION AND MIDCOURSE CORRECTIONS
MARS–EARTH–SUN ANGLE	$E\delta > 5^\circ.0$	COMMUNICATIONS INTERFERENCE FROM SUN WHEN EARTH, SUN, AND MARS ARE IN NEAR ALIGNMENT
MARS APPROACH VELOCITY (HYPERBOLIC EXCESS VELOCITY)	$V_{HP} \leq 3.5$	LOW V_{HP} REDUCES ORBIT INSERTION VELOCITY REQUIREMENTS

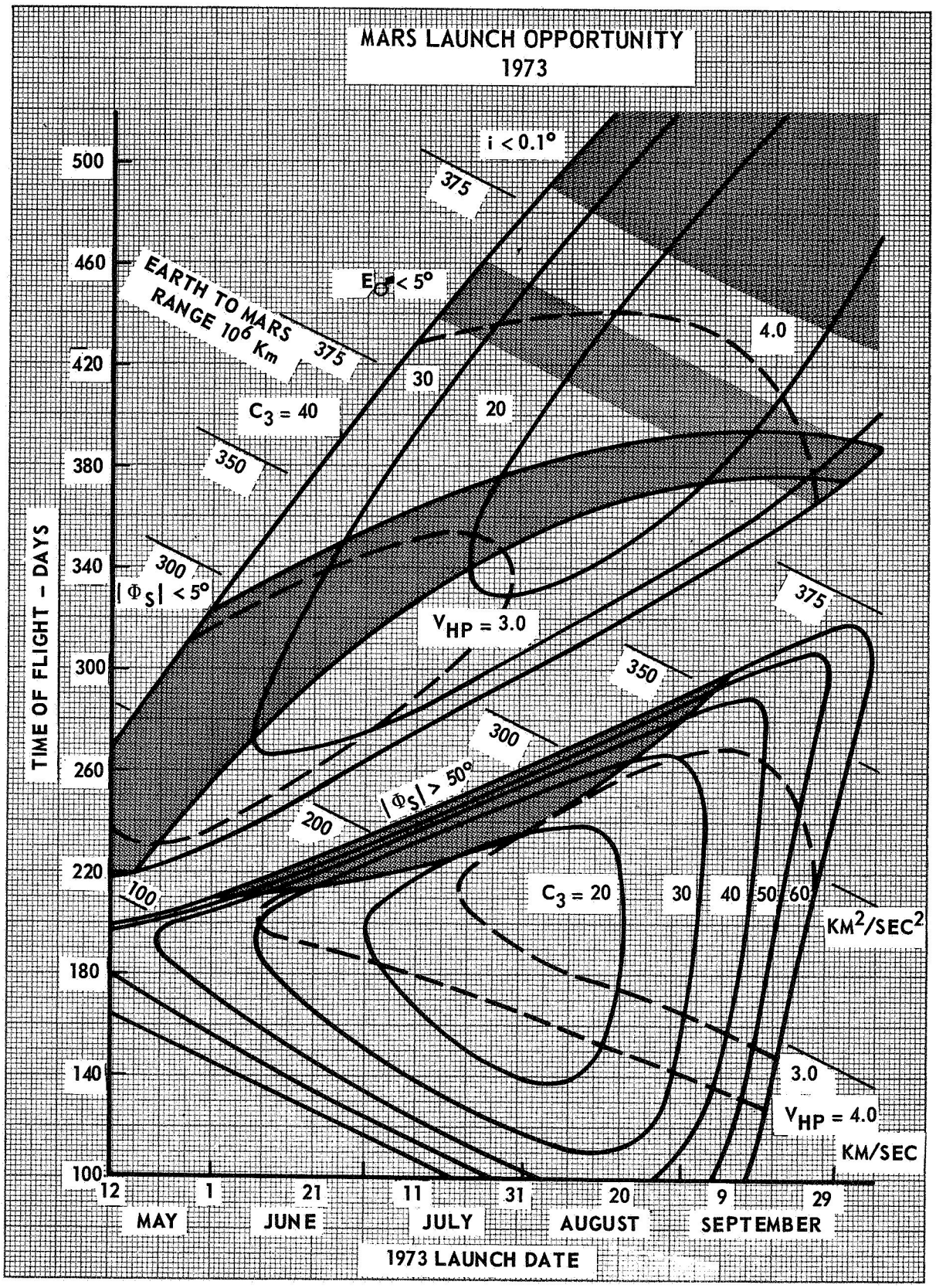
MARS LAUNCH OPPORTUNITY
1973
TIME OF FLIGHT - DAYS
500
460
420
380
340
300
260
220
180
140
100
EARTH TO MARS
RANGE 10^6 Km
375
375
350
300
200
100
i < 0.1°
E♂ < 5°
30
20
4.0
C3 = 40
|Φs| < 5°
VHP = 3.0
375
350
300
|Φs| > 50°
C3 = 20
30
40
50
60
KM²/SEC²
3.0
VHP = 4.0
KM/SEC
12
1
21
11
31
20
9
29
MAY
JUNE
JULY
AUGUST
SEPTEMBER
1973 LAUNCH DATE

FIGURE 3.1.1–1

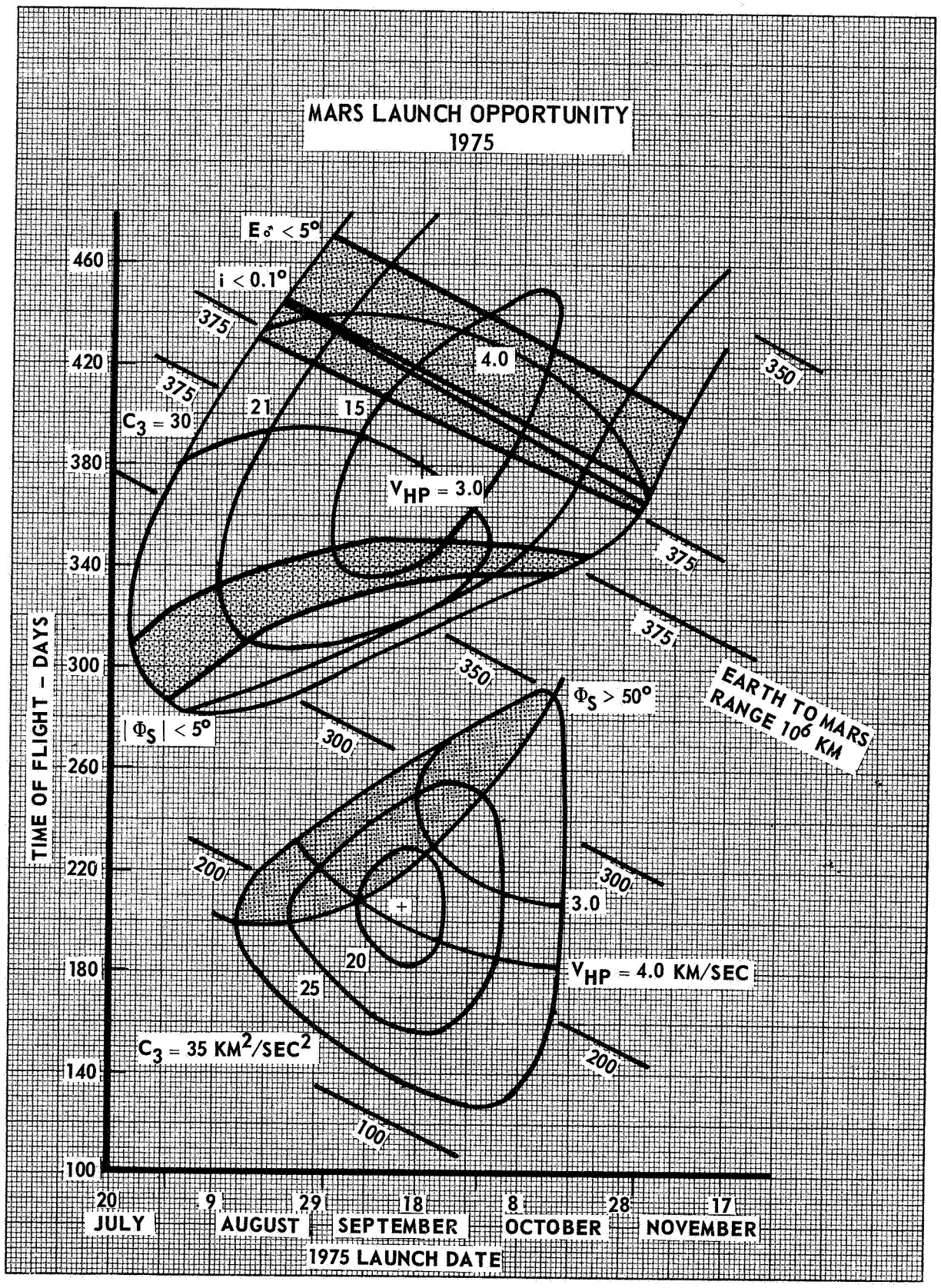
MARS LAUNCH OPPORTUNITY
1975
$E_\delta < 5°$
$i < 0.1°$
375
375
350
4.0
21
15
$C_3 = 30$
$V_{HP} = 3.0$
375
375
350
$\Phi_S > 50°$
EARTH TO MARS RANGE 10^6 KM
$|\Phi_S| < 5°$
300
200
300
3.0
20
25
$V_{HP} = 4.0$ KM/SEC
$C_3 = 35$ KM^2/SEC^2
200
100
TIME OF FLIGHT – DAYS
460
420
380
340
300
260
220
180
140
100
20
9
29
18
8
28
17
JULY
AUGUST
SEPTEMBER
OCTOBER
NOVEMBER
1975 LAUNCH DATE

FIGURE 3.1.1–2

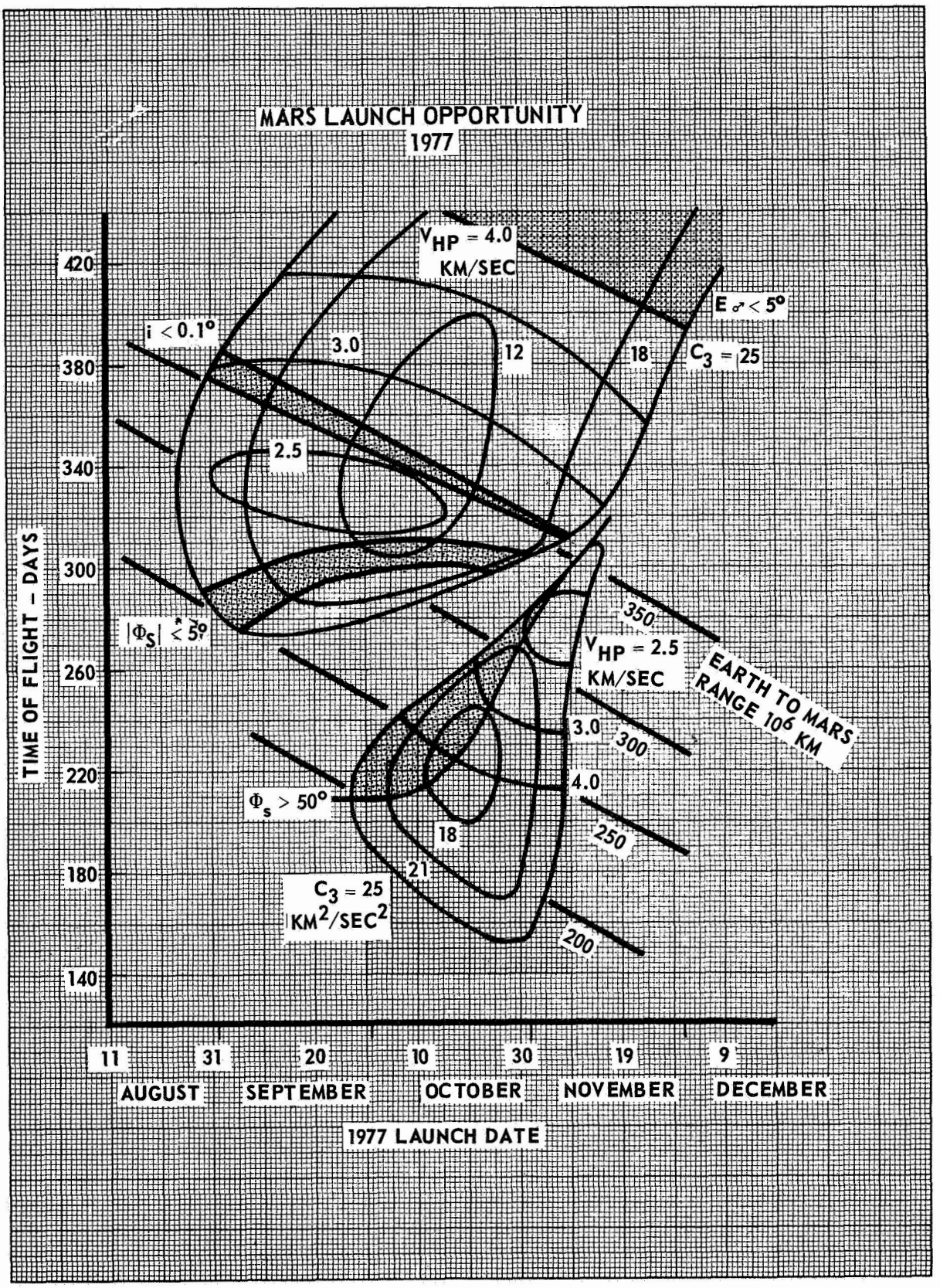
MARS LAUNCH OPPORTUNITY
1977
V_{HP} = 4.0 KM/SEC
$E_{♂} < 5°$
$i < 0.1°$
3.0
12
18
C_3 = 25
2.5
$|\Phi_S| < 5°$
350
V_{HP} = 2.5 KM/SEC
EARTH TO MARS RANGE 10^6 KM
3.0
300
4.0
250
$\Phi_s > 50°$
18
21
C_3 = 25 KM^2/SEC^2
200
TIME OF FLIGHT – DAYS
420
380
340
300
260
220
180
140
11
31
20
10
30
19
9
AUGUST
SEPTEMBER
OCTOBER
NOVEMBER
DECEMBER
1977 LAUNCH DATE

FIGURE 3.1·1–3

TABLE 3.1.1–2

LAUNCH OPPORTUNITIES (WITHOUT CONSTRAINTS)
30 DAY LAUNCH WINDOW

OPPORTUNITY	C_3	LAUNCH DATE	ARRIVAL DATE	MAX V_{HP}
1973 I	16.6	JUL 13, 1973 AUG 12, 1973	18 JAN 1974 17 MAR 1974	4.26
1973 II	16.6	AUG 14, 1973 SEP 13, 1973	21 AUG 1974 30 NOV 1974	4.3
1975 I	22.37	AUG 31, 1975 SEPT 30, 1975	1 MAR 1976 25 MAY 1976	5.78
1975 II	14.2	SEP 6, 1975 OCT 6, 1975	20 AUG 1976 30 NOV 1976	4.0
1977 I	21.22	OCT 4, 1977 NOV 3, 1977	15 APR 1978 31 JUL 1978	6.66
1977 II	12.0	SEP 25, 1977 OCT 25, 1977	6 AUG 1978 26 NOV 1978	3.8

TABLE 3.1.1–3

COMPARISON OF TRAJECTORY TYPE

1973 LAUNCH OPPORTUNITY

PARAMETER	TYPE I	TYPE II	COMMENT
LAUNCH DATE	13 JUL 73 – 12 AUG 73	1 AUG 73 – 31 AUG 73	30 DAY WINDOW
C_3, KM^2/SEC^2	16.6 14.45 MIN.	18.3 16.05 MIN.	LOW C_3 FOR HIGH INJECTED WEIGHT
$5° < \lvert \Phi_s \rvert < 50°$	MINIMUM INTERFERENCE	DIVIDES WINDOW INTO 2 SECTIONS	FIRING WINDOW, LAUNCH AZIMUTH, BOOST TRACKING
$E♂ > 5°$	NO INTERFERENCE	FOR 30 DAY LANDED MISSION, ELIMINATES UPPER WINDOW	SMALL ♂–⊗–⊙ ANGLE INTERFERES WITH COMMUNICATION
V_{HP}, KM/SEC	2.52 MIN.	3.3 MIN.	LOW VELOCITY MINIMIZES ORBIT INSERTION VELOCITY
TIME OF FLIGHT, DAYS	167–221	347–373	PLANETARY VEHICLE OPERATING TIME
COMMUNICATION RANGE, 10^6 KM	150–235	371–393	POWER REQUIREMENTS

3.1.1.2 Arrival conditions. - The three considerations in the choice of suitable arrival conditions are Mars-Earth-Sun angular relationships, Earth-Mars distances, and the approach vector. Small Mars-Earth-Sun angles (E♂) indicate near conjunction of Mars and Earth. Solar interference during this period makes direct communication impractical; consequently, as shown in the launch opportunity figures, these dates are not suitable for arrival.

The Earth-Mars distance, R_C (direct communications distance), has also been indicated on the launch opportunities, Figures 3.1.1-1 through -3. It is apparent that the Type II trajectories will have longer communication ranges.

The approach direction is generally defined by the outgoing S vector which passes through the center of Mars and is parallel to the specific approach asymptote. The declination of the outgoing S vector at Mars defines the minimum possible orbital inclination, and in conjunction with sub-Sun and sub-Earth positions, can give an indication of lighting and landing conditions. Figures 3.1.1-4 through -6 show the position of the S vector in Mars equatorial coordinates for three opportunities (1973 I, 1975 II, and 1977 II), in addition to the corresponding locations of the Sun and Earth. For the 1973 I opportunity the outlines of the 30 day window have been indicated.

The S vector position, the periapses altitude, and the hyperbolic excess velocity determine the locus of natural (no rotation) periapse positions. The periapses are located on a circle of fixed central angle about the S vector. The central angle, the asymptote half angle, is shown in Figure 3.1.1-7 for various V_{HP}'s and periapse altitudes. A specific inclination would permit four possible periapse positions, two retrograde (approach in opposition to planet rotation), and two posigrade (approach with the planet). Those to be considered are posigrade approaching from both the north (posigrade-north) and the south (posigrade-south) over the S vector. Retrograde orbits were rejected to avoid landing in darkness, to prevent Earth occulation before insertion (loss of communication), and to avoid the higher aerodynamic velocities associated with retrograde entry.

3.1.1.3 Orbit and landing location selection. - Table 3.1.1-4 contains a list of secondary constraints which have been considered for the 1973 mission. These constraints have been examined parametrically to evaluate mutual compat-

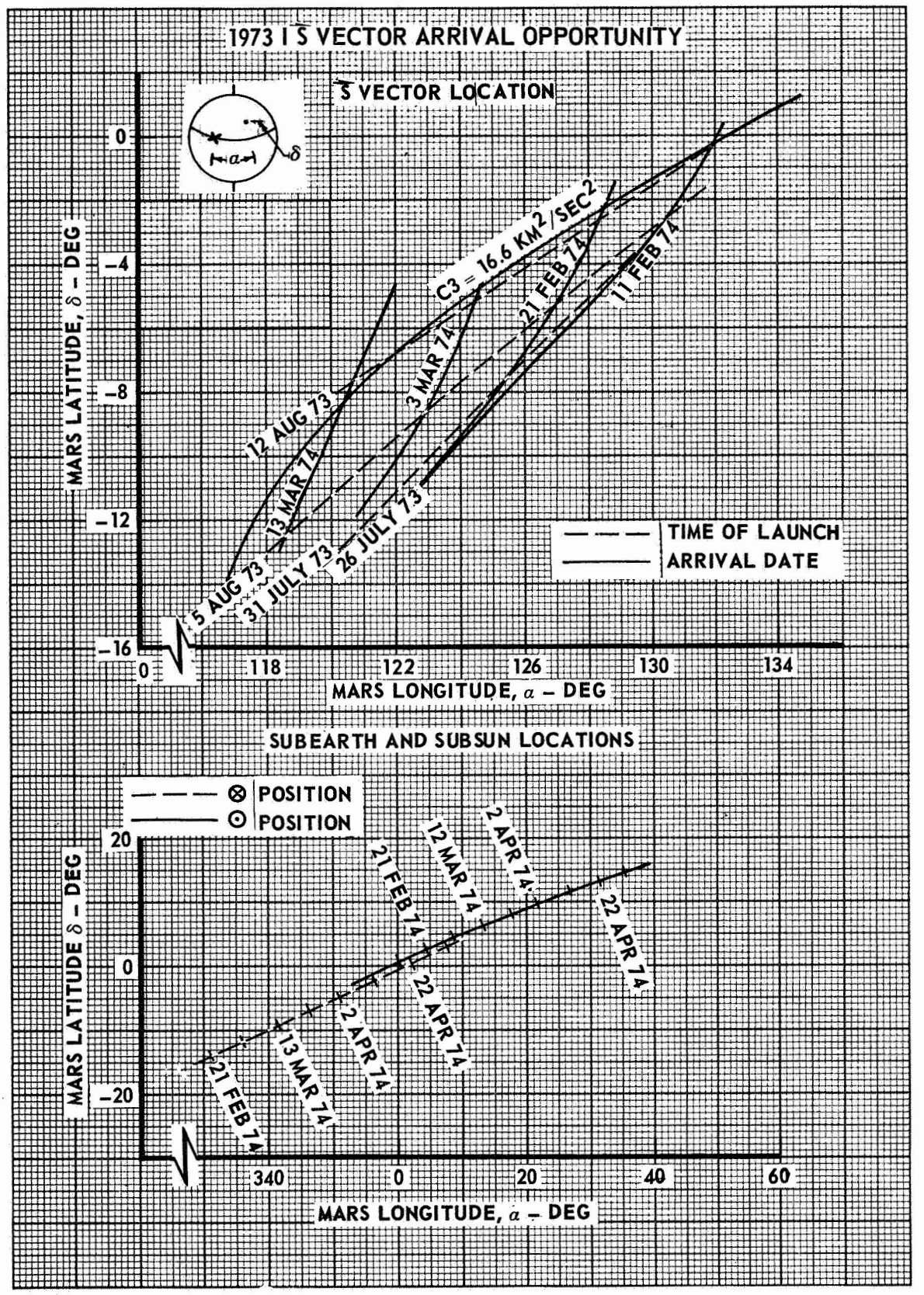
1973 I S VECTOR ARRIVAL OPPORTUNITY
S VECTOR LOCATION
α
δ
MARS LATITUDE, δ – DEG
0
–4
–8
–12
–16
C3 = 16.6 KM²/SEC²
12 AUG 73
13 MAR 74
3 MAR 74
21 FEB 74
11 FEB 74
5 AUG 73
31 JULY 73
26 JULY 73
TIME OF LAUNCH
ARRIVAL DATE
0
118
122
126
130
134
MARS LONGITUDE, α – DEG
SUBEARTH AND SUBSUN LOCATIONS
POSITION
POSITION
MARS LATITUDE δ – DEG
20
0
–20
2 APR 74
12 MAR 74
21 FEB 74
22 APR 74
22 APR 74
2 APR 74
13 MAR 74
21 FEB 74
340
0
20
40
60
MARS LONGITUDE, α – DEG

FIGURE 3.1.1–4

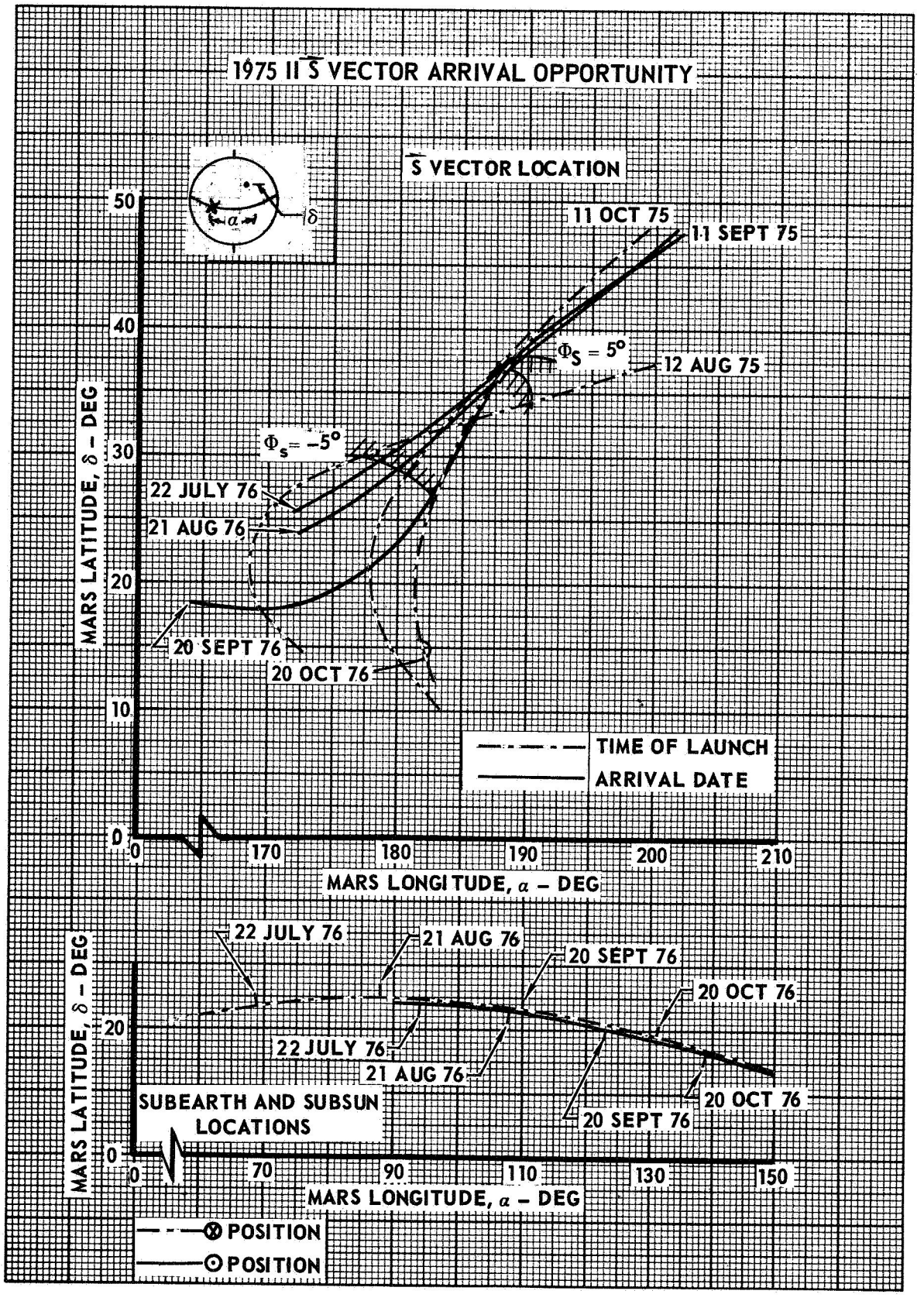
1975 II $\bar{S}$ VECTOR ARRIVAL OPPORTUNITY
$\bar{S}$ VECTOR LOCATION
α
δ
11 OCT 75
11 SEPT 75
$\Phi_S = 5°$
12 AUG 75
$\Phi_S = -5°$
22 JULY 76
21 AUG 76
20 SEPT 76
20 OCT 76
TIME OF LAUNCH
ARRIVAL DATE
MARS LATITUDE, δ – DEG
MARS LONGITUDE, α – DEG
0
10
20
30
40
50
170
180
190
200
210
22 JULY 76
21 AUG 76
20 SEPT 76
20 OCT 76
22 JULY 76
21 AUG 76
20 SEPT 76
20 OCT 76
SUBEARTH AND SUBSUN LOCATIONS
MARS LATITUDE, δ – DEG
MARS LONGITUDE, α – DEG
0
20
70
90
110
130
150
⊗ POSITION
⊙ POSITION

FIGURE 3.1.1–5

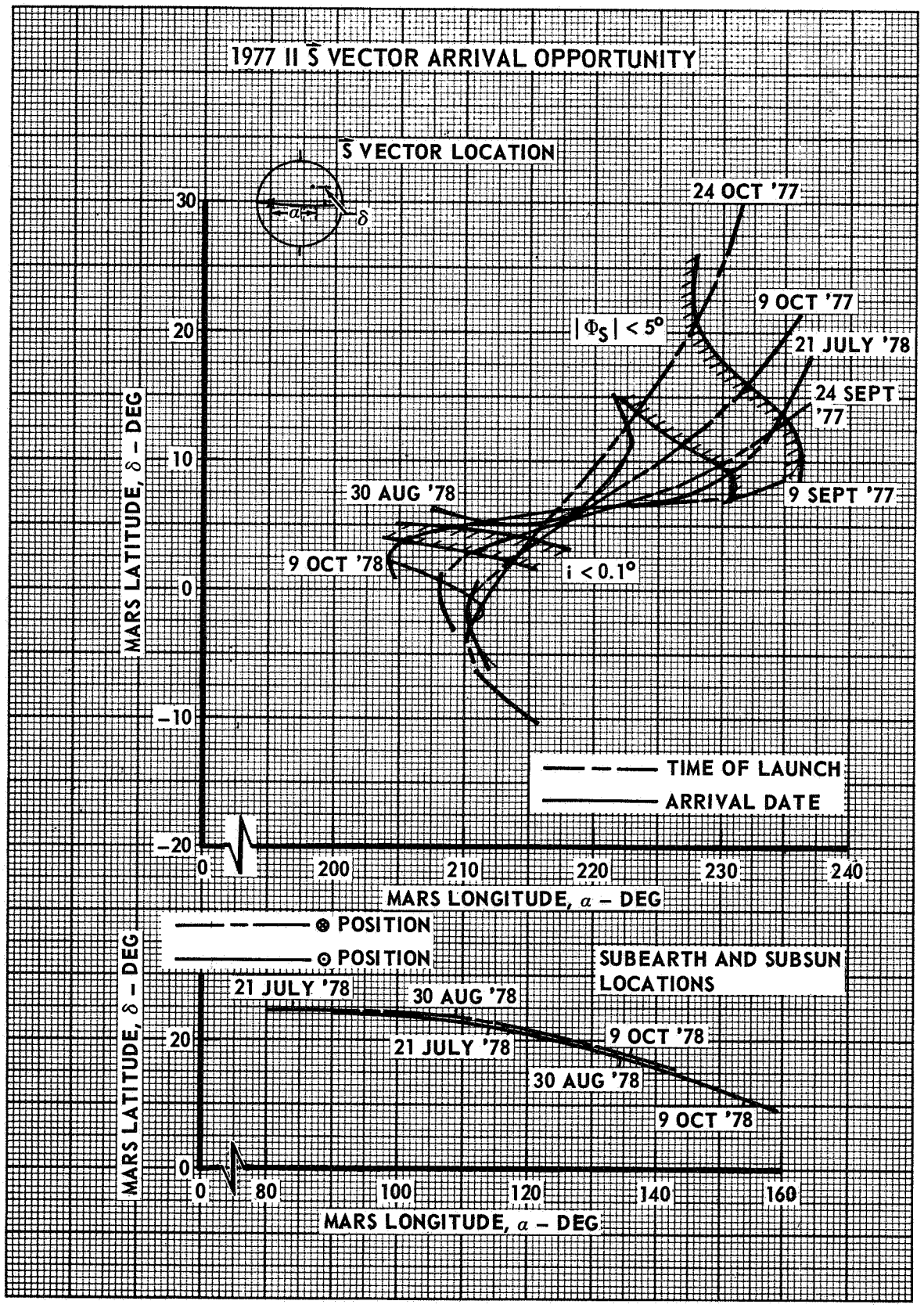
1977 II S̄ VECTOR ARRIVAL OPPORTUNITY
S̄ VECTOR LOCATION
α
δ
24 OCT '77
9 OCT '77
21 JULY '78
24 SEPT '77
9 SEPT '77
30 AUG '78
9 OCT '78
|Φ_S| < 5°
i < 0.1°
TIME OF LAUNCH
ARRIVAL DATE
MARS LATITUDE, δ – DEG
MARS LONGITUDE, α – DEG
30
20
10
0
–10
–20
0
200
210
220
230
240
⊗ POSITION
⊙ POSITION
SUBEARTH AND SUBSUN LOCATIONS
21 JULY '78
30 AUG '78
9 OCT '78
21 JULY '78
30 AUG '78
9 OCT '78
MARS LATITUDE, δ – DEG
MARS LONGITUDE, α – DEG
20
0
0
80
100
120
140
160

FIGURE 3.1.1–6

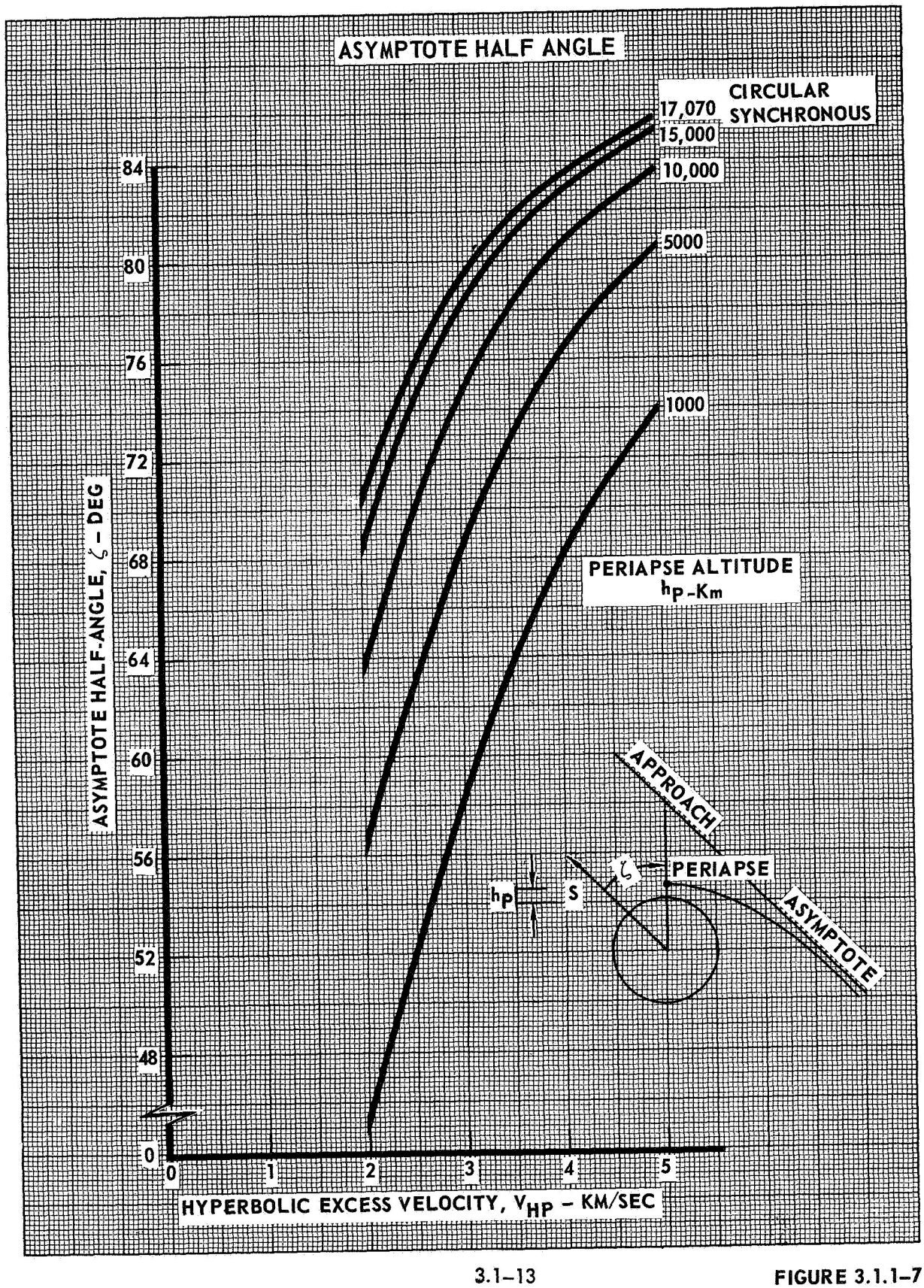
ASYMPTOTE HALF ANGLE
CIRCULAR SYNCHRONOUS
17,070
15,000
10,000
5000
1000
PERIAPSE ALTITUDE
hP -Km
ASYMPTOTE HALF-ANGLE, ζ - DEG
84
80
76
72
68
64
60
56
52
48
0
0
1
2
3
4
5
HYPERBOLIC EXCESS VELOCITY, VHP - KM/SEC
APPROACH
PERIAPSE
ASYMPTOTE
ζ
hP
S

FIGURE 3.1.1–7

TABLE 3.1.1-4

ORBIT AND LANDING CONSTRAINTS

CONSTRAINT	PREFERRED	COMMENT
ORBIT SIZE	PERIOD SYNCHRONOUS	AVAILABLE FOR LANDER SUPPORT FOR A FEW DAYS, THEN ORBIT SIZE MODIFIED FOR MAXIMUM ORBITER UTILITY
LANDING SITE	NEAR EQUATOR	± 20° CONSIDERED AS NEAR EQUATOR
LIGHTING	60° SOLAR ANGLE	PREFERRED FOR CAMERA EXPERIMENTS AT LANDING
DEORBIT ANOMALY		180°–250° CONSIDERED TO MINIMIZE DEORBIT VELOCITY
INCLINATION	0°–60°	ONLY POSIGRADE ORBITS CONSIDERED. 60° INCLINATION DESIRED FOR ORBITER MAPPING
ENVIRONMENT ATMOSPHERE GROUND SLOPE ENTRY CORRIDOR	 VM 1–10 34° V_e: 14,000–15,200 γ_e: GRAZE – –20°	CAPSULE DESIGN CONSTRAINTS TO PROVIDE SOME MISSION FLEXIBILITY IN THE EVENT OF CHANGES IN ORBIT SIZE, VEHICLE WEIGHT, LANDING SITE, ATMOSPHERIC MODELS, ETC.

ibility and applicability to the launch opportunity. Landing at a specific site with these constraints requires:

a) Accurate prediction of the time such that the longitude of the landing site rotates beneath the orbit at the desired time (function of arrival time and wait in orbit).

b) The 60° lighting angle to occur at the selected 10°N latitude for the orbit location (S vector) of that date (function of launch date and arrival date).

c) The orbit periapse to be rotated from the natural periapse such that the landing anomaly will occur at the selected Mars latitude (function of deorbit anomaly, entry angle, atmosphere, etc.).

3.1.1.3.1 Orbital insertion, rotation, and motion: Results of parametric studies for orbit selection and subsequent motion are shown in Figures 3.1.1-8 and -9. Rotation from natural periapse, ρ, the periapse altitude, h_p, and the hyperbolic excess velocity at arrival, V_{HP}, determine the total orbit insertion velocity increment, ΔV. Figure 3.1.1-8a details the advantages of negative rotation using a tangent orbit insertion technique. Figure 3.1.1-8b relates the trade-off between periapse altitude and rotation. The effects of the various periapse altitudes on orbital precession and regression due to the planet oblateness are shown in Figure 3.1.1-9 as a function of orbital inclination.

3.1.1.3.2 Landing locations: The geometry at landing is shown in Figure 3.1.1-10. For this study and its particular specifications the nominal conditions considered are an inclination, i, of 60°, a solar angle, Γs, of 60°, a landing latitude, δ, of 10° N, and a landing anomaly, θ_L, of 355°. The conditions met for the nominal inclination, solar angle, and landing latitude are shown on a Type I opportunity in Figure 3.1.1-11a. The morning landings require much lower C_3 and have longer launch windows than the evening landings; however, when the rotation required to meet the landing anomaly is examined, Figure 3.1.1-11b, the morning landing requires rotations larger than -100°. (An example of rotation computation would be adding the landing anomaly with respect to the hyperbola periapse (e.g., θ = 50° in Figure 3.1.1-11b) to the

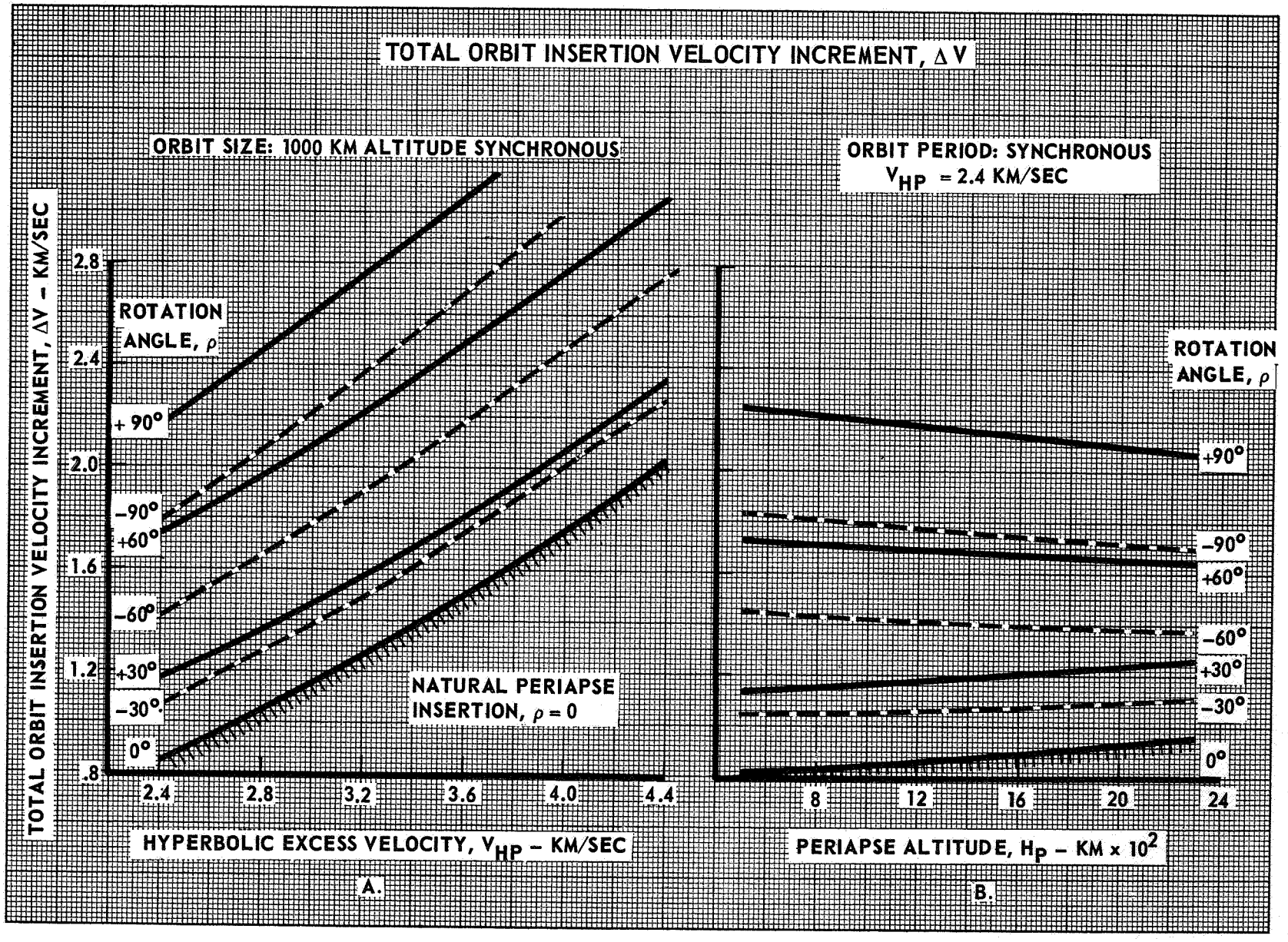
TOTAL ORBIT INSERTION VELOCITY INCREMENT, ΔV
ORBIT SIZE: 1000 KM ALTITUDE SYNCHRONOUS
ROTATION ANGLE, ρ
+ 90°
−90°
+60°
−60°
+30°
−30°
0°
NATURAL PERIAPSE INSERTION, ρ = 0
TOTAL ORBIT INSERTION VELOCITY INCREMENT, ΔV – KM/SEC
2.8
2.4
2.0
1.6
1.2
.8
2.4
2.8
3.2
3.6
4.0
4.4
HYPERBOLIC EXCESS VELOCITY, V_HP – KM/SEC
A.
ORBIT PERIOD: SYNCHRONOUS
V_HP = 2.4 KM/SEC
ROTATION ANGLE, ρ
+90°
−90°
+60°
−60°
+30°
−30°
0°
8
12
16
20
24
PERIAPSE ALTITUDE, H_P – KM x 10^2
B.

FIGURE 3.1.1-8

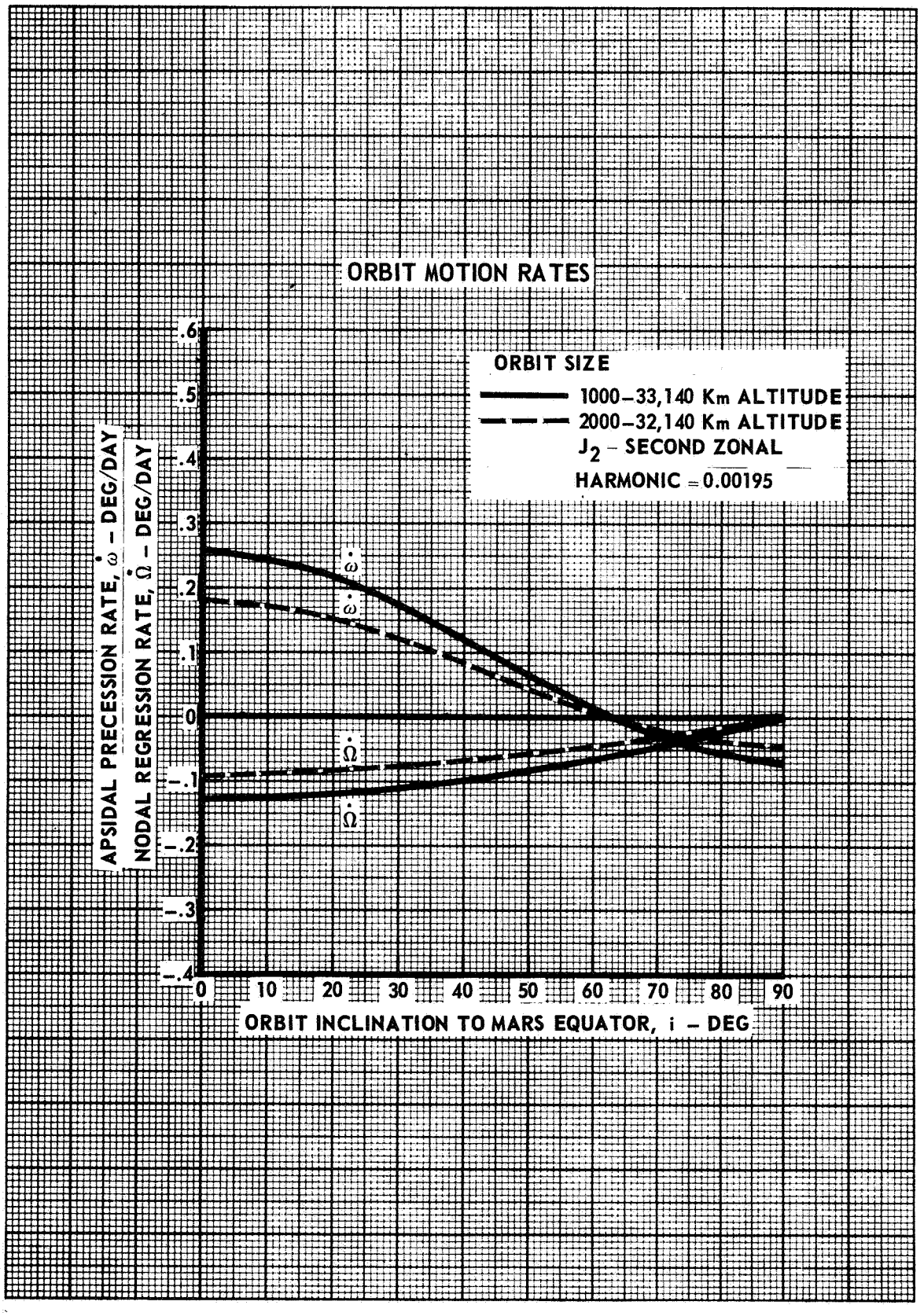
ORBIT MOTION RATES
ORBIT SIZE
1000–33,140 Km ALTITUDE
2000–32,140 Km ALTITUDE
J_2 – SECOND ZONAL
HARMONIC = 0.00195
APSIDAL PRECESSION RATE, $\dot{\omega}$ – DEG/DAY
NODAL REGRESSION RATE, $\dot{\Omega}$ – DEG/DAY
$\dot{\omega}$
$\dot{\omega}$
$\dot{\Omega}$
$\dot{\Omega}$
.6
.5
.4
.3
.2
.1
0
–.1
–.2
–.3
–.4
0
10
20
30
40
50
60
70
80
90
ORBIT INCLINATION TO MARS EQUATOR, i – DEG

FIGURE 3.1.1–9

LANDING GEOMETRY

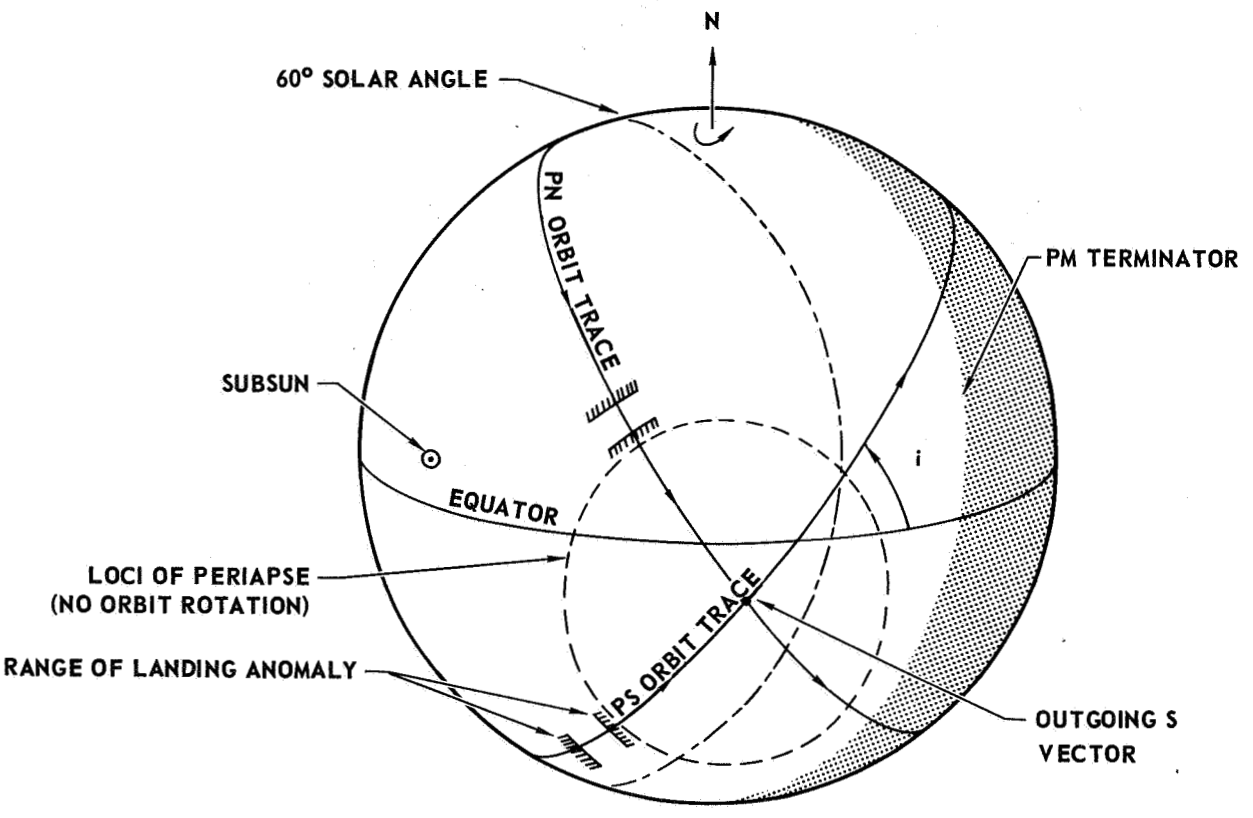

PN – POSIGRADE APPROACH OVER NORTHERN HEMISPHERE
PS – POSIGRADE APPROACH OVER SOUTHERN HEMISPHERE

FIGURE 3.1.1–10

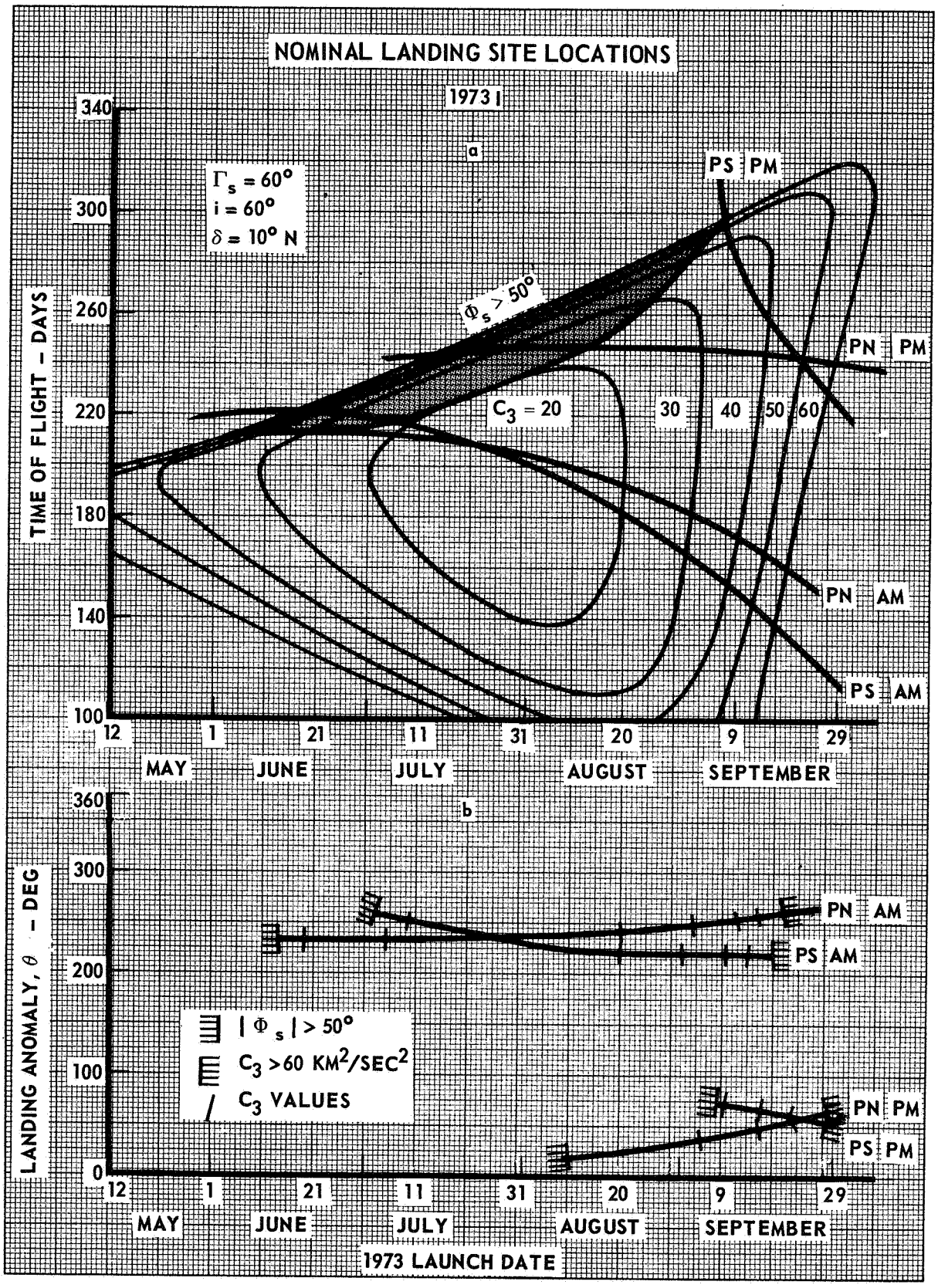

FIGURE 3.1.1–11

landing anomaly with respect to the actual ellipse periapse (θ_L = 355°) and obtaining a rotation of +55°. With a V_{HP} of 2.8 km/sec, Figure 3.1.1-8 indicated a ΔV of 1.85 km/sec for this orbit insertion and rotation.) Thus, the evening landing is more favorable, due to its lower rotation requirements and lower V_{HP}. The posigrade-north evening landing has the advantages of longer launch window and a small C_3, as compared to a posigrade-south evening landing. Therefore it seems to be the most favorable selection.

A note of interest to Figure 3.1.1-11a concerns the two points of commonality between the two sets of landings. These points indicate where the landing occurs directly over either the incoming or outgoing S vector. Thus, the declination of the S vector equals 10°. Also, for these specific launch and arrival trajectories, the 60° solar angle and 10° latitude occur for any possible inclination. By moving 5 to 10 days in time of flight along the contour of δ equal to 10°, the contours of 0° and 20° can be obtained.

The Type II 1973 opportunity has been examined in a region having landing parameters comparable to the landing locations shown in Figure 3.1.1-11. The solar angles shown in Figure 3.1.1-12 indicate that acceptable landing locations can be obtained for Type II trajectories. If the high C_3 required for Type I becomes a critical constraint, further investigation of the Type II trajectories should be made.

3.1.1.3.3 Occultation and landing location: An important aspect to be considered in orbit and landing site selection is the resulting occultation conditions encountered by the orbiting spacecraft. The occultation geometry is shown in Figure 3.1.1-13. The loss of acquisition of any of three celestial bodies, the Sun, Earth, or Canopus, has varying degrees of significance on mission success. Loss of Sun lock could cause failure of the orbiter batteries if the time spent in the shadow requires a deep drain of the stored energy. Loss of Earth lock is also a disadvantage for communications reasons. Canopus loss affects stabilization of the orbiter.

Figure 3.1.1-14 shows a mapping of occultation and solar angle effects on a Martian coordinate grid. For the specific date shown, the sub-Sun point lies nearly on the equator. Both posigrade north and south orbits are shown. If

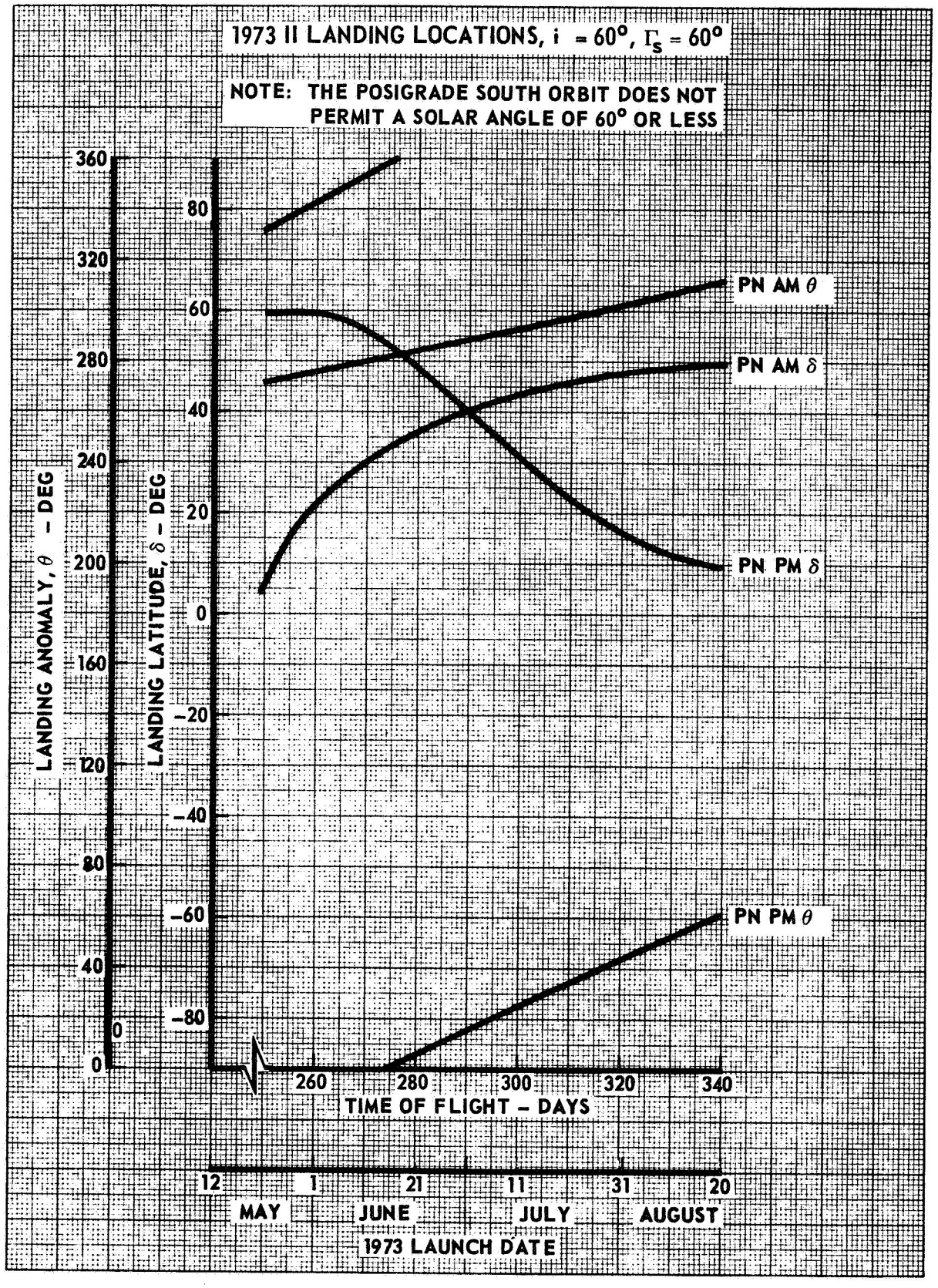

FIGURE 3.1.1–12

OCCULTATION GEOMETRY

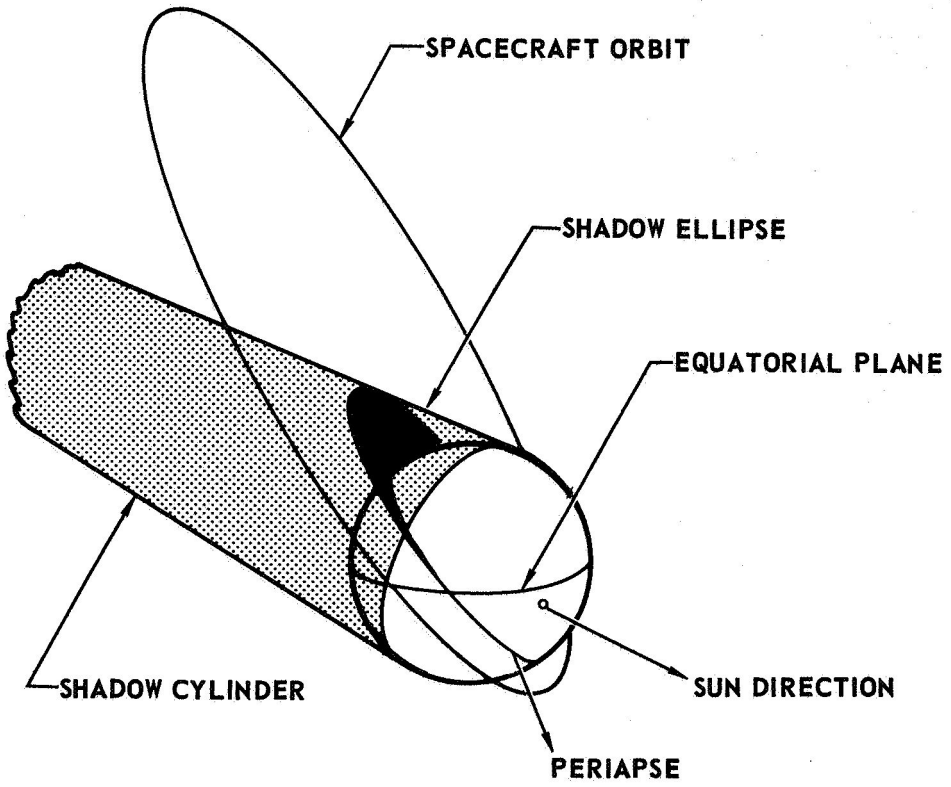

FIGURE 3.1.1–13

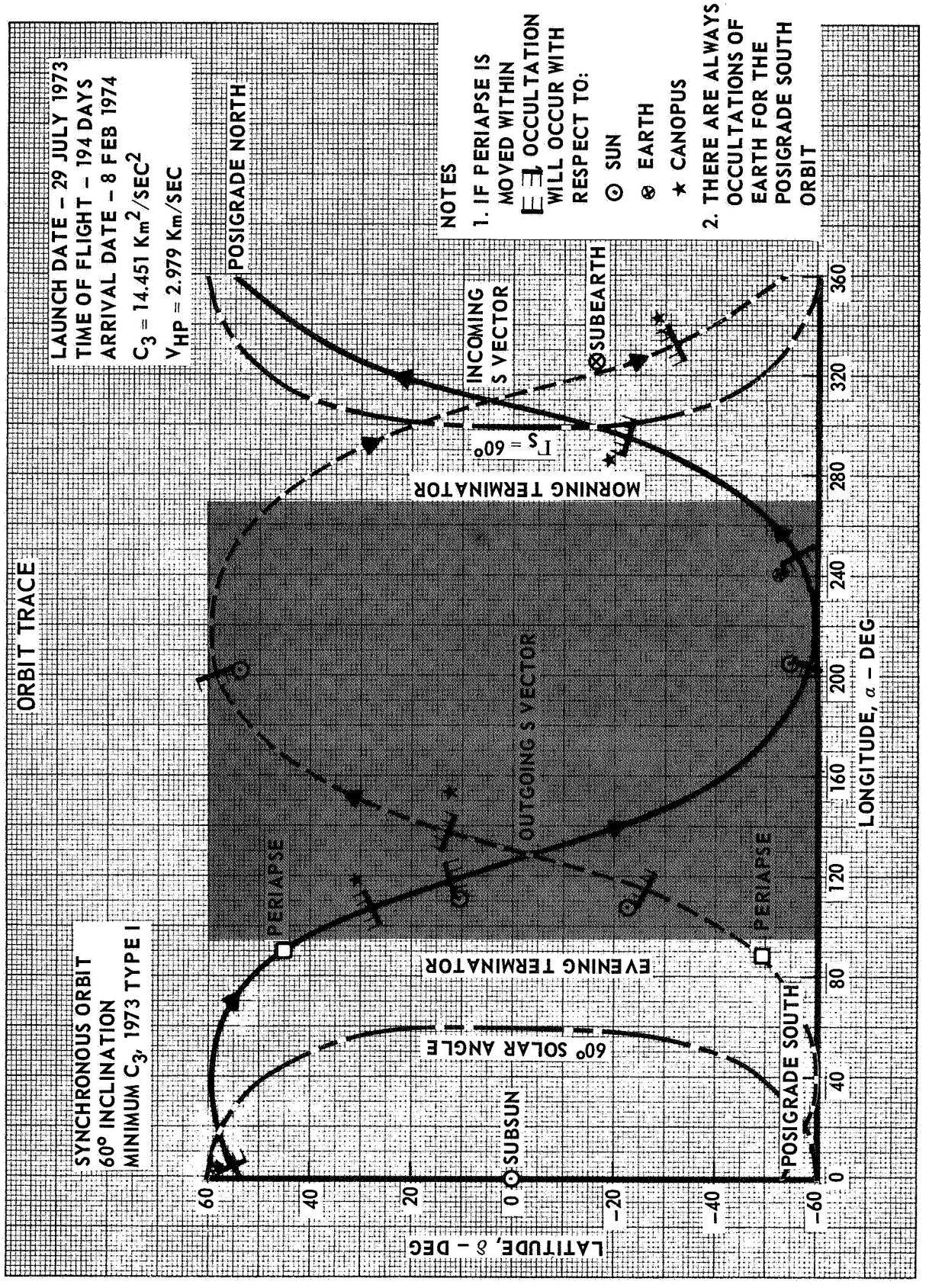

FIGURE 3.1.1–14

the orbit periapse lies in particular regions of the orbit, occultation will occur as noted on the orbit traces.

The resulting occultations to an orbiter of a constrained landing location have been examined for the four possibilities mentioned in the previous section. Figure 3.1.1-15 shows the "absolute" occultation conditions of the three bodies mentioned above for both posigrade orbits. The cross-hatch areas show regions where occultations for that body always occur, regardless of orbit rotation. The shaded areas indicate regions of no occulation regardless of periapse rotation. Note that there are no regions of either all occultation or no occultation for Canopus. In both cases, occulations for Canopus depend on the location of the rotated periapse. Plots of the occultation conditions for the posigrade-north orbit (Figure 3.1.1-16) show the evening landing to be more desirable, because of the absence of Earth and Sun occultations and only some Canopus occultation at the desired landing anomaly. The posigrade-south evening landing is also free of all Sun and Earth occultation, but requires higher C_3's and V_{HP}'s, and has a shorter launch window, making it the less desirable of the two evening landings.

3.1.1.3.4 Landing and occultation flexibility: Since the nominal landing location does not present the optimum solution for a number of variables such as C_3, V_{HP}, and occultation characteristics, studies of other launch and arrival dates in the opportunity have been made. Variations in a wide variety of parameters are presented to show the wide range of flexibility achievable by modifying various constraints.

Figure 3.1.1-17 shows the variation in landing conditions for a constant launch date. Both the latitude and landing anomaly are shown for a solar angle and inclination of 60°. Figure 3.1.1-18 shows the occultation characteristics for an inclination range for both the minimum C_3 and V_{HP} launch trajectories, with corresponding landing conditions as a function of the argument to the periapse, ω. It is defined as the angle measured from the ascending node (where the orbit trace crosses the Martian equator heading north) to the periapse. Figure 3.1.1-19 shows the occultation as a function of orbit rotation rather than the natural periapse location for only the minimum C_3 trajectory.

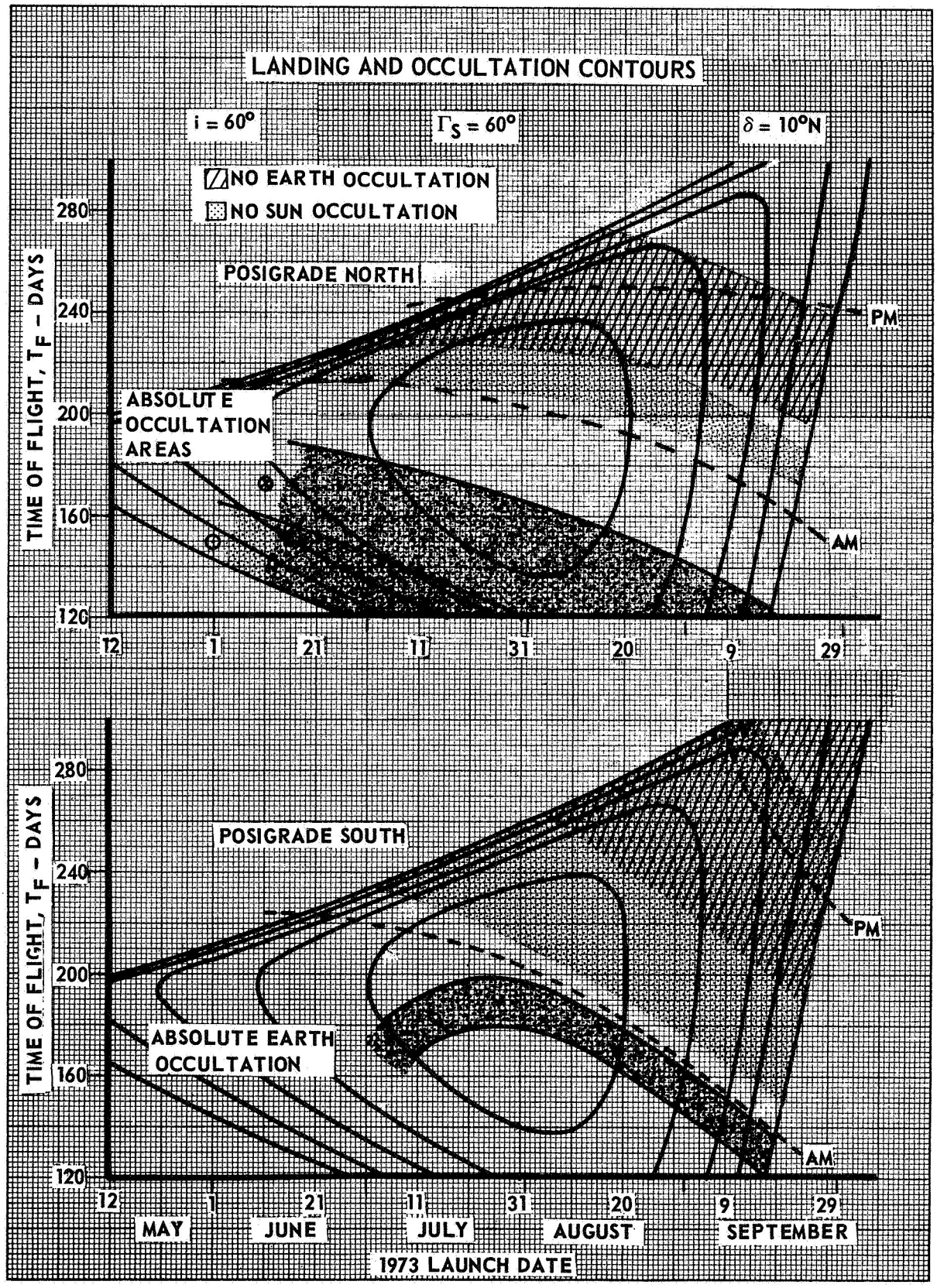

FIGURE 3.1.1–15

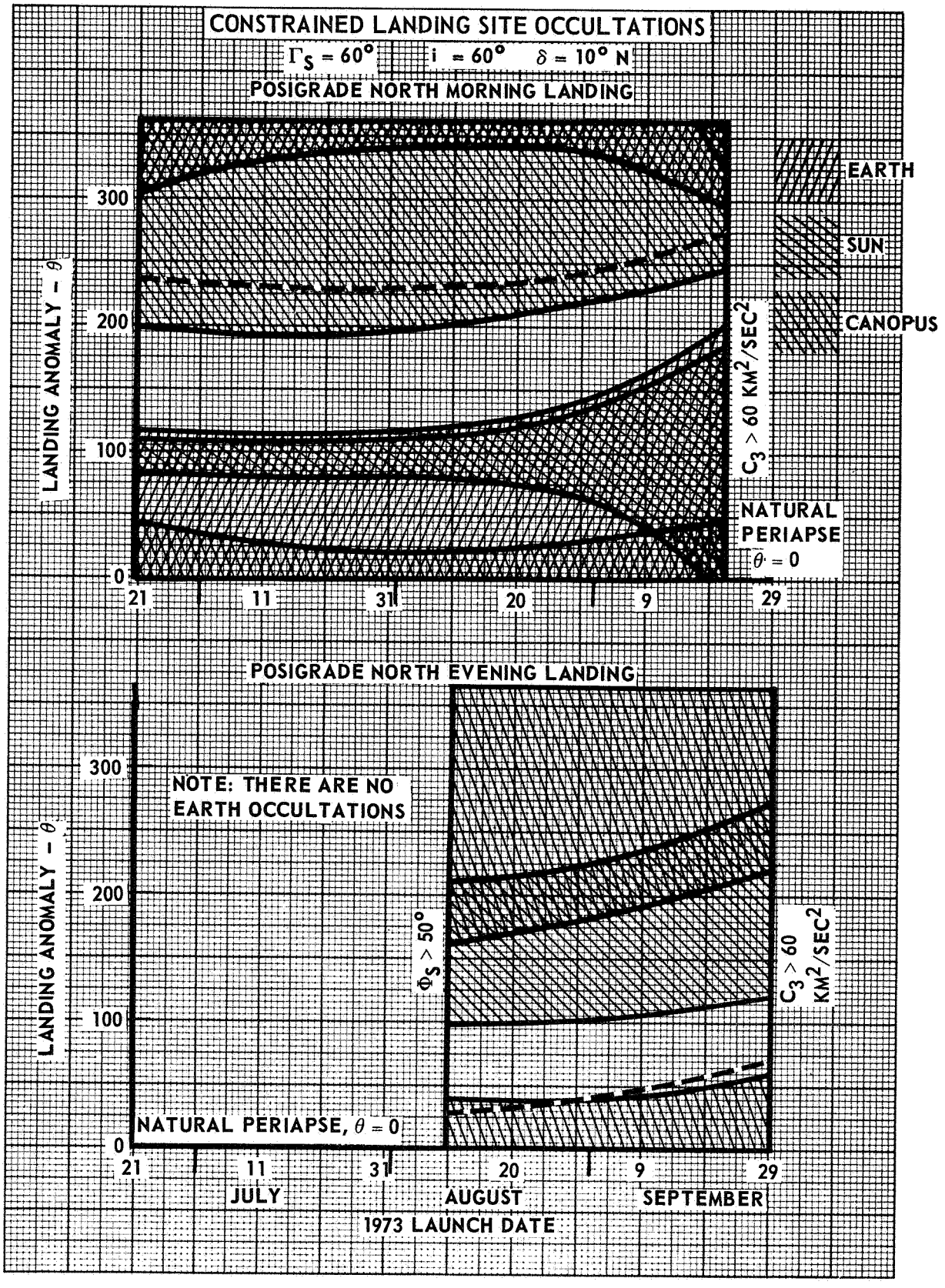

FIGURE 3.1.1–16

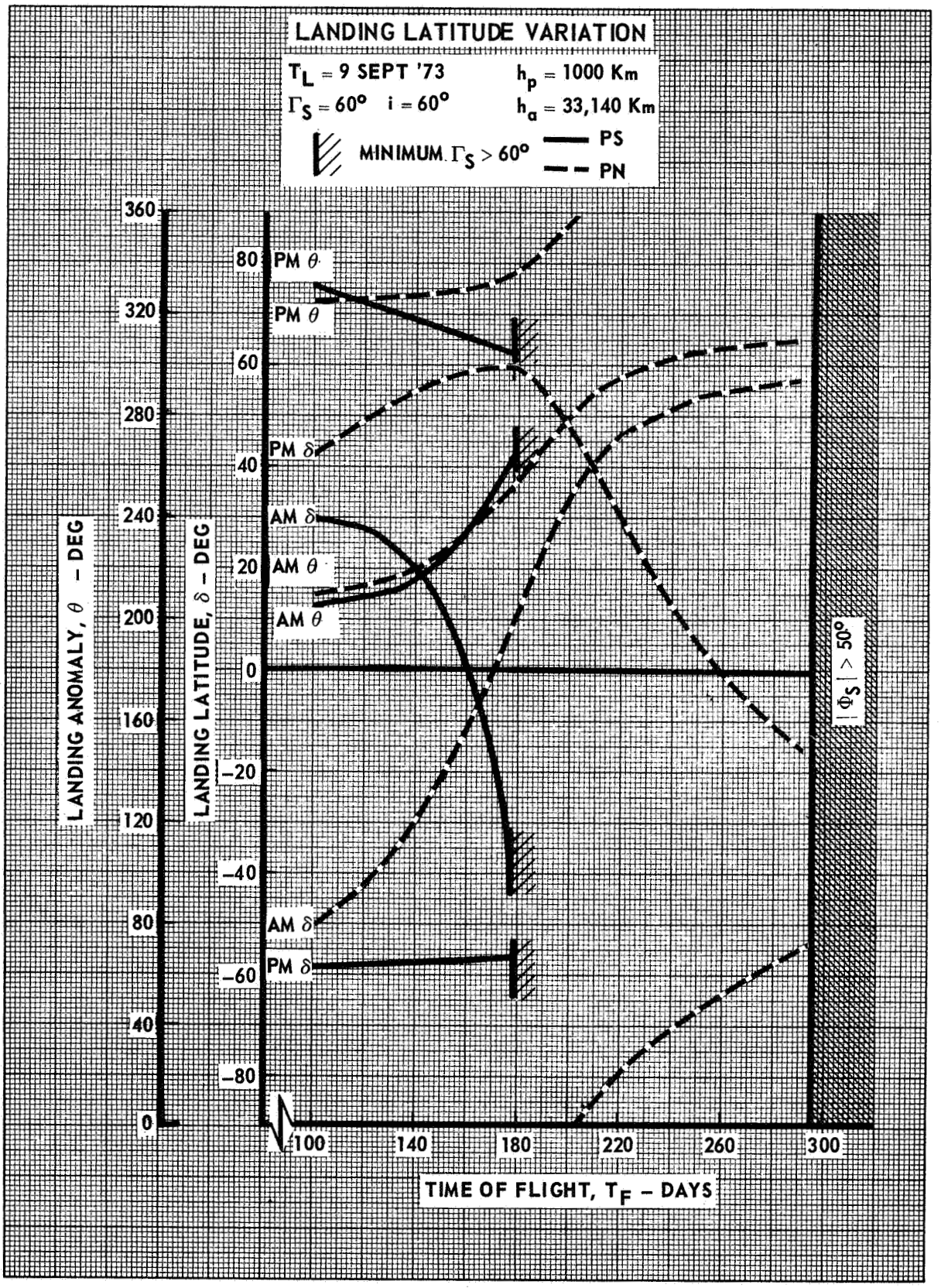

FIGURE 3.1.1–17

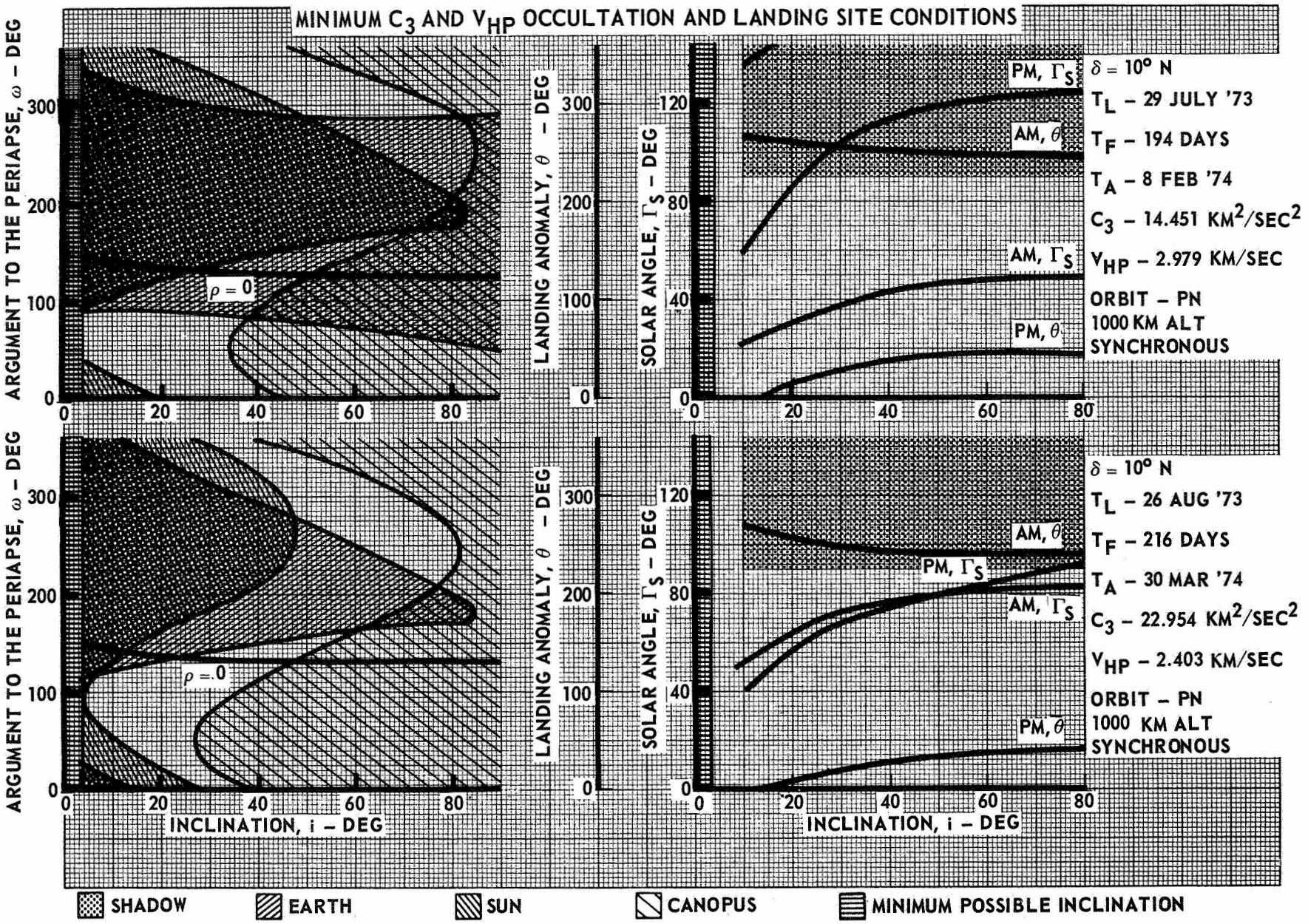

FIGURE 3.1.1–18

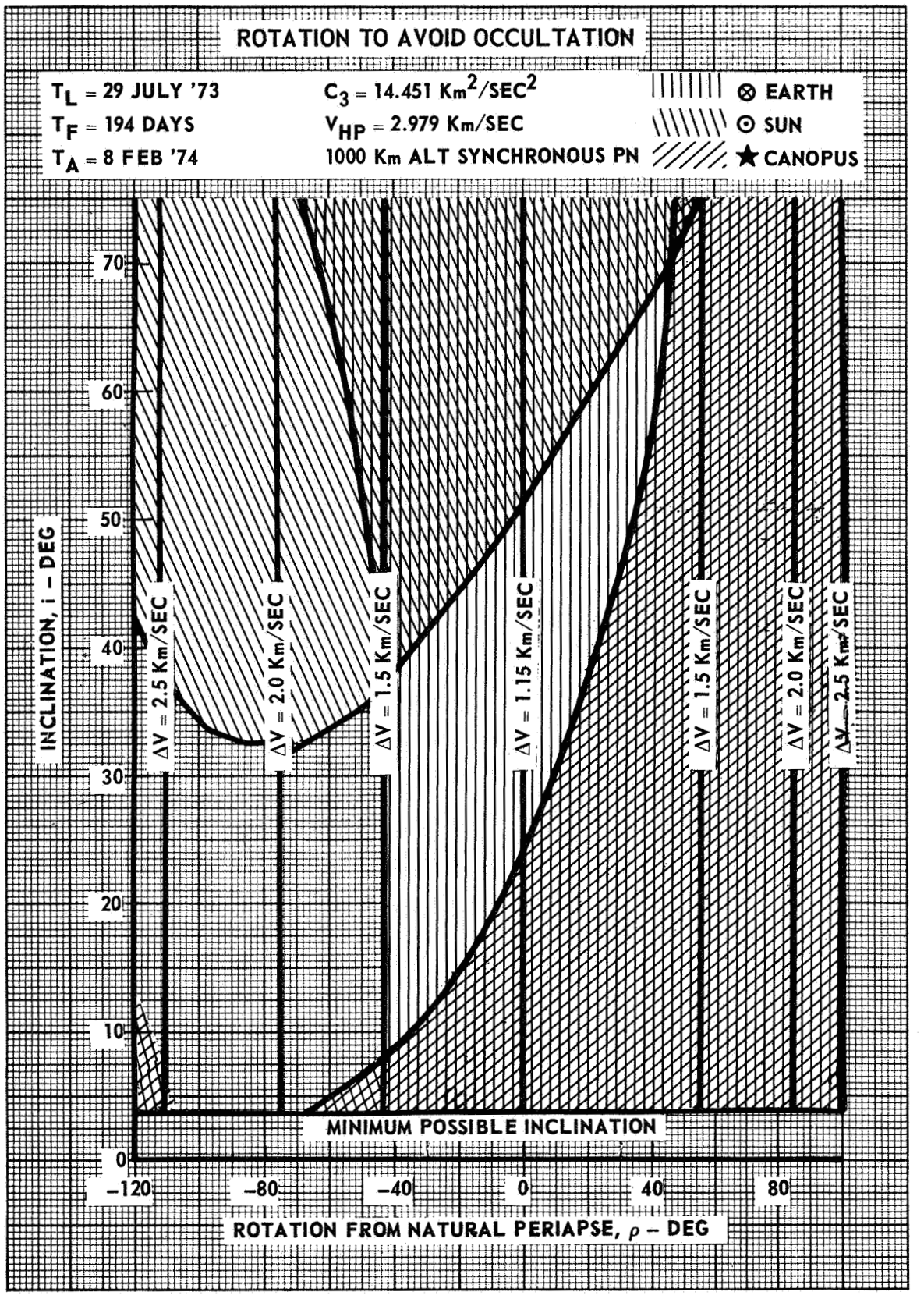

FIGURE 3.1.1–19

Contours of ΔV for orbit insertion are indicated for the solutions. Figure 3.1.1-20 presents a condition where Earth occultation occurs shortly after insertion and then disappears after an additional stay in orbit. For this set of conditions the inclination has been reduced and the periapse altitude increased. Landing sites, while sometimes meeting the solar angle limit, do occur at negative latitudes rather than positive. One advantage, however, of a low inclination orbit, is that it does limit landing latitude while giving a wide range of solar angles. For this case, shadow times and minimum limb angle data have also been presented as functions of rotation and time. Shadow time is defined as the time spent by the orbiter out of sight of the particular celestial body. The limb angle is the central angle between the celestial body and the disk of Mars. The minimum limb angle is the closest distance the celestial body appears to approach the surface of Mars during an orbit.

Figure 3.1.1-21 neglects landing site consideration entirely. Since the shadow time and minimum limb angle are of interest, examples of their fluctuations have been shown for related parameters.

The effect of time in orbit on both occultation and landing site is shown in Figure 3.1.1-22 for the minimum V_{HP} trajectory.

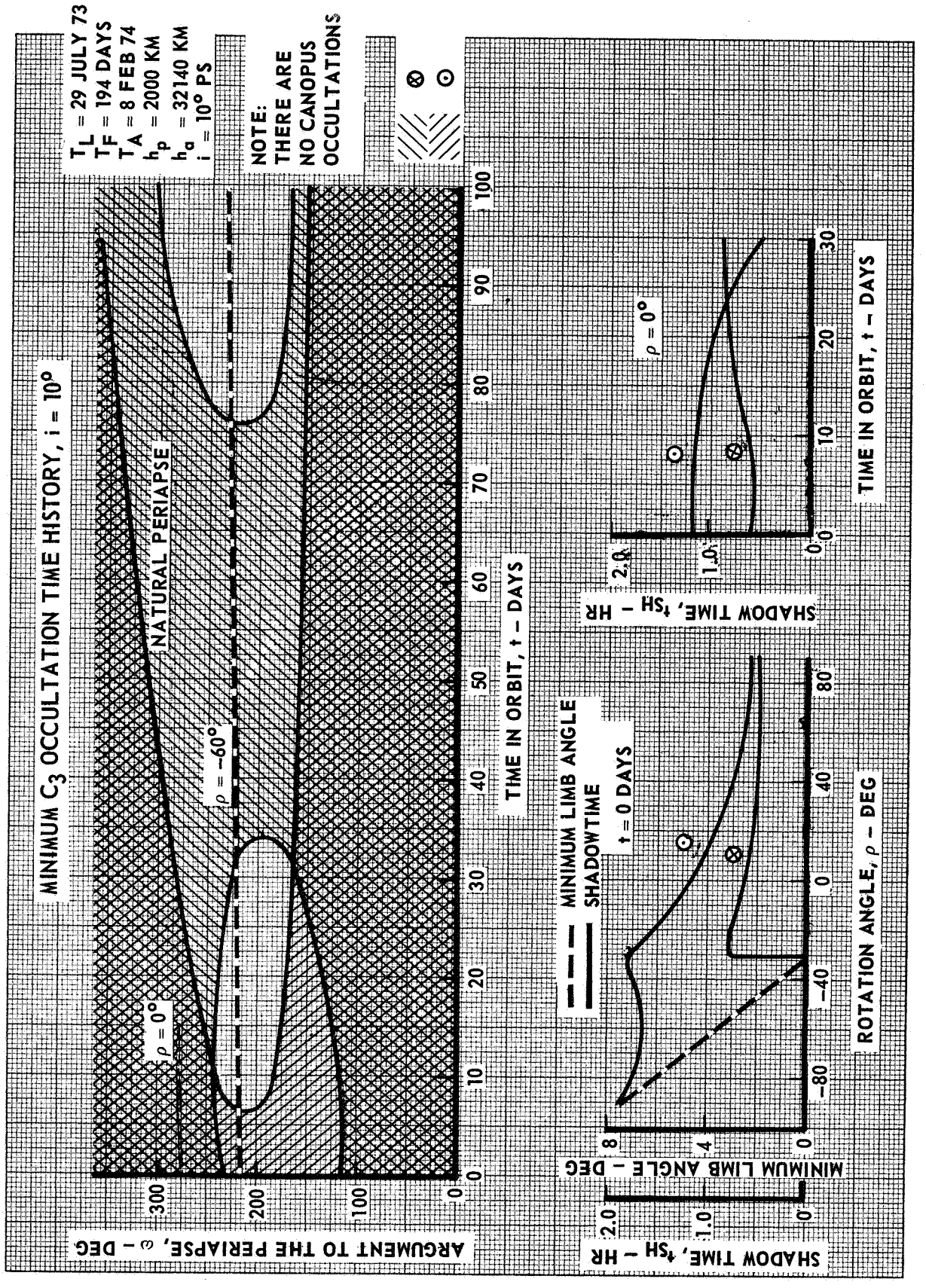

FIGURE 3.1.1–20

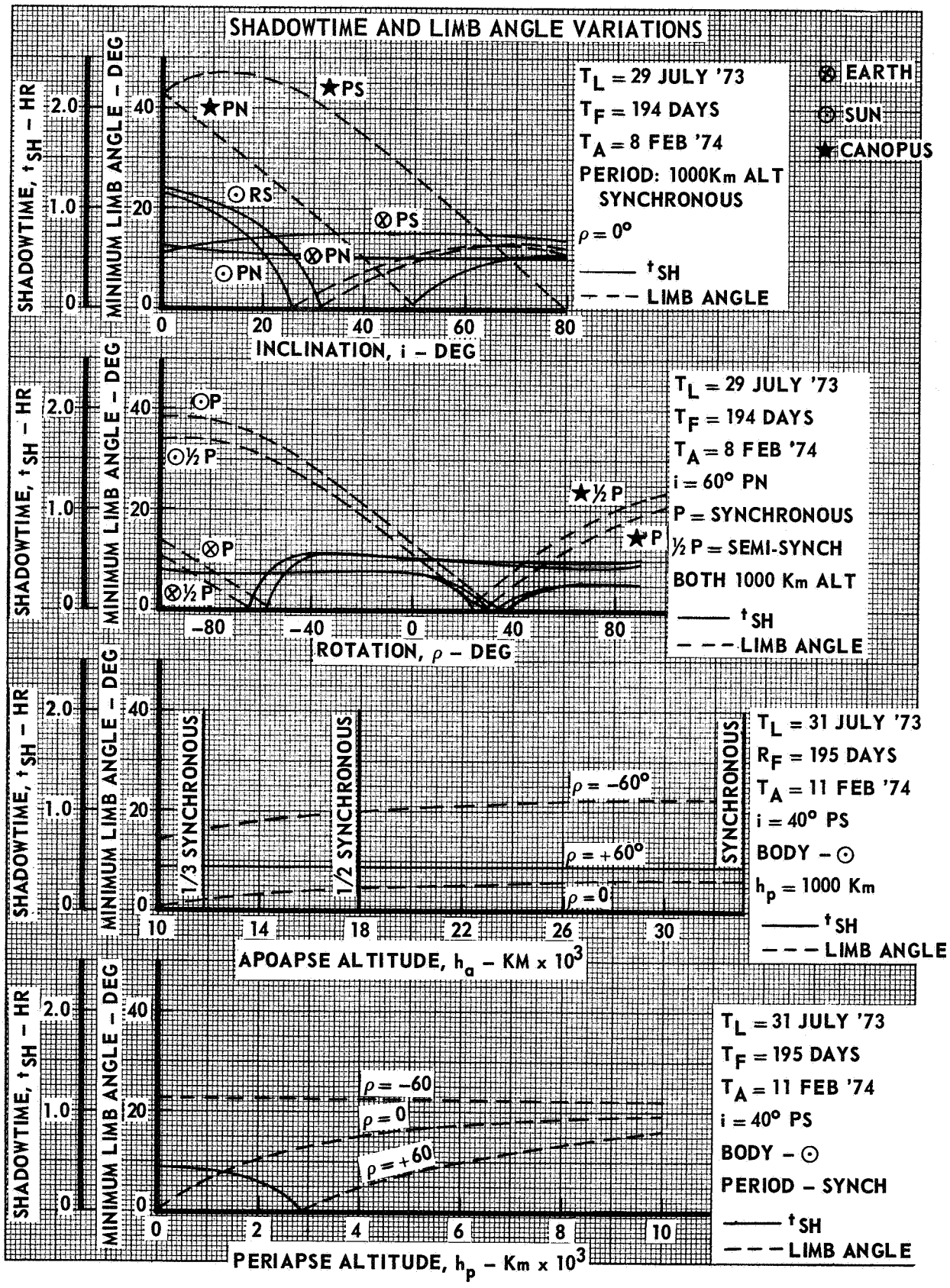

FIGURE 3.1.1–21

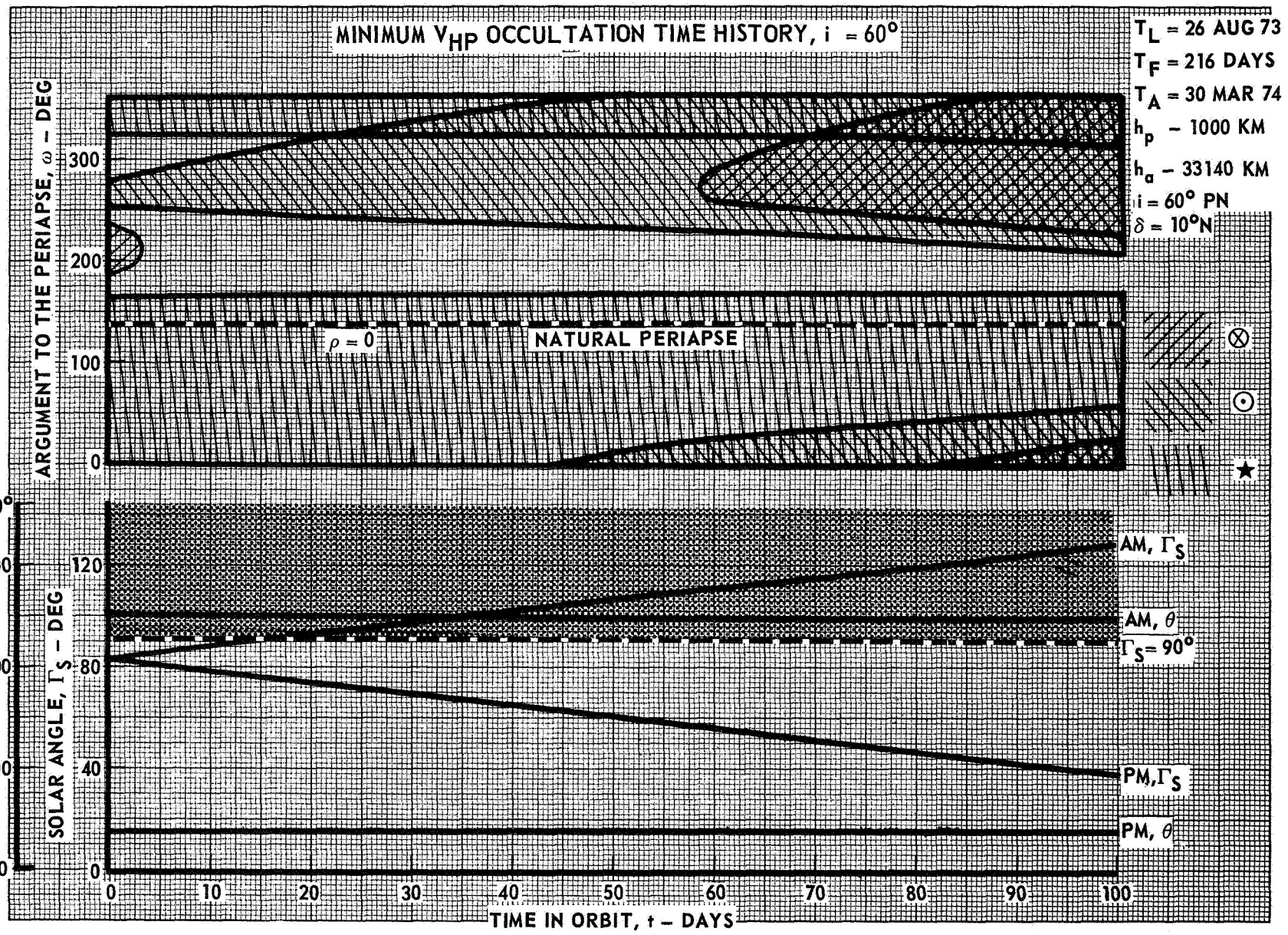

FIGURE 3.1.1-22

3.1.2 DEORBIT AND DESCENT - An important element in the capsule design is the influence of the deorbit maneuver on all subsequent flight conditions and the relative orbiter-capsule geometry during capsule descent and landing. The critical flight parameters are: deorbit velocity increment (propulsion system), descent time (descent power and attitude control systems), the capsule velocity and flight path angle at entry (corridor of initial conditions for atmospheric flight), and the relative capsule orbiter geometry at entry (the degree of multipath interference with capsule-orbiter communications). In addition, it may be desirable for the orbiter to remain in view of the landed capsule long enough to allow relay transmission of the initial data.

The initial conditions of the descent trajectory, which determine these capsule parameters, are established at deorbit. These initial conditions are determined by the orbit size, the true anomaly at deorbit, and the deorbit propulsion system. Variations in the descent trajectory at a given deorbit anomaly are achieved by varying the magnitude and application angle of the deorbit velocity increment.

The following paragraphs present a parametric analysis of the capsule flight as affected by variation of the deorbit maneuver parameters. The analysis is limited by the following constraints:

a) Orbit Size - Emphasis is on a Mars orbit with a synchronous orbital period (1000 - 33 124 km altitude).

b) Deorbit - Deorbit true anomaly limited from 180° to 250° (Logical orientation for Earth and relay communications - reasonable deorbit velocity increment).

c) Entry - Entry angle from graze to -20°. (Provides maximum aerodynamic braking with adequate margins for mission flexibility).

d) Atmosphere - VM-1 to VM-10.

e) Landing View Limits - Lander view of the orbiter for ground slopes of 34°.

Computations were based on Keplerian orbital mechanics with a point-mass analysis of the atmospheric trajectory. The range and time for the atmospheric flight of the capsule were obtained from the parametric data of Section 3.1.3.

3.1.2.1 Deorbit velocity increment and geometry. - The range of deorbit velocities required governs the sizing of the deorbit propulsion system. During the deorbit maneuver the velocity increment is applied to alter the capsule velocity and flight path angle. The capsule subsequently descends on a trajectory which intersects the planetary atmosphere (specified as 800 000 ft altitude). The geometry is shown in Figure 3.1.2-1. A deflection angle (δ) of zero occurs when the deorbit velocity increment (ΔV) is applied directly opposite to the capsule velocity vector. A positive deflection angle results in a steeper capsule flight path angle at the deorbit point; a negative deflection angle causes a more shallow capsule flight path angle. Negative deflection angles at deorbit have not been used because the capsule would be lofted on a trajectory which is initially outside the orbiter path and later would descent below the orbiter. The large variation in relative capsule-orbiter geometry which results would complicate the relay communication between the two vehicles and might require one or more extra reorientations of the capsule attitude. In addition negative deflection angles increase deorbit velocity increment requirements and trajectory error dispersions.

The variation of the deorbit velocity increment with deorbit true anomaly is shown in Figure 3.1.2-2 for a capsule entry angle of -15° and various entry velocities. Minimum deorbit velocity increment (187 ft/sec) occurs at apoapse (θ_{DO} = 180°) with the deflection angle opposing the capsule velocity vector (δ = 0°). The resulting entry velocity is 15 179 ft/sec. As deorbit anomaly is varied away from apoapse the deorbit velocity requirements increase. A similar family of curves is shown in Figure 3.1.2-3 for an entry angle of -20°. For the steeper entry angle the velocity increment requirements are higher. This is more evident in Figure 3.1.2-4, which shows the variation of velocity increment with entry flight path angle for a synchronous orbit and a deorbit deflection angle of 0°. With deorbit at apoapse, the steeper entries

DEORBIT AND ENTRY GEOMETRY

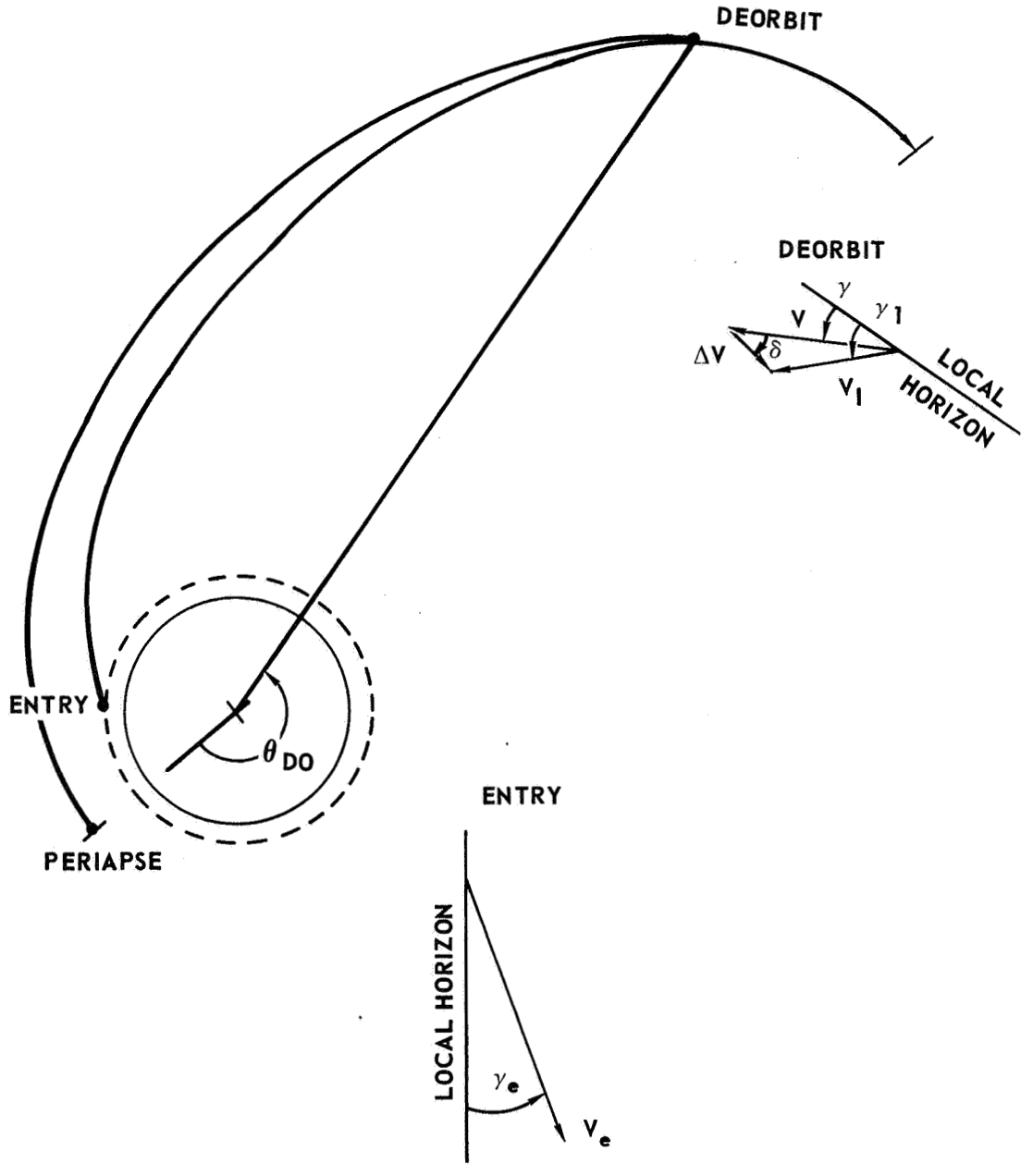

FIGURE 3.1.2–1

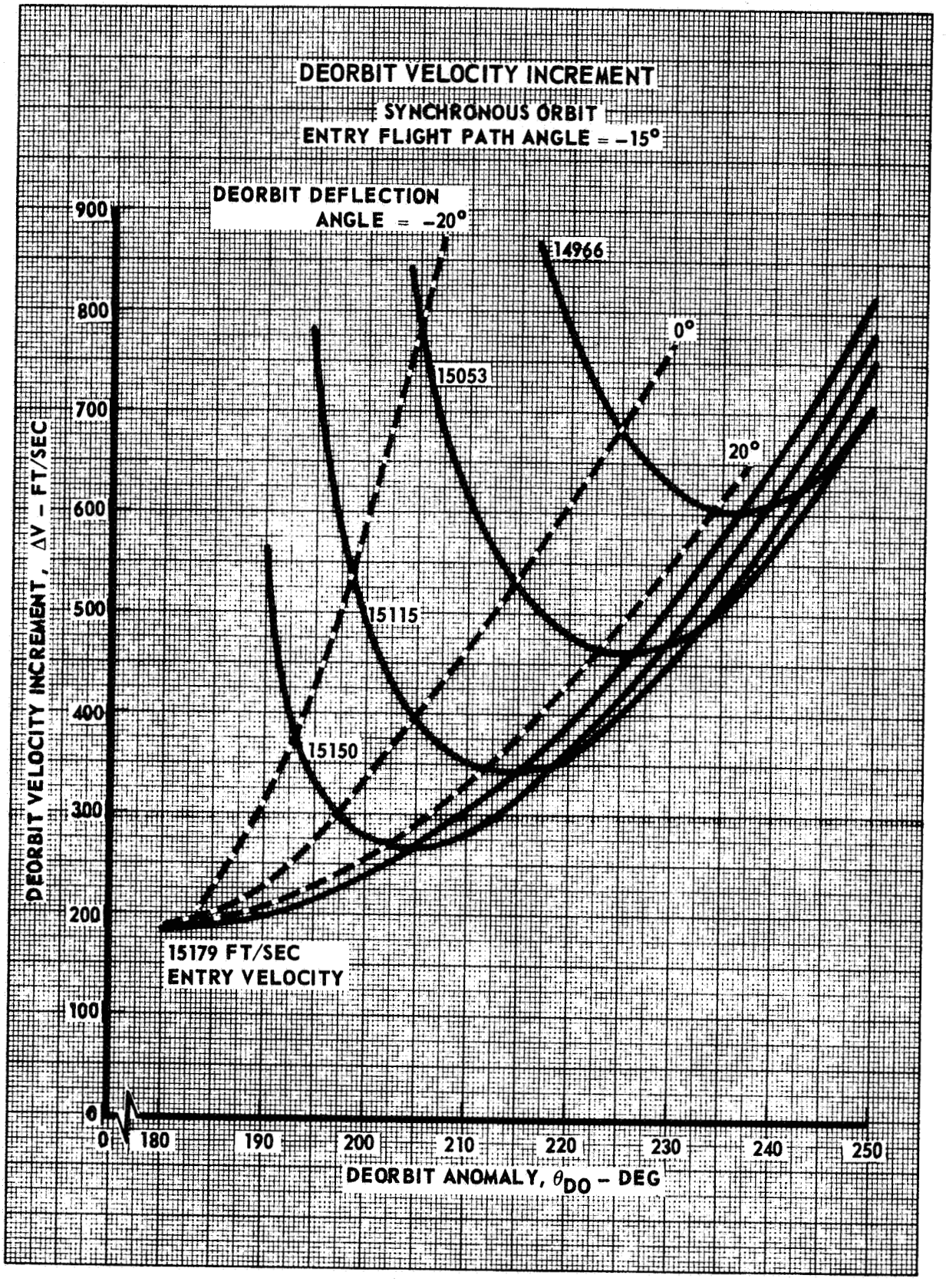
DEORBIT VELOCITY INCREMENT
SYNCHRONOUS ORBIT
ENTRY FLIGHT PATH ANGLE = −15°
DEORBIT DEFLECTION ANGLE = −20°
14966
0°
15053
20°
15115
15150
15179 FT/SEC ENTRY VELOCITY
DEORBIT VELOCITY INCREMENT, ΔV − FT/SEC
900
800
700
600
500
400
300
200
100
0
0
180
190
200
210
220
230
240
250
DEORBIT ANOMALY, θDO − DEG

FIGURE 3.1.2–2

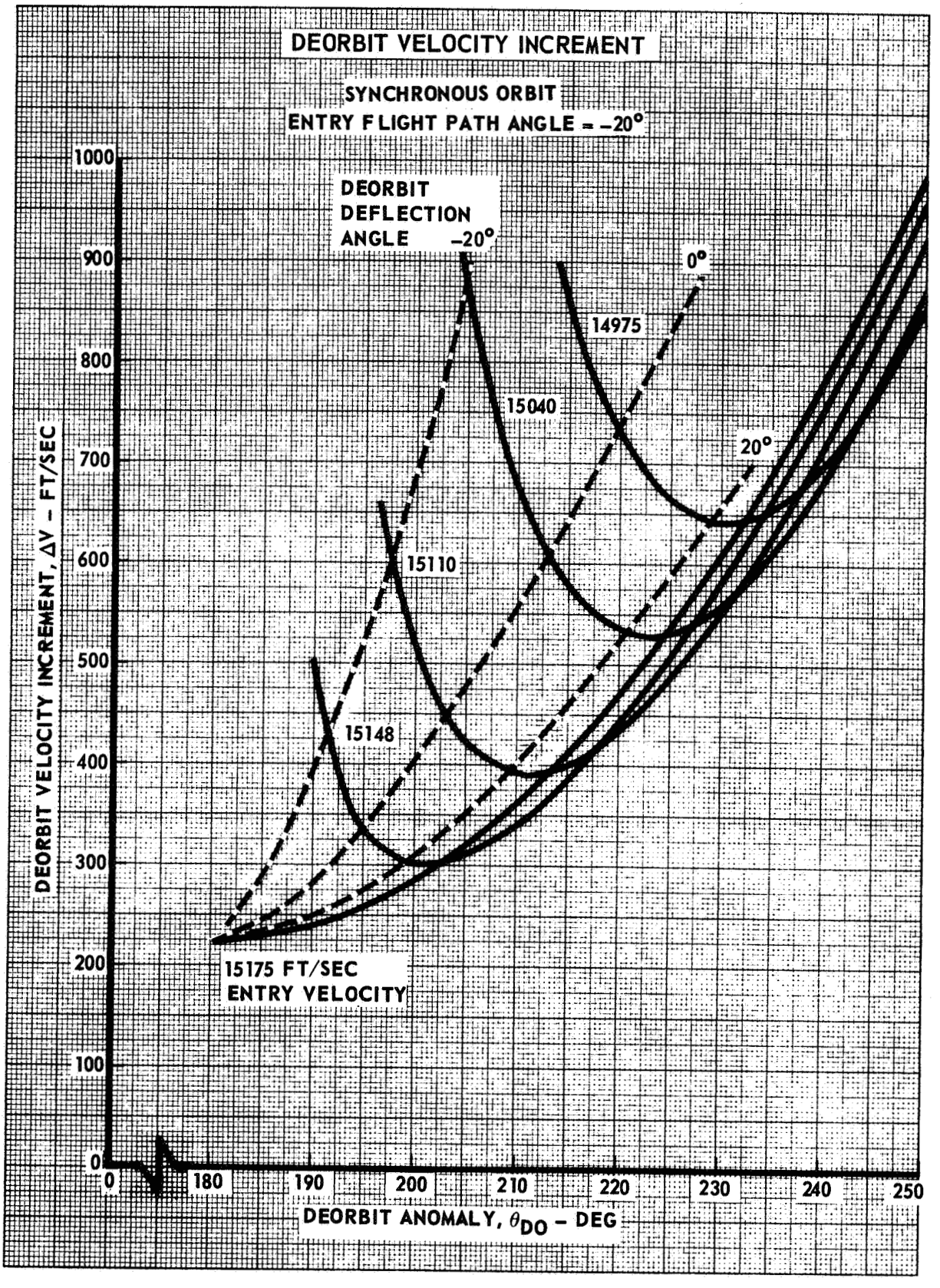
DEORBIT VELOCITY INCREMENT
SYNCHRONOUS ORBIT
ENTRY FLIGHT PATH ANGLE = -20°
DEORBIT
DEFLECTION
ANGLE -20°
0°
20°
14975
15040
15110
15148
15175 FT/SEC
ENTRY VELOCITY
DEORBIT VELOCITY INCREMENT, ΔV - FT/SEC
1000
900
800
700
600
500
400
300
200
100
0
0
180
190
200
210
220
230
240
250
DEORBIT ANOMALY, θDO - DEG

FIGURE 3.1.2-3

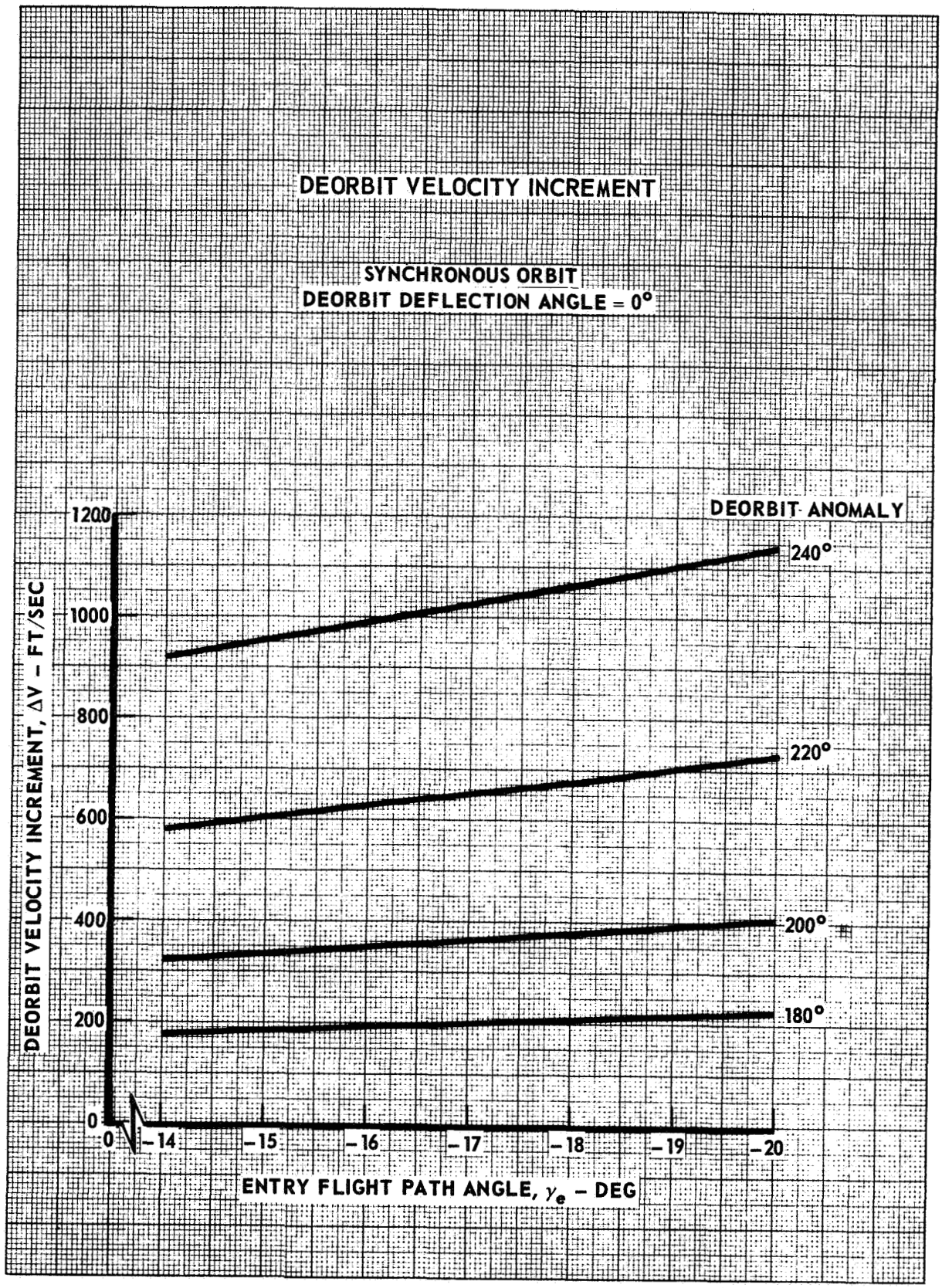
DEORBIT VELOCITY INCREMENT
SYNCHRONOUS ORBIT
DEORBIT DEFLECTION ANGLE = 0°
DEORBIT ANOMALY
240°
220°
200°
180°
DEORBIT VELOCITY INCREMENT, ΔV – FT/SEC
1200
1000
800
600
400
200
0
0
–14
–15
–16
–17
–18
–19
–20
ENTRY FLIGHT PATH ANGLE, γ_e – DEG

FIGURE 3.1.2–4

require 40 to 50 ft/sec more velocity increment. As deorbit anomaly is increased, the velocity increment requirements increase more rapidly for steeper entries. The effect of orbit size on the deorbit velocity increment requirements is shown in Figure 3.1.2-5 for entry with a -15° flight path angle and a deorbit deflection angle of 0°. The orbits have varying apoapse altitude with a periapse altitude of 1000 km. For deorbit at apoapse, the larger orbits require less velocity increment. As deorbit anomaly is varied from apoapse, however, the effect of orbit size diminishes, until it is negligible at a deorbit anomaly of 220°. Above this value, velocity increment requirements increase with the size of the orbits.

The important variations of the deorbit parameters are summarized below:

a) Deorbit velocity increment requirements increase as the maneuver is performed away from apoapse.

b) Steeper entry angles require higher velocity increments.

c) Entry velocity is relatively unaffected by the deorbit velocity increment for the ranges of deorbit anomalies shown.

d) Lower velocity increment requirements are obtained with positive deflection angles.

e) Larger orbits require lower velocity increments for deorbit near apoapse. However, the effect is diminished as deorbit anomaly is increased.

3.1.2.2 Capsule descent time. - The time from deorbit to entry determines the operational period required of the descent power and attitude control systems. The variation in time from deorbit to entry is shown in Figure 3.1.2-6 for variable entry conditions for the synchronous and the semi-synchronous orbits. Figure 3.1.2-7 shows the descent time variation with orbit size for an entry flight path angle of -15° and deorbit deflection angle of 0°. The important variations in descent time are:

a) The larger orbits require longer descent time but the difference decreases rapidly at higher deorbit anomalies.

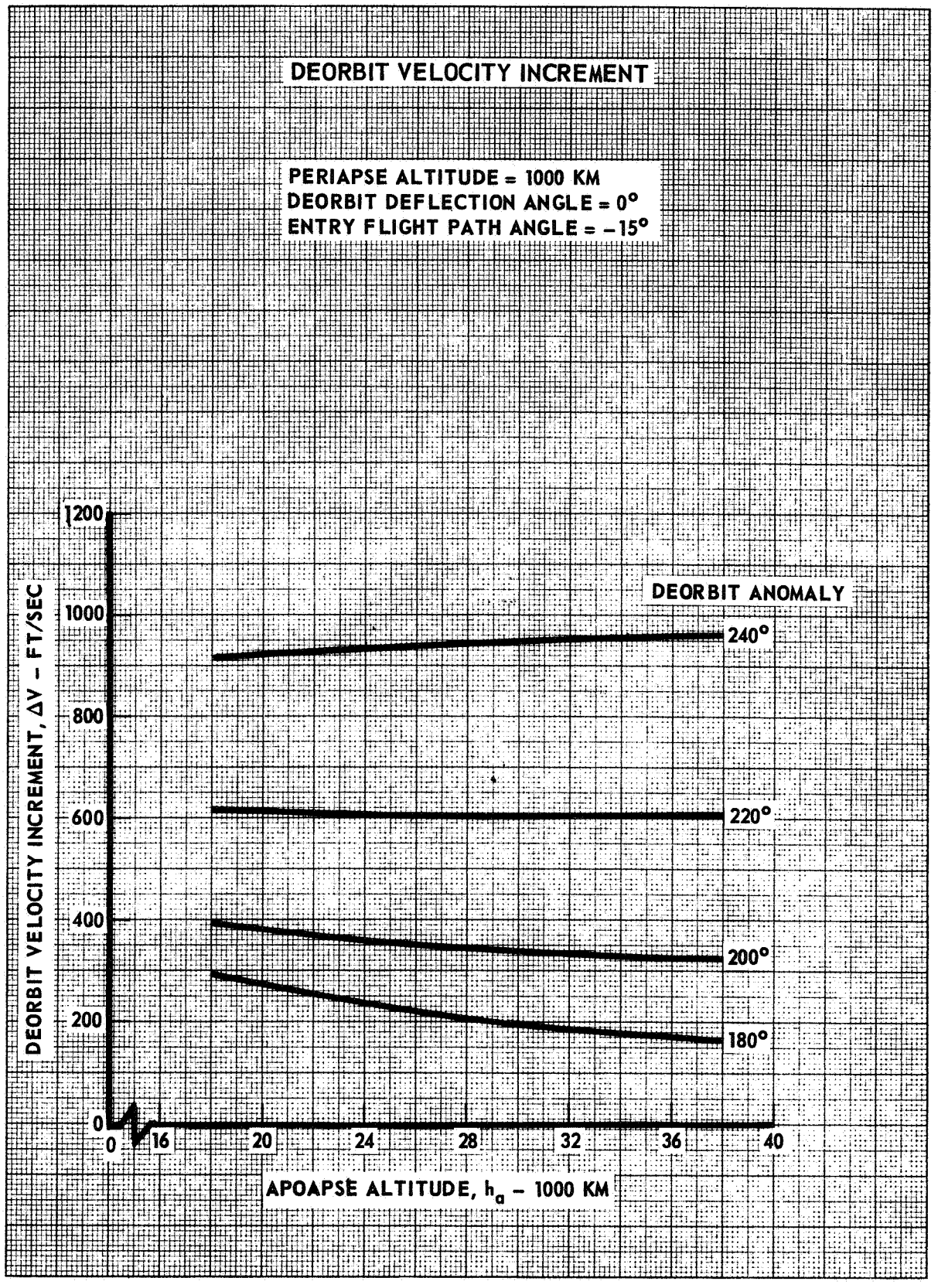
DEORBIT VELOCITY INCREMENT
PERIAPSE ALTITUDE = 1000 KM
DEORBIT DEFLECTION ANGLE = 0°
ENTRY FLIGHT PATH ANGLE = −15°
DEORBIT ANOMALY
240°
220°
200°
180°
DEORBIT VELOCITY INCREMENT, ΔV – FT/SEC
1200
1000
800
600
400
200
0
0
16
20
24
28
32
36
40
APOAPSE ALTITUDE, h_a – 1000 KM

FIGURE 3.1.2–5

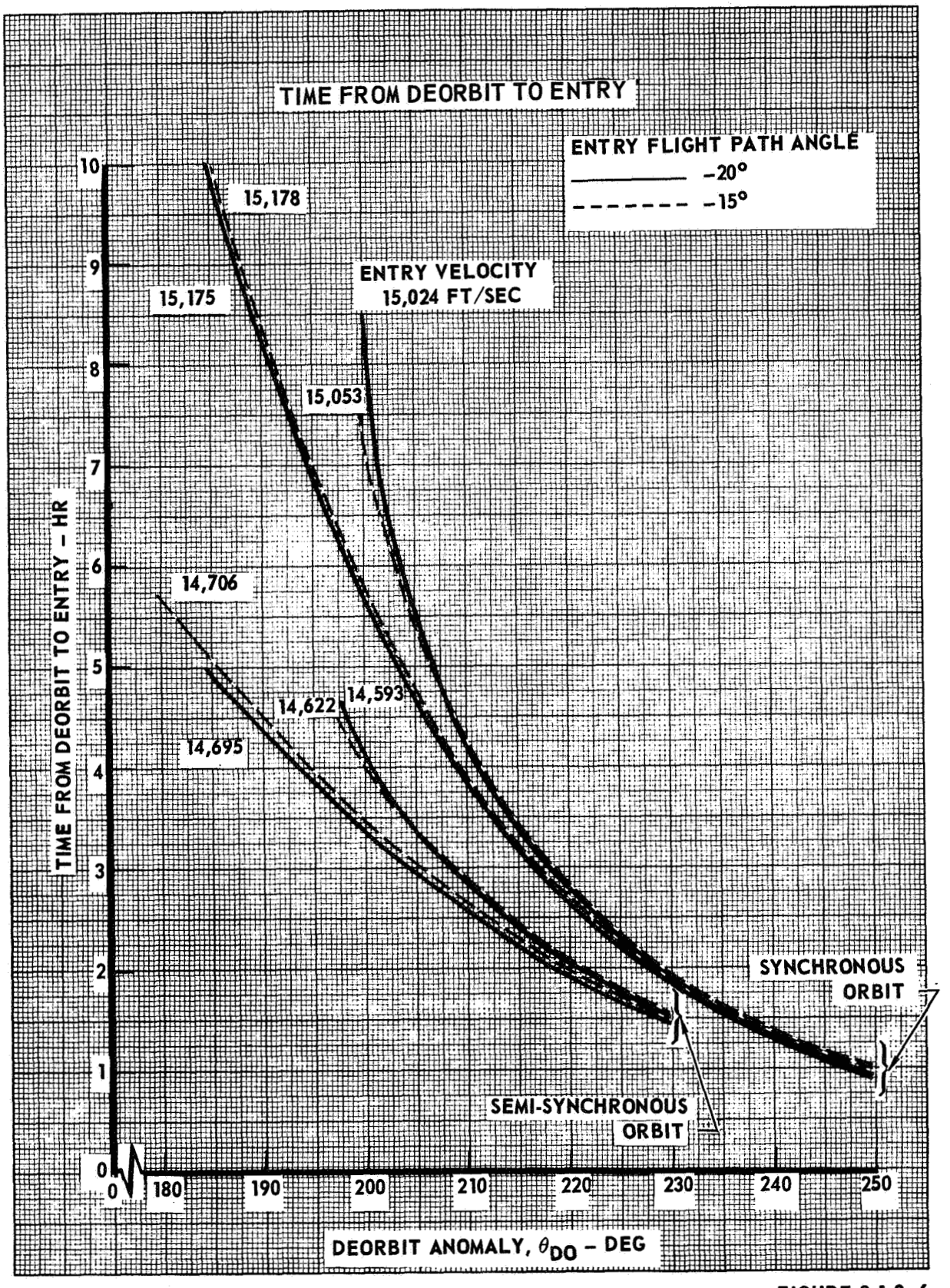
TIME FROM DEORBIT TO ENTRY
ENTRY FLIGHT PATH ANGLE
-20°
-15°
ENTRY VELOCITY
15,024 FT/SEC
15,178
15,175
15,053
14,706
14,622
14,593
14,695
SYNCHRONOUS ORBIT
SEMI-SYNCHRONOUS ORBIT
TIME FROM DEORBIT TO ENTRY - HR
0
1
2
3
4
5
6
7
8
9
10
0
180
190
200
210
220
230
240
250
DEORBIT ANOMALY, θ_{DO} - DEG

FIGURE 3.1.2-6

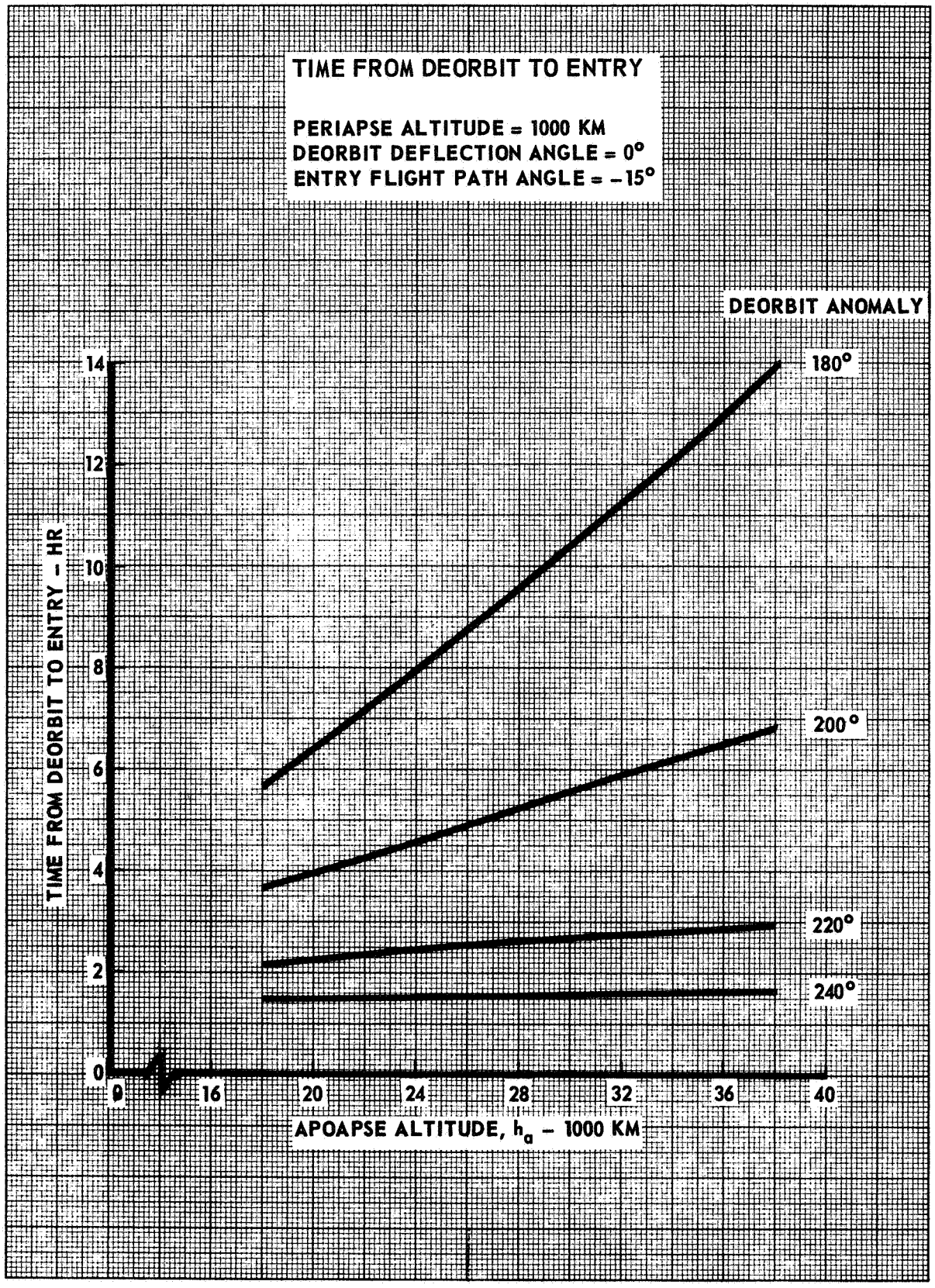
TIME FROM DEORBIT TO ENTRY
PERIAPSE ALTITUDE = 1000 KM
DEORBIT DEFLECTION ANGLE = 0°
ENTRY FLIGHT PATH ANGLE = -15°
DEORBIT ANOMALY
180°
200°
220°
240°
TIME FROM DEORBIT TO ENTRY - HR
0
2
4
6
8
10
12
14
16
20
24
28
32
36
40
APOAPSE ALTITUDE, h_a - 1000 KM

FIGURE 3.1.2-7

b) High deorbit anomalies significantly reduce descent time.

c) Descent time variance with entry flight path angle is negligible for a given entry velocity.

d) Slightly lower entry velocity will increase the descent time significantly at the lower deorbit anomalies.

3.1.2.3 Capsule lead angle. - The capsule lead angle is defined as the true anomaly difference between the capsule and orbiter (see Figure 3.1.2-8). The lead angle is positive when the capsule is ahead of the orbiter. During the terminal portion of the descent trajectory and during capsule entry, signals from the capsule can reflect from the planet surface and interfere with the direct communications from the capsule to the orbiter. This phenomenon, known as multipath interference (see Section 3.2.2), is directly affected by the capsule lead angle.

The capsule lead angle at entry for varying deorbit conditions from a synchronous orbit is shown in Figure 3.1.2-9 with an entry flight path angle of -15°. A similar family of curves is shown in Figure 3.1.2-10 with an entry flight path angle of -20°. The important parametric variations of capsule lead angle are:

a) For a constant deorbit velocity increment, the lead angle can be varied by varying the deorbit deflection angle and deorbit anomaly.

b) Positive deflection angles at deorbit produce greater capsule lead over the orbiter at entry.

c) Velocity increment requirements for a given lead angle and deorbit position are higher for steeper entry angles.

The power level required for capsule relay transmission (Section 3.2.2) is minimized when the capsule lead angle at entry is approximately 5°. The deorbit conditions giving 5° capsule lead at entry and the resulting landing positions are shown in Figure 3.1.2-11. The entry flight path angle is from -15° to -20°. Descent trajectories requiring minimum capsule communications power and giving large flexibility in choice of landing position can be obtained for a given deorbit velocity increment by varying the deorbit anomaly and entry flight path angle.

CAPSULE LEAD ANGLE

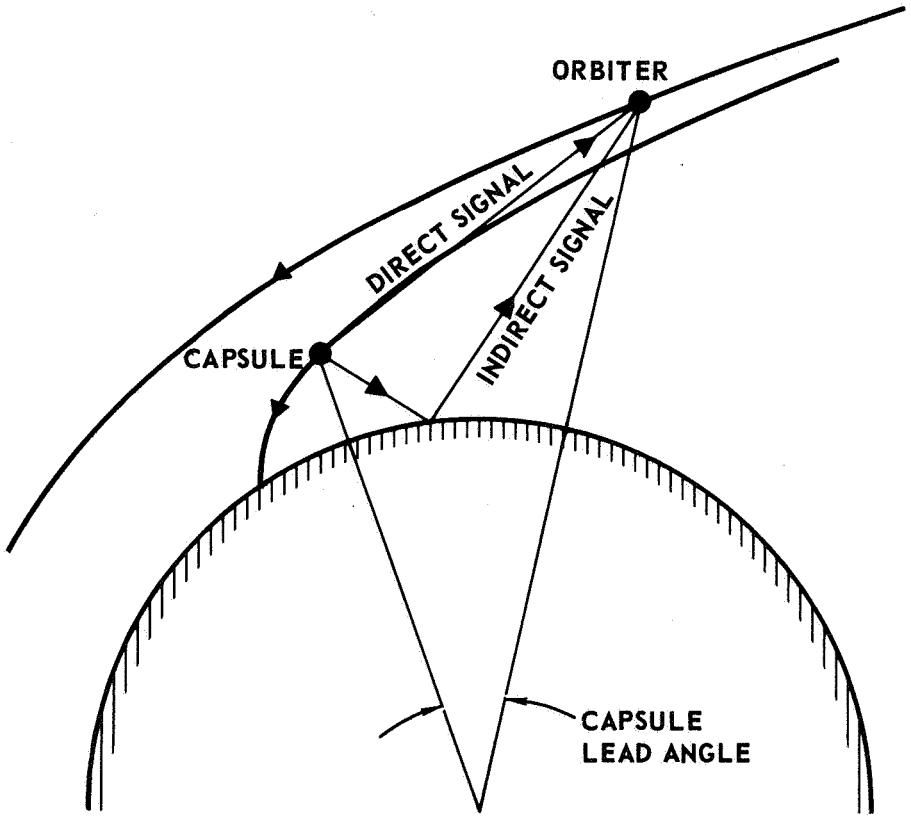

FIGURE 3.1.2–8

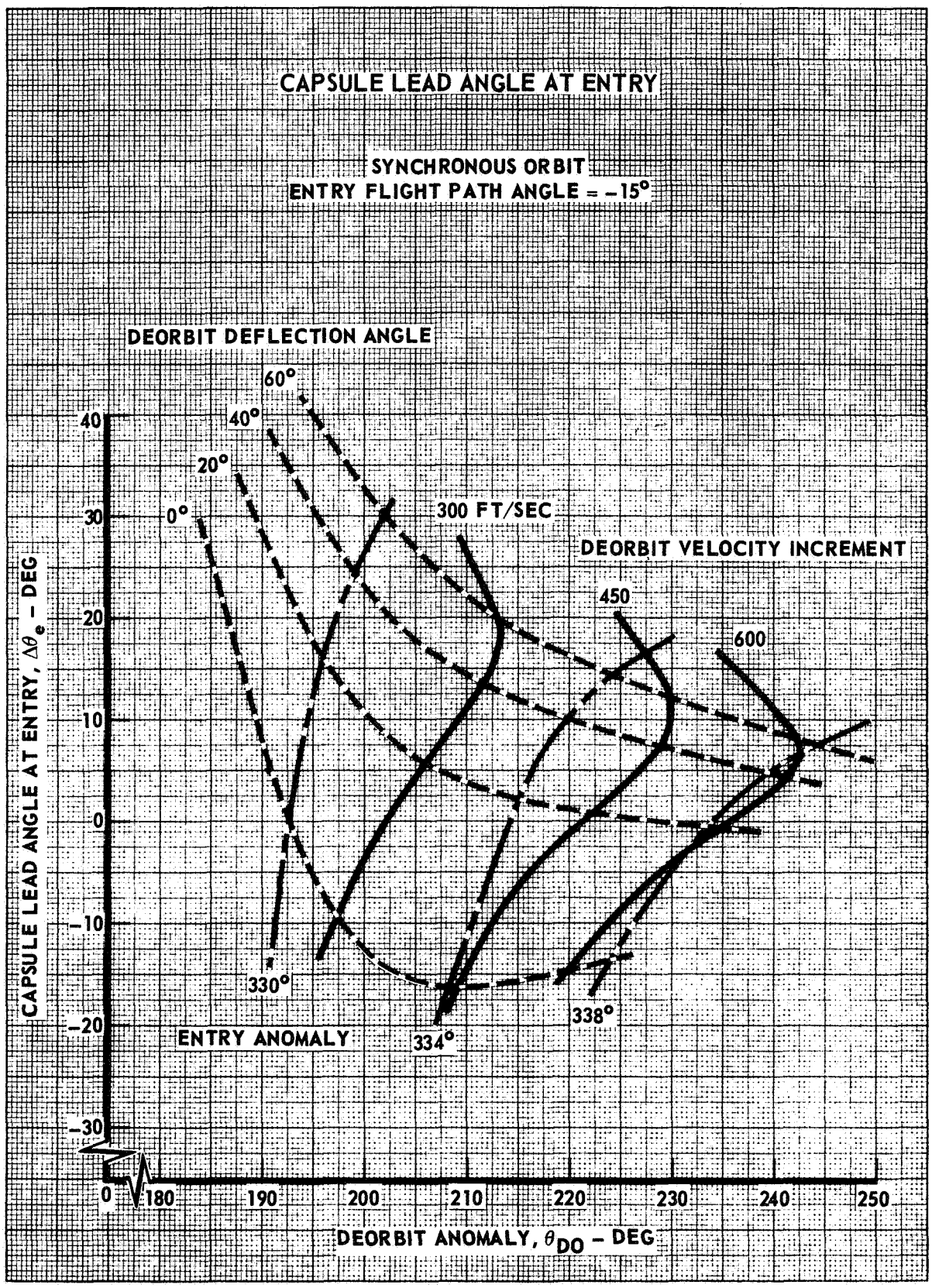
CAPSULE LEAD ANGLE AT ENTRY
SYNCHRONOUS ORBIT
ENTRY FLIGHT PATH ANGLE = −15°
DEORBIT DEFLECTION ANGLE
60°
40°
20°
0°
300 FT/SEC
DEORBIT VELOCITY INCREMENT
450
600
330°
334°
338°
ENTRY ANOMALY
CAPSULE LEAD ANGLE AT ENTRY, $\Delta\theta_e$ – DEG
40
30
20
10
0
−10
−20
−30
0
180
190
200
210
220
230
240
250
DEORBIT ANOMALY, θ_{DO} – DEG

FIGURE 3.1.2–9

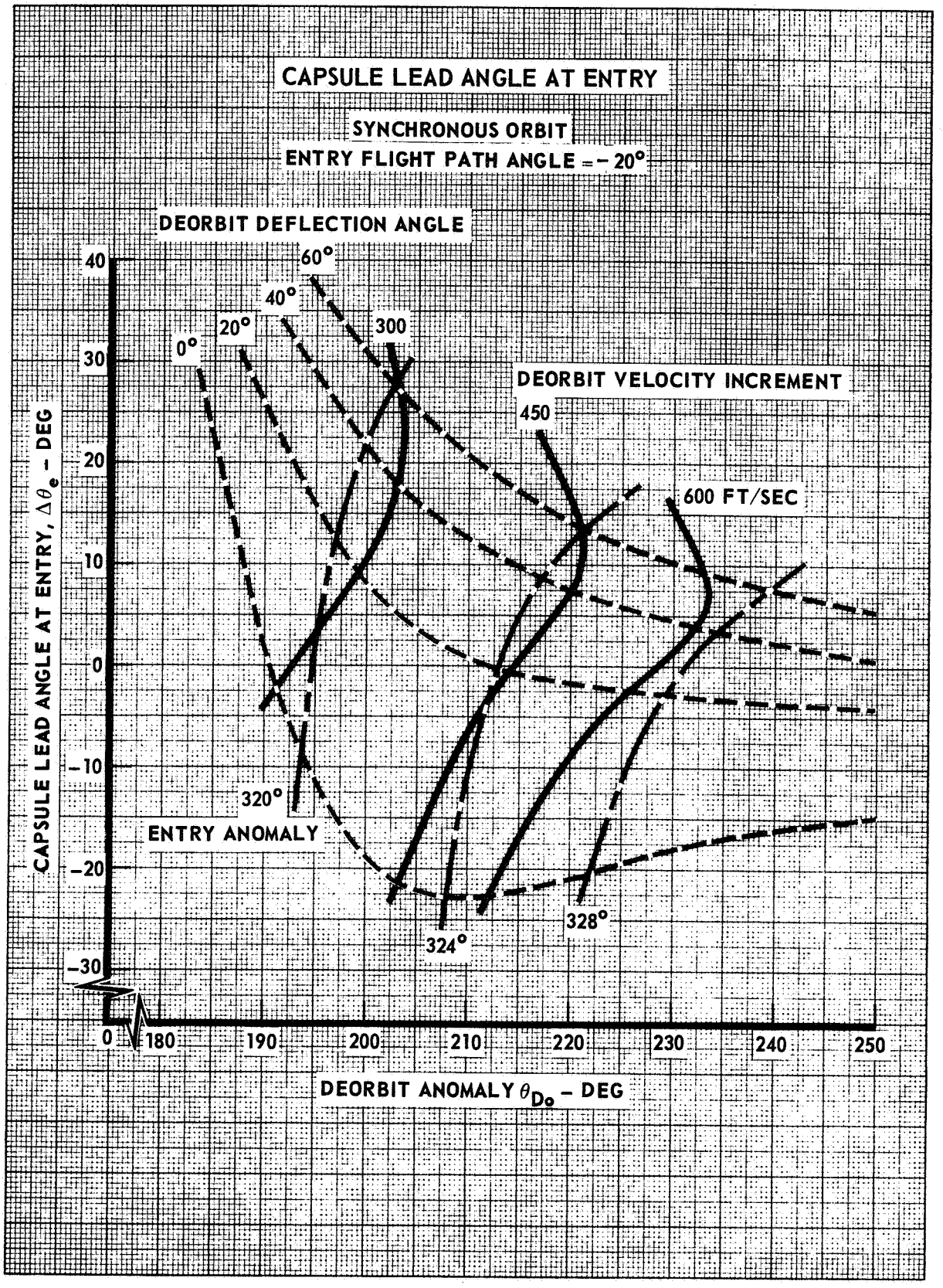

FIGURE 3.1.2–10

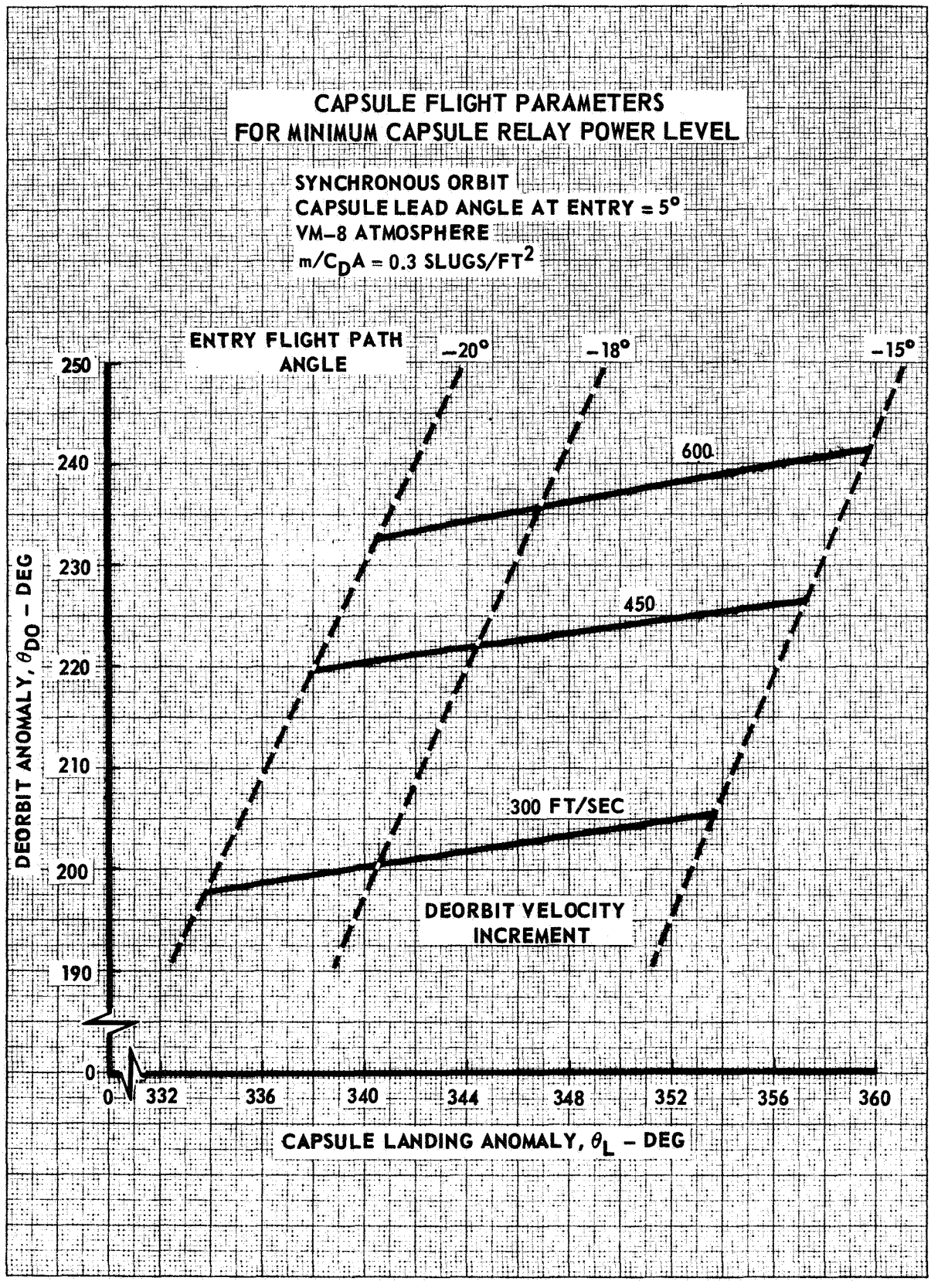

FIGURE 3.1.2-11

3.1.2.4 Landing geometry. - The capsule landing anomaly and the assumed 34° surface slope determine the orbital positions visible from the landing point. The geometry is shown in Figure 3.1.2-12. The ideal descent sequence to maximize the mutual view period would have the orbiter at the trailing view limit at the time of capsule landing. The orbiter would then be in position to receive transmitted data from the landed capsule until it has moved forward past the leading view limit. Design for maximum view at landing is complicated by the uncertainty of the atmosphere encountered during the capsule atmospheric flight. Within the range of atmospheres considered, the more dense atmospheres result in a shorter range and longer descent time for the capsule. (See Figures 3.1.3-5 and 6, Section 3.1.3). To insure that the orbiter always views capsule landing, the deorbit maneuver must be performed so that the orbiter is above the trailing view limit at landing after the capsule descends through the minimum density atmosphere (VM-8). Then if a more dense atmosphere (VM-9) is encountered, the capsule landing anomaly decreases, placing the trailing view limit farther back, but the descent time increases, allowing the orbiter to move farther ahead. The combined effect places the orbiter ahead of the trailing view limit at landing, decreasing the period of mutual view.

The capsule-orbiter locations at landing after deorbit from a synchronous orbit and descent through the VM-8 (least dense) Mars atmosphere are shown in Figure 3.1.2-13 for an entry angle of -15°. The capsule ballistic parameter assumed is .3 slugs/ft^2 with no auxiliary deceleration.

The same parametric variation is shown in Figure 3.1.2-14 for the capsule entry angle of -20°. The region between the trailing and leading view limits is the band of orbiter positions visible above a 34° ground slope at the landing point. The effects of the entry conditions and deorbit parameters on the orbiter-capsule mutual view at landing are as follows:

a) Steeper entry angles result in landing at anomalies farther back from periapse and thus increase the band of visible orbiter positions.

VIEW LIMITS AT CAPSULE LANDING

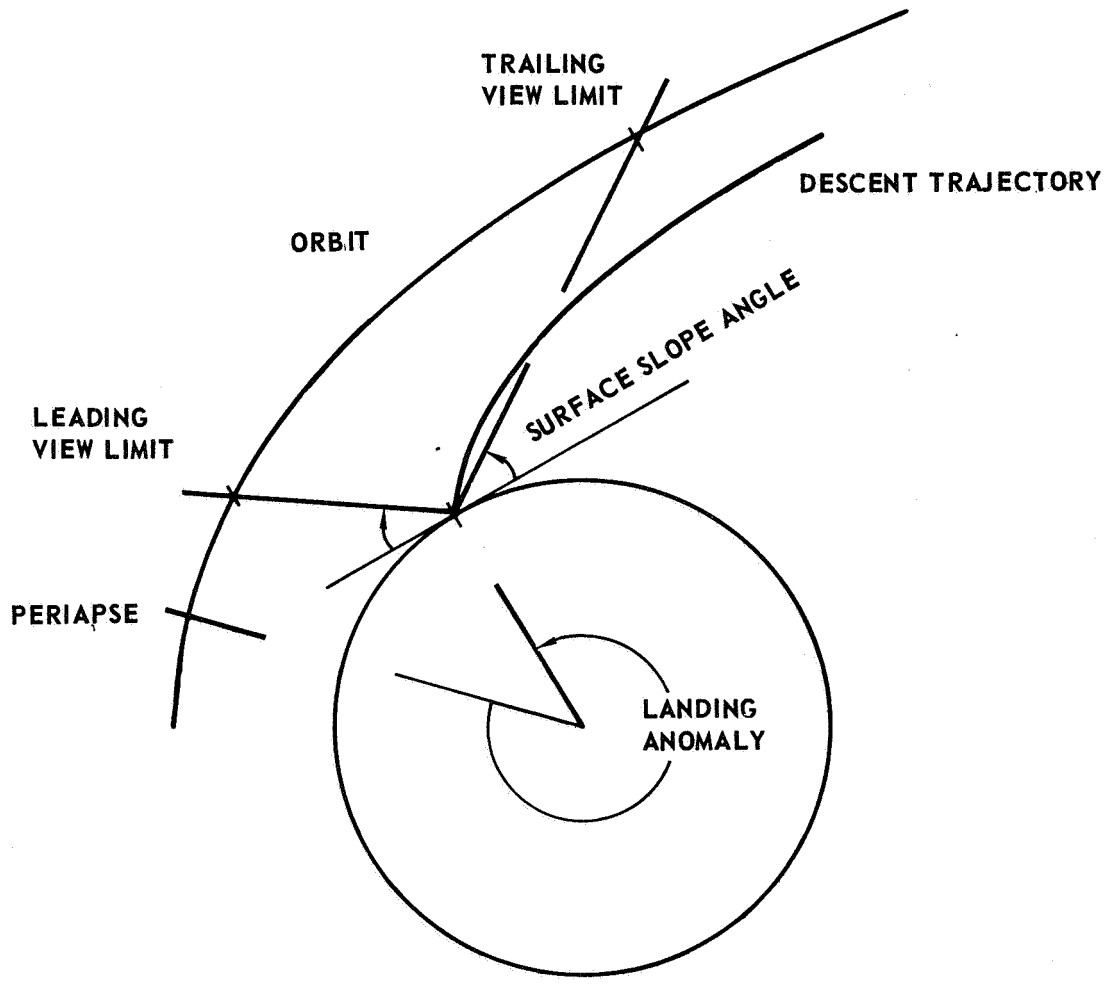

FIGURE 3.1.2–12

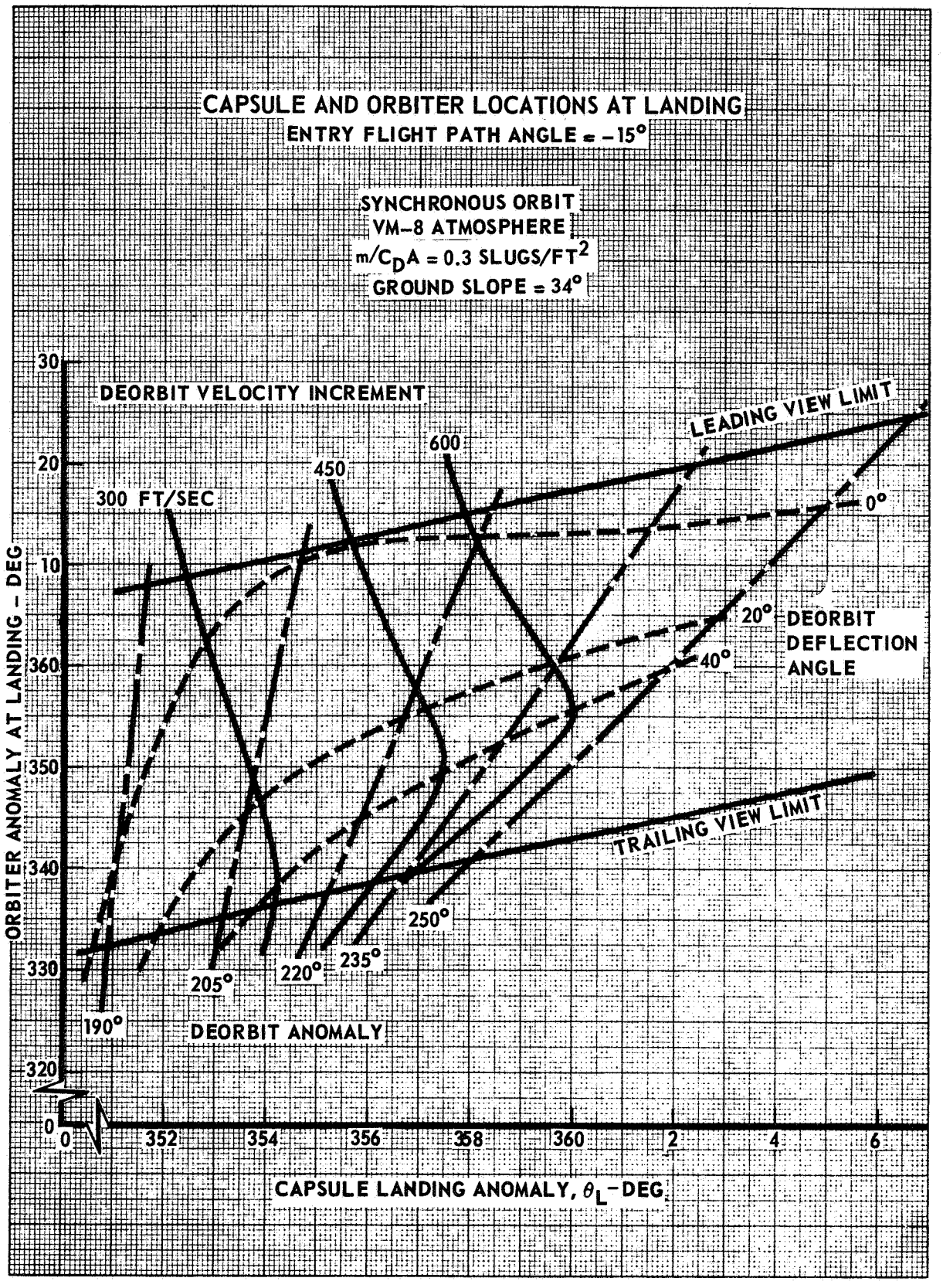

FIGURE 3.1.2-13

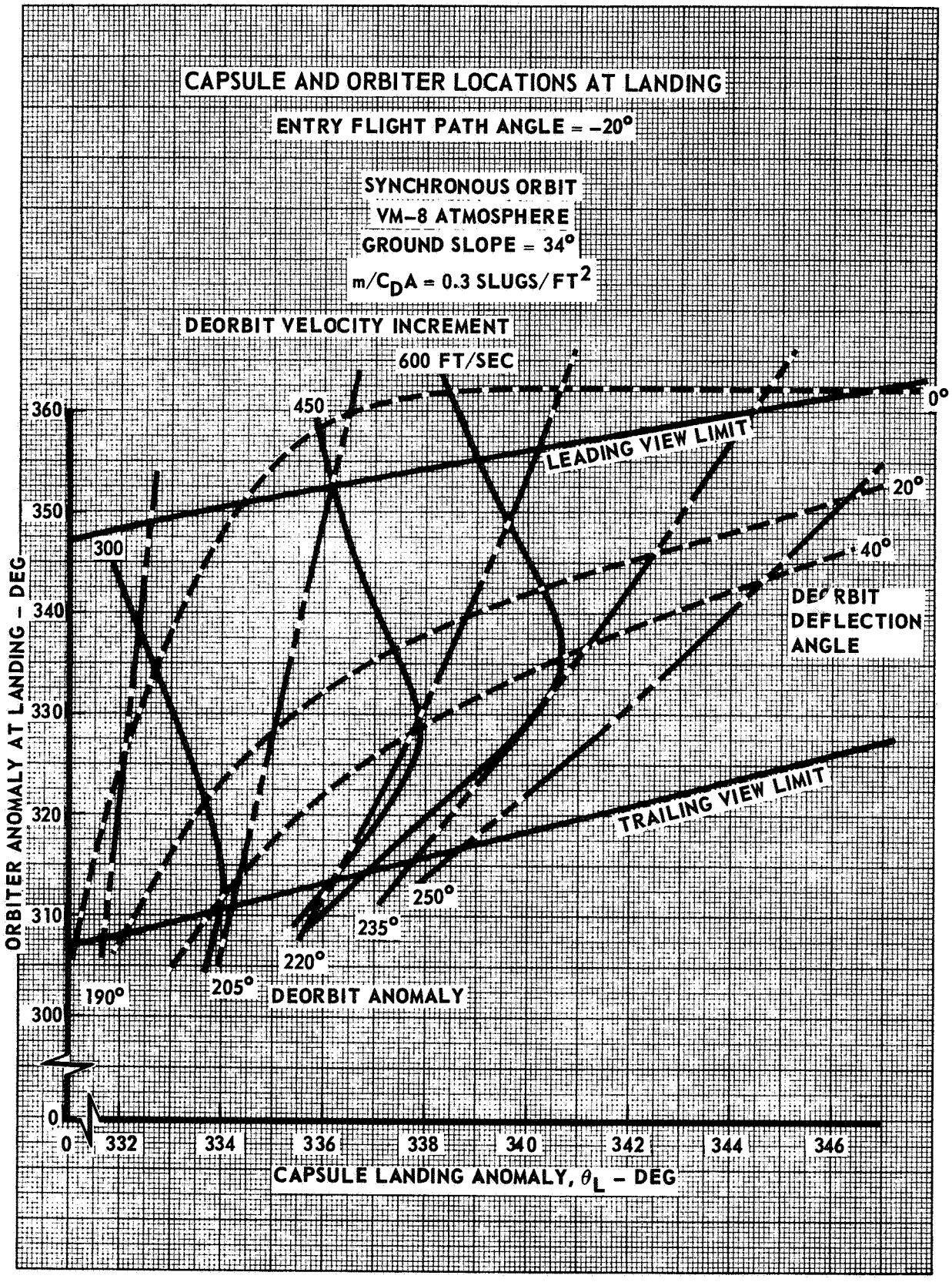

FIGURE 3.1.2–14

b) At a specific deorbit anomaly, more positive deflection angles increase the mutual view period and decrease the required velocity increment.

c) For a constant deorbit velocity increment, deorbit at higher anomalies increases the post-landed view of the orbiter.

d) At a specific deorbit deflection angle, deorbit at higher anomalies requires higher velocity increments and decreases orbiter view.

The ballistic parameter of the capsule and the choice of a final descent system will influence the post-landed geometry. As an example, parachute deployment during terminal descent may delay landing by approximately one minute. Landing anomaly will change slightly while the orbiter will move ahead 2 to 3 degrees before capsule landing.

The result of atmospheric uncertainty on the orbiter position at landing is shown in Figure 3.1.2-15 for entry flight path angles of -15° and -20°. The deorbit velocity increment and deflection angle were chosen to place the orbiter at the trailing view limit after capsule descent through the VM-8 atmosphere. For these deorbit conditions but with entry in the opposite extreme atmosphere (VM-9), the orbiter is ahead of the trailing view limit at landing but still well behind the leading view limit. The band between the two is the maximum uncertainty in viewing positions due to the atmospheric variations.

3.1.2.5 Post-landed view time. - The duration of the post-landed view period determines the amount of data that can be transmitted to the orbiter during the initial pass over the landing site. The length of mutual view depends on the capsule landing anomaly, the orbiter position at capsule landing, and the ground slope. The previous paragraphs showed these positions to be dependent on the deorbit maneuver, the entry conditions and the atmosphere encountered during entry. The effect of these parameters on maximum post-landed view time is shown in Figure 3.1.2-16, assuming a 34° ground slope.

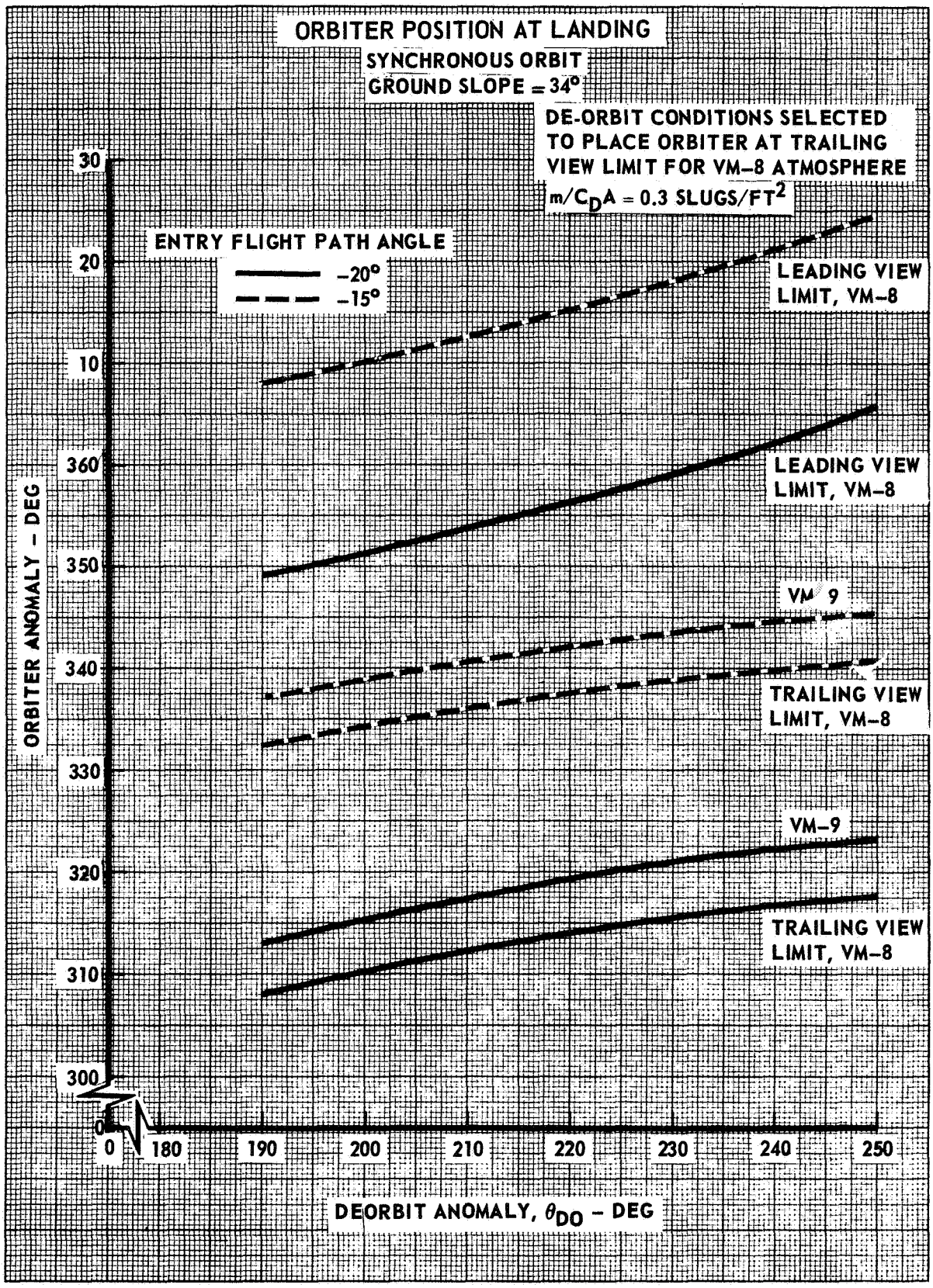

FIGURE 3.1.2-15

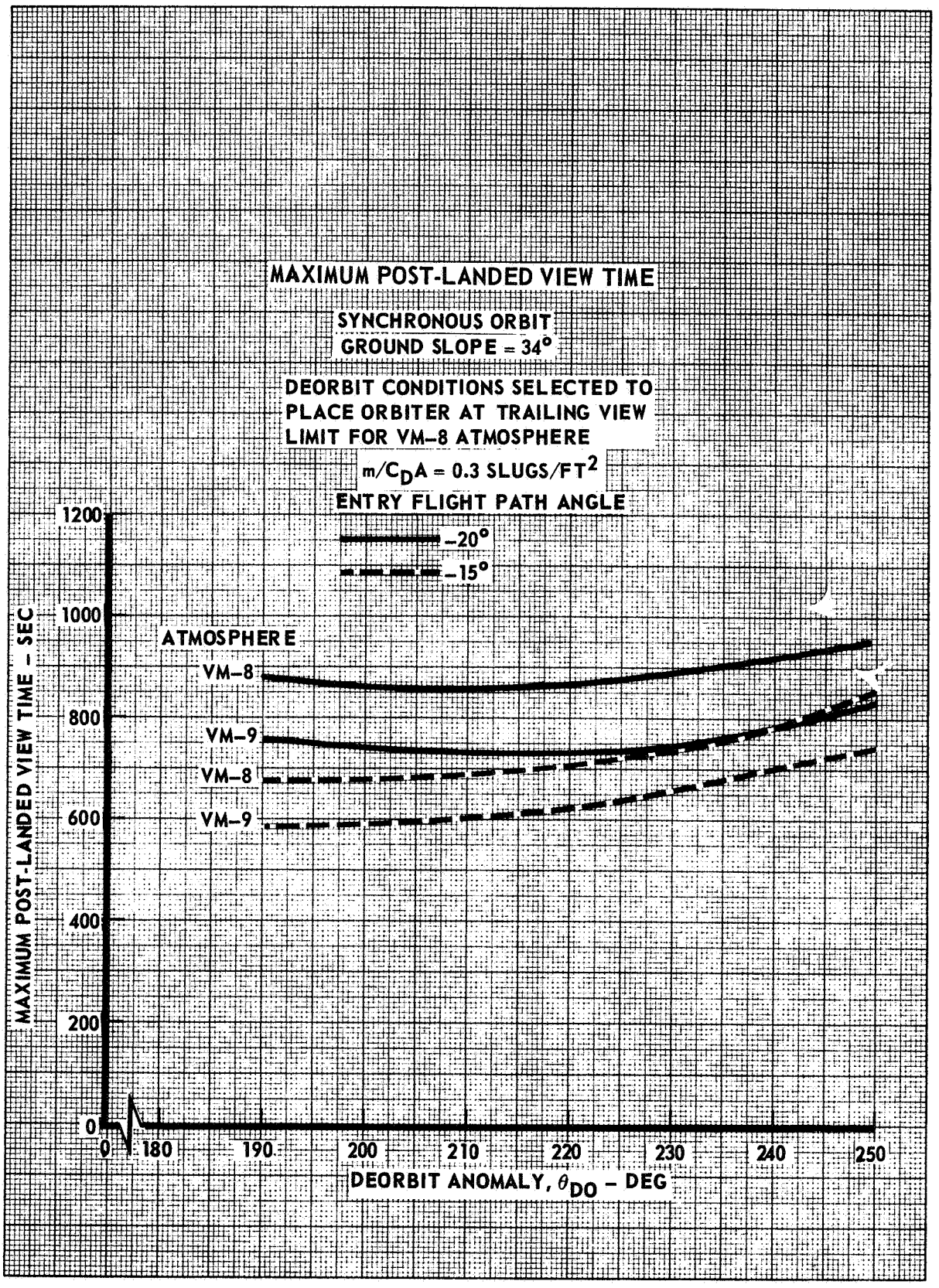

FIGURE 3.1.2-16

The deorbit conditions are those placing the orbiter at the trailing view limit after capsule descent through the VM-8 atmosphere. The effect of atmospheric uncertainty is shown for deorbit from a synchronous orbit with entry at -15° and -20° flight path angles. The important variations are summarized as follows:

a) Steeper entry trajectories increase post-landed view time. (The steeper entries result in landing at anomalies back from periapsis where a greater band of orbital positions can be viewed and the orbiter is moving slower).

b) Maximum view time is increased by choosing larger deorbit anomalies.

c) Deorbit design for the VM-8 atmosphere reduces the post-landed view time by 100 to 120 seconds if the VM-9 is encountered.

3.1.2.6 Entry angle of attack. - Capsule angle of attack at entry influences the degree of pitch attitude oscillations during the atmospheric flight and the accompanying reduction in drag retardation. Before atmospheric entry the capsule attitude will most likely be reoriented to minimize entry angle of attack. In addition, an active damping system will probably be used during the atmospheric flight to reduce pitch oscillations. If no attitude reorientation is performed after deorbit, the entry angle of attack is determined by the capsule inertial orientation at deorbit, the deorbit and entry true anomalies, and the entry flight path angle. The capsule angle of attack at entry is shown in Figure 3.1.2-17 for deorbit at various true anomalies from a synchronous orbit. The capsule attitude is held at the deorbit inertial position and entry is at -15° flight path angle. The loft limit boundary (deorbit deflection angle = 0°) and the trailing view limit boundary for the VM-8 atmosphere are shown. The effect of the deorbit and flight parameters on entry angle of attack assuming no post-deorbit attitude maneuver, are:

a) For a constant deorbit velocity increment, entry angle of attack is decreased at the higher deorbit anomalies.

b) Greater capsule lead angle at entry occurs at the lower entry angles of attack.

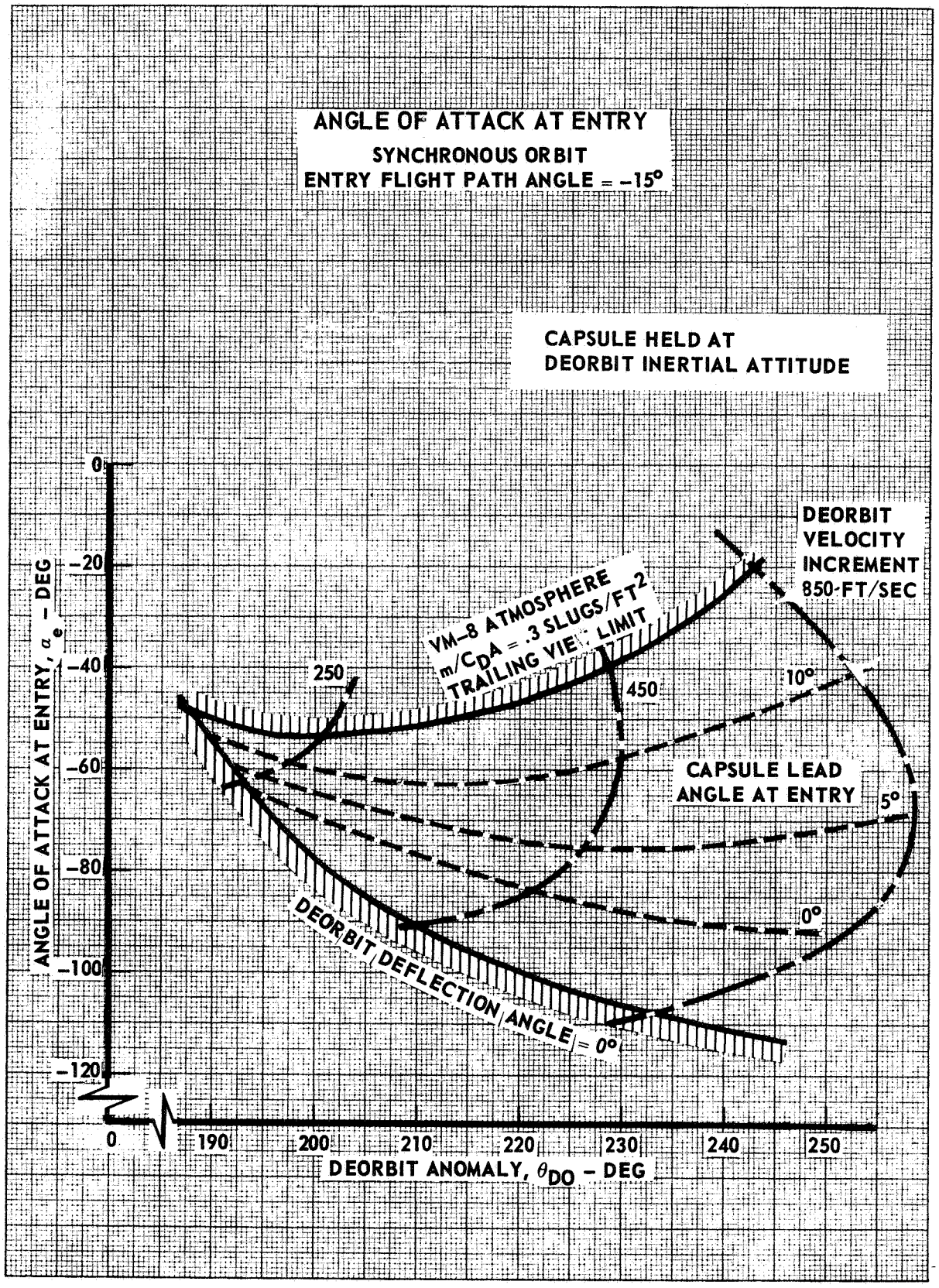

FIGURE 3.1.2–17

c) For maximum post-landed view time, lower entry angles of attack are achieved at the higher deorbit anomalies which require larger deorbit velocity increments.

d) For deorbit deflection angle = 0° (loft limit) the entry angle of attack increases as deorbit is performed away from apoapse.

3.1.2.7 Entry and landing dispersions. - Dispersions result from uncertainties in knowledge of the true orbit parameters, application of the deorbit velocity, and the atmosphere. Estimates of these dispersions are based upon analytical sensitivities for the deorbit phase coupled with digitally simulated entry trajectory data.

Trajectory sensitivities are evaluated for deorbit from a synchronous Mars orbit using deorbit ΔV's which produce a 5 degree capsule lead angle at entry. The partial derivatives of entry conditions with respect to orbit and deorbit conditions at varying deorbit anomalies for -15° and -20° nominal entry flight path angles are shown in Tables 3.1.2-1 through 3.1.2-8. The sources of entry dispersions are:

- Navigation Inaccuracies - Errors in orbit determination prior to deorbit result in errors in the computation of the deorbit impulse. Errors in the Martian mass and radius are also considered.
- Propulsion Subsystem Inaccuracies - The uncertainty in thrust termination is the result of uncertainty in nozzle blow off time and of impulse uncertainty after the nozzle is blown off.
- Attitude Errors During Deorbit - The error is the result of alignment error, attitude reference drift, computation errors, attitude control deadband, and propulsion system misalignment.

The uncertainties in the orbit and deorbit parameters and planet physical constants used in the dispersion analysis are presented in Table 3.1.2-9. The resulting three sigma entry dispersions are shown in Figures 3.1.2-18 and 19. These are significant with respect to deorbit targeting within the design entry corridor and contribute to landing dispersions along with the following atmospheric trajectory considerations:

TABLE 3.1.2–1

KAH2 -- ELLIPTIC ORBIT PARTIAL DERIVATIVES FOR CONSTANT TERMINAL RADIUS

DEORBIT FROM SYNC ORB/CAPSULE LEAD ANG=5DEG/INCLIN=60DEG

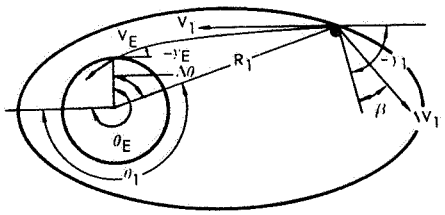

R1	8.9088872E+07	V0	3.3732699E+03	GAM0	-4.9012170E+01	THE1	2.0500000E+02
		DELV	2.9730646E+02	BETA	3.0572221E+01		
		V1	3.0926585E+03	GAM1	-5.0754681E+01		
RE	1.1908789E+07	VE	1.5153122E+04	GAME	-1.5000000E+01	DTHE	1.2703709E+02	DELT 1.7577334E+04
RPL	1.1108789E+07	GRAV	1.5124543E+15				

INDEPENDENT VARIABLES	SENSITIVITIES	DEPENDENT VARIABLES AT ENTRY: TIME	DOWNRANGE ANGLE	CROSSRANGE ANGLE	VELOCITY	FLGHT PATH ANGLE	HEADING ANGLE
	GRAV CONST UNCERTAINTY	3.91599E-13	7.49194E-15	0.	5.20245E-12	3.77336E-15	0.
	ORBIT PERIOD UNCERTAINTY	9.96685E-01	-1.19925E-03	0.	7.45751E-03	-5.08343E-04	0.
	TIME PERIAPS PASS UNCERT	1.00026E+00	-1.04956E-03	0.	1.90167E-03	-4.15993E-04	0.
	PLANET RAD UNCERTAINTY	-1.07518E-04	-1.63307E-06	0.	-7.04767E-04	-6.84912E-07	0.
	PERIAPS ALTITUDE UNCERT	1.47459E-04	1.63226E-05	0.	-9.74221E-07	7.33934E-06	0.
	ARGUMNT OF PERIAP UNCERT	-2.68823E+01	3.62244E-01	0.	3.65380E-01	-2.93598E-01	0.
	ORBIT INCLIN UNCERTAINTY	0.	0.	1.11765E+00	0.	0.	-3.29229E-01
	RIGHT ASCENSION ANG UNCR	-1.34411E+01	1.81122E-01	-7.04207E-02	1.82690E-01	-1.46799E-01	8.96979E-01
	DEORBIT DELTA-V	-2.90014E+00	-1.85125E-01	-0.	-1.91562E-01	-9.13942E-02	-0.
	POINTING -IN-PLANE	2.68823E+01	6.37756E-01	-0.	-3.65380E-01	2.93598E-01	-0.
	OUT-OF-PLANE	-0.	-0.	1.2[illegible]97E-01	-0.	-0.	-1.24029E-01
	DEORBIT TIME	3.12269E-02	2.05336E-04	-0.	-2.66378E-03	6.73487E-04	-0.

ALL DISTANCES IN FEET, TIMES IN SEC, ANGLES IN DEG

TABLE 3.1.2–2

KAH2 -- ELLIPTIC ORBIT PARTIAL DERIVATIVES FOR CONSTANT TERMINAL RADIUS

DEORBIT FROM SYNC ORB/CAPSULE LEAD ANG=5DEG/INCLIN=60DEG

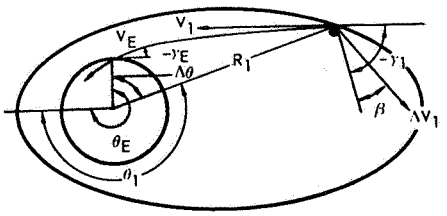

R1	6.4465540E+07	V0	4.9343687E+03	GAM0	-5.1708831E+01	THE1	2.2000000E+02
		DELV	3.9608658E+02	BETA	2.3768704E+01		
		V1	4.5882057E+03	GAM1	-5.4026990E+01		
RE	1.1908789E+07	VE	1.5104144E+04	GAME	-1.5000000E+01	DTHE	1.1469274E+02
RPL	1.1108789E+07	GRAV	1.5124543E+15				

DELT 9.8283422E+03

INDEPENDENT VARIABLES	SENSITIVITIES	DEPENDENT VARIABLES AT ENTRY: TIME	DOWNRANGE ANGLE	CROSSRANGE ANGLE	VELOCITY	FLGHT PATH ANGLE	HEADING ANGLE
	GRAV CONST UNCERTAINTY	3.21960E-13	6.50990E-15	0.	5.20704E-12	3.68064E-15	0.
	ORBIT PERIOD UNCERTAINTY	9.62268E-01	-2.78919E-03	0.	9.52054E-03	-1.22500E-03	0.
	TIME PERIAPS PASS UNCERT	9.63174E-01	-2.73226E-03	0.	3.84658E-03	-1.18150E-03	0.
	PLANET RAD UNCERTAINTY	-8.62246E-05	-1.45243E-06	0.	-7.06746E-04	-6.36456E-07	0.
	PERIAPS ALTITUDE UNCERT	1.69580E-04	1.65033E-05	0.	-6.71178E-07	7.32328E-06	0.
	ARGUMNT OF PERIAP UNCERT	-1.74323E+01	4.90629E-01	0.	1.05818E+00	-2.36042E-01	0.
	ORBIT INCLIN UNCERTAINTY	0.	0.	1.13337E+00	0.	0.	-3.50962E-01
	RIGHT ASCENSION ANG UNCR	-8.71615E+00	2.45315E-01	-1.56951E-02	5.29088E-01	-1.18021E-01	8.71751E-01
	DEORBIT DELTA-V	-2.15789E+00	-1.34270E-01	-0.	-2.62386E-01	-6.88954E-02	-0.
	POINTING -IN-PLANE	1.74323E+01	5.09371E-01	-0.	-1.05818E+00	2.36042E-01	-0.
	OUT-OF-PLANE	-0.	-0.	1.3[illegible]526E-01	-0.	-0.	-9.71725E-02
	DEORBIT TIME	4.48838E-02	-1.50085E-04	-0.	-6.54652E-03	1.06762E-03	-0.

ALL DISTANCES IN FEET, TIMES IN SEC, ANGLES IN DEG

TABLE 3.1.2–3

KBM2 -- ELLIPTIC ORBIT PARTIAL DERIVATIVES FOR CONSTANT TERMINAL RADIUS

DEORBIT FROM SYNC ORB/CAPSULE LEAD ANG=5DEG/INCLIN=60DEG

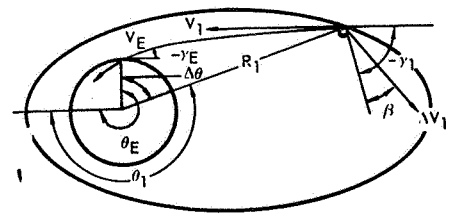

R1	4.6739203E+07	V0	6.4918404E+03	GAM0	-4.9486726E+01	THE1	2.3500000E+02				
		DELV	5.2640731E+02	BETA	1.1933468E+01						
		V1	6.0829788E+03	GAM1	-5.2510175E+01						
RF	1.1908789E+07	VE	1.5042944E+04	GAME	-1.5000000E+01	DTHE	1.0231029E+02	DELT	5.8316848E+03		
RPL	1.1108789E+07	GRAV	1.5124543E+15								

INDEPENDENT VARIABLES	DEPENDENT VARIABLES AT ENTRY: TIME	DOWNRANGE ANGLE	CROSSRANGE ANGLE	VELOCITY	FLGHT PATH ANGLE	HEADING ANGLE
GRAV CONST UNCERTAINTY	2.43990E-13	4.40353E-15	0.	5.20791E-12	2.99588E-15	0.
ORBIT PERIOD UNCERTAINTY	9.01401E-01	-5.84923E-03	0.	1.08449E-02	-2.66282E-03	0.
TIME PERIAPS PASS UNCERT	9.01343E-01	-5.83704E-03	0.	5.00966E-03	-2.64509E-03	0.
PLANET RAD UNCERTAINTY	-6.32160E-05	-9.04698E-07	0.	-7.07756E-04	-3.95364E-07	0.
PERIAPS ALTITUDE UNCERT	1.93629E-04	1.70510E-05	0.	1.19134E-06	7.48287E-06	0.
ARGUMNT OF PERIAP UNCERT	-1.08483E+01	6.74997E-01	0.	2.41661E+00	-1.44077E-01	0.
ORBIT INCLIN UNCERTAINTY	0.	0.	1.13837E+00	0.	0.	-3.66922E-01
RIGHT ASCENSION ANG UNCR	-5.42413E+00	3.37498E-01	3.03675E-02	1.20831E+00	-7.20383E-02	8.56799E-01
DEORBIT DELTA-V	-1.58547E+00	-9.78455E-02	-0.	-3.07137E-01	-5.21433E-02	-0.
POINTING -IN-PLANE	1.08483E+01	3.25003E-01	-0.	-2.41661E+00	1.44077E-01	-0.
OUT-OF-PLANE	-0.	-0.	1.38917 -01	-0.	-0.	-6.75379E-02
DEORBIT TIME	8.85096E-02	-5.17903E-04	-0.	-1.43061E-02	1.96624E-03	-0.

ALL DISTANCES IN FEET, TIMES IN SEC, ANGLES IN DEG

TABLE 3.1.2–4

KAH2 -- ELLIPTIC ORBIT PARTIAL DERIVATIVES FOR CONSTANT TERMINAL RADIUS

DEORBIT FROM SYNC ORB/CAPSULE LEAD ANG=5DEG/INCLIN=60DEG

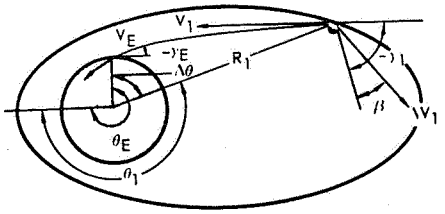

R1	3.5120651E+07	V0	7.9720873E+03	GAM0	-4.5250656E+01	THE1	2.5000000E+02
		DELV	7.0480281E+02	BETA	-5.3060085E+00		
		V1	7.5439760E+03	GAM1	-4.9388054E+01		
RE	1.1908789E+07	VE	1.4992962E+04	GAME	-1.5000000E+01	DTHE	8.9785496E+01 DELT 3.6890442E+03
RPL	1.1108789E+07	GRAV	1.5124543E+15				

INDEPENDENT VARIABLES	SENSITIVITIES	DEPENDENT VARIABLES AT ENTRY: TIME	DOWNRANGE ANGLE	CROSSRANGE ANGLE	VELOCITY	FLGHT PATH ANGLE	HEADING ANGLE
	GRAV CONST UNCERTAINTY	1.62601E-13	1.29962E-15	0.	5.19393E-12	1.70735E-15	0.
	ORBIT PERIOD UNCERTAINTY	8.01467E-01	-1.12051E-02	0.	7.13126E-04	-5.30827E-03	0.
	TIME PERIAPS PASS UNCERT	8.01084E-01	-1.12128E-02	0.	-5.33042E-03	-5.30384E-03	0.
	PLANET RAD UNCERTAINTY	-3.92426E-05	-3.63575E-08	0.	-7.04222E-04	3.55437E-08	0.
	PERIAPS ALTITUDE UNCERT	2.18458E-04	1.79194E-05	0.	7.08898E-06	7.84648E-06	0.
	ARGUMNT OF PERIAP UNCERT	-5.51363E+00	8.98505E-01	0.	5.05114E+00	-2.25057E-02	0.
	ORBIT INCLIN UNCERTAINTY	0.	0.	1.14071E+00	0.	0.	-3.79843E-01
	RIGHT ASCENSION ANG UNCR	-2.75682E+00	4.49253E-01	6.29663E-02	2.52557E+00	-1.12529E-02	8.46726E-01
	DEORBIT DELTA-V	-1.15266E+00	-7.08256E-02	-0.	-2.90802E-01	-3.92105E-02	-0.
	POINTING -IN-PLANE	5.51363E+00	1.01495E-01	-0.	-5.05114E+00	2.25057E-02	-0.
	OUT-OF-PLANE	-0.	-0.	1.435[illegible]5E-01	-0.	-0.	-3.79201E-02
	DEORBIT TIME	1.58429E-01	-1.16701E-03	-0.	-2.48658E-02	3.41461E-03	-0.

ALL DISTANCES IN FEET, TIMES IN SEC, ANGLES IN DEG

TABLE 3.1.2–5

KAM2 -- ELLIPTIC ORBIT PARTIAL DERIVATIVES FOR CONSTANT TERMINAL RADIUS
DEORBIT FROM SYNC ORB/CAPSULE LEAD ANG=5DEG/INCLIN=60DEG

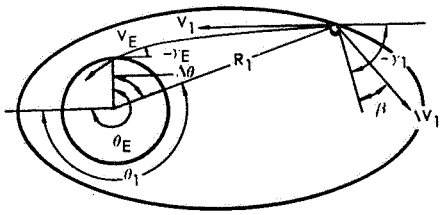

R1	8.9088872E+07	V0	3.3732699E+03	GAM0	-4.9012170E+01	THE1	2.0500000E+02
		DELV	3.4751867E+02	BETA	2.6835643E+01		
		V1	3.0542770E+03	GAM1	-5.1473662E+01		
RE	1.1908789E+07	VE	1.5145335E+04	GAME	-2.0000000E+01	DTHE	1.1690614E+02 DELT 1.7347947E+04
RPL	1.1108789E+07	GRAV	1.5124543E+15				

INDEPENDENT VARIABLES

SENSITIVITIES	DEPENDENT VARIABLES AT ENTRY: TIME	DOWNRANGE ANGLE	CROSSRANGE ANGLE	VELOCITY	FLGHT PATH ANGLE	HEADING ANGLE
GRAV CONST UNCERTAINTY	4.49117E-13	6.32284E-15	0.	5.20363E-12	3.25441E-15	0.
ORBIT PERIOD UNCERTAINTY	9.94213E-01	-1.20484E-03	0.	7.56675E-03	-5.13831E-04	0.
TIME PERIAPS PASS UNCERT	9.97188E-01	-1.09167E-03	0.	1.97391E-03	-4.31502E-04	0.
PLANET RAD UNCERTAINTY	-1.18637E-04	-8.65115E-07	[illegible]	-7.05272E-04	-3.06182E-07	0.
PERIAPS ALTITUDE UNCERT	7.44125E-05	1.23536E-05	0.	-1.11757E-06	5.59363E-06	0.
ARGUMNT OF PERIAP UNCERT	-2.70267E+01	4.99993E-01	0.	5.09918E-01	-2.31867E-01	0.
ORBIT INCLIN UNCERTAINTY	0.	0.	1.13027E+00	0.	0.	-2.56672E-01
RIGHT ASCENSION ANG UNCR	-1.35133E+01	2.49997E-01	-2.36875E-01	2.54959E-01	-1.15933E-01	9.44892E-01
DEORBIT DELTA-V	-2.32961E+00	-1.41095E-01	-0.	-1.83305E-01	-7.19296E-02	-0.
POINTING -IN-PLANE	2.70267E+01	5.00006E-01	-0.	-5.09918E-01	2.31867E-01	-0.
OUT-OF-PLANE	-0.	-0.	1.628[illegible]E-01	-0.	-0.	-1.41954E-01
DEORBIT TIME	2.92020E-02	-8.36090E-05	-0.	-3.02969E-03	5.30393E-04	-0.

ALL DISTANCES IN FEET, TIMES IN SEC, ANGLES IN DEG

TABLE 3.1.2–6

KAH2 -- ELLIPTIC ORBIT PARTIAL DERIVATIVES FOR CONSTANT TERMINAL RADIUS

DEORBIT FROM SYNC ORB/CAPSULE LEAD ANG=5DEG/INCLIN=60DEG

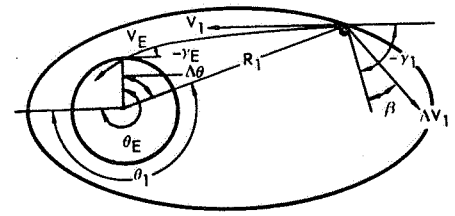

R1	6.4465540E+07	V0	4.9343687E+03	GAM0	-5.1708831E+01	THE1	2.2000000E+02		
		DELV	0.6233193E+02	BETA	1.8848370E+01				
		V1	4.5529286E+03	GAM1	-5.4867335E+01				
RE	1.1908789E+07	VE	1.5093465E+04	GAME	-2.0000000E+01	DTHE	1.0491863E+02	DELT	9.6196763E+03
RPL	1.1108789E+07	GRAV	1.5124543E+15						

INDEPENDENT VARIABLES	SENSITIVITIES	DEPENDENT VARIABLES AT ENTRY: TIME	DOWNRANGE ANGLE	CROSSRANGE ANGLE	VELOCITY	FLGHT PATH ANGLE	HEADING ANGLE
	GRAV CONST UNCERTAINTY	3.64521E-13	5.06960E-15	0.	5.20770E-12	3.06423E-15	0.
	ORBIT PERIOD UNCERTAINTY	9.57405E-01	-2.75675E-03	0.	9.34713E-03	-1.23005E-03	0.
	TIME PERIAPS PASS UNCERT	9.57872E-01	-2.72133E-03	0.	3.60148E-03	-1.19122E-03	0.
	PLANET RAD UNCERTAINTY	-9.33631E-05	-6.24713E-07	0.	-7.07166E-04	-2.29545E-07	0.
	PERIAPS ALTITUDE UNCERT	1.00350E-04	1.25940E-05	0.	-5.91074E-07	5.61987E-06	0.
	ARGUMNT OF PERIAP UNCERT	-1.64031E+01	6.29683E-01	0.	1.43136E+00	-1.71554E-01	0.
	ORBIT INCLIN UNCERTAINTY	0.	0.	1.15236E+00	0.	0.	-2.80914E-01
	RIGHT ASCENSION ANG UNCR	-8.20153E+00	3.14842E-01	-1.76134E-01	7.15681E-01	-8.57771E-02	9.19963E-01
	DEORBIT DELTA-V	-1.71105E+00	-1.01239E-01	-0.	-2.43980E-01	-5.43153E-02	-0.
	POINTING -IN-PLANE	1.64031E+01	3.70317E-01	-0.	-1.43136E+00	1.71554E-01	-0.
	OUT-OF-PLANE	-0.	-0.	1.70509E-01	-0.	-0.	-1.07489E-01
	DEORBIT TIME	4.34507E-02	-5.23874E-04	-0.	-7.21877E-03	8.80756E-04	-0.

ALL DISTANCES IN FEET, TIMES IN SEC, ANGLES IN DEG

TABLE 3.1.2–7

KAM2 -- ELLIPTIC ORBIT PARTIAL DERIVATIVES FOR CONSTANT TERMINAL RADIUS

DEORBIT FROM SYNC ORB/CAPSULE LEAD ANG=50DEG/INCLIN=60DEG

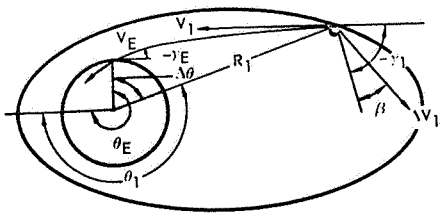

R1	4.6739203E+07	V0	6.4918404E+03	GAM0	-4.9486726E+01	THE1	2.3500000E+02				
		DELV	6.1936656E+02	BETA	4.8503076E+00						
		V1	6.0667394E+03	GAM1	-5.3600115E+01						
RE	1.1908789E+07	VE	1.5036384E+04	GAME	-2.0000000E+01	DTHE	9.2807073E+01	DELT	5.6322934E+03		
RPL	1.1108789E+07	GRAV	1.5124543E+15								

INDEPENDENT VARIABLES	SENSITIVITIES	DEPENDENT VARIABLES AT ENTRY: TIME	DOWNRANGE ANGLE	CROSSRANGE ANGLE	VELOCITY	FLGHT PATH ANGLE	HEADING ANGLE
	GRAV CONST UNCERTAINTY	2.77732E-13	2.77959E-15	0.	5.20499E-12	2.27584E-15	0.
	ORBIT PERIOD UNCERTAINTY	8.93130E-01	-5.72646E-03	0.	8.37250E-03	-2.68415E-03	0.
	TIME PERIAPS PASS UNCERT	8.92768E-01	-5.72725E-03	0.	2.41130E-03	-2.66818E-03	0.
	PLANET RAD UNCERTAINTY	-6.79401E-05	-4.57221E-08	[illegible]	-7.07131E-04	3.90601E-08	0.
	PERIAPS ALTITUDE UNCERT	1.26509E-04	1.31730E-05	0.	2.12631E-06	5.83242E-06	0.
	ARGUMNT OF PERIAP UNCERT	-9.30803E+00	8.13006E-01	0.	3.27915E+00	-7.42964E-02	0.
	ORBIT INCLIN UNCERTAINTY	0.	0.	1.16200E+00	0.	0.	-2.97454E-01
	RIGHT ASCENSION ANG UNCR	-4.65402E+00	4.06503E-01	-1.30580E-01	1.63957E+00	-3.71482E-02	9.06476E-01
	DEORBIT DELTA-V	-1.23501E+00	-7.22463E-02	-0.	-2.66028E-01	-4.07845E-02	-0.
	POINTING -IN-PLANE	9.30803E+00	1.86994E-01	-0.	-3.27915E+00	7.42964E-02	-0.
	OUT-OF-PLANE	-0.	-0.	1.718[illegible]E-01	-0.	-0.	-7.09681E-02
	DEORBIT TIME	8.79136E-02	-1.13471E-03	-0.	-1.48809E-02	1.66375E-03	-0.

ALL DISTANCES IN FEET, TIMES IN SEC, ANGLES IN DEG

TABLE 3.1.2–8

KAM2 -- ELLIPTIC ORBIT PARTIAL DERIVATIVES FOR CONSTANT TERMINAL RADIUS

DEORBIT FROM SYNC ORB/CAPSULE LEAD ANG=5DEG/INCLIN=60DEG

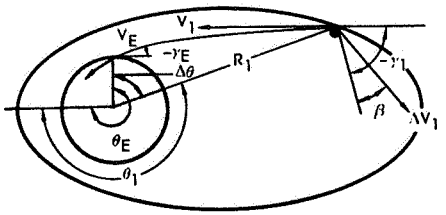

R1	3.5120651E+07	V0	7.9720873E+03	GAM0	-4.5250656E+01	THE1	2.5000000E+02				
		DELV	8.5898721E+02	BETA	-1.5448855E+01						
		V1	7.5887699E+03	GAM1	-5.0915588E+01						
RE	1.1908789E+07	VE	1.5015551E+04	GAME	-2.0000000E+01	DTHE	8.0446773E+01	DELT	3.4909283E+03		
RPL	1.1108789E+07	GRAV	1.5124543E+15								

INDEPENDENT VARIABLES	SENSITIVITIES	DEPENDENT VARIABLES AT ENTRY: TIME	DOWNRANGE ANGLE	CROSSRANGE ANGLE	VELOCITY	FLGHT PATH ANGLE	HEADING ANGLE
	GRAV CONST UNCERTAINTY	1.92969E-13	-4.26232E-16	0.	5.17870E-12	8.45317E-16	0.
	ORBIT PERIOD UNCERTAINTY	7.89604E-01	-1.08900E-02	0.	-1.24405E-02	-5.40308E-03	0.
	TIME PERIAPS PASS UNCERT	7.89014E-01	-1.09057E-02	0.	-1.86853E-02	-5.39872E-03	0.
	PLANET RAD UNCERTAINTY	-4.31266E-05	8.24235E-07	0.	-6.99813E-04	5.04543E-07	0.
	PERIAPS ALTITUDE UNCERT	1.51592E-04	1.40429E-05	0.	1.04280E-05	6.27729E-06	0.
	ARGUMNT OF PERIAP UNCERT	-3.79629E+00	1.03493E+00	0.	6.94135E+00	5.86264E-02	0.
	ORBIT INCLIN UNCERTAINTY	0.	0.	1.16994E+00	0.	0.	-3.08487E-01
	RIGHT ASCENSION ANG UNCR	-1.89814E+00	5.17465E-01	-1.05402E-01	3.47067E+00	2.93132E-02	8.96122E-01
	DEORBIT DELTA-V	-8.59211E-01	-4.97322E-02	-0.	-2.02621E-01	-2.95892E-02	-0.
	POINTING -IN-PLANE	3.79629E+00	-3.49305E-02	-0.	-6.94135E+00	-5.86264E-02	-0.
	OUT-OF-PLANE	-0.	-0.	1.7704[illegible]-01	-0.	-0.	-3.46433E-02
	DEORBIT TIME	1.58628E-01	-2.20932E-03	-0.	-2.22306E-02	2.90531E-03	-0.

ALL DISTANCES IN FEET, TIMES IN SEC, ANGLES IN DEG

TABLE 3.1.2–9

UNCERTAINTY VALUES (3σ)

1	PERIOD	10 SEC
1	TIME OF PERIAPSE PASSAGE	20 SEC
1	PERIAPSE ALTITUDE	10 KM
1	INCLINATION	.5 DEG
1	ARGUMENT OF PERIAPSE	.5 DEG
1	RT. ASCENSION OF ASCENDING NODE	.5 DEG
1	GRAVITATIONAL CONSTANT	24 KM^3/SEC^2
1	PLANET RADIUS	12 KM
2	DEORBIT ΔV	1%
2	IN-PLANE POINTING	.85 DEG
2	OUT-OF-PLANE POINTING	.85 DEG
2	DEORBIT TIME	.05 SEC

1 SPECIFIED BY NASA LRC

2 MDC ANALYSIS OF DEORBIT EXECUTION ERROR

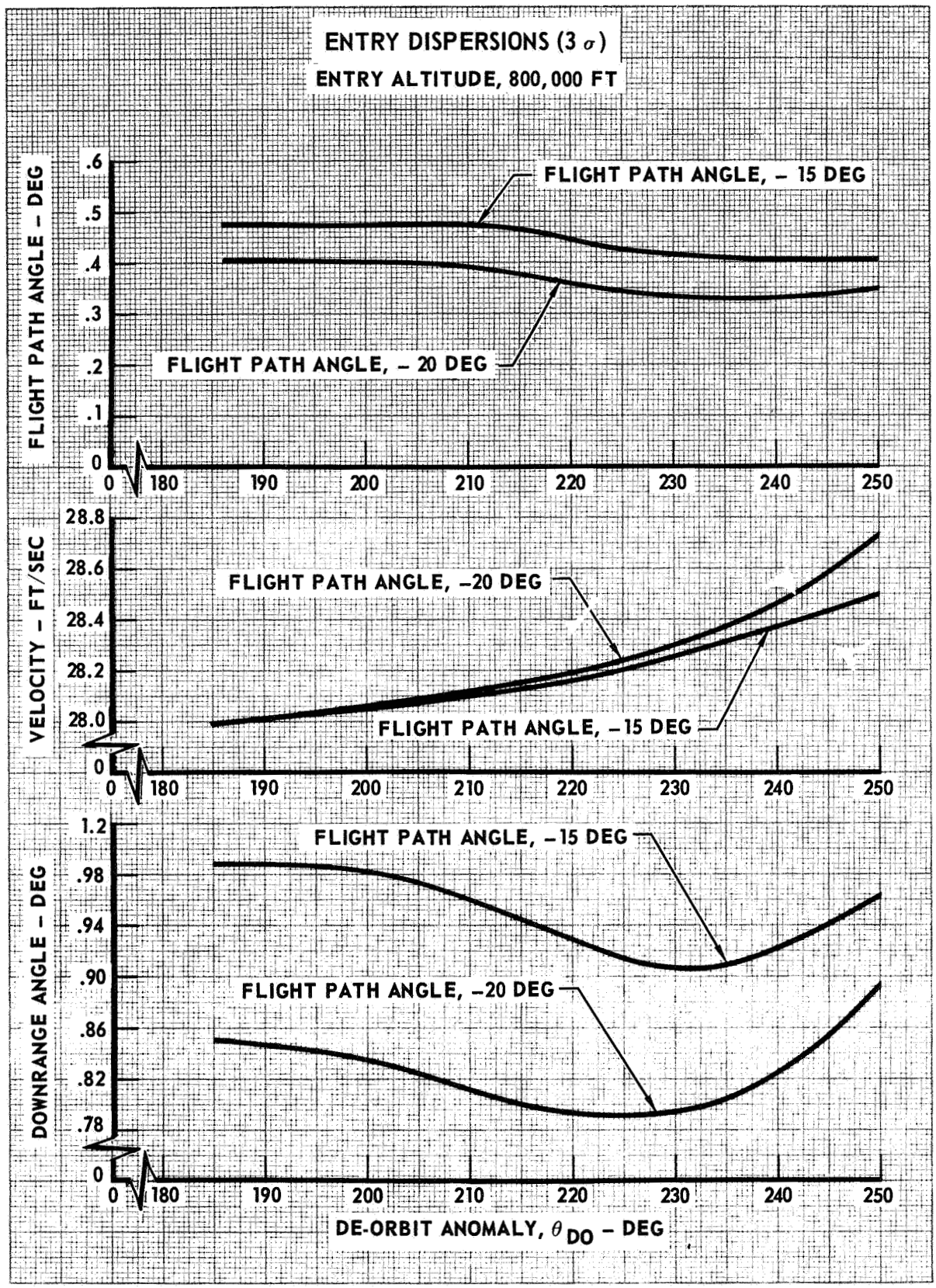

FIGURE 3.1.2–18

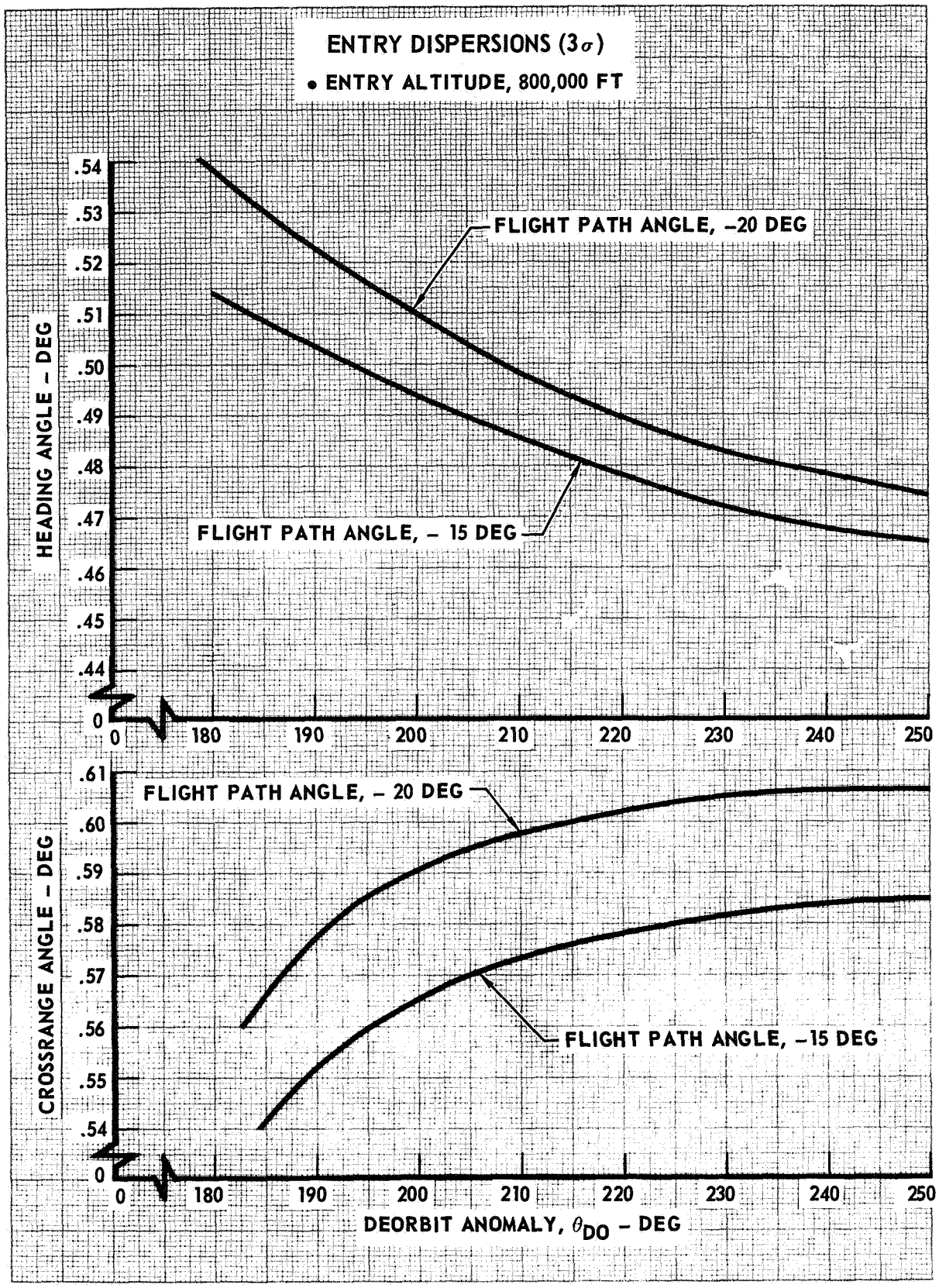

FIGURE 3.1.2–19

- o Atmosphere Model Variations - Different atmosphere models result in different dynamic histories and, therefore, different central angles of travel during entry. Data from VM-8 and VM-9 are assumed to represent a range $\pm 3\sigma$ from nominal. The three sigma variations in landing anomaly are 2° and .8° for -15° and -20° entry flight path angles respectively, for a ballistic parameter of 0.3 slugs/ft^2.
- o Wind - The presence of wind will affect impact by affecting horizontal velocity. A central angle variation of 0.106° is based on trajectories with mean head and tail winds in a VM-8 atmosphere. A correction factor for parachute deployment increases the angle to 0.13°. This is used as the one sigma landing dispersion.
- o Aerodynamic Coefficient Uncertainty - Knowledge of the aerodynamic coefficient affects the accuracy of trajectory prediction. This effect is small compared to atmosphere model variations.

The landing dispersions which result from the above errors are shown in Figure 3.1.2-20. The reduction in landing dispersions as deorbit anomaly increases results from the decreased effect of the deorbit ΔV magnitude and pointing uncertainties.

3.1.2.8 Deorbit and descent selection. - Selection of the deorbit maneuver is based on the capsule flight and post-landed parameters, as well as on the practical limitations on the deorbit propulsion system. A summary of capsule flight and deorbit parameters is shown in Table 3.1.2-10 for a spread of deorbit positions (true anomalies of 195°, 220°, and 245°). The resulting descent trajectories will land the capsule with a maximum view time of the orbiter for the VM-8 atmosphere. The data shown is for deorbit from a synchronous orbit and entry at -15° flight path angle. The trends in the data are summarized below:

a) Deorbit - The requirements for the deorbit propulsion system increase from 224 ft/sec velocity increment to 845 ft/sec as the deorbit position varies from 195° true anomaly to 245°. The required deflection angle increases from +19.6° to +91.2°.

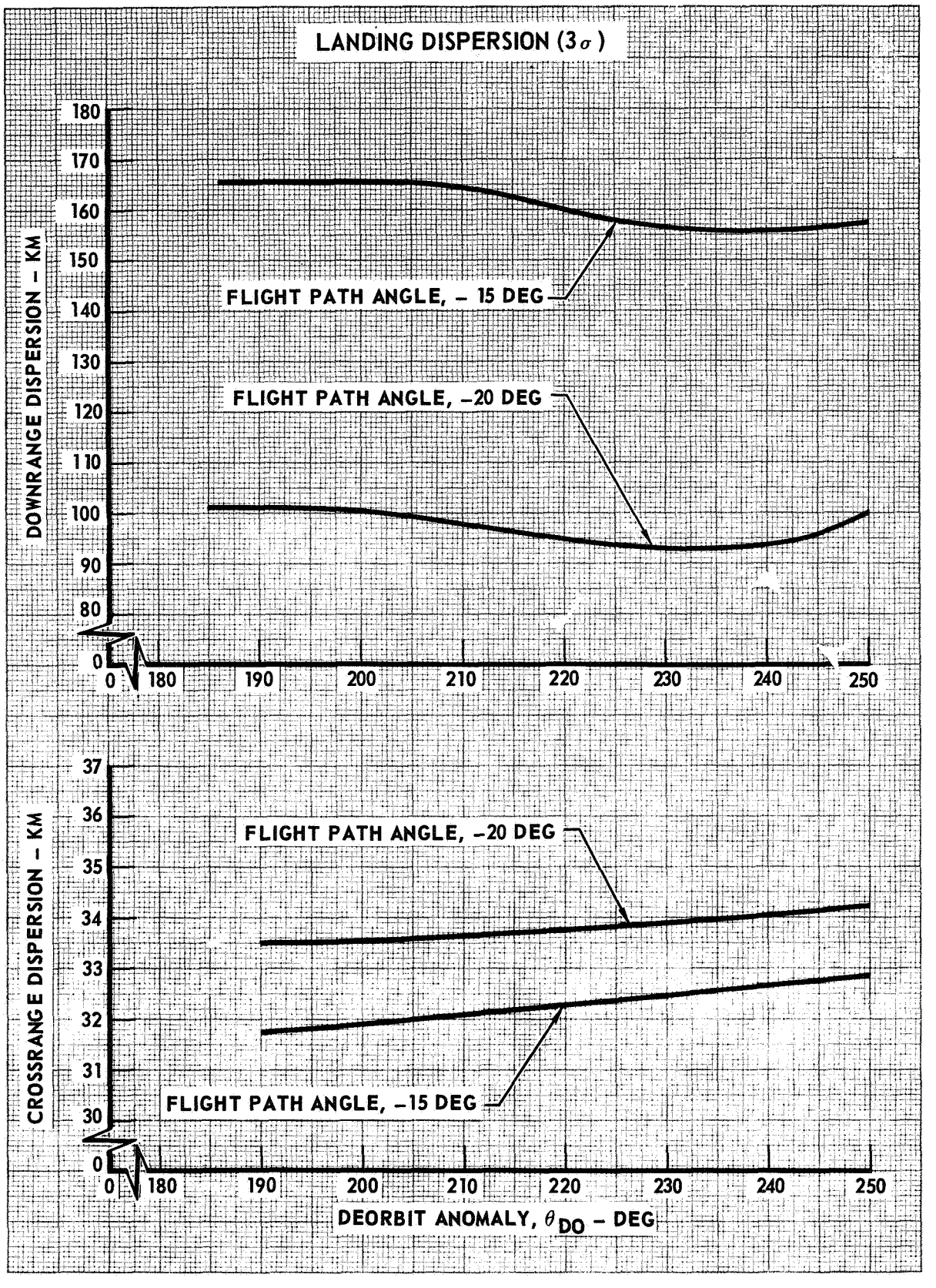

FIGURE 3.1.2–20

TABLE 3.1.2-10

CAPSULE DEORBIT AND FLIGHT PARAMETERS
FOR MAXIMUM POST-LANDED VIEW TIME (VM-8 ATMOSPHERE)

$m/C_DA = 0.3$ SLUGS/FT^2

SYNCHRONOUS ORBIT

ENTRY FLIGHT PATH ANGLE = $-15°$

GROUND SLOPE VIEW LIMIT = $34°$

DEORBIT ANOMALY (DEG)	VELOCITY INCREMENT (FT/SEC)	DEORBIT DEFLECTION ANGLE (DEG)	DESCENT TIME (HR)	ENTRY LEAD ANGLE (DEG)	ENTRY VELOCITY (FT/SEC)	LANDING ANOMALY (DEG)	MAX VIEW TIME (VM-8) (SEC)	VIEW TIME (VM-9) (SEC)
195	224	19.6	7.45	16.6	15166	351.66	680	585
220	354	57.4	2.67	15.4	15141	355.16	721	629
245	845	91.2	1.11	15.2	15262	357.68	821	728

b) Descent - The descent systems must operate for 7.45 hours for deorbit at 195° true anomaly; the requirement is significantly reduced to 1.11 hours for 245° deorbit anomaly.

c) Entry - With entry at -15° flight path angle, the entry velocity and capsule lead angle have little variance with deorbit position. Capsule lead is 15.2° to 16.6° and entry velocity is 15 141 to 15 262 ft/sec.

d) Landing - The capsule landing true anomaly varies from 351.66° to 357.68° for the spread in deorbit positions. The view time is longer for the higher landing anomaly, because the leading view limit extends farther past periapse where the orbiter moves more slowly. The length of post-landed view decreases by approximately 100 sec if the VM-9 atmosphere is encountered.

3.1.3 ENTRY - Entry into the Martian planetary atmosphere is initiated at the prescribed 800 000 ft through an entry corridor (velocity, flight path angle limits) which, in conjunction with the vehicle ballistic parameter (m/C_DA) and the model atmosphere, defines the shape of the trajectory and the magnitudes of the associated forces, times, ranges, thermodynamic environment, etc.

The vehicle drag coefficient is defined by the capsule shape (60° half-angle cone with a 0.5 ratio of nose radius to base radius); thus, ballistic parameter variations imply only vehicle density or diameter variations. A summary of the estimated static and dynamic aerodynamic force and moment coefficients throughout the Mach number and angle of attack ranges is presented for this vehicle in Figure 3.1.3-1. This data was compiled from estimates and wind tunnel tests conducted during or prior to the VOYAGER Phase B study (NASA CR-89675). This data agrees well with the results of static force tests conducted in the Jet Propulsion Laboratory facilities on blunted, large-angle cones (NASA TR 32-1213). The nominal center of gravity location is on the vehicle longitudinal axis at the maximum diameter.

3.1.3.1 Trajectory parameters. - The entry corridor shown in Figure 3.1.3-2 presents the combinations of velocity and flight path angle which produce extremes in the trajectory parameters. The atmospheres in which the extremes occur are shown in Figure 3.1.3-3 where the atmospheres are defined only by surface pressure and scale height. Intermediate atmospheres (not VM) must be constructed such that the other defining parameters (tropopause altitude, adiabatic lapse rate, molecular weight, etc.) conform to known intermediate variations.

In general, an increase in ballistic parameter causes more severe heating rates (see Section 3.2.9) and air loads, a decrease in entry time, and an increase in range. Maximum dynamic pressure, time, and range are shown in Figures 3.1.3-4 through -6 as a function of ballistic parameter in the extreme atmospheres. The ballistic parameter values quoted in this section are for hypersonic speeds but actually vary during descent according to the drag coefficient. Maximum dynamic pressure and the altitude at maximum dynamic pressure have been correlated in nomograph form as a function of entry velocity,

RESULTS OF MCDONNELL POLYSONIC WIND TUNNEL TEST PROGRAM #195

EFFECT OF MACH NUMBER ON AXIAL FORCE COEFFICIENT

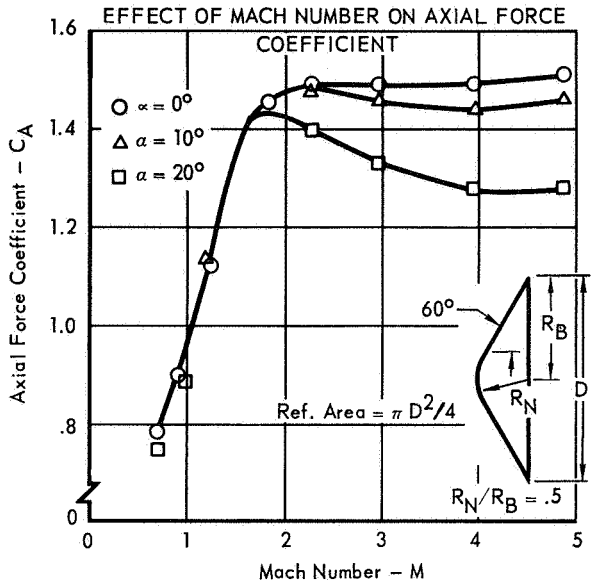

ADDITIONAL AERODYNAMIC CHARACTERISTICS

AEROSHELL AERODYNAMIC COEFFICIENTS OBTAINED FROM MODIFIED NEWTONIAN THEORY

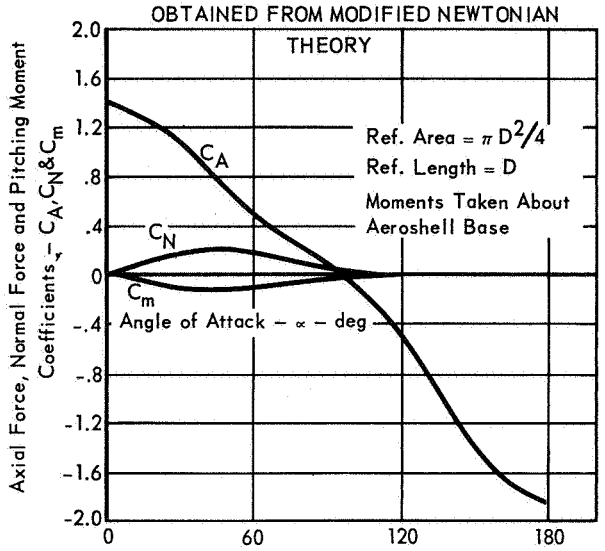

EFFECT OF MACH NUMBER ON NORMAL FORCE COEFFICIENT SLOPE

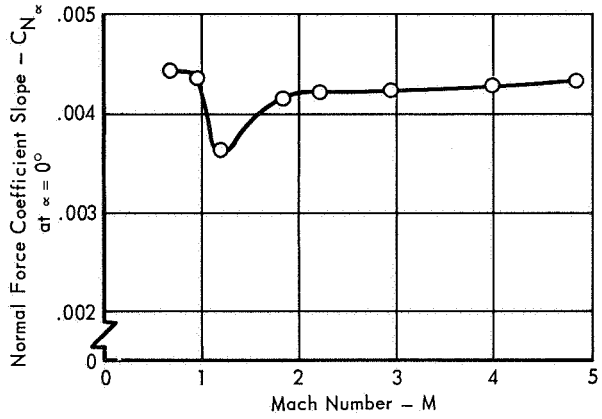

PITCH DAMPING COEFFICIENT FOR MODELS HAVING THE C.G. 8.4% D AND 0% D FORWARD OF THE MAXIMUM DIAMETER

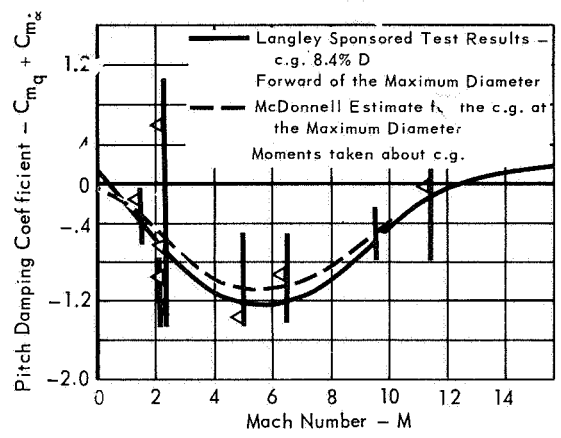

EFFECT OF MACH NUMBER ON PITCHING MOMENT COEFFICIENT SLOPE

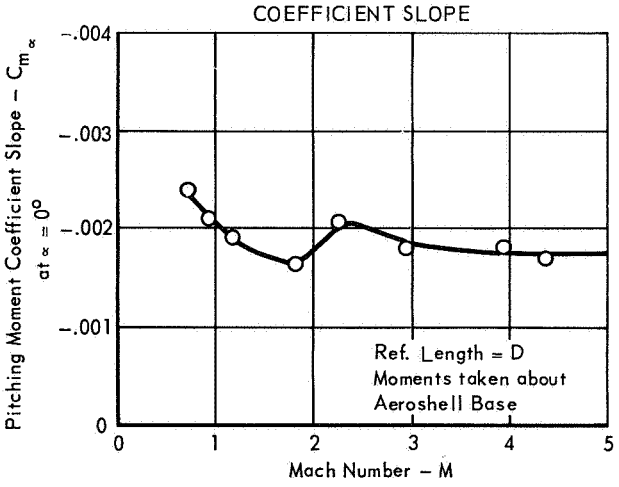

PITCH DAMPING COEFFICIENT FOR MODELS HAVING THE C.G. 1.21% D AFT OF THE MAXIMUM DIAMETER

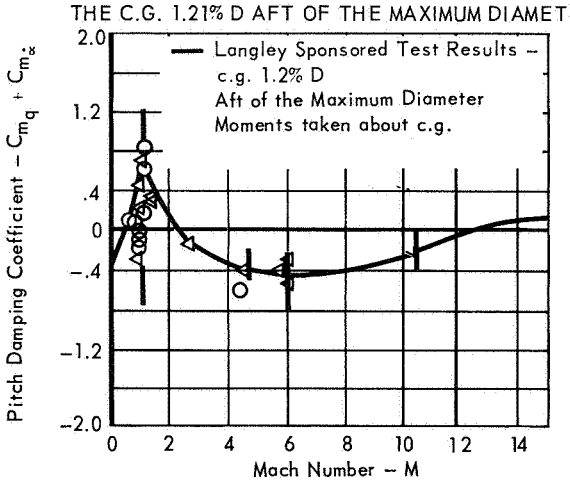

FIGURE 3.1.3–1

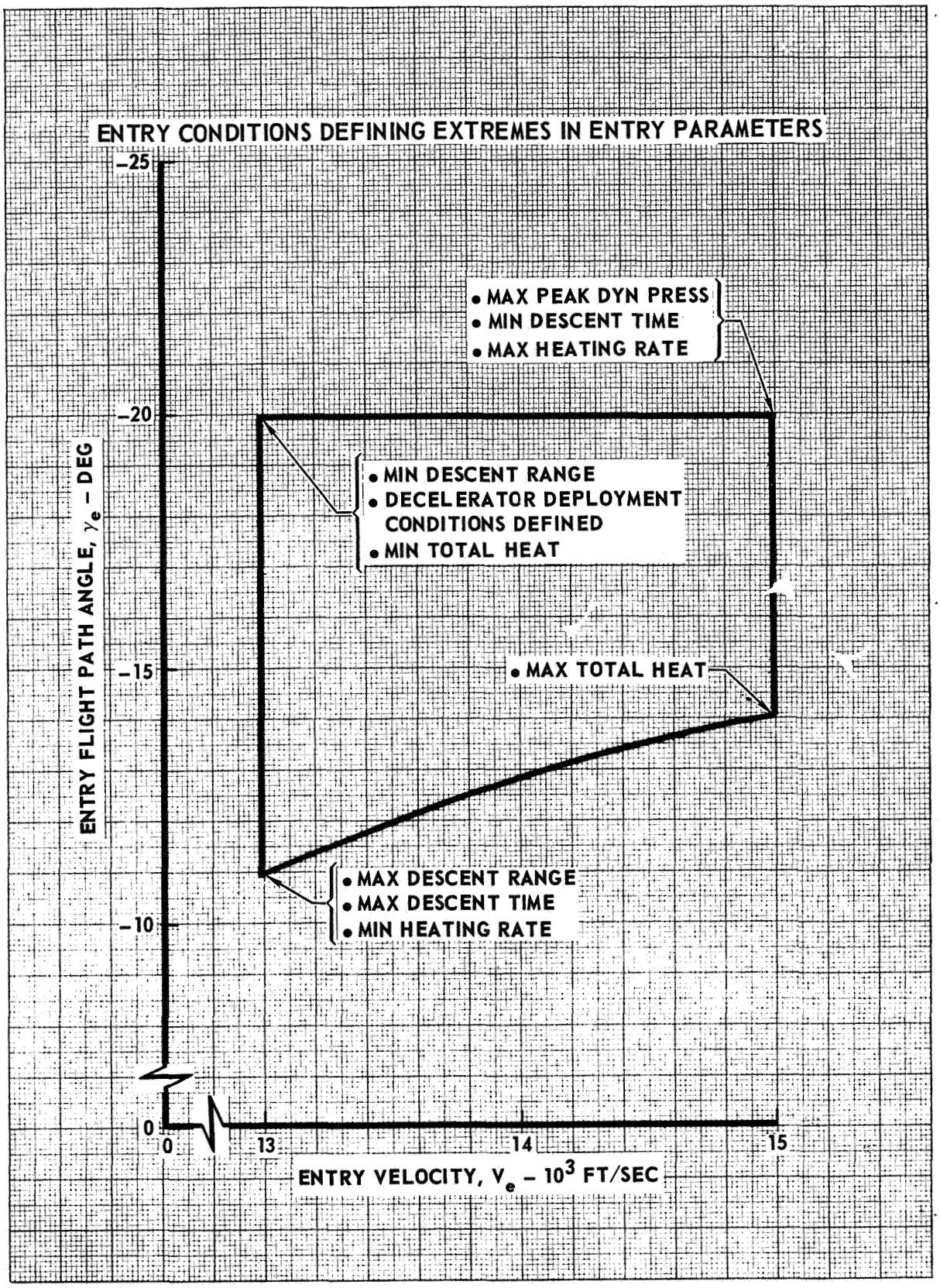
ENTRY CONDITIONS DEFINING EXTREMES IN ENTRY PARAMETERS
-25
-20
-15
-10
0
ENTRY FLIGHT PATH ANGLE, γ_e – DEG
• MAX PEAK DYN PRESS
• MIN DESCENT TIME
• MAX HEATING RATE
• MIN DESCENT RANGE
• DECELERATOR DEPLOYMENT CONDITIONS DEFINED
• MIN TOTAL HEAT
• MAX TOTAL HEAT
• MAX DESCENT RANGE
• MAX DESCENT TIME
• MIN HEATING RATE
0
13
14
15
ENTRY VELOCITY, V_e – 10^3 FT/SEC

FIGURE 3.1.3–2

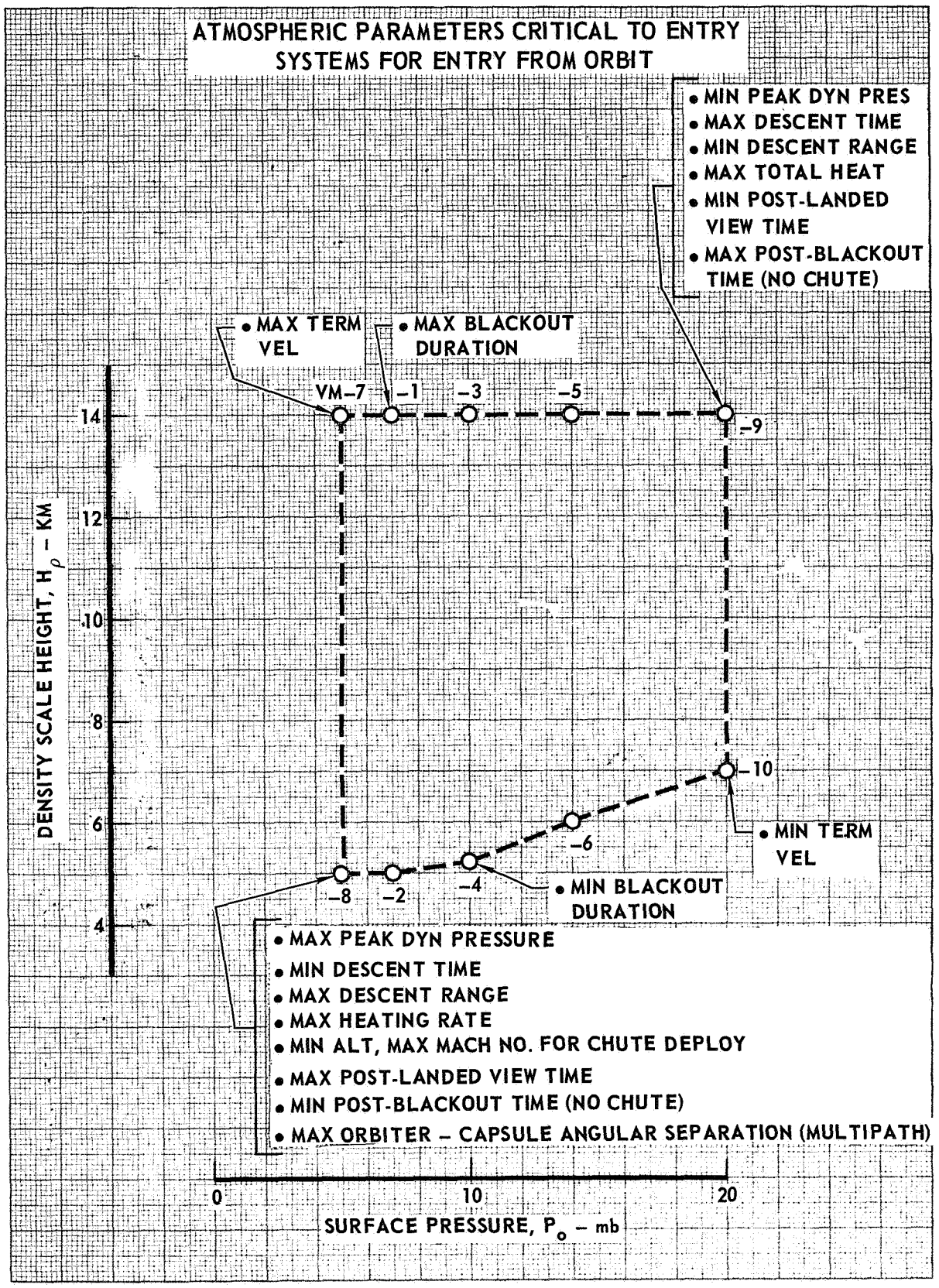
ATMOSPHERIC PARAMETERS CRITICAL TO ENTRY SYSTEMS FOR ENTRY FROM ORBIT
• MIN PEAK DYN PRES
• MAX DESCENT TIME
• MIN DESCENT RANGE
• MAX TOTAL HEAT
• MIN POST-LANDED VIEW TIME
• MAX POST-BLACKOUT TIME (NO CHUTE)
• MAX TERM VEL
• MAX BLACKOUT DURATION
VM–7
–1
–3
–5
–9
–10
–6
–4
–2
–8
• MIN TERM VEL
• MIN BLACKOUT DURATION
• MAX PEAK DYN PRESSURE
• MIN DESCENT TIME
• MAX DESCENT RANGE
• MAX HEATING RATE
• MIN ALT, MAX MACH NO. FOR CHUTE DEPLOY
• MAX POST-LANDED VIEW TIME
• MIN POST-BLACKOUT TIME (NO CHUTE)
• MAX ORBITER – CAPSULE ANGULAR SEPARATION (MULTIPATH)
DENSITY SCALE HEIGHT, H_ρ – KM
14
12
10
8
6
4
0
10
20
SURFACE PRESSURE, P_o – mb

FIGURE 3.1.3–3

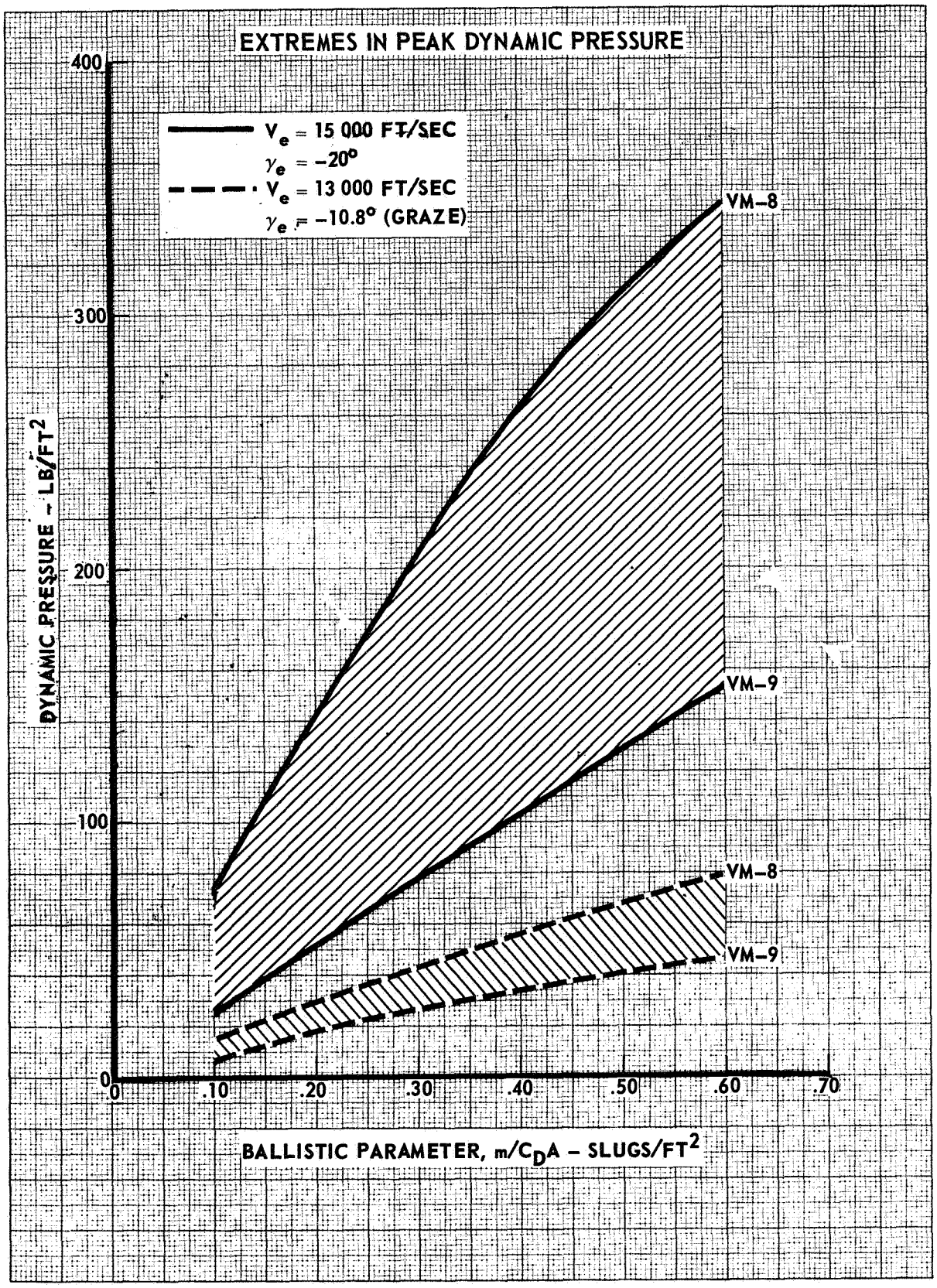
EXTREMES IN PEAK DYNAMIC PRESSURE
V_e = 15 000 FT/SEC
γ_e = −20°
V_e = 13 000 FT/SEC
γ_e = −10.8° (GRAZE)
VM−8
VM−9
VM−8
VM−9
DYNAMIC PRESSURE – LB/FT²
400
300
200
100
0
0
.10
.20
.30
.40
.50
.60
.70
BALLISTIC PARAMETER, m/C_DA – SLUGS/FT²

FIGURE 3.1.3–4

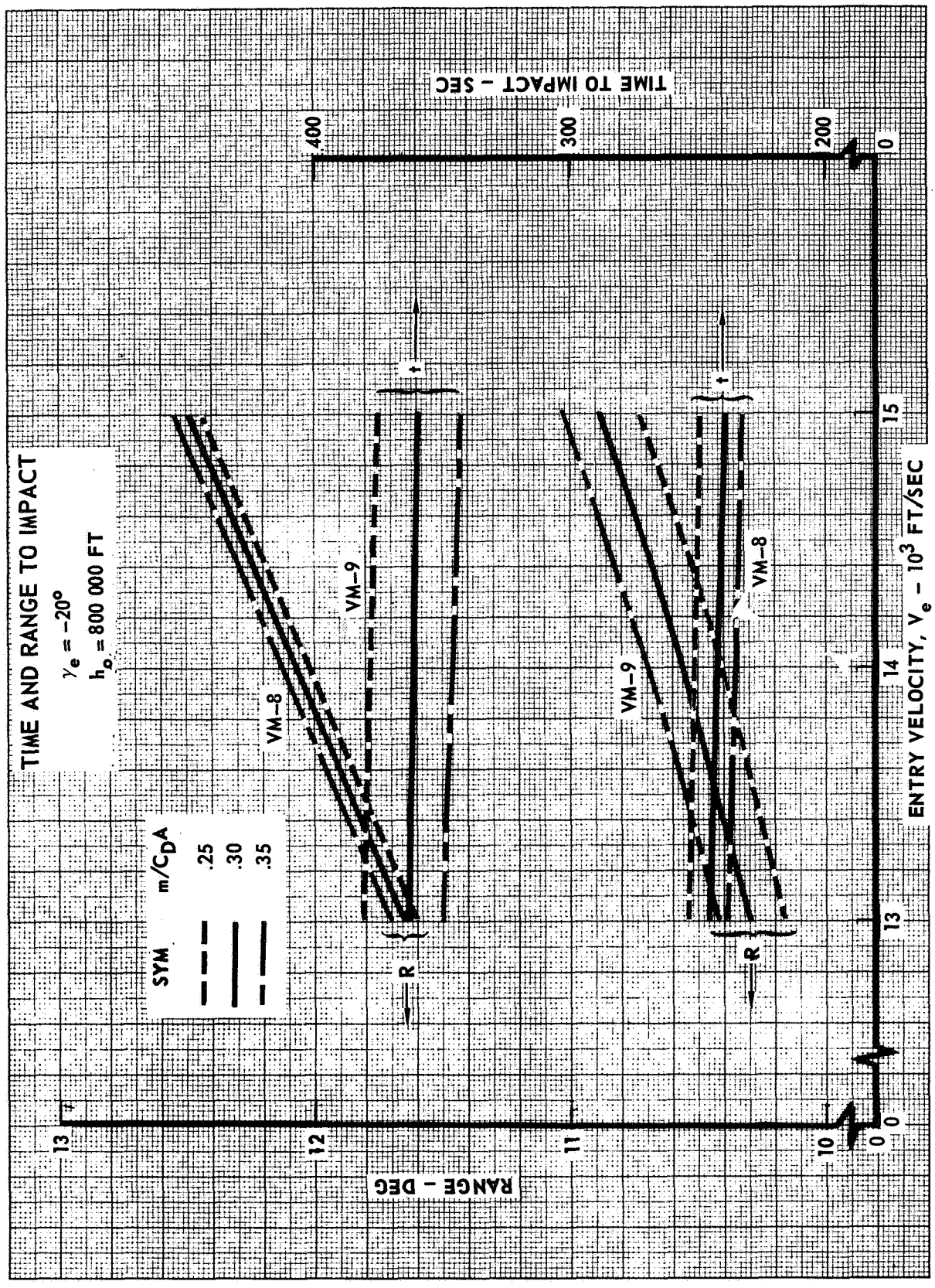
TIME AND RANGE TO IMPACT
$\gamma_e = -20°$
$h_o = 800\ 000$ FT
SYM
m/C_DA
.25
.30
.35
VM-8
VM-9
R
t
RANGE - DEG
TIME TO IMPACT - SEC
ENTRY VELOCITY, V_e - 10^3 FT/SEC
13
12
11
10
0
400
300
200
0
15
14
13

FIGURE 3.1.3-5

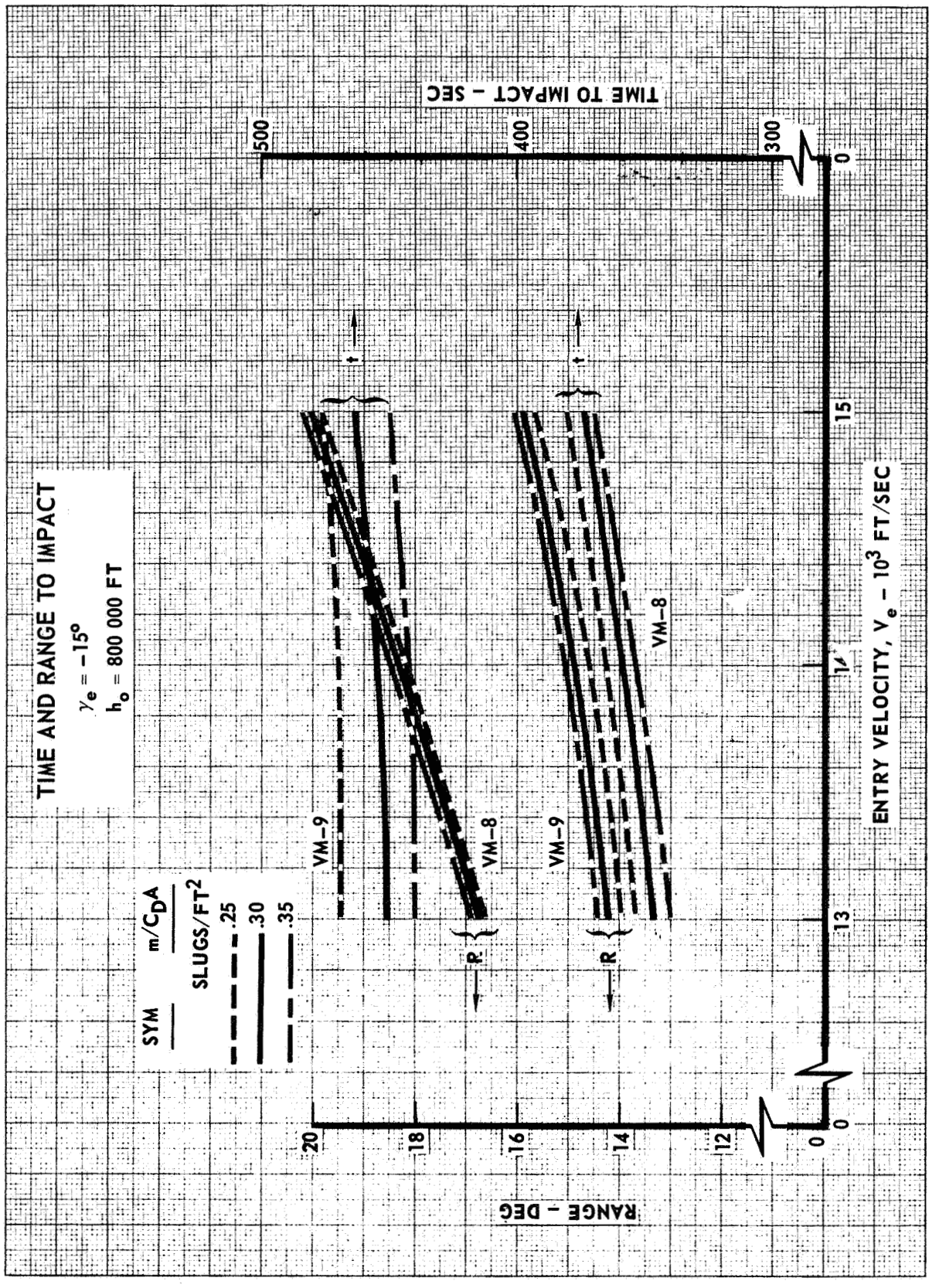
TIME AND RANGE TO IMPACT
$\gamma_e = -15°$
$h_o = 800\ 000$ FT
SYM
m/C_DA
SLUGS/FT^2
.25
.30
.35
VM-9
VM-8
VM-9
VM-8
R
R
TIME TO IMPACT - SEC
500
400
300
0
RANGE - DEG
20
18
16
14
12
0
0
13
14
15
ENTRY VELOCITY, V_e - 10^3 FT/SEC

FIGURE 3.1.3-6

flight path angle, m/C_DA, and atmosphere in Figures 3.1.3-7 through -9. These nomographs provide a convenient source for rapid assessment of parametric effects.

3.1.3.2 Reduced corridor effects. - Reduction of the entry corridor by reducing the maximum entry flight path angle (γ_e) from -20° to -18°, increasing the minimum entry velocity from 13 000 to 14 000 ft/sec, and increasing the minimum entry flight path angle from vacuum graze to -15° affects maximum dynamic pressure and time and range to landing. Figure 3.1.3-10 presents the effects on maximum dynamic pressure caused by the changes in flight path angle. Similarly, time and range variations are presented in Figures 3.1.3-11 and -12, showing the effects of changes in both atmosphere and flight path angle.

Modifying the postulated atmospheric environment by increasing the density scale height from 5 to 8 km and, alternately, reducing the variation in surface pressure from 5-20 mb to 7-14 mb eliminates the atmospheres (VM-8 and VM-9) most critical to maximum dynamic pressure and to time and range. Critical conditions then occur in the low scale height - low surface pressure atmospheres labeled VM-85, -87, denoting atmospheres of 8 km density scale heights and 5 or 7 mb surface pressures, respectively (see Figure 3.1.3-3). The effects of the atmospheric changes on maximum dynamic pressure, time and range to landing are summarized in Figures 3.1.3-13 through -15. Maximum dynamic pressure reflects only changes in density scale height.

The effects on maximum dynamic pressure and time and range to landing of the combined changes in entry corridor and atmosphere are also shown on Figures 3.1.3-13 through -15.

3.1.3.3 Rotating planet effects. - The entry trajectories used in the above analysis were simulated for a non-rotating planet because of the possible variations in orbit inclination. The effects on entry range of orbit inclination with planet rotation are shown in Figure 3.1.3-16, with landing sites on the equator. The effects of planet rotation (zero inclination) on maximum dynamic pressure and maximum convective heating rate are shown in Figures 3.1.3-17 and -18 for trajectories flown in the direction of planet rotation. Both maximum dynamic pressures and heating rates are reduced, while the central angle travers-

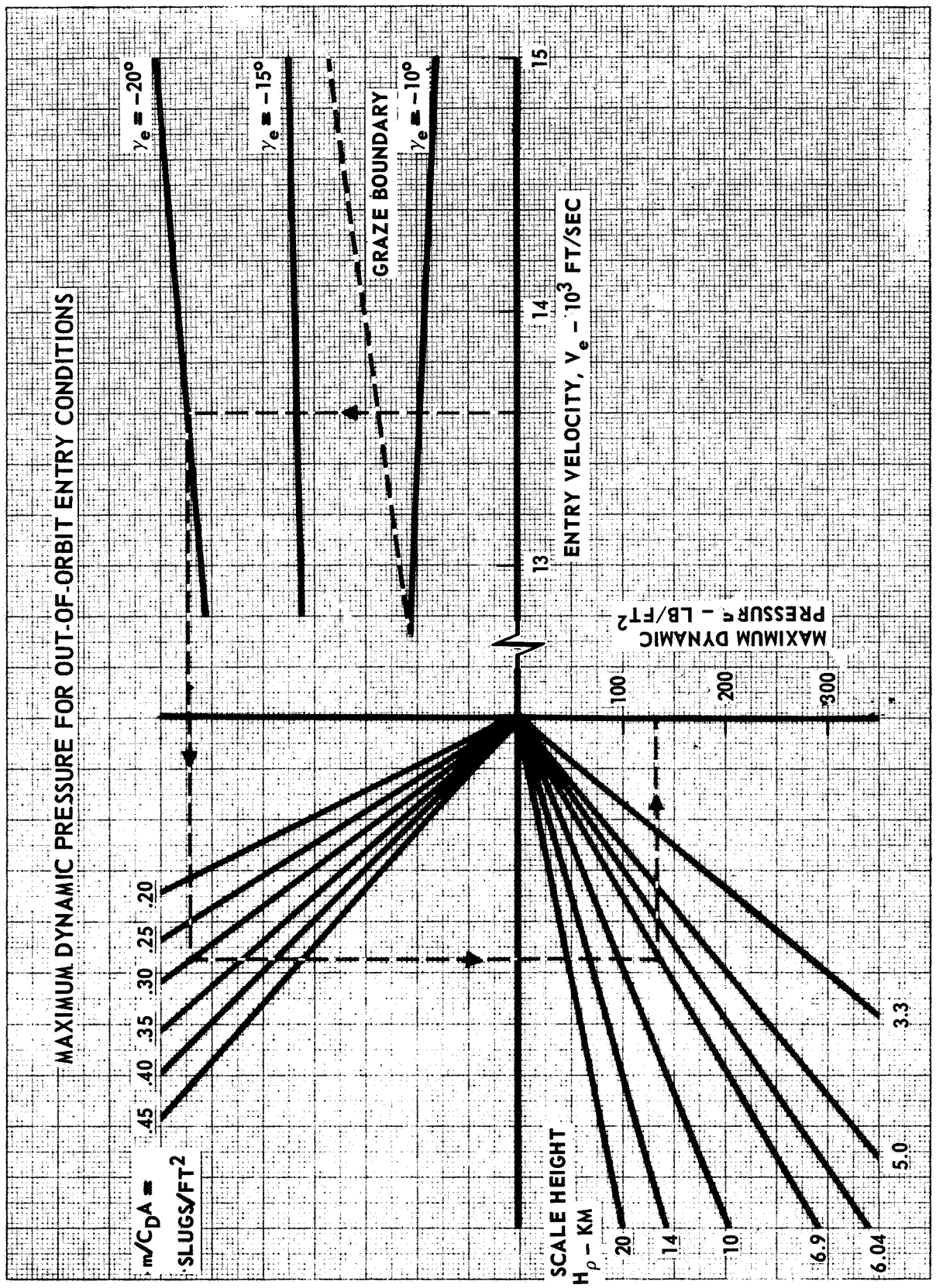
MAXIMUM DYNAMIC PRESSURE FOR OUT-OF-ORBIT ENTRY CONDITIONS
$\gamma_e = -20°$
$\gamma_e = -15°$
GRAZE BOUNDARY
$\gamma_e = -10°$
13
14
15
ENTRY VELOCITY, V_e – 10^3 FT/SEC
MAXIMUM DYNAMIC PRESSURE – LB/FT^2
100
200
300
m/C_DA = SLUGS/FT^2
.45
.40
.35
.30
.25
.20
SCALE HEIGHT H_ρ – KM
20
14
10
6.9
6.04
5.0
3.3

FIGURE 3.1.3–7

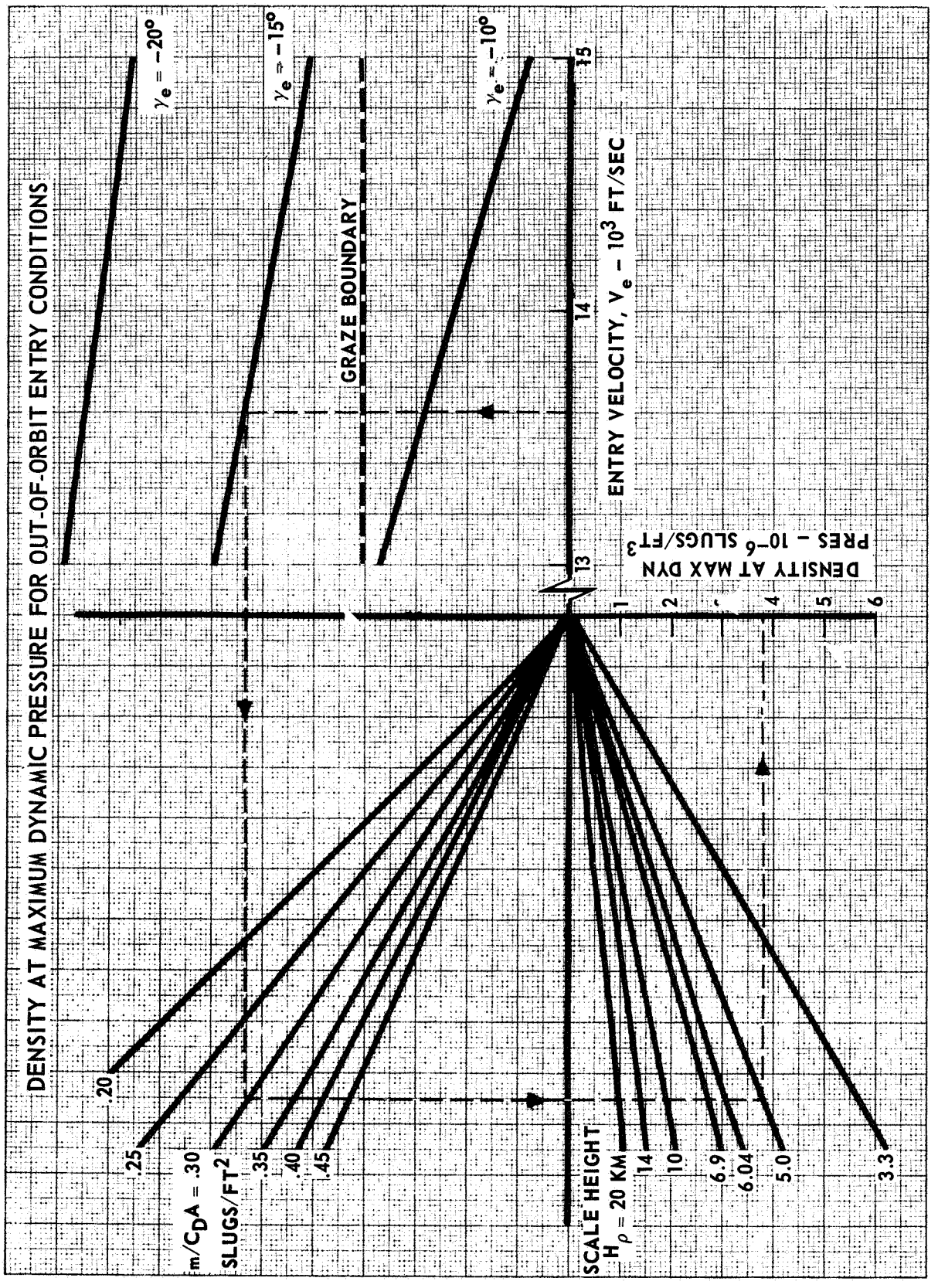
DENSITY AT MAXIMUM DYNAMIC PRESSURE FOR OUT-OF-ORBIT ENTRY CONDITIONS
$\gamma_e = -20°$
$\gamma_e = -15°$
$\gamma_e = -10°$
GRAZE BOUNDARY
ENTRY VELOCITY, $V_e - 10^3$ FT/SEC
13
14
15
DENSITY AT MAX DYN PRES - 10^{-6} SLUGS/FT^3
1
2
4
5
6
m/C_DA = .30 SLUGS/FT^2
.20
.25
.35
.40
.45
SCALE HEIGHT H_ρ = 20 KM
14
10
6.9
6.04
5.0
3.3

FIGURE 3.1.3–8

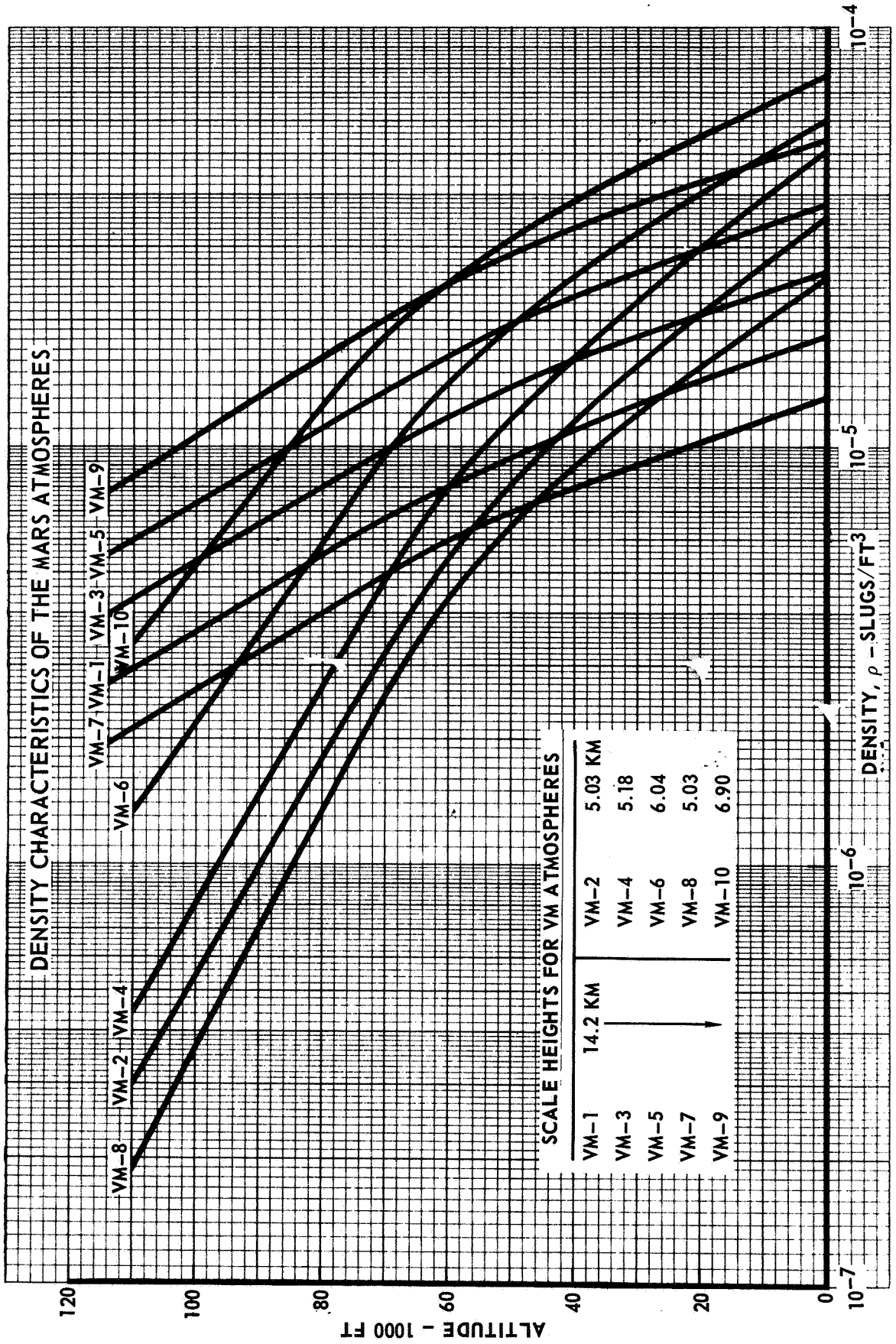
DENSITY CHARACTERISTICS OF THE MARS ATMOSPHERES
VM-8
VM-2
VM-4
VM-7
VM-1
VM-3
VM-5
VM-9
VM-6
VM-10
SCALE HEIGHTS FOR VM ATMOSPHERES
VM-1 14.2 KM
VM-3
VM-5
VM-7
VM-9
VM-2 5.03 KM
VM-4 5.18
VM-6 6.04
VM-8 5.03
VM-10 6.90
ALTITUDE - 1000 FT
120
100
80
60
40
20
0
DENSITY, ρ - SLUGS/FT³
10⁻⁷
10⁻⁶
10⁻⁵
10⁻⁴

FIGURE 3.1.3-9

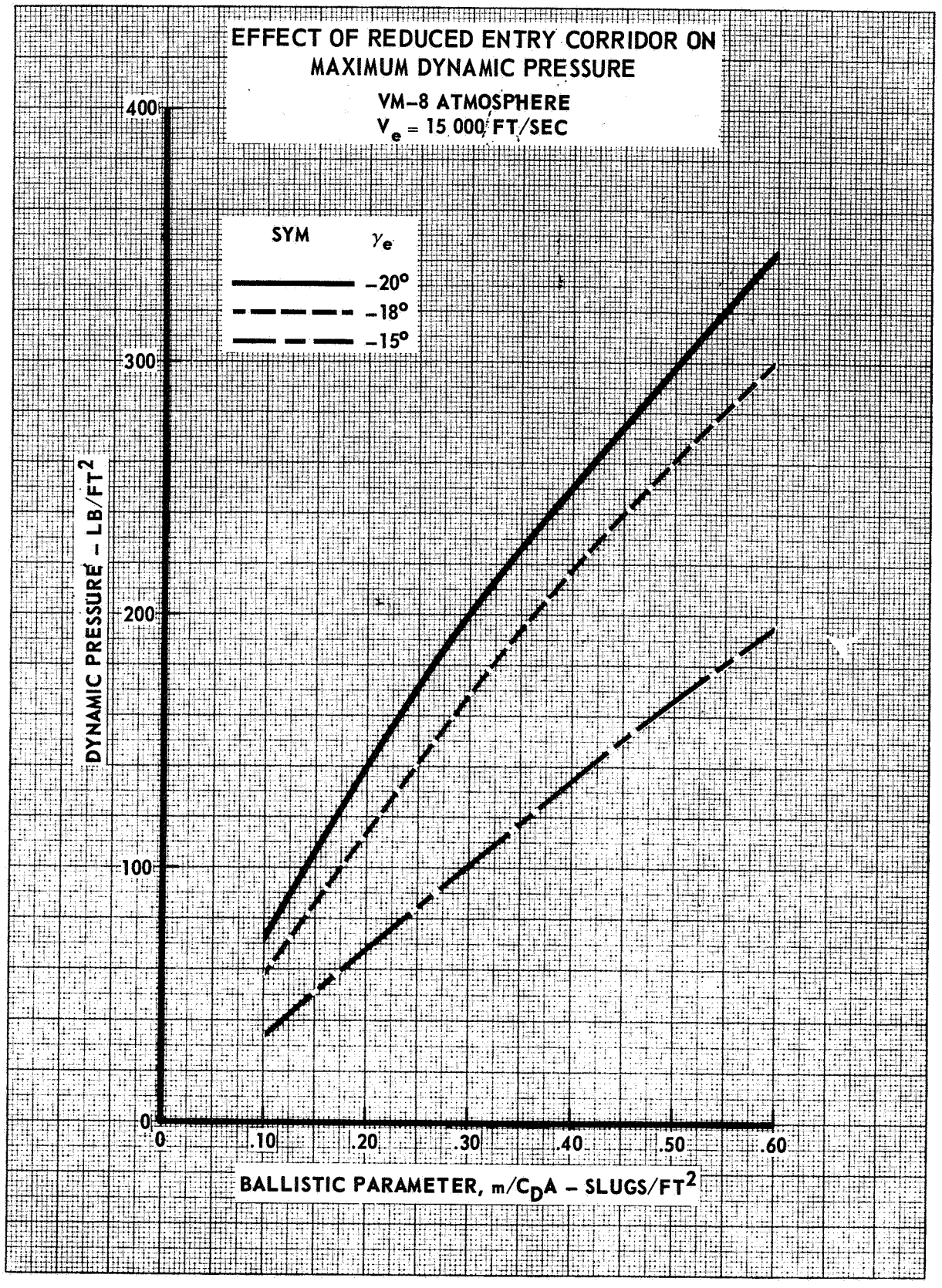

FIGURE 3.1.3-10

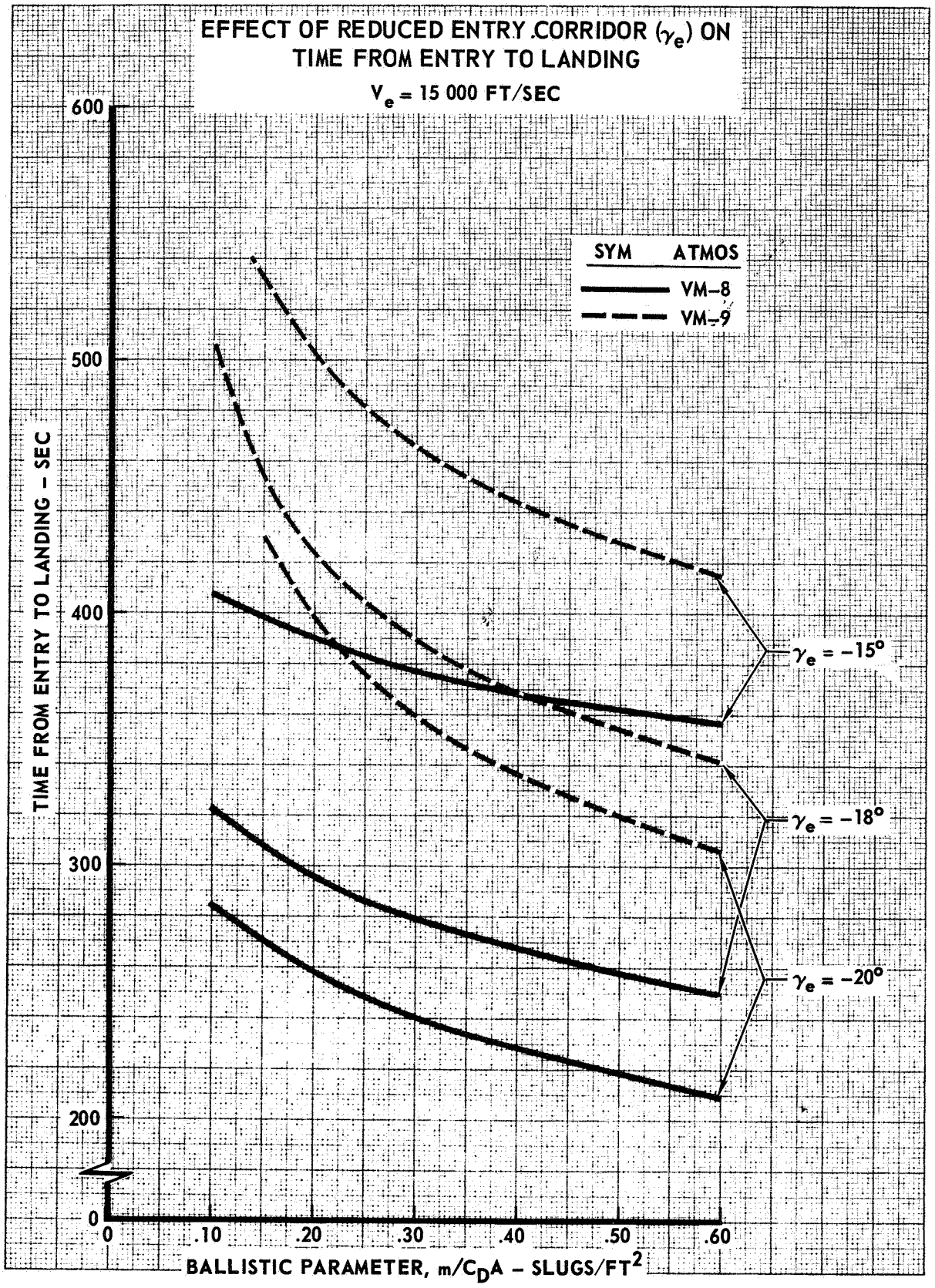

FIGURE 3.1.3–11

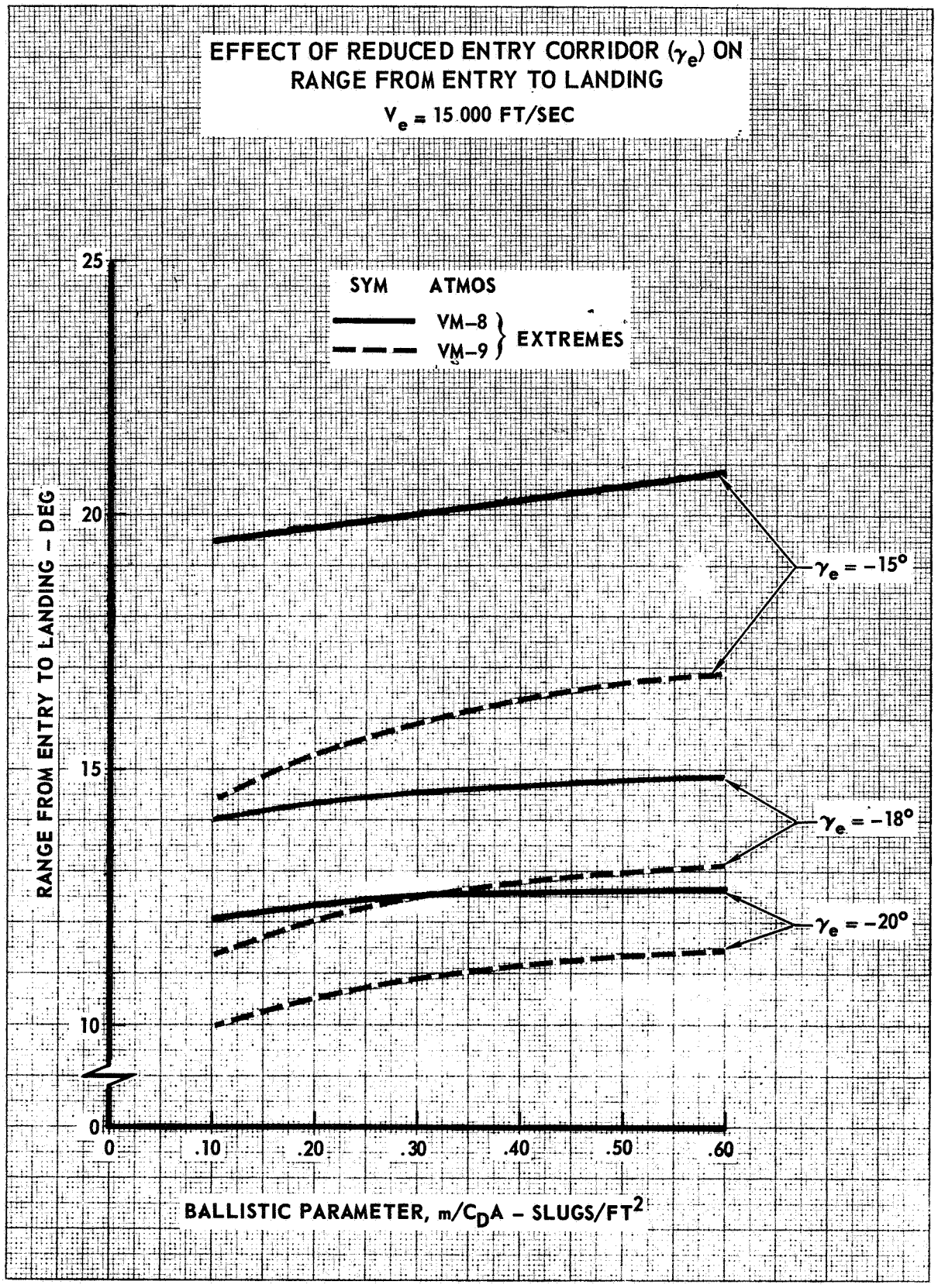

FIGURE 3.1.3-12

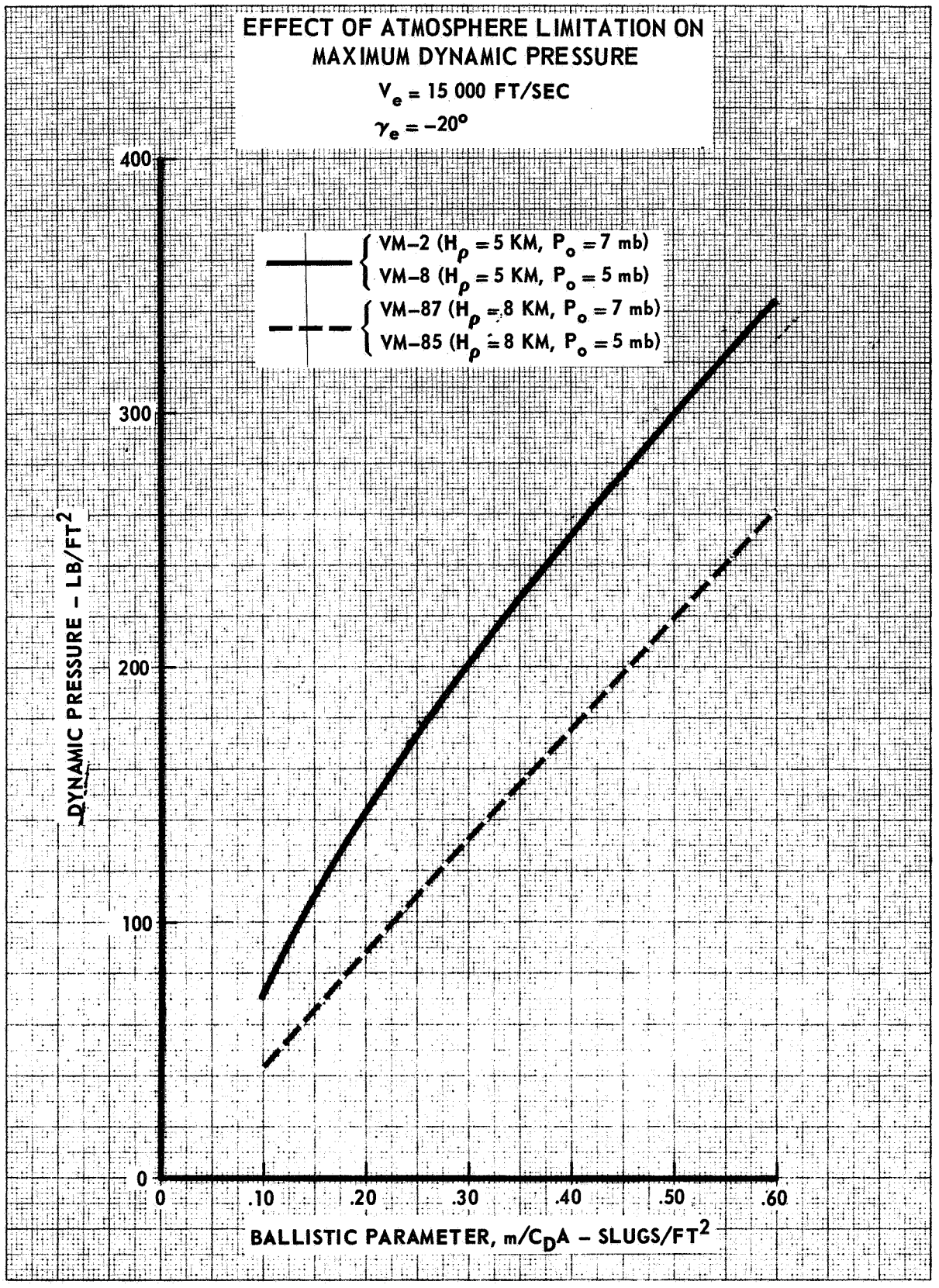

FIGURE 3.1.3-13

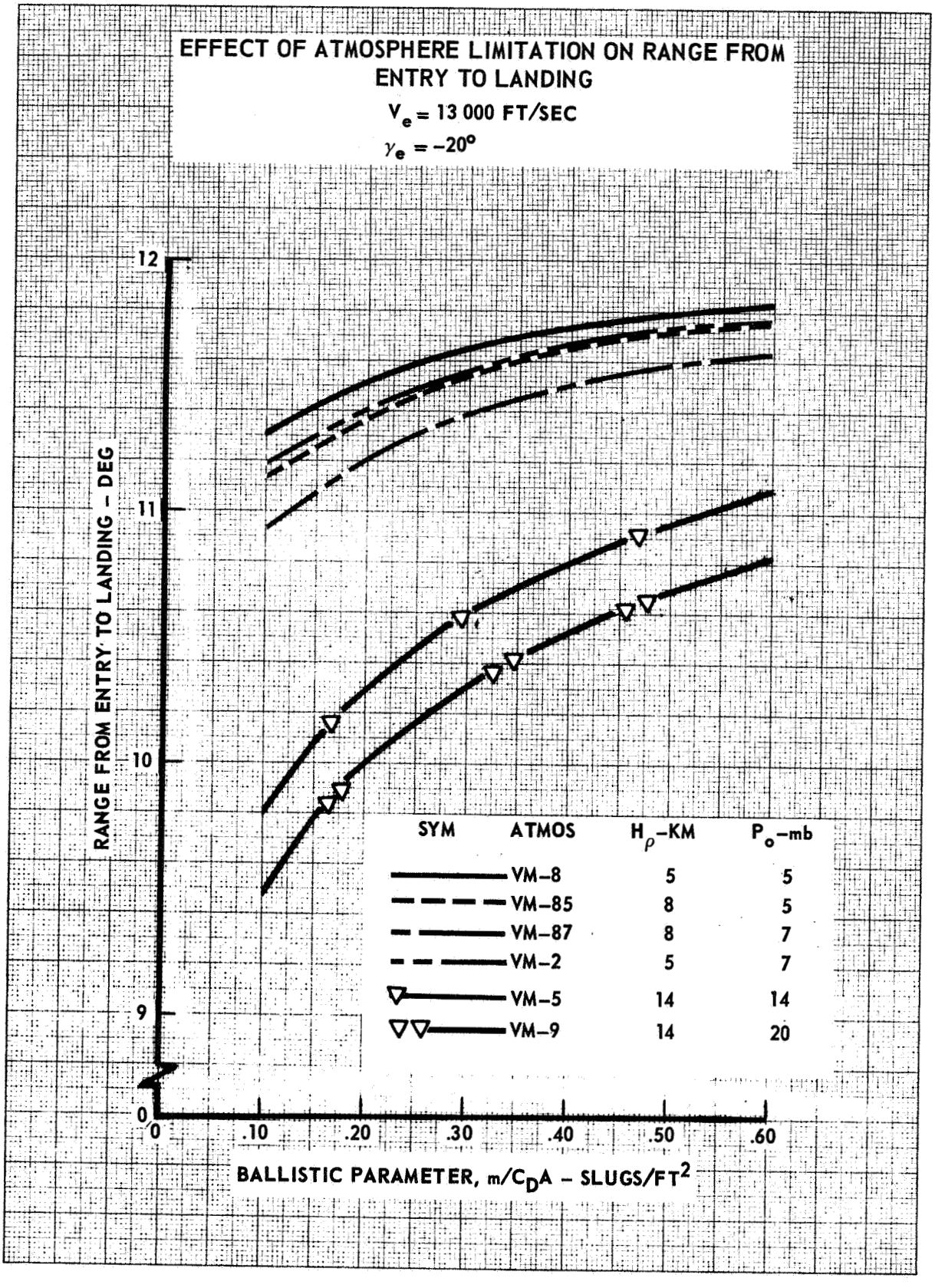

FIGURE 3.1.3–14

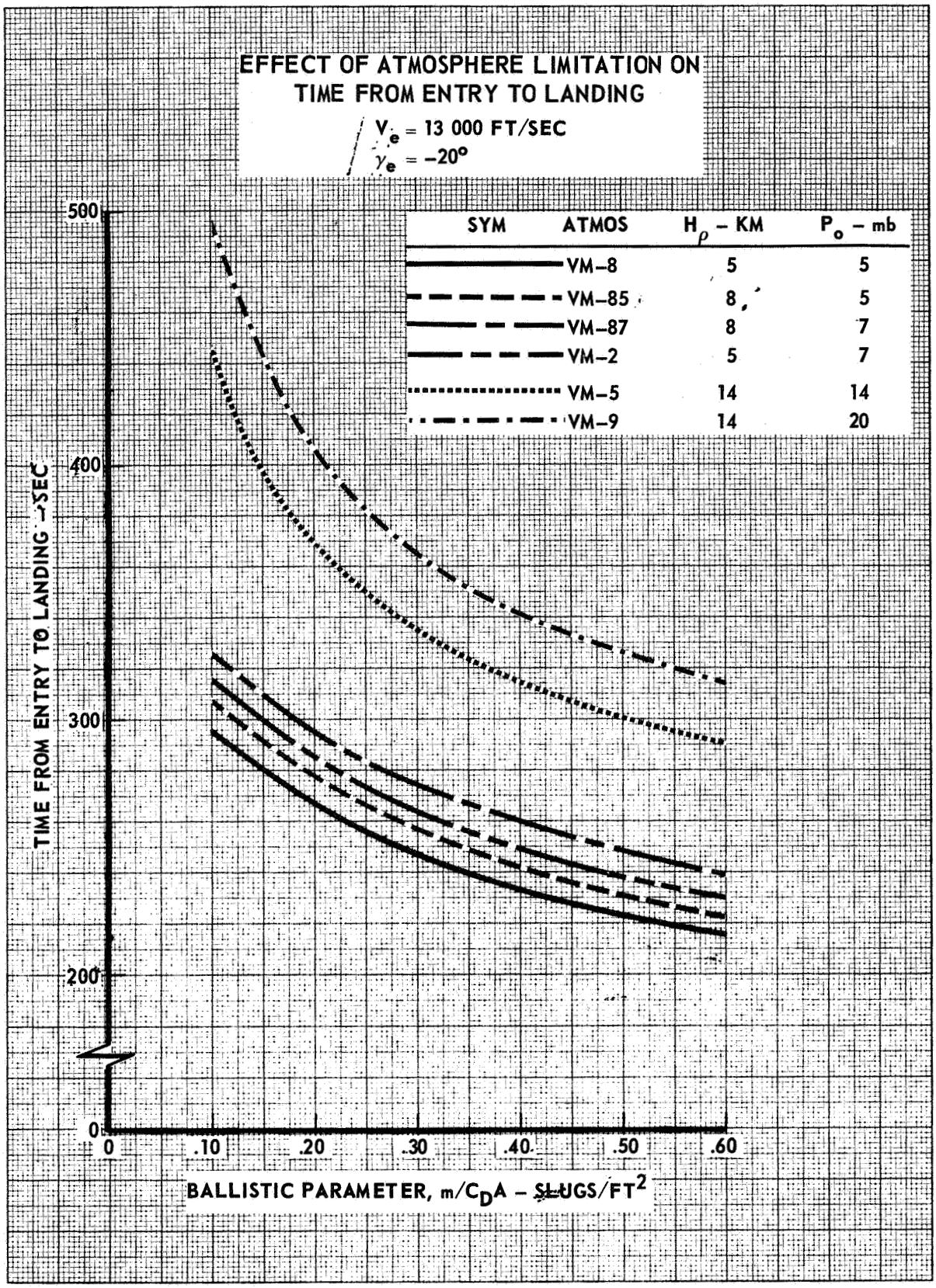

FIGURE 3.1.3–15

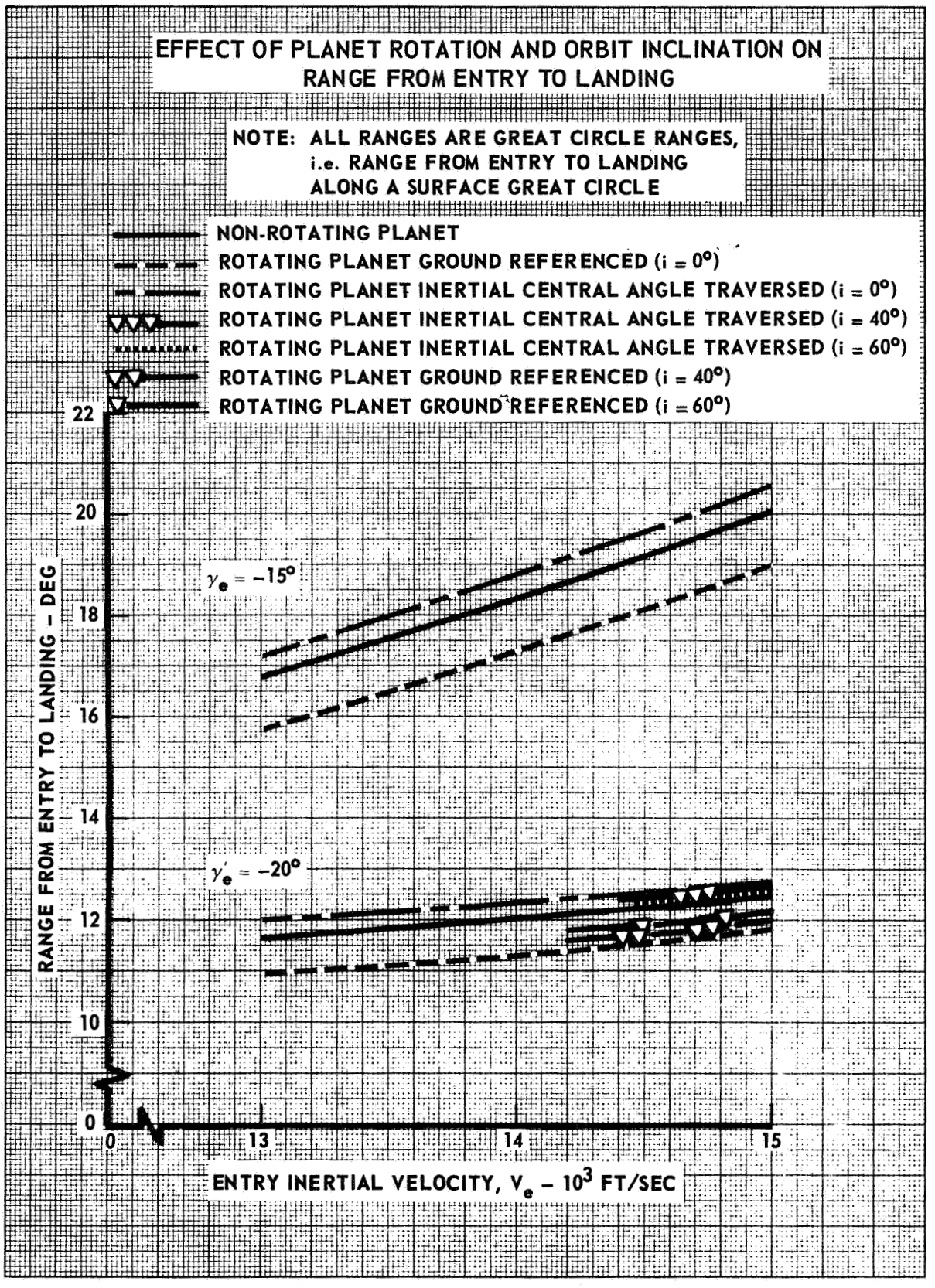

FIGURE 3.1.3-16

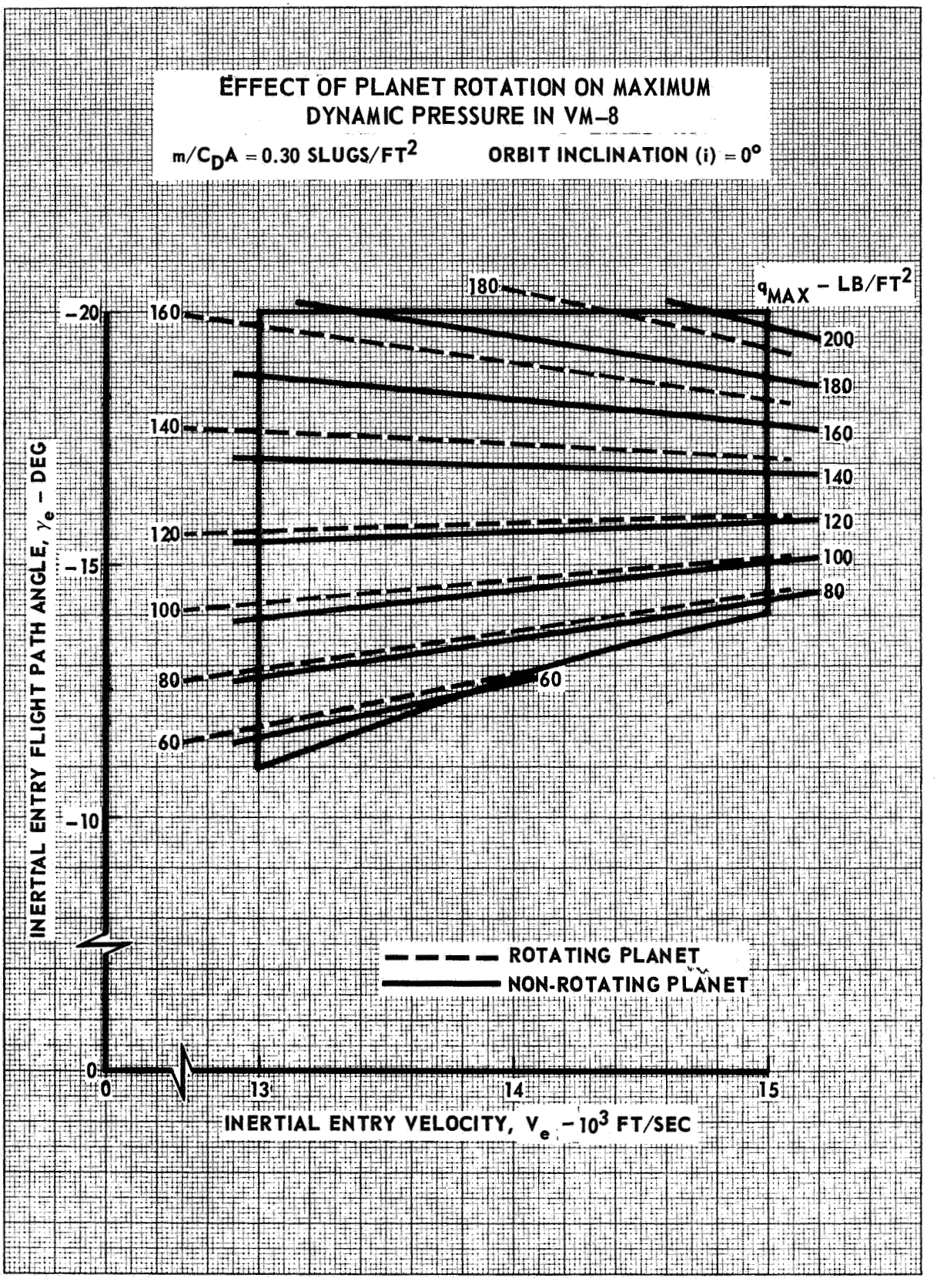

FIGURE 3.1.3-17

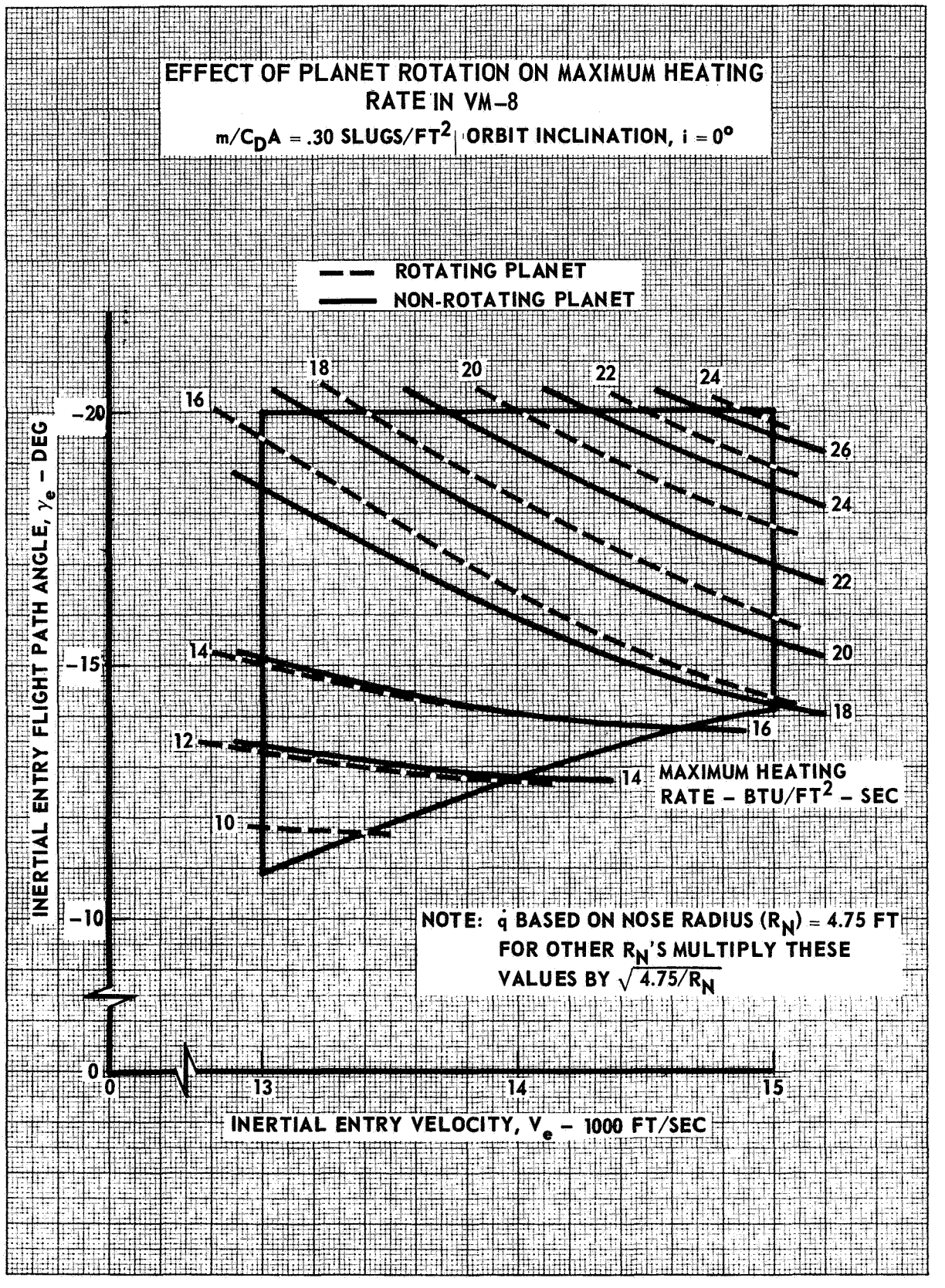

FIGURE 3.1.3-18

ed is slightly larger. The change in entry time is negligible. Increasing orbit inclination lessens the effects of planet rotation until at an orbit inclination of 90° the only effect is a small lateral range increment.

3.1.4 TERMINAL DECELERATION - Deceleration of the entry vehicle to the low surface impact velocities normally associated with "soft landing", including the possibility of strong surface winds, requires the use of a terminal propulsion system. The limiting situation would be a completely propulsive deceleration system. However, because of the high efficiency of auxiliary aerodynamic decelerators in reducing the velocity, combinations of auxiliary aerodynamic decelerators and terminal propulsion systems have received major attention.

For combined terminal deceleration systems, several constraints have been imposed. For aerodynamic decelerators, the deployment has been initiated by radar altimeter, based on VOYAGER Phase B studies of triggering techniques. For a specific capsule size and weight, the maximum deployment altitude is limited by the high speed constraints on the aerodynamic decelerator (Mach 2 for parachutes and temperature limits on fabric strength for attached inflatable decelerators). The minimum deployment altitude must be sufficient for inflation and deceleration. The size of the auxiliary decelerator is governed by its drag efficiency, by differential drag separation of the lander and the aeroshell, by payload velocity at propulsion ignition, and by a landing radar requirement that the aeroshell impacts prior to radar turn-on. For the terminal propulsion system the trade between total impulse and throttle ratio must be examined in conjunction with the guidance system to define the desirable ignition conditions. Separation of the parachute from the lander is triggered by the radar altimeter. Propulsion ignition is timed relative to parachute separation to permit lander stabilization and landing radar acquisition. The total sequence from deployment through landing is shown in a schematic in Figure 3.1.4-1.

Because the mission characteristics of terminal deceleration are primarily functions of the selected parachute and terminal propulsion systems, only the initial auxiliary aerodynamic deployment parametrics are considered in this section. The propulsion system is described in Section 3.2.7.3; the auxiliary aerodynamic decelerator system is described in Section 3.2.8; trend analysis of the combination is described parametrically in Section 3.3.1.2.

TERMINAL DECELERATION SEQUENCE

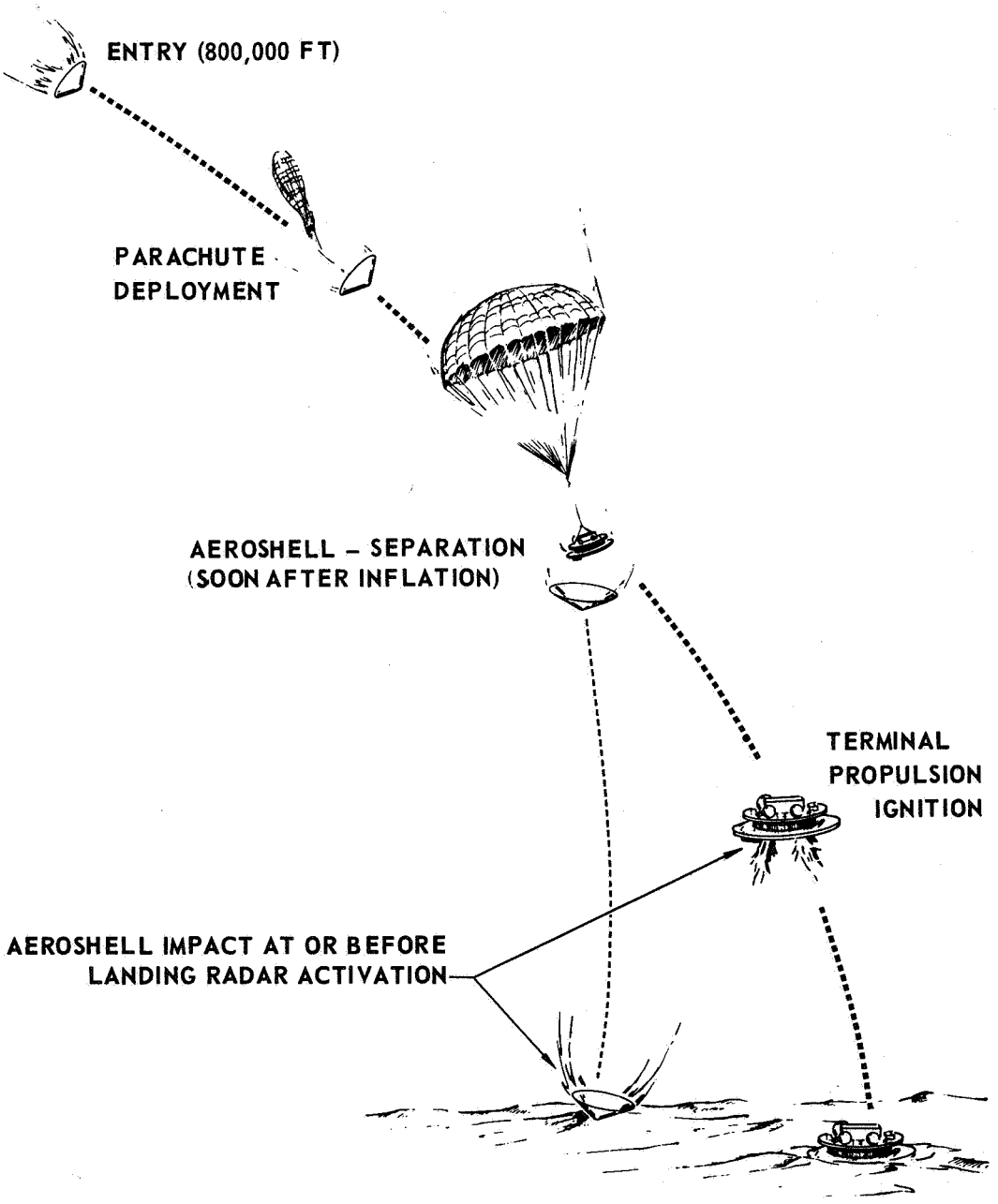

FIGURE 3.1.4–1

3.1.4.1 Deployment altitude. - The most critical atmosphere for parachute deployment in terms of maximum loads and the Mach 2 limit is VM-8 for a steep, slow entry from orbit. Atmosphere VM-8 is shown in Figure 3.1.4-2 to produce the highest deployment Mach number at all altitudes of interest. Figure 3.1.4-3 shows that the VM-8 atmosphere produces the highest deployment dynamic pressures over the normal deployment altitude range (10 000 - 25 000 ft) except for low ballistic parameter values. A summary of the deployment altitudes is shown in Figure 3.1.4-4 for the critical entry conditions. Thus, under the conditions of the entry corridor, the maximum m/C_DA permissible at the desired deployment altitude, or conversely, the minimum altitude for the desired m/C_DA can be selected from Figure 3.1.4-4. The following figure, Figure 3.1.4-5 shows the maximum m/C_DA to produce Mach 2 at a particular altitude for entries at other flight path angles and entry velocities.

3.1.4.2 Aeroshell/lander separation. - The first of the criteria for sizing the auxiliary aerodynamic decelerator is to insure aeroshell/lander separation by differential drag. A minimum relative acceleration between the aeroshell and lander of 0.25 g based on deployment conditions has been assumed as sufficient. Thus, the minimum area of the auxiliary decelerator can be determined from the relative acceleration relation:

$$n = q\left[\left(\frac{C_D S_o}{W}\right)_{\substack{\text{lander}\\ \text{w/chute}}} - \left(\frac{C_D A}{W}\right)_{\text{aeroshell}}\right]$$

where: n = relative acceleration (g)

q = dynamic pressure (lb/ft^2)

C_D = drag coefficient

W = weight (lb)

S_o, A = reference area (auxiliary decelerator and aeroshell, respectively)

It appears from this expression that the dynamic pressure at separation will dominate the relative acceleration. Since the conditions at separation depend on inflation time and decelerator size, the conditions at deployment were used

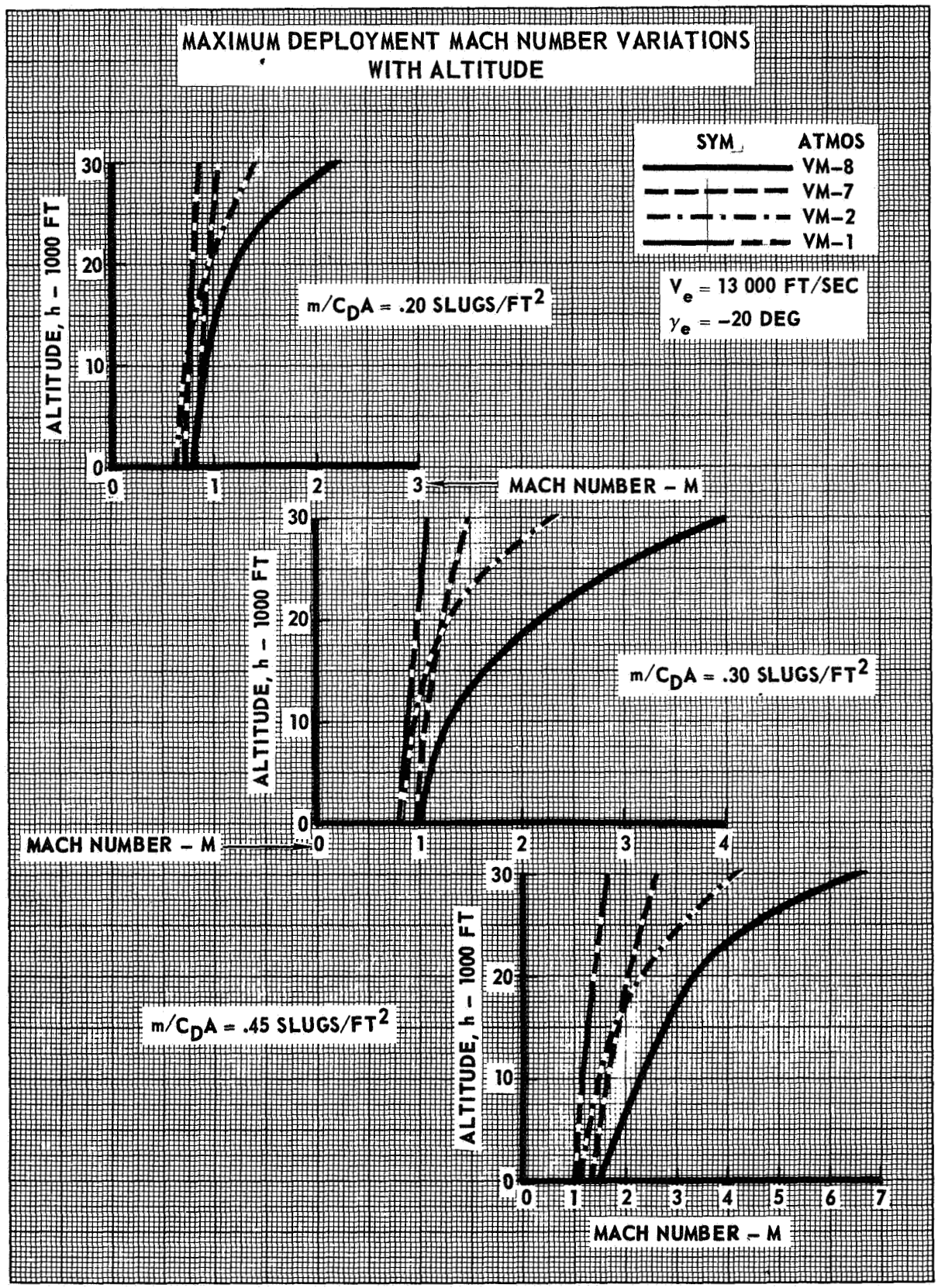
MAXIMUM DEPLOYMENT MACH NUMBER VARIATIONS WITH ALTITUDE
SYM
ATMOS
VM-8
VM-7
VM-2
VM-1
V_e = 13 000 FT/SEC
γ_e = -20 DEG
m/C_DA = .20 SLUGS/FT^2
m/C_DA = .30 SLUGS/FT^2
m/C_DA = .45 SLUGS/FT^2
ALTITUDE, h - 1000 FT
MACH NUMBER - M
0
10
20
30
0
1
2
3
4
5
6
7

FIGURE 3.1.4-2

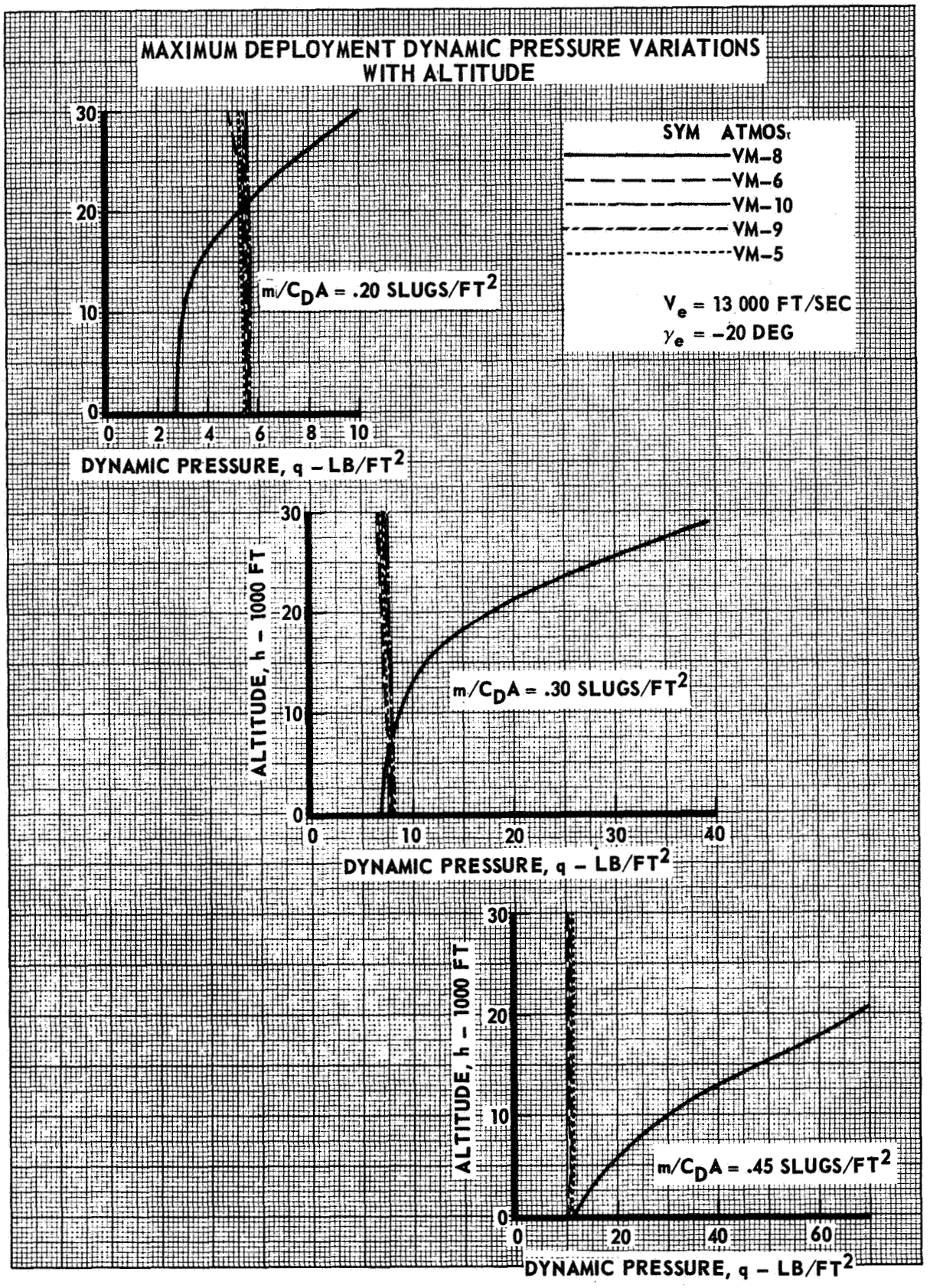
MAXIMUM DEPLOYMENT DYNAMIC PRESSURE VARIATIONS WITH ALTITUDE
SYM ATMOS
VM-8
VM-6
VM-10
VM-9
VM-5
V_e = 13 000 FT/SEC
γ_e = -20 DEG
m/C_DA = .20 SLUGS/FT^2
m/C_DA = .30 SLUGS/FT^2
m/C_DA = .45 SLUGS/FT^2
ALTITUDE, h - 1000 FT
DYNAMIC PRESSURE, q - LB/FT^2

FIGURE 3.1.4-3

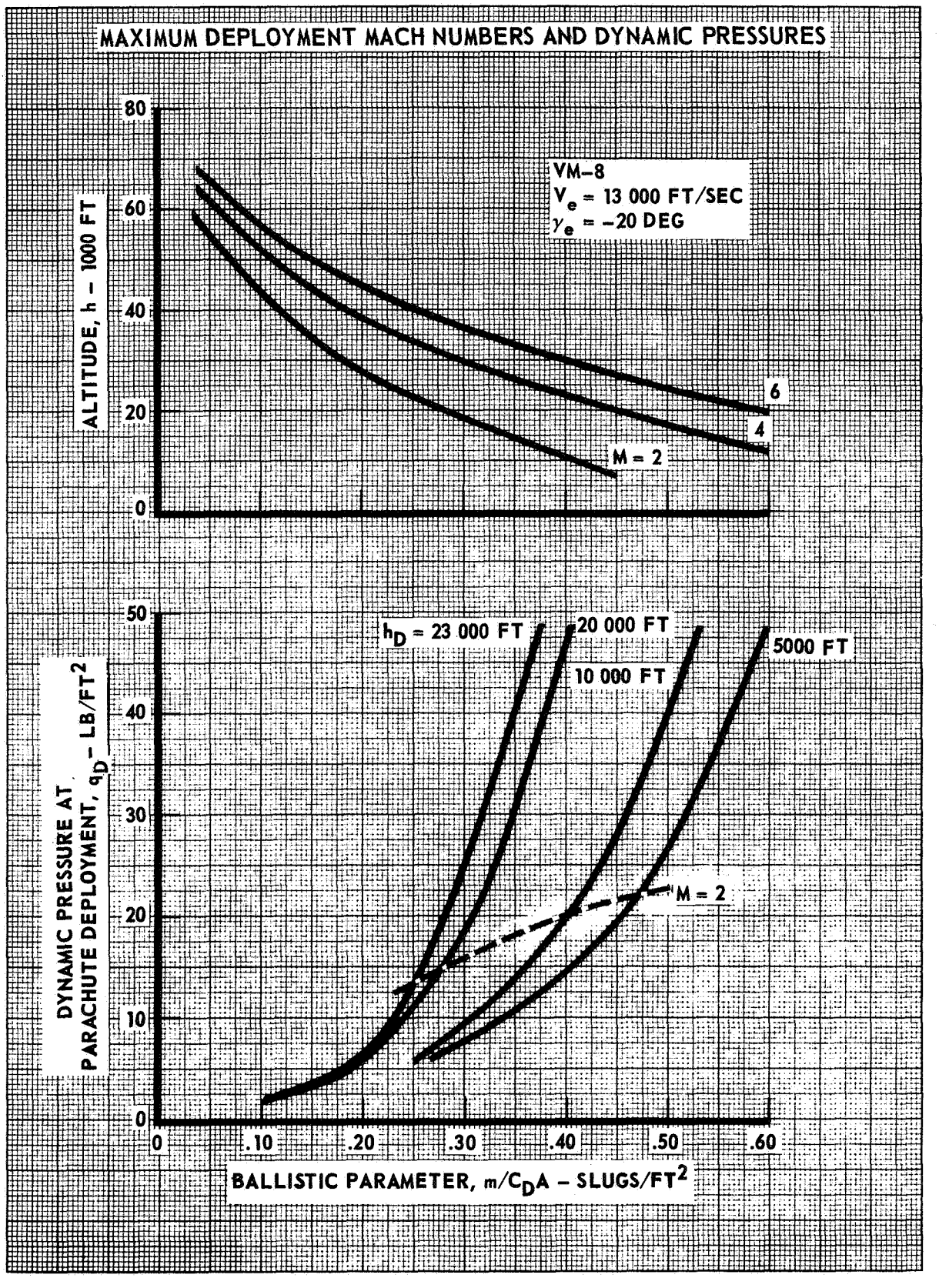
MAXIMUM DEPLOYMENT MACH NUMBERS AND DYNAMIC PRESSURES
VM-8
V_e = 13 000 FT/SEC
γ_e = -20 DEG
ALTITUDE, h - 1000 FT
80
60
40
20
0
6
4
M = 2
DYNAMIC PRESSURE AT PARACHUTE DEPLOYMENT, q_D - LB/FT^2
50
40
30
20
10
0
h_D = 23 000 FT
20 000 FT
10 000 FT
5000 FT
M = 2
0
.10
.20
.30
.40
.50
.60
BALLISTIC PARAMETER, m/C_DA - SLUGS/FT^2

FIGURE 3.1.4-4

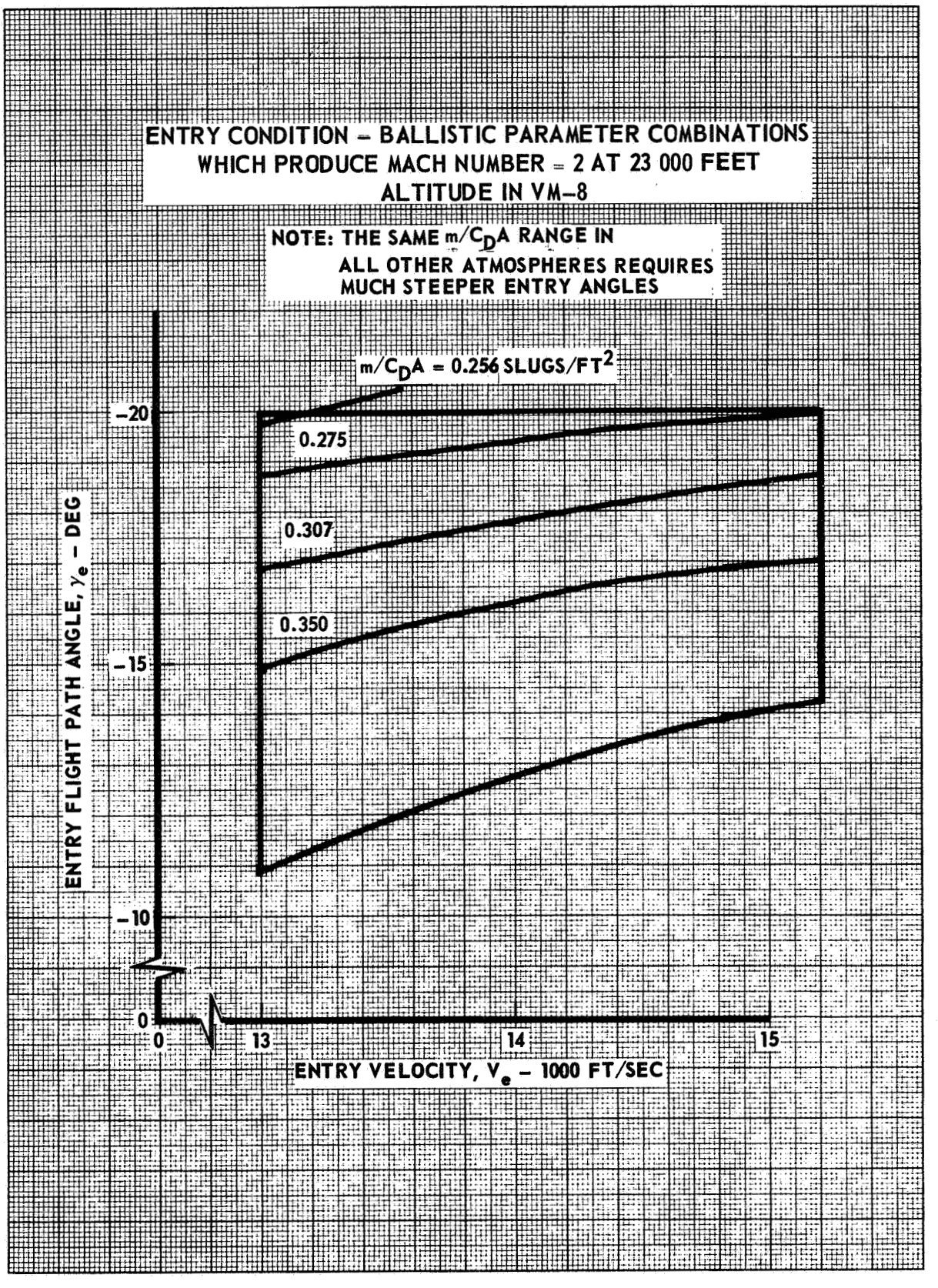
ENTRY CONDITION – BALLISTIC PARAMETER COMBINATIONS WHICH PRODUCE MACH NUMBER = 2 AT 23 000 FEET ALTITUDE IN VM–8
NOTE: THE SAME m/C_DA RANGE IN ALL OTHER ATMOSPHERES REQUIRES MUCH STEEPER ENTRY ANGLES
m/C_DA = 0.256 SLUGS/FT^2
0.275
0.307
0.350
–20
–15
–10
0
ENTRY FLIGHT PATH ANGLE, γ_e – DEG
0
13
14
15
ENTRY VELOCITY, V_e – 1000 FT/SEC

FIGURE 3.1.4–5

as a basis for comparison. As shown in Figures 3.1.4-6 and 3.1.4-7, the minimum deployment dynamic pressure can occur over a range of three or more model atmospheres. Thus, the range of velocities or Mach numbers is also broad. It is the Mach number change which influences the aeroshell drag coefficient (C_D) and produces the change in relative acceleration for nearly constant dynamic pressures. These conditions are summarized in Figure 3.1.4-8 by showing which atmospheres produce minimum dynamic pressures and those which produce minimum relative accelerations.

Using the dynamic pressures at the minimum relative accelerations of Figure 3.1.4-8, the relative acceleration relation above may be solved for a preliminary design value of the parachute diameter.

3.1.4.3 Terminal velocity. - A second sizing criterion is the parachute terminal vertical velocity capability. This terminal velocity (plus winds added vectorally) must be removed by the terminal propulsion system.

Terminal velocity, as a function of parachute diameter, is presented in Figures 3.1.4-9 and -10 for the atmosphere extremes: VM-7 and -10, and representative lander plus parachute weights. Atmospheres VM-8 and -9 are also shown in these figures because of their critical nature with respect to other parameters. The effects of terminal propulsion ignition altitude on terminal vertical velocity are presented in Figure 3.1.4-11 for one atmosphere (VM-8). This effect is small over the range of altitudes of probable terminal propulsion ignition.

Figure 3.1.4-12 presents the weight ratio of parachute system to total vehicle weight as a function of the desired terminal velocity for the atmosphere extremes. Included in the computation are the assumptions about parachute construction and accessory weights that are noted on the figure as derived from our earlier VOYAGER Phase B Study (NASA CR-89673).

3.1.4.4 Entry corridor and atmosphere variations. - The sensitivity of parachute design parameters to a reduced entry corridor is shown in Figure 3.1.4-13 where the maximum deployment dynamic pressure in the worst case atmosphere is reduced by increasing the entry velocity (V_e) and also by

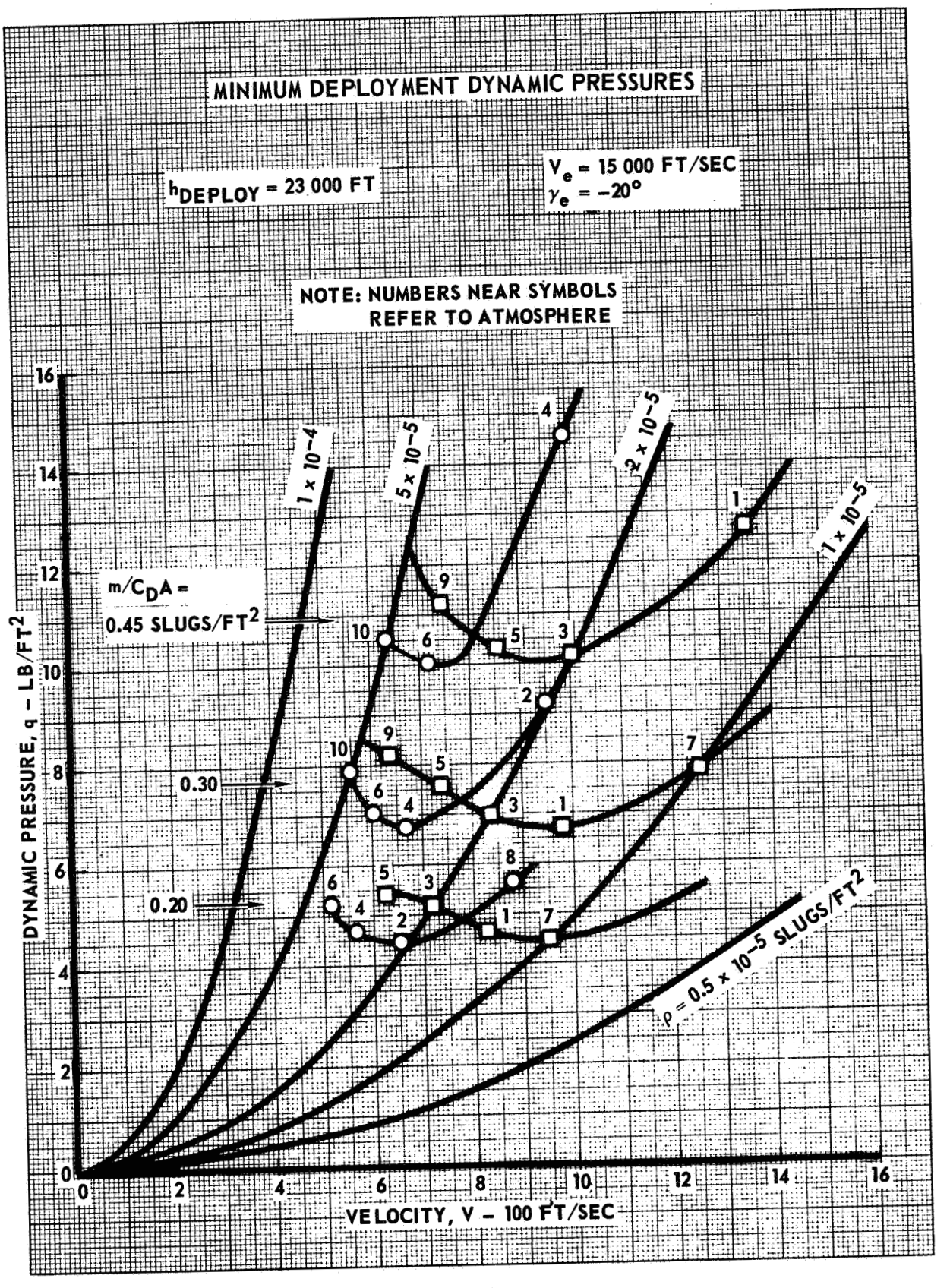
MINIMUM DEPLOYMENT DYNAMIC PRESSURES
h_{DEPLOY} = 23 000 FT
V_e = 15 000 FT/SEC
γ_e = −20°
NOTE: NUMBERS NEAR SYMBOLS REFER TO ATMOSPHERE
m/C_DA = 0.45 SLUGS/FT^2
0.30
0.20
1 × 10−4
5 × 10−5
2 × 10−5
1 × 10−5
ρ = 0.5 × 10−5 SLUGS/FT^2
DYNAMIC PRESSURE, q – LB/FT^2
VELOCITY, V – 100 FT/SEC
0
2
4
6
8
10
12
14
16

FIGURE 3.1.4–6

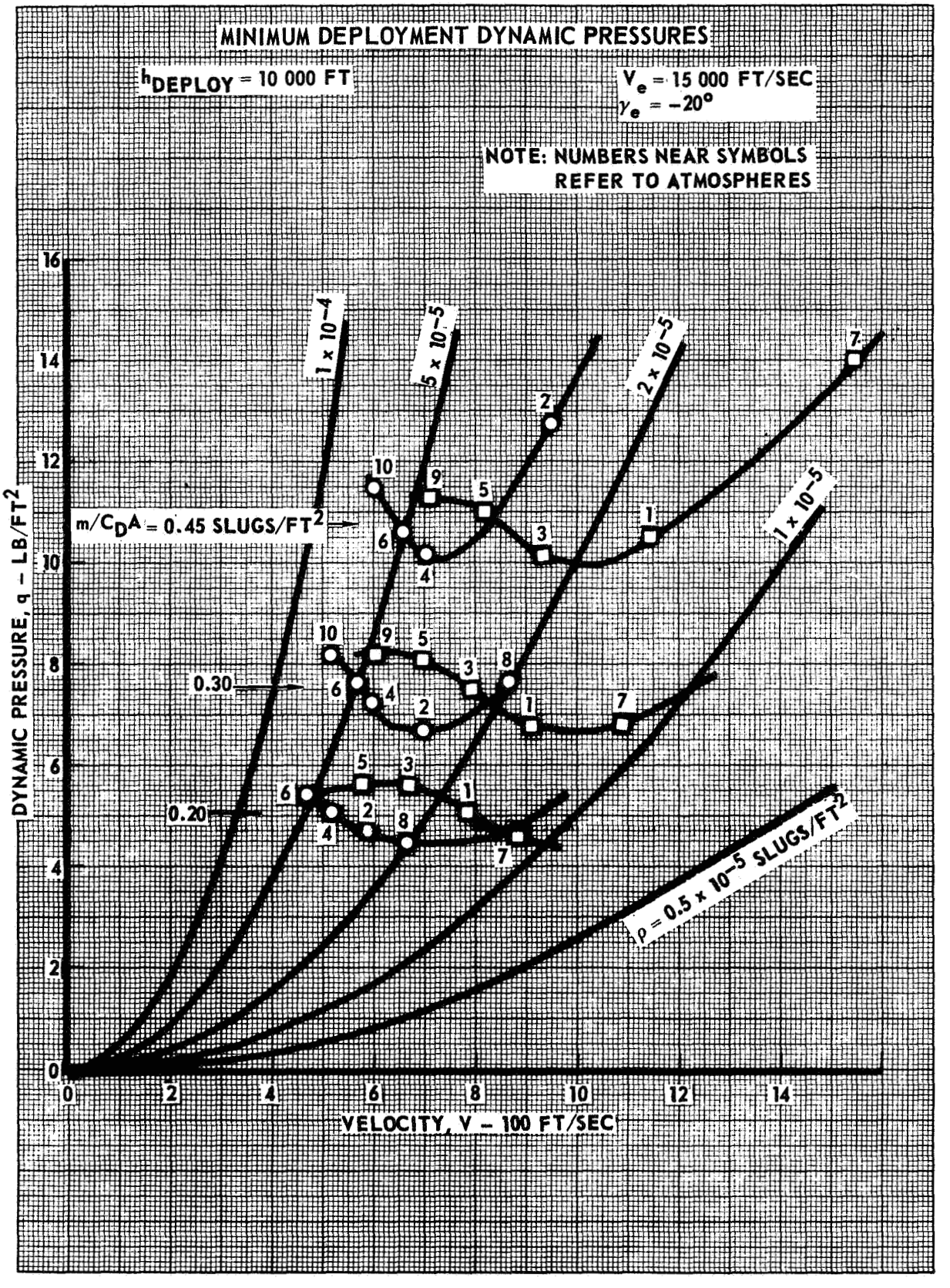
MINIMUM DEPLOYMENT DYNAMIC PRESSURES
h_{DEPLOY} = 10 000 FT
V_e = 15 000 FT/SEC
γ_e = −20°
NOTE: NUMBERS NEAR SYMBOLS REFER TO ATMOSPHERES
m/C_DA = 0.45 SLUGS/FT^2
0.30
0.20
1 × 10−4
5 × 10−5
2 × 10−5
1 × 10−5
ρ = 0.5 × 10−5 SLUGS/FT^2
DYNAMIC PRESSURE, q – LB/FT^2
VELOCITY, V – 100 FT/SEC
0
2
4
6
8
10
12
14
16

FIGURE 3.1.4-7

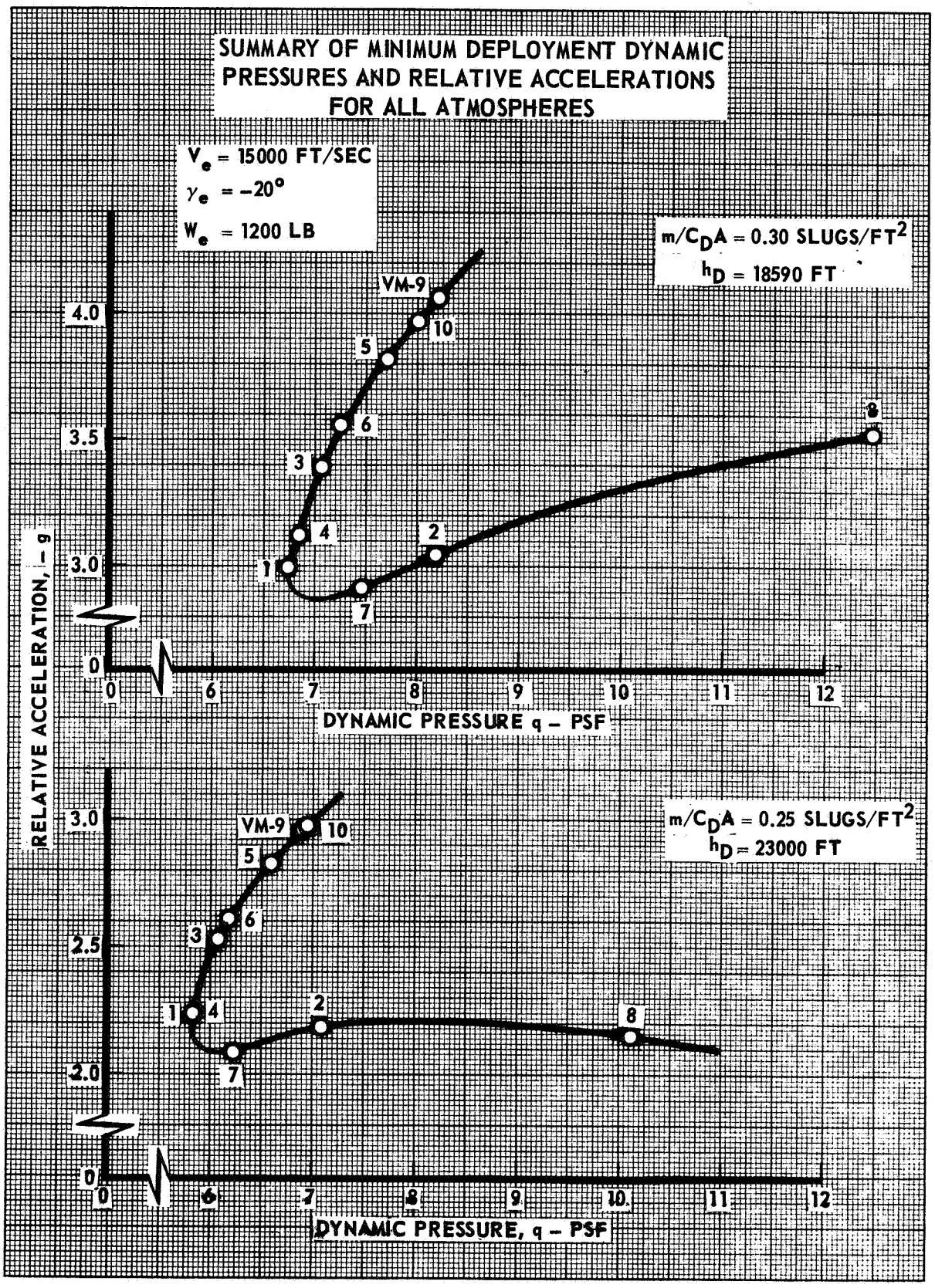
SUMMARY OF MINIMUM DEPLOYMENT DYNAMIC PRESSURES AND RELATIVE ACCELERATIONS FOR ALL ATMOSPHERES
V_e = 15000 FT/SEC
γ_e = −20°
W_e = 1200 LB
m/C_DA = 0.30 SLUGS/FT^2
h_D = 18590 FT
VM-9
10
5
6
3
4
1
2
7
8
4.0
3.5
3.0
0
0
6
7
8
9
10
11
12
DYNAMIC PRESSURE q – PSF
RELATIVE ACCELERATION, – g
m/C_DA = 0.25 SLUGS/FT^2
h_D = 23000 FT
VM-9
10
5
6
3
1
4
2
7
8
3.0
2.5
2.0
0
0
6
7
8
9
10
11
12
DYNAMIC PRESSURE, q – PSF

FIGURE 3.1.4–8

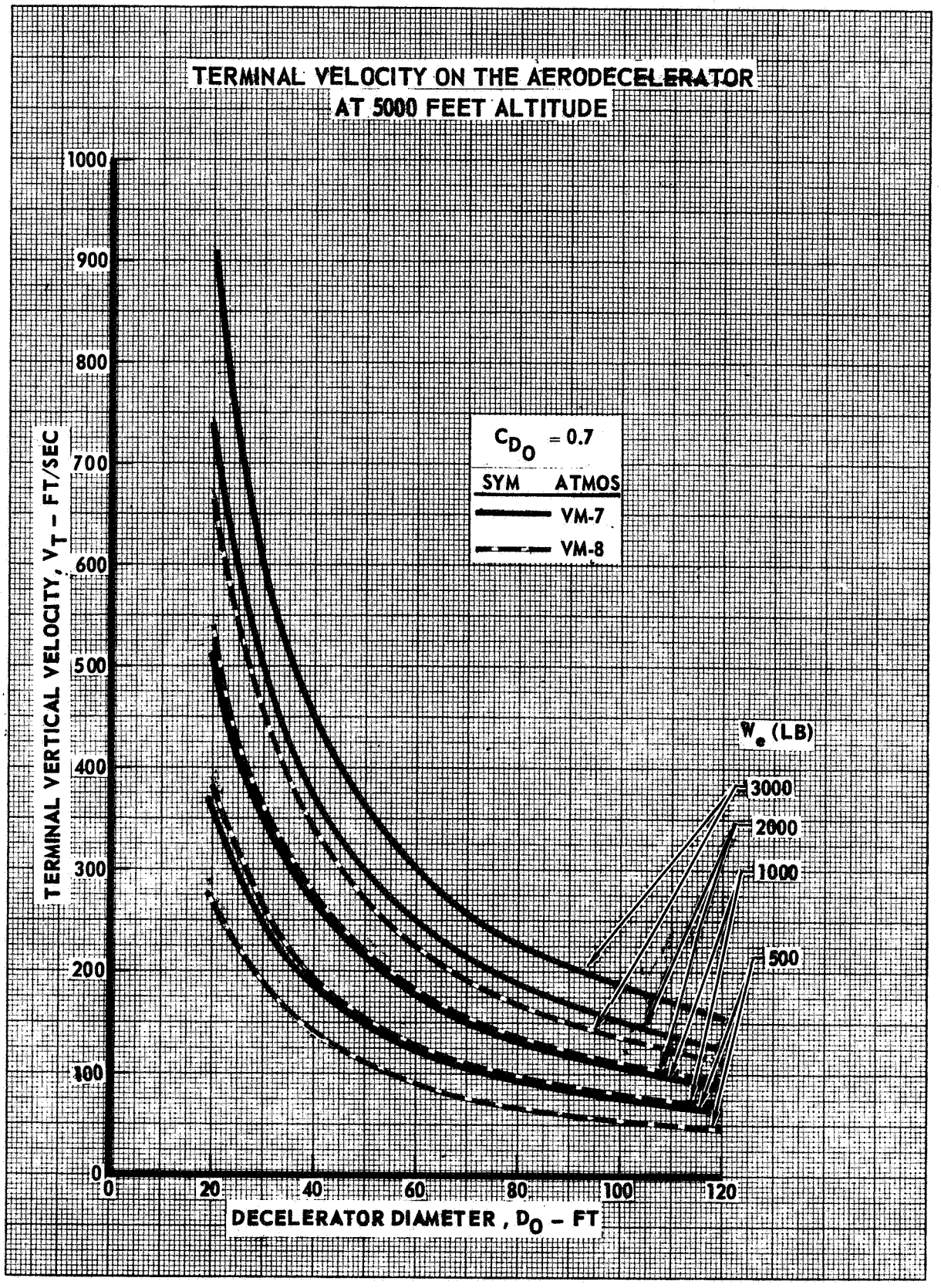
TERMINAL VELOCITY ON THE AERODECELERATOR
AT 5000 FEET ALTITUDE
TERMINAL VERTICAL VELOCITY, V_T – FT/SEC
1000
900
800
700
600
500
400
300
200
100
0
0
20
40
60
80
100
120
DECELERATOR DIAMETER, D_O – FT
C_{D_O} = 0.7
SYM ATMOS
VM-7
VM-8
W_e (LB)
3000
2000
1000
500

FIGURE 3.1.4–9

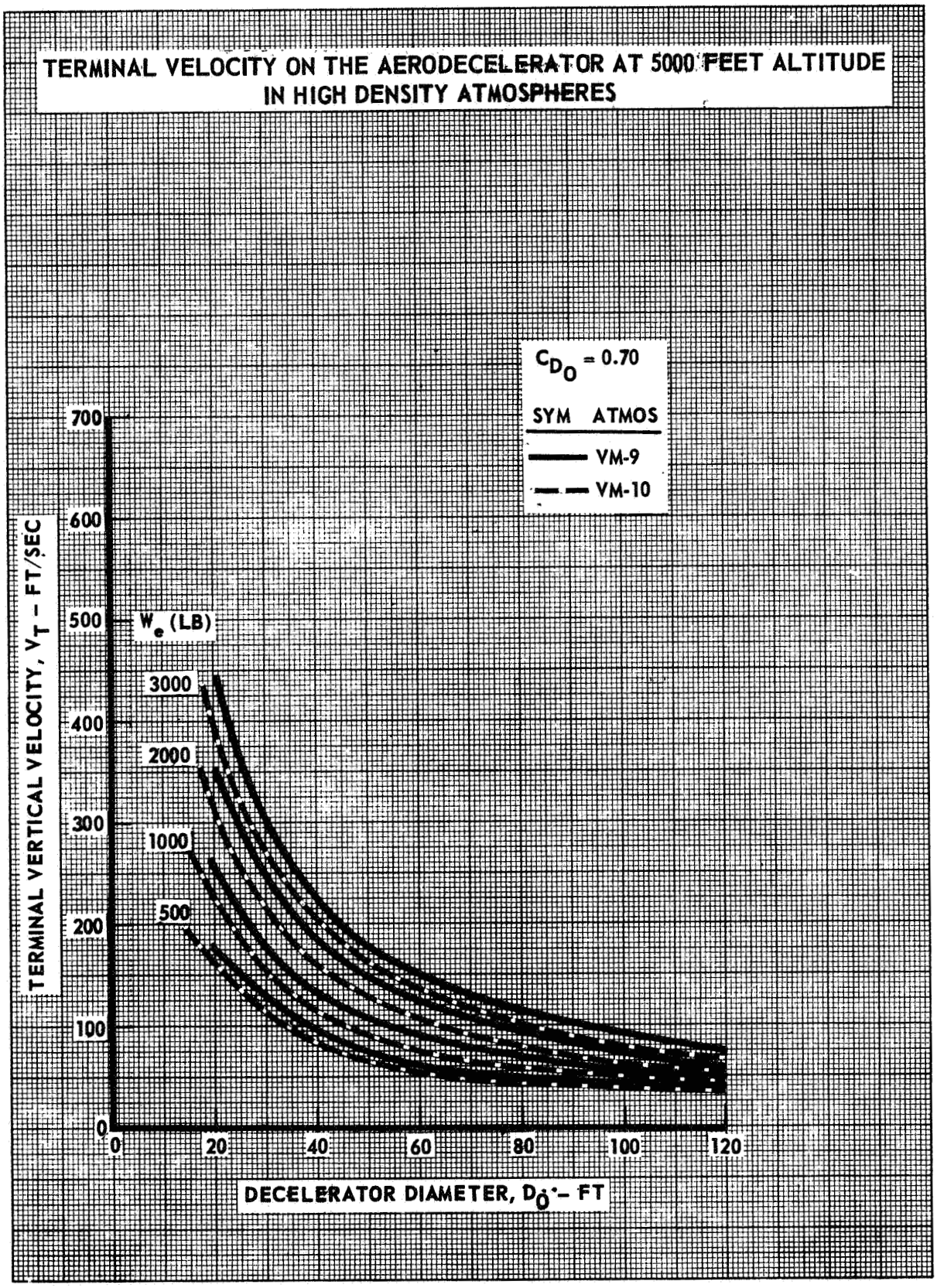

FIGURE 3.1.4–10

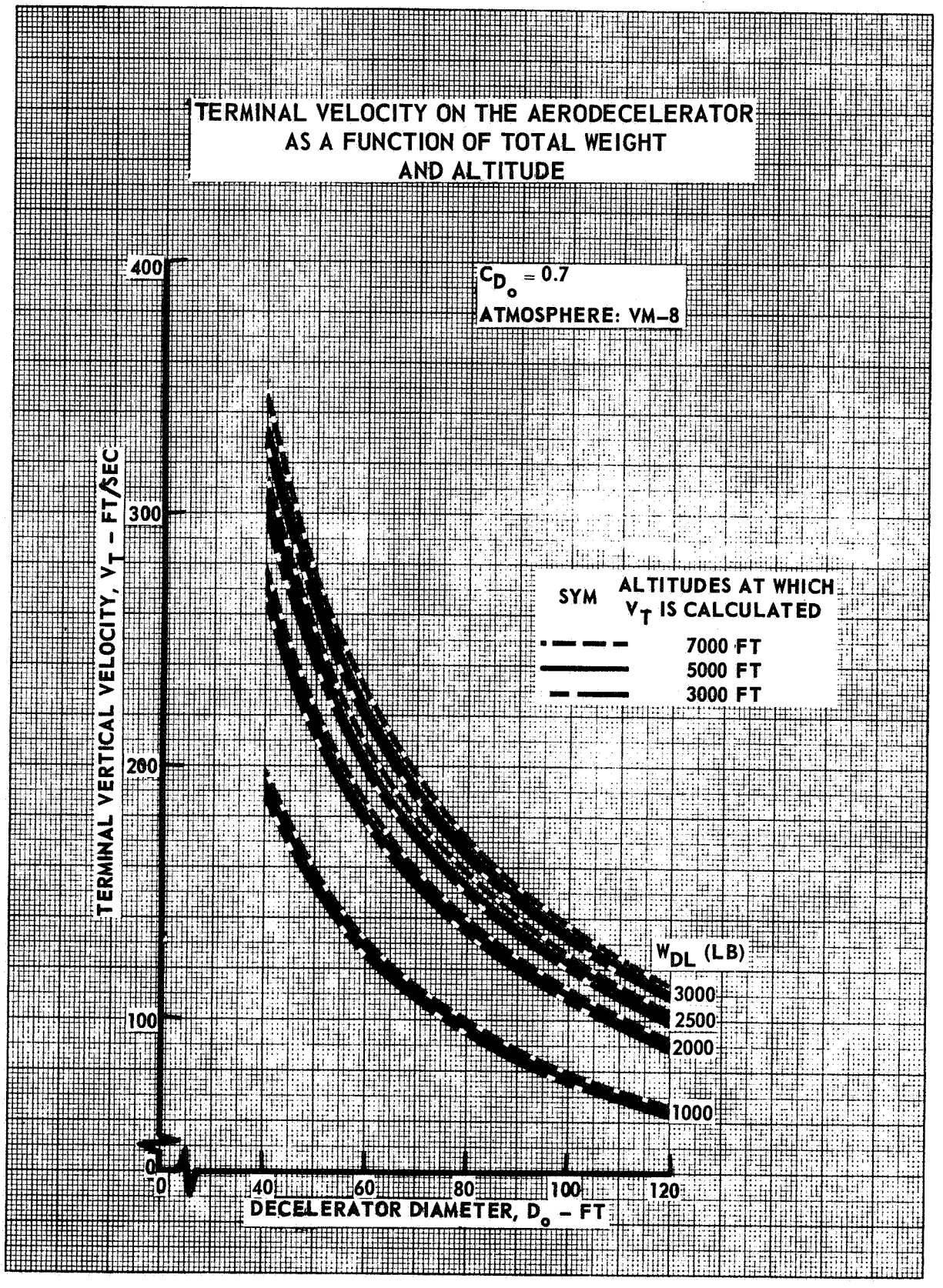

FIGURE 3.1.4-11

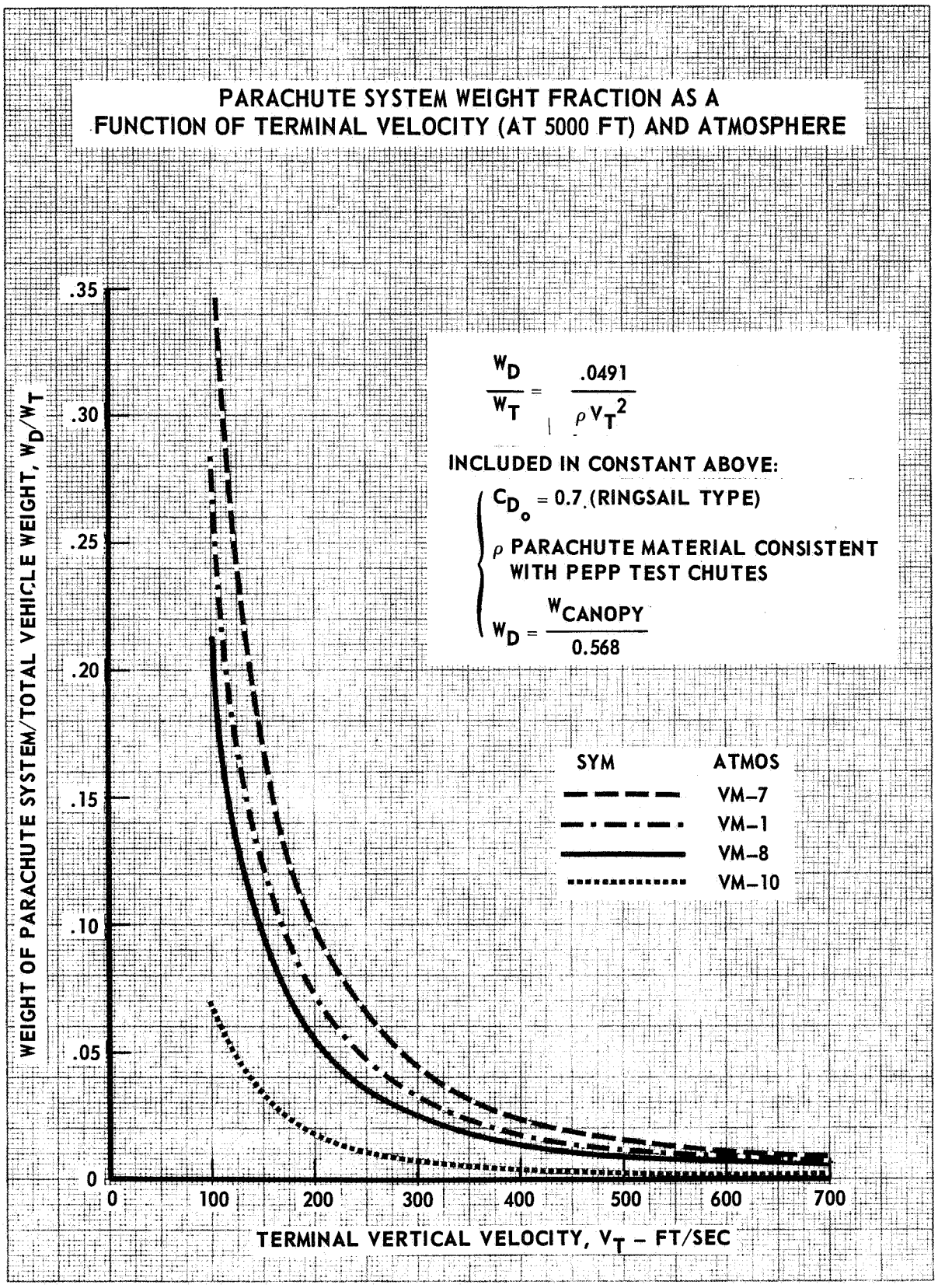

FIGURE 3.1.4–12

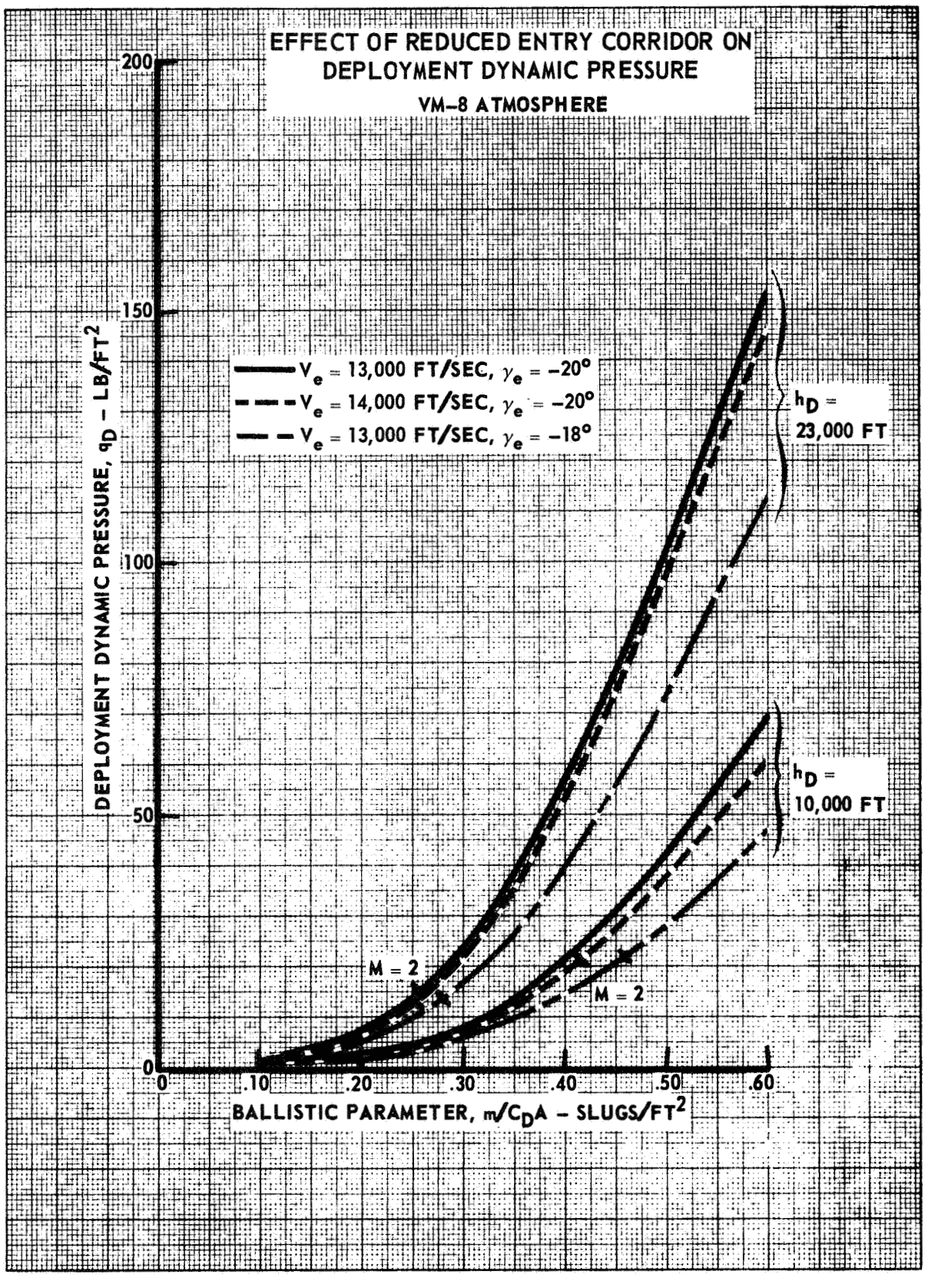

FIGURE 3.1.4–13

decreasing the entry flight path angle (γ_e). In addition, the deployment Mach number-altitude relation to m/C_DA is somewhat eased by movement away from the critical corner of the entry corridor (V_e = 13 000 ft/sec and γ_e = -20 deg), shown in Figure 3.1.4-14.

Modifications to the atmospheric scale height and surface pressure limits affect parachute design most by removing the atmosphere (VM-8) most critical to deployment dynamic pressure and Mach number. These effects are shown in Figure 3.1.4-15 and 3.1.4-16. Higher minimum scale height or higher surface pressure reduces the maximum deployment dynamic pressure, and the combination reduces this value considerably. A higher entry ballistic parameter can also be used with the constraints on deployment at Mach 2 (at a fixed altitude). In addition, the higher minimum surface pressure will decrease the terminal velocity for a given weight, permitting a reduction in parachute size.

The effects on maximum deployment dynamic pressure and on the ballistic parameter limited by deployment Mach number are shown in Figures 3.1.4-15 and 3.1.4-16 for the combination of reduced entry corridor and modified atmospheric environment.

Aeroshell/lander separation requirements are unchanged or possibly slightly improved by the reduced entry corridor (γ_e reduction). The minimum relative accelerations will not be affected by the change in surface pressure limitations, because these were shown (Figure 3.1.4-8) to occur in either atmospheres VM-1 or VM-7. The scale height increase affects only the even numbered atmospheres, while the minimum relative accelerations were shown to occur also in the odd numbered atmospheres.

3.1.4.5 Rotating planet effects. - The above analyses were made over a non-rotating planet. The effects of planet rotation for a posigrade entry trajectory are small, but are in the direction of increasing the criticality of the design parameters. The effects on flight path angle, deployment dynamic pressure, and Mach number-altitude relations are shown in Figures 3.1.4-17 3.1.4-18 and -19 where the effect of increasing orbit inclination is shown to return the rotating planet parameter values to the non-rotating values.

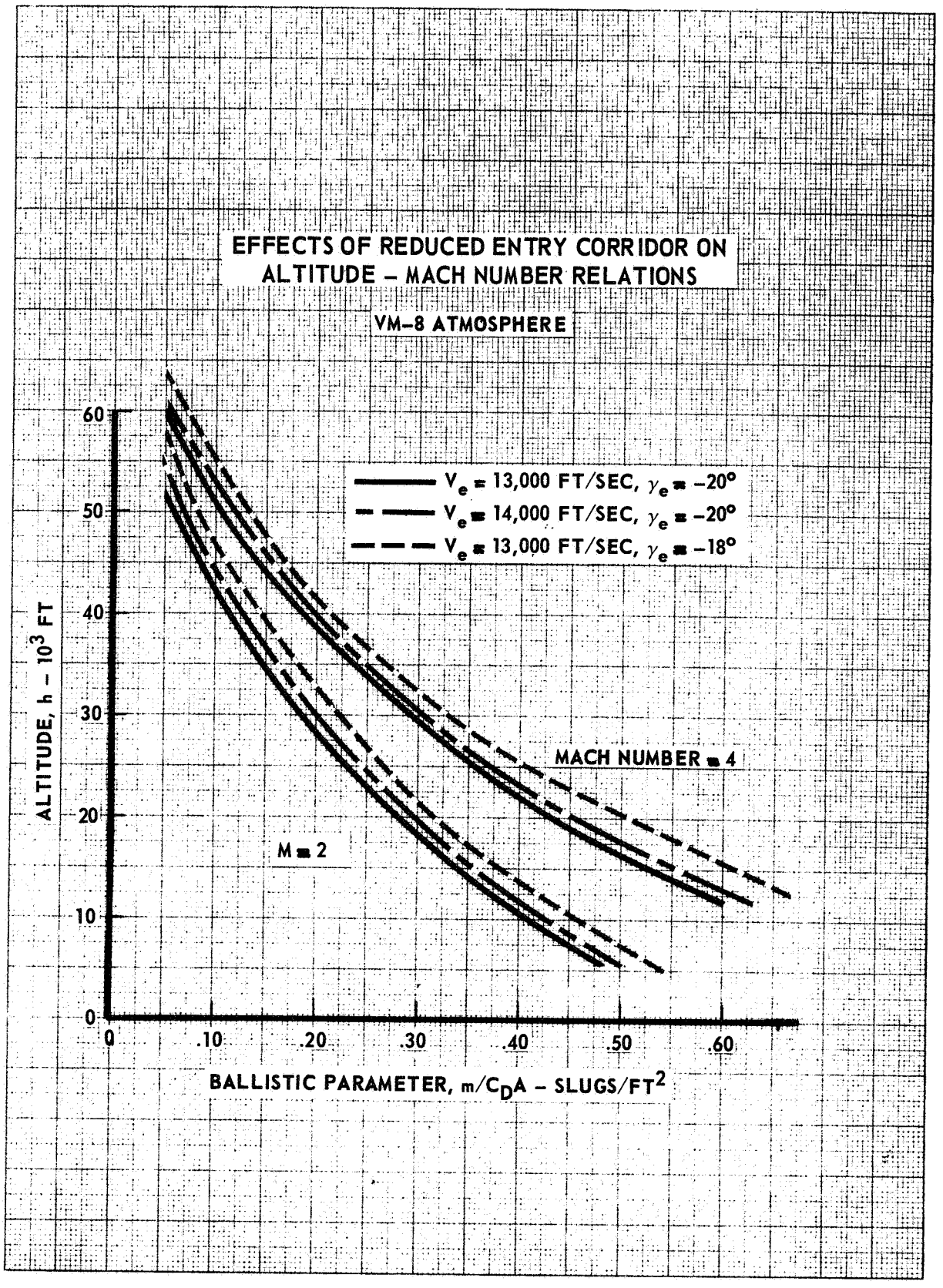

FIGURE 3.1.4–14

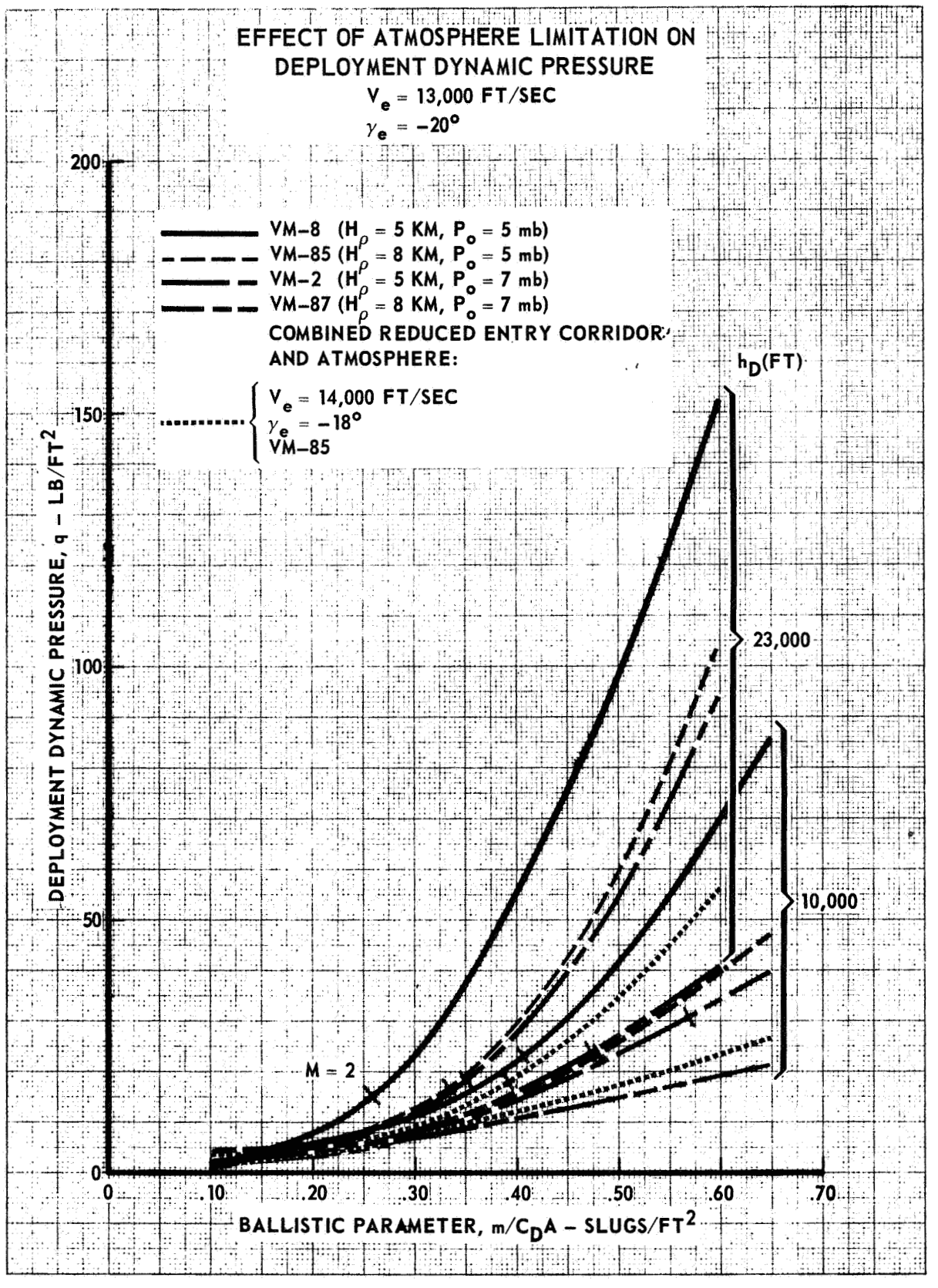

FIGURE 3.1.4–15

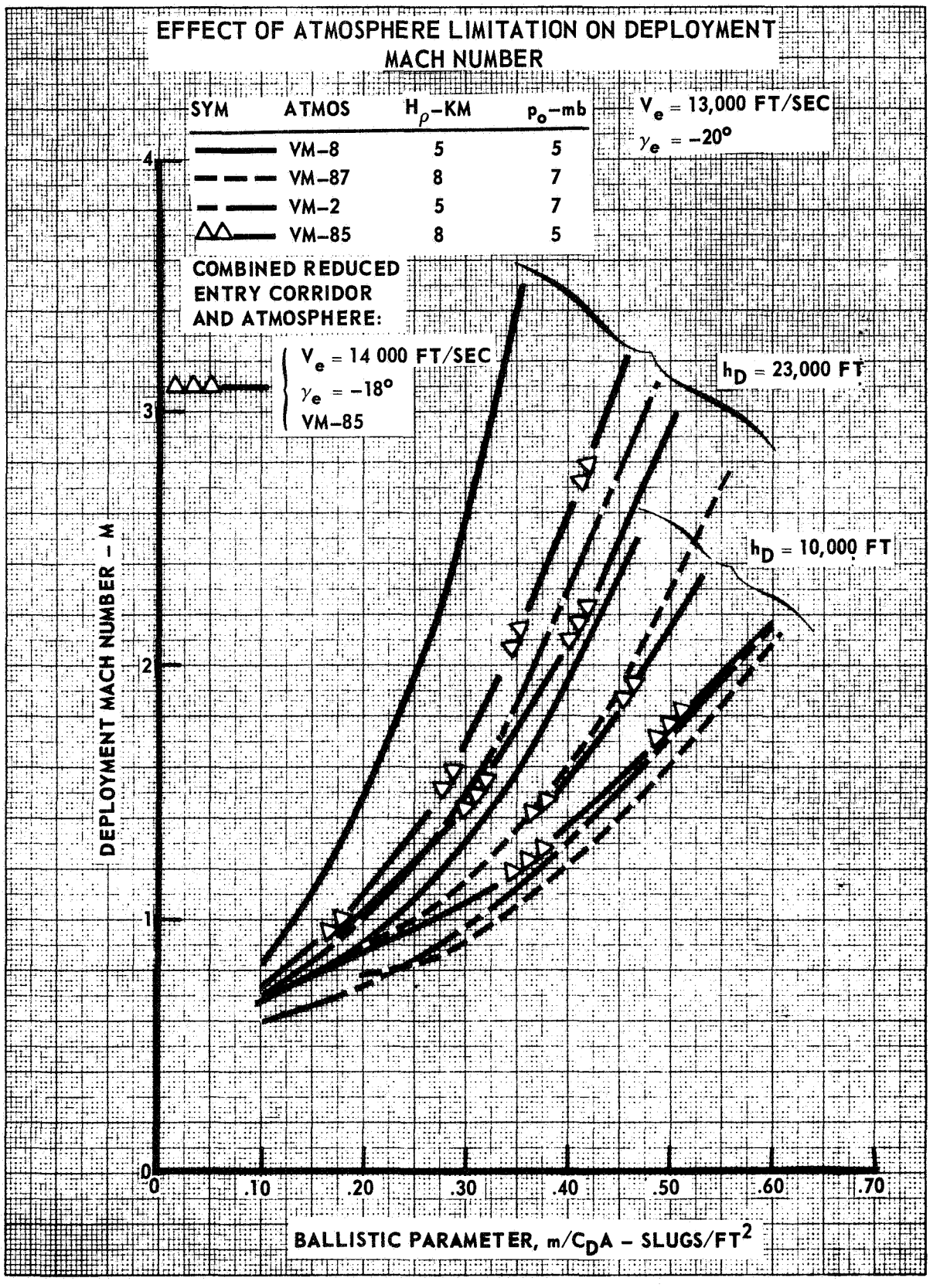

FIGURE 3.1.4–16

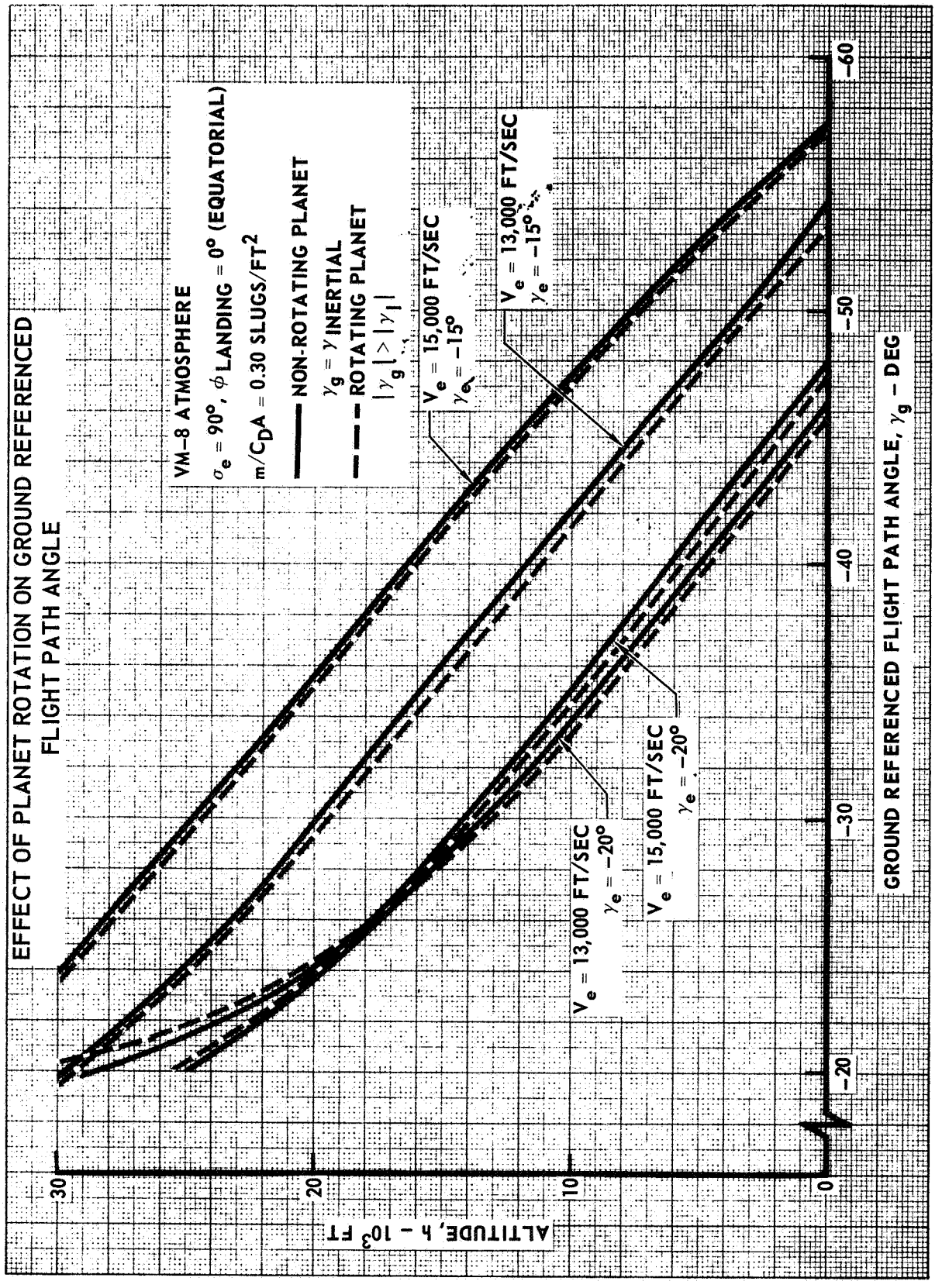

FIGURE 3.1.4–17

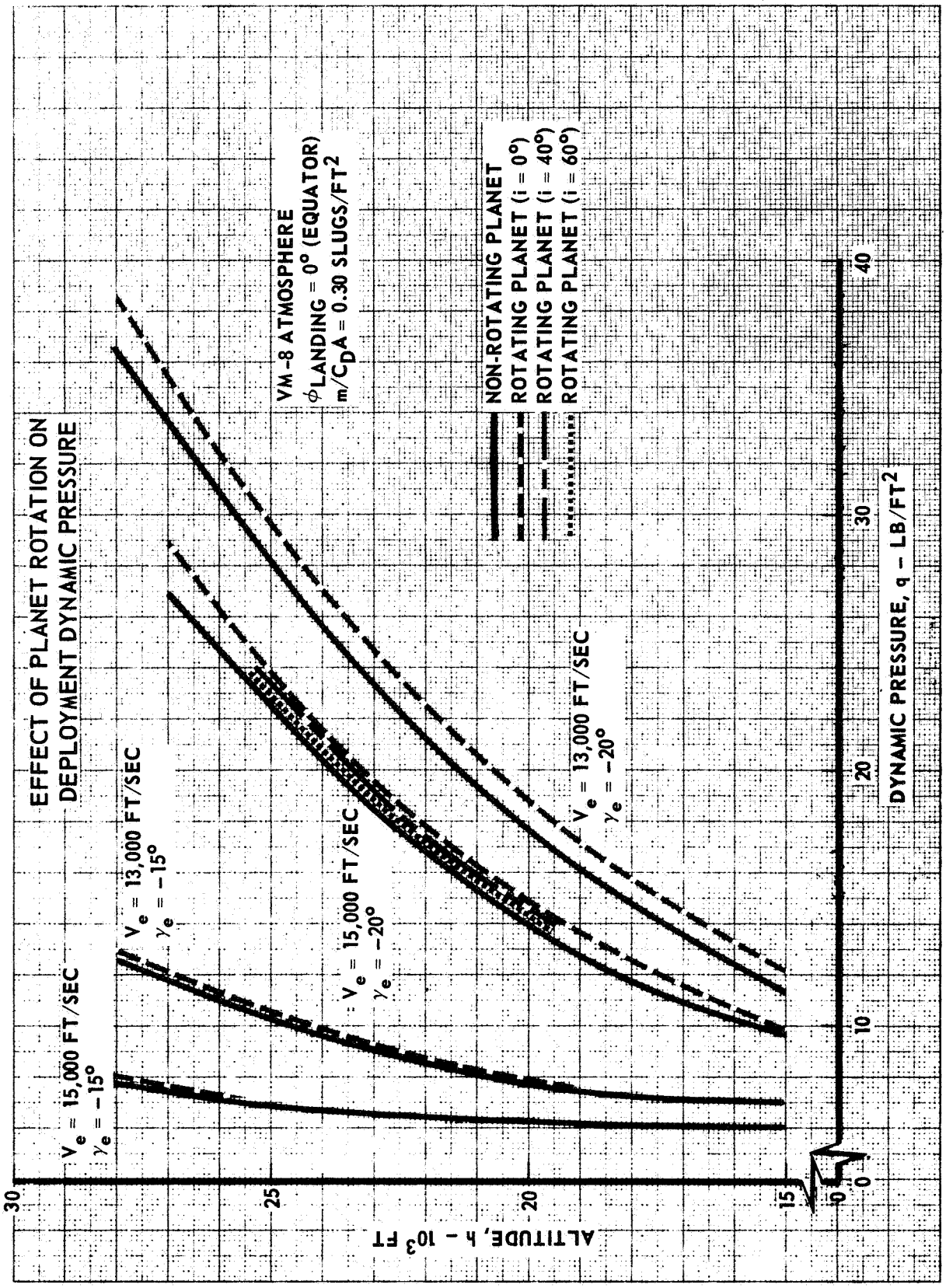

FIGURE 3.1.4–18

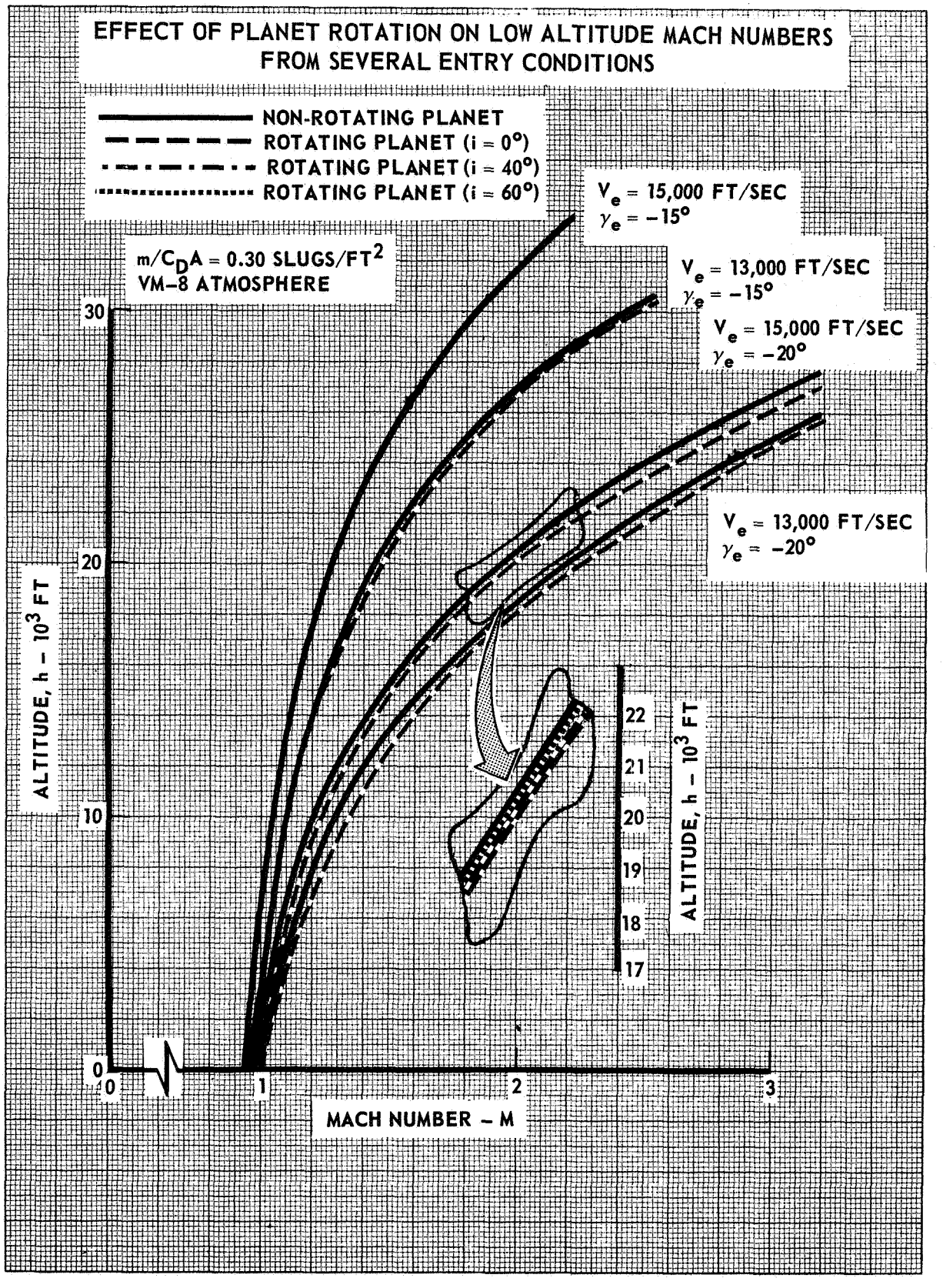

FIGURE 3.1.4–19

3.2 System Parametric Studies

The capsule systems have been studied over a range of parameters suitable for combination into capsules of the 1000-5000 pound weight class. For some of the systems, alternative design approaches have been studied and the results presented below. In these cases the parametric data is supplemented by a summary of the advantages and disadvantages of each approach. For others, the sensitivity of the total capsule to the selection of a particular approach is not great enough to warrant detailed examination of alternate approaches as a part of this limited study. Where choices of design approache are predicated on work publicly reported prior to this study, reference is made to that report and the reasons for selection summarized. Unless specifically noted, the system types described below are sufficiently developed to permit their use in a capsule for the earliest (1973) mission opportunity described in this study.

3.2.1 SCIENCE - The parametric analysis of the science system completed during the study is described in this section while the effect of the science payload weight, data output, and mission duration on the total landed payload system (including the electrical power supply and the communications system) is described in Section 3.3.2, Surface Payload Analysis. This section, 3.2.1, contains the general parametric analysis of the payloads and individual instruments. The application of these parametric analyses in selecting the detail instrument characteristics, operational sequences, and data outputs for the separate point designs is discussed in the science sections for each concept.

Although the scope of this study did not permit a detailed analysis to be carried out on every instrument, a parametric analysis of many of the instruments was completed which resulted in several conclusions:

a) No serious difficulty is expected in obtaining instruments which will be satisfactory for carrying out the scientific measurements. In many cases, a moderate amount of development effort will produce an increased measurement capability that will greatly enhance the suitability of the data for interpretation.

b) Since a large diameter lens will be required for the high resolution camera in order to obtain a reasonable light level sensitivity within the available scan times, it will be necessary to control the focus of the facsimile camera for objects near the lander.

c) The atmospheric humidity is expected to be extremely low during the early part of the 1974 landing opportunity while later in the opportunity the humidity is expected to have a much higher value. Diurnal variations in the surface atmospheric humidity are expected for the higher humidity conditions in the later part of the opportunity.

d) Significant variations of the atmospheric humidity with altitude are expected. The time constant of aluminum oxide humidity sensor is believed to be sufficiently short to follow the humidity variation with altitude during entry, however, lab tests to verify the shortness of the time constant are desirable.

e) Calculated performance values indicate that the addition of an electron multiplier detector to the mass spectrometer should make it possible to measure minor constituents in the atmosphere such as water vapor. A significant increase in the measurement accuracy will be obtained if the scan time is increased for operation of the mass spectrometer on the surface after landing.

f) A counting system should be added to the alpha spectrometer in order to reduce the data output to a value which is reasonable for Mars missions. Additional or longer half-life radioactive sources will be required to obtain sample measurement times which are reasonable for the short duration missions.

3.2.1.1 Landed Science Payload. - Although a wide range of payloads was considered during the study, the 30 lb. minimum science payload received most emphasis. This payload consists of 10 lb. for surface imaging, 10 lbs. for meterology measurements, and 10 lb. for the determination of the composition of the surface material.

The Mars mission objectives for the use of the 30 lb. surface science payload is summarized by the measurement requirements in Table 3.2.1-1. The required accuracies are not only moderate in comparison with the capability of presently available instruments but are also sufficiently precise so that meaningful data interpretation and conclusions will be possible. In several cases, such as for the wind velocity threshold of 5 meters/sec, a lower value for a design goal or requirement is desirable.

Payload Characteristics - Of the three payloads approved for use in the point designs in Table 3.2.1-2, only the 30 lb. payload was utilized. The point designs for the heavier capsules in this study utilized the additional weight for an extended duration mission rather than for increasing the surface science payload weight.

The 30 lb. science payload includes 6.5 lb. for a high resolution fascimile camera to obtain 5° x 5° images of the surface with a scanning element diameter of 0.01° and a wide angle facsimile camera to obtain four 70° high x 25° wide frames using a scan element diameter of 0.1°. Since the

TABLE 3.2.1-1

SURFACE SCIENCE MEASUREMENT REQUIREMENTS

IMAGERY*

"WIDE ANGLE"

RESOLUTION: 0.1°/LINE

COVERAGE: 4 SCENES LOCATED AT RIGHT ANGLES. SCENE SIZE OF 25° IN AZIMUTH AND 70° IN ELEVATION

COLOR: NO REQUIREMENT FOR MINIMUM LIFE; HOWEVER, CAPABILITY (RED AND GREEN FILTERS) TO BE PROVIDED FOR POTENTIAL USE IF ADDITIONAL LIFETIME IS ACHIEVED

"HIGH RESOLUTION"

RESOLUTION: 0.01°/LINE

COVERAGE: 4 SCENES LOCATED WITHIN "WIDE ANGLE" COVERAGE. SCENE SIZE OF 5° x 5°

COLOR: NO

TOTAL IMAGE DATA: APPROXIMATELY 10^7 TOTAL BITS

METEOROLOGY

	ACCURACY
PRESSURE VARIATIONS WITH TIME	± 5 PERCENT OF VALUE AT KNOWN TIME 0.5 MB THRESHOLD
TEMPERATURE VARIATIONS WITH TIME	± 2 PERCENT OF VALUE AT KNOWN TIME 3°K THRESHOLD
WIND VELOCITY VARIATIONS, WITH TIME	± 5 PERCENT OF VALUE AT KNOWN TIME 5 METERS/SEC THRESHOLD
WIND DIRECTION VARIATIONS WITH TIME	± 10° AT KNOWN TIME
SPECIFIC HUMIDITY (ATMOSPHERE) VARIATIONS WITH TIME	DEW/FROST POINT OF ± 2°C

SOIL COMPOSITION

SAME AS SURVEYOR α-SPECTROMETER EXPERIMENT

*TO BE OBTAINED WITHOUT RELIANCE ON REGENERATED POWER

THE DESIGN GOAL IS TO OBTAIN AS MUCH ADDITIONAL IMAGERY DATA AS POSSIBLE; IF REGENERATED POWER IS AVAILABLE, TIME SEPARATION BETWEEN VIEWINGS IS DESIRED TO STUDY SEASONAL VARIATIONS. IT IS ALSO A GOAL TO HAVE THE CAPABILITY TO COMMAND THE SYSTEM TO EXAMINE A DESIRED LOCATION

LANDER LIFETIME

MINIMUM: A LIFETIME SUFFICIENT, WITHOUT DEPENDENCE ON REGENERATED POWER, TO ACCOMPLISH: THE INITIAL IMAGERY EXPERIMENT, THE SOIL COMPOSITION EXPERIMENT AND, FOR ONE DIURNAL CYCLE, THE METEOROLOGICAL EXPERIMENT

GOAL: EXPENDABLES AND MINIMUM LIFETIME EQUIPMENT TO BE DESIGNED FOR A LIFETIME OF 90 MARS DAYS USING REGENERATED POWER

TABLE 3.2.1–2

SURFACE SCIENCE
POINT DESIGN PAYLOADS

	MINIMUM 30 LB	INCREASED CAPABILITY	MAXIMUM 118 LB
FACSIMILE CAMERAS	(10)	(10)	(10)
WIDE ANGLE	3.5	3.5	3.5
HIGH RESOLUTION	6.5	6.5	6.5
ATMOSPHERIC PACKAGE	(10)	(10)	(10)
PRESSURE	4	4	4
TEMPERATURE	2	2	2
WIND	2	2	2
HUMIDITY	2	2	2
SURFACE COMPOSITION	10	10	10
SUBSURFACE PROBE		6	6
GAS CHROMATOGRAPH		10	15
LIFE DETECTION			30
SPECTRO–RADIOMETER			10
SAMPLE GATHERING			27
TOTAL	30	46	118

data rates, the sequence in which the images are taken, and the other operational procedures vary from one concept to another, the instrument data and operation are discussed in the separate point design sections. It is possible to obtain both the high resolution images and the wide angle images using a single 6.5 lb camera. The use of two 6.5 lb cameras for redundancy would, however, require more than the total alloted weight of 10 lb. By using both a wide angle and a high resolution camera, it is possible to either obtain redundancy for the wide angle images or the high resolution camera can be simplified since it is not necessary to obtain both the wide angle and high resolution images with the 6.5 lb camera.

The 10 pounds alloted to the atmopsheric package should make it possible to make relatively precise measurements of the atmospheric pressure, temperature, wind velocity and direction, and humidity. A two pound design goal is a reasonable value for each of the transducers with a two pound margin which can be used for any one of the four. A four pound weight is shown for the pressure transducer in Table 3.2.1-2, however, it is more likely that the wind instrument would require 4 lb and 2 lb should be more than adequate for the pressure sensors.

Ten pounds is alloted for the surface composition measurement using the alpha spectrometer. The 10 lb normally consists of 3 lb for the sensor, 5 lb for the electronics package, and 2 lb for the deployment mechanism. However, for the Mars mission it will be necessary to add 3 lb for a counting system to reduce the total transmitted data for the alpha spectrometer. The counters can most likely be included in the instrument within the 10 lb weight allotment if the deployment mechanism weight is charged to the structural support system rather than to the instrument weight.

The 46 lb increased-capability payload in Table 3.2.1-2 was not used for any of the point designs. The reason for adding the subsurface probe to the other measurements was to obtain a direct measurement of the temperature and subsurface H_2O which are the most important quantities for determining whether or not the surface environment is suitable for the evolution or existence of microorganisms. The gas chromatograph was added to detect the presence of any subsurface or atmospheric organic gases. However, atmospheric

organic gases may be present only in trace amounts. On Earth, the largest organic gas in the atmosphere is methane which represents only $1.5 \times 10^{-4}\%$ of the Earth's atmosphere by volume at the surface. Thus, it appears that a better payload to use for the increased capability would be a 56 lb. payload which includes a 15 lb. gas chromatograph with pyrolysis chamber for heating solid surface samples and a 5 lb. surface sampler to provide finely divided samples to the gas chromatograph pyrolysis chamber. This payload would have the capability of detecting organic compounds in the surface material.

The third payload, 118 lb., includes 30 lb. for life detection. It is felt that the first payload that includes life detectors should have at least 30 lb. allocated to the life detection instruments. This will make it possible to use many different techniques for detecting life so that there is a reasonable probability for life detection if microorganisms are present. It would be reasonable to include the 30 lb. of life detection instruments in payloads lighter than 118 lb. for missions following the landers using the 30 lb. minimum payload.

Since it appeared that the constraints on the study would permit larger payloads than 118 lb. an instrument list for a 200 lb. payload was identified, Table 3.2.1-3. Even with this large payload weight, several compromises were required in order to keep the weight within 200 lb. For example, for the high priority seismic measurements, it was necessary to use a lightweight 8 lb. single-axis unit rather than a 25 lb, 3-axis sophisticated unit suitable for detecting both long period and short period seismic activity on Mars.

Conclusions - The 30 lb. payload consisting of 10 lb. for facsimile cameras, 10 lb. for an atmospheric package and 10 lb. for an alpha spectrometer should be adequate for obtaining the required high and low resolution images, the meteorology measurements of pressure, temperature, wind, and humidity and the determination of the Mars surface material composition. The instrument operation and data produced is discussed in the separate sections for each of the point design concepts.

3.2.1.2 Entry Science Payload. - The 23 lb. entry science payload, Table 3.2.1-4, selected for making the entry science measurements listed in

TABLE 3.2.1–3

SURFACE SCIENCE

200 LB PAYLOAD

INSTRUMENTS	(160)
IMAGERY	(43)
CAMERA	20
MICROSCOPE	23
ATMOSPHERIC PACKAGE (P, T, W, & H)	10
SURFACE COMPOSITION	(62)
ALPHA/X-RAY SPECTROMETER (ELEMENTS)	15
X-RAY DIFFRACTOMETER (MINERALS)	20
GAMMA RAY SPECTROMETER (ISOTOPES)	12
GAS CHROMATOGRAPH (ORGANIC VOLATILES)	15
SPECIFIC LIFE DETECTORS	30
SEISMOMETER	8
SOLAR AND COSMIC RADIATION	7
SAMPLE ACQUISITION AND PROCESSING	25
	185
MARGIN	15
TOTAL	200

TABLE 3.2.1–4

ENTRY SCIENCE
POINT DESIGN PAYLOAD

INSTRUMENT	WEIGHT (LB)
MASS SPECTROMETER	9
MOISTURE SENSOR	1
TEMPERATURE SENSORS (2)	1
PRESSURE SENSOR (ATMOSPHERIC) (2)	2
PRESSURE SENSOR (AEROSHELL NOSE) (4)	3
ACCELEROMETER (TRI-AXIS)	2
MARGIN	5
TOTAL	23

Table 3.2.1-5 includes a mass spectrometer, moisture sensor, temperature and pressure sensors, and a dual range tri-axis accelerometer. One other entry science payload considered during this study consisted of this payload with an additional 14 lb. for an entry television resulting in a total entry science payload weight of 37 lb. This 37 lb. payload was initially utilized in the Concept IV point design which was, however, not completely developed in order to do a more thorough analysis of the lighter weight capsules.

In addition to the instruments listed in Table 3.2.1-4, other equipment will provide measurements which are of use for the atmospheric profile analysis. For example, the radar altimeter will provide altitude measurements below 60 km and the systems monitoring instrumentation will provide data such as the high temperature of the beryllium nose cap caused by the entry heating.

3.2.1.3 Lander Facsimile Camera. - A facsimile camera is suitable for obtaining high resolution photographs of the Mars surface with a quality comparable to that obtained on Surveyor. The facsimile has the advantage that it is much lighter than a television camera. Two facsimile cameras, one for wide angle coverage and one for high resolution coverage, weigh less than 10 lb, compared to 20 lb. for one Surveyor type TV camera. The facsimile camera has the further advantage that the data can be read directly into the transmitter without using a data storage.

Measurements - The required images corresponding to the minimum data of approximately 10^7 bits consist of four high resolution frames (5° x 5°) with a scan element size of 0.01° and four wide angle (70° x 25°) frames with a 0.1° scan element size. (The four wide angle frames are separated by approximately 90°.) The low light levels on Mars make it necessary to have a luminance threshold between 1 and 3 ft-Lamberts for the two cameras. The values used to calculate the threshold luminance values in Table 3.2.1-6 include an 80% atmospheric transmission and a surface reflectance of 30%. The atmospheric haze brightness measured by Mariner IV is in reasonable agreement with these values. According to Reference 3.2.1-1, the haze ranges from 30 to 50% of the average intensity of light reflected from Mars. If 80% of the radiation is transmitted by the atmosphere, then less than 20% will be reflected as haze radiation. For a surface reflectivity of 30% and an 80%

TABLE 3.2.1–5

ENTRY SCIENCE MEASUREMENT REQUIREMENTS

PRESSURE VARIATION WITH ALTITUDE

ALTITUDE RANGE: FROM 60 Km TO AS LOW AN ALTITUDE AS PRACTICAL

ACCURACY: ± 5 PERCENT OF VALUE AT KNOWN ALTITUDE, THRESHOLD ACCURACY 0.5 MB

DENSITY VARIATION WITH ALTITUDE

ALTITUDE RANGE: FROM 60 Km TO AS LOW AN ALTITUDE AS PRACTICAL

ACCURACY: ± 5 PERCENT OF VALUE AT KNOWN ALTITUDE, THRESHOLD ACCURACY 1×10^{-6} GM/CM^3

TEMPERATURE VARIATION WITH ALTITUDE

ALTITUDE RANGE: FROM 60 Km TO AS LOW AN ALTITUDE AS PRACTICAL

ACCURACY: ± 2 PERCENT OF VALUE (°K) AT KNOWN ALTITUDE, THRESHOLD ACCURACY 3°K

COMPOSITION VARIATION WITH ALTITUDE (INCLUDING WATER VAPOR)

ALTITUDE RANGE: BELOW 50 Km

MASS NO. RANGE: 10–60 (REQUIRED DETECTION CAPABILITY FOR CO_2, N_2, Ar, AND H_2O)

ACCURACY: ± 5 PERCENT IF GREATER THAN 50 PERCENT OF TOTAL
± 10 PERCENT FOR OTHER CONSTITUENTS

TABLE 3.2.1–6

FACSIMILE CAMERA SENSITIVITY

SURFACE RADIANCE FACTOR

INCIDENT SOLAR RADIATION: MARS SUN SEPARATION = 1.57 AU (8 FEBRUARY 1974)	0.057 WATTS/CM^2
SOLAR RADIATION IN DETECTOR SPECTRAL BAND: (55%)	0.031 WATTS/CM^2
RADIATION TRANSMITTED BY ATMOSPHERE: (~80%)	0.025 WATTS/CM^2
RADIATION REFLECTED BY SURFACE: (~30%)	2.4 MW/CM^2/STER
MINIMUM REFLECTED RADIATION: (EXPOSURE LATITUDE OF 20)	1.2×10^{-4} W/CM^2/STER

transmission through the atmosphere, both for the radiation going in and the radiation coming out, the surface radiation as viewed through the atmosphere will be approximately 19% of the incident radiation. The haze radiation and the surface radiation are thus nearly equal (for the maximum haze) which agrees with the 50% minimum value obtained from Mariner IV.

At the time of the 1974 landing, the radiation reflected by the surface, as evaluated in Table 3.2.1-6, is approximately 2.4 $mW/cm^2/ster$. This value corresponds to a 90° sun angle near noon. Areas in the shadows and areas with a surface reflectance of less than 30% will thus have a brightness of less than 2.4 $mW/cm^2/ster$. If an exposure latitude of 20 is used to account for the reduced brightness, then the resulting minimum reflected radiation from the surface is 1.2×10^{-4} $W/cm^2/ster$. For a luminance efficiency of approximately 80 lumens per watt for solar radiation, this minimum reflected radiation corresponds to approximately 28 ft-Lamberts. Taking into account the requirement for obtaining images early in the morning or late in the afternoon or with cloudy conditions, a value of 1 to 3 ft-Lamberts appears to be a reasonable threshold luminance requirement.

The spectral characteristics of the solar radiation, the atmospheric transmission, the surface reflectivity, and the detector sensitivity were used to arrive at the percentages in Table 3.2.1-6. Most of the solar radiation energy, Figure 3.2.1-1, is in a region in which the atmospheric transmission on Mars should be high, Figure 3.2.1-2. The concentration of CO_2 of 65 meter atmospheres in Figure 3.2.1-2 may be slightly low. Astronomical observations during the 1965 opposition indicated that the concentration of CO_2 is 90 ± 27 meter atmospheres. Figures 3.2.1-3 and -4 indicate that both the surface reflectivity and the camera detector sensitivity are high in the region in which there is a large amount of solar radiation.

Instrument Characteristics - The use of two facsimile cameras, one to obtain the high resolution images and one to obtain the wide angle images will reduce the complexity of the facsimile camera. The high resolution camera requires a larger lens and hence a larger camera, as shown in Table 3.2.1-7. The wide angle camera is similar to the lunar ranger facsimile camera. In order to obtain a reasonable scan period for the high resolution camera, a lens diameter of 0.5 to 1 inch will be required and for a lens this large, it will be necessary to focus the camera when looking at areas close to the lander.

FACSIMILE CAMERA SENSITIVITY
SOLAR RADIATION FACTOR

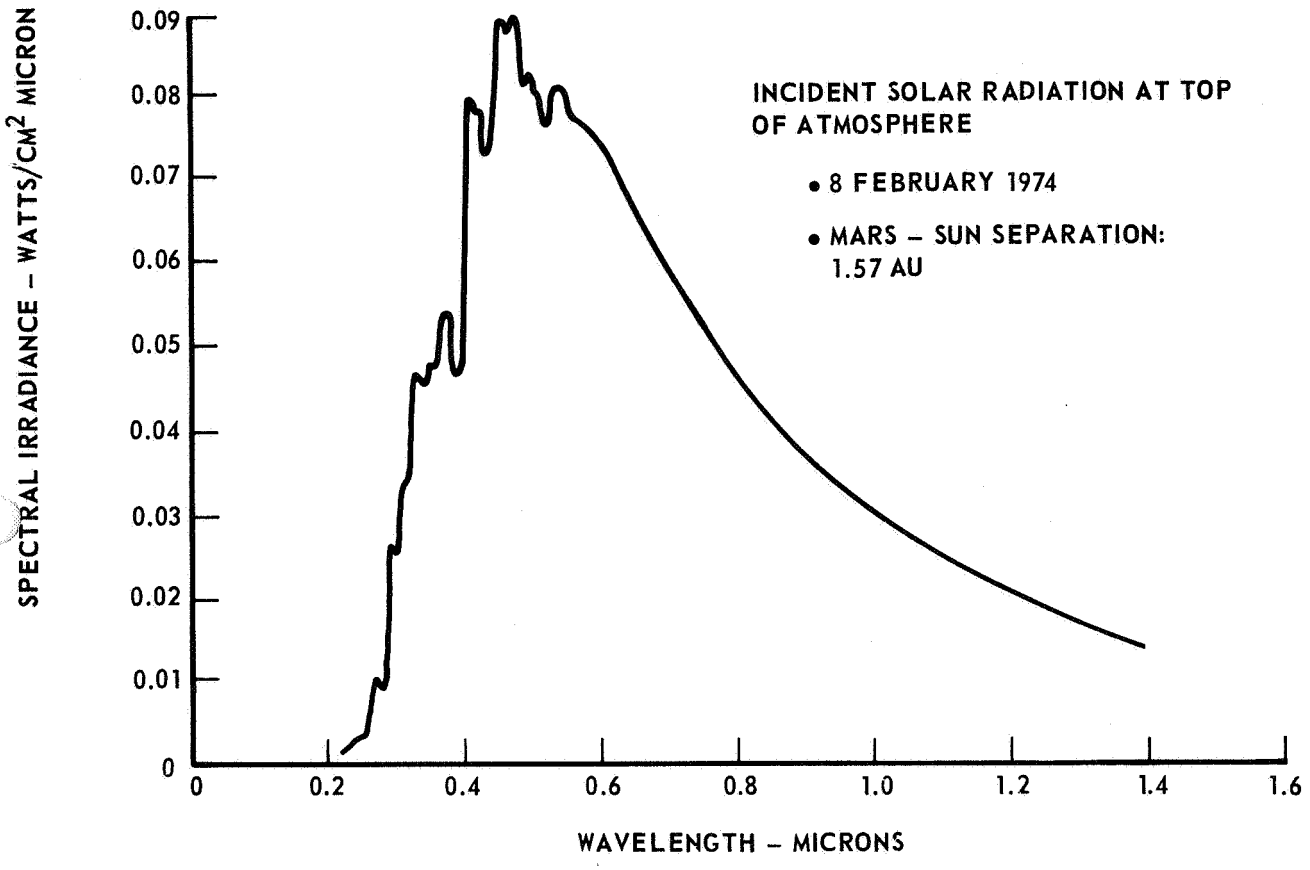

FIGURE 3.2.1–1

FACSIMILE CAMERA SENSITIVITY
ATMOSPHERIC TRANSMISSION FACTOR

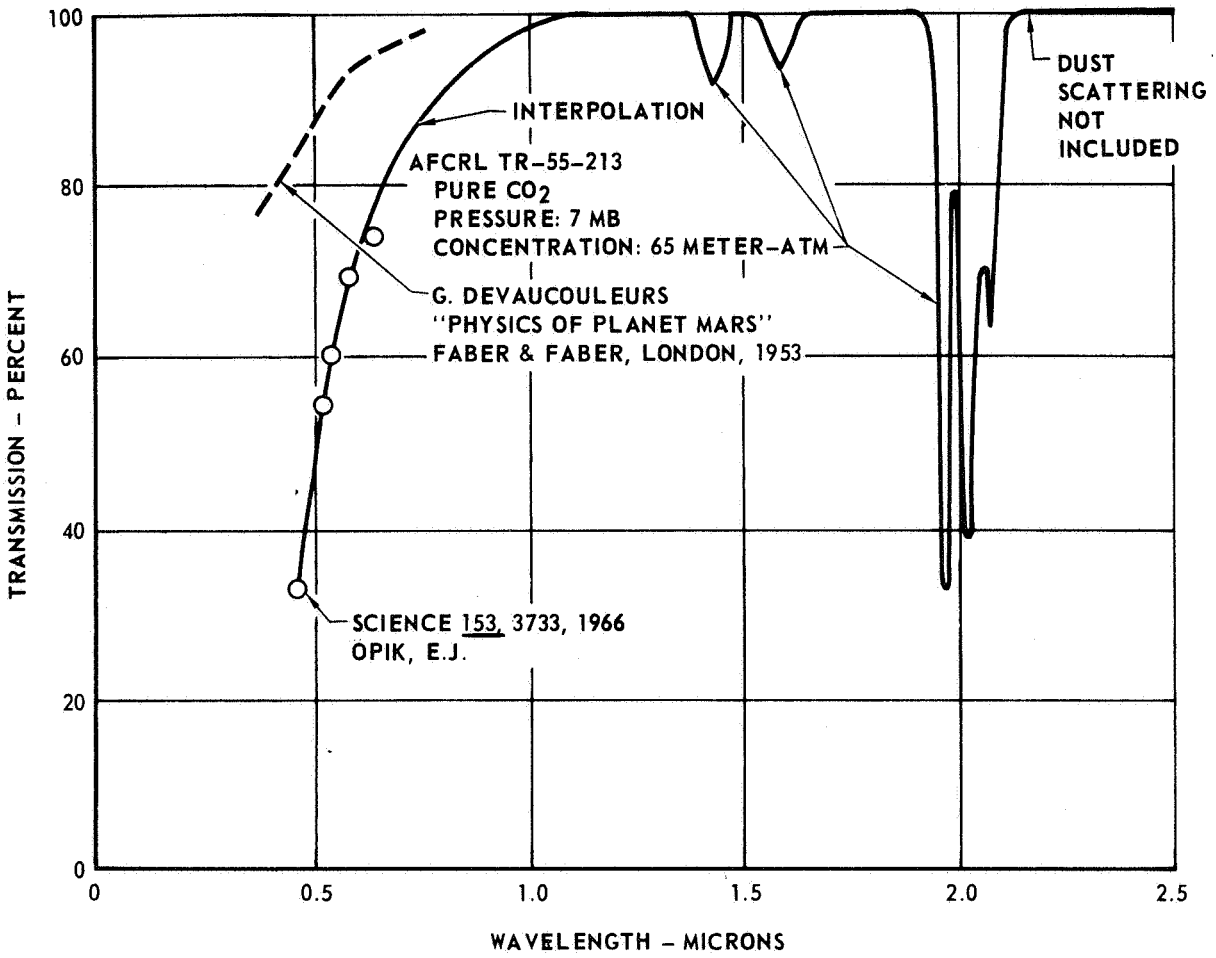

FIGURE 3.2.1–2

FACSIMILE CAMERA SENSITIVITY
SURFACE SPECTRAL REFLECTIVITY FACTOR

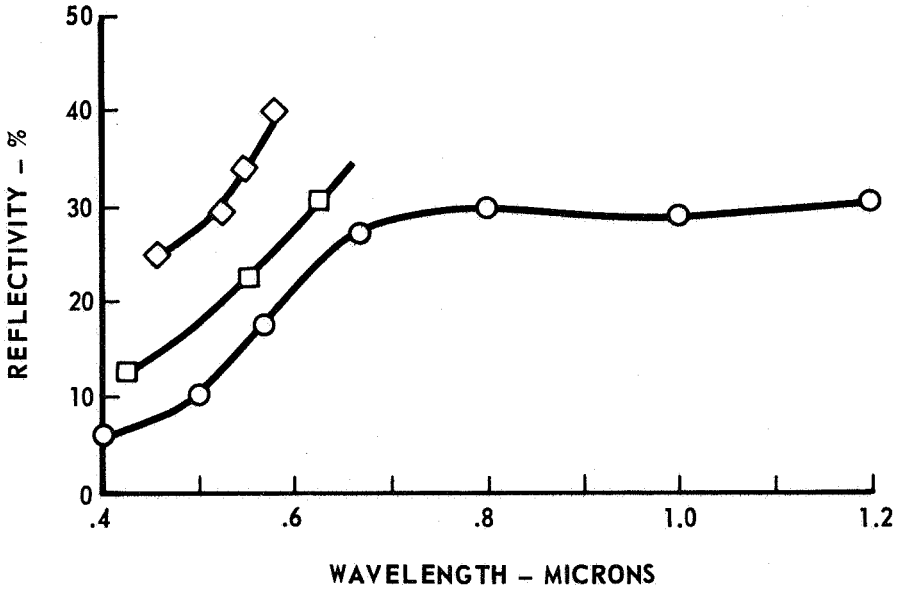

◇ E.J. OPIK, SCIENCE 153 257, 1966

□ G. DeVAUCOULEURS, PHYSICS OF THE PLANET MARS, 1953

○ R. G. TULL, ICARUS 5 513, 1966

FIGURE 3.2.1–3

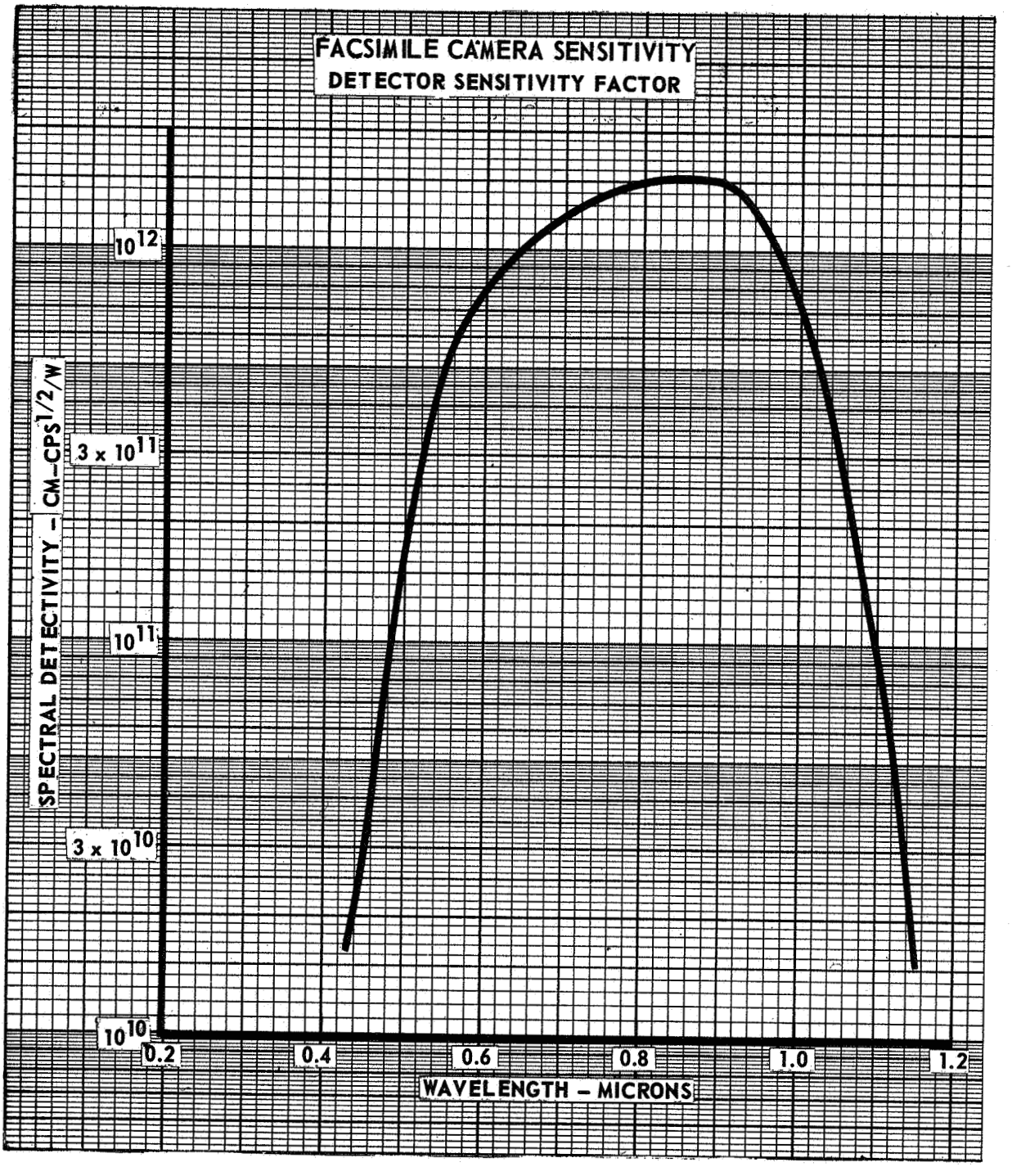
FACSIMILE CAMERA SENSITIVITY
DETECTOR SENSITIVITY FACTOR
SPECTRAL DETECTIVITY – CM-CPS$^{1/2}$/W
10^{12}
3×10^{11}
10^{11}
3×10^{10}
10^{10}
0.2
0.4
0.6
0.8
1.0
1.2
WAVELENGTH – MICRONS

FIGURE 3.2.1–4

TABLE 3.2.1–7

FACSIMILE CAMERA CHARACTERISTICS

CAMERA	SCAN ELEMENT SIZE	IMAGES	SIZE	WEIGHT LB	POWER WATTS	DATA BITS
HIGH RESOLUTION	0.01°	4 FRAMES (5° x 5°)	3'' DIA x 18''	6.5	15	6×10^6
WIDE ANGLE	0.1°	4 FRAMES (70° x 25°)	1.5'' DIA x 10''	3.5	10	4.2×10^6
		TOTAL		10 LB		1.02×10^7 BITS

The high sensitivity of the facsimile camera with a lens as large as one inch in diameter is illustrated by the calculations in Table 3.2.1-8. The bandwidth of 1000 hz is sufficient to scan a 5° x 5° field with a scan element size of .01° in a little less than 9 minutes and the resulting noise equivalent radiance for this bandwidth is 2.4×10^{-5} W/cm^2/ster. which is 1/5 the minimum reflected radiation, 1.2×10^{-4} W/cm^2/ster, in Table 3.2.1-8. If a half-inch lens is used, the same noise equivalent radiance can be obtained using a decreased bandwidth and a scanning period of about 2.3 hours.

The relations between the field of view, detector characteristics, and optical characteristics of the facsimile camera and the scan element size in Table 3.2.1-9 were used to obtain the parametric dependence of the noise equivalent radiance on the scan period and the lens diameter. The resulting values in Figure 3.2.1-5 illustrate that it will be necessary to use a lens between one-half and one inch in diameter in order to obtain a noise equivalent radiance of 10^{-5} W/cm^2/ster. for a scan period of 0.7 to 10 hours. The use of a light chopper at the detector will increase the NER by approximately a factor of two. Since such large lenses of 0.5 to 1 inch are required, it is necessary to focus the high resolution camera for photographs of the surfaces near the lander. An attempt to scan the wide angle field of the 0.1 wide angle camera in a few minutes will not produce severe focus problems as illustrated by Figure 3.2.1-6. A sensitivity of 6×10^{-6} watts/cm^2/ster. with a lens as small as 0.2 inches is possible with scan times less than 5 minutes. Figure 3.2.1-7 illustrates the limited depth of field for a high resolution camera with a scan element diameter of 0.01° and a lens diameter of 0.5 inches. The resolution loss factor of 2 means that the resolution at the extremes of the field is only half the resolution at the mean level surface indicated by the solid line.

The need for a controlled focus for the high resolution camera is further illustrated in Figure 3.2.1-8. In this figure the scan element diameter at the object being photographed is shown as a function of the distance to the surface or object. Values are shown for three camera systems, having lenses of 0.1 inches, 0.33 inches, and 1 inch. The corresponding scan element diameter for these three cameras are 0.1°, 0.03°, and 0.01°. Since the product of

TABLE 3.2.1–8

FACSIMILE CAMERA SENSITIVITY

SILICON SENSOR DETECTIVITY: 1.5×10^{12} CM/(WATT SEC$^{1/2}$)

NEP (CELL SIZE: 1 MM x 1 MM, Δf: 1000 CPS): 0.21×10^{-11} WATTS

NER, NOISE EQUIVALENT RADIANCE:

($\theta = 0.01°$, LENS DIA = 1 INCH, OPTICAL TRANSMISSION = 80%)

$$(NER) = (NEP) \left(\frac{\pi\theta^2}{4}\right)^{-1} \left(\frac{\pi D^2}{4}\right)^{-1} T^{-1}$$

$$NER = (0.21 \times 10^{-11} \text{ WATTS}) \left[\frac{\pi}{4} (17.45 \times 10^{-5} \text{ RAD})^2\right]^{-1} \left[\frac{\pi (2.54 \text{ CM})^2}{4}\right]^{-1} (0.8)^{-1}$$

$$NER = 2.2 \times 10^{-5} \text{ WATTS/CM}^2 \text{ STER}$$

TABLE 3.2.1–9

FACSIMILE CAMERA SENSITIVITY
EFFECT OF SCAN PERIOD ON SENSITIVITY

1. ELECTRICAL BANDWIDTH

$$\Delta f = \frac{2\,\theta_V\,\theta_H}{\eta\,T\,\delta^2}$$

δ – SCAN ELEMENT DIAMETER (0.01°)

T – SCAN TIME

θ_V – VERTICAL SCAN ANGLE (5°)

θ_H – HORIZONTAL SCAN ANGLE (5°)

η – SCAN EFFICIENCY (0.97)

2. NOISE EQUIVALENT POWER

$$NEP = \sqrt{A\Delta f}\,/D^*$$

A – DETECTOR AREA (10^{-2} CM^2)

D* – DETECTIVITY 1.5×10^{12} CM $CPS^{1/2}/W$

3. NOISE EQUIVALENT RADIANCE

$$NER = NEP\left(\frac{\pi\delta^2}{4}\right)^{-1}\left(\frac{\pi D^2}{4}\right)^{-1} t^{-1}$$

t – OPTICAL TRANSMISSION (0.8)

FACSIMILE CAMERA SENSITIVITY

EFFECT OF SCAN PERIOD ON SENSITIVITY

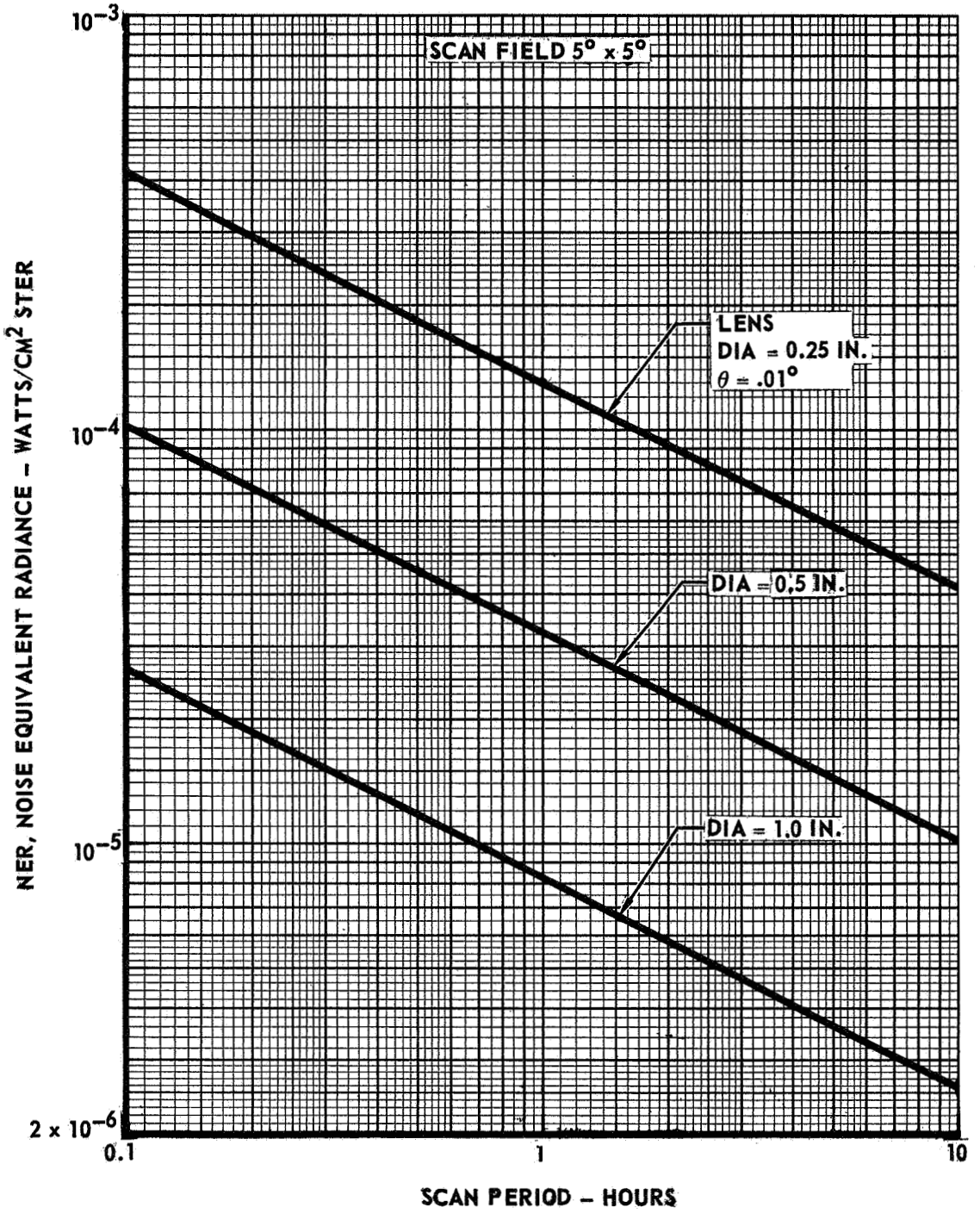

FIGURE 3.2.1–5

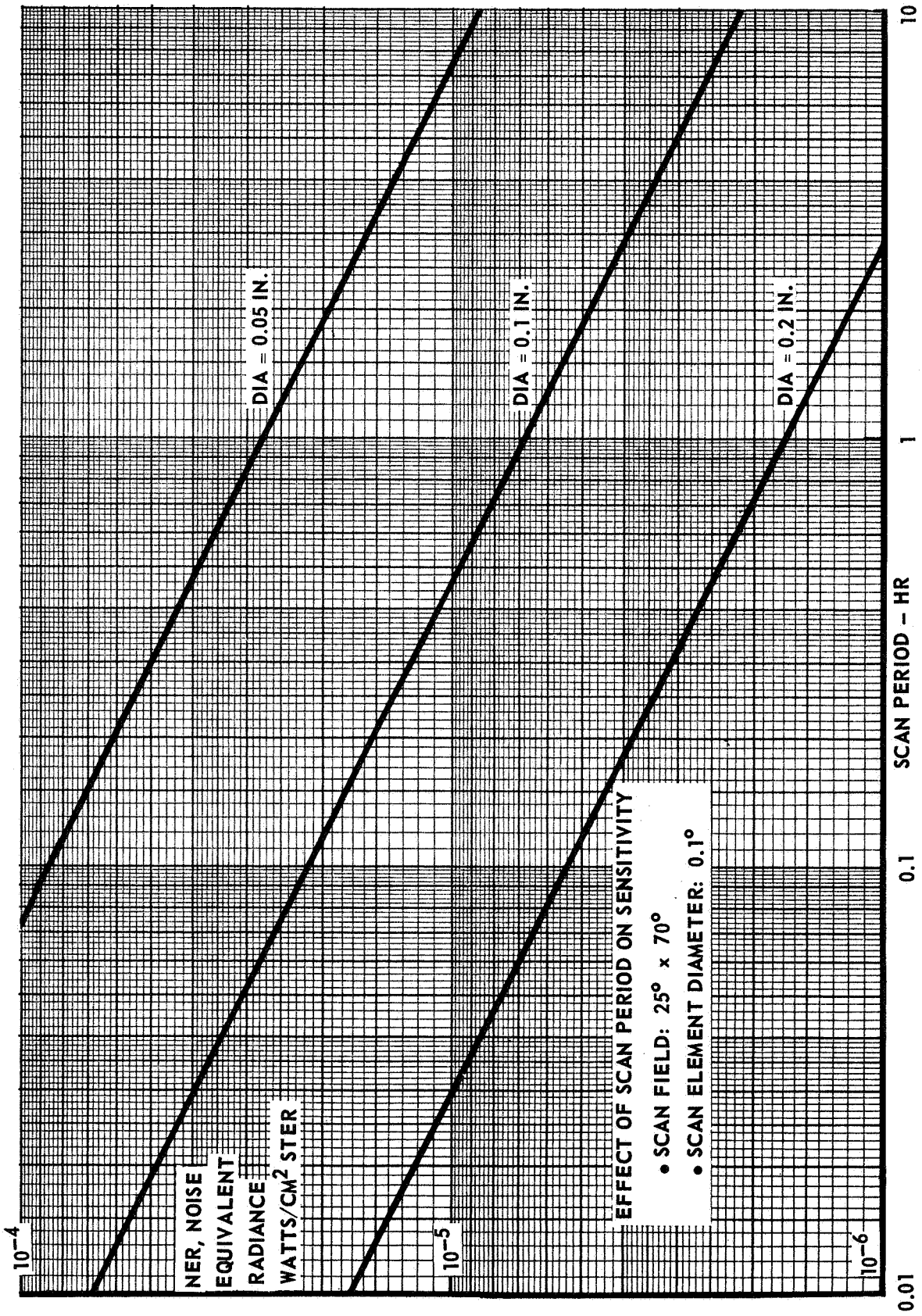
NER, NOISE EQUIVALENT RADIANCE WATTS/CM^2 STER
10^{-4}
10^{-5}
10^{-6}
DIA = 0.05 IN.
DIA = 0.1 IN.
DIA = 0.2 IN.
EFFECT OF SCAN PERIOD ON SENSITIVITY
• SCAN FIELD: 25° x 70°
• SCAN ELEMENT DIAMETER: 0.1°
0.01
0.1
1
10
SCAN PERIOD – HR

FIGURE 3.2.1–6

FACSIMILE CAMERA RESOLUTION
EFFECT OF DEPTH OF FIELD ON RESOLUTION

- CAMERA HEIGHT: 4 FT
- SCAN ELEMENT DIAMETER: 0.01°
- LENS DIAMETER: 0.5 IN.
- RESOLUTION LOSS FACTOR: 2

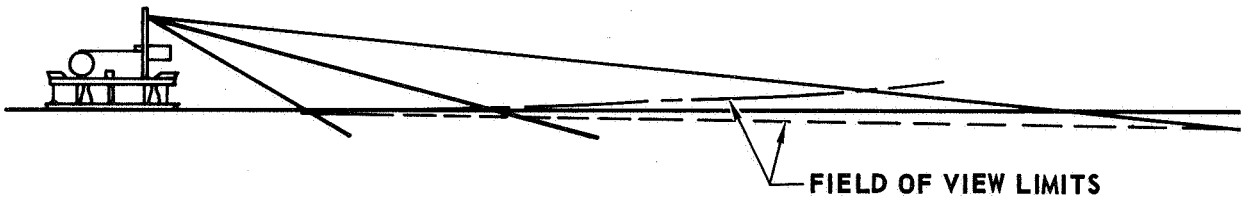

FIGURE 3.2.1–7

FACSIMILE CAMERA RESOLUTION

EFFECT OF FIXED AND VARIABLE FOCUS ON RESOLUTION

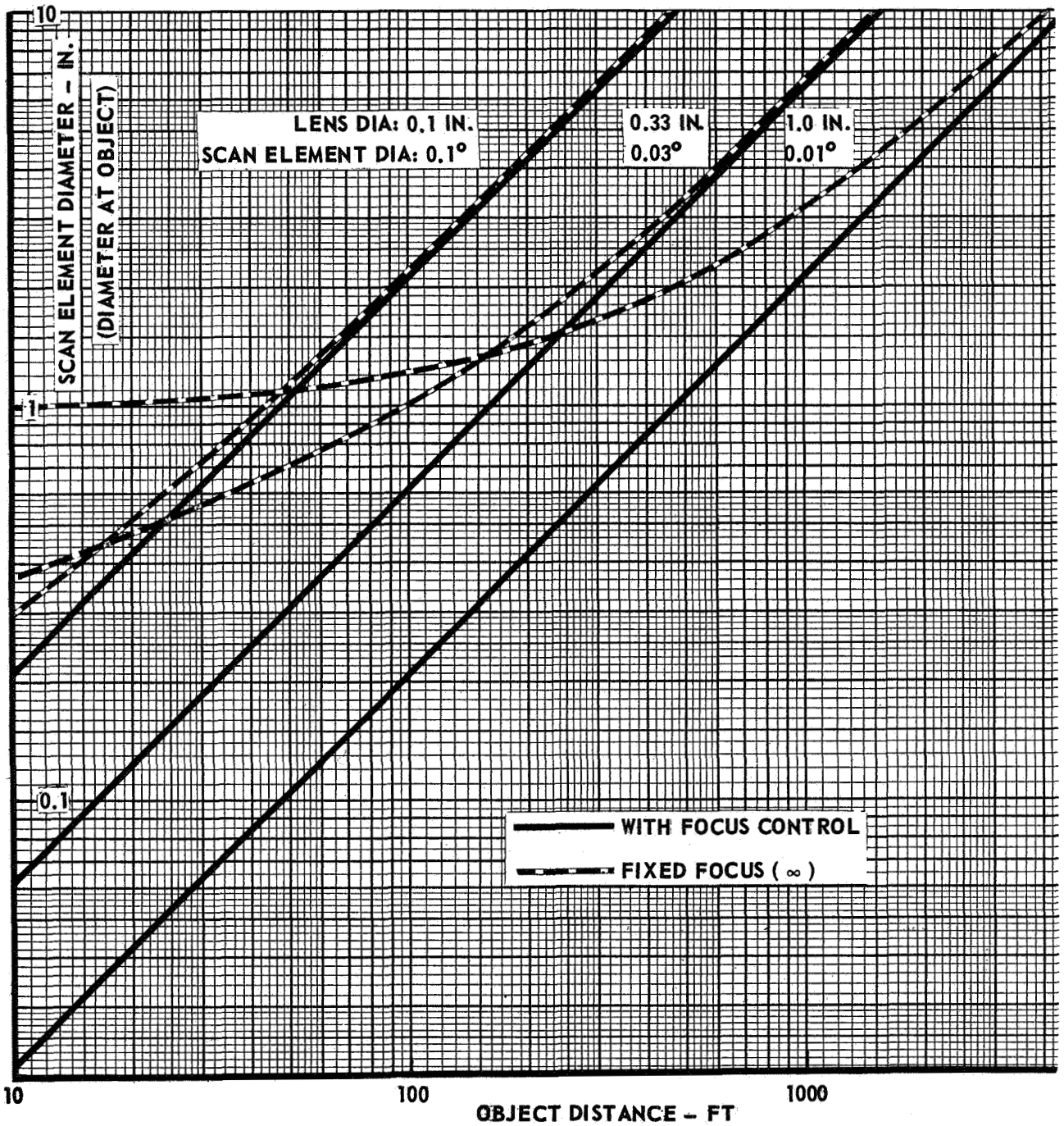

FIGURE 3.2.1–8

the lens diameter and the scan element diameter is approximately 0.01 inches x degrees in all three cases, these three cameras have nearly the same radiation sensitivity. That is, the luminance threshold is equivalent for the 3 cameras. The first low resolution camera, 0.1°, has a resolution which doesn't depend greatly on whether or not a focus control is used. (The solid line shows the resolution which will be obtained if a focus control is used and the dashed line the resolution without focus control. For the fixed focus the camera is in critical focus at infinity.)

For object distances of 10 ft. and greater only a small loss in resolution is incurred by using the fixed focus for the 0.1° low resolution camera as illustrated in Figure 3.2.1-8. The resolution loss for the 0.03° camera, however, becomes very significant at distances of 10 ft. Near 100 ft. the resolution loss becomes fairly small. For the 0.01° camera with the one inch lens, even at 100 ft. there will be a significant loss in resolution unless focus control is utilized. It is possible to obtain resolutions of a few hundredths of inch using the .01° system with a focus control whereas if the fixed focus is used for this camera, then the resolutions obtained is limited to more than one inch.

The depth of field was evaluated for a wide range of combinations of scan element diameter and lens diameter and resolution loss factors. The reason that these curves do not show a depth of field extending to infinity is that the resolution shown is a linear value rather than an angular value. This is illustrated by the geometry used for the depth of field calculations in Figure 3.2.1-9. The camera is in critical focus at a distance L and the scan element diameter in the object field is d. The defocused scan element diameter is defined as 2d for a resolution loss factor of 2. However, the value of d_2 must be larger than twice d at a distance twice the critical focus distance. The far field thus cannot extend over a factor of twice the critical focus distance for a resolution loss factor of 2. Therefore the far field limits in Figures 3.2.1-10 through -15 are not as useful for interpretation and for drawing conclusions as the near field limits for large critical focus distances.

FACSIMILE CAMERA RESOLUTION

GEOMETRY FOR DEPTH OF FIELD CALCULATION

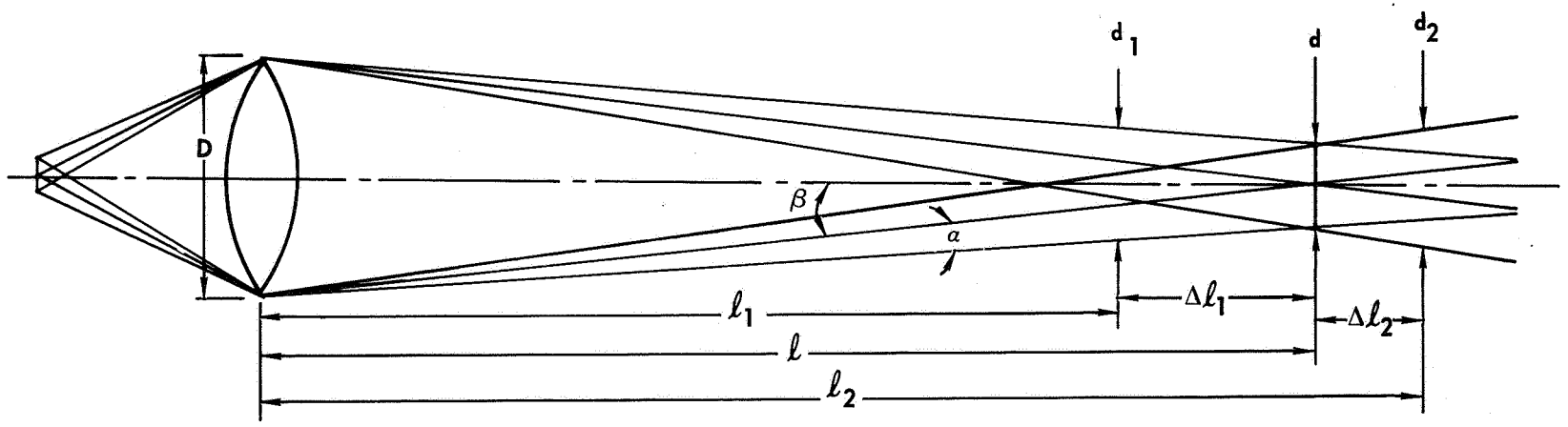

$d \sim 2\,\alpha\ell$	SCAN ELEMENT DIAMETER
$d_1 \sim 2(\alpha\ell_1 + \beta\Delta\ell_1)$	DEFOCUSED SCAN ELEMENT DIAMETER
$d_2 \sim 2(\alpha\ell_2 + \beta\Delta\ell_2)$	DEFOCUSED SCAN ELEMENT DIAMETER
$K = d_1/d = d_2/d$	RESOLUTION LOSS FACTOR
$D \sim 2\,\beta\ell$	LENS DIAMETER

FIGURE 3.2.1–9

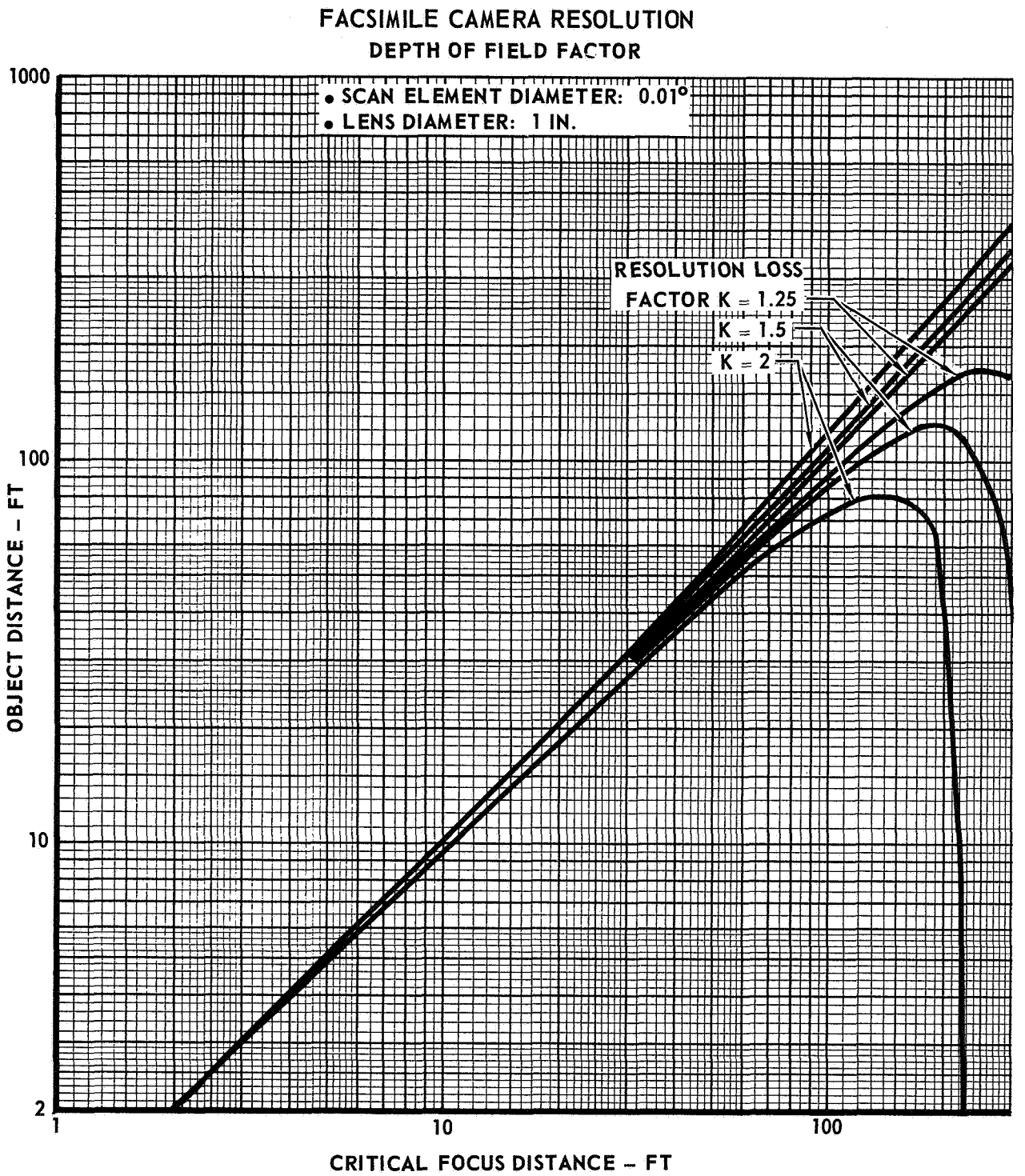

FIGURE 3.2.1–10

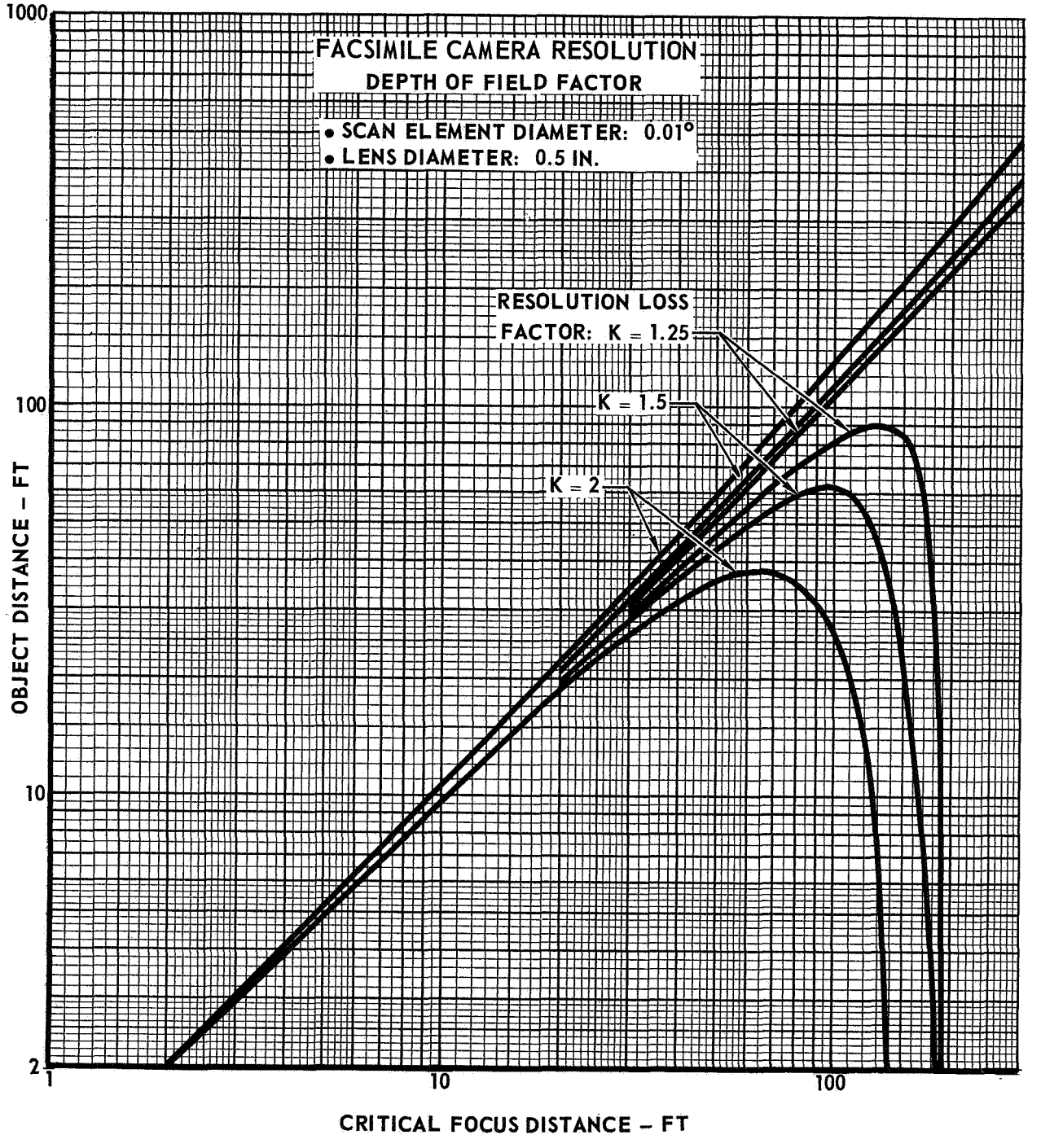

FIGURE 3.2.1–11

FACSIMILE CAMERA RESOLUTION

DEPTH OF FIELD FACTOR

- SCAN ELEMENT DIAMETER: 0.01°
- LENS DIAMETER: 0.25 IN.

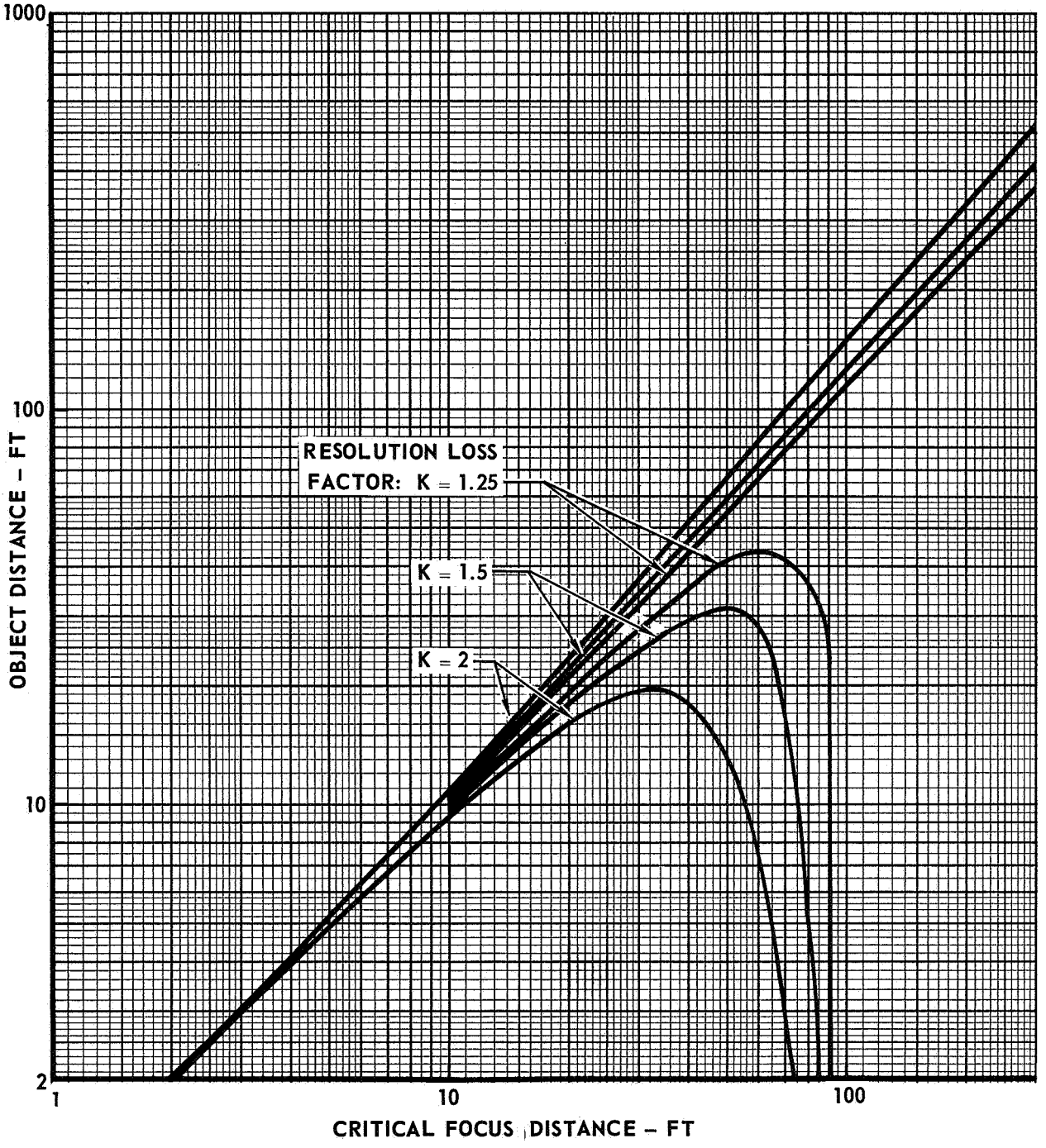

FIGURE 3.2.1–12

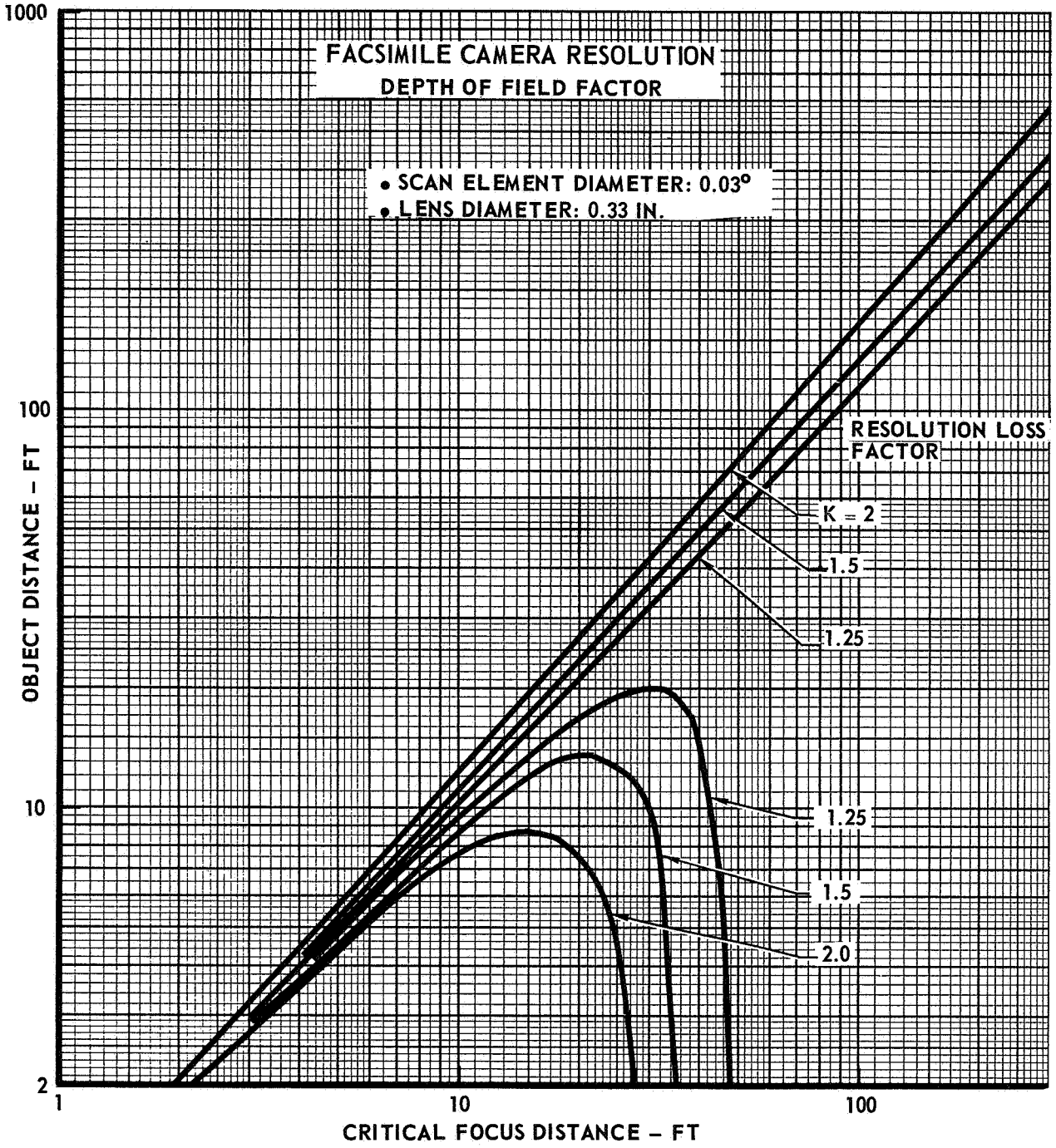

FIGURE 3.2.1–13

FACSIMILE CAMERA RESOLUTION

DEPTH OF FIELD FACTOR

- SCAN ELEMENT DIAMETER: 0.03°
- LENS DIAMETER: 0.17 IN.

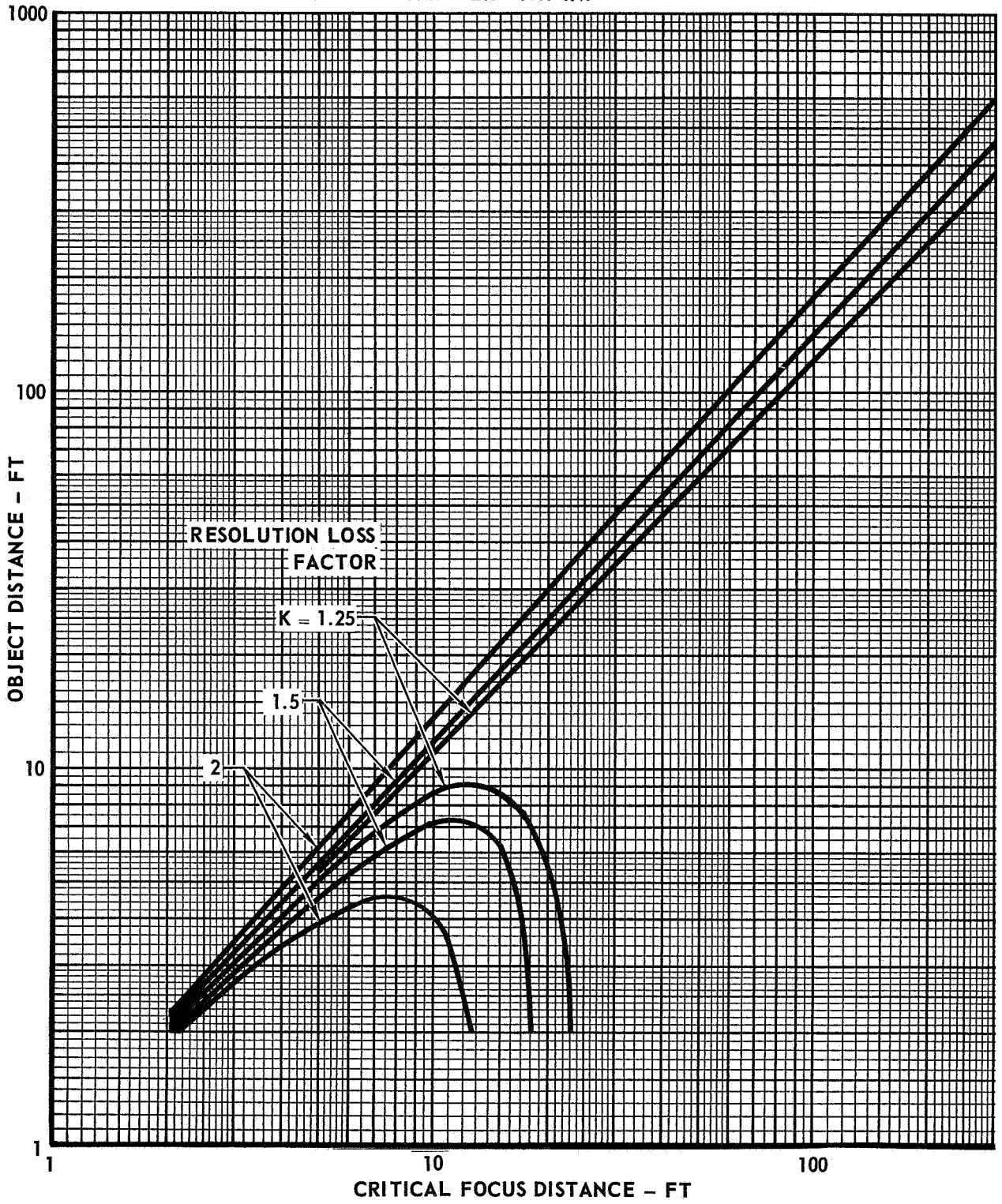

FIGURE 3.2.1–14

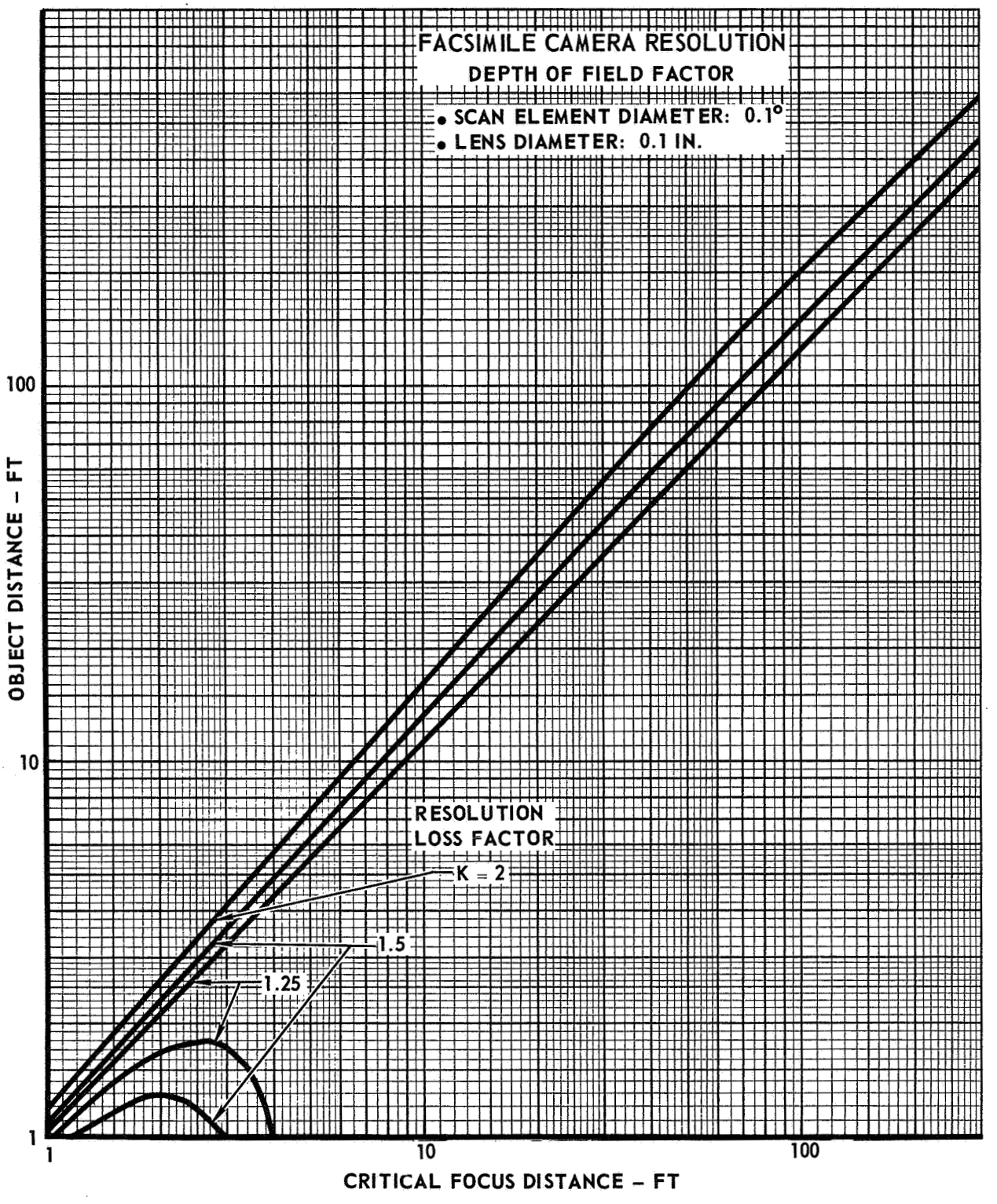

FIGURE 3.2.1–15

Figure 3.2.1-10 illustrates the extreme focus requirements for a 0.01° camera with a one inch lens diameter. If an object at 10 ft. is photographed, the depth of field will not even extend to 9 ft, and at 9 ft the camera will have to be refocused unless a resolution loss factor greater than 2 is tolerated. The use of a high resolution camera with a 0.01 degree scan element diameter and a lens diameter between 0.5 and one inch will thus require focus control in order to get good close up images of surface near the lander. On the other hand, for a 0.1° scan element diameter camera with a lens diameter of a tenth of an inch, Figure 3.2.1-15 and critical focus at an object distance of 10 ft, the resolution loss factor will be less than 1.25 even at a distance of only 1 ft. from the camera.

Several techniques are available for obtaining the information necessary to focus the camera. First, it can be assumed that the lander is sitting on a level surface and the camera can be focused for a mean level surface as illustrated in Figure 3.2.1-7. However, it can be seen in this figure that for a resolution loss factor of 2, it is not very likely that the surface will turn out to be within the rather narrow limits indicated by the two dashed lines. As already indicated the near field limit has more significance than the far field limit. However, even taking this into account, it is apparent that having a nominal focus for a level surface is not likely to produce good in-focus images for a surface with any degree of roughness or for a landing on slopes.

A second method is to focus the camera for the high resolution images based on the low resolution facsimile images. That is, first, the wide angle low-resolution images are taken and transmitted to Earth. Then using the shadows and the appearance of the surface around the spacecraft the distance to the various portions of the surface can be calculated.

A third alternate for obtaining the surface distance information necessary to focus the camera is to move the low resolution camera slightly and repeat a small fraction of the low resolution images to provide a stereo ranging capability. The stereo ranging capability is accurate enough that it will be possible to obtain distance information for objects on the surface and focus the camera to an accuracy better than the depth of field limits. The

technique used to calculate the stereo ranging capability, as listed in Table 3.2.1-10, utilizes a parallax factor of 2.5. That is, the ratio of the accuracy to which two stereo images can be matched is even better than the resolution of the individual images by a factor of 2.5. This value is a result of experimental measurements made in plotting surface altitude contours from aerial photographs. Figure 3.2.1-16 compares the stereo ranging accuracy with the depth of field limits. It is evident that small displacements of the wide angle camera which has a 0.1° scan element diameter can provide a stereo ranging accuracy which is more than adequate for focusing the camera.

Conclusions - It will be possible to obtain high resolution photographs of the Mars surface using a facsimile camera with a reasonable scan period. For close up views of the surface near the lander, it will be necessary to control the focus of the high resolution camera.

3.2.1.4 Lander Atmospheric Pressure Transducer. - Presently available pressure transducers appear to be suitable for making measurements of the diurnal and seasonal fluctuation of atmospheric pressure on the surface of Mars. These units are capable of withstanding both the sterilization procedure and the shock and vibration environment of launch and landing.

Measurements - Four quantities are important in determining the methods of measuring pressure on the surface of Mars. First, the range of pressure measurements; second, the accuracy with which the measurements are to be made; third, how often measurements are made; and fourth, the period or length of time over which they are made.

The range of expected surface pressure values corresponding to the spectrum of VM atmospheres is from 5 to 20 millibars. These pressure values take into account the effects of altitude variations. The effect of these variations can be estimated from the distribution of altitudes on Earth and on the Moon. The distribution of altitudes on Earth is described in Figure 3.2.1-17. The solid line shows the actual distribution of solid surface altitudes, ranging from 6 km below sea level to 4 km above sea level (the fraction beyond these limits is insignificant).

TABLE 3.2.1–10

FACSIMILE CAMERA RESOLUTION

STEREO RANGING CAPABILITY FACTOR

FACSIMILE CAMERA RESOLUTION

$$\Delta y = \frac{2(L\delta)}{0.7} \text{ FEET/LINE PAIR}$$

L– OBJECT DISTANCE

δ – SCAN ELEMENT ANGULAR DIAMETER

STEREO RANGING ACCURACY

$$\Delta L = \frac{\Delta y}{K} \frac{L}{b}$$

b – STEREO BASE

K – PARALLAX FACTOR (2.5)

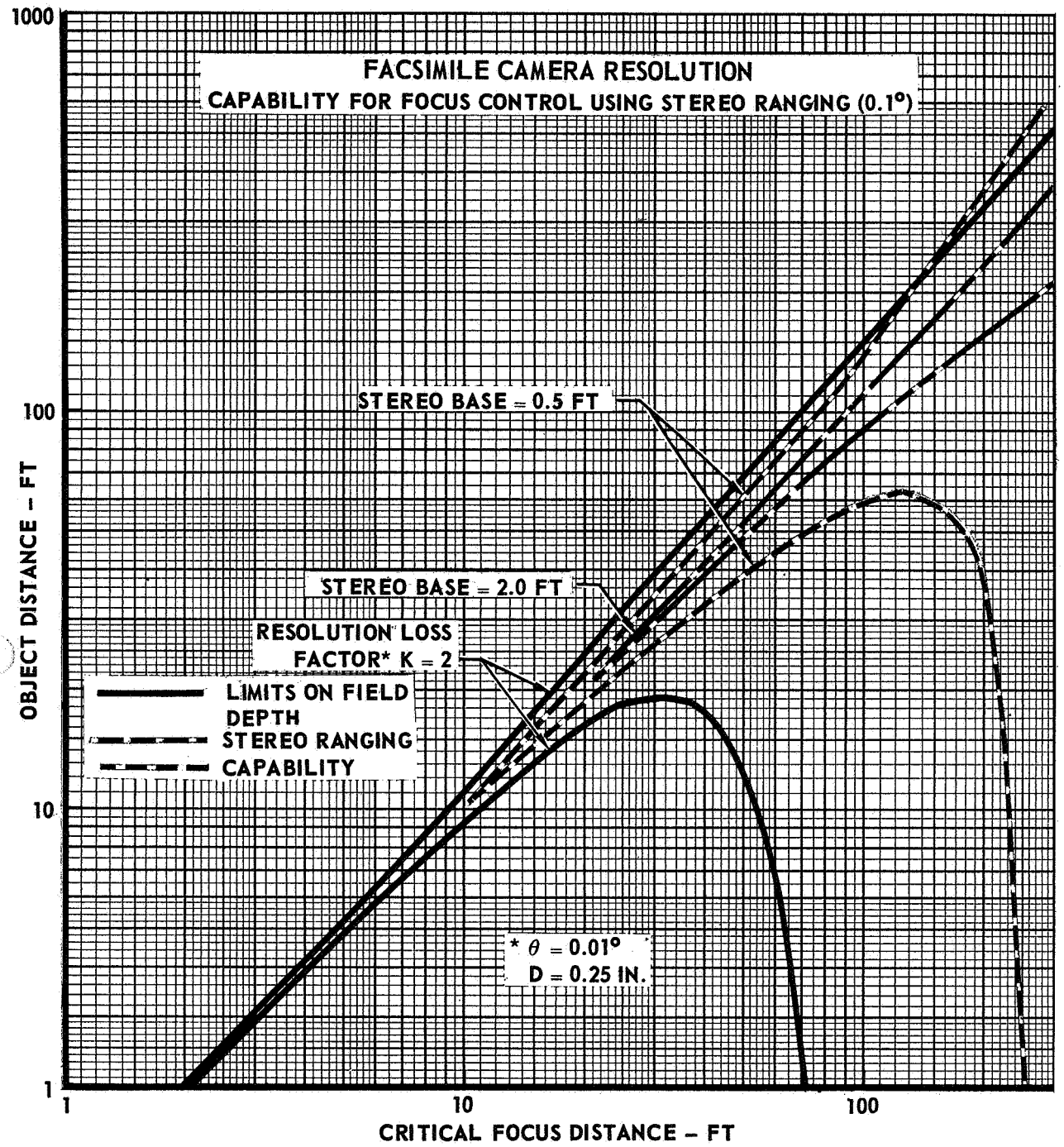

FIGURE 3.2.1–16

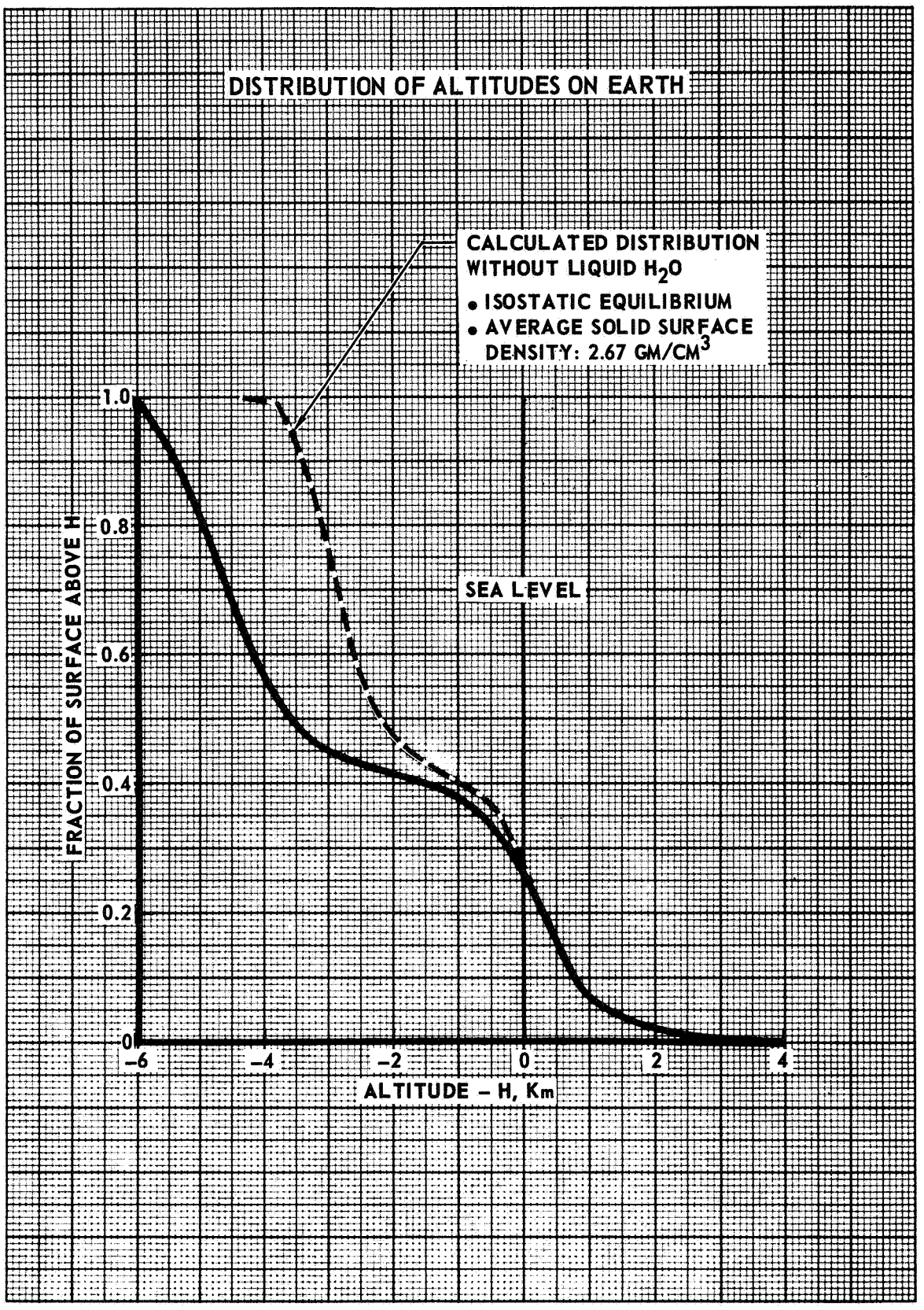

FIGURE 3.2.1–17

In the absence of the water in the ocean, it would be expected, however, that the fraction of the surface below sea level would not be as great. In order to calculate this factor, an isostatic equilibrium was assumed, that is, if the water were removed, the solid surface would rise until the weight of solid material was equal to the weight of water removed. An average density of 2.67 g/cm^3 was used for the solid material. The correction to the distribution is -2 to +6 km from the 50% point (-2.2 km). If this same distribution in altitudes occurs on Mars then it would be expected that the range in surface pressures would be from 2.7 mb to 22.3 mb, for the maximum altitude, as illustrated in Figure 3.2.1-18 for the 10 June 1968 model atmospheres.

The much more restricted distribution of altitudes on the Moon, however, as illustrated in Figure 3.2.1-19, indicates that a much smaller distribution of altitudes than -2 to +6 may be expected on Mars. If the distribution of altitudes on Mars ranges from -1.5 to + 4.5 Km, a range obtained by interpolation between the Earth and Moon, then the range in surface pressures will be 3.3 mb to 21.7 mb (0.048 to 0.315 psi). A more than adequate range for the pressure transducer thus appears to be 0 to 0.4 psi. (0 to 28 mb).

The second quantity of interest for making measurements of pressure is the accuracy with which the pressure measurements are made. If the diurnal variation of pressure is to be measured it will be necessary to make accurate surface pressure measurements. If only gross mean surface pressure measurements are required, less precise measurements will be satisfactory. The diurnal pressure variation is indicated by Figures 3.2.1-20 and -21. The values in Figure 3.2.1-20 are for the northern hemisphere vernial equinox, which is near an early 1974 landing date. In both cases it can be seen that the surface pressure varies by less than 0.6 mb (less than ± 6% of 5 mb). In order to have good resolution of the diurnal pressure variation, it will thus be necessary to have an accuracy of ± 1% of the measured value or better. Since the mean value of the surface pressure is so uncertain, and the accuracy of the pressure transducer is also the order of ± 1% of full scale, it will be necessary to have at least two pressure transducers with different ranges, so that one range is close to the value of the mean surface pressure. If the transducer temperature is measured in order to obtain an overall transducer

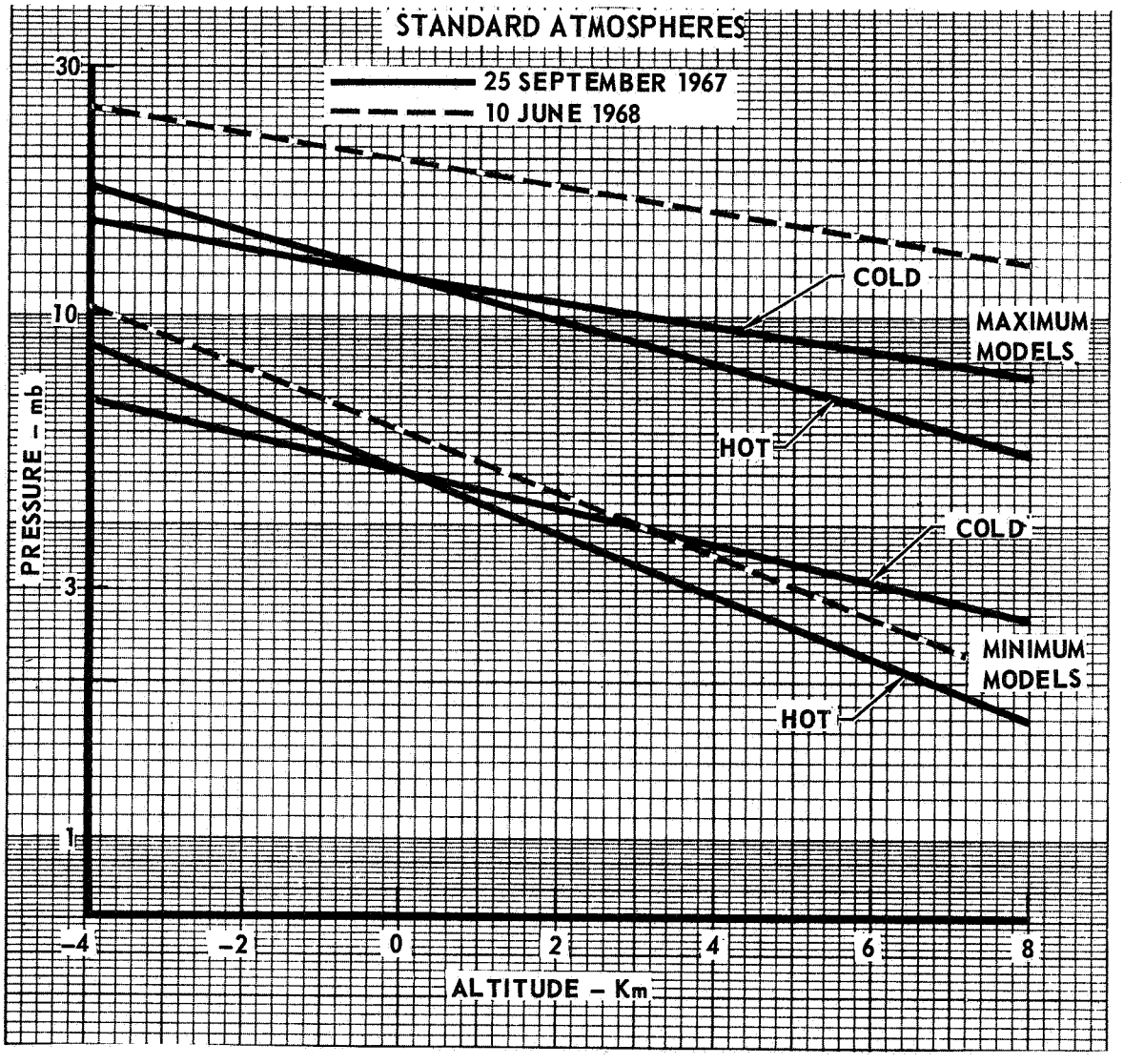

FIGURE 3.2.1–18

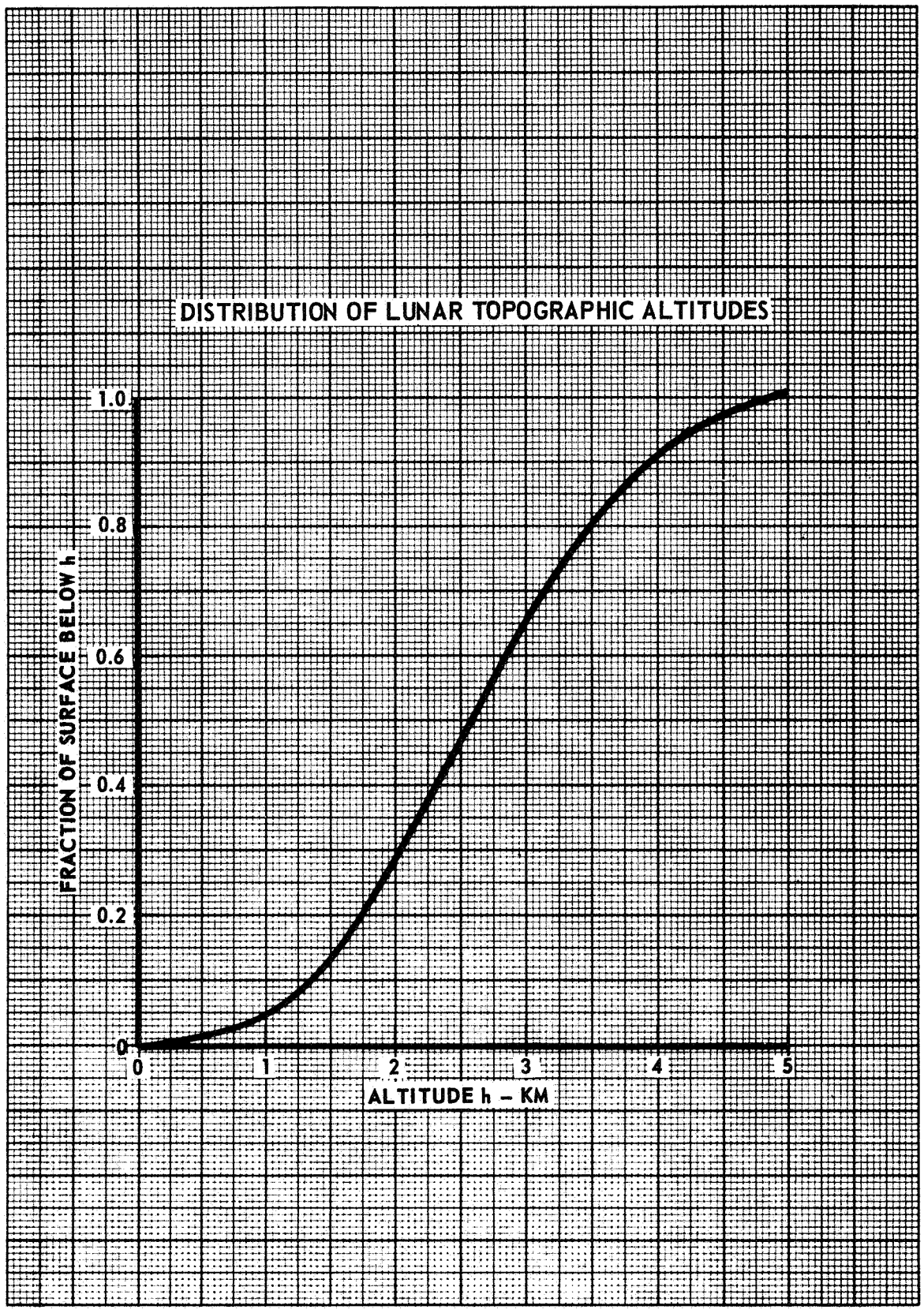

FIGURE 3.2.1–19

SURFACE PRESSURE

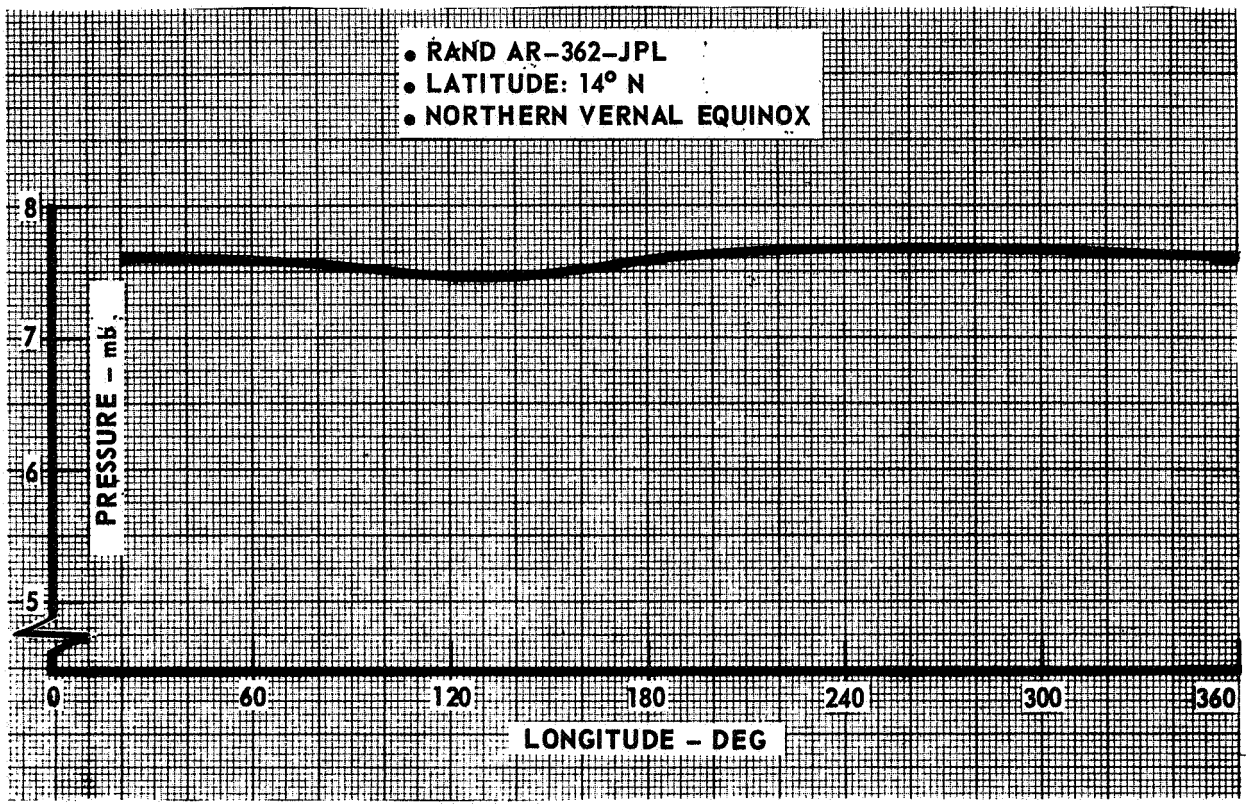

FIGURE 3.2.1-20

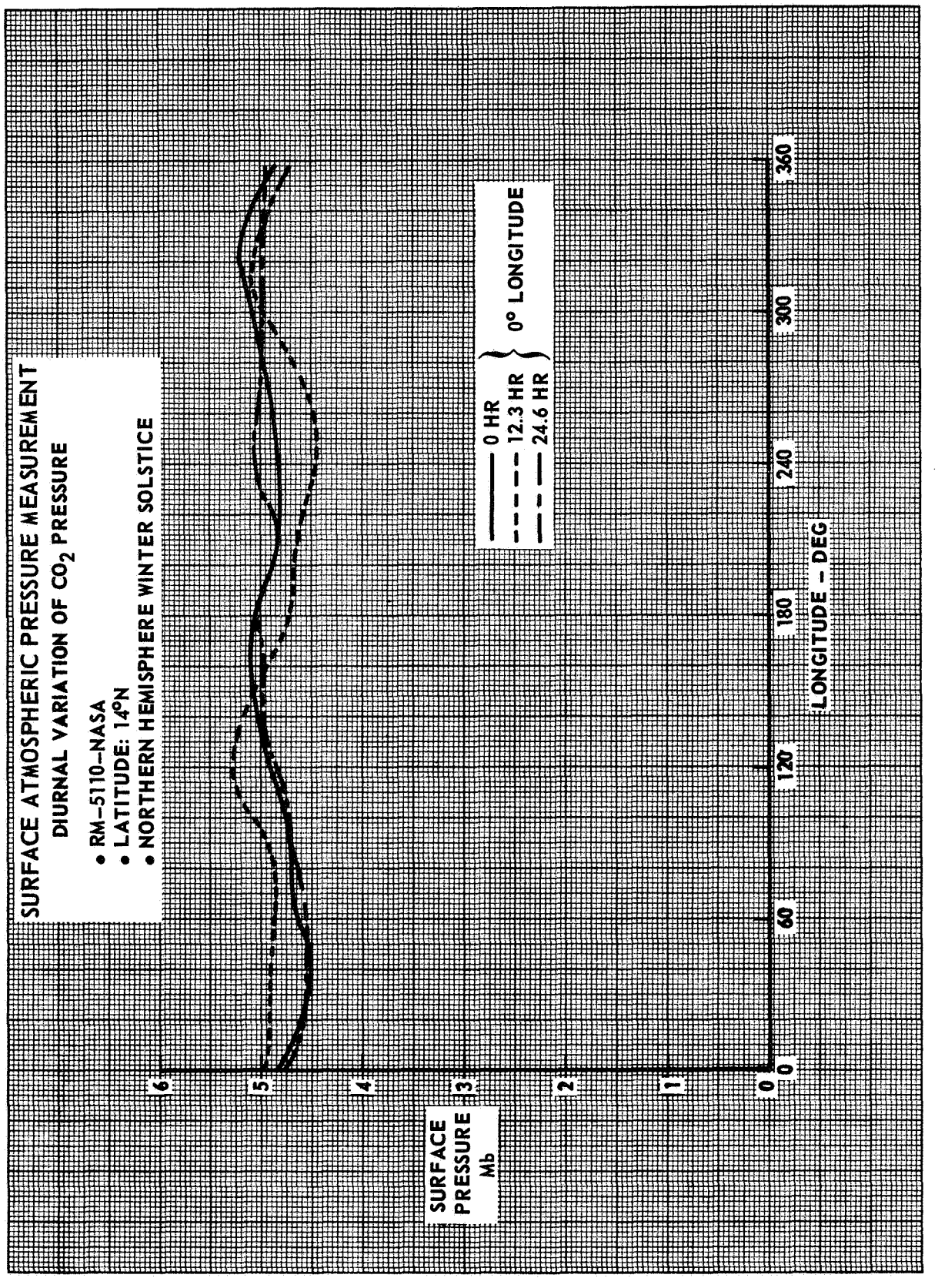

FIGURE 3.2.1-21

accuracy of approximately 0.5% and two units are used, 0-5 mb and 0-28 mb, the accuracy of the 28 mb unit will be ± 0.14 mb. This accuracy is equivalent to ± 2% for a 7 mb surface pressure measurement.

The diurnal surface pressure variations in Figures 3.2.1-20 and -21 were calculated using a general atmospheric circulation computer program, Reference 3.2.1-2 and -3. Further analysis with an increase in the number of layers may reduce the diurnal pressure variation below the values shown, but it is expected however, that there will still be a few tenths of a millibar variation in the surface pressure over a single diurnal cycle over most of the surface. It can be seen in Figure 3.2.1-21 that there is a much smaller diurnal variation at some longitudes than at others. This pressure variation with longitude is due to the high and low pressure areas caused by differential heating of the surface. That is, the dark areas absorb more sunlight and become warmer than the light areas, and also the areas which have the higher solar radiation input near noon are warmer than the other areas.

The next quantity of interest for making pressure measurements is the frequency with which the measurements are made. Since the diurnal fluctuation is so small compared with the accuracy of the instrument, a measurement period of 1 or 2 hours is necessary. However, other measurements are made every fifteen minutes, so for correlation with wind and temperature measurements it appears that it would be desirable to make surface pressure measurements every fifteen minutes.

The fourth and last quantity necessary for planning the pressure measurements is the total period or duration over which measurements are made. In order to observe the complete diurnal variation in surface pressure, at least one diurnal cycle is necessary. Since at some longitudes the pressure variation will be very low, it is desirable to make measurements over several diurnal cycles. If the high and low pressure area locations are such that there is only a small diurnal variation there will be a later time when the high and low pressure areas move so that the variation in pressure will increase. In order to observe the seasonal variation of pressure it will be necessary to make measurements at widely separated times. This is due to the fact that the seasonal variation in pressure is not extremely large compared

with the diurnal variation and also due to the pressure variation caused by the movement of the high and low pressure areas.

Figure 3.2.1-22 illustrates the calculated variation in surface pressure due to the melting and freezing of the polar caps. Near a landing early in the 1974 opportunity the polar caps will be large and a significant amount of the atmospheric carbon dioxide is expected to be in the polar caps so that the surface pressure will be low. After a period of 120 to 150 days, the total amount of CO_2 in both polar caps is reduced and the amount of CO_2 in the atmosphere has been increased. This causes the surface pressure to increase. Even over this long period, only about 1 mb seasonal change in surface pressure is expected. Since the fluctuation due to the weather is a few tenths of a millibar, it will be necessary to make measurements over a large fraction of the 120 to 150 days to be certain that the change in surface pressure observed is due to seasonal rather than weather effects.

Instrument Characteristics - The pressure transducer characteristics summarized in Table 3.2.1-11 illustrate that this unit can withstand the sterilization procudure, since the unit has a temperature tolerance of up to + 135°C when non operating. Also, the unit is not affected by the gases used during sterilization. In addition, the ability to withstand shock, vibration, and acceleration is more than sufficient for the expected soft lander dynamic environment. It would be desirable to have a better accuracy than 1% of full scale. Most of the 1% inaccuracy in the reading is due to the temperature variation of the unit. By simply monitoring the temperature of the transducer and transmitting the temperature along with the pressure data, it will be possible to correct for most of the inaccuracy due to temperature fluctuations. The primary remaining sensor error will be due to non-linearity, which is 0.3% of the full scale.

Thus, a 0.5% error (full scale) is a reasonable value for the pressure sensor. If two units are used, one with a range from 0 to 7 mb, and the other with a range of 0 to 27 mb, then the corresponding errors for a half of a percent accuracy are 0.035 and 0.135 mb. The 0.035 mb is more than sufficient for measuring a diurnal fluctuation of a few tenths of a millibar. If the surface pressure is higher it is possible that the diurnal variation in pressure will be greater so that the 0.135 mb accuracy will be sufficient for higher pressures.

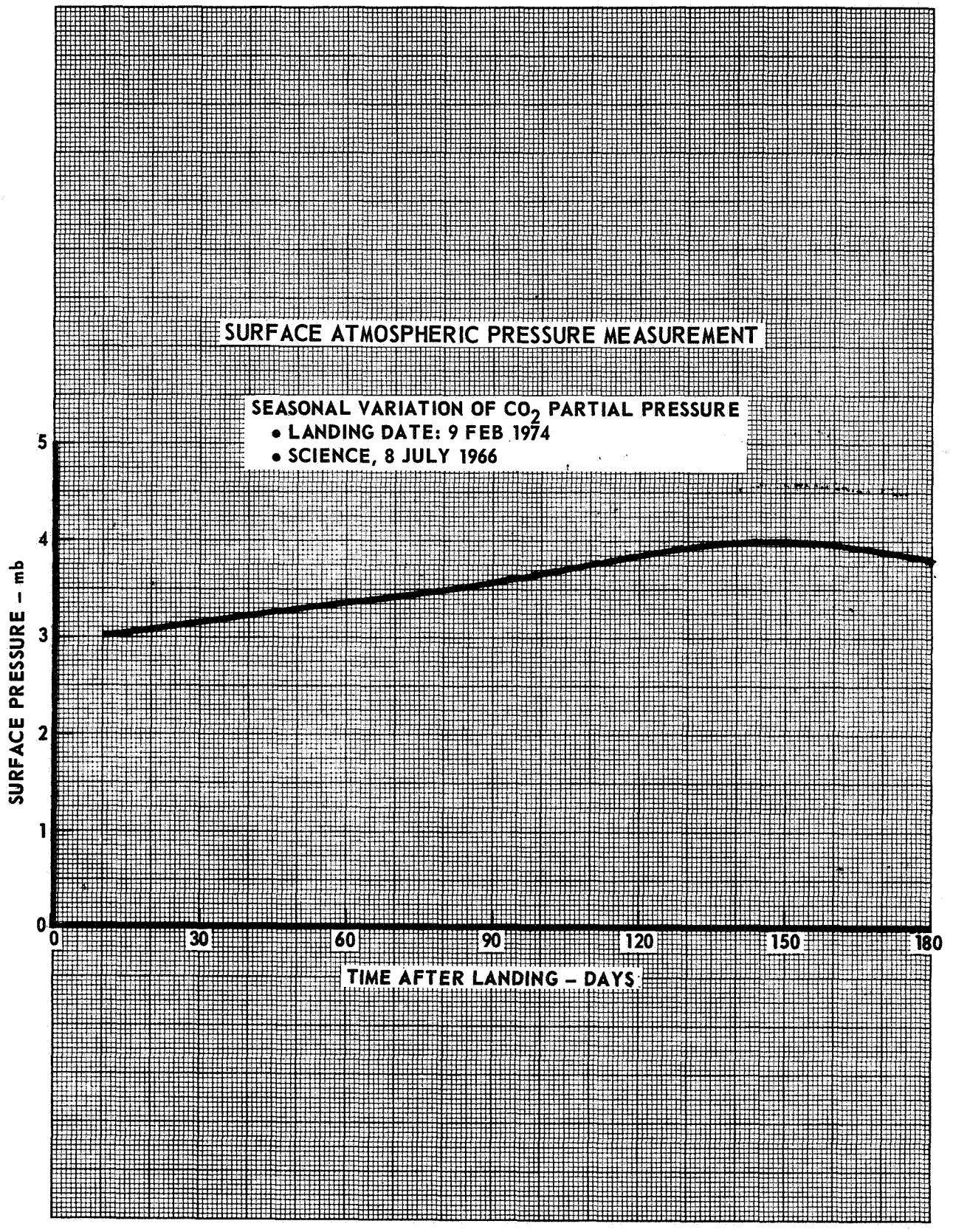

FIGURE 3.2.1–22

TABLE 3.2.1–11

PRESSURE TRANSDUCER CHARACTERISTICS

• VARIABLE CAPACITANCE UNIT

QUANTITY	VALUE
RANGE	0–7 MB, 0–28 MB (~0–0.1 PSIA, 0–0.4 PSIA)
SIZE, IN.	2 DIA x 4
POWER	1.4 W AT 28 V
ACCURACY	
OVERALL ACCURACY	1% (RSS)
TEMPERATURE STABILITY	
ZERO SHIFT	0.01% FULL SCALE/°F
SLOPE CHANGE	0.01% FULL SCALE/°F
NON LINEARITY	0.3% FULL SCALE
ENVIRONMENT TOLERANCE	
SHOCK	300 g (0.5 MSEC)
VIBRATION	25 g (RANDOM VIBRATION 20 TO 2000 CPS)
ACCELERATION	150 g
TEMPERATURE	–80°F TO +275°F (+135°C) NON-OPERATING –65°F TO +200°F OPERATING
OVERPRESSURE	20 PSIA
BURST PRESSURE	> 200 PSI
CORROSIVE GAS	NOT AFFECTED BY ETHYLENE OXIDE AND FREON

The small size of the unit is illustrated in Figure 3.2.1-23 and the principle of operation is shown in Figure 3.2.1-24. As gas is emitted to the chamber on the left, the flat center plate between the two reference plates deflects to the right. The capacitance between the two right hand plates will therefore increase while the capacitance between the left hand plate and the center plate will decrease. The dielectric constant of the atmosphere will not significantly affect the measurements since it will cause a change of the capacitance of less than .001 to .002%. A zero shift, due to a small pressure change on the evacuated side from outgassing and leakage, is expected. This small change in calibration can be made prior to and during the flight. Ths use of a barium or other type of getter may be feasible, to eliminate the need for this change in calibration. Even without a getter, the zero shift for a 0.1 psi full scale unit is less than 0.5% in a 6-month period.

As can be seen in Figure 3.2.1-24, the support of the center plate is much thinner than the center plate, enabling the center plate to deflect as a nearly free plate. This provides a good linearity between the capacitance and surface pressure and also reduces the effects of strain induced in the plate by the external portion of the transducer. A capacitance bridge, Figure 3.2.1-25, is used to measure the deflection of the center plate. Since the temperature tolerance of the standard unit goes down to only -65°F it will be necessary to locate the pressure senser in the equipment compartment where the temperatures ranges from 0 to 100°F rather than outside, where the temperature can go as low as -190°F. The use of a short vent tube to the atmosphere will minimuze the temperature corrections required for the pressure measurements.

Conclusions - The variable capacitance diaphragm pressure transducer appears to be suitable for making observations of the diurnal and seasonal variations in surface pressure on Mars. If the unit is located in the equipment compartment of the lander, special provisions will not have to be made for developing a unit which will tolerate extremely low temperatures such as -190°F. By using dual range instruments it will be possible to observe the diurnal fluctuation and surface pressure, if this fluctuation is as large as is presently predicted. It may not be possible to observe the seasonal fluctuation in surface pressure unless the mission duration is a large fraction of the 120 to 150 days required for a significant variation.

SURFACE PRESSURE TRANSDUCER SIZE
(CAPACITANCE TYPE)

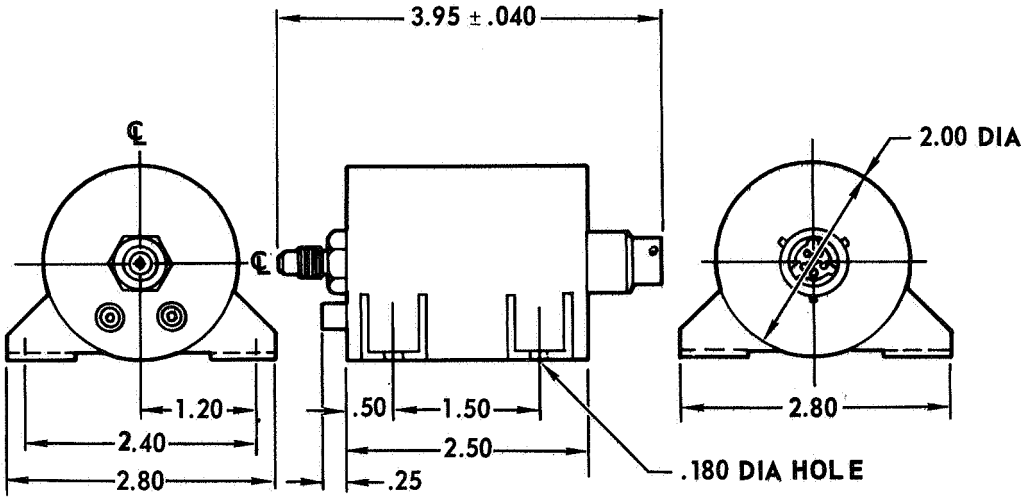

FIGURE 3.2.1–23

VARIABLE CAPACITANCE PRESSURE TRANSDUCER

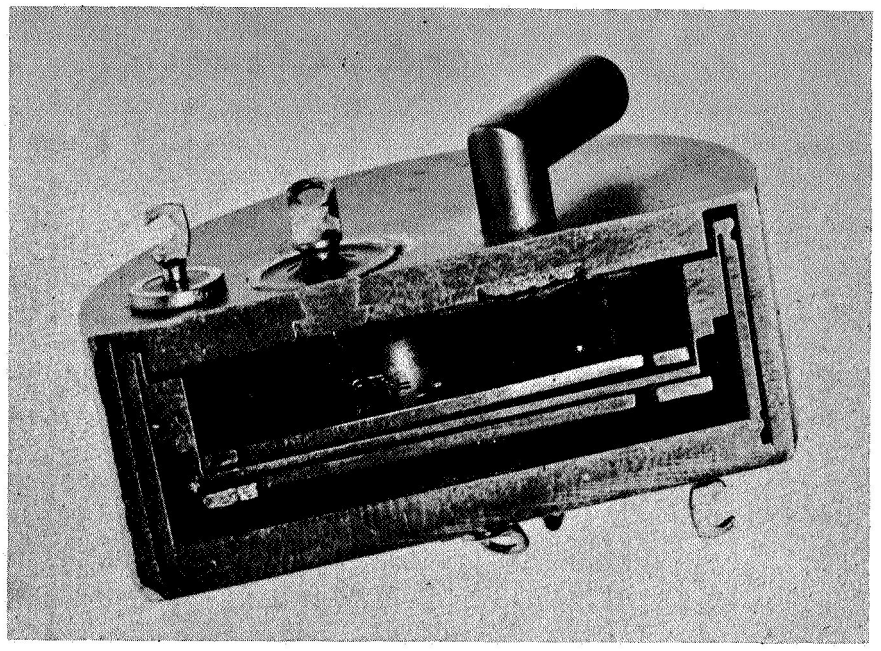

FIGURE 3.2.1–24

PRESSURE TRANSDUCER BLOCK DIAGRAM

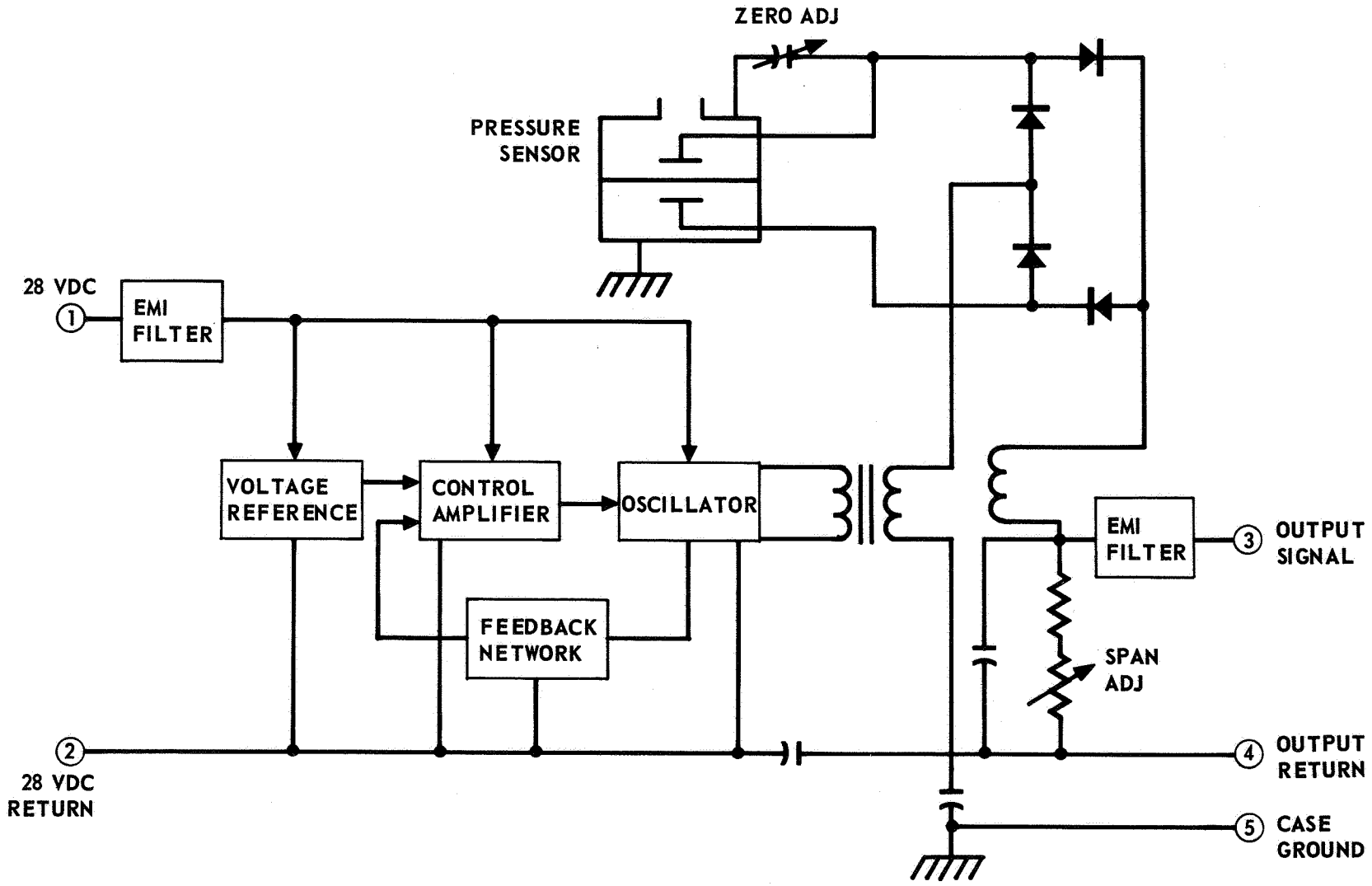

FIGURE 3.2.1–25

3.2.1.5 Lander Atmospheric Temperature Transducer. - The measurement of the surface atmospheric temperature and its diurnal variation is not expected to offer any serious problems. The measurement of the vertical temperature profile near the surface, however, is expected to be difficult, since the change in temperature with height over the first two meters can be very small.

Measurements - The range of expected temperatures for the surface atmosphere for a typical set of conditions is approximately - 102°C to + 19°C at 10° N latitude. These values were obtained from a calculation using a surface thermal conductivity of 6×10^{-5} cal/(cm sec)°K, an emissivity of 0.85, and a solar radiation absorption factor of 0.15. A slightly lower minimum temperature of -104°C was obtained by Leighton & Murray, Reference 3.2.1-4, for the 10° N latitude and a landing time near northern vernal equinox, while for a landing at 30° N latitude, the minimum temperature is -108°C, Figure 3.2.1-26. At the equator, the maximum temperature range, including both seasonal and diurnal effects, is expected to be approximately -105°C to +45°C. A range of -130 to +50°C should thus be more than adequate for landings at low latitudes, even for long duration missions.

The desired temperature measurement accuracy is determined by several factors. First, one quantity related to the suitability of the surface environment to support microorganisms is the fraction of the day during which the surface (and the near surface atmosphere) has a temperature greater than 0°C. If the peak temperature only goes to +5°C, as opposed to the calculated value of 19°C, an accuracy of much better than 5° will be necessary to accurately determine the time when the temperature is over 0°C.

A second factor which determines the temperature measurement accuracy desired is the diurnal fluctuation in temperature. The temperature accuracy should be much better than the diurnal temperature range. This is not a problem, since the calculated range is 121° near northern vernal equinox (-102°C to +19°C) and the diurnal change at a different season (solstice) is also 121°C, Reference .

The last factor which determines the desired accuracy for the temperature measurement is the variation in temperature with height near the surface. If

MINIMUM DIURNAL TEMPERATURE

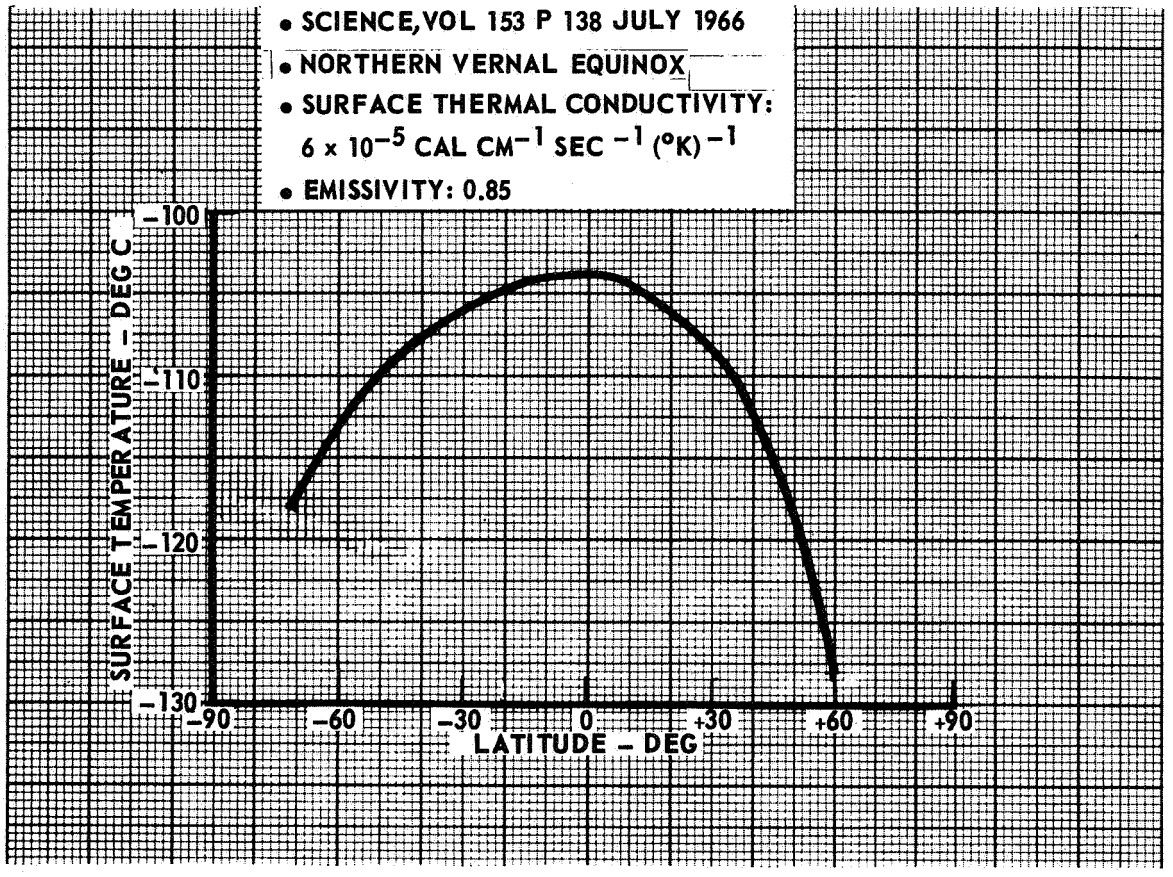

FIGURE 3.2.1–26

two temperature sensors are used, one at only a few centimeters from the surface and the other at one to two meters above the surface, the expected temperature difference between the two heights may be less than the measurement accuracy of the transducer. A typical temperature profile for the Earth's atmosphere, over a surface which does not have vegetation, has very small temperature differences at these heights, typical values being less than 2°C, Figure 3.2.1-27. Since the thermal conductivity of the Mars atmosphere is expected to be approximately 1/3 that of the Earth's atmosphere, the Mars near-surface temperature profile may have slightly larger temperature differences than the Earth's atmospheric temperature profile shown in Figure 3.2.1-27. Even with a temperature difference of 6°C, however, it can be seen that an accuracy of ± 2% of the absolute temperature (± 5.5°C at 0°C) will make it impossible to measure the variation in temperature with height.

It is possible that a larger temperature gradient will be present on Mars, since the diurnal temperature variation is so great. However, it may be necessary to use two temperature sensors in a bridge circuit in order to detect the temperature differences with height above the surface.

The frequency with which atmospheric temperature measurements are made is determined by the maximum rate of the diurnal variation in temperature, which is approximately 0.4°C per min, in the morning. Thus, if a 10 to 15 minute period is used between measurements, the change in temperature from one measurement to the next will be 4 to 6°C, a reasonable value in comparison with the expected accuracies for the temperature measurement.

Instrument Characteristics - A platium wire resistance sensor has the advantage that the resistance varies linearly with temperature and has a very high accuracy, as good as 0.5°C. The temperature measurement accuracy is thus limited not by the sensitivity of the sensor but rather by the technique used to measure the sensor output. A typical platinum wire resistance sensor has a resistance, as shown in Figure 3.2.1-28, which varies from 460 to 1210 ohms for a temperature range from -130°C to +50°C. If the resistance is measured with a ± 1% accuracy, then the absolute temperature will be accurate to within ± 1%. It is evident than an accuracy of better than ± 1% would be useful in interpreting temperature data. However, whether or not an accuracy better than the ± 1% is practical is yet to be determined.

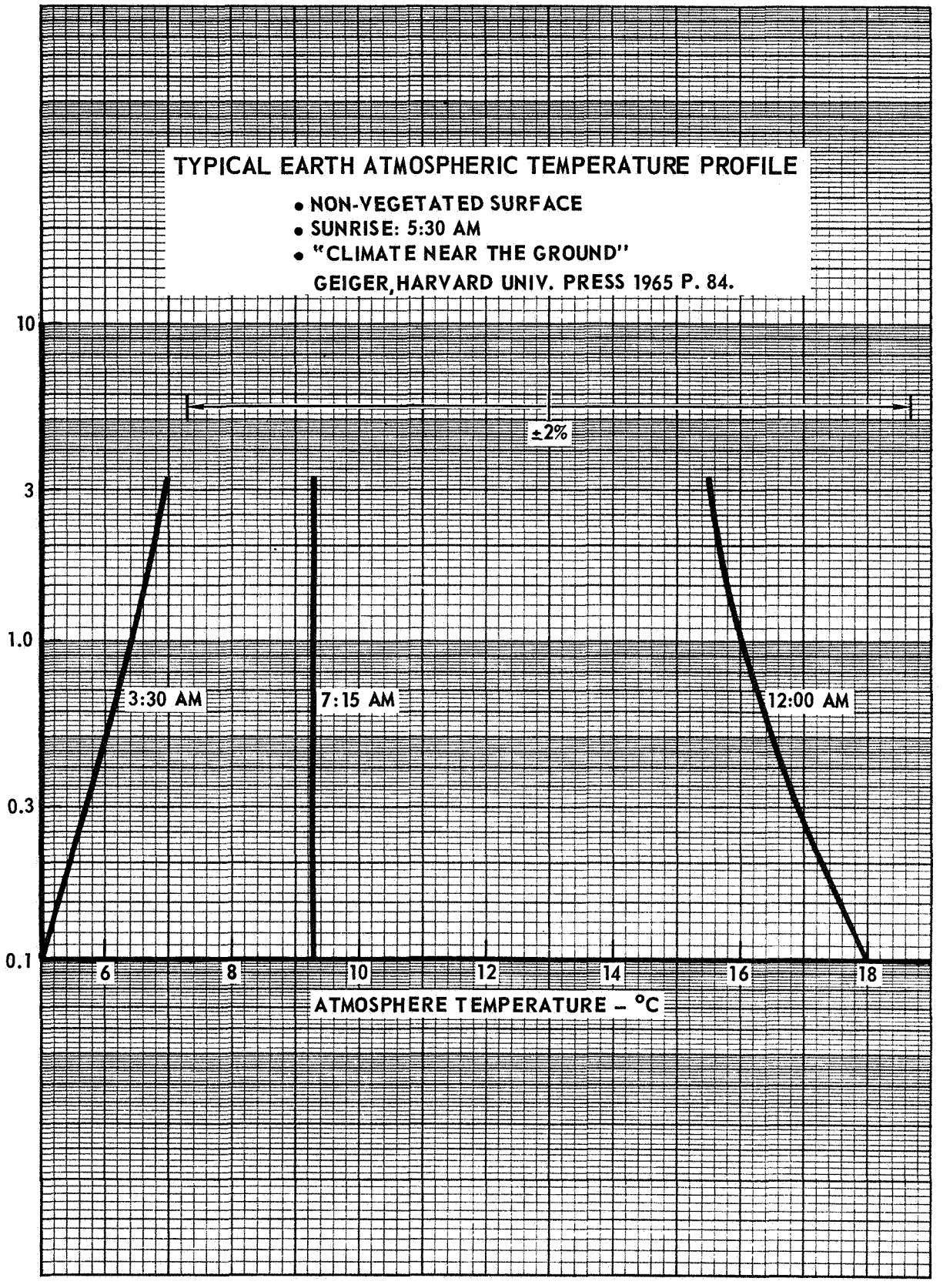

FIGURE 3.2.1–27

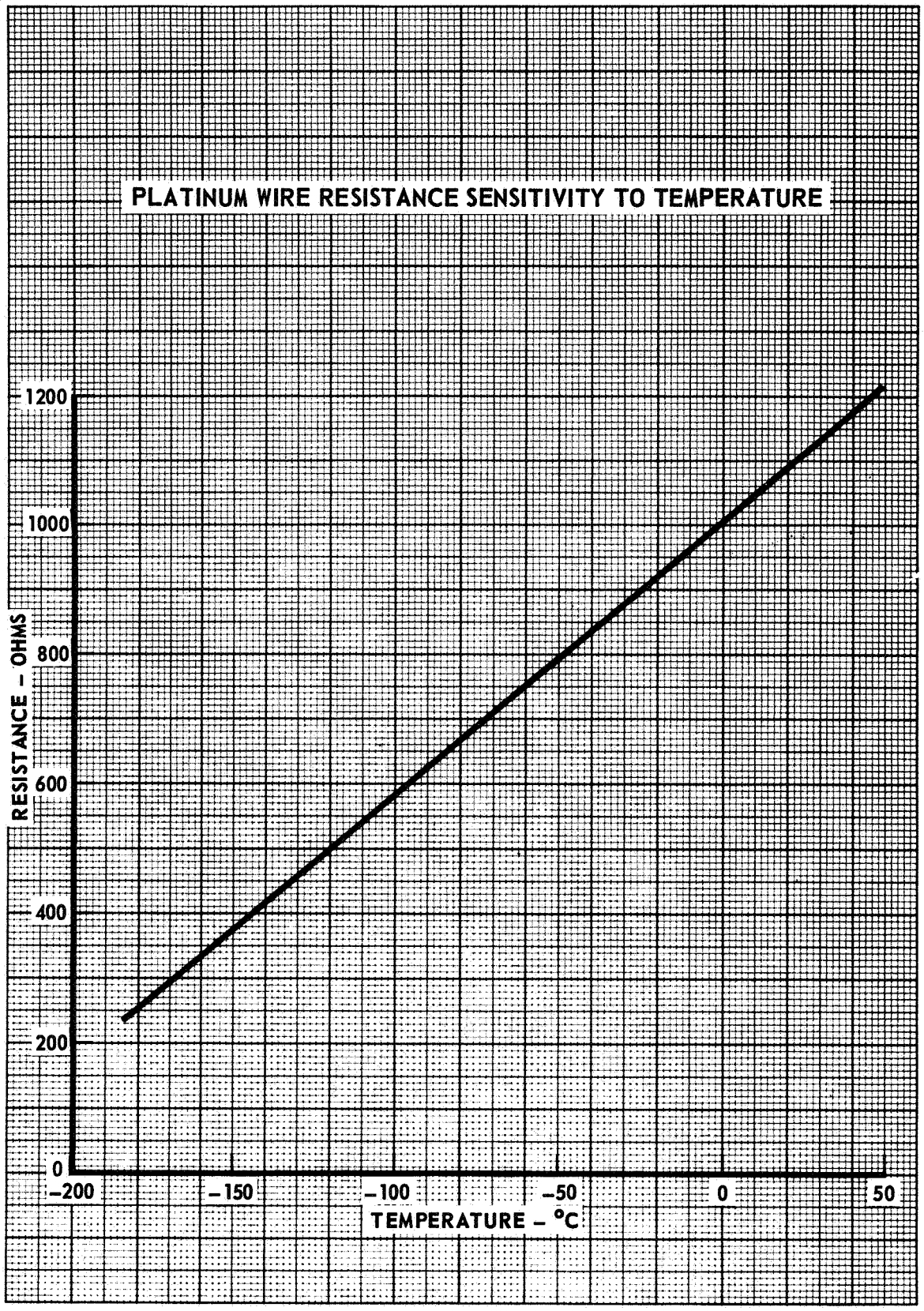

FIGURE 3.2.1–28

One of the primary instrument problems associated with measurement of the atmospheric temperature is obtaining a sensor temperature which is equal to the atmospheric temperature rather than a temperature which is determined by the sensor container. Radiation shields will be required around the sensor to prevent the sunlight from directly impinging on the temperature sensor, and consideration of the thermal properties of the shield around the sensor will be important.

Conclusions - It is not expected that any serious difficulties will be encountered in measuring the atmospheric temperature of Mars to an accuracy of ± 2% of the absolute temperature. At 0°C, however, the 2% accuracy is equivalent to a temperature accuracy of ± 5.5°C which will severely limit the interpretation of the atmospheric temperature data. A consideration of techniques for obtaining a higher accuracy is desirable, and in addition the determination of a technique for measuring the small temperature differences due to the change in temperature with height above the surface would be useful.

3.2.1.6 Lander Wind Sensor - At the time of the 1974 landing near the northern vernal equinox it is expected that the wind velocities at the surface of Mars will be low. Therefore, a wind sensor with a threshold value as low as 1 to 2 meters per second will be necessary, in order to measure wind velocities for a significant fraction of the time, based on the calculated surface wind velocity distribution of Leovy and Mintz, Reference 3.2.1-3. In order to keep the total amount of data for the wind measurement to a reasonably low value, wind measurements can be made over a fifteen minute period. During this period, the maximum, the minimum, and the average wind can be determined, and these three values, along with the instantaneous wind at the end of the fifteen minute period, can be transmitted. The instantaneous wind reading in two directions is necessary in order to determine the direction of the wind at the end of the fifteen minute period.

Measurements - The general numerical atmospheric circulation calculation of Leovy and Mintz, Reference 3.2.1-3, was used to determine the surface wind velocity distribution in Figure 3.2.1-29. The low winds near the northern vernal equinox correspond to a landing early in the 1974 opportunity. The winds, for a two meter altitude were obtained by taking the winds, at approximately 1 km, given in the report, and dividing them by the recommended value of two.

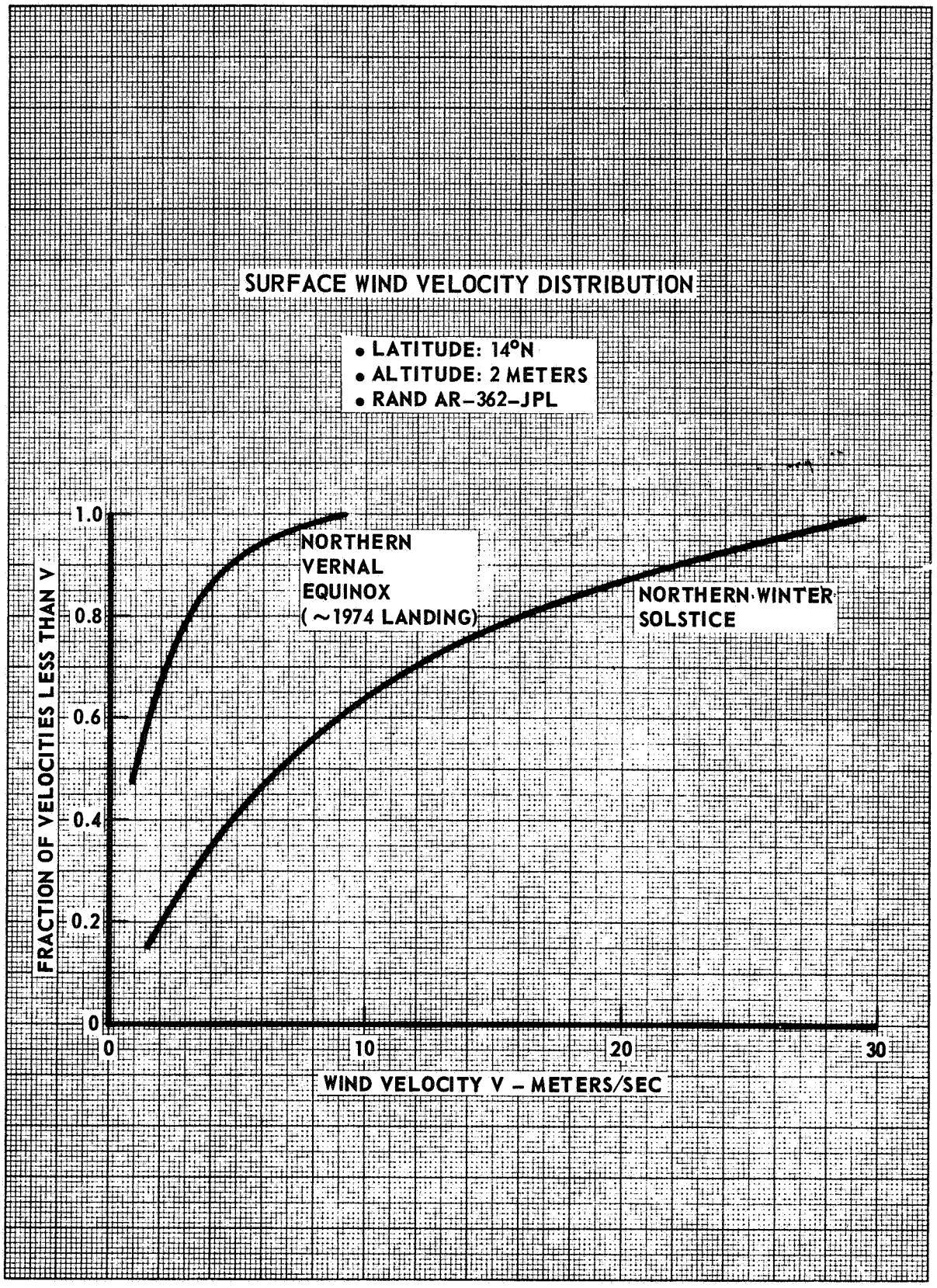

FIGURE 3.2.1–29

If a threshold wind velocity of 5 mps is used for the wind sensor, then the threshold will be exceeded only 10% of the time. Even a 1 meter per second threshold would be exceeded only 50% of the time, indicating that the total time during each 15 minute period that the threshold of the sensor is not exceeded should be transmitted along with the wind data.

The large seasonal variation of the winds is illustrated by the fact that for the 14° N latitude the winter solistic winds are more than three times as strong as those at the vernal equinox in Figure 3.2.1-29. Since the winds were evaluated at only a few discrete times in Reference 3.2.1-3 it was not possible to calculate the wind velocity distribution with time at a given location. In order to approximate this distribution, however, the distribution of winds as a function of longitude at a given latitude was used in Figure 3.2.1-29. The results of calculating the general atmospheric circulation indicated that in many cases there will be very large diurnal variations in the wind velocity.

The wind velocity distribution obtained from the calculation general atmospheric circulation is in reasonable agreement with that obtained from observing the motion of yellow clouds. The 50% value for the yellow cloud velocity distribution in Figure 3.2.1-30 is a little greater than 10 meters per second. Extrapolating this velocity to the surface, using the factor of 2, provides 5 meters per second as the 50% value at the surface. In comparison, the general atmospheric circulation calculation values in Figure 3.2.1-29 range from 1 to 6.5 meters per second as the 50% level.

Instrument Characteristics - The anemometer for measuring winds on the surface of Mars should have a threshold as low as possible, approaching 1 to 2 mps. The range of the measurement should extend up to as high as 35 mps in order to detect the higher winds which will occur later in the season for long duration missions.

3.2.1.7 Lander Atmospheric Humidity Sensor. - The aluminum oxide hygrometer appears to be suitable for measuring the humidity in the atmosphere near the surface of Mars. The surface temperatures at night are low enough that the water vapor in the atmosphere near the surface will be condensed out of

VELOCITY OF WINDS AND YELLOW CLOUDS

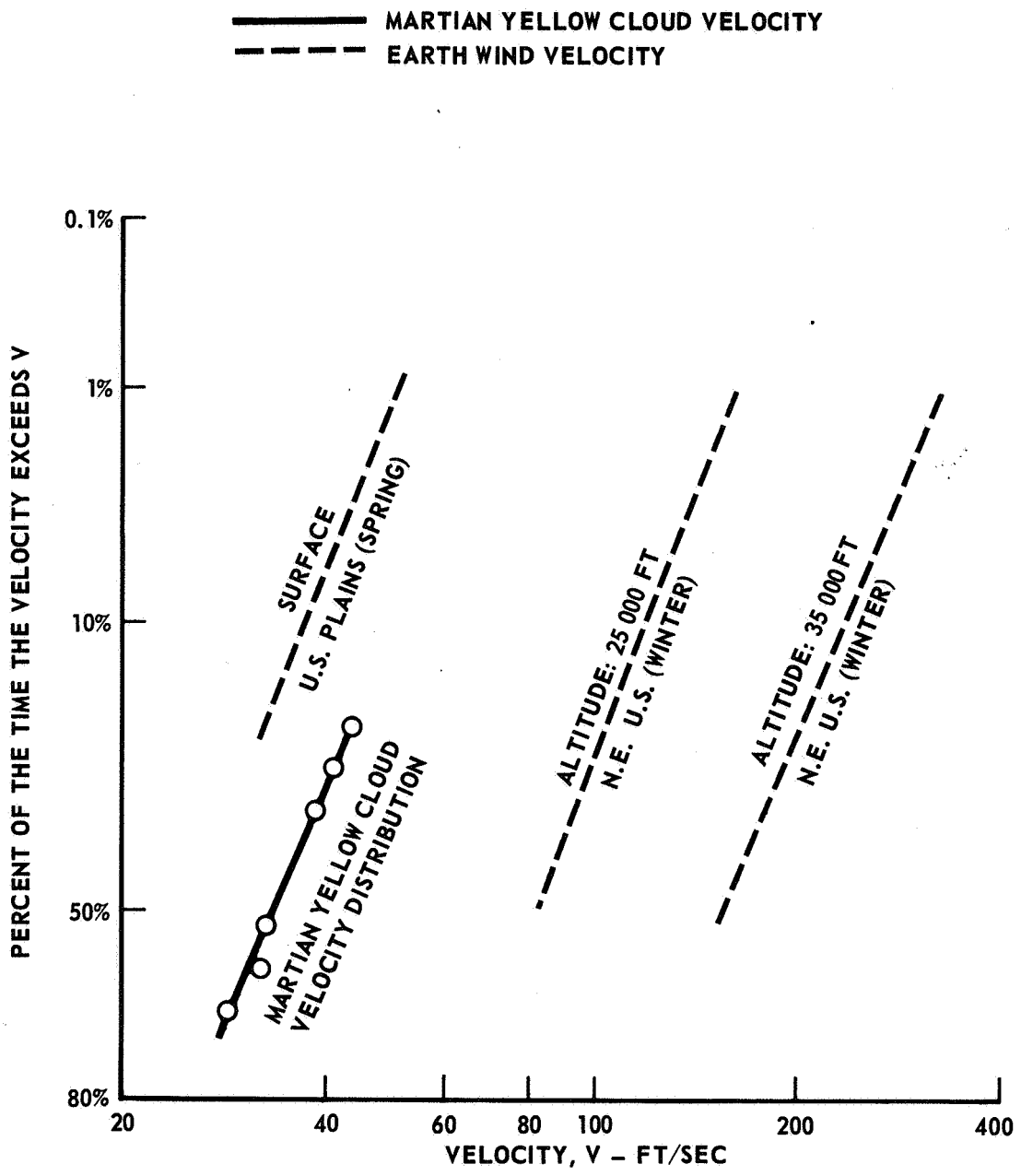

FIGURE 3.2.1–30

the atmosphere onto the surface. The night time atmospheric humidity thus should be much lower than the day time humidity. A seasonal variation is expected to produce low humidities early in the 1974 opportunity and high humidities during the later available landing dates.

Measurements - Astronomical observations of the water vapor content of the Martian atmosphere during the 1965 opposition indicated that there is a seasonal variation in the water vapor content of the atmosphere. As the northern polar cap melted, the water vapor content increased until it was great enough to be detected. In the early winter, before the polar cap started melting, it was not possible to detect it. These results were applied to the 1974 opportunity to estimate the expected seasonal variation in the humidity at the surface. Since the accuracy with which the water vapor content can be measured from Earth is limited, it is not possible to tell exactly how low the humidity is during the northern winter.

If the atmosphere is circulating so that most of the atmosphere comes into contact with the northern polar cap, then the air would be freeze dried to a frost point corresponding to the temperature of the northern polar cap. A frost point of -129°C is shown in Figure 3.2.1-31 for the very dry air at the time of vernal equinox, which corresponds to the 3 February landing in 1974. At high latitudes, the calculated minimum diurnal surface temperatures are low enough to cause CO_2 condensation. The temperatures are near -129° at 60° latitude, which is within the region of the northern polar cap. At the Mars northern vernal equinox, which occurred in September of 1964, the northern polar cap extended all the way down to a 57° latitude. At the 57° latitude, the calculated minimum surface temperature can be seen in Figure 3.2.1-27 to be about - 125°C; at a 60° latitude the temperature is closer to - 129°. If the partial pressure of CO_2 is 4 mb or greater, then the - 129°C temperature is sufficiently low to cause carbon dioxide to condense out of the atmosphere onto the surface, as illustrated in Figure 3.2.1-32.

As the atmosphere is circulated past the polar cap, the water vapor in the atmosphere will be frozen out onto the carbon dioxide polar cap, and the remaining atmosphere will then have a frost point of - 129°C. If the mixing of the atmosphere is not complete, then the atmosphere will not be completely

SEASONAL VARIATION IN SURFACE ATMOSPHERIC HUMIDITY

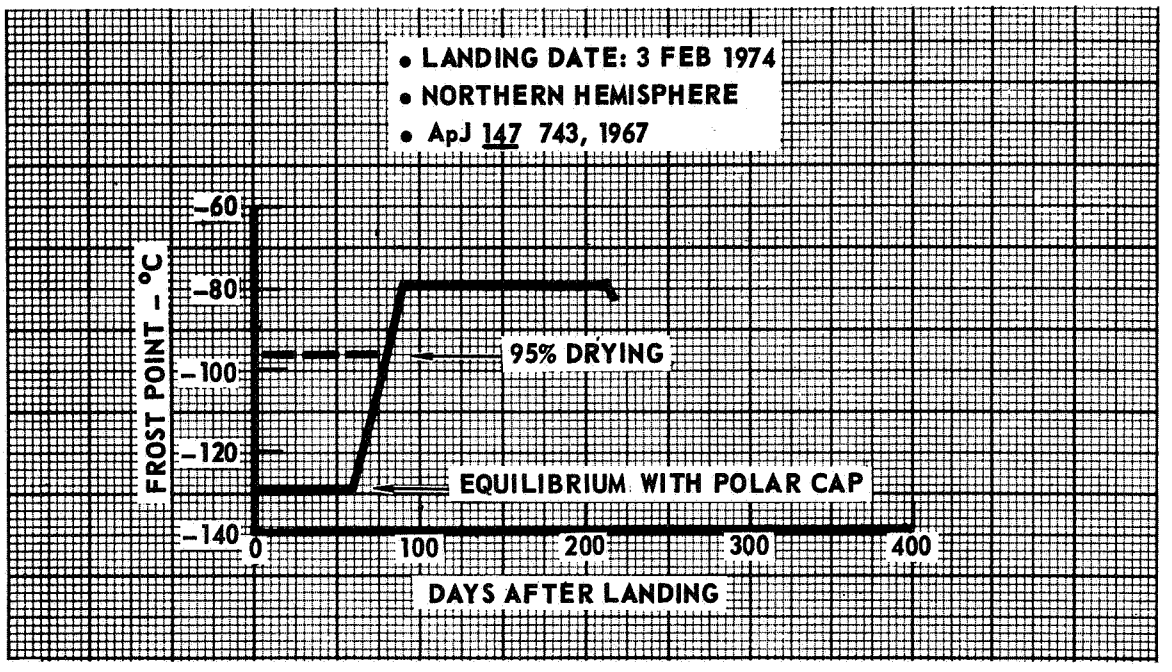

FIGURE 3.2.1–31

CARBON DIOXIDE CONDENSATION TEMPERATURE

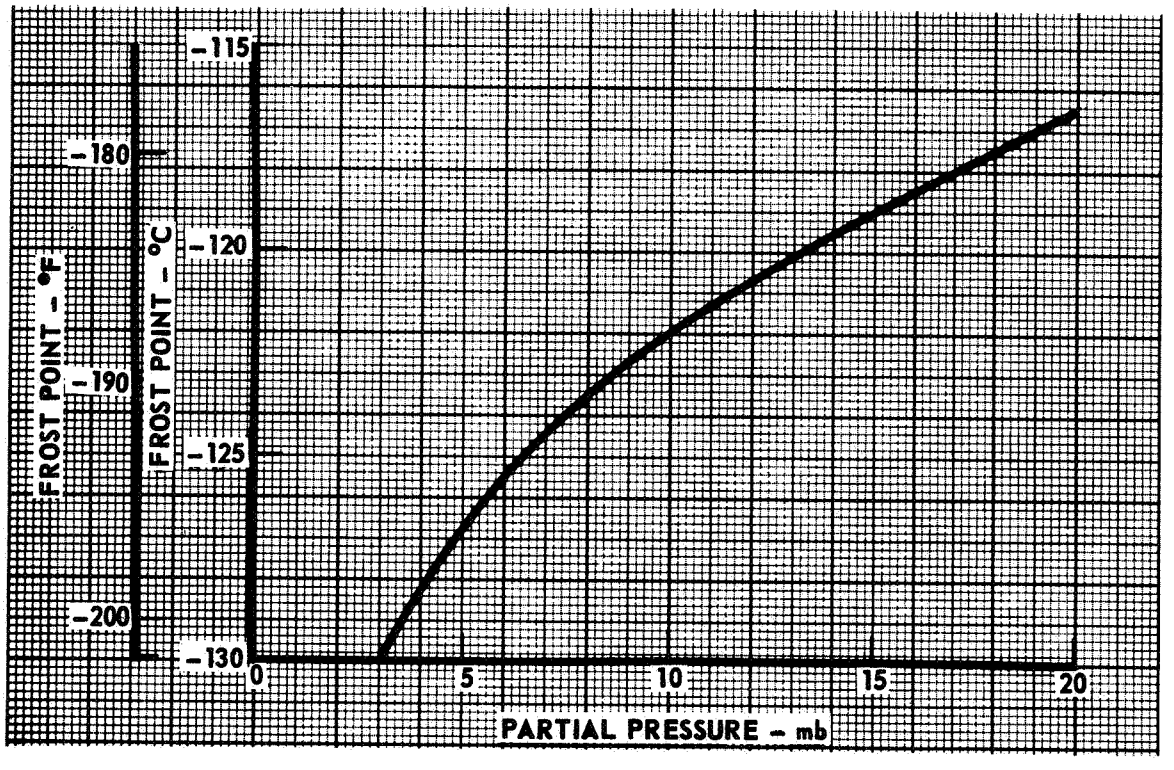

FIGURE 3.2.1–32

dried to a - 129°C frost point. If the circulation is such that only 95% drying takes place, then instead of 20 microns percipitable water vapor in the atmosphere, there will be only 1 micron of water vapor left. For a 1 micron water vapor concentration, the frost point will be - 95°C rather than - 129°C as illustrated in Figure 3.2.1-33.

The astronomical observations of the water vapor in the Mars atmosphere were, unfortunately, not sufficiently accurate to determine whether or not the water vapor concentration was 1 micron or much less than 1 micron. The extremely small amount of water vapor corresponding to a 20 micron precipitable water vapor content is illustrated in Figure 3.2.1-34. The surface pressure corresponding to 20 microns of precipitable water vapor is 7.5×10^{-4} mb of water vapor. If the total surface pressure is 20 mb, then the water vapor partial pressure will be less than 0.004% of the total pressure.

Late in the northern spring on Mars during 1965, as the temperature increased and the northern polar cap started to melt, water vapor was observed in the atmosphere. Before the cap started to melt, it was not possible to detect water vapor. Approximately 15 microns of water vapor was detected, which corresponds to a frost point of - 80°C. The period over which this increase in humidity took place was not precisely defined. However, it corresponds to a period of approximately 60 to 90 days following vernal equinox, as illustrated in Figure 3.2.1-31. Thus, for approximately 60 to 90 days following a 3 February 1974 landing, the frost point will be very low, from -95°C to as low as - 129°C. After a period of 60 to 80 days following landing, the humidity should start rising toward a frost point of approximately -80°. If a landing is made during the later part of the opportunity, then the higher humidities will be observed both during entry and on the surface.

The predicted diurnal humidity in Figure 3.2.1-35 is for landings during the later part of the opportunity. During the early part of the opportunity, the humidity values will not go over - 95°C for a 95% drying of the atmosphere. If the atmosphere is nearly in equilibrium with the polar cap, then the humidity will not vary with time during the day and the atmosphere will have a constant - 129°C frost point.

WATER VAPOR FROST POINT

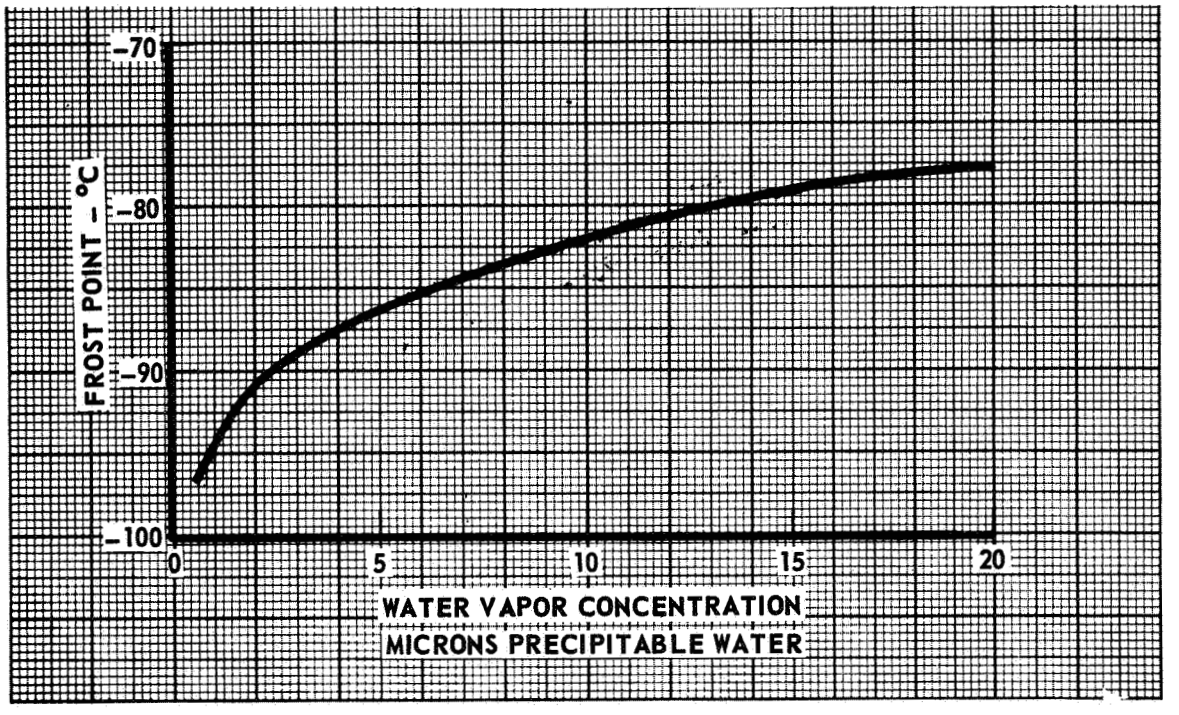

FIGURE 3.2.1–33

WATER VAPOR PARTIAL PRESSURE AT THE SURFACE

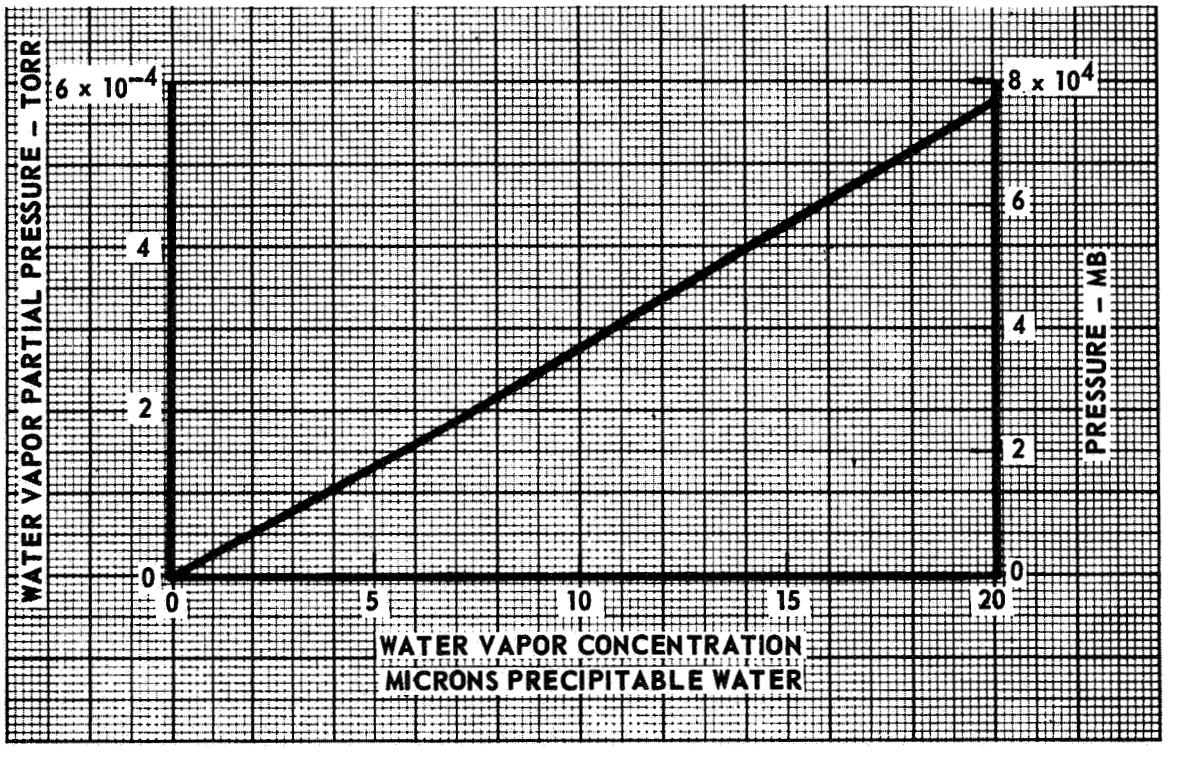

FIGURE 3.2.1–34

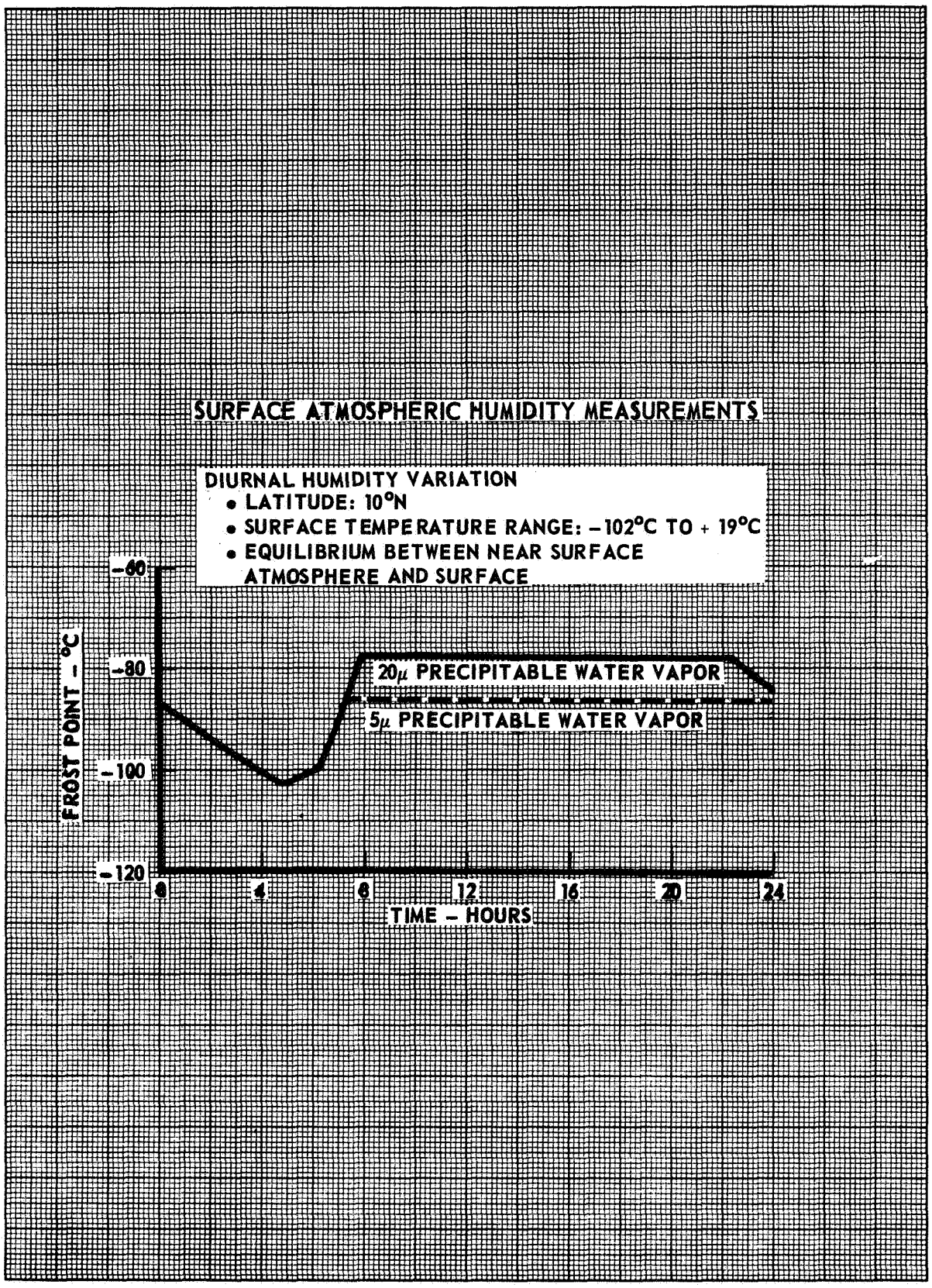

FIGURE 3.2.1–35

During the formation of the northern polar cap, the winds will be toward the pole as the CO_2 is frozen out of the atmosphere onto the surface. These winds will carry the wet atmosphere toward the cap, where the water will be removed when it comes in contact with the low temperature CO_2. After most of the water vapor is frozen out of the atmosphere, the water will remain in the polar cap, which stays at a constant temperature depending on the CO_2 partial pressure (see Figure 3.2.1-32).

In the spring, when the polar cap starts to melt, the water vapor will flow away from the polar cap with the winds caused by the CO_2 release from the melting polar cap. As the water vapor is released near the edge of the polar cap, it will flow away from the polar cap. Thus, the melting of the polar cap near the edge of the cap in the spring appears to be a suitable explanation of the observed changes in humidity.

The predicted diurnal variation in the surface humidity in Figure 3.2.1-35 was obtained from the calculated diurnal variation in surface temperature. For a typical set of surface conditions and a 10° N latitude, it was found that the surface temperature varied from a low during the night of 102°C to a high during the day of + 19°C. During the day the atmospheric temperature near the surface is higher than the frost point, corresponding to 5 to 20 microns of precipitable water vapor, which is - 78 to - 86°C. However, during the evening the surface temperature is lower than the frost point. Therefore, water vapor from the atmosphere will condense on the surface if the humid air comes in contact with the surface. When the surface is cooled, there should be down drafts, so that the air is continually circulated past the surface. The air close to the surface will be dry since the water will condense out of the atmosphere onto the surface. For an equilibrium between the near surface atmosphere and the cold surface, the frost point of the atmosphere will approach the surface temperature. Therefore, the frost point of the atmosphere near the surface should follow the surface temperature profile during the night. When the surface reaches the frost point corresponding to the average amount of water vapor in the atmosphere, then the water from the surface will be exhausted and no more water vapor will be added to the atmosphere. The frost point for the atmosphere near the surface will then be

in equilibrium with the atmosphere at higher altitudes and the frost point will be independent of the time as shown in the figure. If, during the early part of the mission, the atmosphere is much drier and contains only 1 micron of precipital water vapor, then the level portion of the curve will be at - 95°C and there will only be a small dip in frost point during the night. If the atmosphere is even drier due to water vapor being frozed out of the atmosphere at the polar caps, there will not be a diurnal variation in the humidity. The combination of the orbiter and lander humidity measurements will be particularly useful in analyzing the diurnal, seasonal, and geographical variations in humidity.

Instrument Characteristics - The aluminum oxide humidity sensor is suitable for making the surface atmospheric humidity measurements and also the entry humidity measurements. This instrument is described in detail in the entry humidity sensor section, 3.2.1.11. The low time constant required for entry humidity measurements is of course not necessary for surface humidity measurements. The slow variation in humidity with time is illustrated in Figure 3.2.1-35.

Conclusions - The 1974 mission offers a unique opportunity for observing the seasonal variations in surface humidity near the Mars vernal equinox. An early landing occurs in a period when the atmosphere should be very dry while a late landing occurs in a period when the humidity should have significantly increased. An early landing with the extended mission duration will make it possible to determine the exact extent of the seasonal variation in atmospheric humidity. The aluminum oxide humidity sensor is sufficient for making the measurements, however the range should be extended as far below - 110°C as possible. A - 130°C frost point capability would be desirable.

3.2.1.8 Landed Mass Spectrometer Operation. -There appears to be only one problem with using the entry mass spectrometer for measurements on the surface. If the mass spectrometer is located on the lander, a long sample tube extending from the mass spectrometer to the aeroshell nose will be required. The length required for this tube is approximately 2 to 4 ft, whereas normally the tube is kept to a maximum length of 1 ft. It will be necessary to carry out tests to determine the extend to which outgassing from this tube will contaminate the

atmospheric samples due to tube wall outgassing and to investigate the possibility of locating the leak near the mass spectrometer far from the inlet.

Measurements - One potential use for the landed mass spectrometer is to measure the diurnal variation in humidity. As discussed in Section 3.2.1.7, the aluminum oxide humidity sensor has an accuracy that permits the measurement of the water vapor to within a factor of 2. As indicated in Section 3.2.1.12, it may be feasible to measure the water vapor in the atmosphere with an accuracy of as low as ± 16% for water vapor concentrations above 10 microns precipitable water. A scanning mass spectrometer which covers the entire range from 10 to 90 mass units is desirable in order to determine if there are any minor constituents in the atmosphere, in addition to water vapor, which have a diurnal variation. Development tests are necessary to determine whether or not the shot noise limited accuracy can be obtained for a mass spectrometer using an electron multiplier detector and if the values in Section 3.2.1.12 for the mass spectrometer accuracy are achievable.

Instrument Characteristics - This instrument which is used both during entry and on the surface, is described in the section on the Entry Mass Spectrometer, Section 3.2.1.12. A value to switch the mass spectrometer to a second inlet leak just prior to aeroshell separation is necessary to continue measurement during the remaining part of the descent and following landing.

Conclusions - It appears to be feasible to make measurements after landing using the entry mass spectrometer. The only question is related to the use of a long sample tube during entry. Lab tests will be necessary to determine whether or not a very long sample tube is practical and if the tube outgassing will be low enough so that the atmospheric composition measurements can be made with a reasonable accuracy.

3.2.1.9 Lander Alpha Spectrometer. -The alpha spectrometer used for making lunar surface composition measurements on Surveyor is suitable for making measurements on the surface of Mars. However, there are three problem areas in which a development effort is required. First, the long transit time will produce a decrease in the intensity of the radioactive sources, so that the counting time will be increased for the Mars mission unless the number of sources or the type of source is changed. Second, the data transmission capability

utilized for Surveyor is much larger than that which will be available for the Mars soft lander , and third, an improved deployment mechanism, with a higher reliability, should be developed.

Measurements - The lunar surface composition measured by the alpha spectrometer is a good first approximation to the expected composition on the surface of Mars. For long duration missions and high latitude landing sites, the alpha spectrometer can be raised off the surface during the night and placed on the surface again during the morning to determine if it is possible to detect any condensed carbon dioxide on the surface.

Instrument Characteristics - The first problem associated with using the alpha spectrometer for the Mars soft lander is the decrease in intensity of the radioactive sources during the transit time. A decrease in the average alpha count rate from 2 counts per second initially to an average of 0.72 counts per second at the end of a 240 day nominal transit time will result if the present Curium 242 radioactive source is used, Figure 3.2.1-36. This source has a 163 day half-life and the decrease in average counting rate will have a significant effect on the operation of the alpha spectrometer. Two ways in which this problem may be reduced are to use a radioactive source that has a longer half-life or to increase the number of sources.

The decrease in source intensity due to the long transit time will increase the counting time from the 8 hour period used for lunar measurements to 22.2 hours on the surface of Mars, Figure 3.2.1-37. A counting time of 1 hour can be used to illustrate how these values were obtained. The average alpha count rate on Surveyor V of 2 counts per second for 1 hour produces 7200 counts. Dividing by the number of alpha channels, 128, provides the average number of counts per channel, 56. The RMS variation in an average number of counts of 56 is the square root of 56 which is 7.5. The relative accuracy is thus 7.5 divided by 56 which equals 13% and the 3σ variation in the number of counts per channel is therefore 39%, as shown in Figure 3.2.1-37. However, if the same system is used on Mars, the average alpha count rate will decrease to 0.72 counts per second. The resulting average accuracy per channel will be increased by the square root of the ratio of the count rates so that the average accuracy per channel becomes 67% for a 1 hour counting period. On Surveyor, counting

ALPHA SPECTROMETER DATA RATE DECREASE

• SOURCE: 163 d Cm^{242}

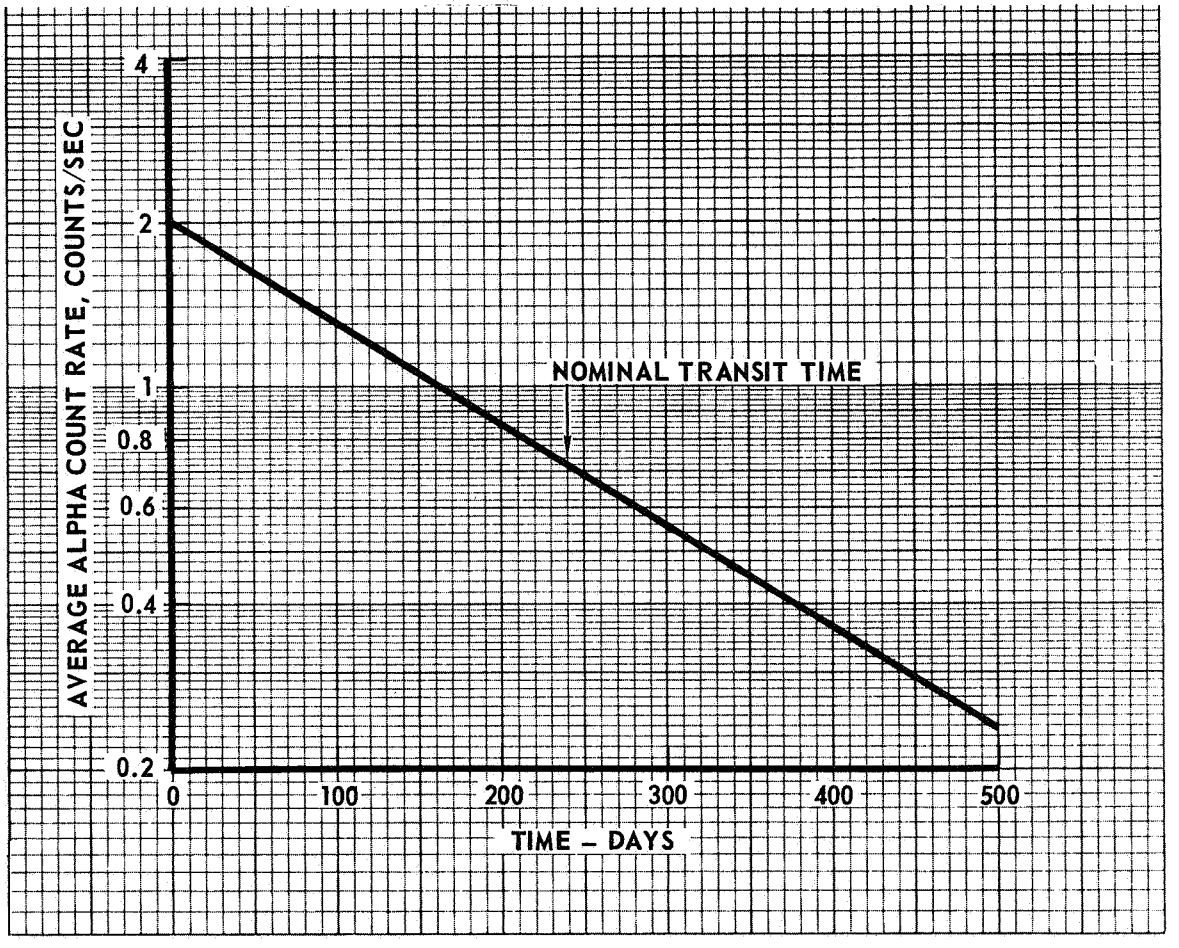

FIGURE 3.2.1–36

ALPHA SPECTROMETER ACCURACY

• 128 ALPHA CHANNELS

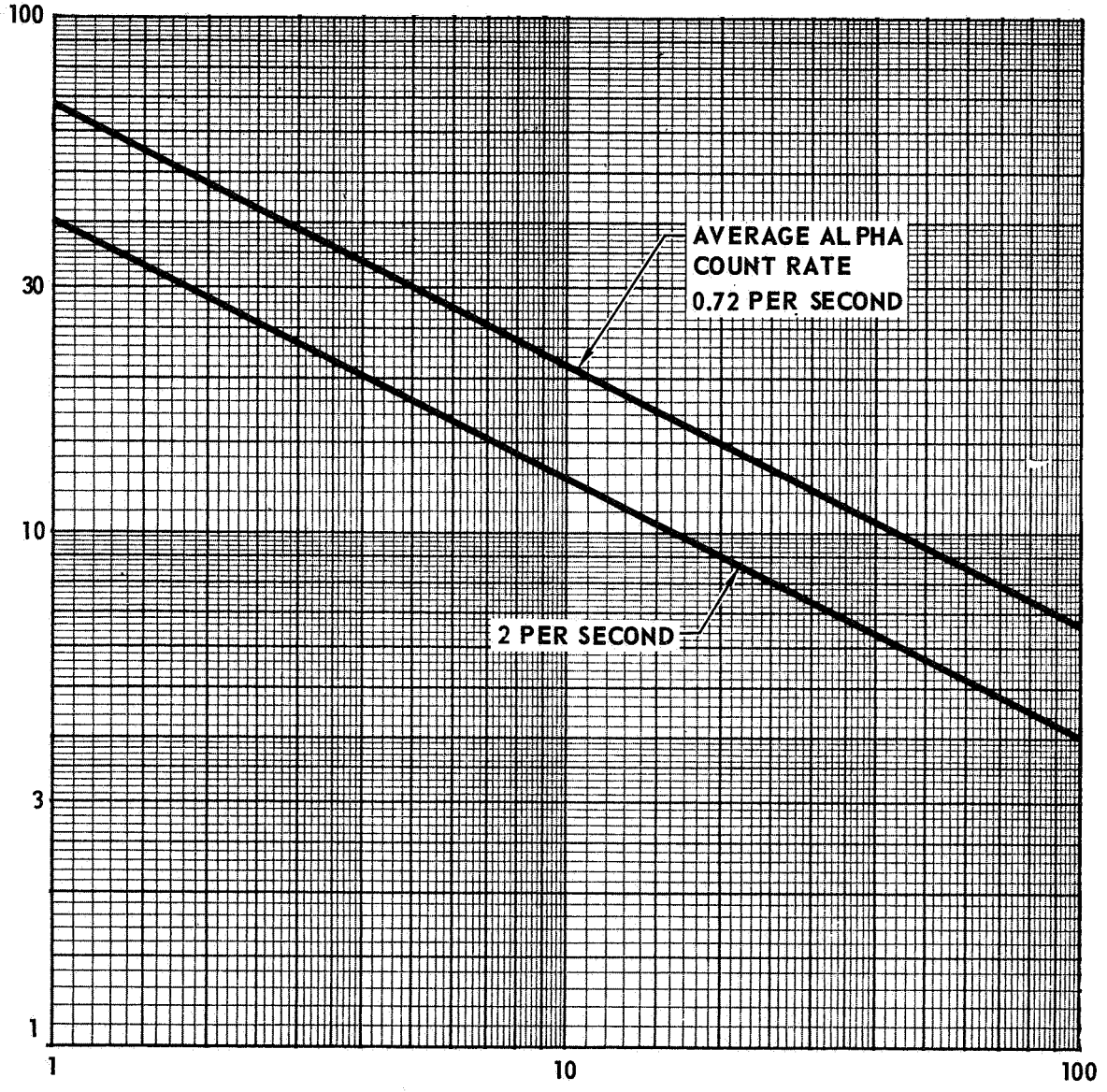

ALPHA SPECTROMETER COUNTING TIME – HOURS

FIGURE 3.2.1–37

times as long as 17 hours produced average calculated accuracies of better than 10%. To obtain an equivalent accuracy on Mars, an extremely long period, approximately 47 hours, would be required. Since the alpha spectrometer is not normally operated during the night, the short day makes the counting time requirement an even more severe problem on Mars than on the moon where the day is long. A development effort is thus required to find some technique for obtaining a reasonable counting time for short duration missions on Mars.

The second problem associated with using the alpha spectrometer on Mars is data transmission. For Surveyor, 1.5×10^8 bits of data could be transmitted over the channel used for the alpha spectrometer in a 15 hour period. Since the total transmission capability for the minimum mission for Mars is only 10^7 bits, it will be necessary to use a different technique for transmitting the alpha spectrometer data. Fortunately, counters can be added to the alpha spectrometer which will greatly reduce the amount of data to be transmitted. It is estimated that approximately 3 pounds will be required for the 256 counters and other electronics required for the data processing. During the present study it has been assumed that this count capability will be included in the alpha spectrometer design for the Mars mission.

The present 10 pounds alloted to the alpha spectrometer will be sufficient for the unit with the counters only if the present weight of the alpha spectrometer is reduced. It is estimated that if the present type unit is not significantly changed, 3 pounds will be required for alpha spectrometer head, 5 pounds for the electronics package, and 2 pounds for the deployment mechanism which results in a total 10 pound package. In order to add 3 pounds for the counting system the weight of the other units will have to be reduced or the deployment mechanism weight charged to the structural support weight. By utilizing the counters, the alpha spectrometer total data output is reduced to less than 2×10^4 bits.

Conclusions - The alpha spectrometer used for lunar composition measurements will be satisfactory for making Mars surface composition measurements if the unit is modified to account for the reduced data rate after the long transit time and the requirement to keep the total data low for the short duration missions.

3.2.1.10 Entry Pressure, Temperature, and Acceleration Sensors. - It is not expected that any serious difficulty will be encountered in obtaining entry pressure, temperature and acceleration measurements suitable for reconstructing the Mars atmosphere within the required accuracy. Many techniques are available for making these measurements, however, the scope of this study did not permit a detailed parametric trade-off analysis to be made in order to select the best techniques for making the entry measurements. In order to define the point designs, a typical set of measurement techniques and instruments was selected.

Measurements - The entry measurements were selected using the requirements for the atmospheric reconstruction of:

a) Pressure variations with altitude, Altitude range: from 60 km to as low an altitude as practical. Accuracy: $\pm$ 5% of value at known altitude, Threshold accuracy, 0.5 mb.

b) Density variations with altitude, Altitude range: from 60 km to as low an altitude as practical. Accuracy: $\pm$ 5% of value at known altitude, Threshold accuracy: 1×10^{-6} g/cm^3.

c) Temperature variations with altitude, Altitude range: from 60 km to as low an altitude as practical. Accuracy: $\pm$ 2% of value (°K) at known altitude, Threshold accuracy: 3°K.

The use of the threshold accuracy along with the altitude range greatly simplifies the measurements necessary to obtain the required accuracies for the minimum model atmosphere since the 0.5 mb threshold occurs at 18 km and the 10^{-6} g/cm^3 density occurs at 23 km. Thus for the minimum model atmosphere, measurements are necessary over an altitude range from 0 to 23 km rather than the full range from 0 to 60 km. The threshold accuracies correspond to the atmospheric values at approximately 60 km for the maximum model atmosphere. The typical measurements used for the point designs include the stagnation region pressure, the base pressure, the wall pressure, stagnation temperature, base temperature, and the acceleration of the capsule c.g. Typical values for the expected stagnation pressure and acceleration are illustrated by Figures 3.2.1-38 through -43. Other measurements, such as the altitude from the radar altimeter and the berylluim nose cap temperature, are also available for the atmospheric reconstruction.

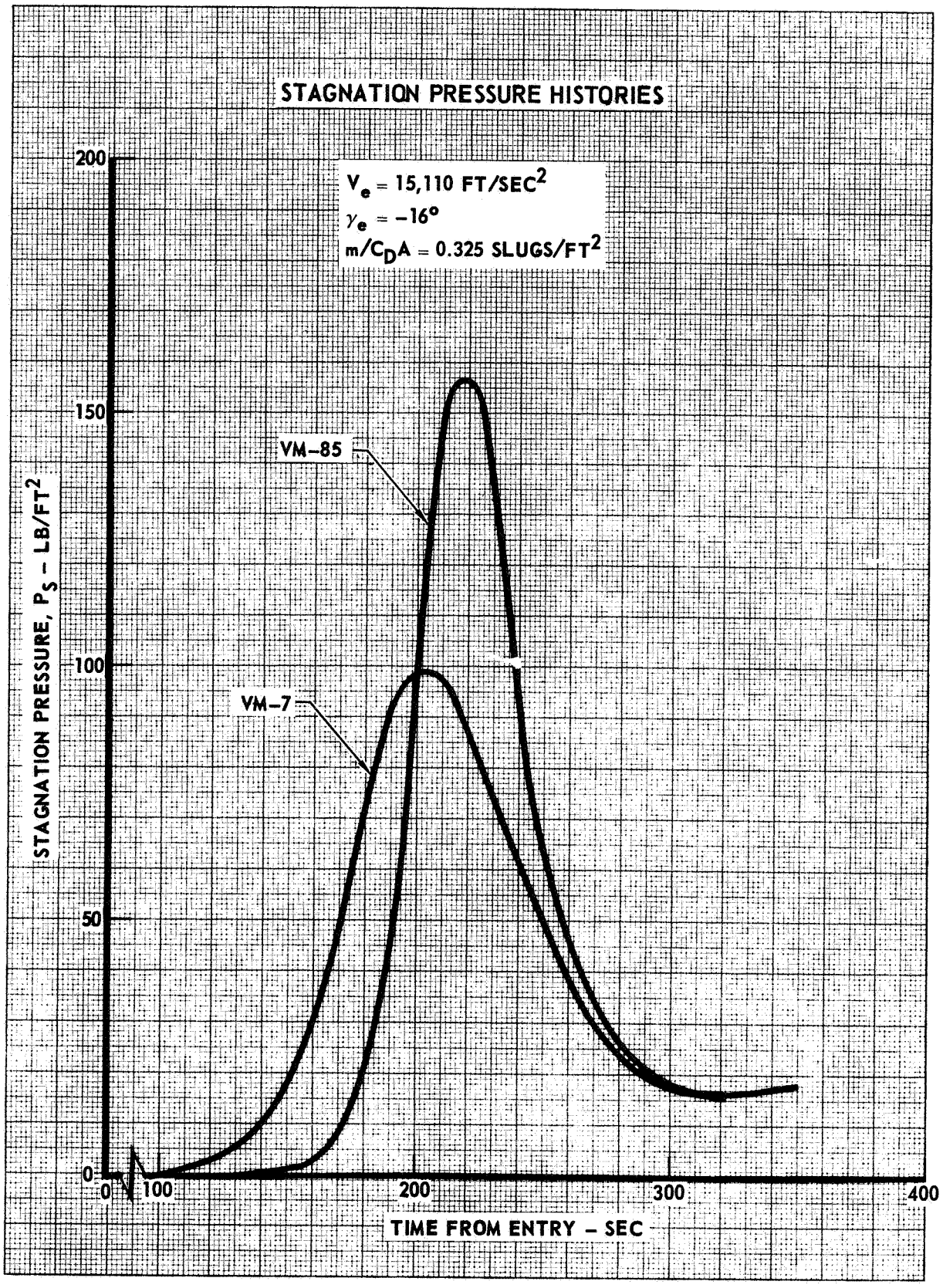

FIGURE 3.2.1−38

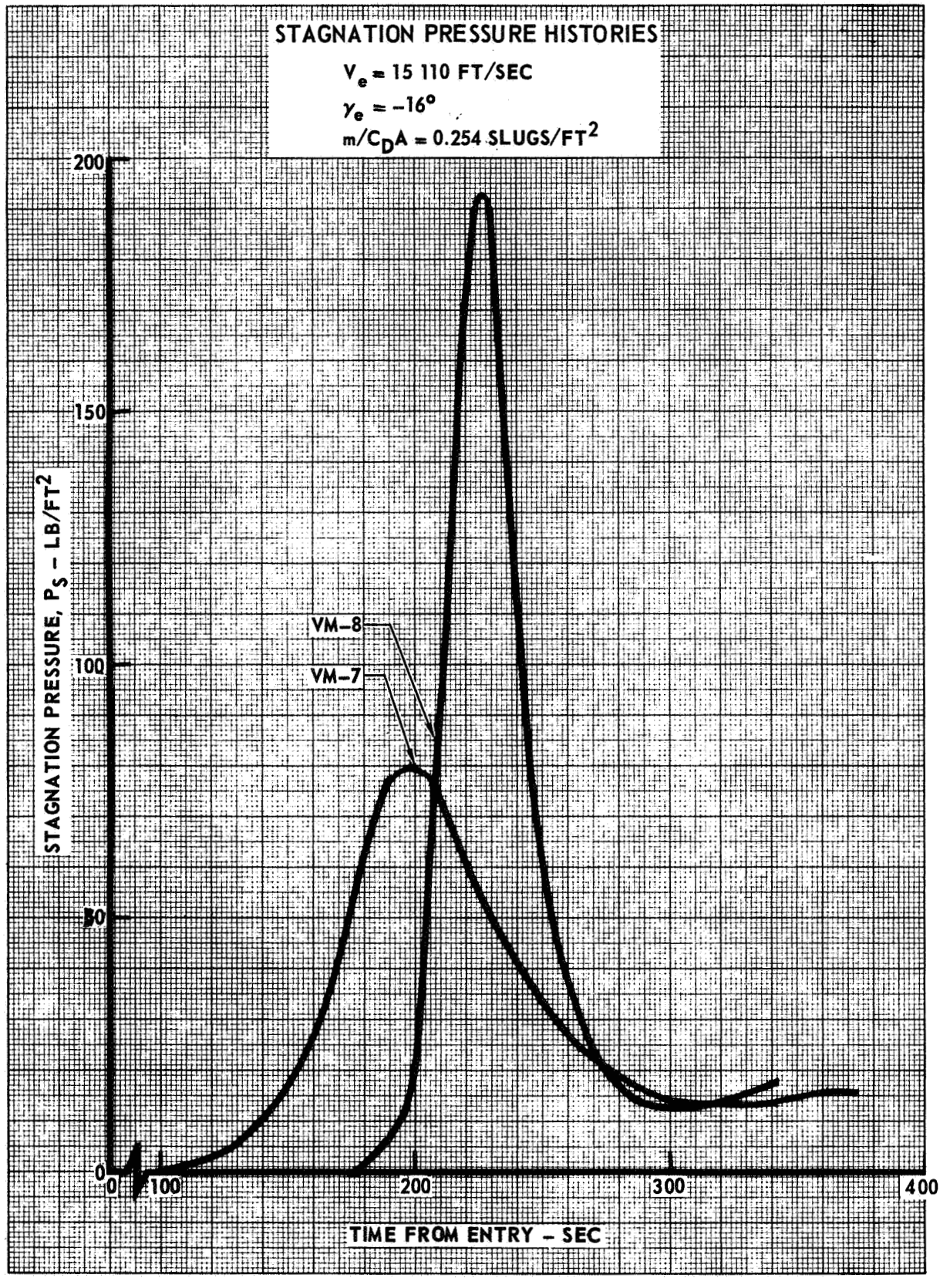

FIGURE 3.2.1–39

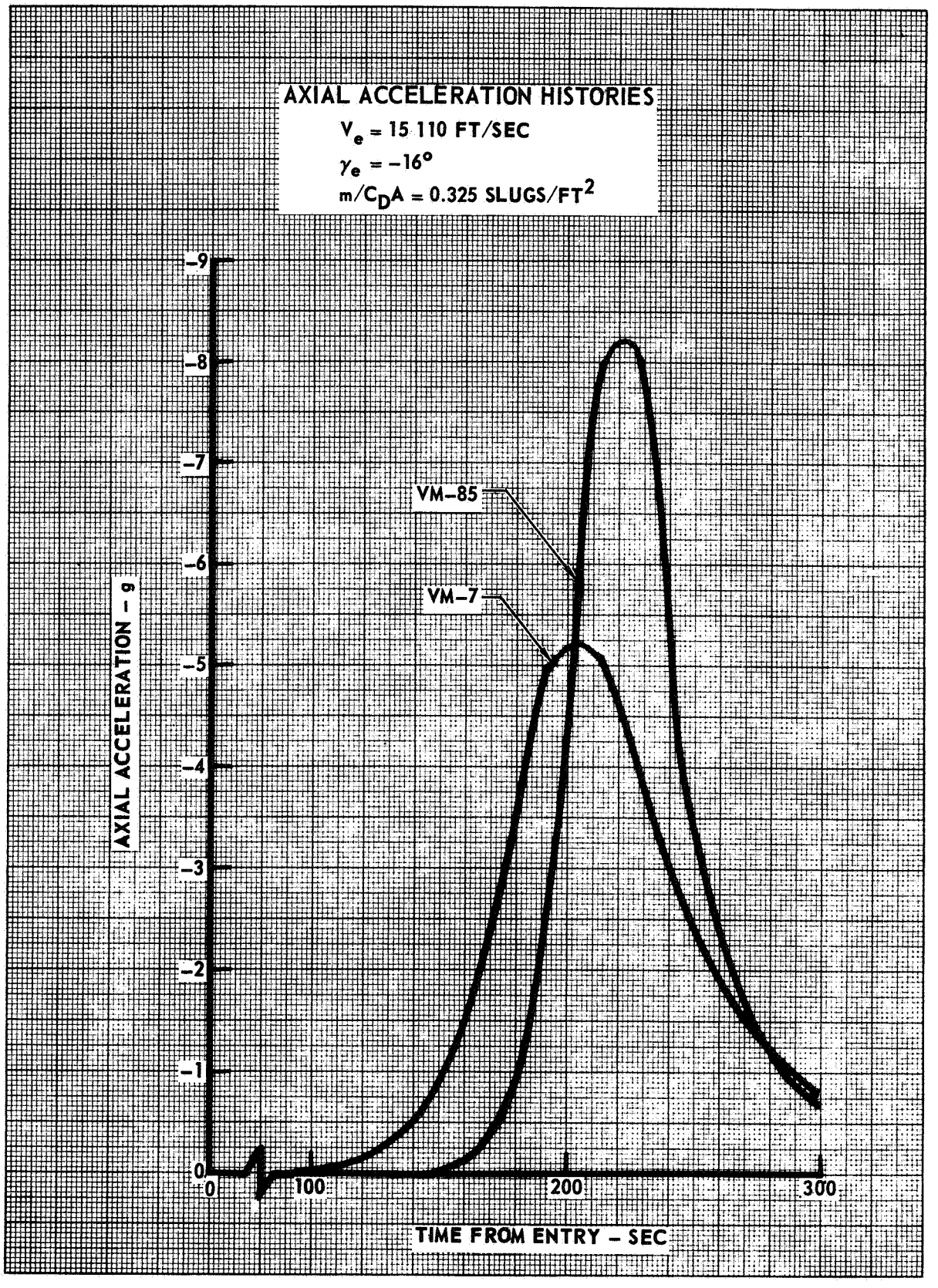

FIGURE 3.2.1−40

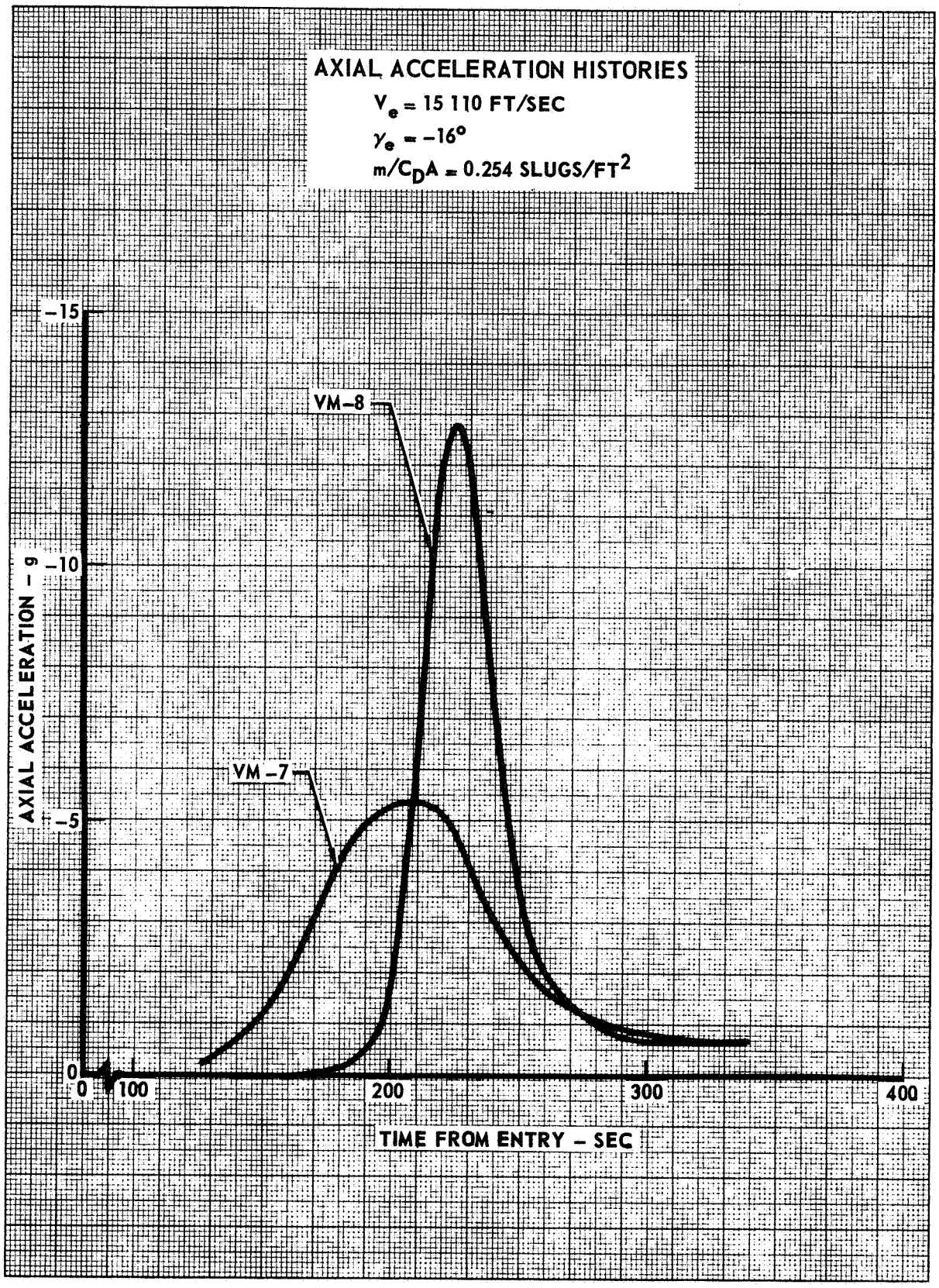

FIGURE 3.2.1–41

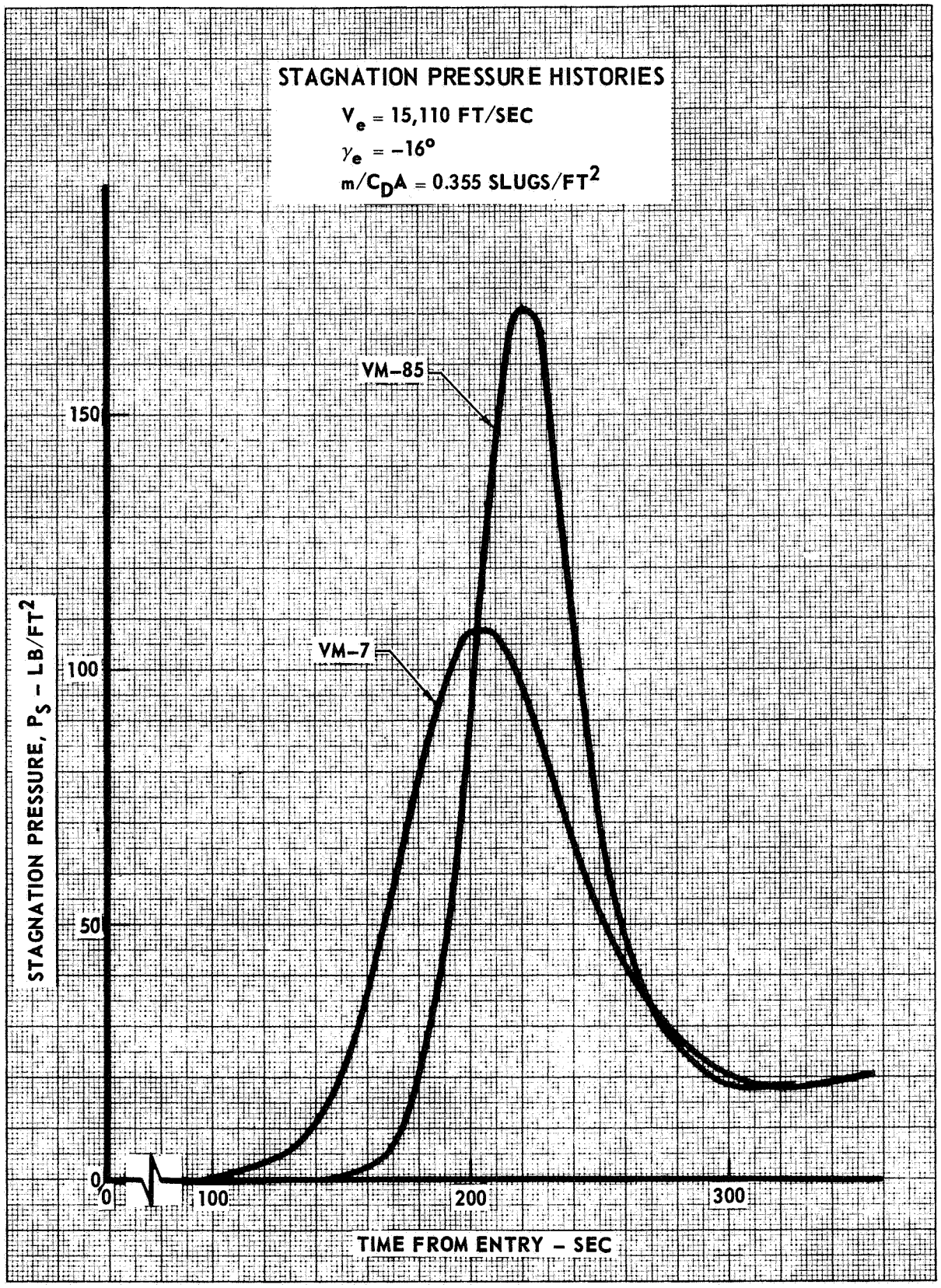

FIGURE 3.2.1–42

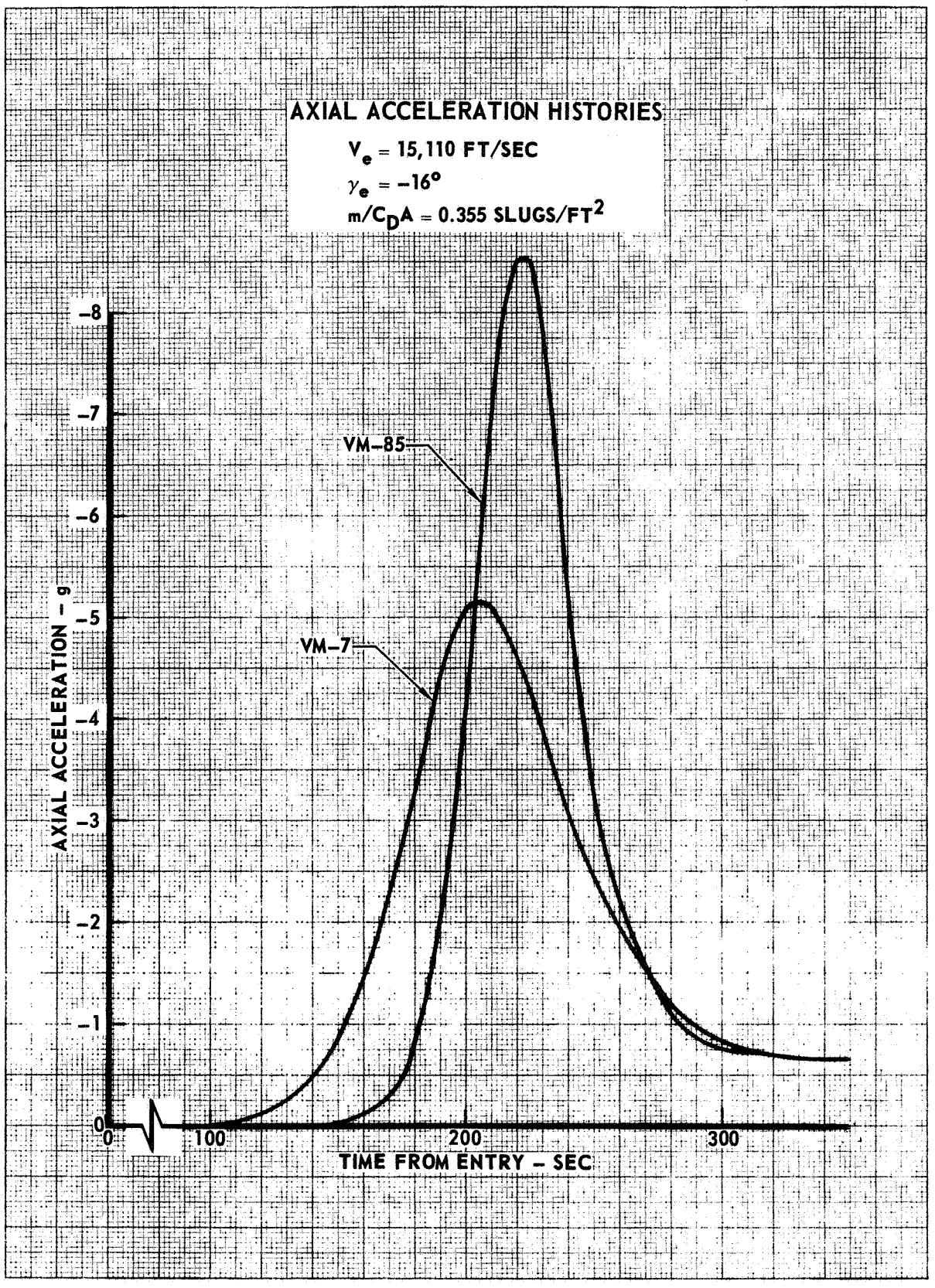

FIGURE 3.2.1−43

Instrument Characteristics - The two temperature sensors weigh approximately 0.5 lb each for a total of 1 lb. The stagnation and the base pressure sensors each weigh 1 lb for a total of 2 lbs and the four wall pressure sensors weigh 12 oz each for a total of 3 lbs. The tri-axis accelerometer with dual ranges is estimated to weigh approximately 2 lbs. These weights are only tentative and depend on a more refined analysis of the atmospheric reconstruction techniques. A five pound margin has been included in the entry science payload total weight to account for any changes in the entry instrument weights.

There are several trade-off analyses which significantly effect the capsule design. One example is the analysis of the tube used to provide samples to the mass spectrometer and the temperature sensor. A tube which has a port on the front of the capsule and vents at the base region has been provided in previous capsule designs to provide continuous fresh atmospheric samples to the mass spectrometer leak input and to the stagnation region temperature sensor. An alternate technique is to use a port which provides samples directly to the mass spectrometer leak inlet without using a vent to the base region. If the leak inlet to the mass spectrometer is kept near the surface of the aeroshell, then the samples will be mixed by the turbulent flow near the aeroshell surface and the mass spectrometer can obtain continuous fresh samples. Also the temperature sensor can be placed in the beryllium nose cap, the nose cap temperature measured, and the stagnation region gas temperature calculated using the beryllium nose cap temperature. Although the instrumentation is simplified in comparison with a temperature sensor in the gas flow, it is not expected that the measurements will be as accurate. A detailed trade-off analysis is necessary to determine which of these two design techniques is best for making the measurements during entry.

A second trade-off analysis which significantly affects the capsule design is related to the question of the use of the radar altimeter to define the altitudes at which the pressure and temperature measurements are made. Since an altimeter is required for determining the time for parachute deployment which occurs at an altitude of approximately 40 000 ft, the altitude determination at 40 000 ft. is available for the atmospheric reconstruction without

any additional capsule weight requirement. However, since the atmospheric reconstruction requirement includes altitudes as high as 60 km it would be desirable to measure the altitude to this height. Since most of the altimeter weight is necessary for the electronics, the extension of the altimeter measurements from 40 000 ft to 200 000 ft (approximately 60 km) requires an additional altimeter weight of only a few pounds.

This radar altimeter has an accuracy which is more than sufficient for use in reconstructing the atmospheric pressure profile with an accuracy of better than 5%. At an altitude of 15 km, where the pressure is 0.77 mb for the minimum atmosphere, a 5% decrease in pressure corresponds to a 1630 ft increase in altitude. Since the altimeter accuracy is approximately 700 ft, the altitude measurements will be sufficiently accurate for use in the atmospheric profile determination. This is also the case for the maximum atmosphere. At a height of 60 km where the pressure is 0.29 mb, a 5% reduction in pressure will occur for an increase in altitude of approximately 2300 ft. In comparison, the altimeter accuracy is approximately 1000 ft (3σ).

Conclusions - Although a detailed analysis of the entry instruments and the atmospheric reconstruction has not been carried out, it appears that serious difficulties will not be encountered in achieving the required atmospheric profile determination accuracy.

3.2.1.11 Entry Humidity Sensor. - The aluminum oxide humidity sensor appears to be suitable for making measurements of the humidity profile during entry into the atmosphere of Mars. The unit has been demonstrated to be sterilizable and can withstand a long term period in vacuum during transit. The primary problems associated with the humidity measurements are obtaining a sample which has a humidity that is representative of the ambient humidity. The sampling tube around the humidity sensor tends either to absorb humidity from the gas or to outgas and add water vapor to the atmospheric sample, unless extreme care is taken in maintaining the temperature of the sample tube. It appears that the time constant of the sensor is short enough to follow the humidity profile during entry. However, an experimental lab test is necessary to verify that the sensor will actually follow the frost point profile.

Measurements - The expected variations in humidity with altitude for a constant mixing ratio are illustrated in Figure 3.2.1-44. The atmospheres with a 20 mb surface pressure, VM-10 and VM-9, have a total water vapor content of 20 microns of precipitable water and the models with a 5 mb surface pressure, VM-7 and VM-8, have a water vapor content of 5 microns of precipitable water vapor. The other atmospheres have water vapor contents in proportion to their surface pressures, so that the water vapor ratio is the same for all of the curves.

The frost points corresponding to the extremely low water vapor pressures in Figure 3.2.1-45 were used to determine the variation in frost point with altitude in Figure 3.2.1-46 (dashed lines). Since the atmospheric temperatures for the odd numbered model atmospheres are higher than the frost point temperatures, condensation and cloud formation will not take place. For the even numbered atmospheres at altitudes from 5000 to 10 000 ft and above, the atmospheric temperature is less than the frost point temperature. Thus, the water vapor can condense out into an ice particle haze. The frost point will decrease with increasing altitude. Thus, the partical pressures of water vapor for the even numbered atmospheres in Figure 3.2.1-44 will be even less for the higher altitudes. The expected variation in frost point with time during entry into the atmosphere for a model MV-8 atmosphere is illustrated in Figure 3.2.1-47. It is apparent that a time constant of a few seconds will be required for making measurements during the entry.

As discussed in Section 3.2.1.7, the seasonal humidity change will greatly reduce the humidities for the early part of the 1974 opportunity.

Instrument Characteristics - The one pound allotted to the humidity sensor should be more than adequate, since present units being used in balloon tests weigh as little as 4 to 5 oz, including the electronics. The 0.02 watt electrical power value, Table 3.2.1-12, is sufficient, since an average of only 2 mw is required for the sensors and electronics.

The low temperatures of the even number model atmospheres in Figure 3.2.1-46 indicate that it would be desirable to extend the range below - 110°C. Measurements have been made as low as - 140°C but the values become very inaccurate.

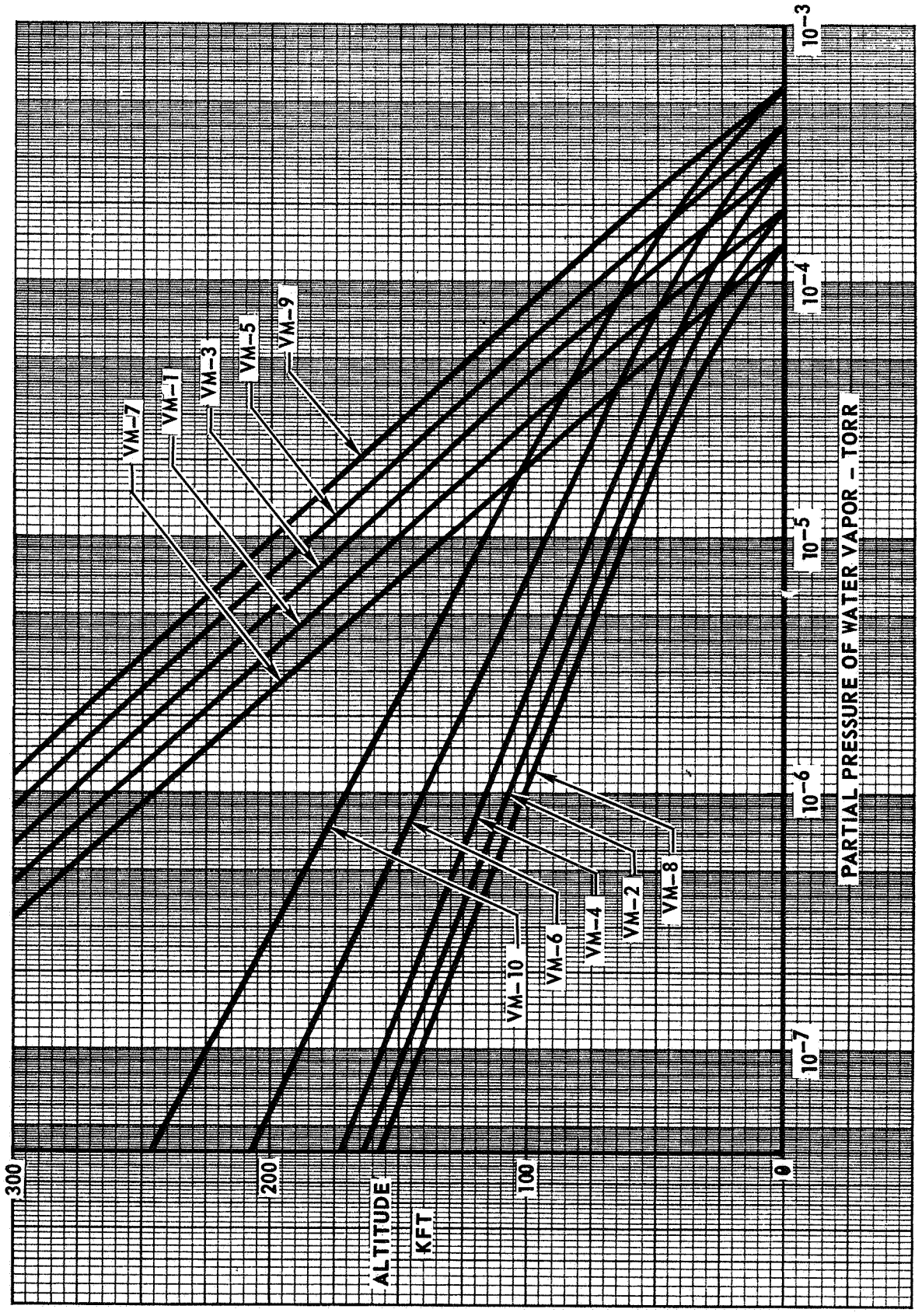

FIGURE 3.2.1–44

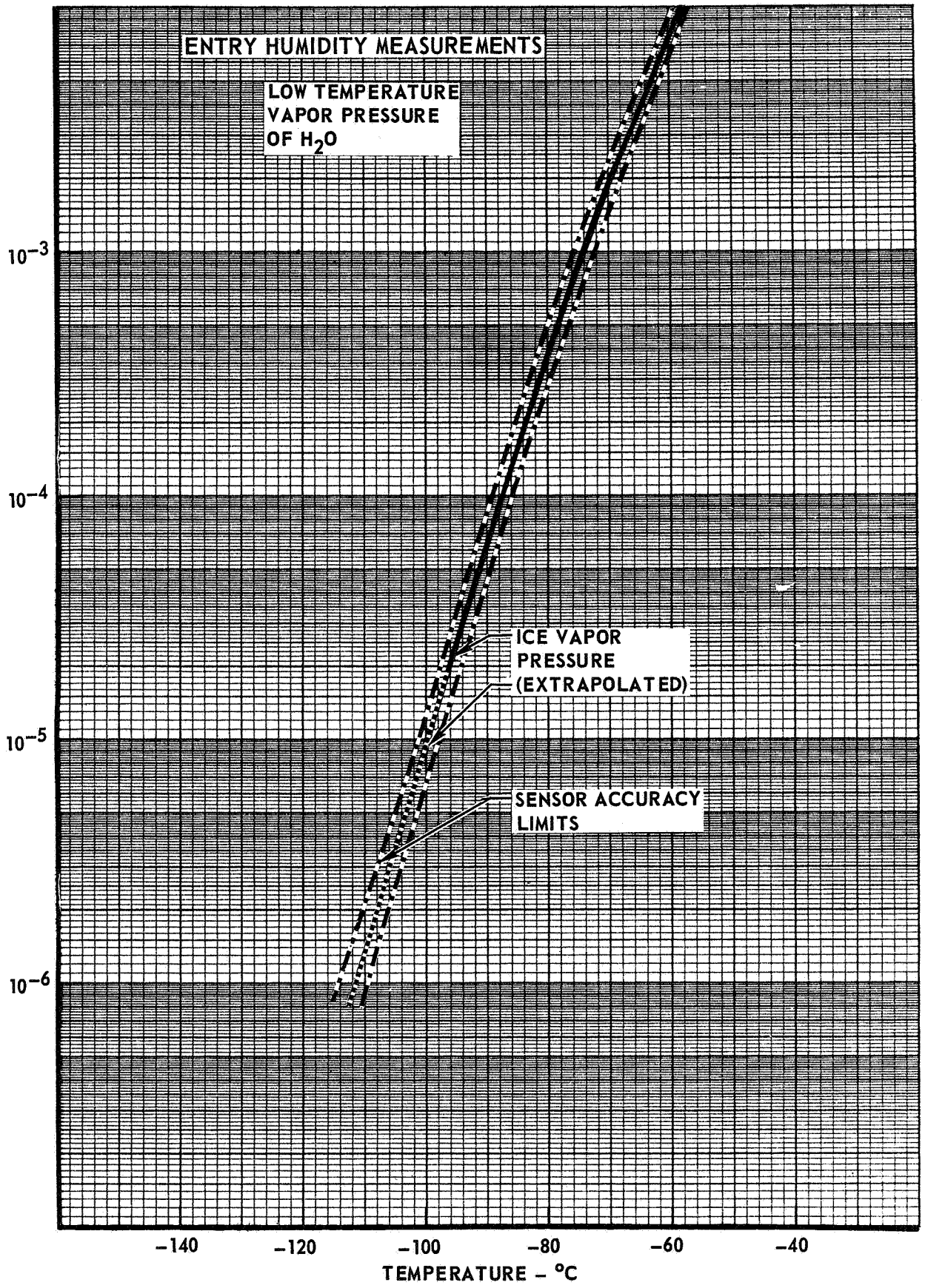

FIGURE 3.2.1–45

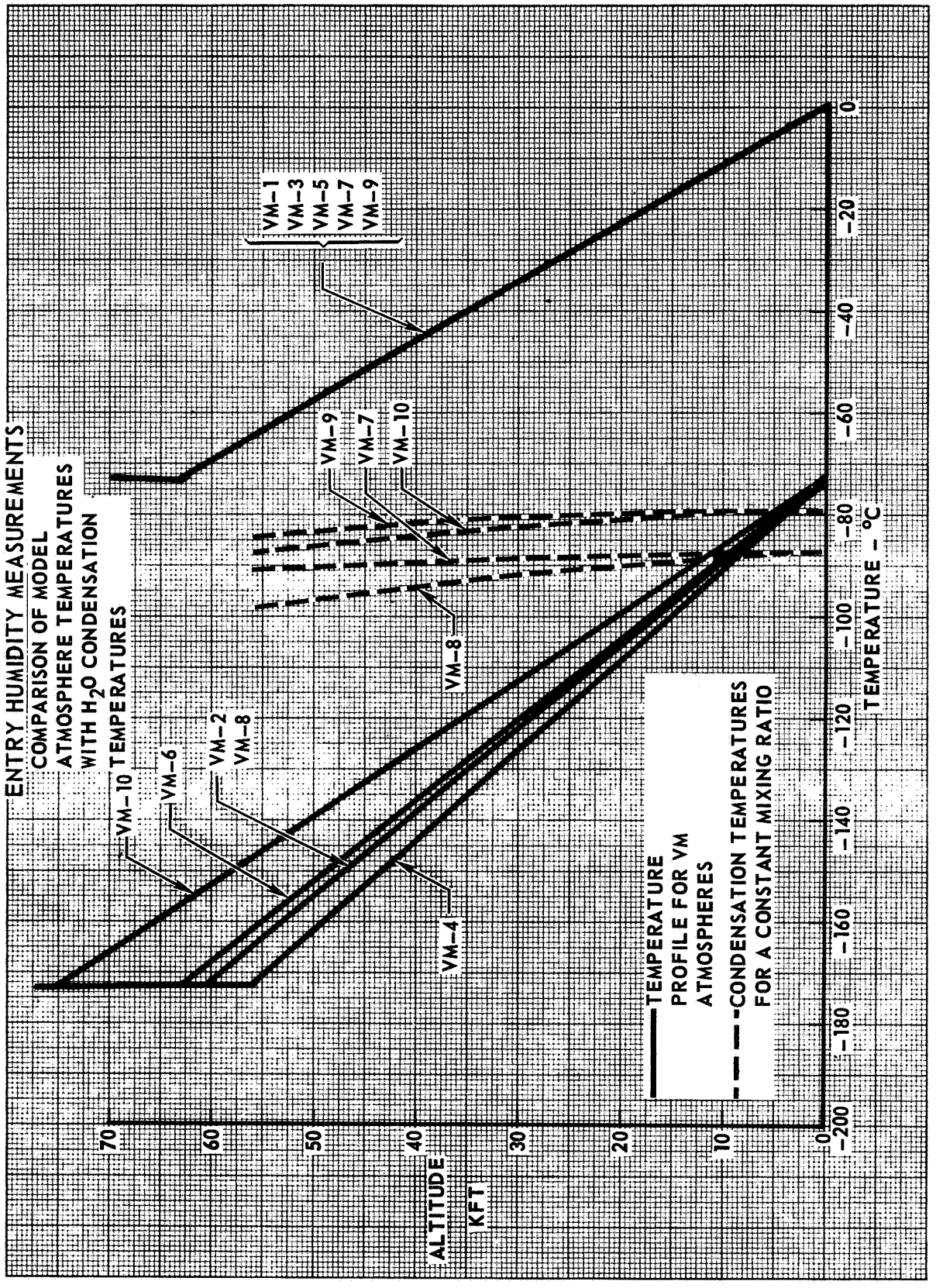

FIGURE 3.2.1-46

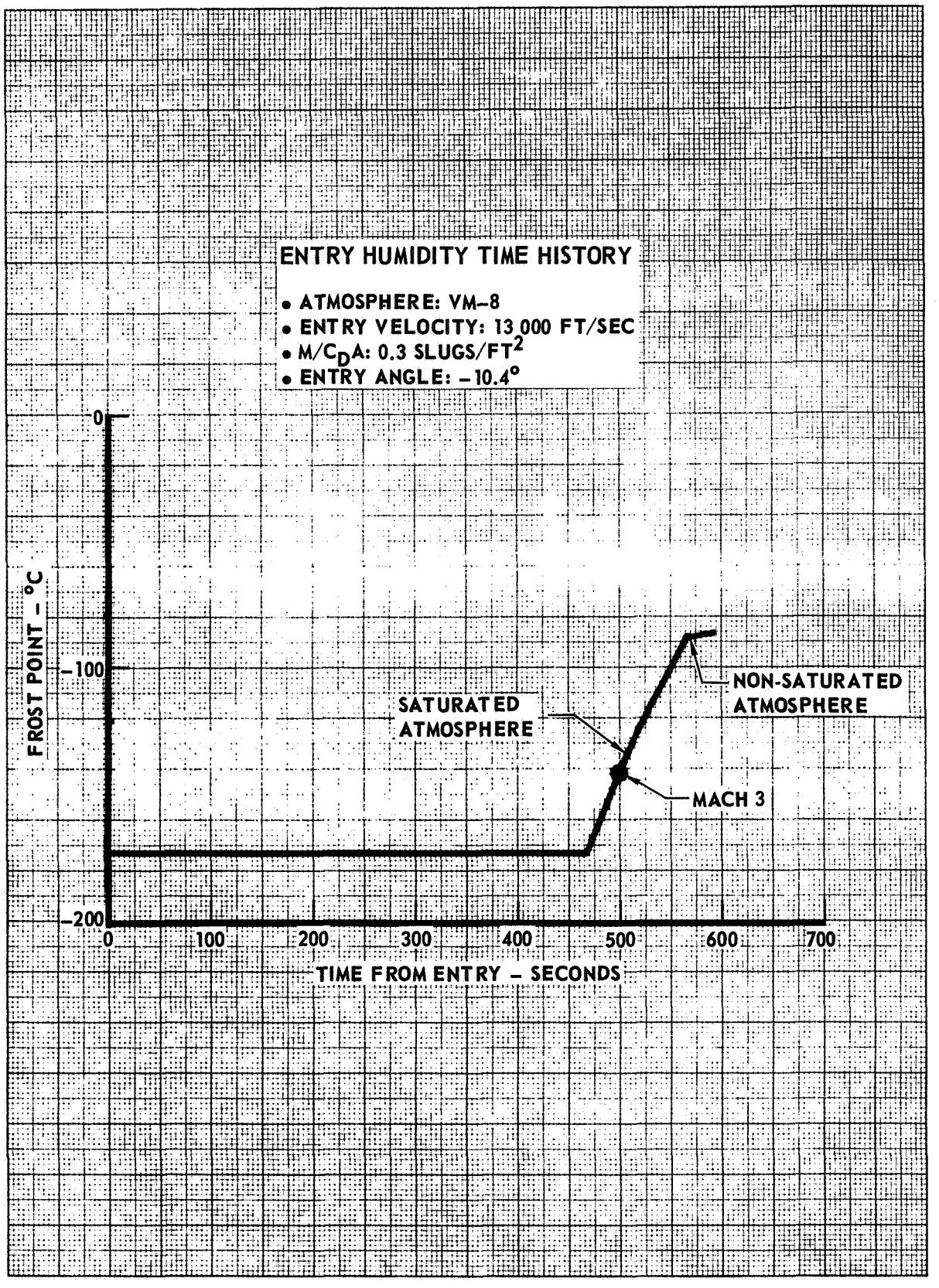

FIGURE 3.2.1-47

TABLE 3.2.1–12

ALUMINUM OXIDE HUMIDITY SENSOR CHARACTERISTICS

RANGE:	–40°C TO –110°C	
ACCURACY:	±2°C	
SIZE:	0.5'' DIA x 2''	SENSOR
	2'' x 3'' x 0.5''	ELECTRONICS
WEIGHT:	0.5 LB	SENSOR
	0.5 LB	ELECTRONICS
	1 LB	TOTAL
POWER:	0.02 WATTS	
DEVELOPMENT STATUS:	DEMONSTRATED TO WITHSTAND HEAT STERILIZATION AND 5 MONTH STORAGE IN VACUUM.	

The amount to which the range can be extended below -110°C is still not well defined. The accuracy of ±2°C is reasonable for the absolute accuracy with which the measurements can be made, taking many factors into account. (The sensitivity of the humidity measurement to small temperature differences is much better than the ±2°C.)

The sensing element is a 3/16 inch by 5/8 inch anodized aluminum foil with a 1/16 x 3/8 inch evaporated metal outer electrode, as illustrated in Figure 3.2.1-48. Water is absorbed from the atmosphere surrounding the sensing element, and this changes the capacitance between the evaporated electrode and the aluminum foil base. The water vapor is absorbed in the thin aluminum oxide coating. This coating, approximately 2 microns thick, produces a fast response to changes in the atmospheric humidity.

At very low humidity levels, the capacitance changes only slightly with changes in frost point, as illustrated in Figure 3.2.1-49. Therefore, assuming an accuracy of 0.5% of the full scale output, the absolute accuracy will decrease for the low frost points. An accuracy of at least ±2°C is expected in the normal range of humidity in the atmosphere of Mars. However, at the high altitudes where the atmospheric temperature is below the frost point, as shown in Figure 3.2.1-46, the atmospheric humidity will correspond to values below -90°C. At -110°C, an accuracy of only ±3 1/2°C is indicated in Figure 3.2.1-50.

The relationship between the frost point accuracy and the vapor pressure accuracy in Figure 3.21-45 makes it evident that the accuracy with which the water vapor pressure can be measured is approximately a factor of 2. This is not much better than the presently predicted uncertainty in the astronomical spectral measurements of the total water vapor on Mars (7 to 21 microns of water vapor total, a factor of three). This might be interpreted to mean that it is not really worthwhile to make the direct measurements in the atmosphere, since the accuracy with which we know the humidity cannot be greatly improved. However, the 7 to 21 microns measurement is subject to some question. Also the direct measurement of the humidity as a function of altitudes will provide a measure of the distribution of humidity with altitude and also give a measurement of the humidity in the localized regions during the entry.

ALUMINUM OXIDE HUMIDITY SENSOR

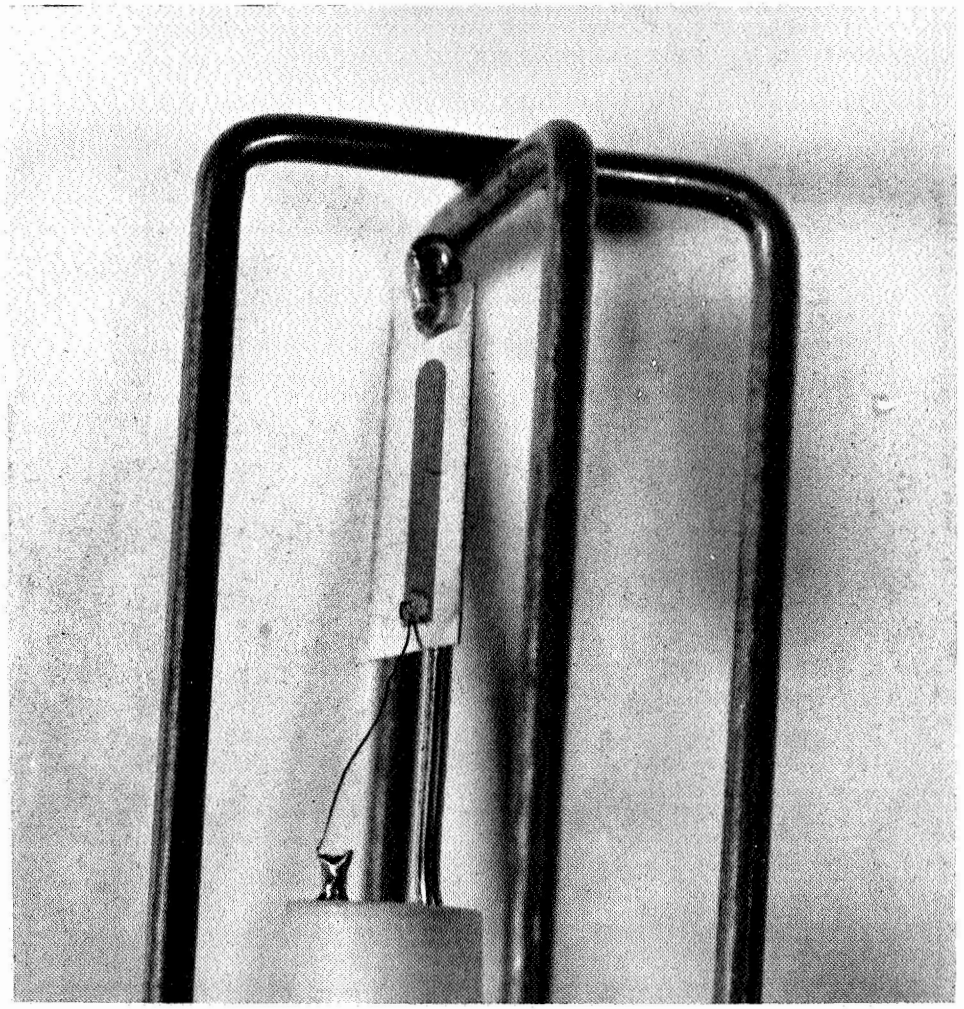

FIGURE 3.2.1–48

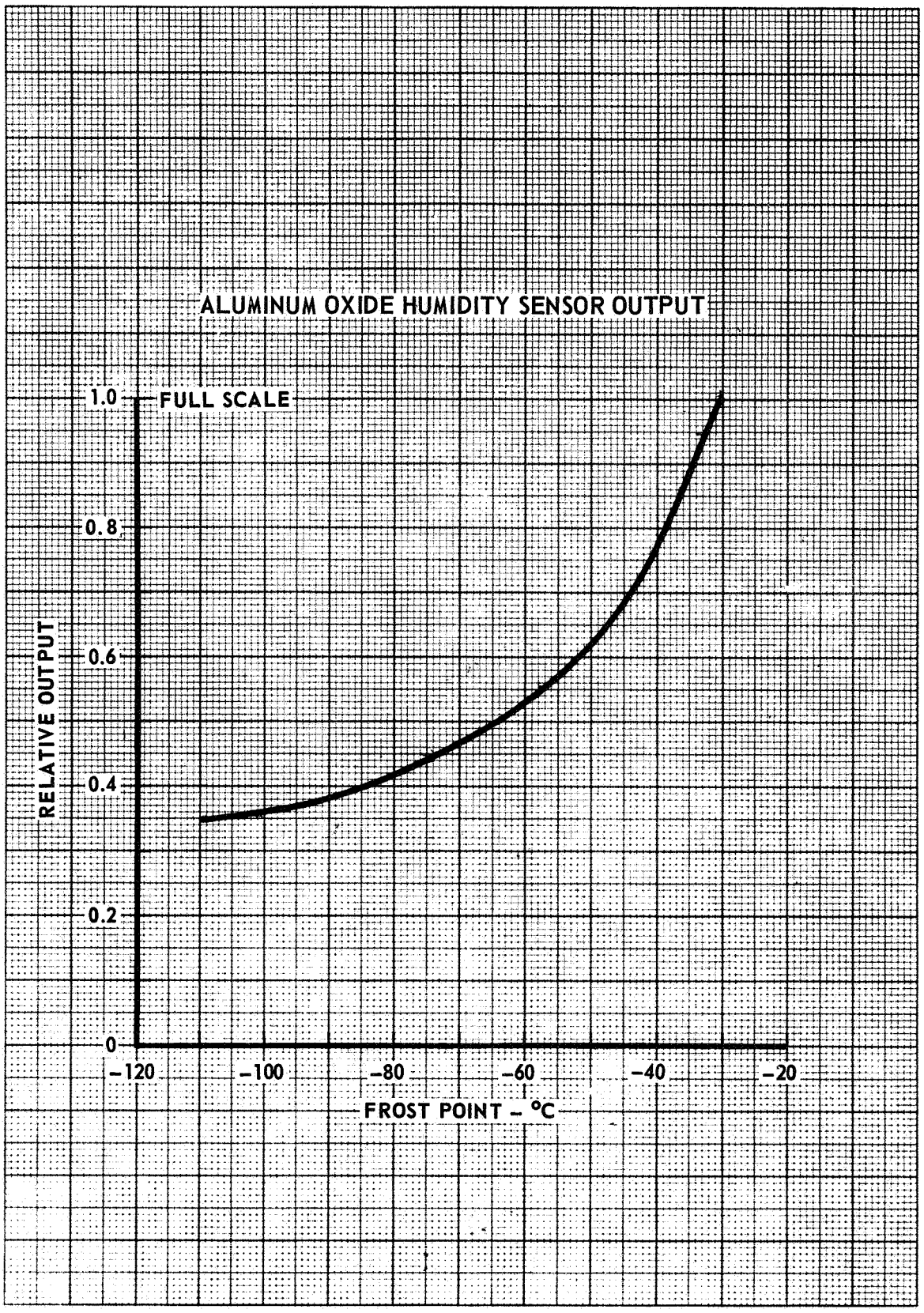
ALUMINUM OXIDE HUMIDITY SENSOR OUTPUT
1.0
FULL SCALE
0.8
0.6
0.4
0.2
0
RELATIVE OUTPUT
-120
-100
-80
-60
-40
-20
FROST POINT – °C

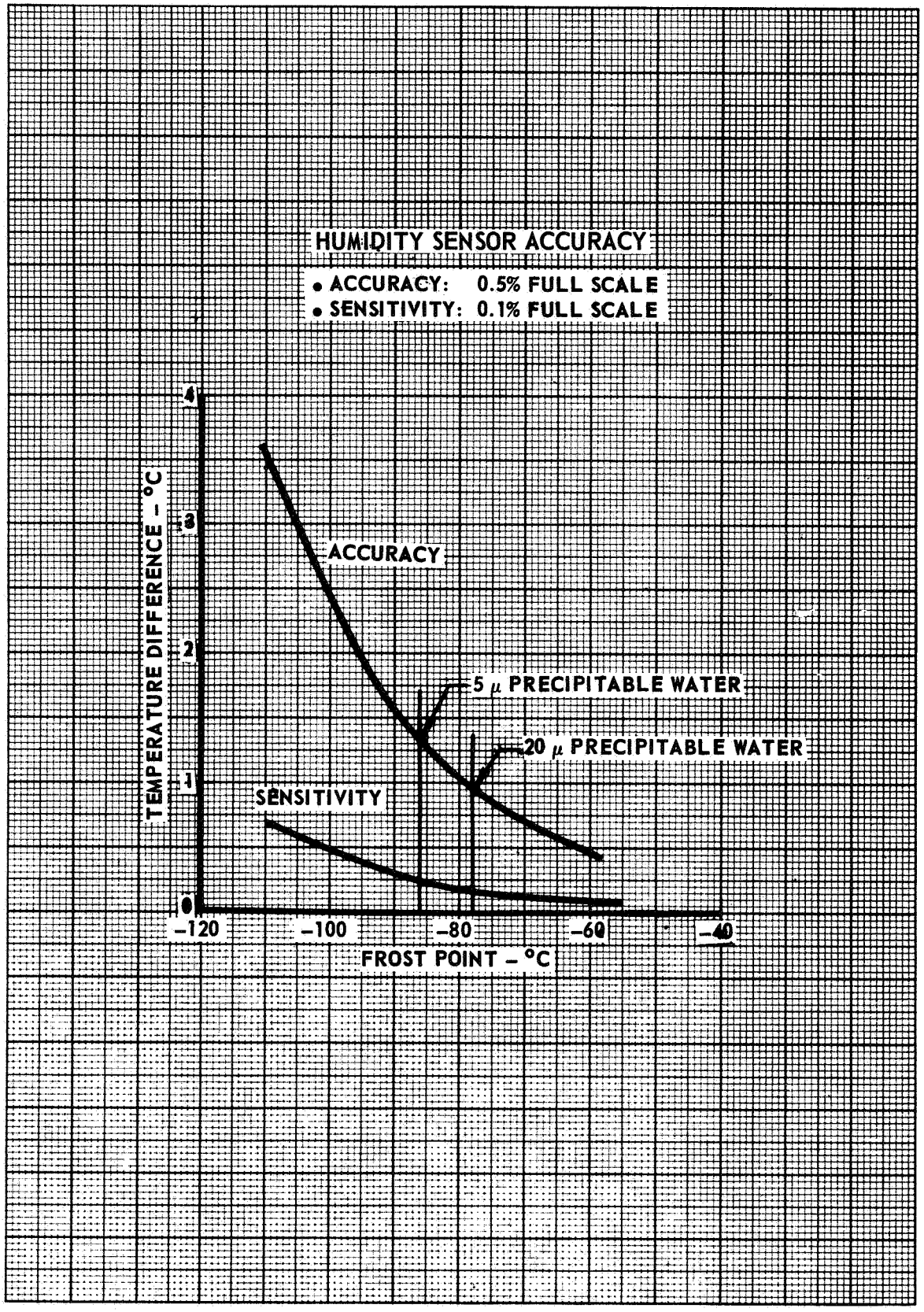

FIGURE 3.2.1–50

An absolute accuracy requirement for the humidity sensor of $\pm 2°C$ appears to be a reasonable value. The best standard provided by the National Bureau of Standards is only $\pm 1.2°C$ at a frost point of -70°C. The use of a mass spectrometer or optical transmission measurements to determine the humidity profile on Mars does not appear to be a better approach than the use of the aluminum oxide sensor. On Earth, where frost points go down as low as -100°C at very high altitudes, the use of optical transmission or mass spectrometer measurements is rarely used for determining the atmospheric humidity, since the aluminum oxide hydrometer and mechanical hydrometers provide convenient and more accurate measurements.

Many difficulties are encountered in trying to determine the time constant of the humidity sensor at very low vapor pressures. This is due to the outgassing and absorption of water vapor by apparatus walls. Time constants of the order of 1 to 2 minutes are not an uncommon result in attempts to make laboratory measurements of changes in humidity at water vapor pressures corresponding to the water vapor pressure on Mars, Figure 3.2.1-51. It is believed that if a test is properly set up to eliminate the effects of the wall or to make the wall effect negligible compared to the time constant of the sensor, the sensor will respond to a step change from -120 to -80°C within a 1 second period.

This measurement will most likely require a dual chamber system in which there is one very large chamber at -80°C frost point and a second very small chamber at -120°C. The sensor would be moved from the -120°C chamber to the -80°C in a small fraction of a second. The -120°C chamber has to be very small compared to the -80°C chamber so that it will not effectively act as a cryo pump and reduce the ambient humidity that the sensor is exposed to when it is moved.

Some measurements have already been made in which a long 4 or 5 ft tube was used. The inside of the tube was coated with ice. One end of the tube was placed in liquid nitrogen to produce a temperature gradient along the tube. The air in the tube was saturated with water vapor from the ice coated walls. It was possible to move the sensor from a region in which the frost point corresponded to room temperature down to a point in the tube where the frost point

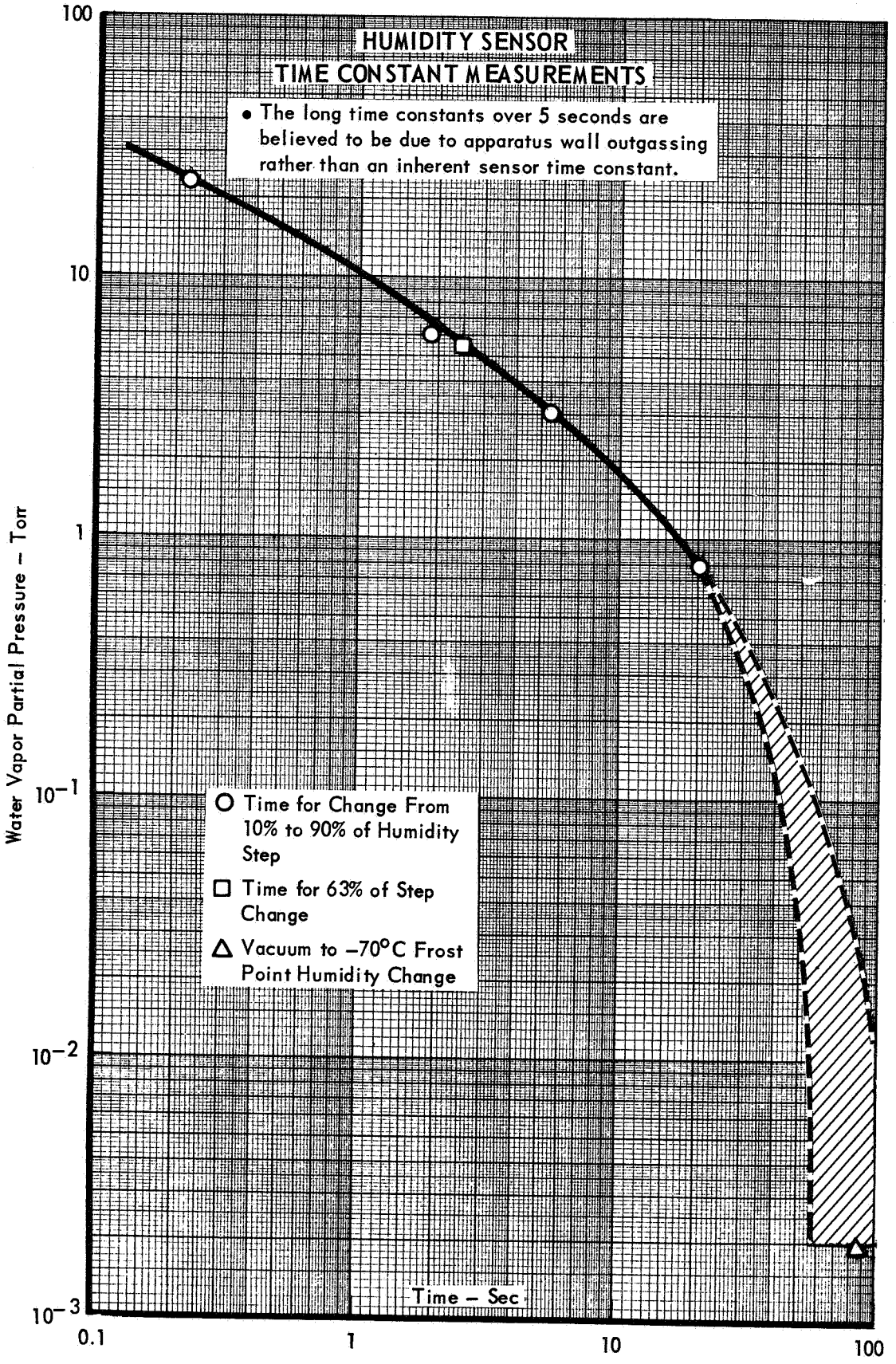

FIGURE 3.2.1–51

was from -80 to -90°C, and the sensor responded to this step change in humidity within 10 seconds.

Conclusions - The aluminum oxide sensor appears to be suitable for making measurements of the humidity profile during entry into the atmosphere of Mars. If the atmospheric temperature profile is such that very low temperatures are encountered at high altitudes, then extremely large variations in the humidity content with altitude may be encountered. If the atmospheric temperature is somewhat higher, the humidity content as a function of altitude may change only slightly. That is, there will be only a small change in the frost point with time during entry.

The time constant for the humidity sensor is expected to be satisfactory. However, to verify that it will be small enough so as not to affect the measurements significantly, it will be necessary to carry out a lab experimental verification of the response of the humidity sensor to a step change in humidity from an extremely low frost point, of the order of -110 to -120°C, up to a frost point comparable to that expected near the surface of Mars, -78 to -86°C.

3.2.1.12 Entry Mass Spectrometer. - Presently available mass spectrometers are suitable for measuring the major components in the Mars atmosphere. To measure the minor constituents of the atmosphere, such as water vapor, however, a modified mass spectrometer, using an electron multiplier will be required. Since it is desired to make long term measurements on the surface following landing, as well as composition measurements during entry, an ion pump is preferred over a vacuum reservoir for evacuating the mass spectrometer. The vacuum reservoir is suitable only for very short measurement periods.

Measurements - The measurement of the major components of the atmosphere of Mars is not expected to be difficult since presently developed units, such as the quadrupole mass spectrometer, will measure atmospheric composition with a threshold as low as 0.01%. The miniature quadrupole mass spectrometer has a range from 16 to 50 mass units and five selected masses can be detected in one second.

The objective for the Mars Soft Lander is to cover a wide range, from 10 to 60 mass units. A parametric analysis was carried out to determine the

trade-off between the composition measurement accuracy, the scanning rate, and the use of a scanning mass spectrometer which covers the whole mass range versus a non-scanning spectrometer which will detect only individual masses. Since it will not be difficult to detect the major components in the atmosphere, the parametric analysis applies primarily to the accuracy with which the minor atmospheric constituents can be measured.

As one result of the parametric analysis, it was determined that it will be possible to detect water vapor in the atmosphere using a mass spectrometer if an electron multiplier detector is used in the analyzer. If an electron multiplier detector is used, then the analyzer noise will be simple shot noise and is easily evaluated. The RMS fluctuation in the analyzer current is the square root of $2\ eI\Delta f$, where e is the electron charge, I is the analyzer current corresponding to a particular component of the atmosphere, and Δf is the bandwidth of the amplifier. A typical value for the ionization efficiency of the mass spectrometer is 5×10^{-6} amp/torr and a reasonable value for the chamber total pressure is 10^{-4} torr. It is desired to have the pressure as high as possible in order to have a high output current. However, if the pressure is too high then there will be a problem with the filament lifetime, if an electrically heated filament is used to provide electrons for the ionization process. With the 5×10^{-6} amps/torr efficiency and 10^{-4} torr pressure, the total current out of the analyzer will be 5×10^{-10} amps. If a single component represents 10^{-3}% of the total current, then the current corresponding to that component will be 5×10^{-15} amps.

In order to calculate the shot noise corresponding to this current, it is necessary to know the amplifier bandwidth. This bandwidth is determined by the mass range, the mass accuracy, and the scan time. For a mass spectrometer range from 10 to 90 units, a 2 second scan time, and a resolution of 1/2 mass unit, the bandwidth will be 2 x the mass unit range (80), divided by the mass resolution (1/2), divided by the scan time, (2 seconds) which results in a 160 Hz bandwidth.

The shot noise is simply $\sqrt{2\ eI\Delta f}$. This is the RMS fluctuation in the output current. If we divide by the current to obtain the relative fluctuation

in the output current, then the noise ratio becomes $\sqrt{2\ e\Delta\ f/I}$.

The accuracy required for the water vapor composition measurement was determined by first converting the water vapor concentration in microns to the water vapor concentration in terms of percent of the total atmosphere. (Ten microns of water vapor corresponds to a little less than .004% of the total atmosphere if the atmosphere contains 10 microns for a 10 millibar surface pressure.) The composition measurement accuracy was then calculated using the shot noise equation as providing the 1σ measurement accuracy. The 3σ noise level for water vapor detection as a function of the water vapor concentration ranges from 50% at 1 micron to 11% at 20 microns as illustrated in Figure 3.2.1-52.

If instead of scanning the range from 10 to 90 mass units, which requires a 160 cycle bandwidth, several individual masses are detected, the entire 2 second time can be made available for making each mass measurement. The bandwidth is then reduced from 160 Hz to 1 Hz. Much more accurate measurements are then possible, the increase in accuracy being the square root of the ratio of the bandwidths, (12.7).

By using an electron multiplier, it is evident that water vapor measurements will be possible using either a scanning mass spectrometer or a non-scanning mass spectrometer. Even if it is not possible to obtain completely shot-noise-limited measurements, reasonable accuracies should still be possible.

The miniature quadrupole mass spectrometer, which does not have an electron multiplier detector, is not suitable for making measurements on water vapor. The detection limit for this unit is 100 parts per minute, or .01%, while the expected amount of water vapor corresponding to 7 to 20 microns of precipital water is 13 to 150 parts per million (1.3×10^{-3}% to 1.5×10^{-2}%). In addition to the water vapor, there are many other compounds that may be present as minor constituents of the Mars atmosphere. The upper limits that have been determined for the abundance of several compounds, as listed in Table 3.2.1-13, range from 0.08 to 20 cm atmospheres. For a total atmospheric abundance of 100 meter atmospheres, 1 cm atmosphere will correspond to ~0.01% of the total. It is evident in Table 3.2.1-13 that several compounds of interest have upper limits of less than 1 cm atmosphere and an accuracy for the

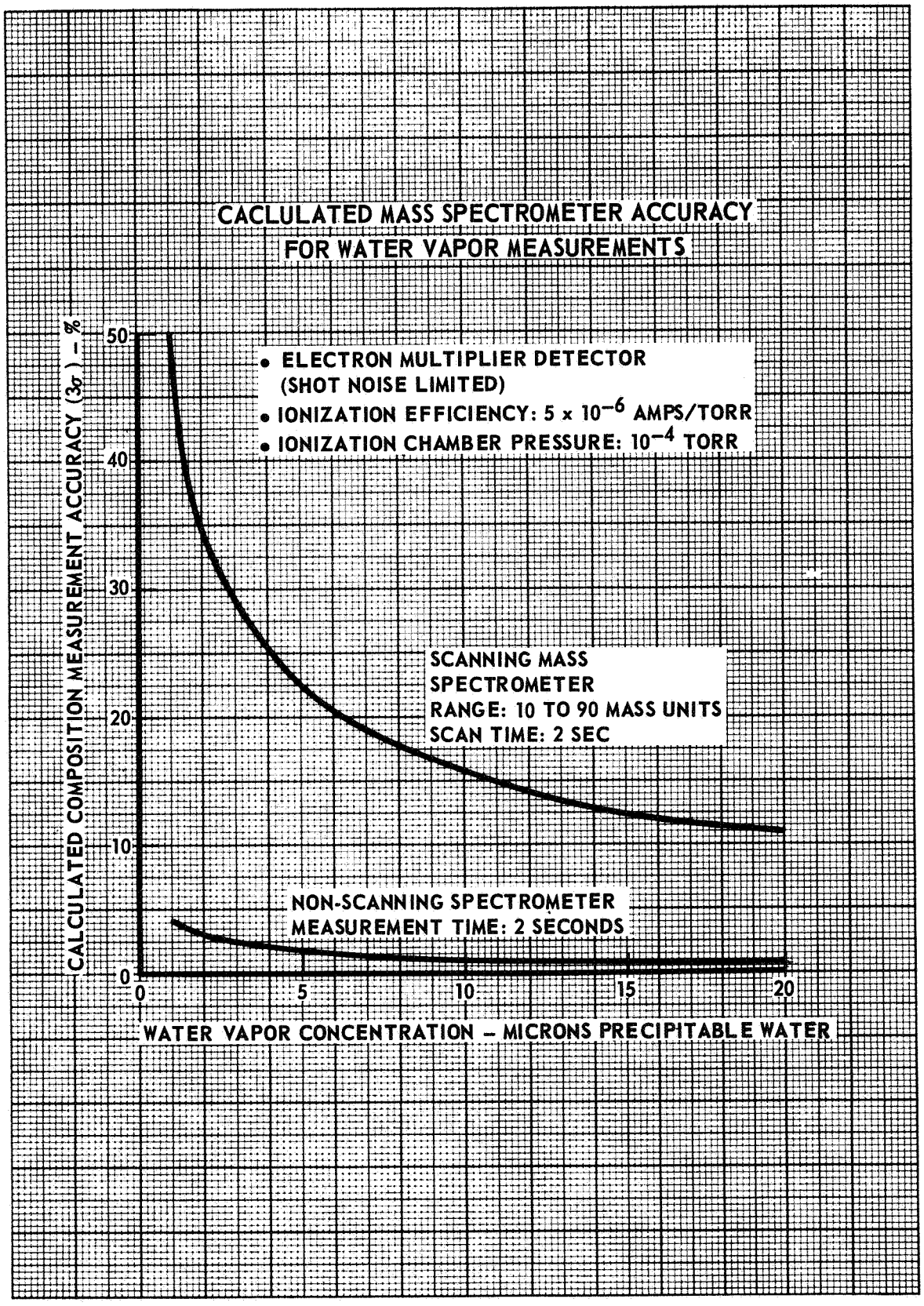

FIGURE 3.2.1–52

TABLE 3.2.1–13

ATMOSPHERIC COMPOSITION

UPPER LIMIT ON ABUNDANCES

COMPONENT	UPPER LIMIT CM ATM
NO	20
CO	10
H_2S	7.5
O_2	2
H_2CO	0.3
COS	0.2
CH_4	0.1
NH_3	0.1
N_2O	0.08

abundance measurement of less than 1 cm atmosphere is therefore desirable.

To obtain measurements with an accuracy of better than the 0.01% corresponding to 1 cm atmosphere for most scan times, it will be necessary to go to an electron multiplier detector as illustrated in Figure 3.2.1-53. For the mass range from 10 to 90 mass units, a scan time of 2 seconds, a 1/2 mass unit resolution and a 160 Hz bandwidth, the accuracy with which the .001% constituent can be measured is ±30%. If the bandwidth is reduced to 16 Hz then a .001% component can be measured with an accuracy of ±10%.

Making measurements on selected mass units using multiple detectors greatly improves the accuracy, as shown. However, only a limited number of detectors is feasible, so the number of mass units or the number of compounds which can be detected is reduced. Extrapolating the 2 second scan time line in Figure 3.2.1-53 to higher component fractions indicates that the measurements for the major components of the atmosphere will be accurate to better than 1%. Other factors, such as outgassing of the sampling system, and ionization effects, can prevent this high accuracy from being attained.

As the atmosphere moves past the shock front it will be heated and the gas composition will change. The large changes that take place during the initial part of the entry completely change the composition, as illustrated in Figure 3.2.1-54. At 400 000 ft for entry into the VM-10 atmosphere, the Mach number is approximately 21 for a 13 000 ft/sec entry at a 10.4° angle. It can be seen that the carbon dioxide in the atmosphere is almost completely dissociated. For much lower Mach numbers at this altitude, such as Mach 4, the composition will not be affected by the stagnation region heating. Although calculations have not been made over the full range of entry conditions, Mach numbers, and altitudes, it appears, at the present, that the composition behind the shock front will not be greatly different than the composition of the ambient atmosphere if measurements are made only below Mach 4.

Instrument Characteristics - Either a double focusing magnetic or a quadrupole mass spectrometer should be satisfactory for making the entry composition measurements. Originally, the quadrupole mass spectrometer was chosen, since magnetic measurements were planned on the surface. Since magnetic

CALCULATED MASS SPECTROMETER ACCURACY FOR MINOR CONSTITUENTS

- ELECTRON MULTIPLIER DETECTOR (SHOT NOISE LIMITED)
- IONIZATION EFFICIENCY: 5×10^{-6} AMPS /TORR
- IONIZATION CHAMBER PRESSURE: 10^{-4} TORR

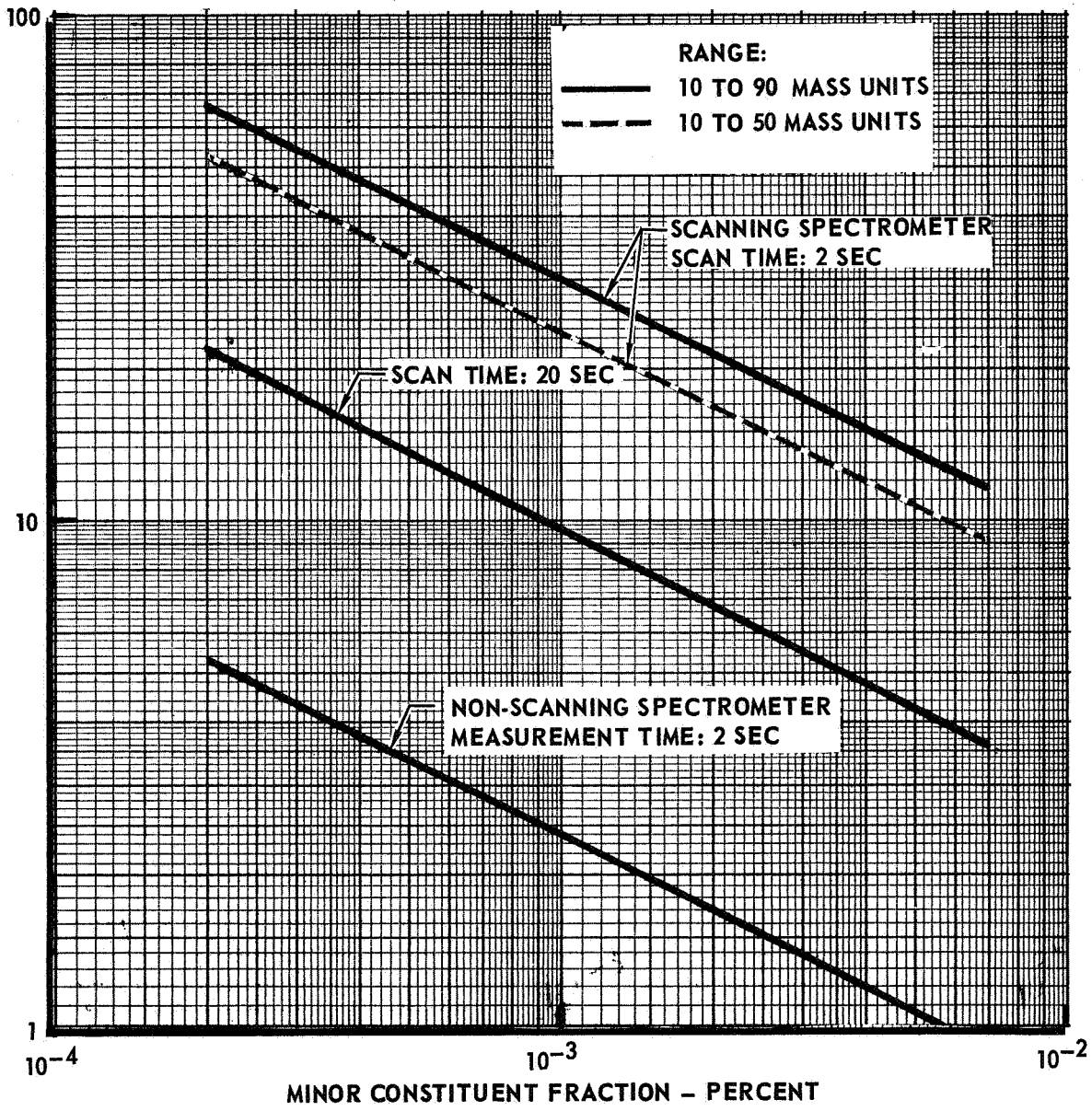

FIGURE 3.2.1–53

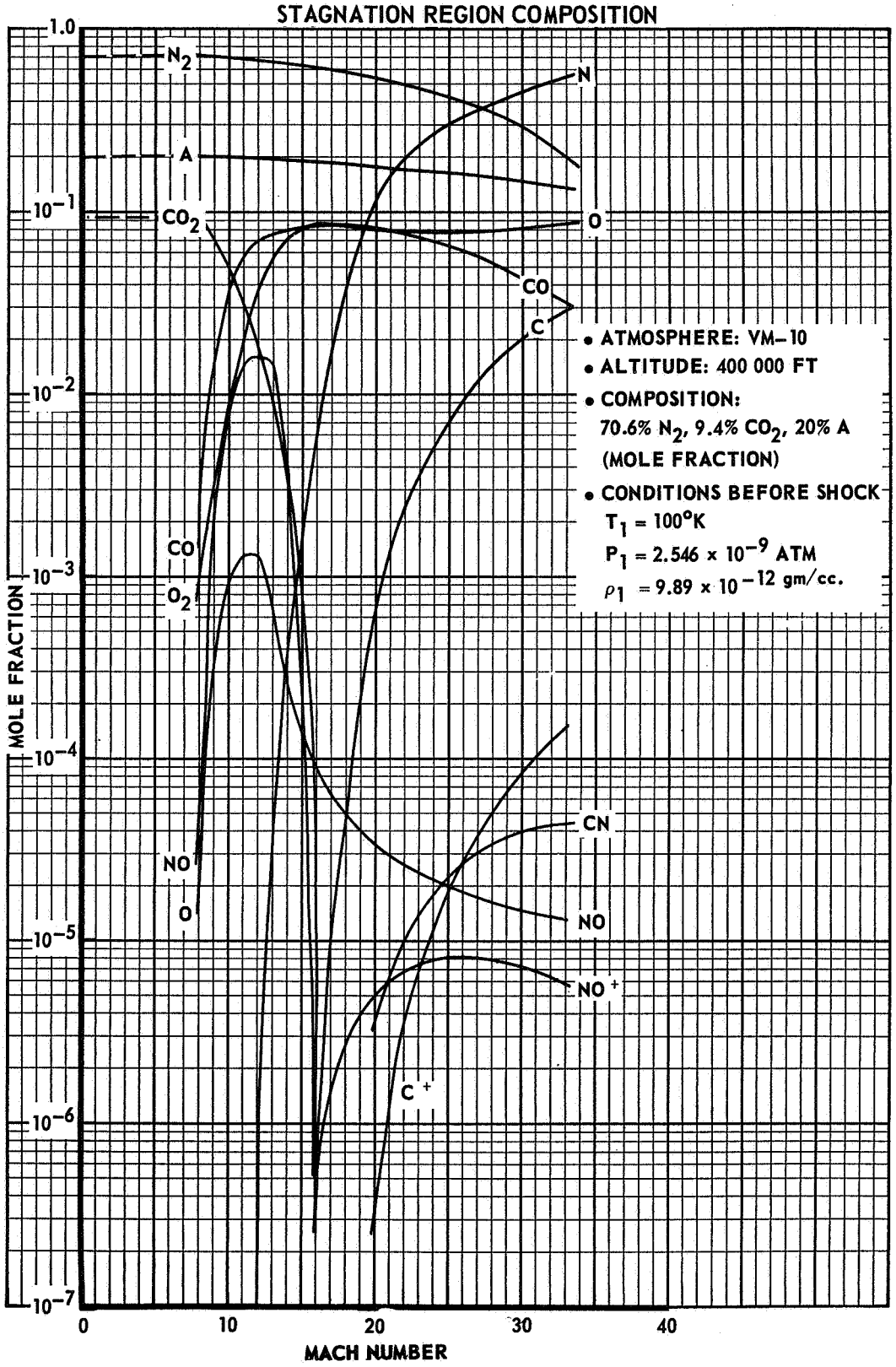

FIGURE 3.2.1–54

measurements are not now included, it is not necessary to restrict the type of unit to a quadrupole instrument. The weight for either type of mass spectrometer is estimated to be between 9 and 10 pounds.

In order to use the mass spectrometer for atmospheric composition measurements both during entry and on the surface, a special sampling tube system design will be necessary. A sample tube which would reach from the stagnation region portion of the heat shield to the mass spectrometer mounted on the lander would be very long, about 2 to 4 ft. For normal measurements, the length of this tube is restricted to 1 ft or less and a very small diameter capillary tube is used with the molecular leak input at the end of the tube away from the mass spectrometer. The very small diameter tube is used to keep the total surface area of the inside portion of the tube small. This reduces the potential contamination of the sample from the outgassing of the internal walls. Lab tests will be required to determine whether or not the outgassing will seriously contaminate the sample for the longer capillary tubes.

An alternate technique to having the leak inlet near the aeroshell nose port is to place the leak near the mass spectrometer far from the inlet. This eliminates the capillary outgassing problem but introduces the problem of composition changes along the tube.

A study was made to determine whether or not the ion pump used to evacuate the mass spectrometer could be replaced by a vacuum bottle. This parametric analysis compared the weight for a vacuum reservoir evacuation system with the weight of presently available ion pumps. To make high accuracy measurements, a pumping speed of approximately 1 meter per second will be required to maintain the ionization chamber at 10^{-4} torr while the analyzer region is at a lower pressure. The weight of a 1 meter per second ion pump, as shown in Figure 3.2.1-55, is approximately 2.6 lb. A 3 meter vacuum bottle which would provide only 3 seconds of operation would weigh approximately 2.2 lb, including 1 lb for valving and tubing while a 25 liter bottle to provide 25 seconds of operation at 1 liter per second weighs approximately 6.2 lb. It is expected that the 6.2 lb weight of the 25 liter bottle would increase the weight of the mass spectrometer to approximately 14 lb. The weight required for the high voltage power supply and batteries to operate the ion

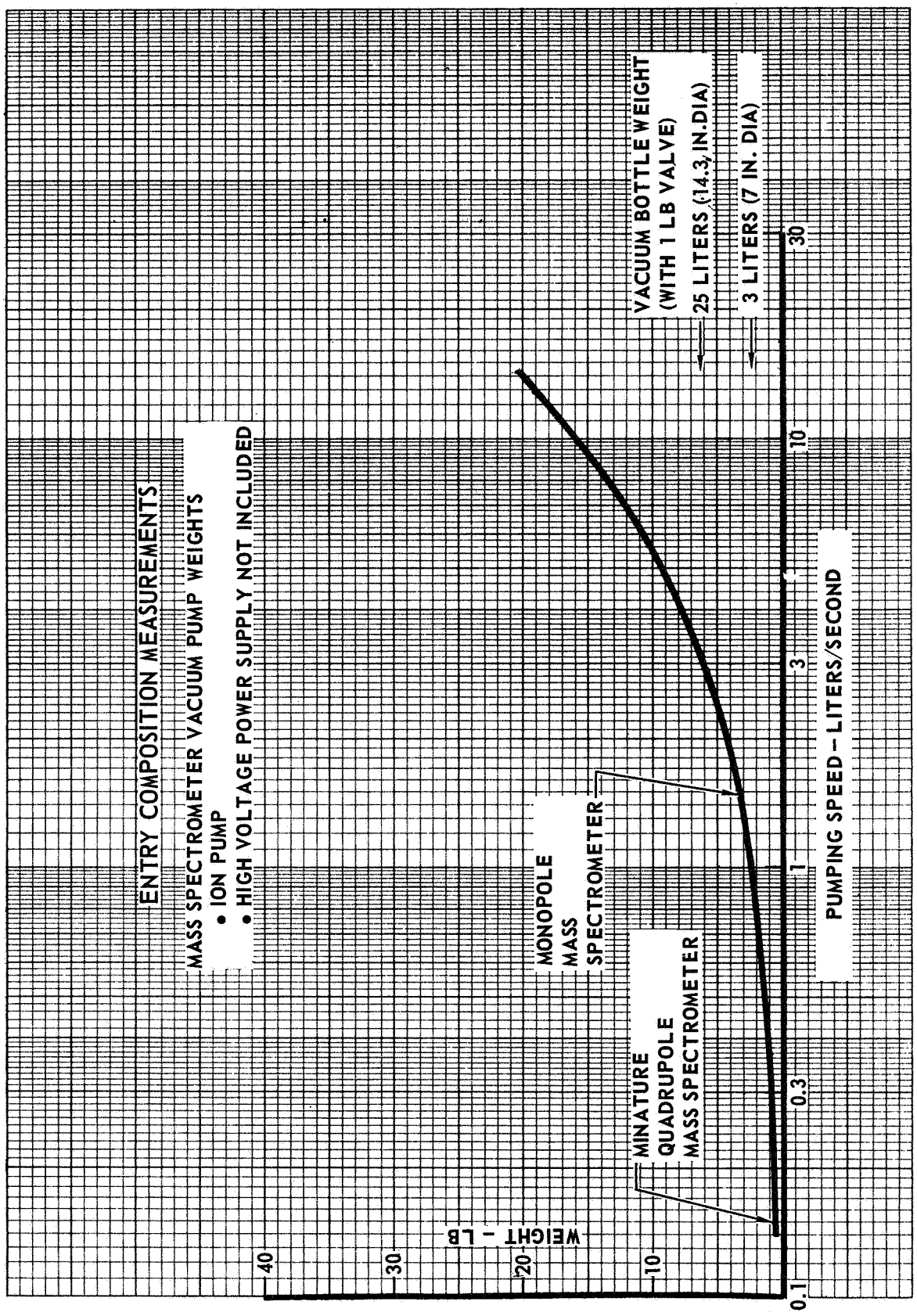

FIGURE 3.2.1–55

pump has not been included in the ion pump weight in Figure 3.2.1-55. The operating power requirements are very small, however, and adding in the weight required for the electrical power is not expected to greatly affect the curves shown in Figure 3.2.1-55.

It is evident that for the miniature quadrupole mass spectrometer which detects only 5 particular compounds has such a small pumping speed, 0.15 liters per second, that the 3 liter reservoir would be satisfactory for 20 seconds of operation. However, the ion pump is still preferred over the vacuum bottle even for this low pumping speed since a 0.15 liter per second ion pump weighs only about 1/2 lb. and provides very long term operation. The high voltage power supply weight has not been included in the ion pump weight, however, even if the power supply weight is included, it is not expected that the vacuum reservoir will be preferred over the ion pump (especially if measurements of atmospheric composition are made on the surface over a long period of time).

The ion pump weights in Figure 3.2.1-55 are for presently available units. These pumps were not necessarily designed to minimize weight, and special pump designs directed toward keeping the weight down should significantly reduce the weight.

It is expected that at lower altitudes, where measurements will be made at velocities below Mach 4, the composition of the atmosphere will not change with altitude. However, for the very high altitudes, from 70 to 100 km and above, it is expected that the atmospheric composition will change with altitude. It would probably be necessary to use a separate mass spectrometer in order to measure the atmospheric composition at very high altitudes before the high temperature portion of the entry. The present entry science payload for the Mars Soft Lander does not include provisions for making these very high altitude measurements since the instrument payload was kept as low as possible. It would, however, be desirable to include a second mass spectrometer for a high altitude measurement for heavier payloads.

One problem associated with this type of measurement is that the transition region from compositions which vary with altitude to compositions that are uniform with altitude comes at altitudes where high entry heating temperature will occur. These high temperatures will make it difficult to determine

the composition in this region.

Conclusions - Presently available mass spectrometers are suitable for measuring the major components of the Mars atmosphere. Special mass spectrometers will need to be developed if the minor constituents of the atmosphere are to be measured. The operation of the mass spectrometer using a long scan time on the surface will greatly increase the accuracy of the mass spectrometer for measuring the amount of minor constituents which are present in the atmosphere. An ion pump is preferred rather than a vacuum reservoir for evacuating the mass spectrometer.

References for 3.2.1

3.2.1-1 Leighton, R. B. et al, Mariner IV Pictures of Mars. NASA CIT/JPL TR 32-884, 1967.

3.2.1-2 Leovy, C. B.; and Mintz, Y.: A Numerical General Circulation Experiment for the Atmosphere of Mars. Rand RM-5110-NASA, Dec. 1966.

3.2.1-3 Leovy, C. B.; and Mintz, Y.: Numerical Simulation of the General Atmospheric Circulation and Climate on Mars. Rand AR-362-JPL, Jan. 1968.

3.2.1-4 Leighton, R. B.; and Murray, B. C.: Behavior of Carbon Dioxide and Other Volatiles on Mars. Science, Vol. 153, 8 July 1966, pp 136-144.

3.2.2 COMMUNICATIONS - The communications system includes the equipment necessary for the processing, transmission, and reception of science and engineering data and commands. This includes the telemetry, data storage, transmission and reception, and antenna equipment located on the capsule and supporting equipment mounted on the orbiter. For convenience, the communication system is discussed in two parts: the equipment associated with the capsule descent, entry, and landing functions, and that associated with operations of the surface payload.

3.2.2.1 Entry communications. - The entry communications are concerned with telemetering information from the entering capsule to the orbiting spacecraft. The most important factor in defining the link is the relative positions of the spacecraft and the capsule. This factor is subdivided into two problems: that of the relative positions at the time of entry, and that of the relative positions during parachute oscillation.

3.2.2.1.1 Performance analyses: One of the more critical entry communications parameters is the transmitter power required during entry. This is a function not only of the transmission range and the antenna patterns, but also of the interference created by the signal reflected from the surface of the planet. Figure 3.2.2-1 illustrates the geometry of the entry communications problem. The problem can be subdivided into two parts; the definition of the "geometry" and the definition of the effects of the interference on the modulation.

The "geometry" is the determination of the range and look angles and the amount of reflected power from the surface for the trajectories in question. The geometric investigation has two principal outputs in addition to the transmission ranges and look angles: the ratio of the direct path signal power to the reflected path signal power (D/J) and the ratio of specular (or constant component) power to diffuse (or Rayleigh component) power of the reflected signal (ξ). Components of these two parameters are the differential antenna gains (transmitting and receiving) of the two propagation paths (ΔAG), the differential free space attenuation of the paths (ΔFS), the fresnel reflection coefficient (RC), the specular power (α_J^2), and the diffuse power ($2\sigma_J^2$).

ENTRY COMMUNICATIONS GEOMETRY

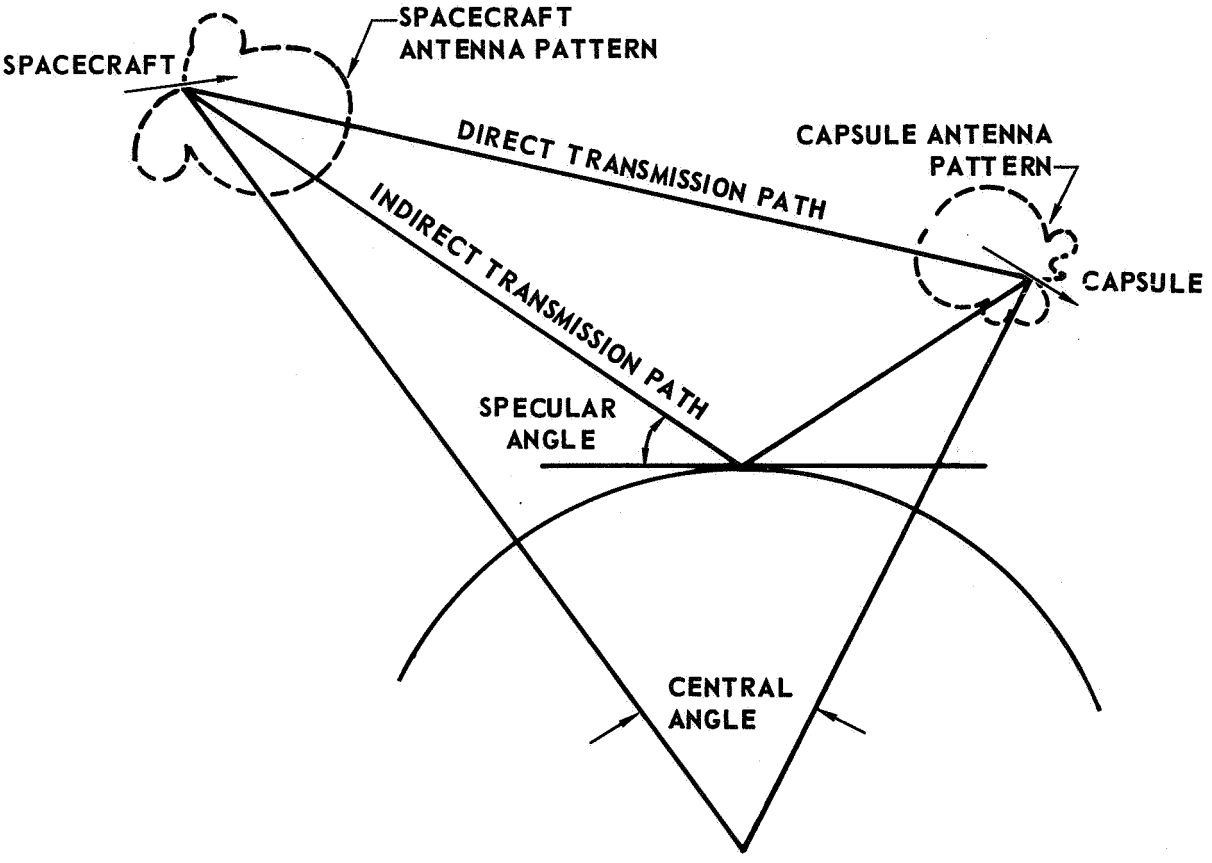

FIGURE 3.2.2–1

For this investigation the reflected power is computed from a horizontally polarized signal over a finite conductivity, smooth, spherical surface and the resultant power is apportioned to specular and diffuse components. Table 3.2.2-1 lists the complete trajectories investigated. These trajectories were chosen because they bound the problem.

TABLE 3.2.2-1

ENTRY TRAJECTORIES INVESTIGATED

Atmosphere	Entry Angle	Capsule Lead Angle at Entry
VM-8	-15°	-5°, 0°, 5°, 10°, 15°, 25°
VM-8	-20°	-5°, 0°, 5°, 10°, 15°, 25°
VM-9	-15°	-5°, 0°, 5°, 10°, 15°, 25°
VM-9	-20°	-5°, 0°, 5°, 10°, 15°, 25°

For each of these 24 trajectories, the power required for a 1×10^{-3} error rate was determined for a noncoherent 2FSK modulation, where both of the receiver outputs and the composite interference signal are taken as modified Rayleigh functions. Two fundamental interference situations may arise: first, the reflected symbol may be the same as the direct symbol (as seen by the receiver), which is termed Mark Mark interference; and, second, the reflected symbol may be different from the direct symbol, defined as Mark Space interference. The Mark Mark situation may be subdivided into three conditions, where the RF interference phasor is "in phase," "out of phase," or "in quadrature" with the RF direct phasor. For our analysis we have investigated the Mark Mark "out of phase" phasor situation. The probability of error in this situation is termed as PEMM (MAX). This is generally the worst case.

The required transmitter power over a trajectory is then

$$P = K + E/No\ (D/J,\ \xi)$$

where K is the link figure of merit, including range and look angle sans the threshold, and E/No is the threshold power, which is a function of D/J and ξ. This link is defined further by the Link Table of Table 3.2.2-2 . Figure 3.2.2-2 is typical of the power requirements for a typical entry.

TABLE 3.2.2–2

ENTRY LINK TABLE

PARAMETER	VALUE	TOLERANCE	NOTES
TRANSMITTER POWER	$+P_o$ dBm	+.5 –.5	TO BE DEFINED
TRANSMIT CIRCUIT LOSS	–.5 dB	+.2 –.3	ASSUMED
TRANSMIT ANTENNA GAIN	+XAG	+.5 –.5	TO BE DEFINED
SPACE LOSS (400 MHz)	$-84.5 - 20\ \mathrm{LOG}_{10} d$	+0 –0	d IN KILOMETERS
POLARIZATION LOSS	+0 dB	+0 –.5	ASSUMED
RECEIVING ANTENNA GAIN	+RAG	+0 – 3	TO BE DEFINED
RECEIVING CIRCUIT LOSS	–1 dB	+.2 –.2	ASSUMED
TOTAL RECEIVED POWER	$P_o + \mathrm{XAG} + \mathrm{RAG} - 86 - 20\ \mathrm{LOG}_{10} d$	+1.4 –5.0	
NOISE DENSITY (555°K)	–171.2 dBm/Hz	+.2 –.7	+25° –80°K
BIT RATE	$+10\ \mathrm{LOG}_{10} R$ (BPS)	+0 –0	TO BE DEFINED
THRESHOLD	$+E/N_o$	+0 –0	TO BE DEFINED
BT AND SYNCHRONIZER DEGRADATION	+2 dB	+0 –0	ASSUMED
SENSITIVITY	$-169.2 + E/N_o + 10\ \mathrm{LOG}_{10} R$	+.2 –.7	
MARGIN	+5.2 dB	+2.1 –5.2	WORST CASE

TRANSMITTER POWER $P_o = -\mathrm{XAG} - \mathrm{RAG} - 78 + E/N_o + 10\ \mathrm{LOG}_{10} R + 20\ \mathrm{LOG}_{10} d$,

WHERE $\mathrm{XAG} = 10\ \mathrm{LOG}_{10}\ 3.6\ \cos^2 \Delta_c$

AND $\mathrm{RAG} = 44.3136 + 20\ \mathrm{LOG}_{10} \dfrac{1}{BW_s} \cos \dfrac{1.57\ \Delta_s}{BW_s}$

WITH Δ_c AND Δ_s THE ANGLES OFF BORESIGHT AND BW_s THE SPACECRAFT BEAMWIDTH (TYPICALLY 55°)

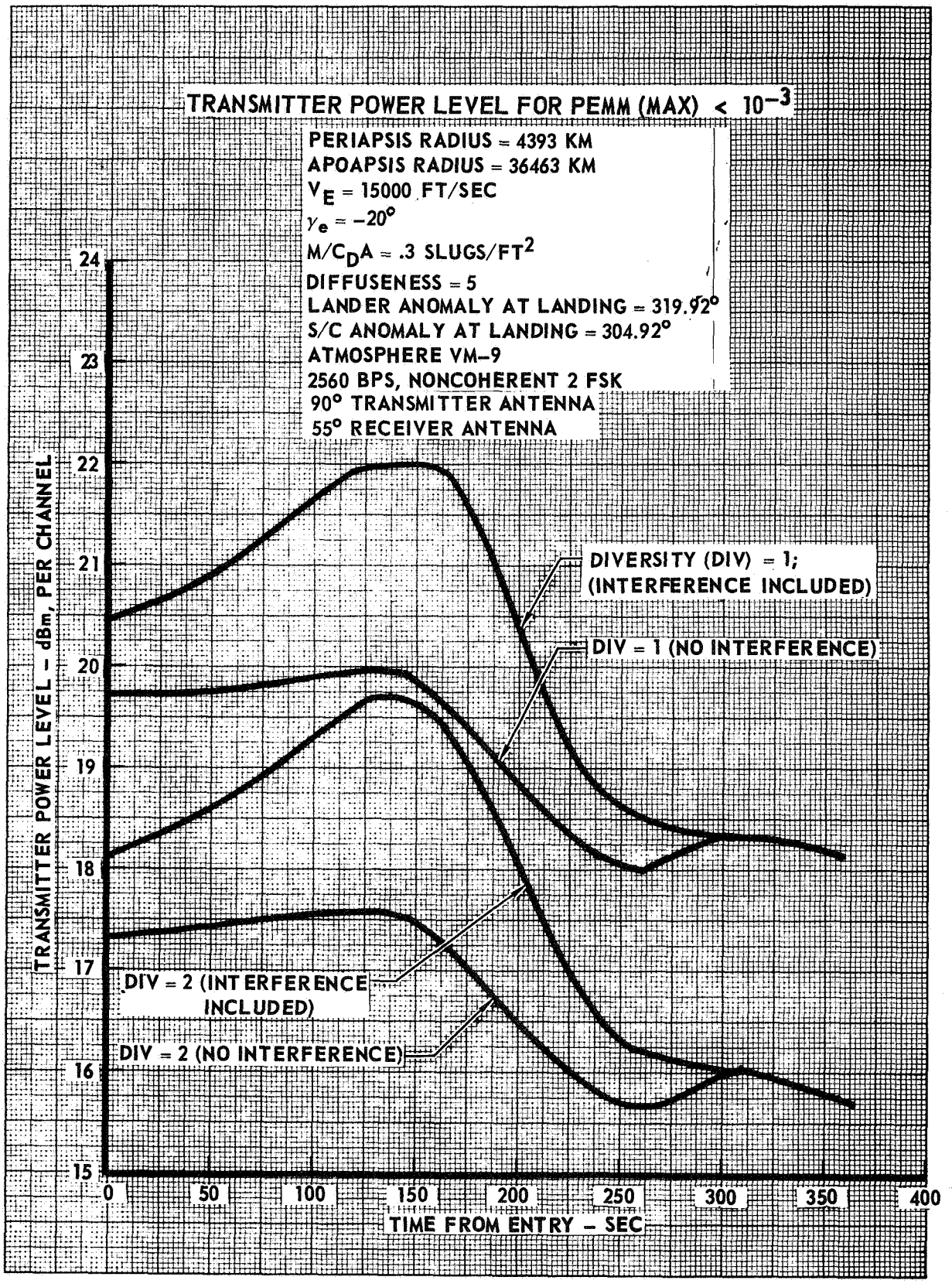
TRANSMITTER POWER LEVEL FOR PEMM (MAX) < 10^{-3}
PERIAPSIS RADIUS = 4393 KM
APOAPSIS RADIUS = 36463 KM
V_E = 15000 FT/SEC
$\gamma_e = -20°$
M/C_DA = .3 SLUGS/FT^2
DIFFUSENESS = 5
LANDER ANOMALY AT LANDING = 319.92°
S/C ANOMALY AT LANDING = 304.92°
ATMOSPHERE VM-9
2560 BPS, NONCOHERENT 2 FSK
90° TRANSMITTER ANTENNA
55° RECEIVER ANTENNA
DIVERSITY (DIV) = 1; (INTERFERENCE INCLUDED)
DIV = 1 (NO INTERFERENCE)
DIV = 2 (INTERFERENCE INCLUDED)
DIV = 2 (NO INTERFERENCE)
TRANSMITTER POWER LEVEL - dBm, PER CHANNEL
24
23
22
21
20
19
18
17
16
15
0
50
100
150
200
250
300
350
400
TIME FROM ENTRY - SEC

FIGURE 3.2.2–2

The results of this investigation are shown in Figures 3.2.2-3, 4, 5, 6 and 7. A 10° tolerance has been added to the capsule orientation to account for the cumulative attitude uncertainties during descent from orbit and the resultant entry oscillations. Note that each point on these curves represents the greatest power required on a complete entry trajectory to maintain an error rate of 10^{-3} for a 2FSK modulation in a Mark Mark out-of-phase phasor interference situation. The figures illustrate, respectively (a) the individual effects of the atmospheres and entry angles both with and without the reflected signal interference, (b) the effect of diversity on the transmission system, (c) the effect of the degree of diffuseness of the reflected signal, and (d) the extremes of these conditions (VM-8, -15°, and $\xi = 1$).

It is apparent from this investigation that the choice of capsule lead angle at the time of entry significantly affects the power required for data transmission. If no reflected signal were present, the allowable capsule lead angles would be constrained only by the range and antenna look angle considerations, or to essentially -3 deg. to greater than +25 deg. The interfering signal, however, narrows this lead angle window to 4 deg, $\pm$ 5 deg. Outside these ranges, the transmitter power requirement increases rapidly.

Within this central angle the use of diversity is not warranted. For example, in a VM-8, -15° entry with a central angle of 5° at entry, diversity saves the vehicle only 1/4 decibel in transmitter power. However, when the central angle at entry goes to 25°, a diversity transmission system would save the vehicle 3.6 dB of radiated power.

The surface roughness, or the diffuseness of the reflected signal, is a less significant parameter, and within the central angle window, only influences the power level about 1.5 db. When all of the extremes are compounded, i.e., a VM-8, -15° entry and a diffuseness of 1, the "acceptable" capsule lead angle moves to about 2-1/2 deg $\pm$ 5 deg when no diversity is used, and 9 deg $\pm$ 12 deg when diversity 2 is used.

During the parachute descent phase of the mission, the induced or natural oscillations of the lander on the parachute can also have a significant effect on the entry transmitter power level. As in the preceding case, this results from the geometric effects on antenna gain, etc., and is sensitive to capsule

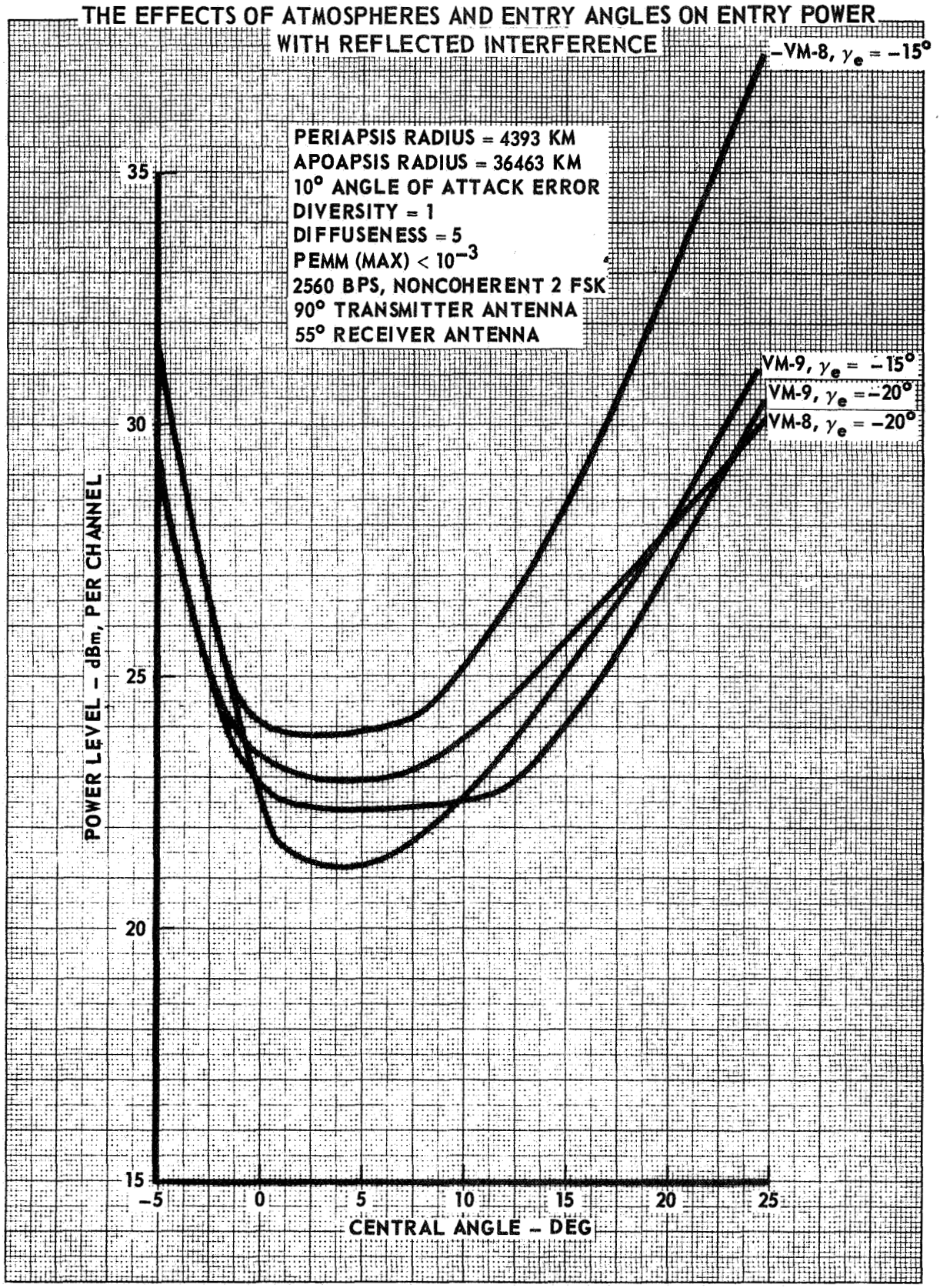
THE EFFECTS OF ATMOSPHERES AND ENTRY ANGLES ON ENTRY POWER WITH REFLECTED INTERFERENCE
PERIAPSIS RADIUS = 4393 KM
APOAPSIS RADIUS = 36463 KM
10° ANGLE OF ATTACK ERROR
DIVERSITY = 1
DIFFUSENESS = 5
PEMM (MAX) < 10^-3
2560 BPS, NONCOHERENT 2 FSK
90° TRANSMITTER ANTENNA
55° RECEIVER ANTENNA
VM-8, γe = −15°
VM-9, γe = −15°
VM-9, γe = −20°
VM-8, γe = −20°
POWER LEVEL – dBm, PER CHANNEL
35
30
25
20
15
−5
0
5
10
15
20
25
CENTRAL ANGLE – DEG

FIGURE 3.2.2–3

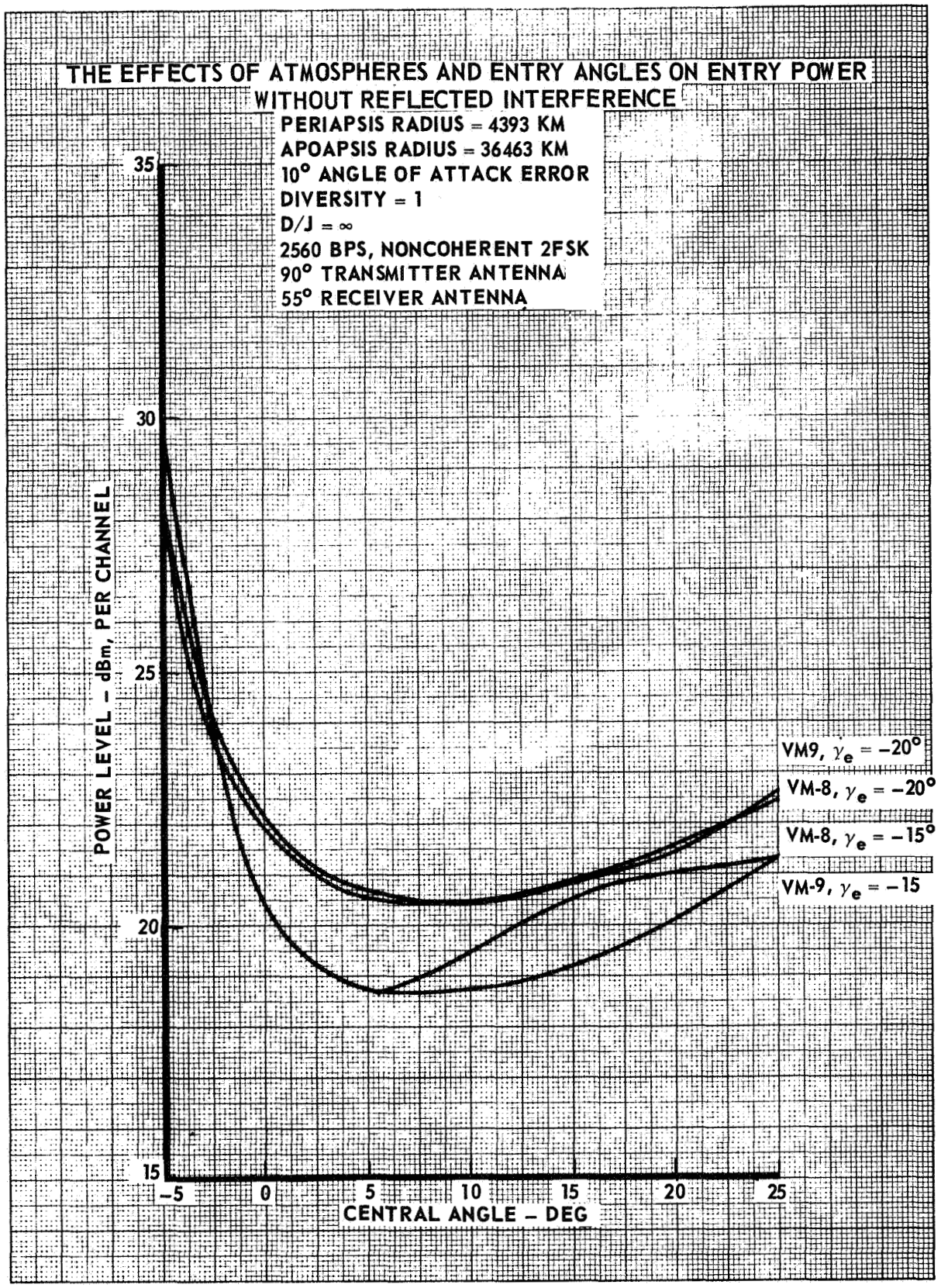
THE EFFECTS OF ATMOSPHERES AND ENTRY ANGLES ON ENTRY POWER
WITHOUT REFLECTED INTERFERENCE
PERIAPSIS RADIUS = 4393 KM
APOAPSIS RADIUS = 36463 KM
10° ANGLE OF ATTACK ERROR
DIVERSITY = 1
D/J = ∞
2560 BPS, NONCOHERENT 2FSK
90° TRANSMITTER ANTENNA
55° RECEIVER ANTENNA
POWER LEVEL – dBm, PER CHANNEL
35
30
25
20
15
–5
0
5
10
15
20
25
CENTRAL ANGLE – DEG
VM9, $\gamma_e = -20°$
VM-8, $\gamma_e = -20°$
VM-8, $\gamma_e = -15°$
VM-9, $\gamma_e = -15$

FIGURE 3.2.2–4

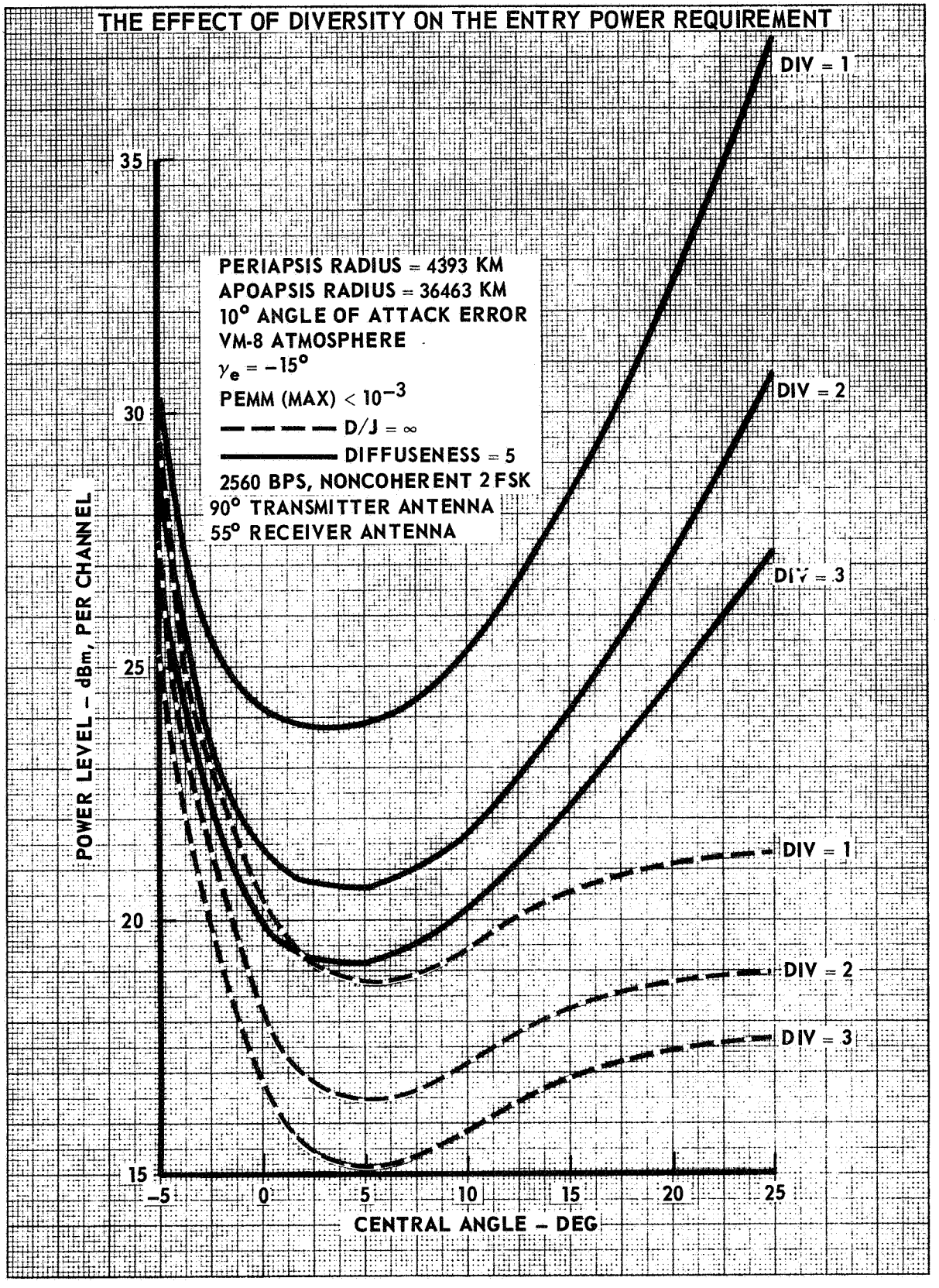
THE EFFECT OF DIVERSITY ON THE ENTRY POWER REQUIREMENT
PERIAPSIS RADIUS = 4393 KM
APOAPSIS RADIUS = 36463 KM
10° ANGLE OF ATTACK ERROR
VM-8 ATMOSPHERE
$\gamma_e = -15°$
PEMM (MAX) < 10^{-3}
D/J = ∞
DIFFUSENESS = 5
2560 BPS, NONCOHERENT 2 FSK
90° TRANSMITTER ANTENNA
55° RECEIVER ANTENNA
DIV = 1
DIV = 2
DIV = 3
DIV = 1
DIV = 2
DIV = 3
POWER LEVEL – dBm, PER CHANNEL
35
30
25
20
15
–5
0
5
10
15
20
25
CENTRAL ANGLE – DEG

FIGURE 3.2.2–5

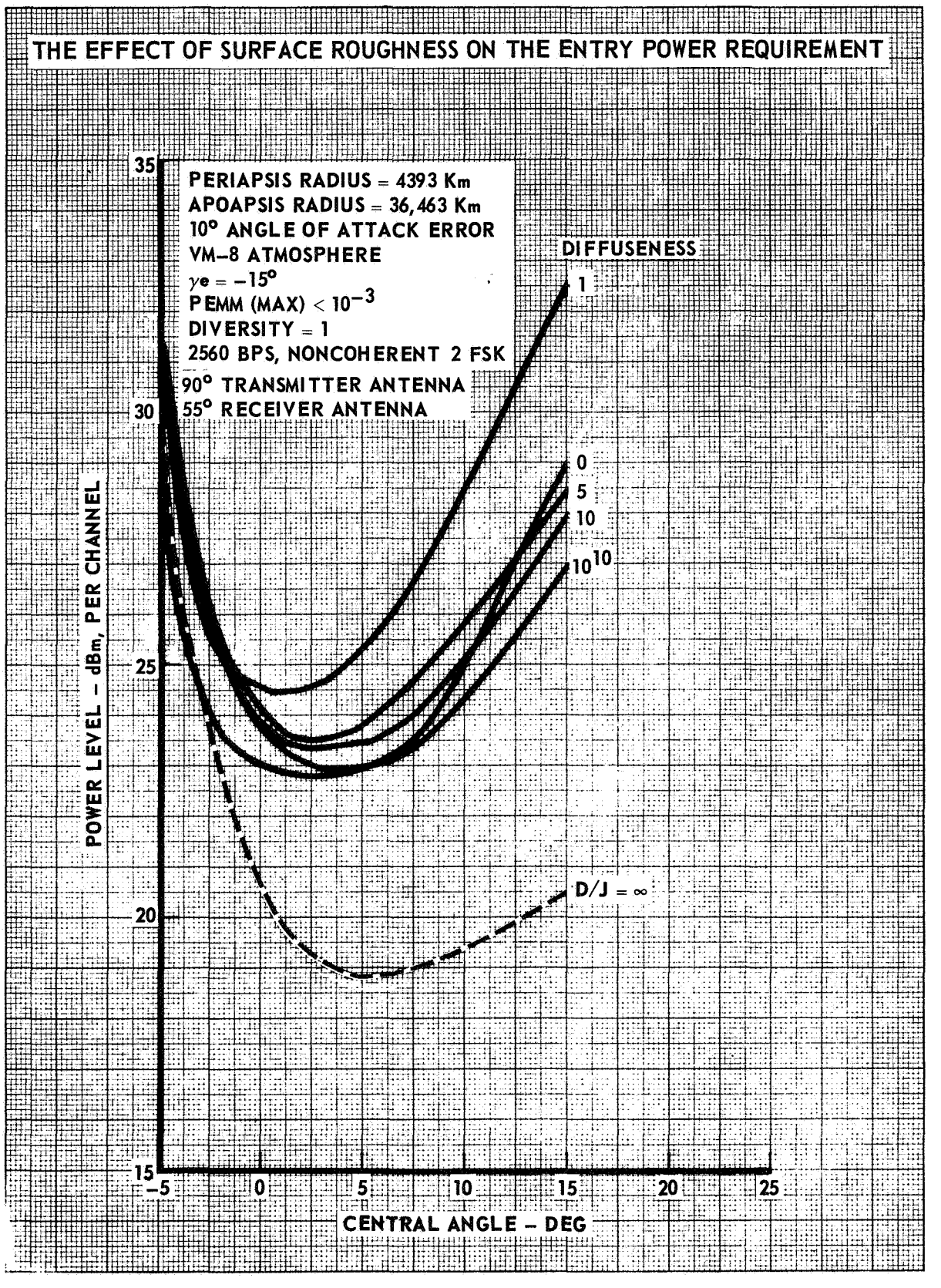
THE EFFECT OF SURFACE ROUGHNESS ON THE ENTRY POWER REQUIREMENT
PERIAPSIS RADIUS = 4393 Km
APOAPSIS RADIUS = 36,463 Km
10° ANGLE OF ATTACK ERROR
VM-8 ATMOSPHERE
γe = −15°
PEMM (MAX) < 10^−3
DIVERSITY = 1
2560 BPS, NONCOHERENT 2 FSK
90° TRANSMITTER ANTENNA
55° RECEIVER ANTENNA
DIFFUSENESS
1
0
5
10
10^10
D/J = ∞
POWER LEVEL – dBm, PER CHANNEL
35
30
25
20
15
−5
0
5
10
15
20
25
CENTRAL ANGLE – DEG

FIGURE 3.2.2–6

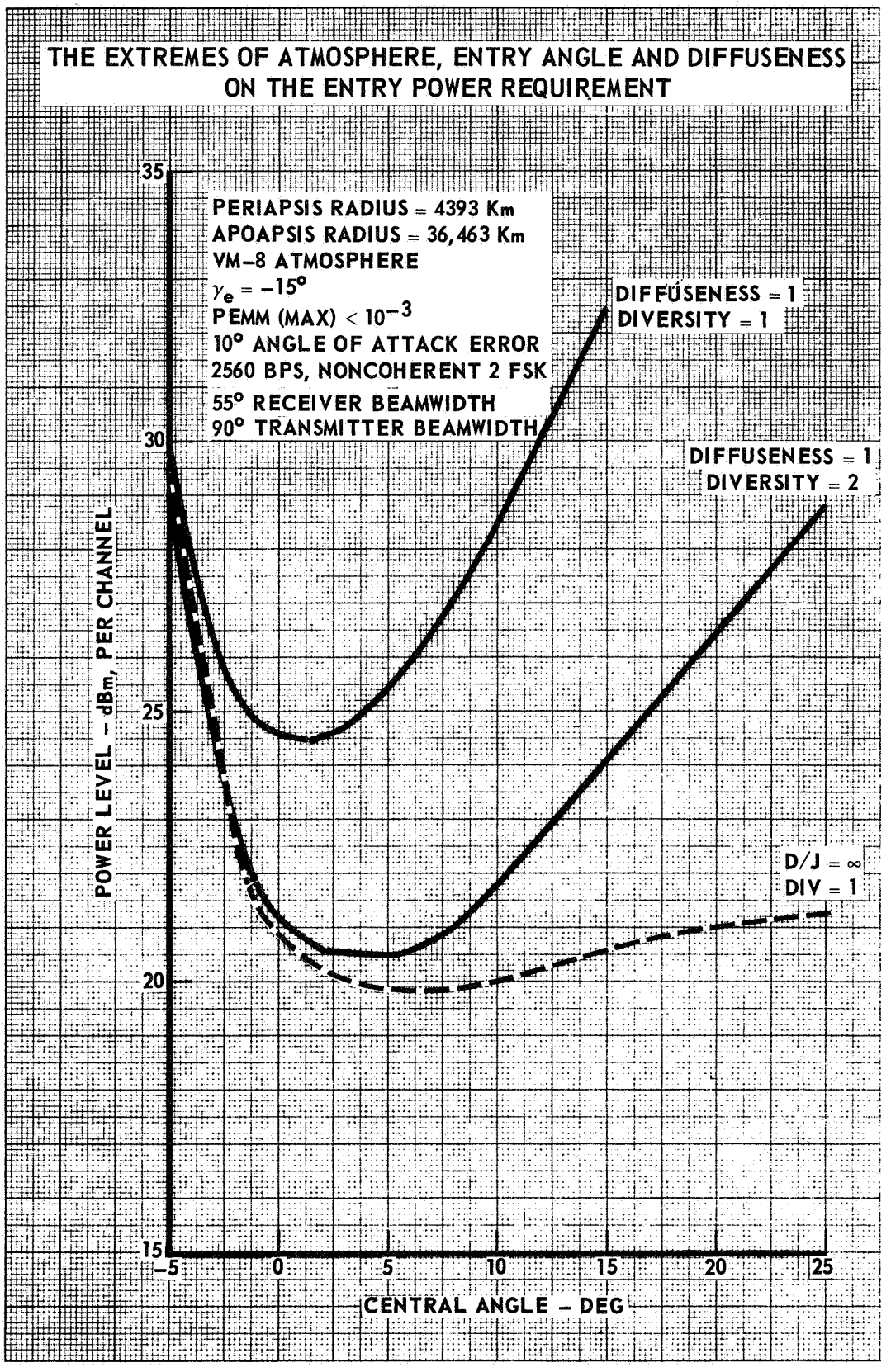
THE EXTREMES OF ATMOSPHERE, ENTRY ANGLE AND DIFFUSENESS ON THE ENTRY POWER REQUIREMENT
PERIAPSIS RADIUS = 4393 Km
APOAPSIS RADIUS = 36,463 Km
VM-8 ATMOSPHERE
$\gamma_e = -15°$
PEMM (MAX) < 10^{-3}
10° ANGLE OF ATTACK ERROR
2560 BPS, NONCOHERENT 2 FSK
55° RECEIVER BEAMWIDTH
90° TRANSMITTER BEAMWIDTH
DIFFUSENESS = 1
DIVERSITY = 1
DIFFUSENESS = 1
DIVERSITY = 2
D/J = ∞
DIV = 1
POWER LEVEL – dBm, PER CHANNEL
35
30
25
20
15
–5
0
5
10
15
20
25
CENTRAL ANGLE – DEG

FIGURE 3.2.2–7

position. These effects are defined in the same manner as those preceding, i.e., first a definition of the geometry factors, and second a definition of the modulation factors; however, the point of analysis is a 20 000 ft altitude for all trajectories.

Figure 3.2.2-8 shows the two entries into the VM-8 atmosphere and the power necessary to maintain communications with 30 deg parachute oscillations. Higher oscillations were not shown, due to the excessive power requirements. Figure 3.2.2-9 and 10 show the power requirements for the VM-9 cases and parachute oscillations of 30°, 45°, and 60°.

When the parachute oscillations are moderate, say less than 30°, and entry occurs in the window defined from the entry power requirements study, the transmitter power requirements during parachute oscillations are less than those during entry. However, when the parachute oscillations are not moderate, and entry does not occur in the "proper" window, the transmitter power requirements are increased.

3.2.2.1.2 Equipment considerations: The entry system components are for a 400 MHz pulse code modulation system. The parametric (size, weight, and power) for each component are given below. The components are "packaged," i.e., the parametrics are for a unit package, rather than just for the component subassemblies. Each component contains its own DC-to-DC converter to convert the raw bus voltage to that required for component operation.

Figures 3.2.2-11, 12 and 13 illustrate how the parametrics are derived. These figures show the size, weight and power characteristics of typical missile and satellite tape recorders, plotted as a function of a "sensitive" parameter. In the case of the size and weight the parameter is tape length, and power is a factor proportional to the energy required to move the tape.

In the lists below, size (S) is given in cubic inches, weight (W) in pounds, and power (P) in watts.

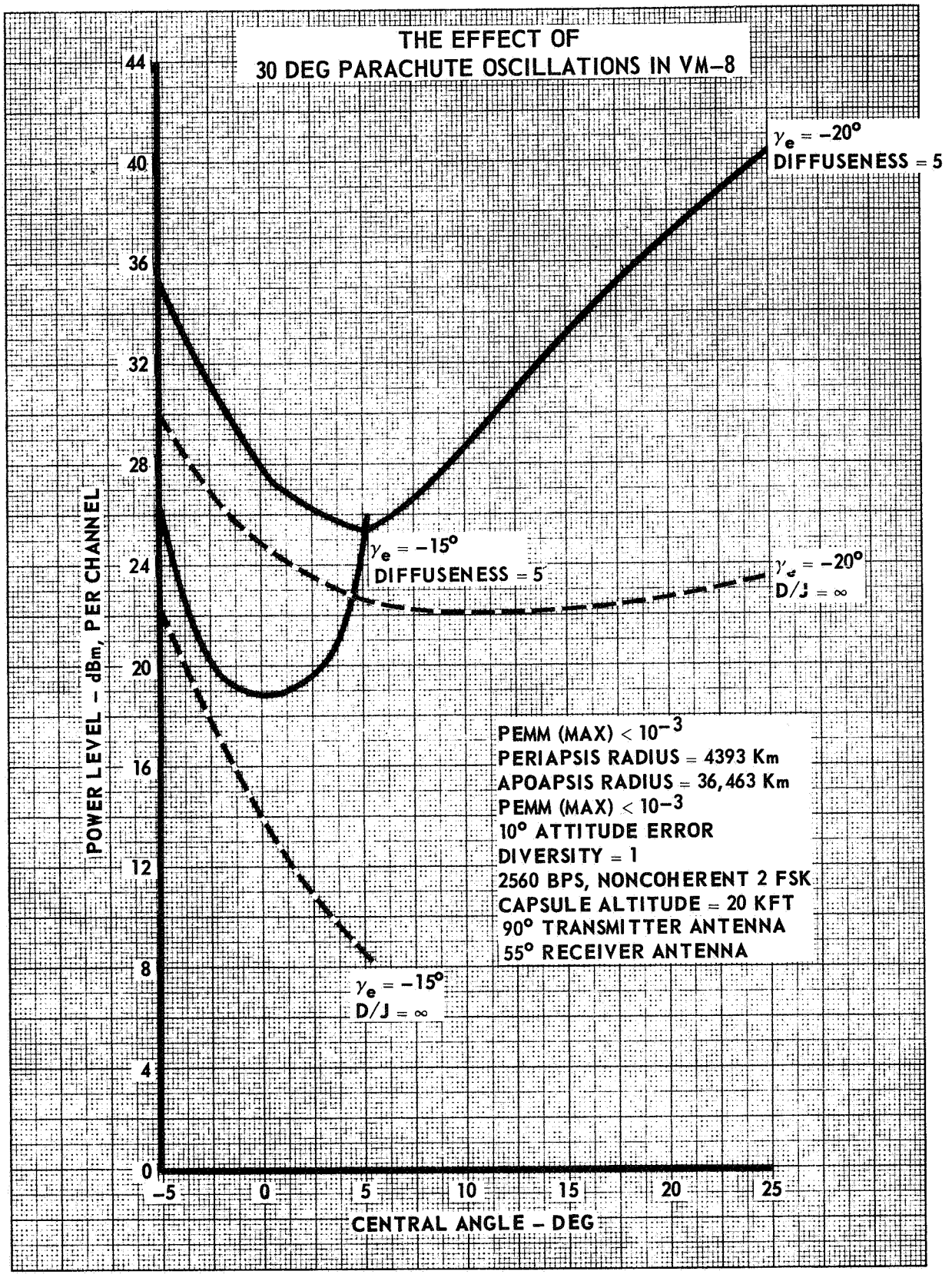
THE EFFECT OF
30 DEG PARACHUTE OSCILLATIONS IN VM-8
$\gamma_e = -20°$
DIFFUSENESS = 5
$\gamma_e = -15°$
DIFFUSENESS = 5
$\gamma_e = -20°$
D/J = ∞
$\gamma_e = -15°$
D/J = ∞
PEMM (MAX) < 10^{-3}
PERIAPSIS RADIUS = 4393 Km
APOAPSIS RADIUS = 36,463 Km
PEMM (MAX) < 10^{-3}
10° ATTITUDE ERROR
DIVERSITY = 1
2560 BPS, NONCOHERENT 2 FSK
CAPSULE ALTITUDE = 20 KFT
90° TRANSMITTER ANTENNA
55° RECEIVER ANTENNA
POWER LEVEL – dBm, PER CHANNEL
44
40
36
32
28
24
20
16
12
8
4
0
–5
0
5
10
15
20
25
CENTRAL ANGLE – DEG

FIGURE 3.2.2–8

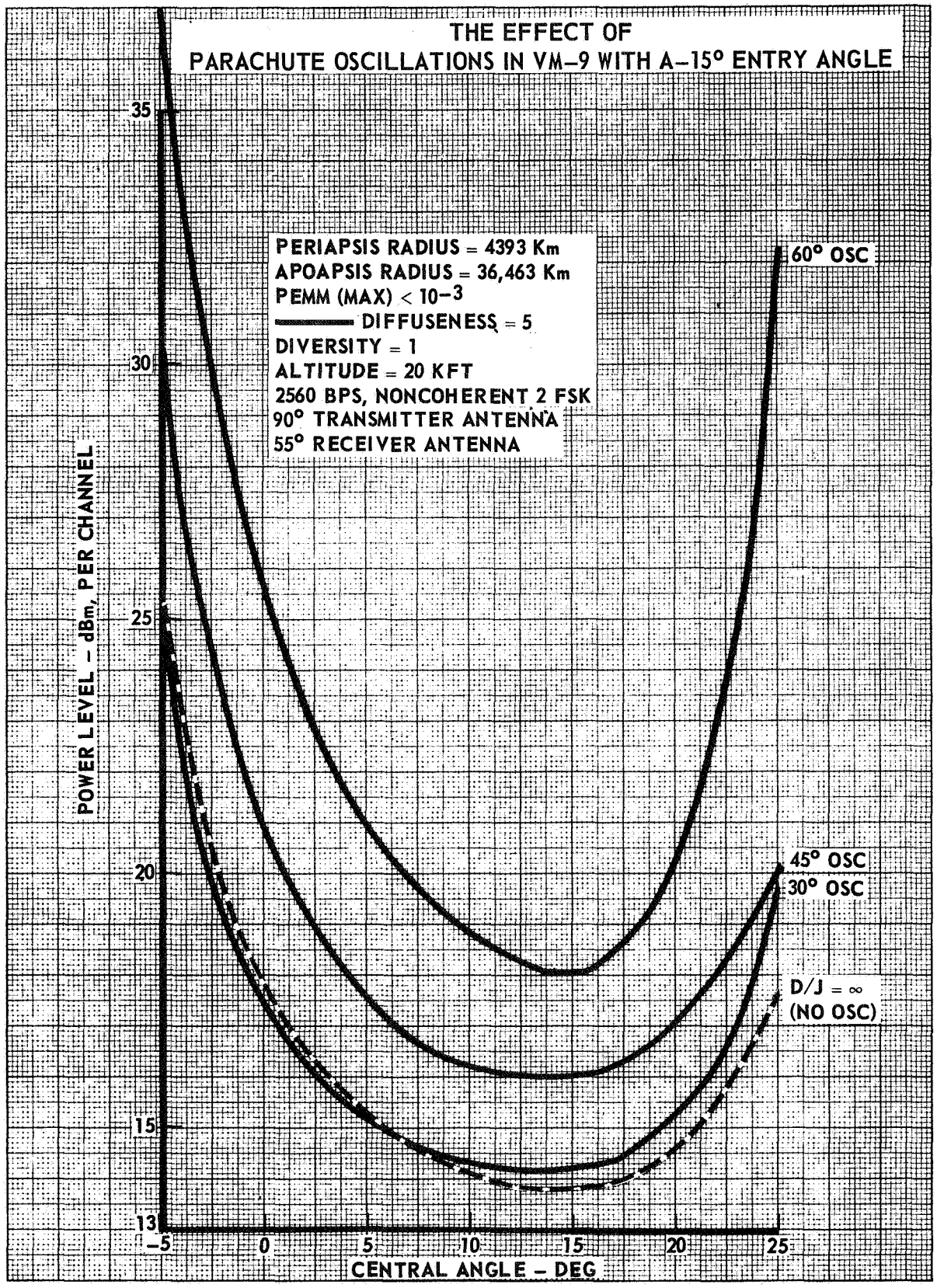
THE EFFECT OF
PARACHUTE OSCILLATIONS IN VM-9 WITH A-15° ENTRY ANGLE
PERIAPSIS RADIUS = 4393 Km
APOAPSIS RADIUS = 36,463 Km
PEMM (MAX) < 10-3
DIFFUSENESS = 5
DIVERSITY = 1
ALTITUDE = 20 KFT
2560 BPS, NONCOHERENT 2 FSK
90° TRANSMITTER ANTENNA
55° RECEIVER ANTENNA
60° OSC
45° OSC
30° OSC
D/J = ∞
(NO OSC)
POWER LEVEL – dBm, PER CHANNEL
35
30
25
20
15
13
-5
0
5
10
15
20
25
CENTRAL ANGLE – DEG

FIGURE 3.2.2-9

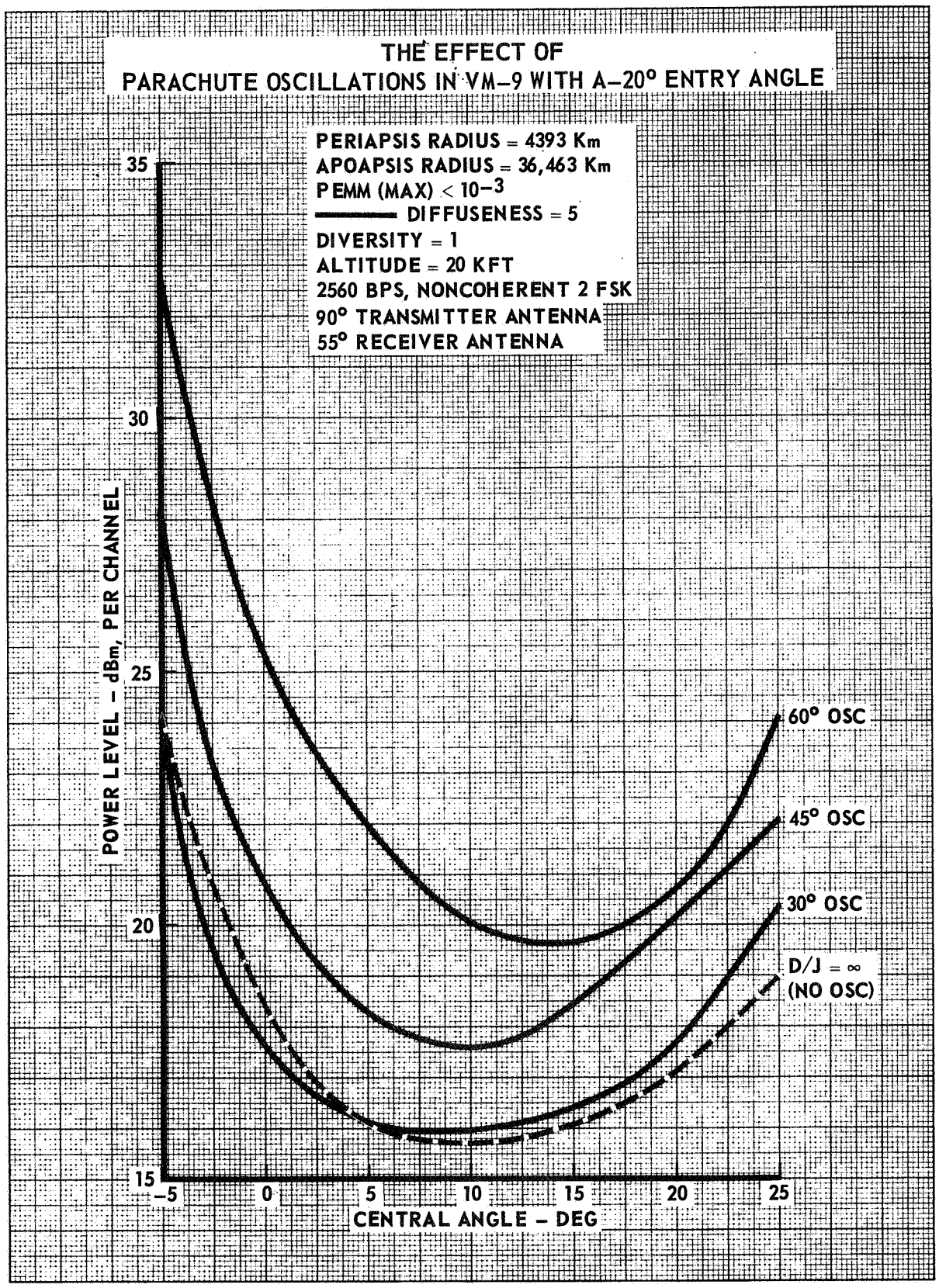

FIGURE 3.2.2-10

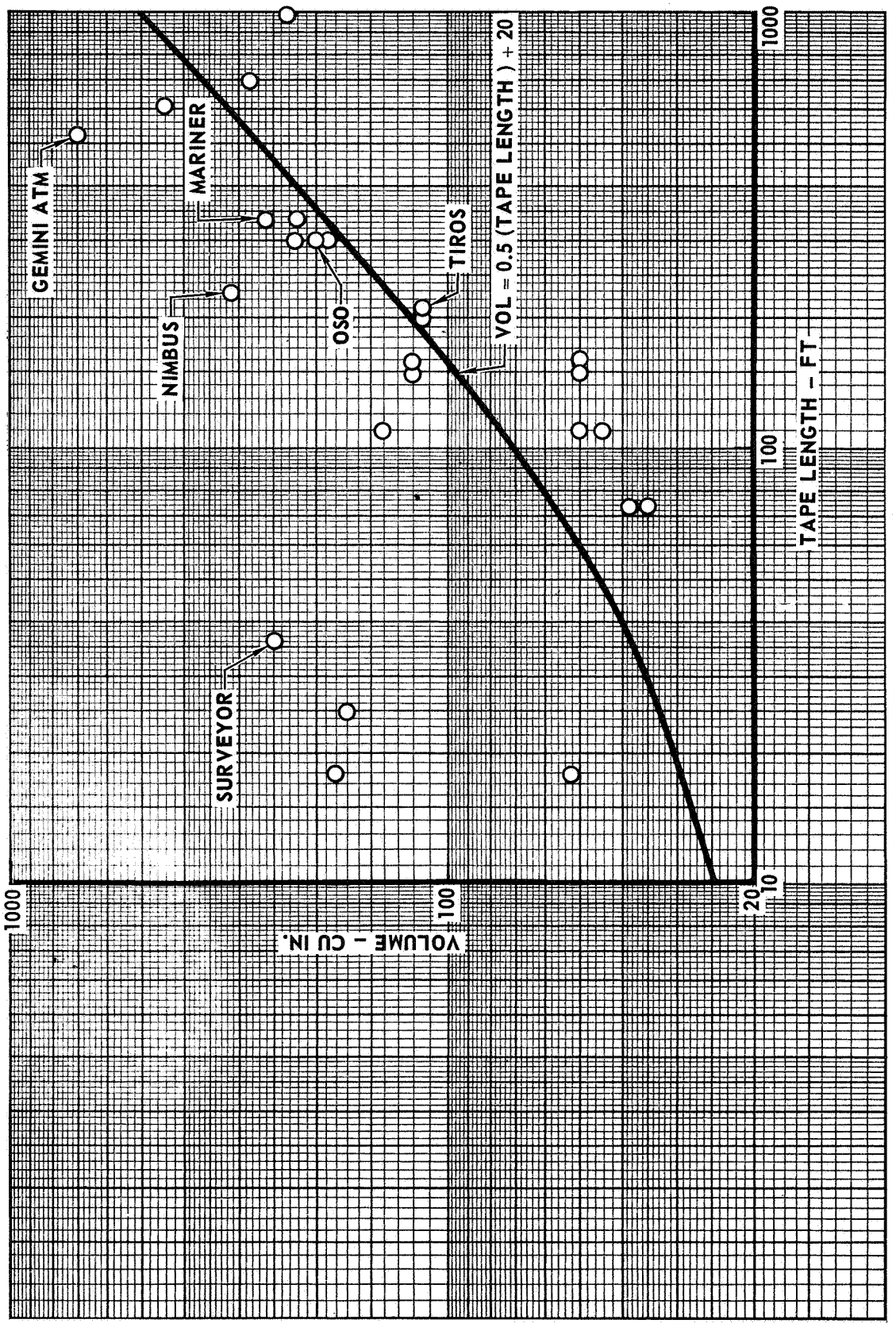

FIGURE 3.2.2–11

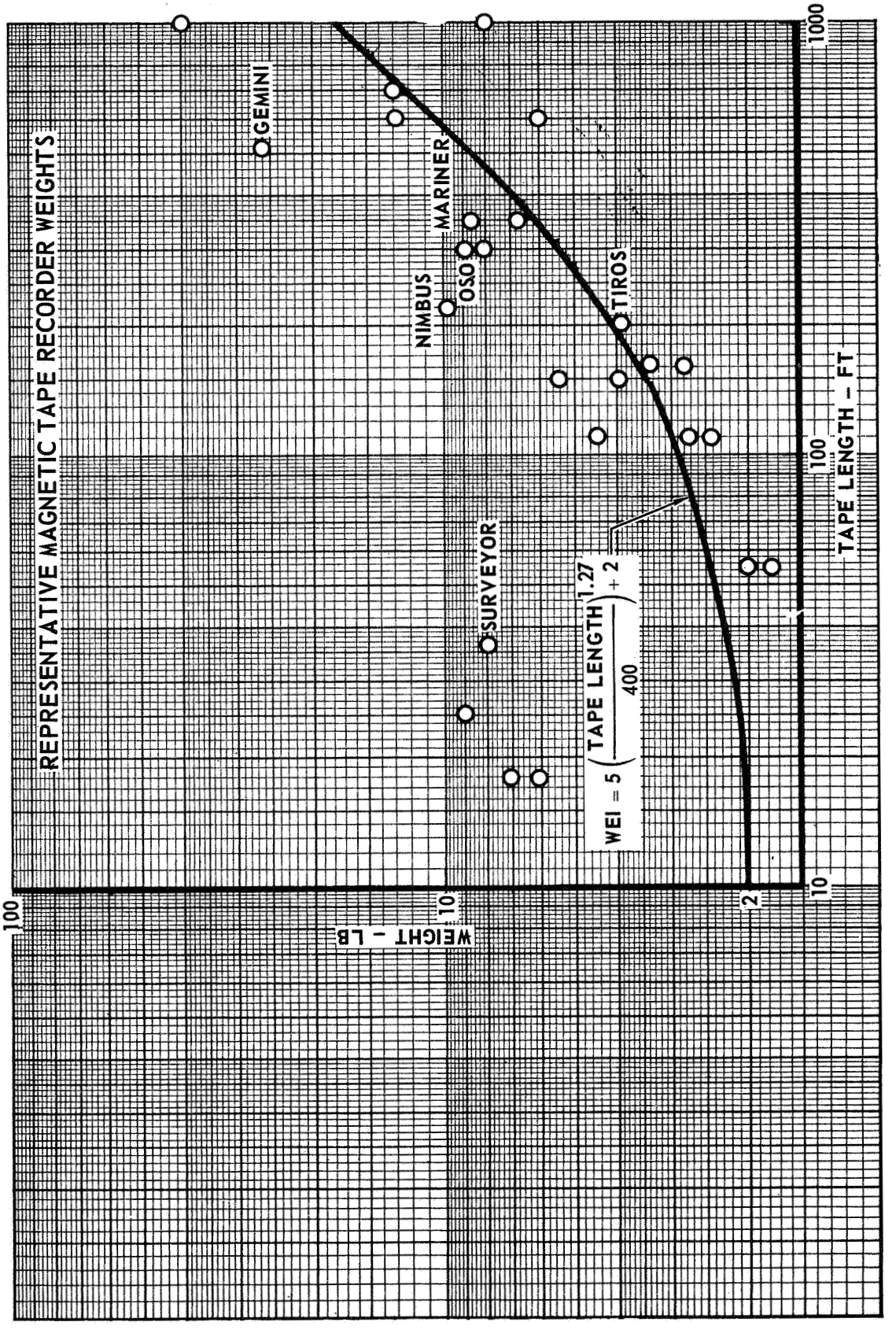

FIGURE 3.2.2–12

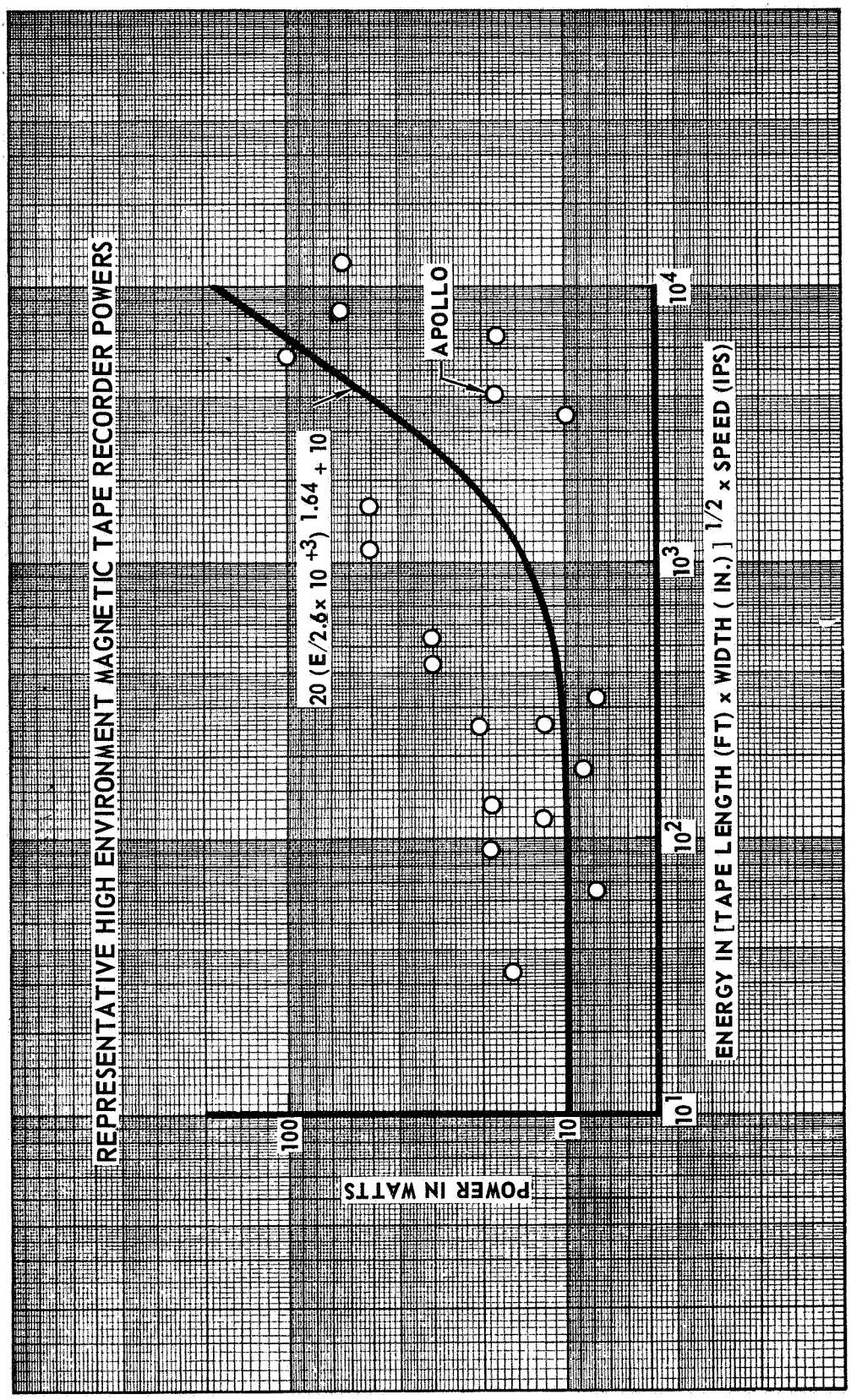

FIGURE 3.2.2–13

a) Magnetic tape recorders are used to store large amounts of data, such as are accumulated from the imaging experiment or relayed data received by the orbiter. The parametrics, including peripheral electronics, are:

$$S = 0.5T + 20$$

$$W = 5(T/400)^{1.27} + 2$$

$$P = 20\ (E/2.6 \times 10^{+3})^{1.64} + 10 \text{ ("missile" type)}$$

$$P = 2(E/140)^{1.36} + 1 \text{ ("satellite" type)}$$

where $E = (Tw)^{1/2}$ $S_p = \dfrac{B_{TOT}^{\ 3/2}}{181.5\ T_d\ \ D^{3/2}\ w}$

and $T = B_{TOT}/\ 168\ Dw$

given T is the tape length in feet, w is the tape width in inches, S_p is the tape speed in inches per second, B_{TOT} is the total number of bits on the tape, D is the bit packing in bits per inch per track, and T_d is the read or write time in seconds.

b) Magnetic core storage is used to store intermediate amounts of data, generally less than 10^5 bits. The parametrics, including peripheral electronics are:

$$S = .294(C/10^{+3})^{1.27} + 40$$

$$W = .131(C/10^{+3})^{.813} + .5$$

$$P = 0.3 \times 10^{-3} R\ (C/30 \times 10^{+3})^{0.263} + 1.66 \times 10^{-6}\ C$$

where C is the number of cores, and R is the rate of operation in bits per second.

c) A 400 MHz solid state transmitter would be used for the entry system, and the landed relay system. The parametrics are:

$$S = 69\ (P_o/20)^{0.655} + 21$$

$$W = 6.5\ (P_o/20)^{0.655} + 2$$

$$P = 5.4P_o^{\ 0.885} + 1$$

where P_o is the radio frequency power output in watts.

d) The data commutator is the device which assembles the various data sources into a coherent bitstream. The parametrics include the gates, gate drivers, analog to digital converter, differential amplifier, programming, and synchronization generators. The expressions are:

$$S = 1 \text{ Ch}$$

$$W = .04 \text{ Ch}$$

$$P = (1.3 \times 10^{-3} R^{0.28} + 2 \times 10^{-3}) \text{ Ch}$$

where Ch is the number of data channels.

e) The 400 MHz antenna on the capsule will be nearly a hemispheric coverage device (typically a spiral), while that on the spacecraft will be directive (typically a helix). The parametrics, without mounting provisions and the ground plane, are:

W (hemispheric) = 3; Diameter (hemispheric) = 13.5 in.

W (helix) = 0.1 G; Diameter (helix) = 9.4 in.;

Length (helix) = 5.32 G in.

where G is the power ratio antenna gain. The beamwidth of a helix is

$$BW = 174 \, G^{-1/2}$$

assuming a 70% efficiency.

f) The other entry communications subsystem components are essentially "fixed", i.e., their size, weight and power are essentially invariant. Table 3.2.2-3 lists these components.

As an example, consider the conventional 400 MHz entry telemetry system in Figure 3.2.2-14. For a design transmission range of 3000 km the system would occupy approximately 253 cubic inches, weigh about 20 pounds and consume about 9.4 watts. Figure 3.2.2-15 shows how these parametrics vary with the design transmission range. At a 10 000 km range, although the size and weight of the system have not changed significantly, the power consumption has increased to 29 watts.

TABLE 3.2.2–3

INSTRUMENTATION PARAMETRICS

COMPONENT	S(c.i.)	W (LB)	P (W)
TEMPERATURE SENSOR	.32	.018	$.2 \times 10^{-3}$
PRESSURE TRANSDUCER	2.2	.313	1.25×10^{-3}
ACCELEROMETER	7.87	.5	14×10^{-3}
INSTRUMENTATION POWER SUPPLY*	$35\ P_o$	$2\ P_o$	$3\ P_o$
DCVM**	5.8	.1725	.276
ACVM**	11.6	.345	.552
PSD**	17.4	.5175	.828
SPACECRAFT-MOUNTED TM RECEIVER***	120	5.7	2.9
SC/MTD–TM RCV'R WITH DIVERSITY 2 ***	200	12	5.75

* WHERE P_o IS THE REGULATED POWER OUTPUT IN WATTS

** COMPONENTS OF THE TELEMETRY SIGNAL PROCESSOR

*** INCLUDING THE BIT SYNCHRONIZER

AN EXAMPLE ENTRY COMMUNICATIONS SYSTEM

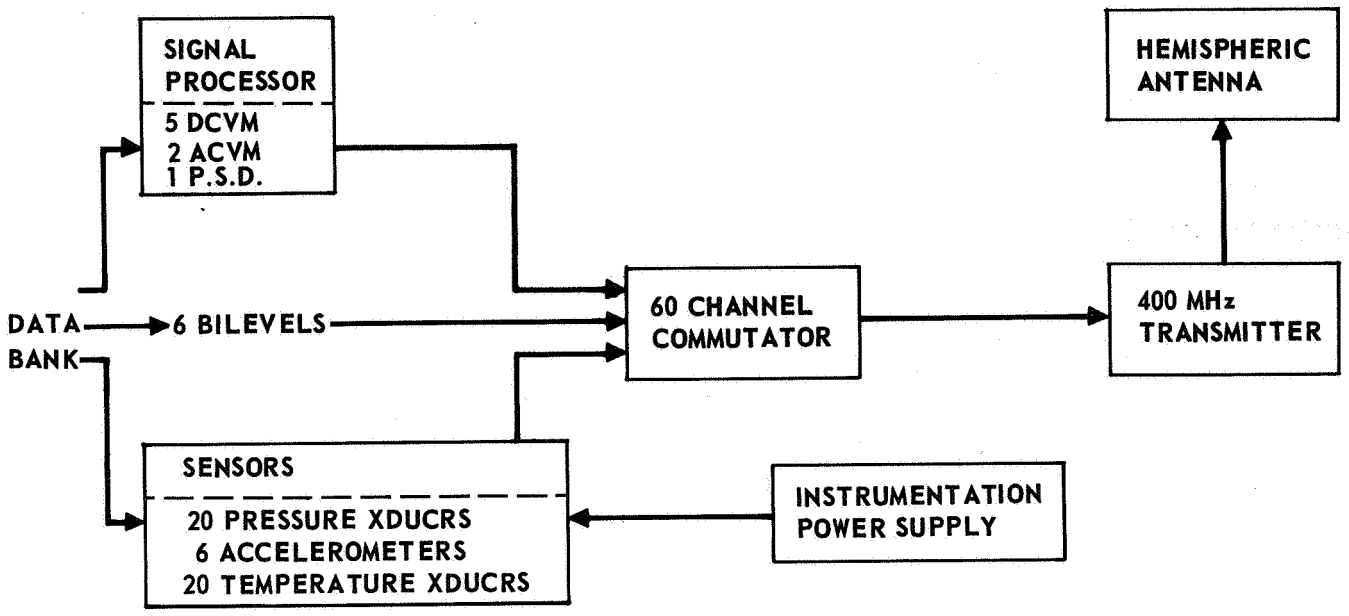

ASSUMING: TRANSMITTING ANTENNA GAIN = 0 dB
RECEIVING ANTENNA GAIN = +6 dB
THRESHOLD = 11 dB (ERROR RATE = 10^{-3})
BIT RATE = 1KBPS
TRANSMISSION RANGE = 3000 KM

ITEM	SIZE (c.i.)	WEIGHT (LB)	POWER (W)
SIGNAL PROCESSOR	64.6	2.07	3.312
INSTRUMENTATION	97.62	9.62	–
INSTRU. POWER SUPPLY	3.955	0.226	0.339
COMMUTATOR	60	2.4	1.8
ANTENNA	–	3.0	–
TRANSMITTER	27.14	2.578	3.94
TOTALS	253.315	19.894	9.391

FIGURE 3.2.2–14

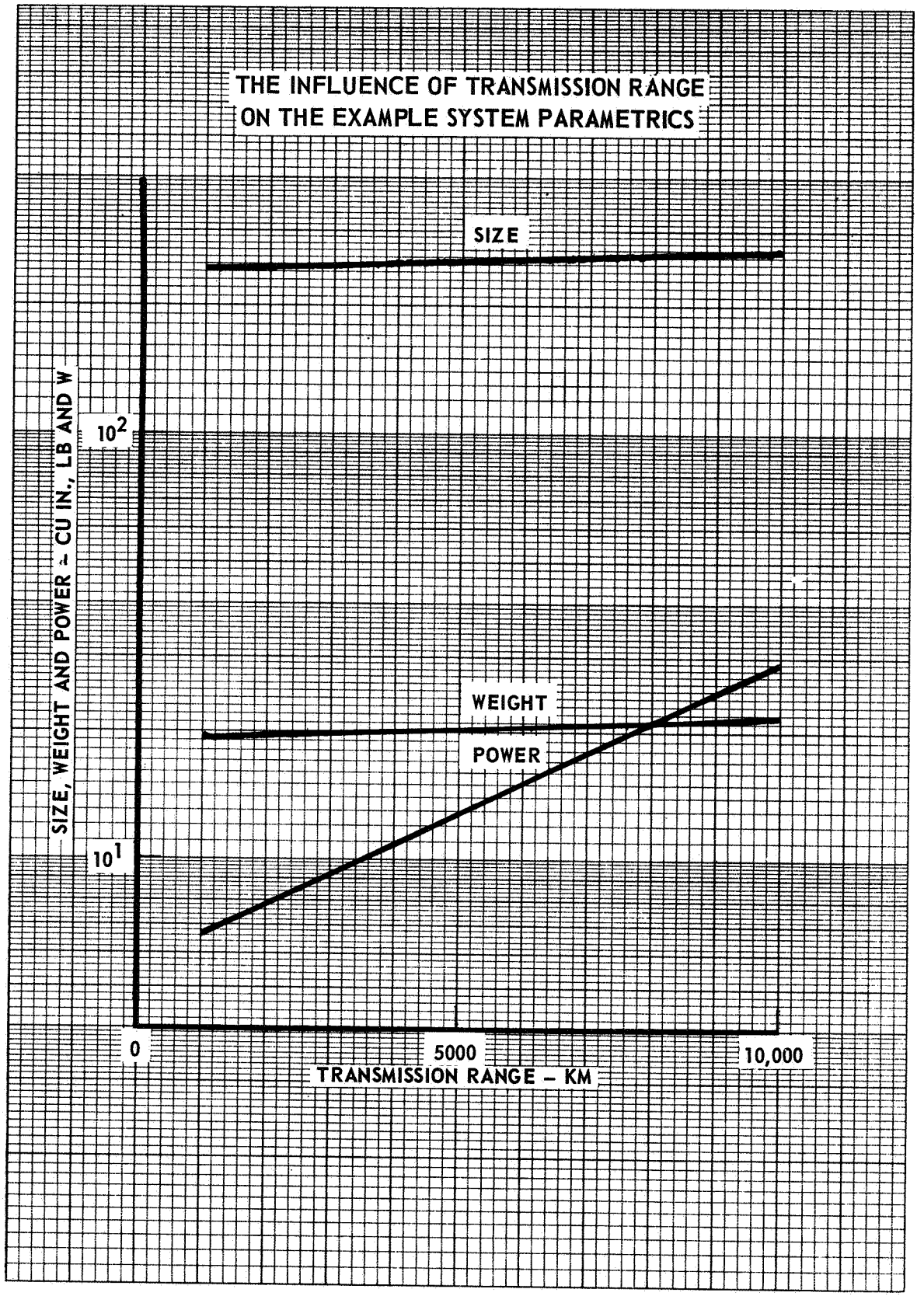

FIGURE 3.2.2–15

3.2.2.2 Landed communications. - Landed communications include the telemetry, storage, transmission, and command equipment required to support the operation of the surface payload. The primary considerations are the transmission range, the landing latitude, and the orbiter period (for the relay communications).

The landed communication parametrics section is subdivided into three parts. The first part describes the influence of the interplanetary range upon the direct communications. The second part defines the influence of the orbiting spacecraft characteristics upon the relay communications. The third part defines the size, weight, and power characteristics of the communication system components.

3.2.2.2.1 Landed direct communications: There are three probable direct to earth communications links: a data transmission link with a low gain, nonpointed antenna, a data transmission link with a high gain, pointed antenna, and a command link with a low gain, nonpointed antenna. The most probable modulation schemes for these links are noncoherent multiple frequency shift keying (MFSK) for the low rate data link, coherent phase shift keying (PSK) with convolutional encoding for the high rate link, and coherent PSK with Bose-Chandhuri coding for the command link. Details of these links are given in the component parametrics section.

Table 3.2.2-4 summarizes the general performance characteristics of the MFSK low rate link. Figure 3.2.2-16 shows the effect of ground slopes on the time history data transmission rate of the MFSK low rate link. The effect of east-west slopes is to change the "phase" of the transmission, while north-south slopes vary the amount of data transmitted. By computing the total number of bits transmitted per day from such data rate history information, as shown in Figure 3.2.2-17, the optimum rate to maximize the information transfer can be determined. Figure 3.2.2-18 shows the total quantity of data which can be transmitted per day at the optimal transfer rate from February to August of 1974. The variation in the total number of daily bits, and consequently rate, is a function of the transmission range. Figure 3.2.2-19 shows that the optimum transmission time, in order to maximize the information transfer from February to August, is a constant six hours.

TABLE 3.2.2–4

LOW RATE DIRECT LINK TABLE

PARAMETER	VALUE	TOLERANCE	NOTES
TRANSMITTER POWER	$+P_o$ dBm	+.5 –.5	TO BE DEFINED
TRANSMIT CIRCUIT LOSS	–.7 dB	+.1 –.1	ASSUMED
TRANSMIT ANTENNA GAIN	+XAG	+1 –1	TO BE DEFINED
SPACE LOSS (2295 MHz)	$-99.85 - 20\ LOG_{10}d$	+0 –0	d IN KILOMETERS
POLARIZATION LOSS	–.1 dB	+.1 –.6	
RECEIVING ANTENNA GAIN	+61	+1 –1	210 FT DISH
POINTING LOSS	–.1 dB	+.1 –.1	
RECEIVING CIRCUIT LOSS	–.1 dB	+.1 –.1	
TOTAL RECEIVED POWER	$P_o + XAG - 39.85 - 20\ LOB_{10}d$	+2.9 –3.4	
NOISE DENSITY	–182.1 dBm/Hz	+.9 –1.1	45°K ± 10°K
BIT RATE	INC IN S/N_o LINE	+0 –0	TO BE DEFINED
THRESHOLD	S/N_o	+0 –1.1	SEE NOTE BELOW
SENSITIVITY	$-182.1 + S/N_o$	+.9 –2.2	
MARGIN	+4.3 dB	+5.1 –4.3	WORST CASE

NOTE:

$$S/N_o = \begin{cases} 7.5 & ;\ 0 \le R \le .75 \\ 8.4 + 7.3\ LOG_{10}R & ;\ .75 \le R \le 8.4 \\ 5.9 + 10\ LOG_{10}R & ;\ 8.4 \le R \le \infty \end{cases}$$

$$\text{TRANSMITTER POWER } P_o = \begin{cases} -XAG - 130.45 + 20\ LOG_{10}d \\ -XAG - 129.55 + 20\ LOG_{10}d + 7.3\ LOG_{10}R \\ -XAG - 132.05 + 20\ LOG_{10}d + 10\ LOG_{10}R \end{cases}$$

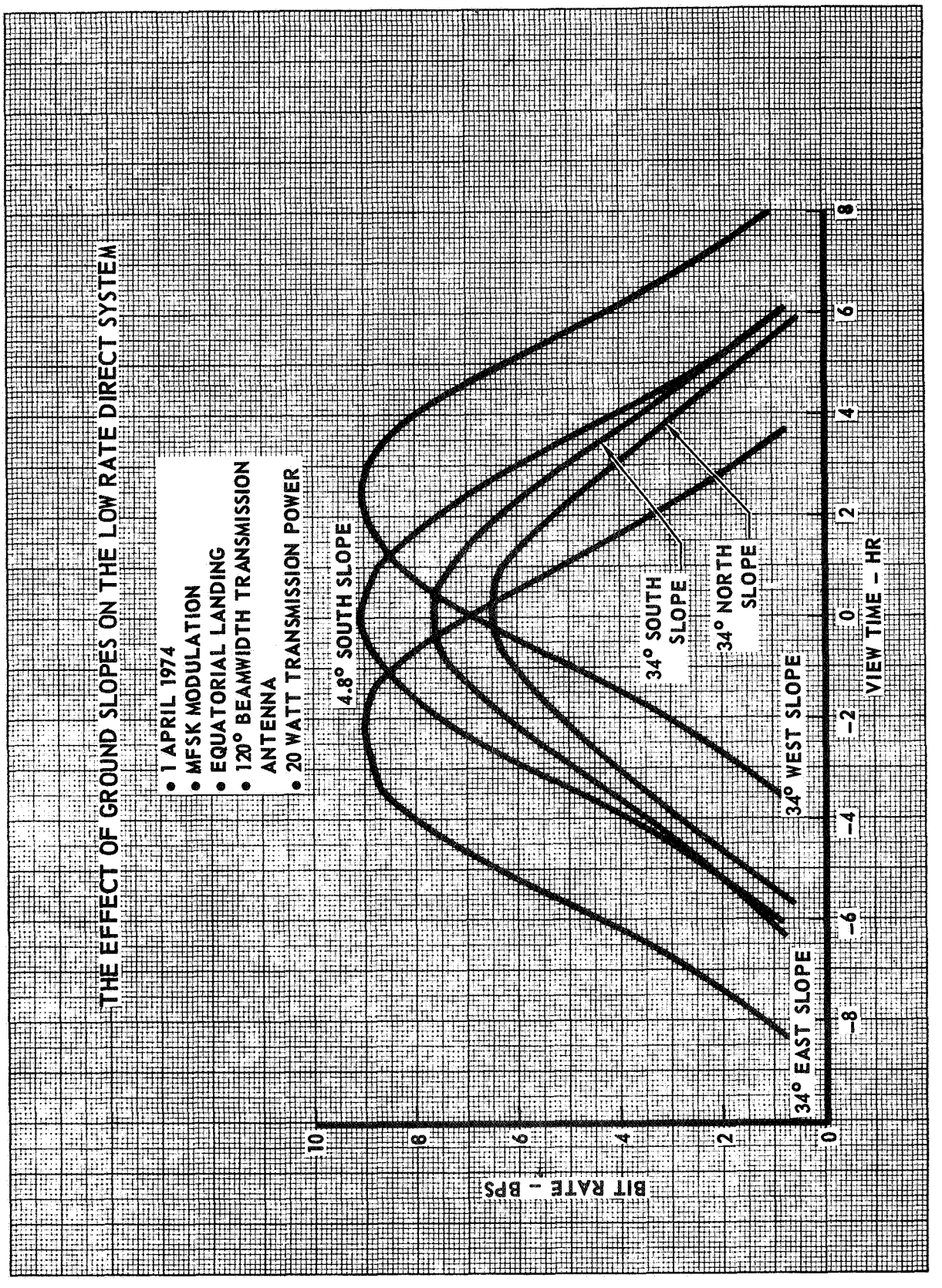

FIGURE 3.2.2–16

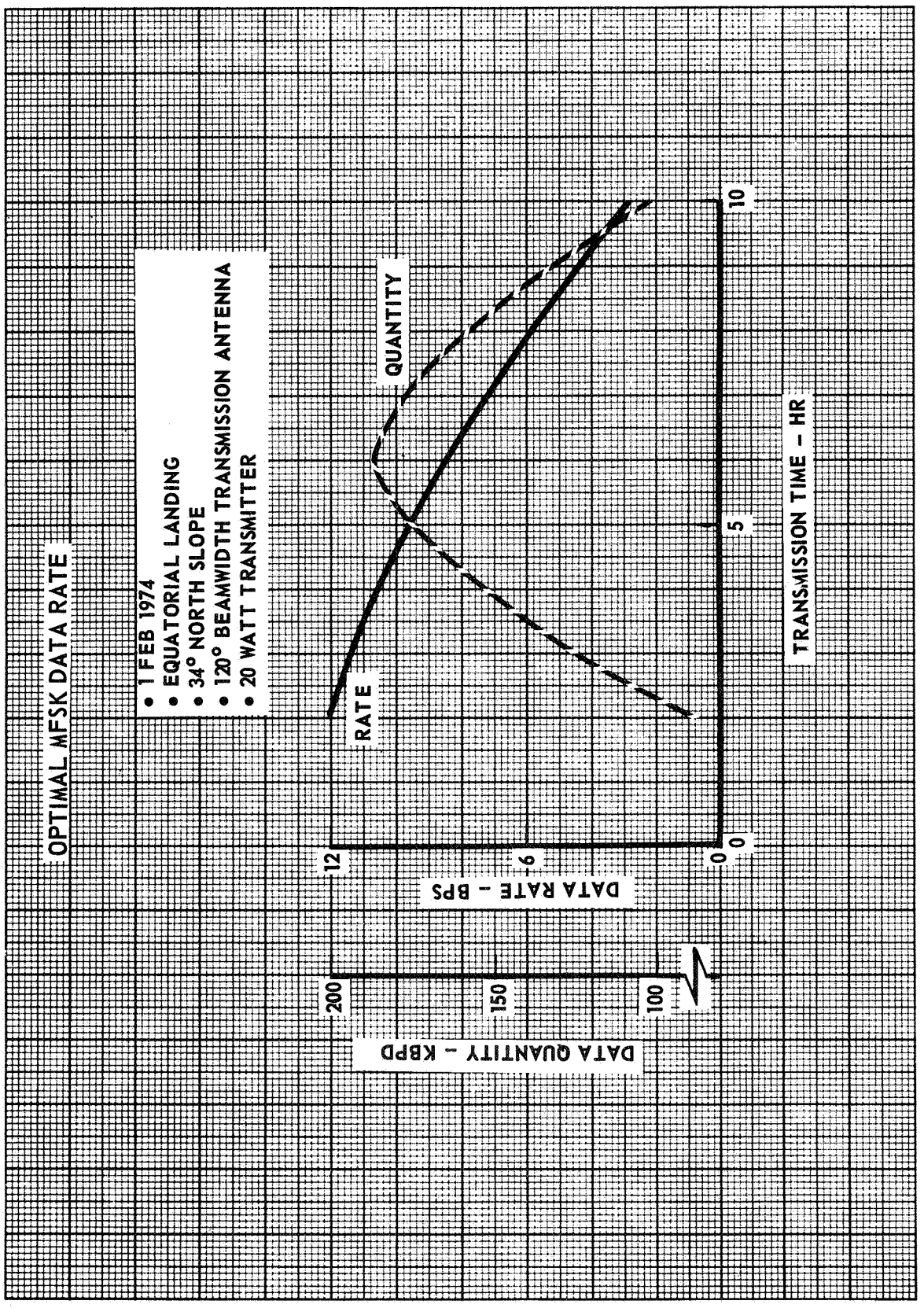

FIGURE 3.2.2–17

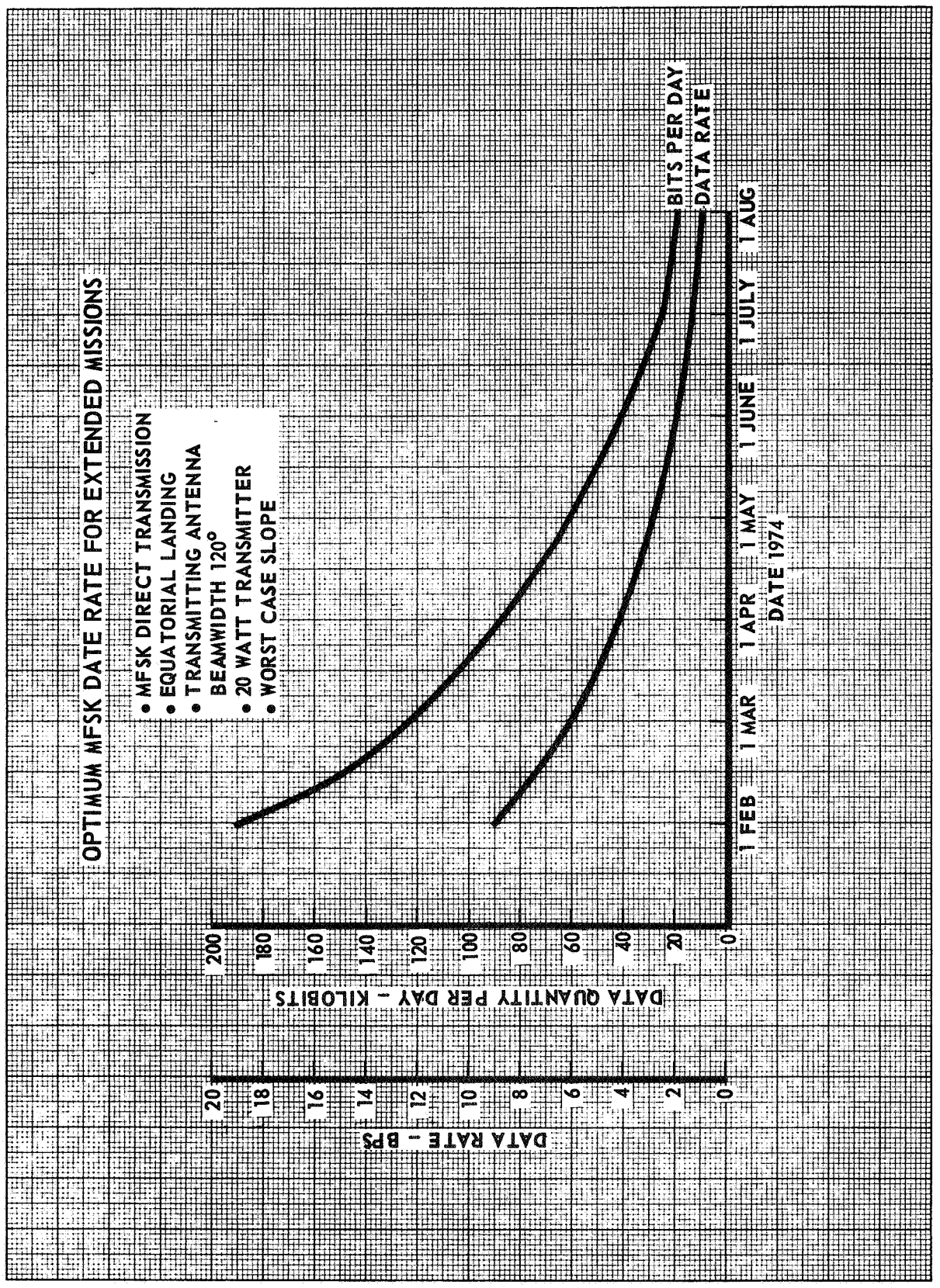

FIGURE 3.2.2-18

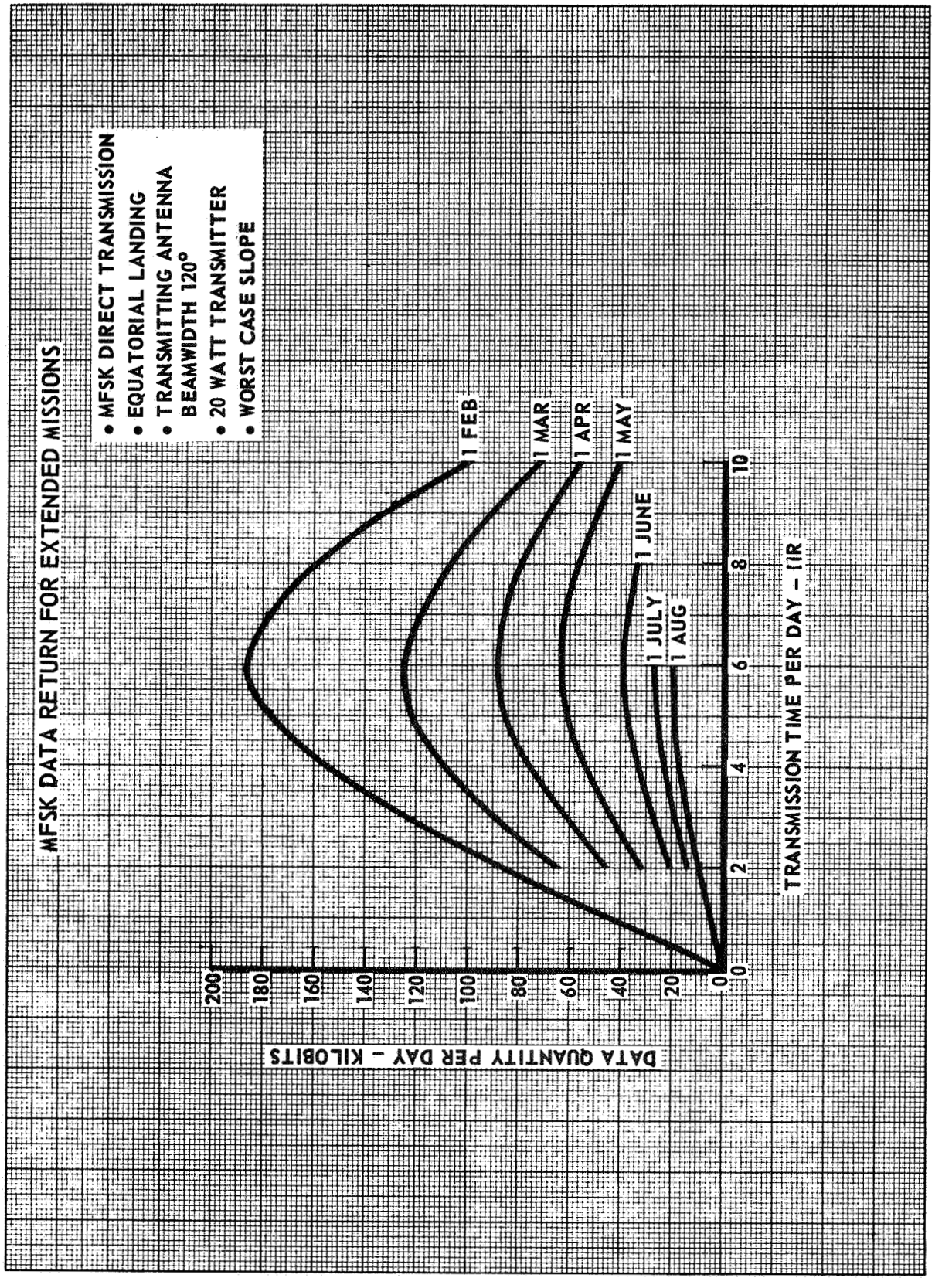

FIGURE 3.2.2–19

Table 3.2.2-5 illustrates the performance characteristics of the PSK high rate link. Figure 3.2.2-20 illustrates the data rate and view times for the high rate direct link communication system. In this case the transmitting antenna is steered, thus the view time limits are constrained by the "horizon," herein defined by the maximum ground slopes of 34°.

Table 3.2.2-6 illustrates the performance characteristics of the command link. Figure 3.2-21 shows the command system margin as a function of the ground slopes. For example if 2 hours of command time is required on 1 April 1974, the link will operate with a margin of +2.75 dB. Figure 3.2.2-22 shows how this margin varies with the mission date. Note that the 10 kilowatt transmitter will only be effective until June 1974, but the 100 kilowatt transmitter will provide more than adequate margin until after August 1974.

3.2.2.2.2 Landed relay communications: The landed relay communications parametrics are divided into two subsections: one for the synchronous equatorial orbit case, and one for the inclined orbit case. The inclined orbit case is further subdivided into synchronous and nonsynchronous cases. For each of the foregoing cases both the near periapse and near apoapse transmission periods are considered. The most probable modulation scheme for the landed relay communications would be a 400 MHz noncoherent two frequency shift keyed (2 FSK) link. The details of this link are given in the entry parametrics section Table 3.2.2-2, where E/N_o is 10.95 dB.

Figure 3.2.2-23 illustrates the significance of the ground slopes for the synchronous orbit/periapse transmission case. If, for example, a 10 kilobit per watt rate is to be supported, 6-1/2 minutes of view time is available with a maximum east/west slope. The absolute time uncertainty with slope, however, is 3-1/4 minutes. This implies that the data must be transmitted more than once during a pass, in order to assure a complete return.

Figure 3.2.2-24 illustrates the importance of the spacecraft antenna beamwidth. It is interesting to note that at moderate data rates, say 3 kilobits per watt, the wider beamwidth, lower gain antenna will support transmission for a longer period of time than the narrower beamwidth, higher gain antenna.

TABLE 3.2.2–5
HIGH RATE DIRECT LINK TABLE

PARAMETER	VALUE	TOLERANCE	NOTES
TRANSMITTER POWER	P_o dBm	+.6 –.6	TO BE DEFINED
TRANSMIT CIRCUIT LOSS	–1.3 dB	+.3 –.3	
TRANSMIT ANTENNA GAIN	XAG	+0 –.5	TO BE DEFINED
TRANSMIT POINTING LOSS	0 dB	+0 –4.4	
SPACE LOSS (2295 MHz)	$-99.85 - 20 \text{ LOG}_{10}d$	+0 –0	d IN KILOMETERS
POLARIZATION LOSS	–0.1 dB	+.1 –.4	
RECEIVING ANTENNA GAIN	+61 dB	+1 –1	210 FOOT DISH
RECEIVING ANTENNA POINTING LOSS	–.1 dB	+.1 –.1	
RECEIVING CIRCUIT LOSS	–.1 dB	+.1 –.1	
TOTAL RECEIVED POWER	$P_o + XAG - 40.45 - 20 \text{ LOG}_{10}d$	+2.2 –7.4	
NOISE DENSITY (45°K)	–182.1 dBm/Hz	+.9 –1.1	+10° –10°K
CARRIER MODULATION LOSS	–7.7 dB	+.8 –.8	CALCULATED
RECEIVED CARRIER POWER	$P_o + XAG - 48.15 - 20 \text{ LOG}_{10}d$	+3 –8.2	
CARRIER APC NOISE BANDWIDTH	7 dB/Hz	+0 –0	($2B_{LO}$ 5 Hz)
CARRIER PERFORMANCE TRACKING – ONE WAY			
THRESHOLD SNR IN $2B_{LO}$	0 dB	+0 –0	
THRESHOLD CARRIER POWER	–175.1 dBm	+.9 –1.1	
PERFORMANCE MARGIN	$P_o + XAG + 126.95 - 20 \text{ LOG}_{10}d$	+4.1 –9.1	
CARRIER PERFORMANCE TRACKING – TWO WAY			
THRESHOLD SNR IN $2B_{LO}$	2.0 dB	+1 –1	
THRESHOLD CARRIER POWER	–173.1 dBm	+1.9 –2.1	
PERFORMANCE MARGIN	$P_o + XAG + 124.95 - 20 \text{ LOG}_{10}d$	+5.1 –10.1	
CARRIER PERFORMANCE TELEMETRY			
THRESHOLD SNR IN $2B_{LO}$	16 dB	+0 –0	
THRESHOLD CARRIER POWER	–159.1 dBm	+.9 –1.1	
PERFORMANCE MARGIN	$P_o + XAG + 110.95 - 20 \text{ LOG}_{10}d$	+4.1 –9.1	
DATA CHANNEL			
MODULATION LOSS	–.8 dB	+.2 –.2	CALCULATED
RECEIVED DATA SUB-CARRIER POWER	$P_o - 41.25 - 20 \text{ LOG}_{10}d + XAG$	+2.4 –7.6	
BIT RATE	$10 \text{ LOG}_{10}R$	+0 –0	TO BE DEFINED
REQUIRED E/NO.	2.9 dB	+.1 –0	
THRESHOLD SUBCARRIER POWER	$-179.2 + 10 \text{ LOG}_{10}R$	+1 –1.1	
PERFORMANCE MARGIN	$P_o + XAG + 137.95 - 20 \text{ LOG}_{10}d - 10 \text{ LOG}_{10}R$	+3.5 –8.6	

AT DATA RATES LESS THAN 505 BPS THE CARRIER PERFORMANCE–TELEMETRY IS THE LIMITING CASE, THUS

$$\text{EXCESS MARGIN} \quad P_o + XAG + 101.85 - 20 \text{ LOG}_{10}d$$

AT DATA RATES GREATER THAN 505 BPS THE DATA CHANNEL IS THE LIMITING CASE, THUS

$$\text{EXCESS MARGIN} = P_o + XAG + 129.35 - 10 \text{ LOG}_{10}R - 20 \text{ LOG}_{10}d$$

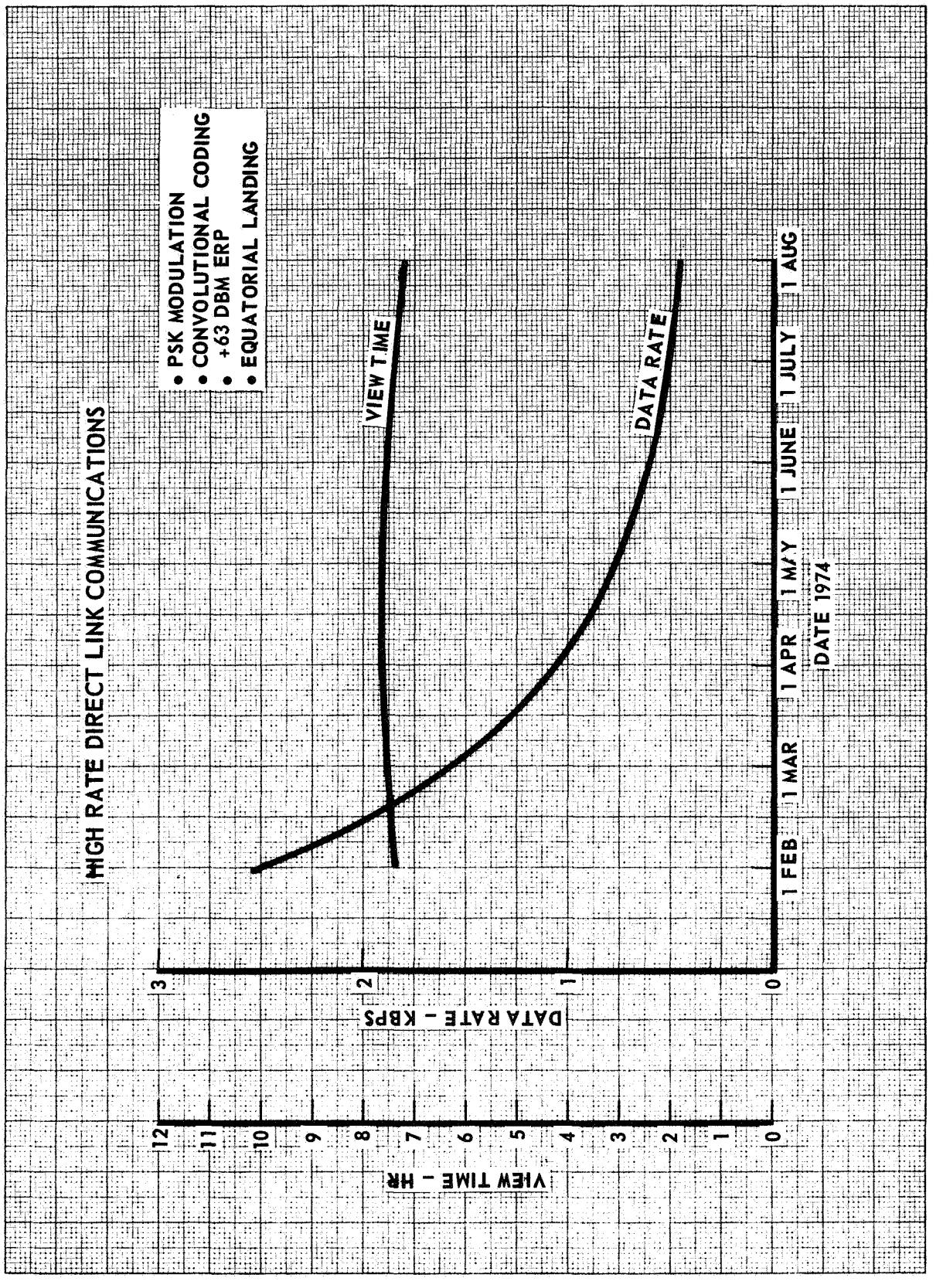

FIGURE 3.2.2–20

TABLE 3.2.2–6

COMMAND LINK TABLE – DIRECT

PARAMETER	VALUE	TOLERANCE	NOTES
TRANSMITTER POWER	+70 dBm	+.5 –.5	10 KW
TRANSMIT CIRCUIT LOSS	–.4 dB	+.1 –.1	
TRANSMIT ANTENNA GAIN	+60 dB	+.8 –.8	210 FOOT DISH
POINTING LOSS	–.1 dB	+ 0 –.1	
SPACE LOSS (2113 Mhz)	$-99.45 - 20 \log_{10} d$	+ 0 – 0	d IN. KILOMETERS
POLARIZATION LOSS	–.1 dB	+ .1 – .6	
RECEIVING ANTENNA GAIN	+ RAG	+ 1. –1.	TO BE DEFINED
RECEIVING CIRCUIT LOSS	– 1.3 dB	+.2 – .2	ASSUMED
TOTAL RECEIVED POWER	$RAG + 28.65 - 20 \log_{10} d$	+2.7 –3.3	
NOISE DENSITY (644°K)	–170.5 dBm/Hz	+.8 –.4	+ 136° – 55°
CARRIER MODULATION LOSS	–2.4 dB	+.3 –.3	
RECEIVED CARRIER POWER	$RAG + 26.25 - 20 \log_{10} d$	+ 3 –3.6	
CARRIER APC NOISE BW	13 dBHz	+ 0 – 1	($2B_{LO}$ = 20 Hz)
CARRIER PERFORMANCE TELEMETRY			
THRESHOLD SNR_{IN} $2B_{LO}$	8.0 dB	+1 – 1	
THRESHOLD CARRIER POWER	–149.5 dBm	+1.8 –2.4	
PERFORMANCE MARGIN	$RAG + 175.75 - 20 \log_{10} d$	+5.4 –5.4	
DATA CHANNEL			
MODULATION LOSS	–8.5 dB	+.2 –.2	
RECEIVED DATA SUBCARRIER POWER	$RAG + 20.15 - 20 \log_{10} d$	+ 2.9 –3.5	
BIT RATE	OdB Hz	+ 0 – 0	1BPS
REQUIRED E/N_0	15.7 dB	+1. –1.	
THRESHOLD SUBCARRIER POWER	–154.8 dBm	+1.8 –1.4	
PERFORMANCE MARGIN	$RAG + 174.95 - 20 \log_{10} d$	+4.3 – 5.3	
SYNCHRONIZATION CHANNEL			
MODULATION LOSS	– 5.5	+.2 – .3	
RECEIVED SYNC SUBCARRIER POWER	$RAG + 23.15 - 20 \log d$	+ 3 –3.6	
SYNC APC NOISE BW	+3dB Hz	+ 0 – 0	($2B_{LO}$ = 2 Hz)
THRESHOLD SNR IN $2B_{LO}$	+15.7 dB	+ 1 –1	
THRESHOLD SUBCARRIER POWER	–151.8	+1.8 –1.4	
PERFORMANCE MARGIN	$RAG + 174.95 - 20 \log_{10} d$	+4.4 – 5.4	

THE WORST CASE PERFORMANCE MARGIN/TOLERANCE MARGIN IS FOR THE SYNCHRONIZATION CHANNEL, THUS:

$$\text{EXCESS MARGIN} = RAG + 169.55 - 20 \log_{10} d$$

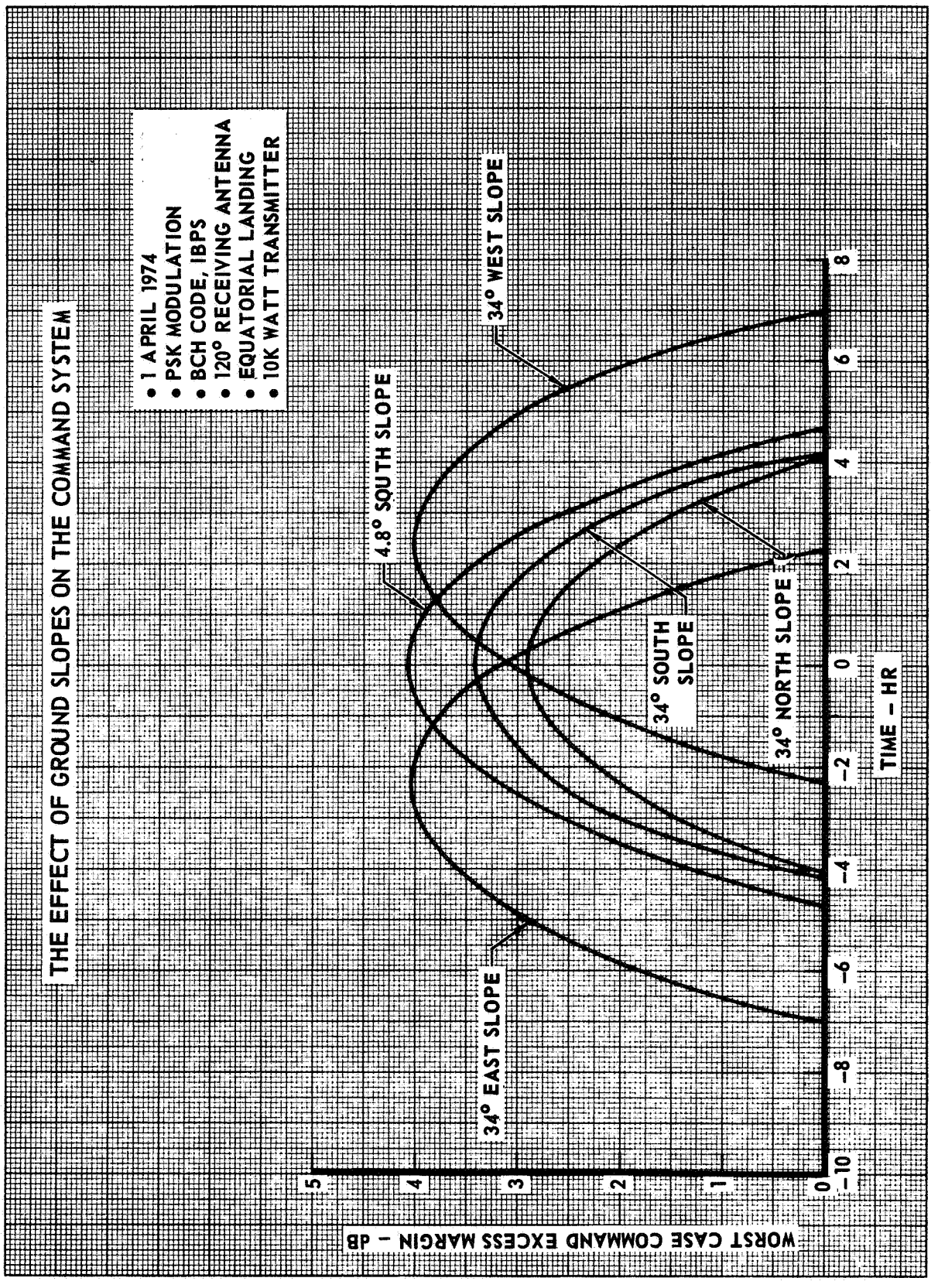

FIGURE 3.2.2–21

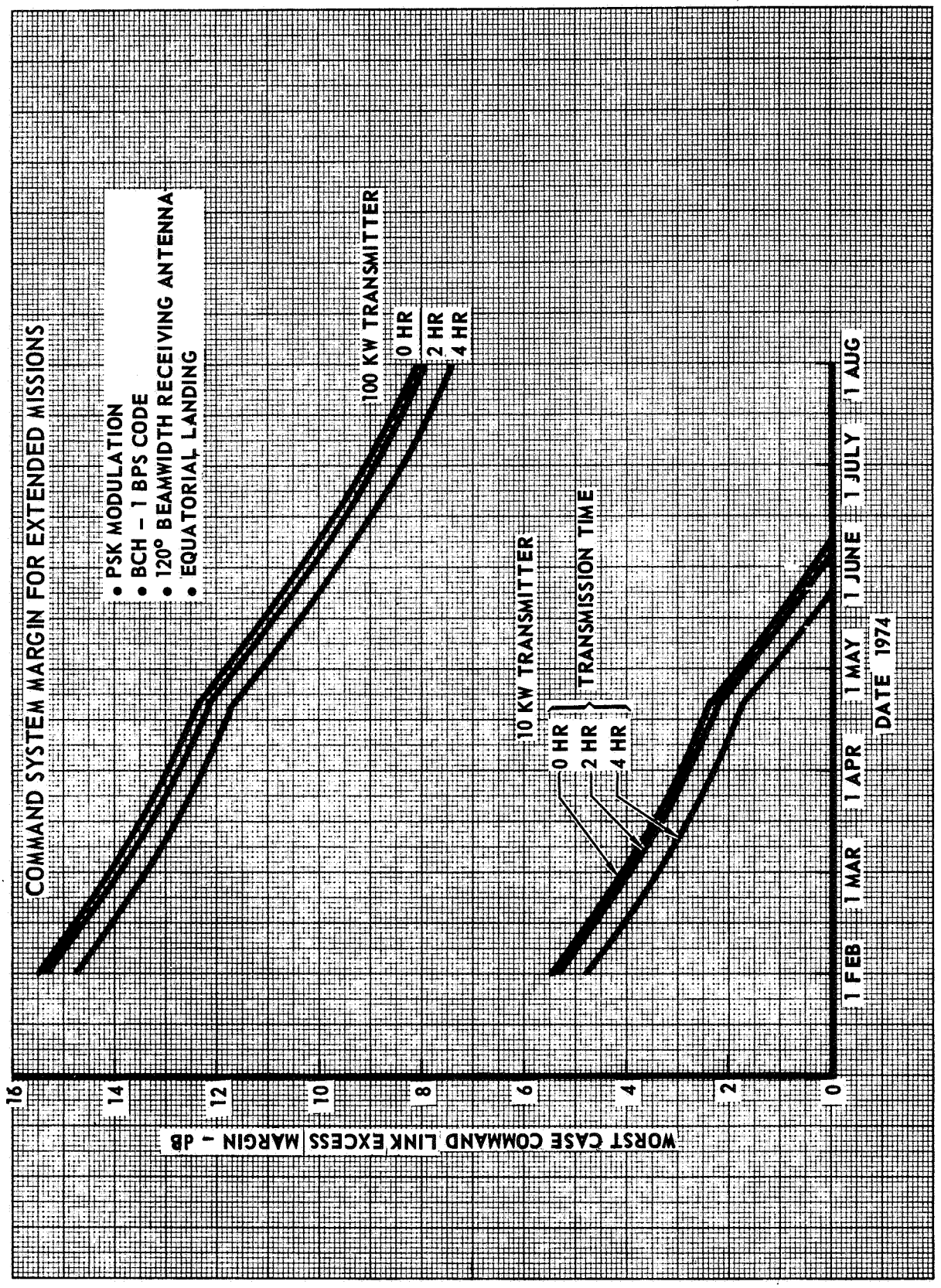

FIGURE 3.2.2–22

THE EFFECT OF GROUND SLOPES ON PERIAPSIS RELAY COMMUNICATIONS

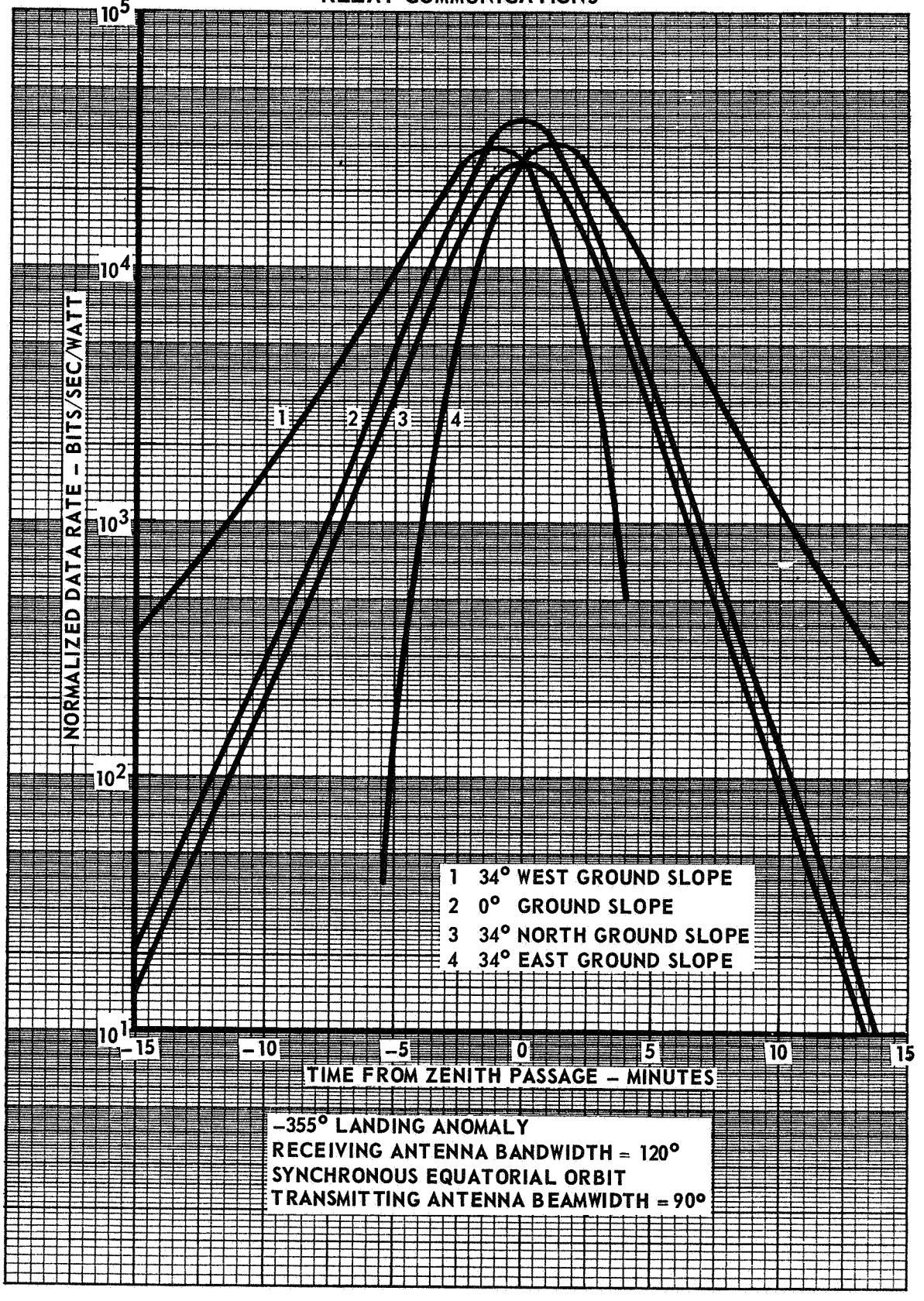

FIGURE 3.2.2–23

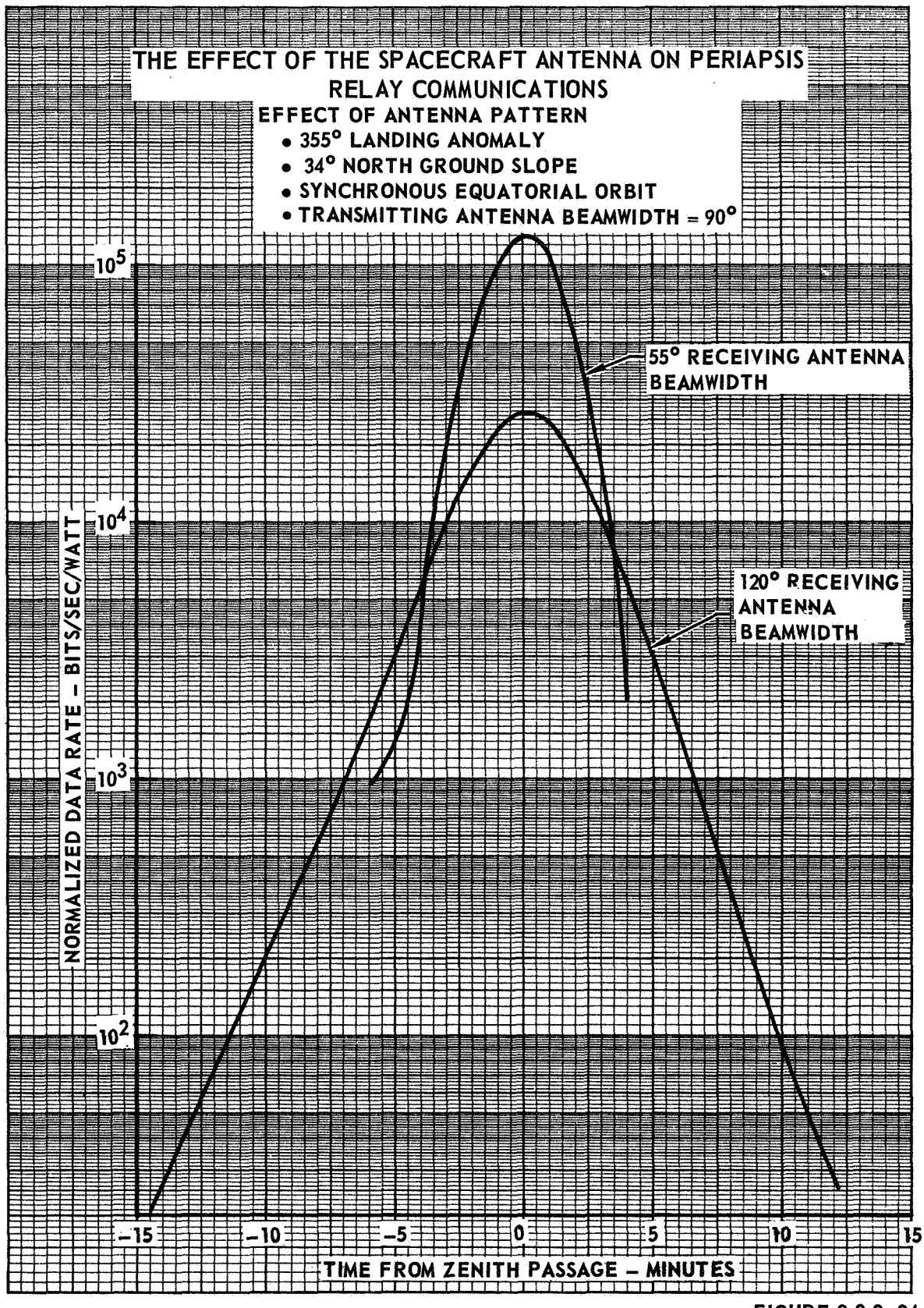

FIGURE 3.2.2–24

Figure 3.2.2-25 shows the total data return per pass at periapse. The narrow beamwidth (55°) spacecraft antenna will support over 3 times as much data as the wide beamwidth (120°) antenna. Figure 3.2.2-26 shows the transmitter power required to support 10^7 bits per pass at periapse.

Figure 3.2.2-27 illustrates the significance of the ground slopes for the synchronous orbit/apoapse transmission case. The slope at apoapse is just as important as it is at periapse. If, for example, a 100 bit per watt rate is to be supported, although a 10 hour window is available, its relative absolute time uncertainty may be 4 hours. Figure 3.2.2-28 shows that at apoapse the power optimal transmission time is 5 to 6 hours, and is essentially independent of the range of spacecraft beamwidths investigated.

The total data return per pass at apoapse is shown in Figure 2.2.2-29. Note that the amount of apoapse data is a critical function of the spacecraft antenna gain. Figure 3.2.2-30 shows the transmitter power required to support 10^7 bits per pass at apoapse.

Figure 3.2.2-31 illustrates the data rate possible for a 60 deg inclined synchronous orbit at periapse with a landing at a 10° latitude. The total data return for this condition is shown in Figure 3.2.2-32. Note that for a data return of five megabits per watt, any rate from 15K to 29K bits per second would be acceptable. Figure 3.2.2-33 shows the maximum data rate possible for apoapse communication as a function of total transmission time, e.g., 200 bps/w can be supported for 5-1/2 hours. The data return from apoapse is shown in Figure 3.2.2-34. The data return is the same as that for the synchronous equatorial orbit.

Figure 3.2.2-35 illustrates the data rate possible for a 60 deg inclined nonsynchronous orbit at periapse. The maximum rate decreases from 3.9×10^4 bps/w immediately after landing to 8×10^3 bps/w by the fifth orbit. The total daily bit transfer degrades from 5.25 M-bit/w to 2.34 M-bit/w from the first to the fourth orbit, as shown in Figure 3.2.2-36.

The data rate possible for a 60 deg inclined nonsynchronous orbit at apoapse is shown in Figure 3.2.2-37. The maximum rate decreases from 385 bps/w during the first orbital pass to 40 bps/w by the 45th orbit. The total

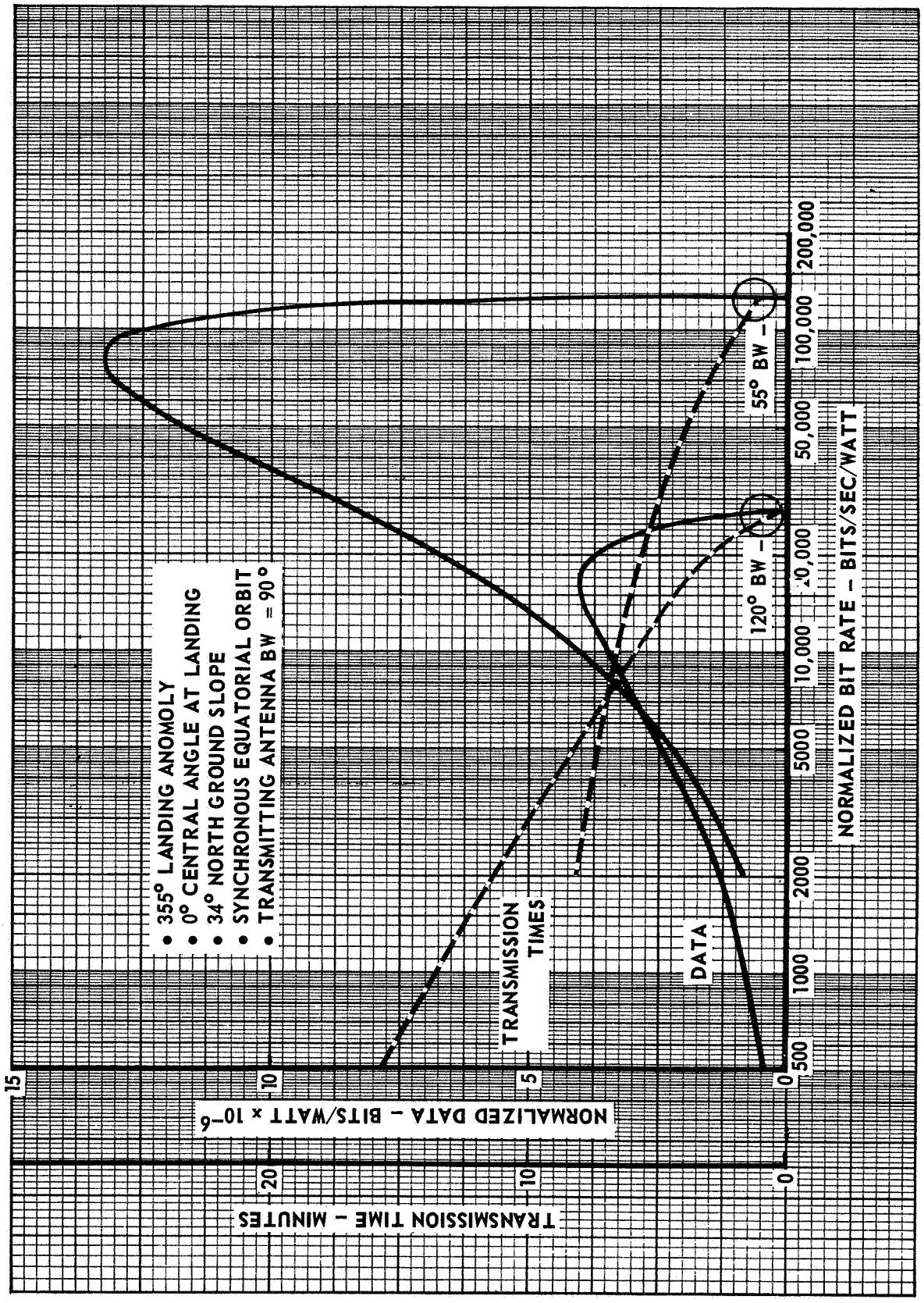

FIGURE 3.2.2–25

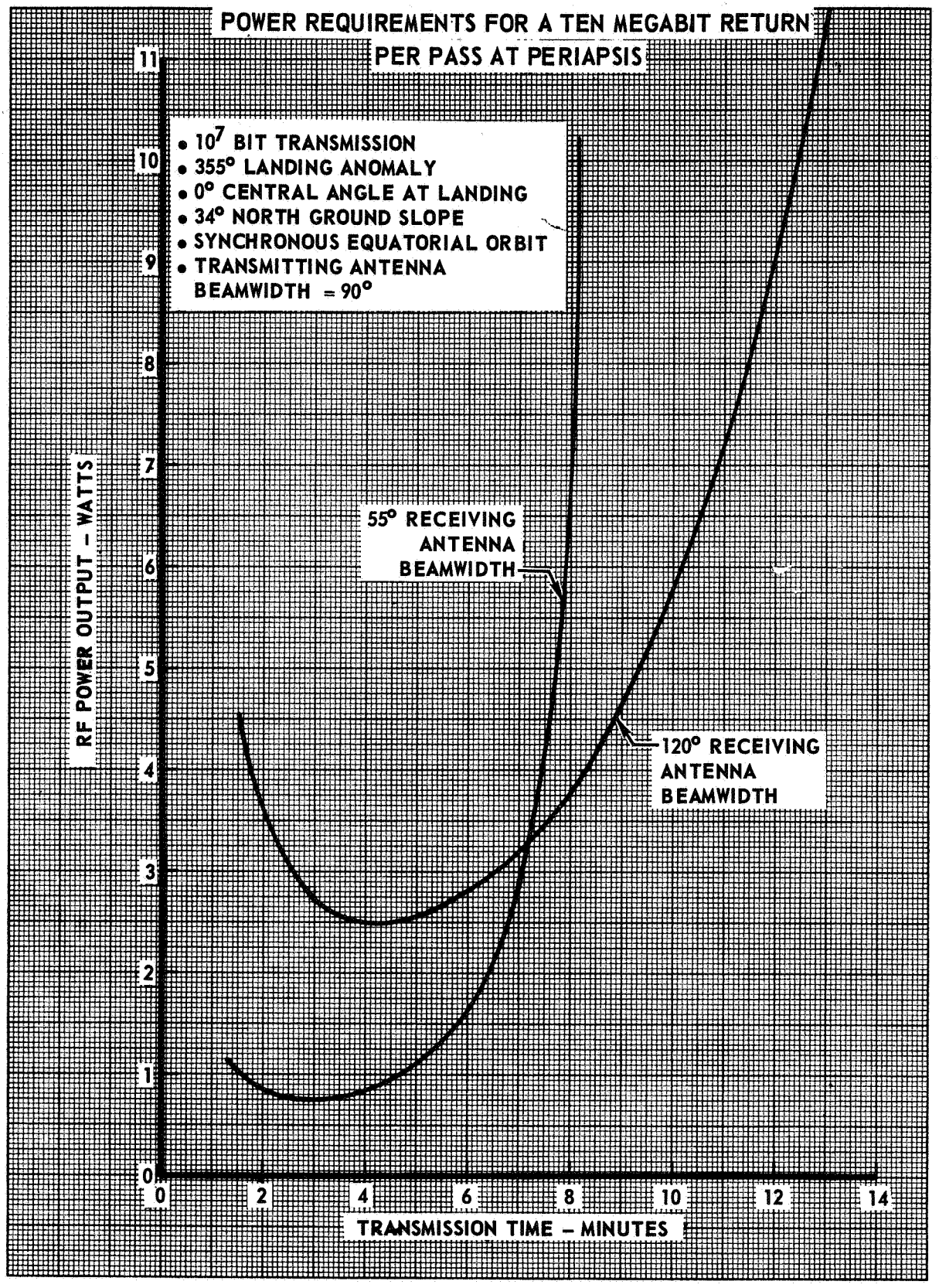

FIGURE 3.2.2–26

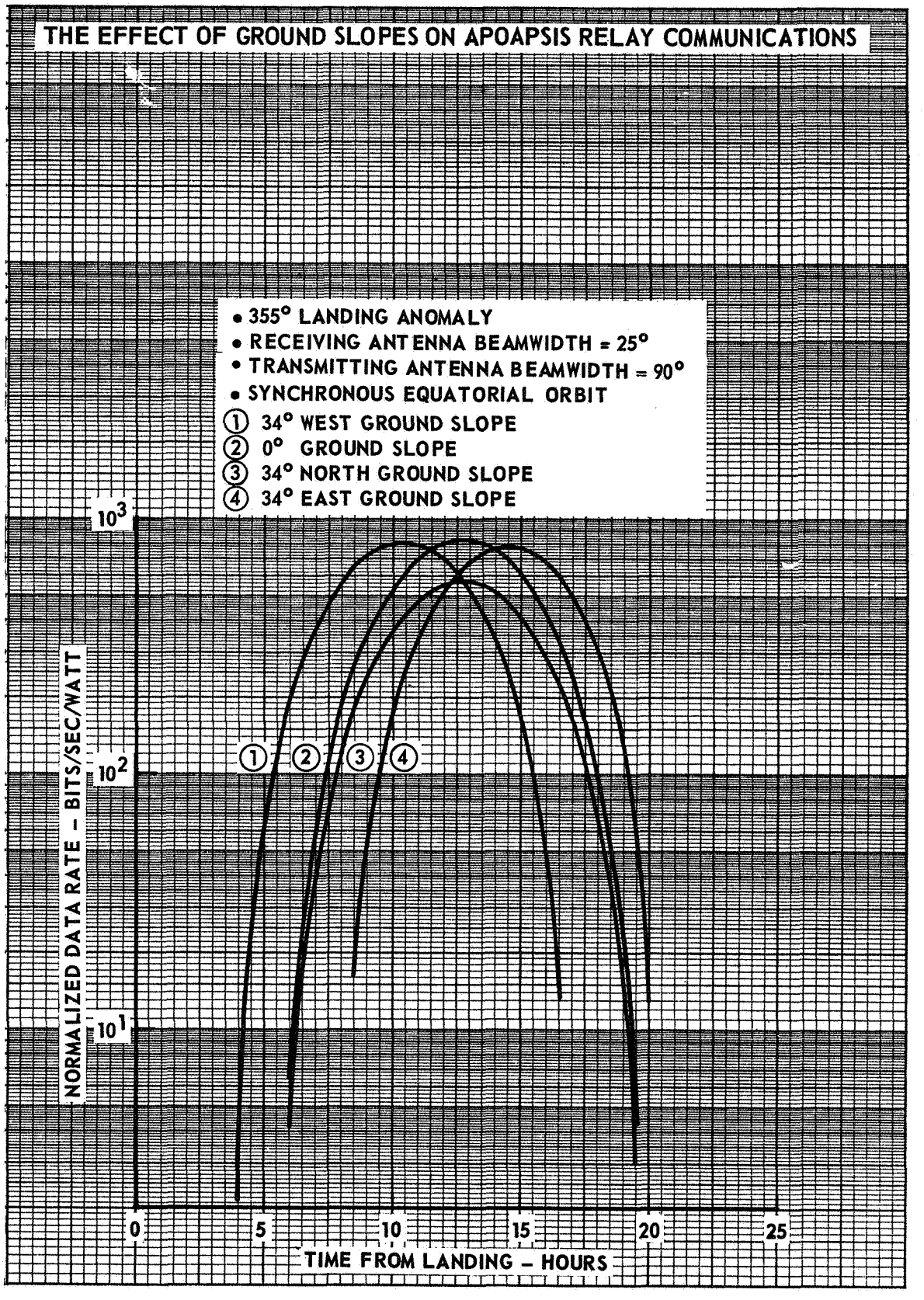

FIGURE 3.2.2–27

THE EFFECT OF THE SPACECRAFT ANTENNA ON APOAPSIS RELAY COMMUNICATIONS

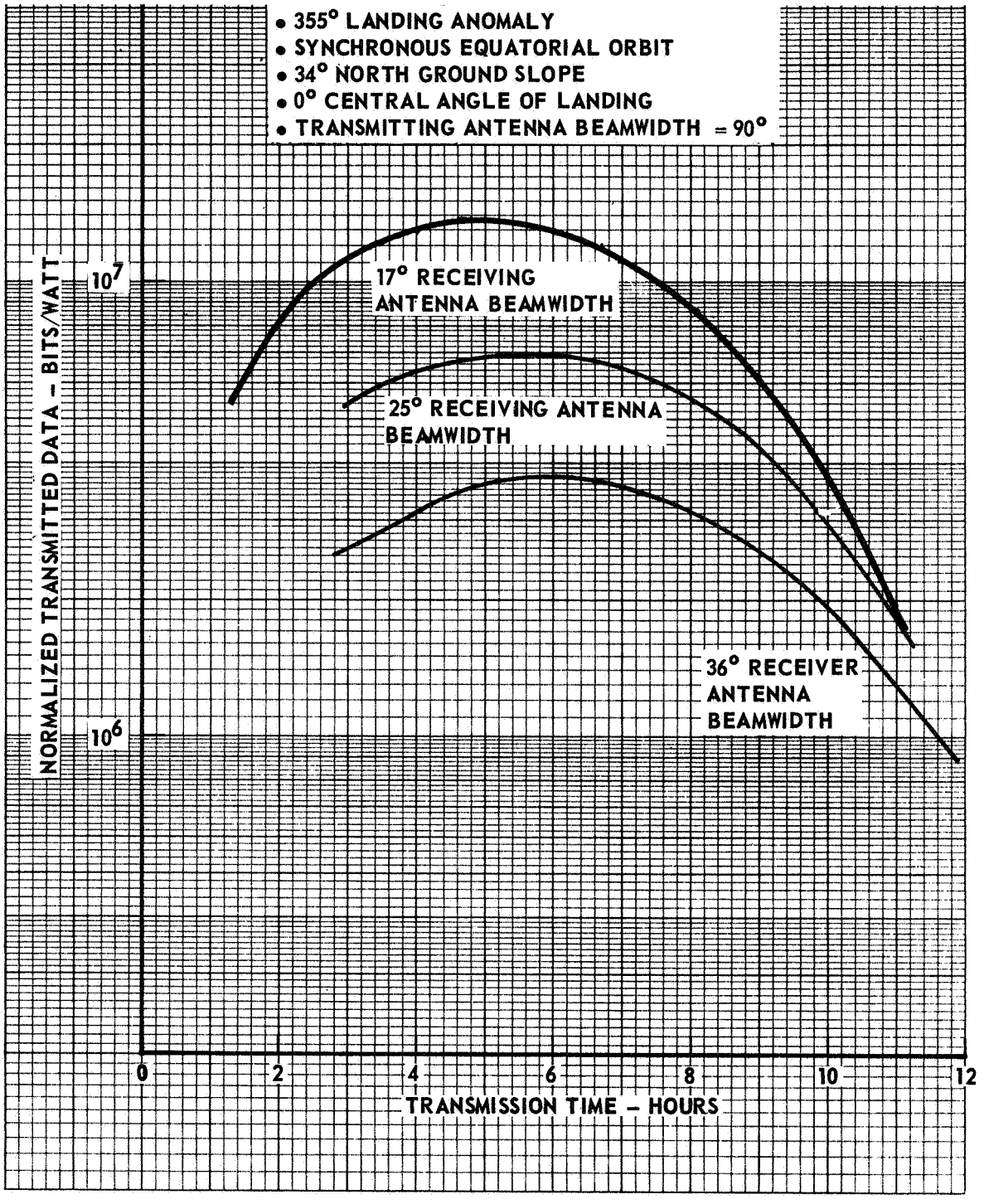

FIGURE 3.2.2–28

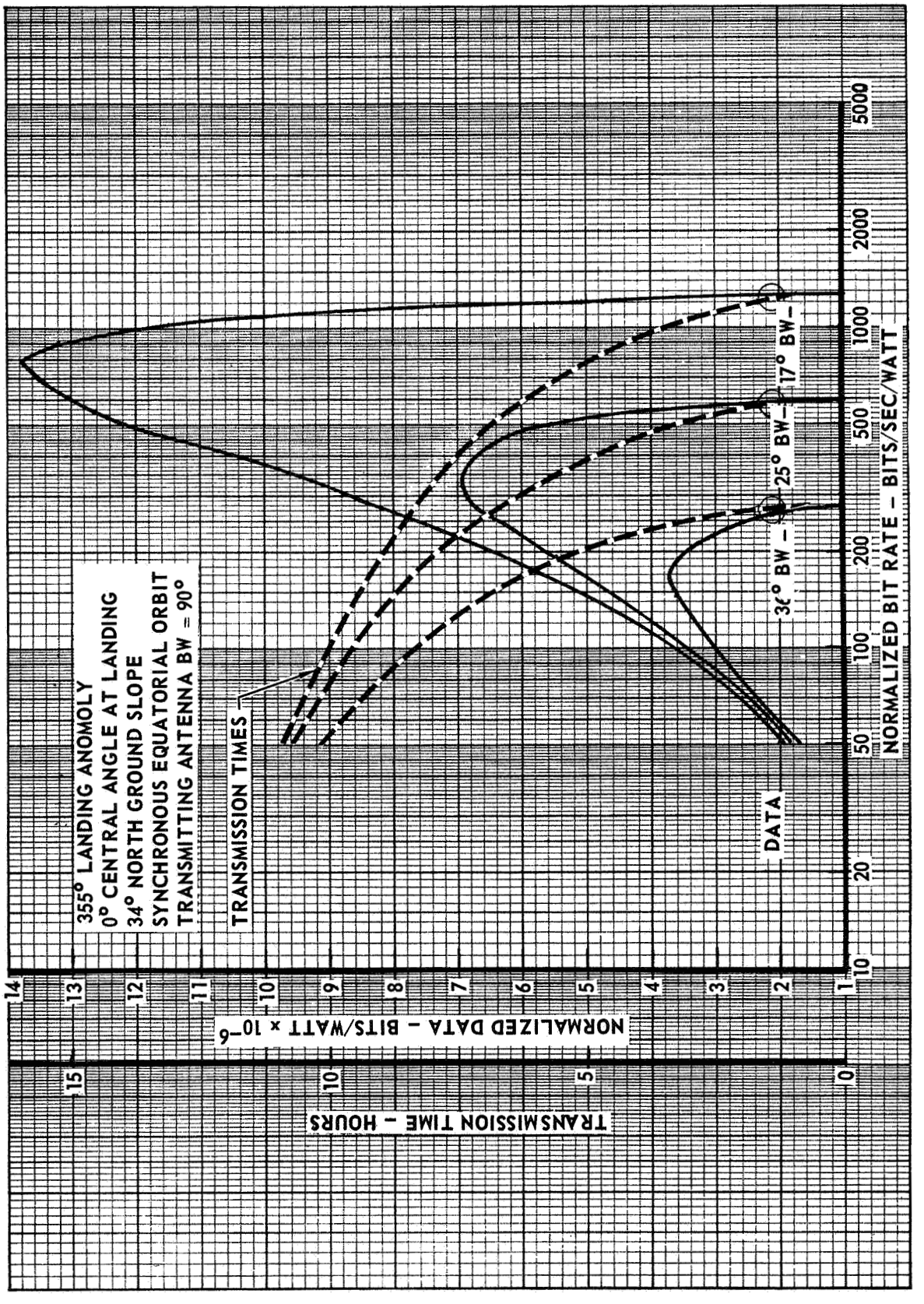

FIGURE 3.2.2–29

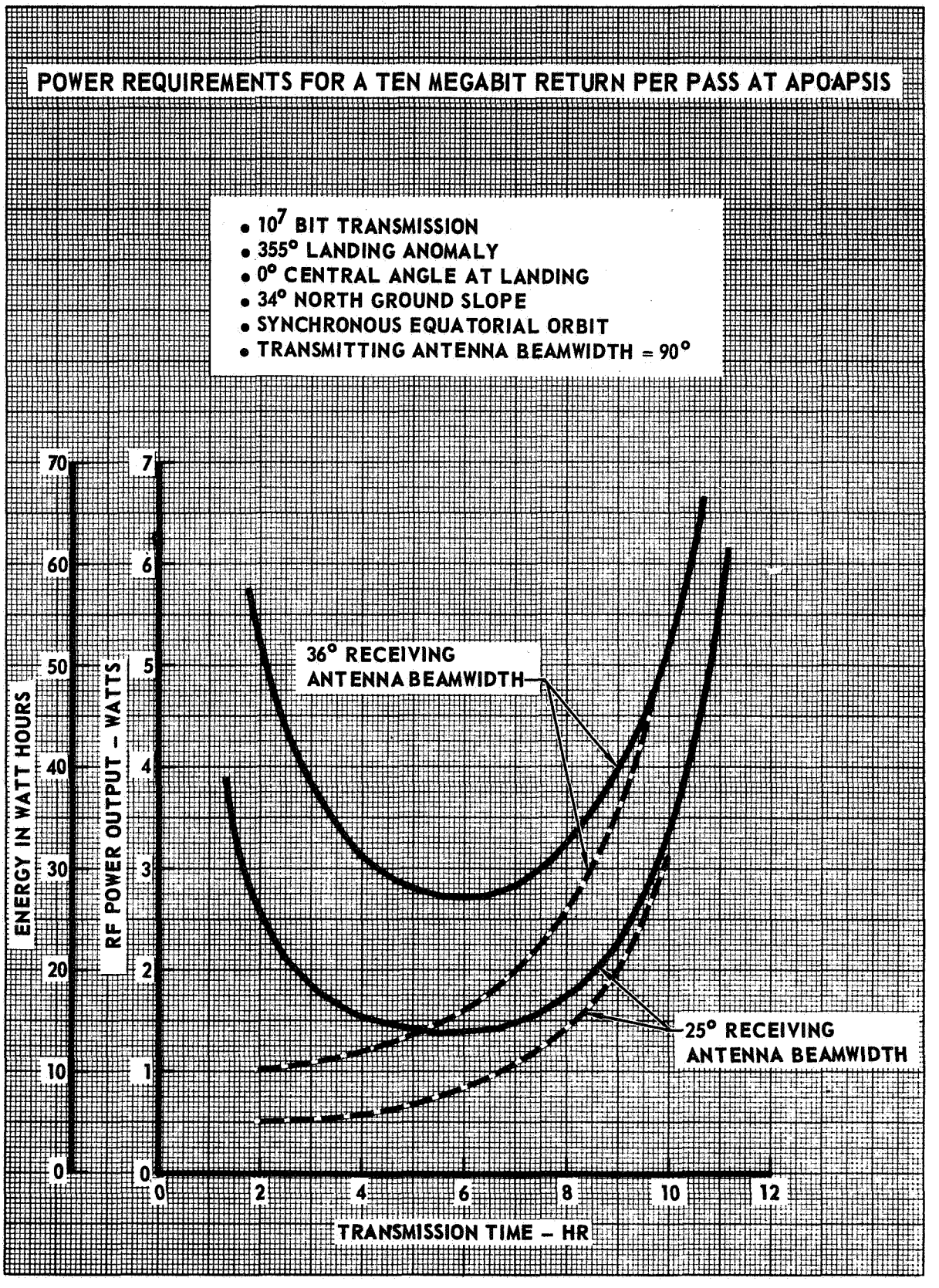

FIGURE 3.2.2–30

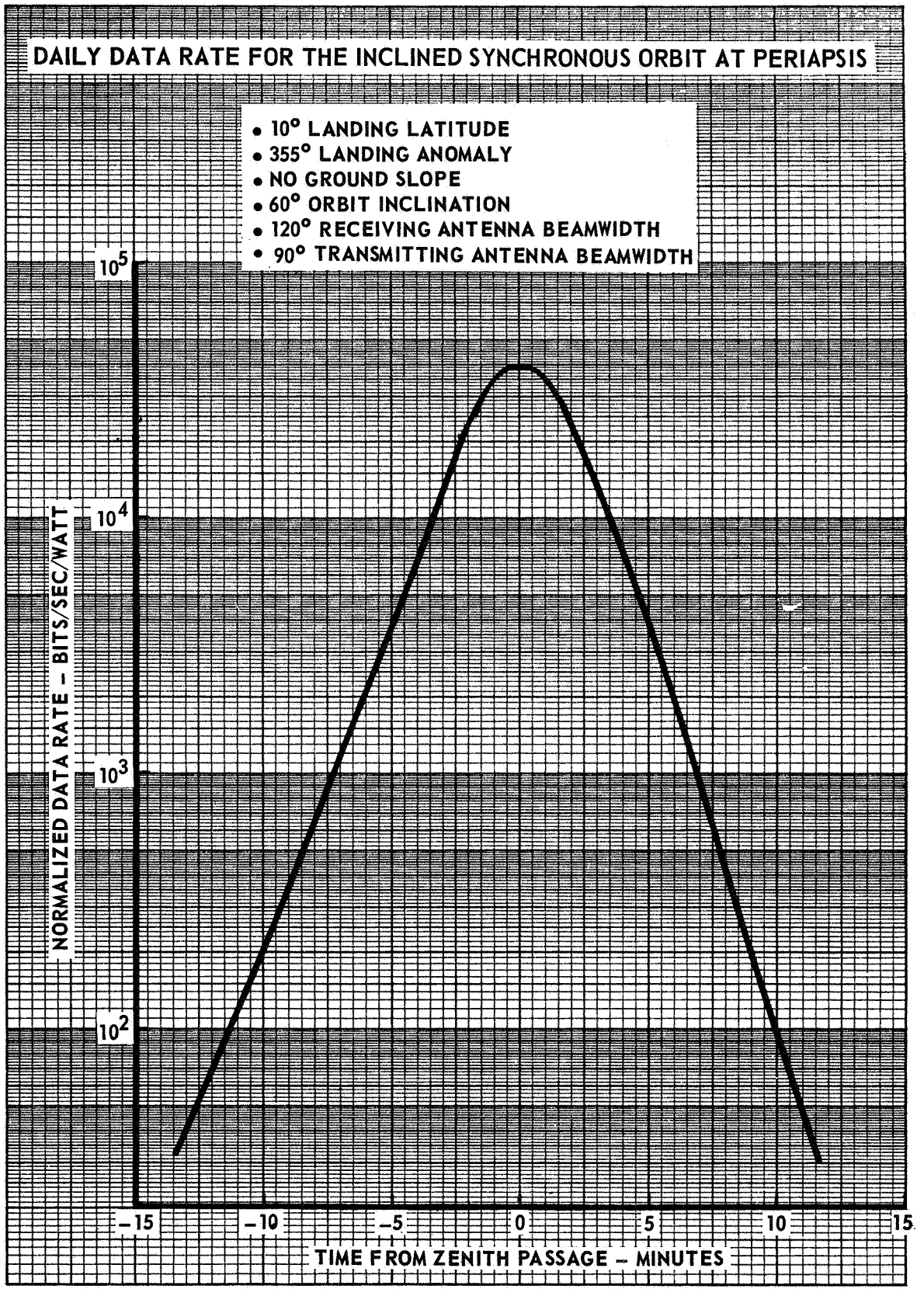

FIGURE 3.2.2–31

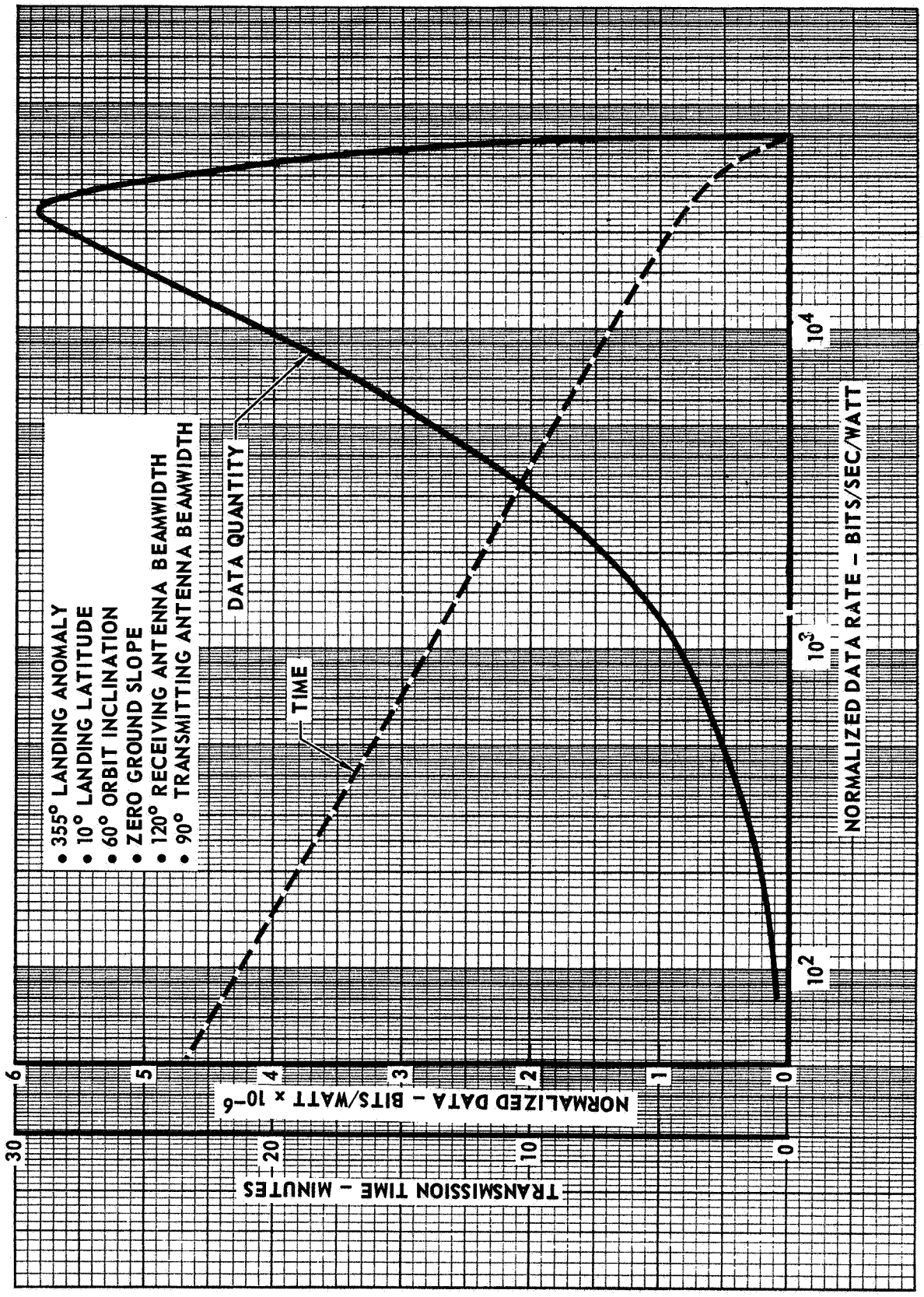

FIGURE 3.2.2–32

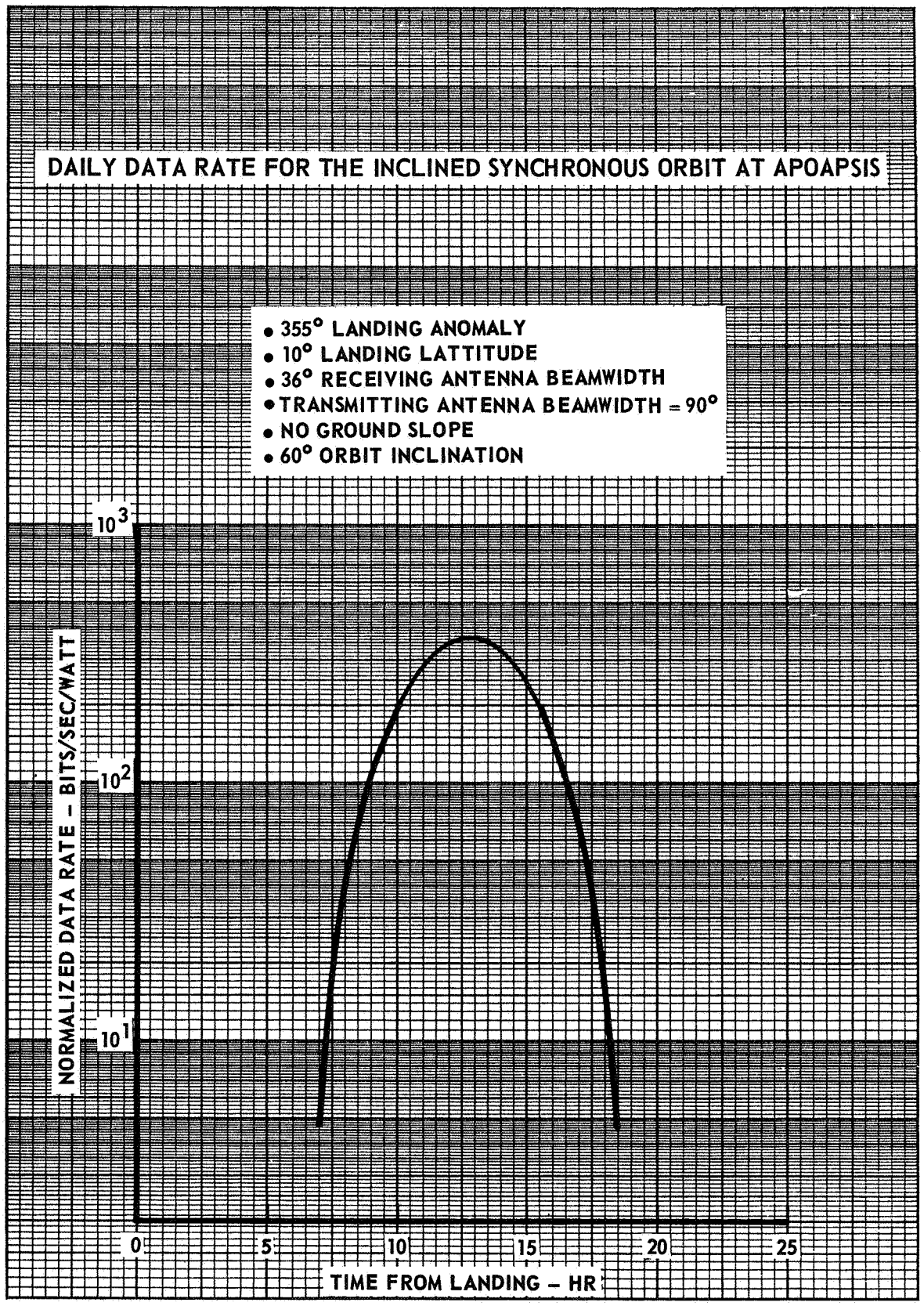

FIGURE 3.3.2–33

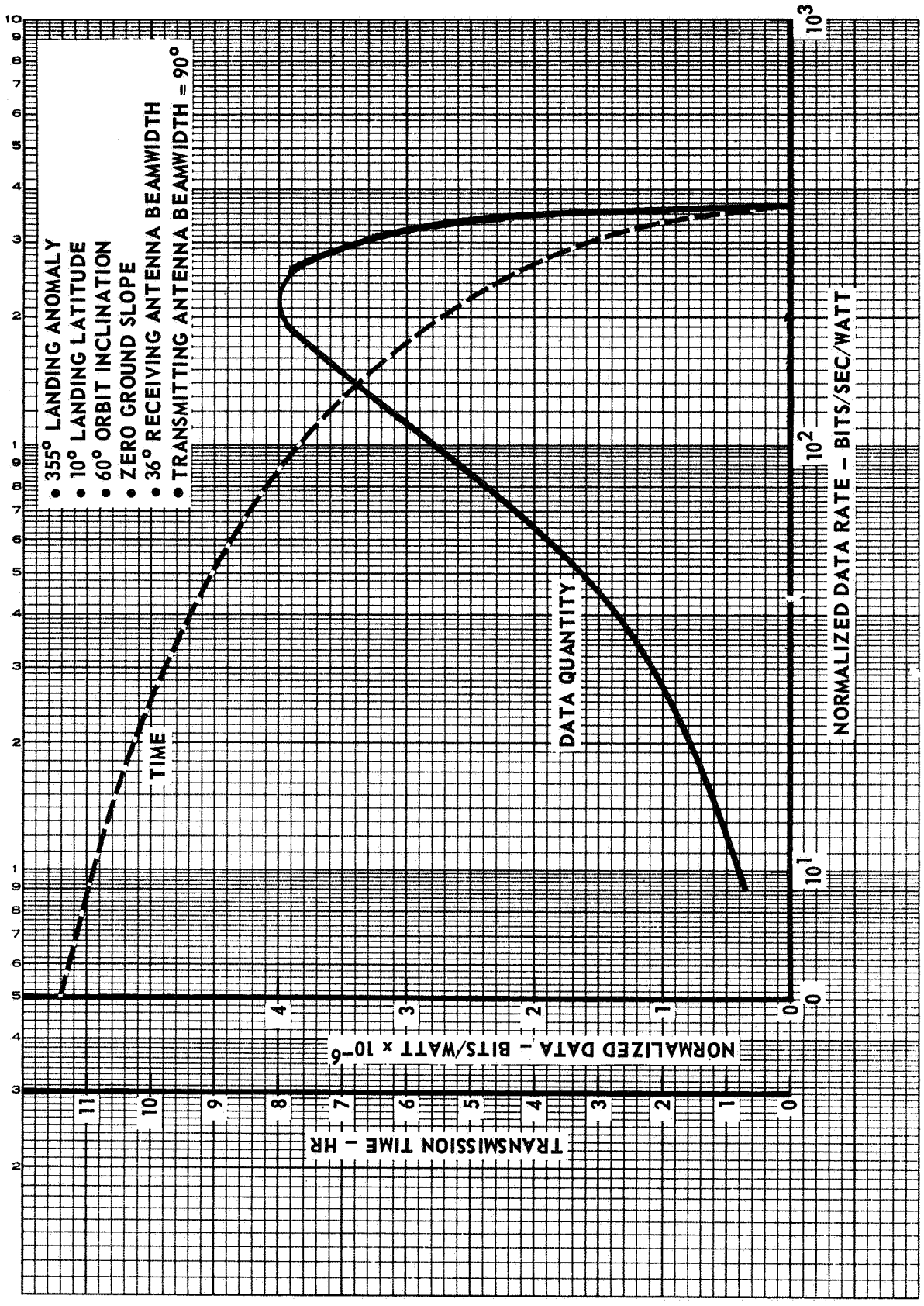

FIGURE 3.2.2–34

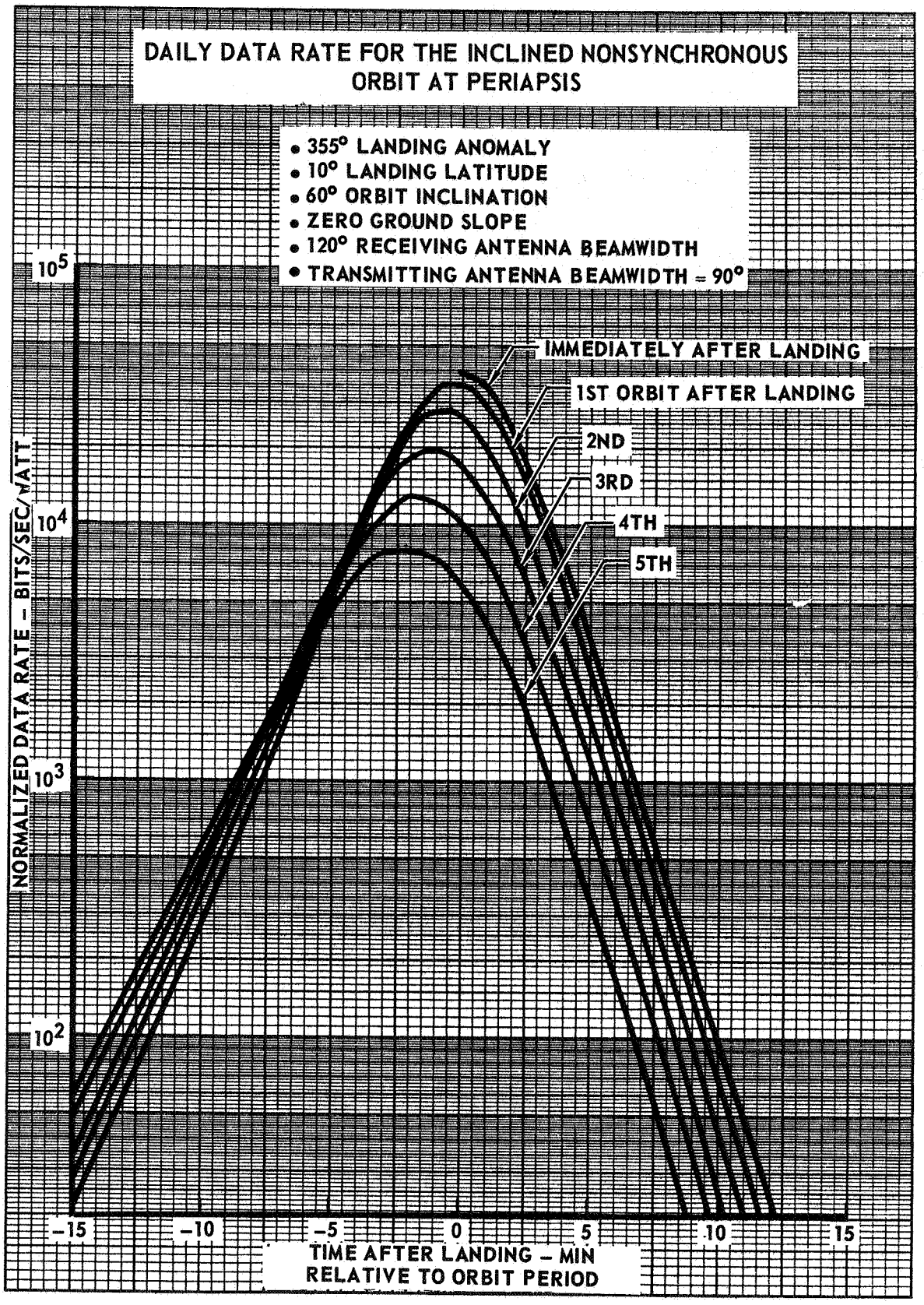

FIGURE 3.2.2–35

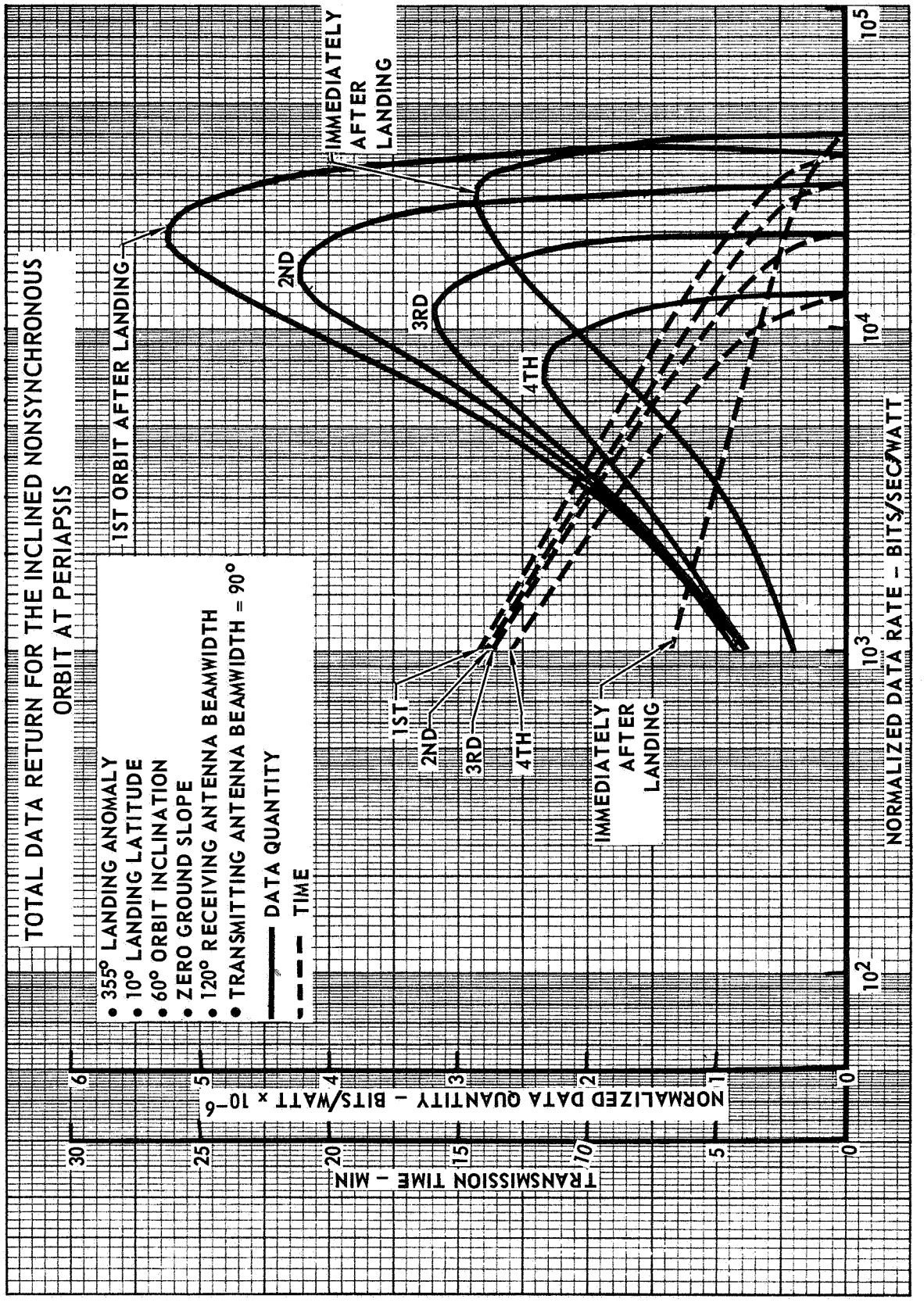

FIGURE 3.2.2–36

DAILY DATA RATE FOR THE INCLINED NONSYNCHRONOUS ORBIT AT APOAPSIS

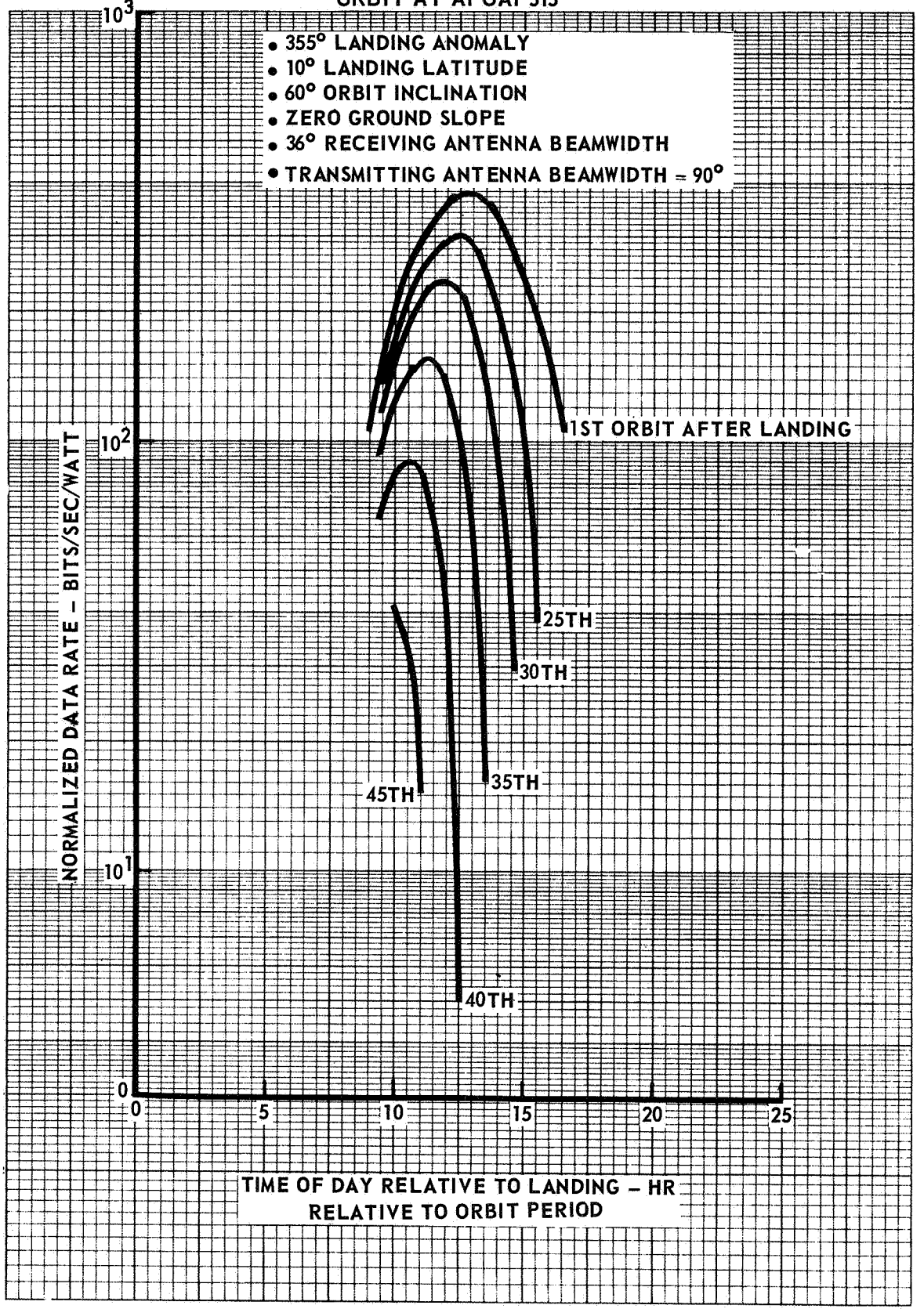

FIGURE 3.2.2–37

maximum daily bit transfer degrades from 4.05 M-bit/w to 0.45 M-bit/w in the 40th orbit, as shown in Figure 3.2.2-38.

3.2.2.2.3 Equipment considerations: The landed communication system includes components for a 400 MHz, two frequency shift keyed relay link; for a 2300 MHz, M-ary frequency shift keyed, low rate direct link; and for a 2300 MHz, convolutionally coded, coherent phase shift keyed, high rate direct link. The parametrics for each component are given below. The components are "packaged," i.e., the parametrics are for a unit package rather than just the component subassemblies. Each component contains its own DC-to-DC converter to convert the raw bus voltage to that required for component operation. Figures 3.2.2-39, -40 and -41 illustrate how the parametrics are derived. These figures show the size, weight, and power characteristics of typical missile and satellite S-band power sources.

In the list below, size (S) is given in cubic inches, weight (W) in pounds, and power (P) in watts.

a) A solid state S-band transmitter would most probably be employed if the output power requirement were less than 10 watts. The parametrics are:

$$S = 45\ (P_o/7.5)^{3.68} + 40$$

$$W = 4\ (P_o/7.5)^{1.95} + 4$$

$$P = 15.4\ P_o^{\ 0.793}$$

Where P_o is the RF output power in watts.

b) A traveling wave tube S-band transmitter would most probably be employed if the output power requirement were greater than 10 watts. The TWTA parametrics are:

$$S = 30\ (P_o/30)^{.564} + 80$$

$$W = (P_o/20)^{.975} + 4.5$$

$$P = 5.8\ P_o^{.845}$$

where P_o is the RF output power in watts. Add S = 40, W = 4 and P = 8.9 for a modulator-driver plus S = 25, W = .8 for an output filter.

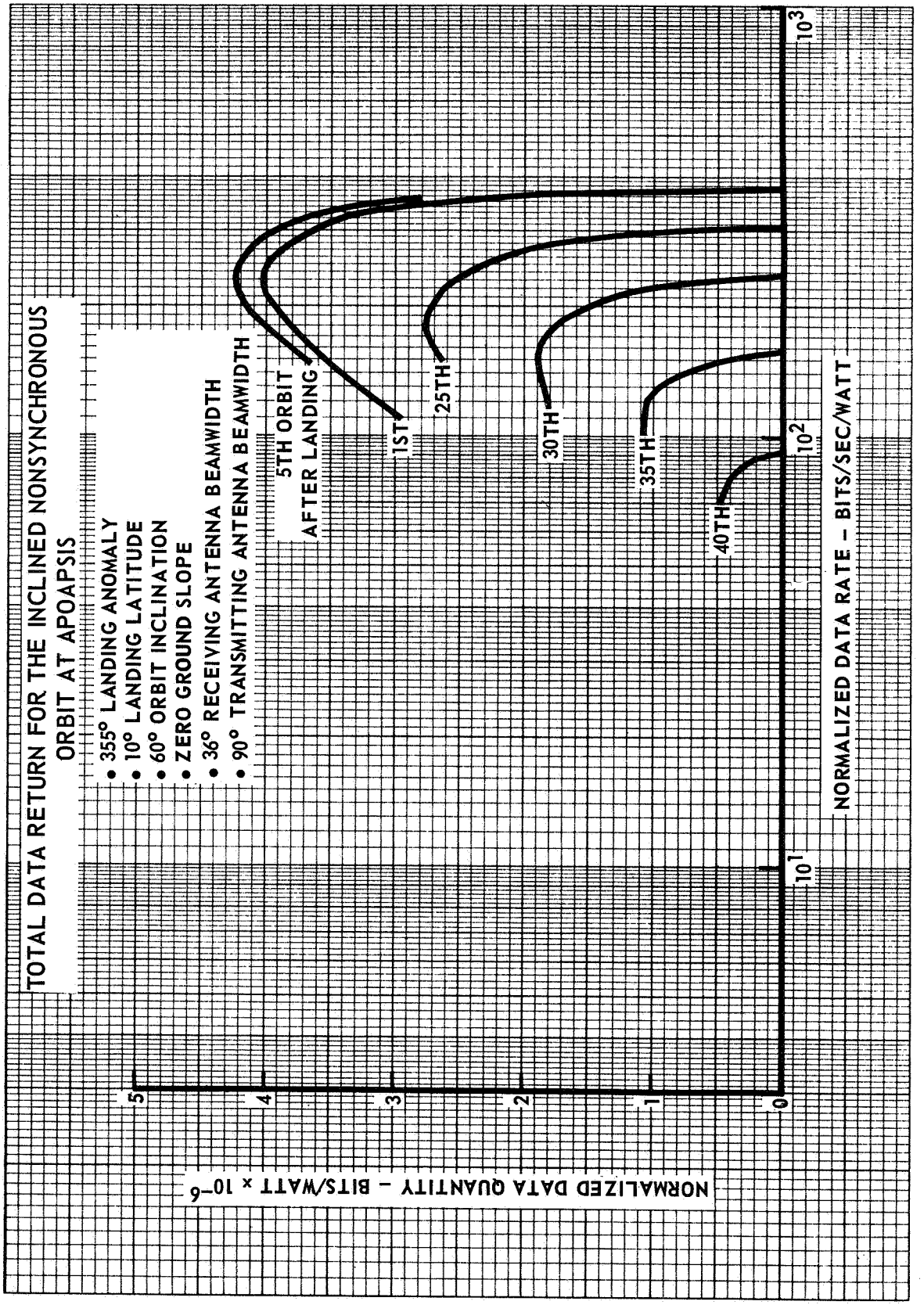

FIGURE 3.2.2–38

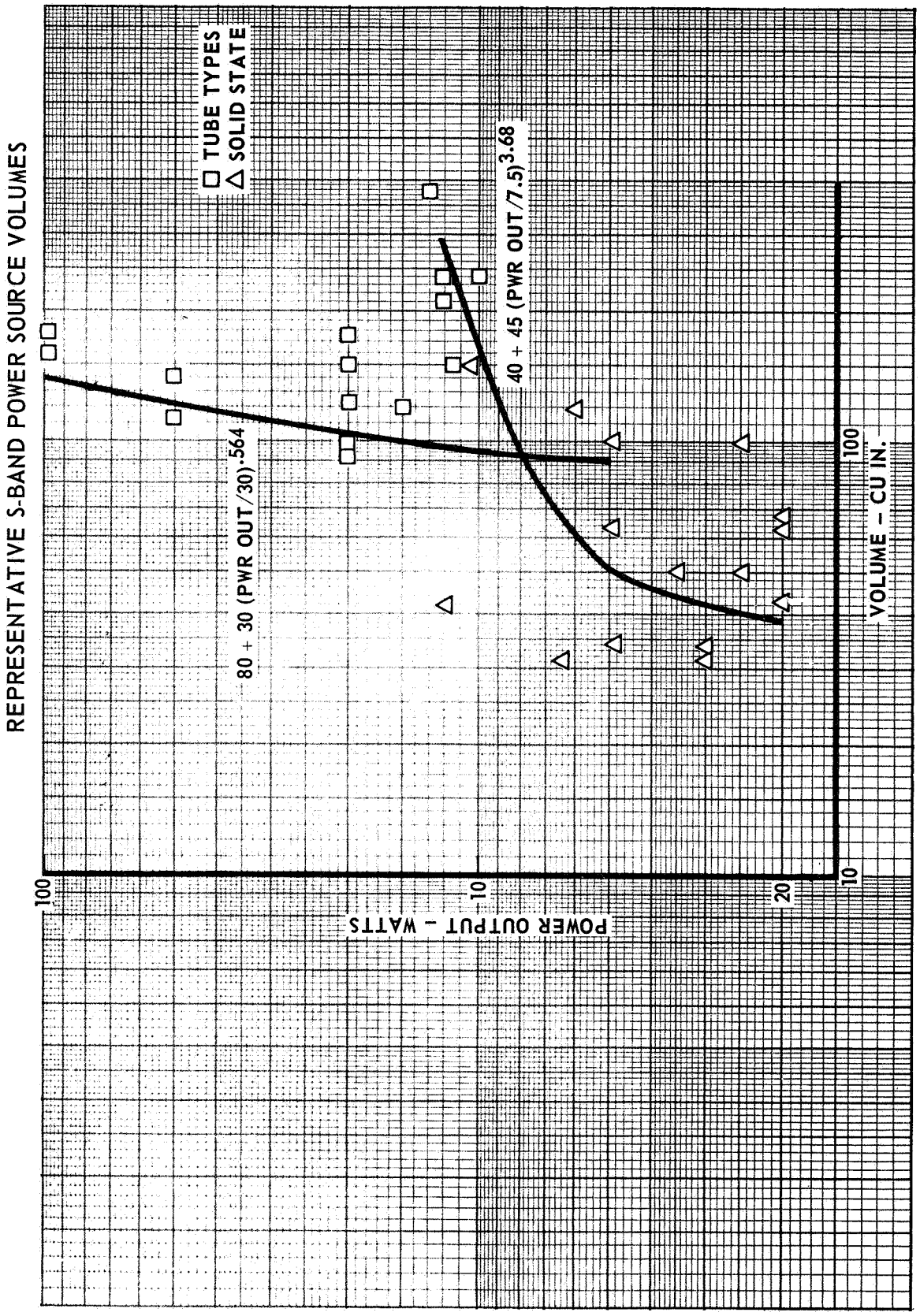

FIGURE 3.2.2–39

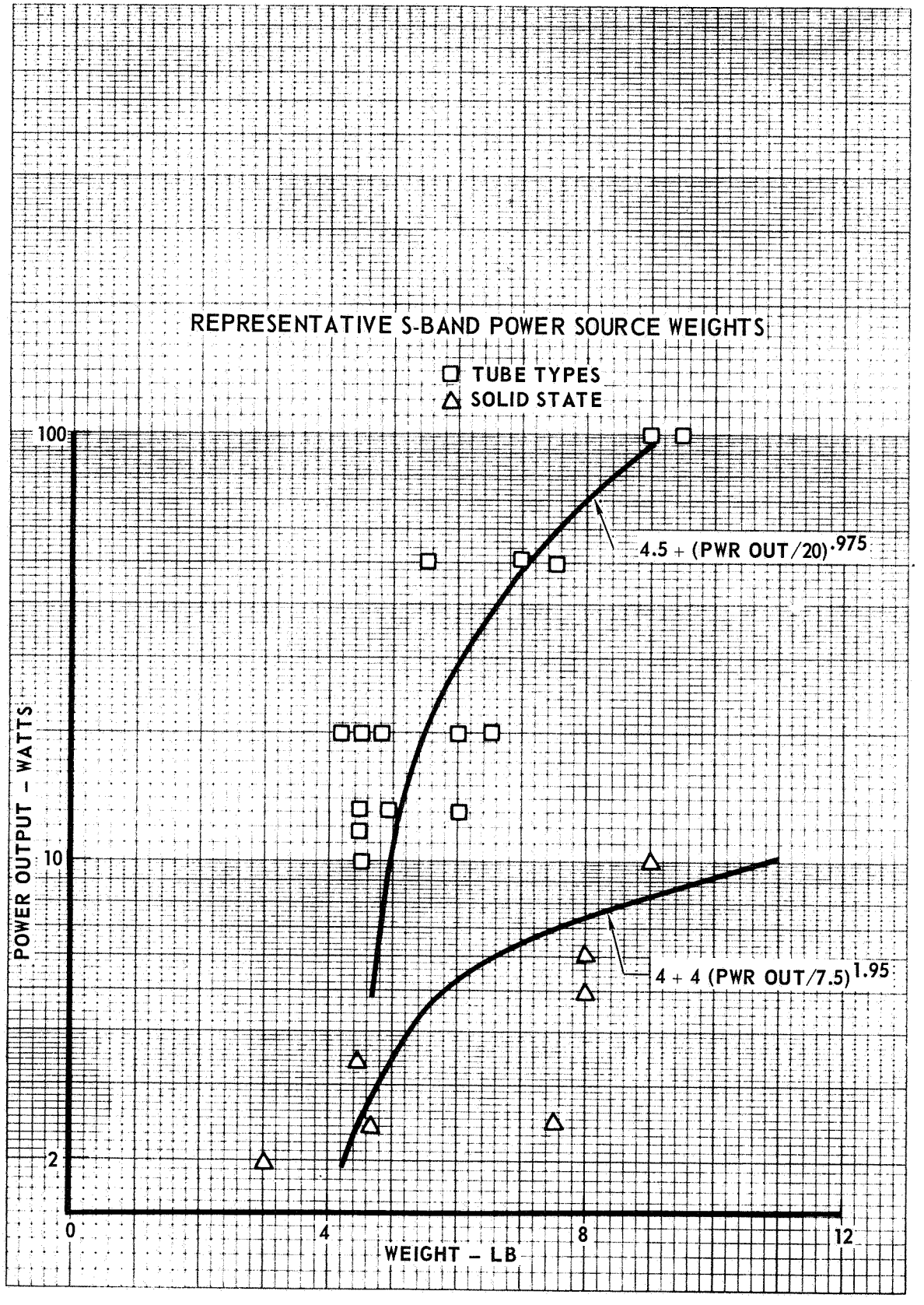

FIGURE 3.2.2–40

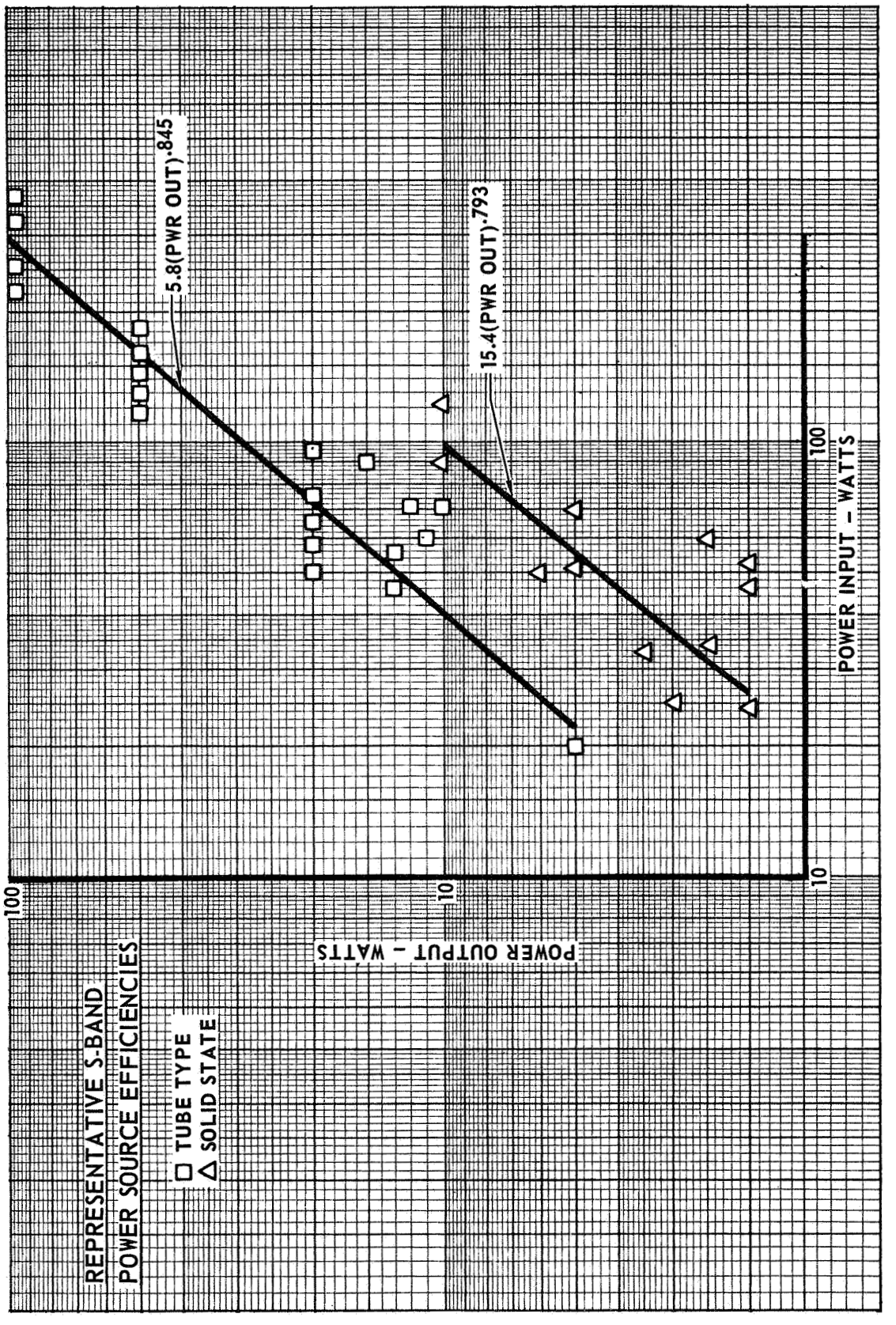

FIGURE 3.2.2–41

c) A MFSK generator and frequency translator is required to condition the data commutator output prior to S-band transmission. The characteristics of the generator/translator are:

$$S = 97.5$$

$$W = 4.48$$

$$P = 2.78$$

d) A command receiver may be required on extended missions to update the capsule sequences. The characteristics of the receiver are:

$$S = 40$$

$$W = 2.3$$

$$P = 2.5$$

e) The command decoder interfaces between the command receiver and the using subsystems. The parametrics are:

$$S = 70\ (Co/100)^{1.7} + 29$$

$$W = 2.5\ (Co/100)^{1.66} + .5$$

$$P = .5\ (Co/100)^{2.06} + .12,$$

where Co is the number of commands.

f) For the 400 MHz antennas, use the same expressions shown in the entry communications component parametrics section. For a S-band hemispheric,

$$W = 0.3, \text{ Diameter} = 2.3 \text{ in.}$$

For a S-band parabola,

$$W = 0.7\ D^2$$

or $W = 0.7 \times 10^{0.1G(dB) - 1.47}$

Where D is the diameter in feet, and G (dB)is the gain in decibels.

For the pointing and control electronics, up to a three foot diameter dish,

$S = 127.8$

$W = 7.08$

$P = 6.0$

Which is independent of the warm-up and "stepping" power.

g) All of the other components are the same as those given in the entry communications component parametrics.

As an example of the parametrics, consider the simple landed system of Figure 3.2.2-42 operating at 2300 MHz MFSK. For a design transmission range of 3×10^8 km the system would occupy approximately 480 cubic inches, weigh about 25 pounds and consume about 84 watts. Figure 3.2.2-43 illustrates the effect of transmission range on the transmitted bit rate, for 20 watts of transmitter power.

3.2.2.3 Total Data Return Analysis. - Figure 3.2.2-44 compares the relative data return of a UHF 2FSK relay link with that of an S-band PSK direct to earth link. The data for the relay periapsis case is taken from the total daily periapsis relay communications data return figure, while that for the direct case is taken from the high rate direct link communications figure. It is interesting to note that pound for pound or watt for watt, the relay mode is always more advantageous up to a daily return of approximately 6.5×10^7 bits.

The relay communication system is capable of returning a significant quantity of data immediately after landing. The performance of the link at this time is a function of the capsule-orbiter geometry at landing, and therefore is determined by the capsule-orbiter geometry at entry. This geometric relationship is further influenced by the choice of entry angle and the uncertainty in atmospheric characteristics.

The immediate post landed view time is shown in Table 3.2.2-7 for six cases. Cases 1 through 4 illustrate the variation of view time with atmosphere and entry angle for a constant 5 degree capsule lead angle at entry. Cases 4

AN EXAMPLE OF A LANDED COMMUNICATION SYSTEM

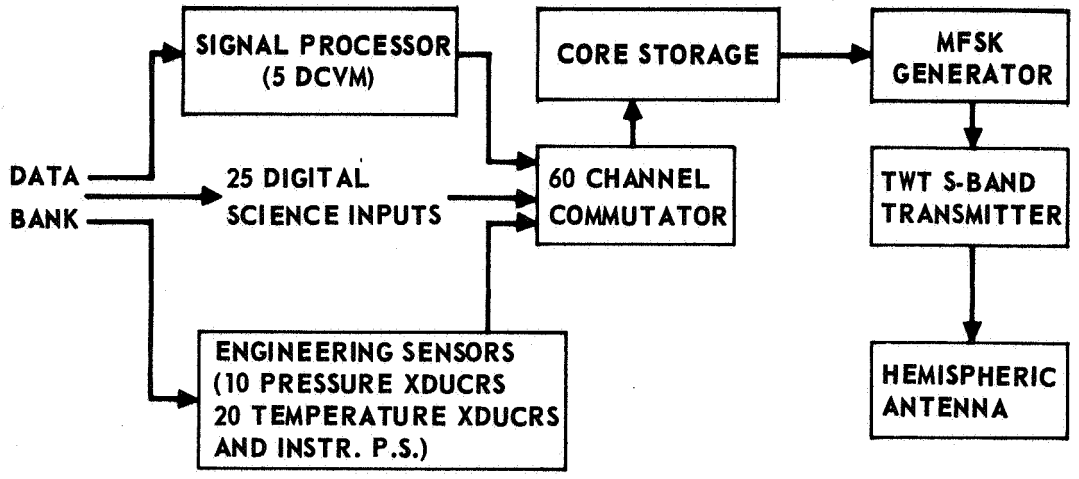

ASSUMING: DATA DUMP IS 4 HOURS
DATA COLLECTION IS 24 HOURS AT 5/6 BPS
TRANSMITTER ANTENNA GAIN IS + 2.5 dB
TRANSMISSION RANGE IS 3×10^8 KM

ITEM	SIZE (c.i.)	WEIGHT (LB)	POWER (ω)
SIGNAL PROCESSOR	29.	.862	1.38
ENGINEERING SENSORS	34.16	3.523	.0495
COMMUTATOR	60.	2.4	1.8
CORE STORAGE	104	4.75	.121
MFSK GENERATOR	97.5	4.48	2.78
TRANSMITTER	166.8	10.154	78.8
ANTENNA	–	.3	–
TOTALS	491.46	26.469	84.9305

FIGURE 3.2.2–42

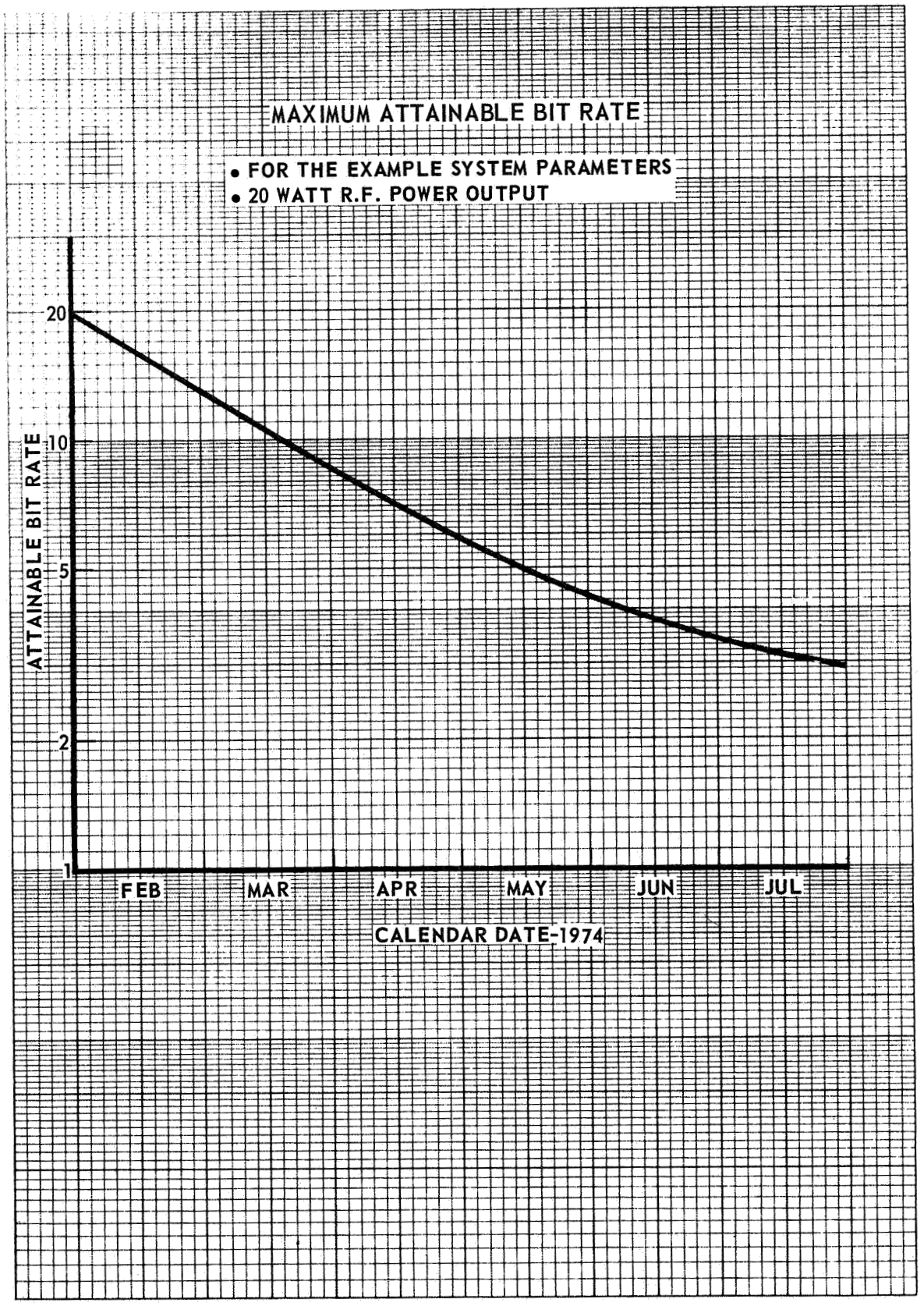

FIGURE 3.2.2–43

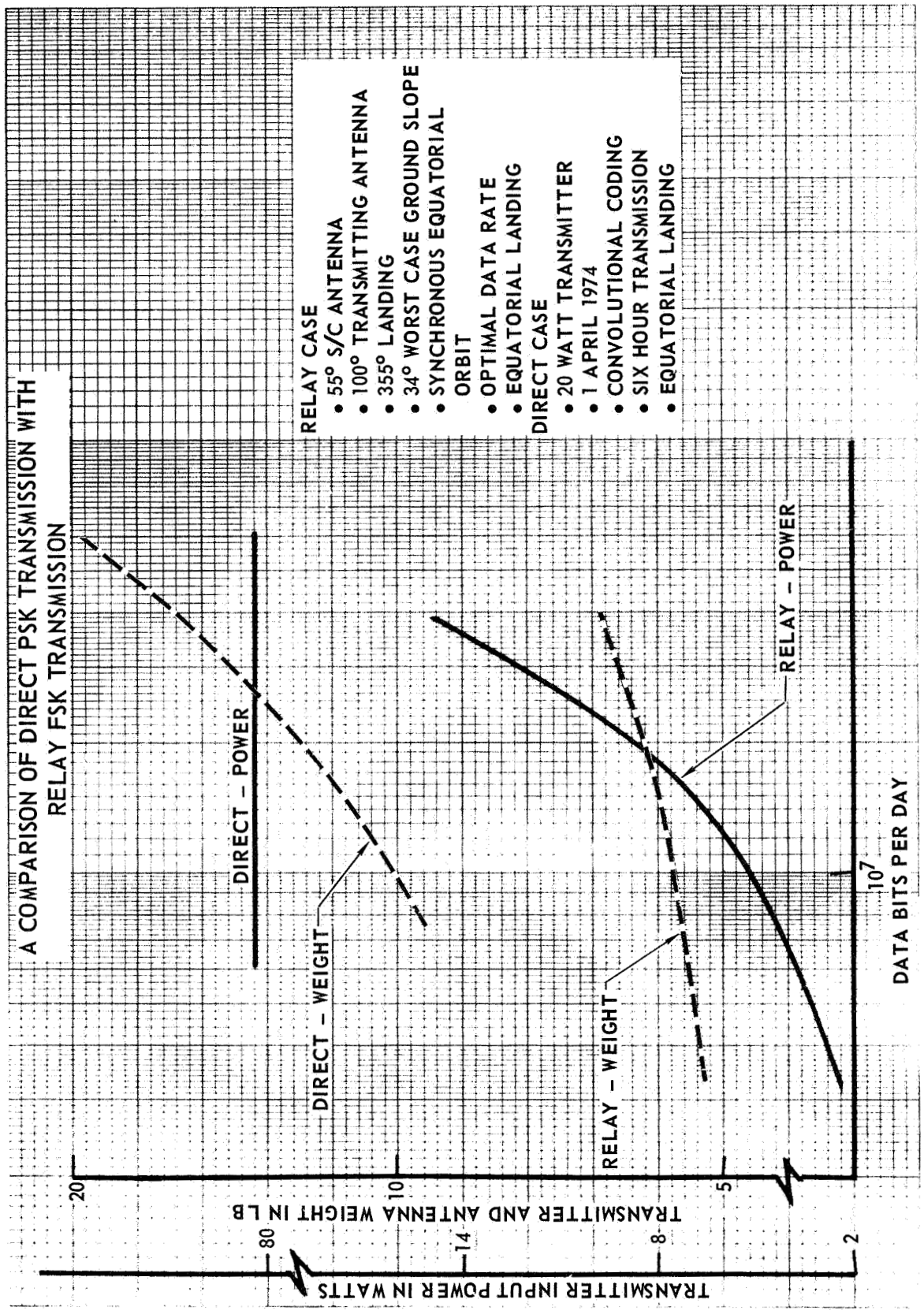

FIGURE 3.2.2–44

TABLE 3.2.2.-7

IMMEDIATE POST LANDED VIEW TIME

- ZERO GROUND SLOPE
- SYNCHRONOUS EQUATORIAL ORBIT
- EQUATORIAL LANDING
- LINK OF TABLE 3.2.2-2
- 120° BEAMWIDTH TRANSMITTING AND RECEIVING ANTENNAS
- DATA THRESHOLD OF 11.4 dB
- SPACECRAFT ANTENNA POINTED AT THE CAPSULE AT THE TIME OF LANDING
- TYPICAL SYSTEM IS 5 WATTS, 41.6 Kbps

TRAJECTORY					OPTIMAL DATA SYSTEM			TYPICAL SYSTEM	
CASE	VM	ENTRY ANGLE (DEG)	CAPSULE LEAD ANGLE AT ENTRY (DEG)	CAPSULE LANDING ANOMALY (DEG)	MAXIMUM VIEW TIME (MIN)	OPTIMAL DATA RATE (BITS/SEC/WATT)	MAXIMUM INFORMATION TRANSFER BITS/WATT	VIEW TIME (MIN)	INFORMATION TRANSFER (BITS)
1	8	−15	+5	351.5	7.35	14×10^3	2.76×10^6	4.40	10.98×10^6
2	9	−15	+5	347.4	4.65	11×10^3	1.39×10^6	2.66	6.65×10^6
3	8	−20	+5	332.4	8.35	9×10^3	2.52×10^6	4.96	12.38×10^6
4	9	−20	+5	330.8	5.73	9.5×10^3	1.67×10^6	3.29	8.21×10^6
5	9	−20	−5	330.8	1.62	6×10^3	0.36×10^6	0	0
6	9	−20	+15	330.8	10.27	6×10^3	2.40×10^6	4.28	10.69×10^6

through 6 illustrate the variation of view time with capsule lead angle at entry for one atmosphere and entry angle. The view periods for these cases are shown for a 1 watt data system optimized to the specific atmosphere/ trajectory/entry lead angle, and also for a "typical" system of 5 watts transmitter power at a data rate of 41.6 K bps. With a fixed 5° entry lead angle, the effects of atmospheric and trajectory variation do not appreciably affect the immediate post landed view time. For a given atmosphere and entry angle, increasing the entry central angle increases the physical post landed view time. However the allowable data rate decreases as a result of increased communication distance and decreased antenna gain.

3.2.3 POWER - The electrical power system provides the entire electrical energy storage, power regeneration, and power distribution for all the capsule and lander subsystems. Energy storage and, for extended duration missions, power regeneration are the major functions that influence power system design.

3.2.3.1 Requirements. - The capsule power system provides the electrical energy during the interplanetary cruise period when orbiter power is not available and during the descent to the surface. The lander power system provides the electrical energy during landed operations.

Cruise - During interplanetary cruise the capsule power system receives electrical energy from the orbiter and distributes this energy to the capsule thermal control subsystem for heat, to the instrumentation subsystem to monitor the capsule performance, and to the battery charger to maintain capsule battery capacity during the interplanetary travel period. When orbiter energy is not available (during midcourse maneuvers), the power system utilizes the capsule batteries to maintain continuous thermal control and performance monitoring. The batteries are recharged after each such use. The depth of discharge is minimal (5-10%) in normal use.

Descent and Entry - From the time of orbiter separation through initial operations on the surface, the delivery capsule battery provides the energy for the electrical power system. Figure 3.2.3-1 is a typical power profile for pre-separation checkout, descent, and entry. This power profile is sensitive to deorbit duration and added entry science requirements, but is not affected by other capsule and lander parameters, such as size, weight, and landed mission requirements.

Landed Operations - Power demands on the lander have a broad spectrum of profiles. Three distinct types of profiles exist depending on the type of communication systems employed; relay at periapse, relay at apoapse, and direct. Figure 3.2.3-2 is the power profile for direct communications, with duration of communication the variable. Figures 3.2.3-3 and 3.2.3-4 are the power profiles for relay communications, with transmitter power the major variable. The power required for night operation is another variable, and these power profiles show a minimum level of night power.

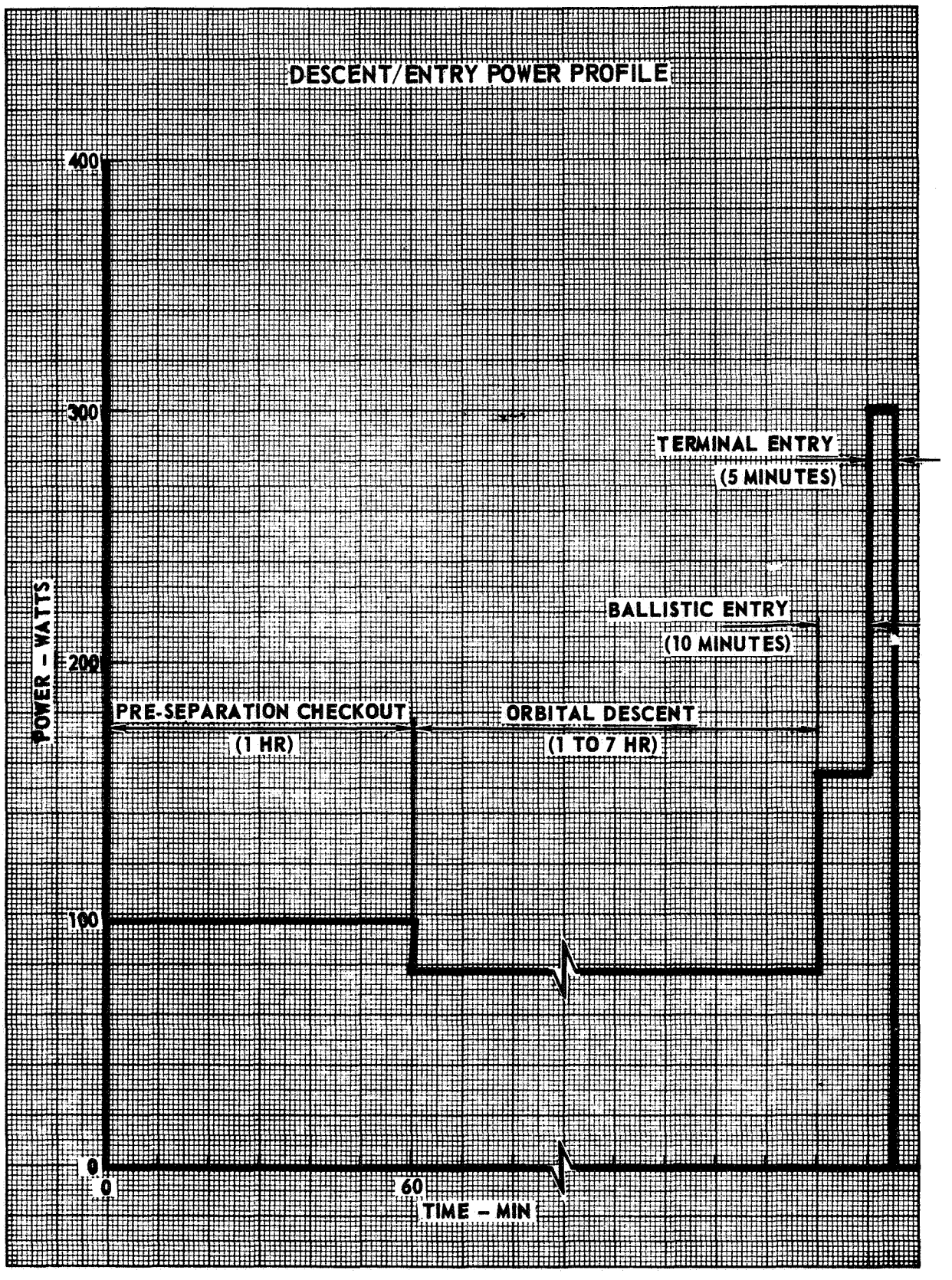
DESCENT/ENTRY POWER PROFILE
400
300
200
100
0
POWER – WATTS
TERMINAL ENTRY
(5 MINUTES)
BALLISTIC ENTRY
(10 MINUTES)
PRE-SEPARATION CHECKOUT
(1 HR)
ORBITAL DESCENT
(1 TO 7 HR)
0
60
TIME – MIN

FIGURE 3.2.3–1

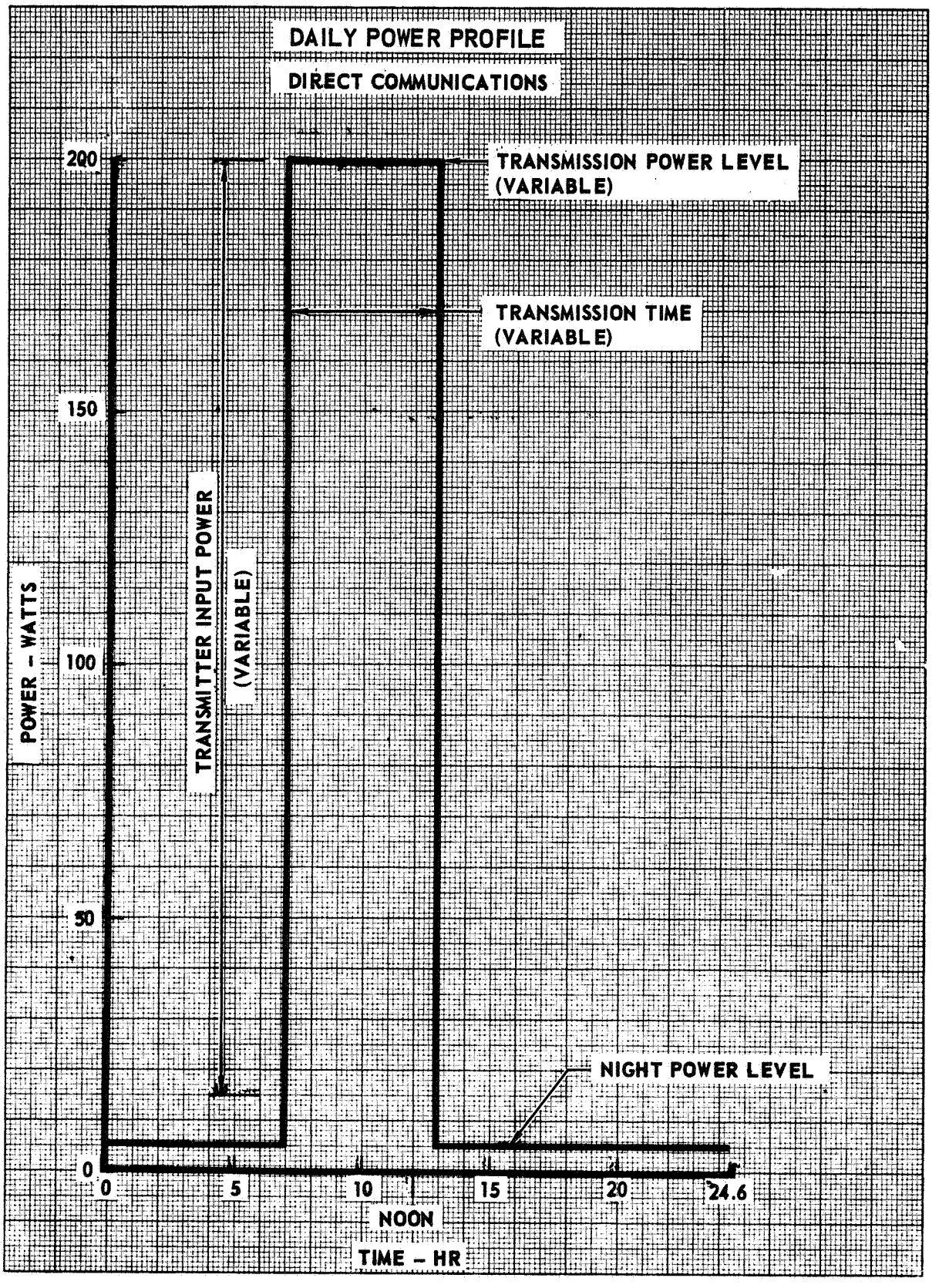
DAILY POWER PROFILE
DIRECT COMMUNICATIONS
TRANSMISSION POWER LEVEL (VARIABLE)
TRANSMISSION TIME (VARIABLE)
TRANSMITTER INPUT POWER (VARIABLE)
NIGHT POWER LEVEL
POWER - WATTS
200
150
100
50
0
0
5
10
15
20
24.6
NOON
TIME - HR

FIGURE 3.2.3-2

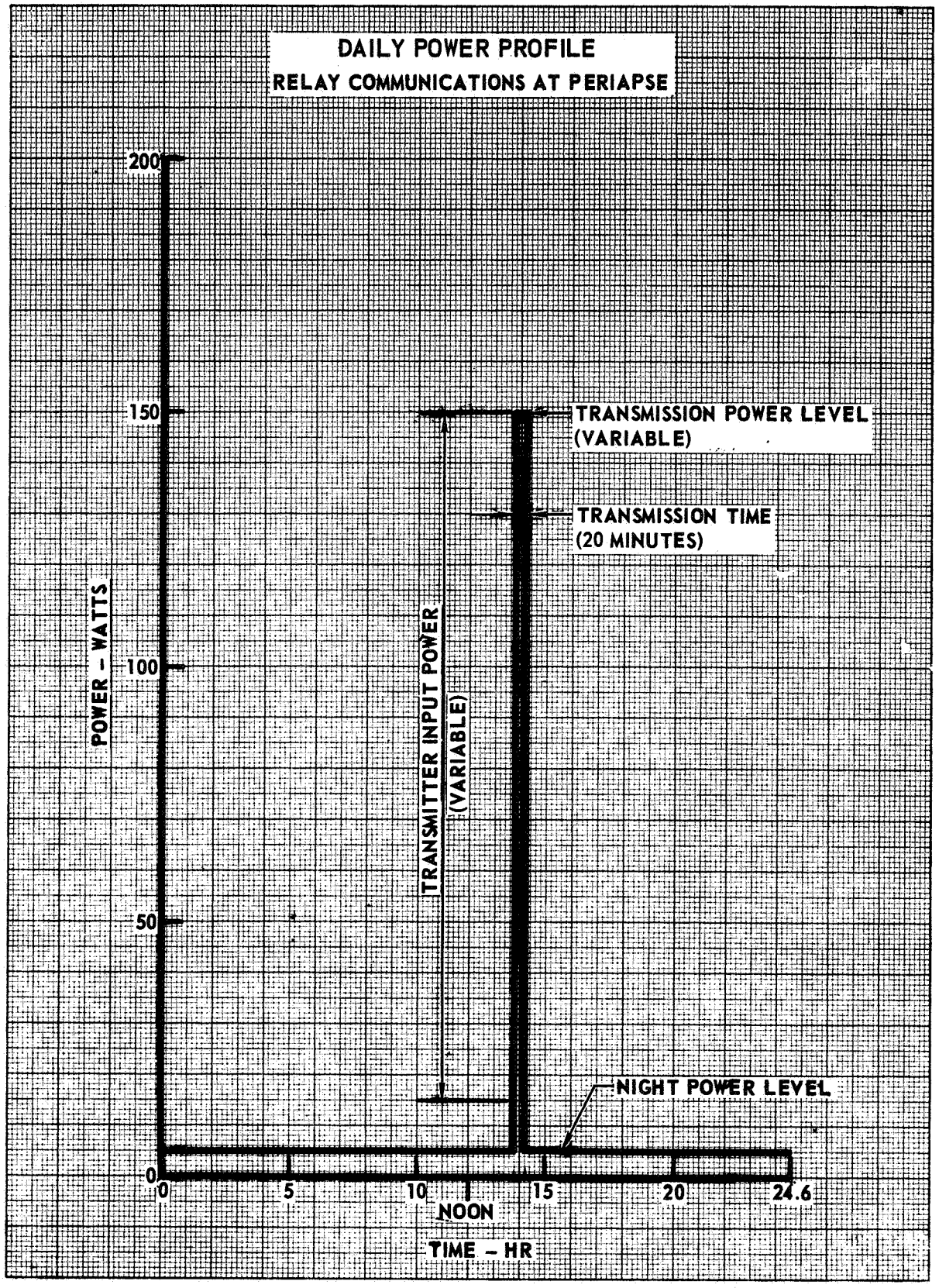
DAILY POWER PROFILE
RELAY COMMUNICATIONS AT PERIAPSE
200
150
100
50
0
POWER – WATTS
TRANSMISSION POWER LEVEL
(VARIABLE)
TRANSMISSION TIME
(20 MINUTES)
TRANSMITTER INPUT POWER
(VARIABLE)
NIGHT POWER LEVEL
0
5
10
15
20
24.6
NOON
TIME – HR

FIGURE 3.2.3–3

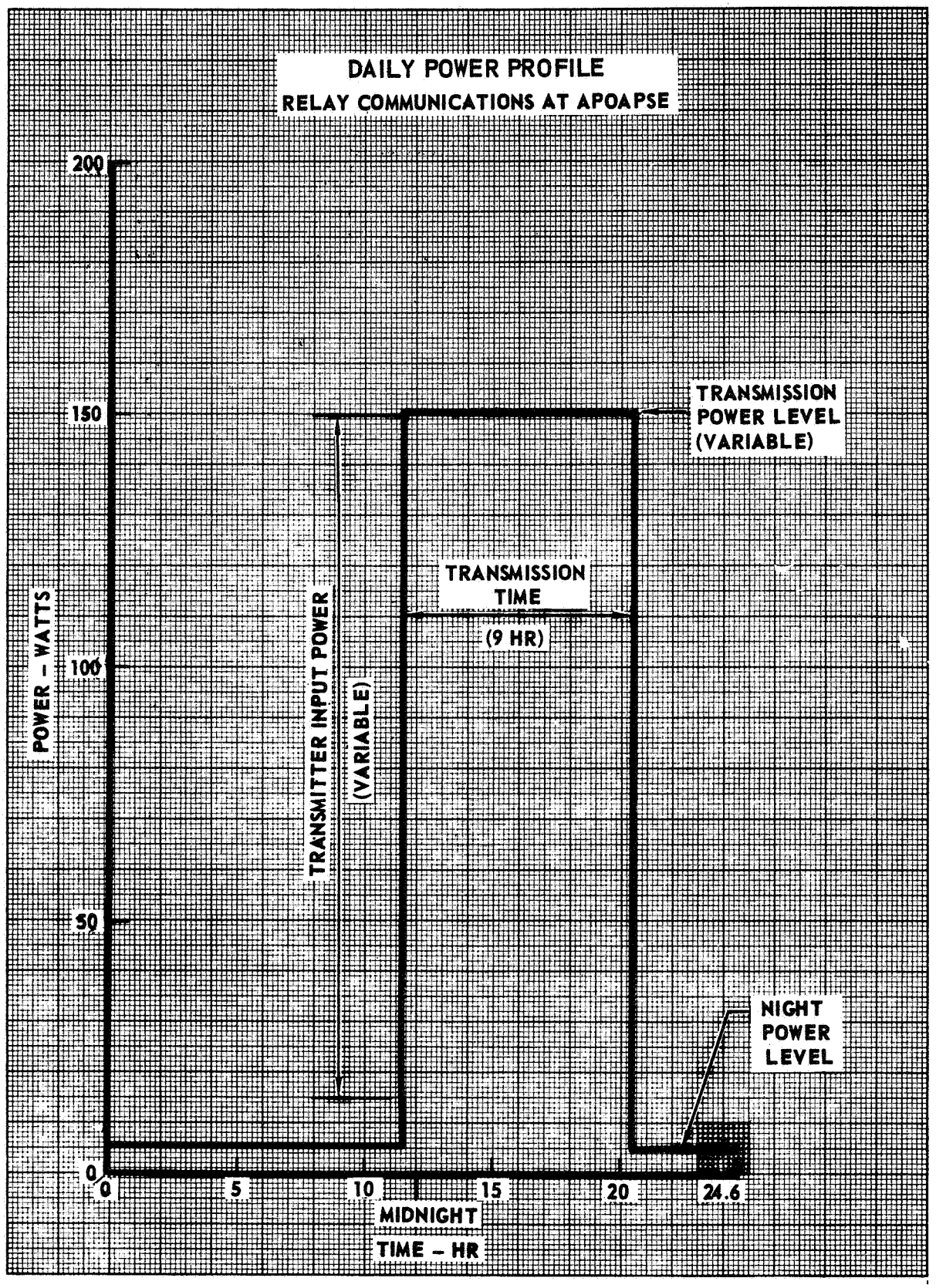
DAILY POWER PROFILE
RELAY COMMUNICATIONS AT APOAPSE
200
150
100
50
0
POWER – WATTS
TRANSMITTER INPUT POWER
(VARIABLE)
TRANSMISSION POWER LEVEL (VARIABLE)
TRANSMISSION TIME
(9 HR)
NIGHT POWER LEVEL
0
5
10
15
20
24.6
MIDNIGHT
TIME – HR

FIGURE 3.2.3–4

A minimum science mission of short duration, utilizing relay link communications, has the minimum energy requirement as shown in Figure 3.2.3-5. This power profile has low total energy but relatively large peak power demands during communications periods. An ambitious science program (extensive imaging), coupled with direct communication, results in a relatively large energy requirement as is shown in Figure 3.2.3-6. This profile has large total energy but the peak-power-to-energy ratio is small.

3.2.3.2 Candidate subsystems. - Three types of energy sources are appropriate for a soft Martian lander: batteries, solar cells, and radioisotope thermoelectric generators (RTG). A typical capsule power system uses manually activated, silver-zinc batteries for the main electrical load and automatically activated, silver-zinc batteries for momentary, high current loads such as pyrotechnics, solenoid valves in the attitude control system, and deployment mechanisms. For missions of short duration, 1 to 3 days, primary batteries would supply the electrical energy requirement. However, as mission duration is extended beyond a few days, battery weight becomes prohibitive and a regenerative source of energy is required. Both solar cells and RTG require a secondary battery, though, to provide peak power capability at minimum cost and weight, or to provide energy when solar cells are inoperative (night).

Batteries - Two battery systems, nickel-cadmium (Ni-Cd) and silver-zinc (Ag-Zn), are currently under development to provide a heat sterilizable battery for planetary landers. In the unsterilized condition Ni-Cd has excellent cycle life and wet life capability but exhibits a low energy density (8 to 15 watt hours per pound). Sterilized Ni-Cd cells have shown up to 30% loss in initial capacity. Unsterilized Ag-Zn cells have relatively excellent energy density of 60 to 100 watt hours per pound while the wet life is adequate. The cycle life is relatively poor, but a very high cycle life (over 1000 cycles) is not required. A cycle life of 90 or more (reasonable with a secondary, Ag-Zn cell design), gives a significant extended mission capability, with one cycle per day. For such a case, the weight penalty for Ni-Cd would be objectionable, since sterilizable Ag-Zn batteries are projected to have energy densities at least 3 times those of sterilizable Ni-Cd batteries.

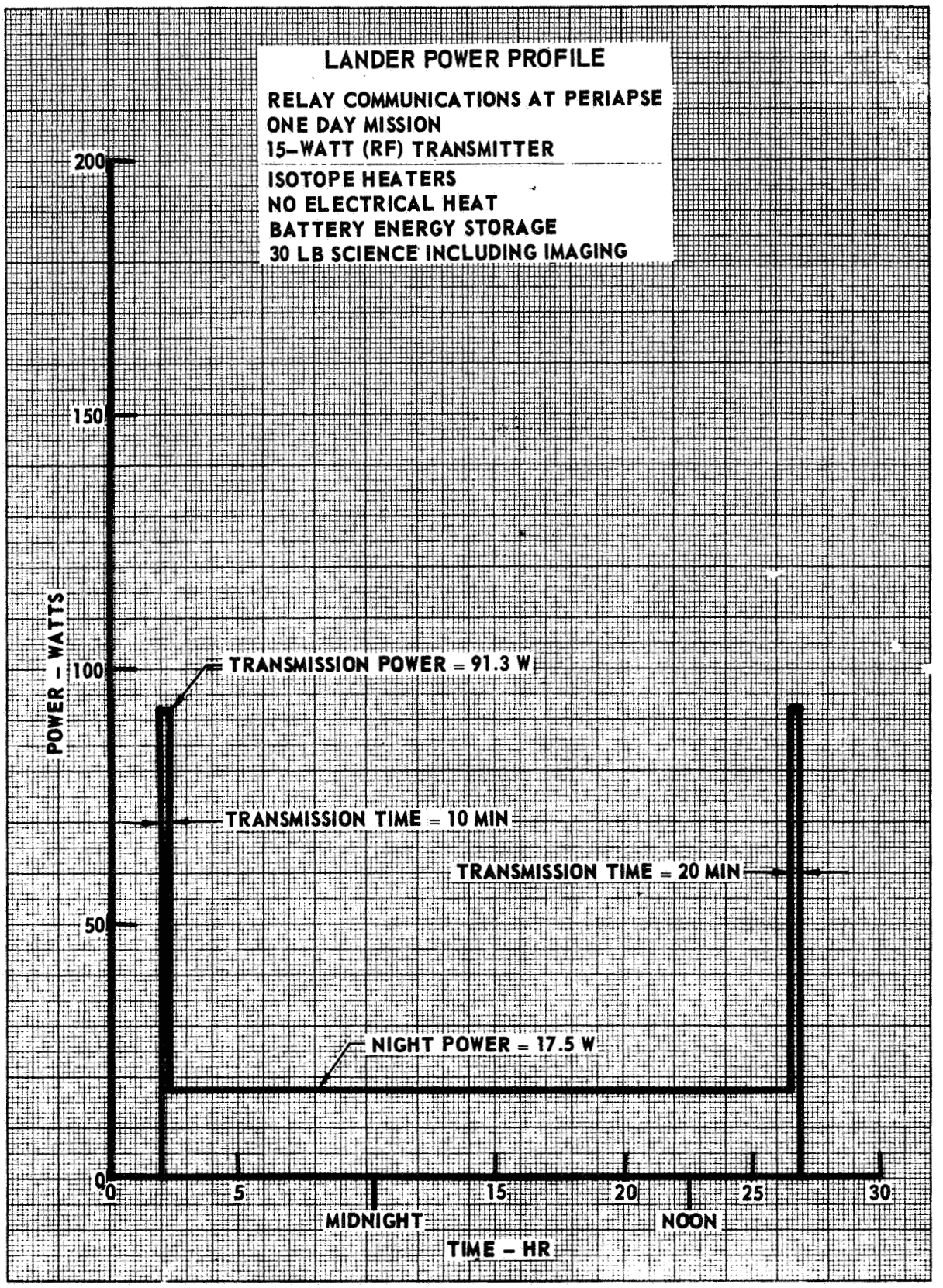
LANDER POWER PROFILE
RELAY COMMUNICATIONS AT PERIAPSE
ONE DAY MISSION
15-WATT (RF) TRANSMITTER
ISOTOPE HEATERS
NO ELECTRICAL HEAT
BATTERY ENERGY STORAGE
30 LB SCIENCE INCLUDING IMAGING
POWER - WATTS
200
150
100
50
0
TRANSMISSION POWER = 91.3 W
TRANSMISSION TIME = 10 MIN
TRANSMISSION TIME = 20 MIN
NIGHT POWER = 17.5 W
0
5
15
20
25
30
MIDNIGHT
NOON
TIME - HR

FIGURE 3.2.3-5

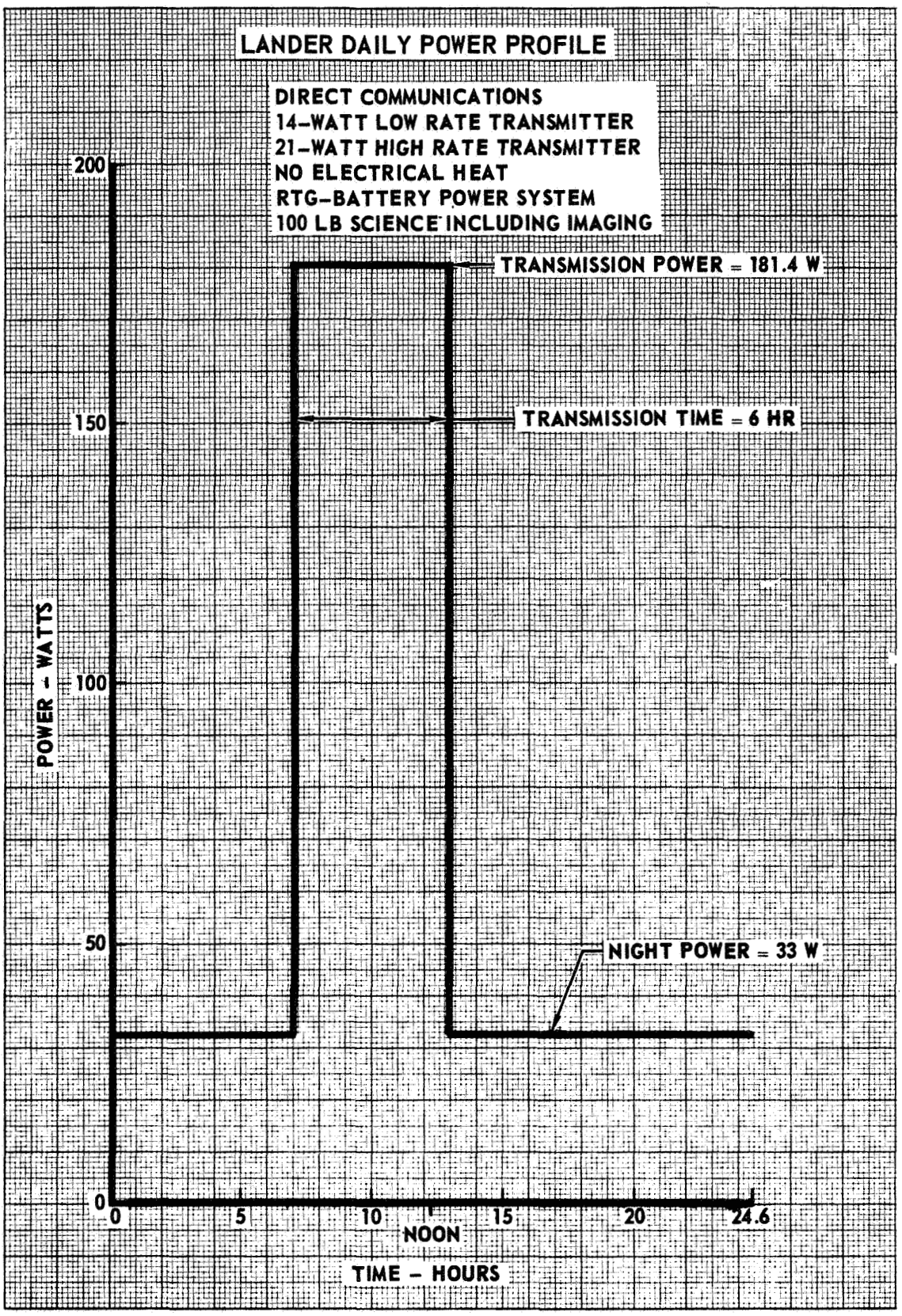
LANDER DAILY POWER PROFILE
DIRECT COMMUNICATIONS
14-WATT LOW RATE TRANSMITTER
21-WATT HIGH RATE TRANSMITTER
NO ELECTRICAL HEAT
RTG-BATTERY POWER SYSTEM
100 LB SCIENCE INCLUDING IMAGING
TRANSMISSION POWER = 181.4 W
TRANSMISSION TIME = 6 HR
NIGHT POWER = 33 W
POWER - WATTS
200
150
100
50
0
0
5
10
15
20
24.6
NOON
TIME - HOURS

FIGURE 3.2.3-6

Battery development is critical for a 1973 launch date. Maximum development effort is required in order to obtain adequate engineering data of wet life, cycle life, and loss rates on heat sterilizable batteries (whether they be the Ni-Cd or Ag-Zn system). Currently, little data exists on wet life and cycle life of heat sterilizable systems. Such data that does exist is based on a statistically inadequate sample of one or two cells. Data is urgently needed on the cycle life capability after the extended wet stand period of interplanetary cruise. This data is required in order to size and plan battery capacity for proper depth of discharge to provide the cycle life required for a specific mission. Since the interplanetary cruise period is about 220 days, and a 90-day surface mission capability is desirable, a program to provide this data will require at least a year or more of testing before significant data is obtained. Therefore, immediate initiation of such a program is imperative to provide adequate data for design of a vehicle for the 1973 launch date.

An alternate solution to wet heat sterilization of sealed, Ag-Zn batteries is sterile activation of a dry, heat-sterilized battery and electrolyte and subsequent sterile insertion or assembly into the flight capsule. This technique has been proven feasible with no failure of the sterilization procedure. Furthermore, long wet life, silver-zinc batteries of current, non-sterile technology were tested, indicating that little development may be required to extend current technology to a sterile battery by this technique. An energy density of over 60 watt hours per pound, with no apparent initial degradation due to sterilization, was realized in an initial feasibility demonstration reported in Reference 1.

Solar Cells - For extended operation of a Martian lander, a solar cell array offers an attractive power source that is not weight sensitive to total energy output. However, many parameters that affect solar cell output are undefined such as atmosphere transmissibility with cloud cover, wind blown sand and dust degradation of cells, daily temperature variations, and heat transfer to the local environment. Consequently, parametric data must be more conservative than would otherwise be necessary if the uncertainty of the predicted Martian surface environment was eliminated. Thus, conservative

design must be applied in the use of solar cells, or a considerable risk will be assumed.

In addition to the environmental limitation on solar cells, the vehicle volume and shape available for packaging and storing an array, limits the feasible size of any solar cell array. Fixed arrays of cylindrical, conical, and flat shapes are suitable, since they are easily packaged within a typical lander configuration and require little if any deployment. A sun tracking panel produces considerably more power output per unit area of array, but requires extensive deployment and continuous tracking resulting in lower reliability.

Radioisotope Thermoelectric Generators - For extended missions on the Martian surface, an RTG is an especially suitable power source because of its inherent long life, excellent reliability, relative insensitivity to the local environment, and the independence of its total energy output to weight. However, an RTG presents a complex set of problems. Accommodating the RTG waste heat is difficult, without overheating adjacent equipment or employing an active cooling system such as heat pipes, shutters, or a pumped liquid cooling loop. Providing earth entry of the radioisotope fuel requires previously qualified entry capsules that meet the requirements of intact entry and intact impact. Very long lead time is required to design, develop, produce, and qualify an entry capsule and RTG. Only the SNAP-19 and SNAP-27 programs have progressed sufficiently to meet a 1973 launch date. However, an immediate commitment is required to initiate the modifications necessary for this Martian application.

3.2.3.3 Performance. - The performance parameters of each of the candidate power sources -- batteries, solar cells, and radioisotope thermoelectric generator -- are uniquely different. Battery size is directly dependent on total energy requirements, but only slightly affected by peak power demands. On the other hand, an RTG is size dependent on power demand and is essentially independent -- for a long half-life fuel -- of total energy requirement. Solar cells are size dependent on power requirements, but on diurnal energy

requirements rather than total energy requirements. In addition, solar cells are dependent upon Sun illumination parameters.

Batteries - The requirement for a primary battery of reasonable energy density dictates the use of a silver-zinc battery. No other battery system of current technology has been adequately qualified, even nonsterilized, with higher energy density. However, sterilization is a critical problem and requires continued, concentrated investigation and development to meet a 1973 launch date. Assuming continuing progress, Figure 3.2.3-7 is a conservative projection of energy densities for wet, heat sterilizable, silver-zinc batteries.

o Capsule - The typical capsule power system uses a manually activated, silver-zinc, primary battery for energy storage. The entry power peak determines the discharge rate of the battery. This power peak occurs at the end-of-life of the battery capacity, is consequently more severe, and requires serious consideration to minimize this peak power requirement to maintain adequate voltage regulation without unnecessarily oversizing the battery. Total battery capacity is dependent upon the duration of descent but is not too strongly reflected in battery weight. Figure 3.2.3-8 shows battery weight versus descent duration for the power profile of Figure 3.2.3-1. The slope of the battery weight curve indicates a battery incremental energy density of 43 watt hours per pound. This result reflects the decreased battery discharge rate and increased battery capacity with increased descent time. The actual overall battery energy density is 25 watt-hours per pound for a 7-hour descent period while only 13 watt-hours per pound at the one-hour descent.

o Lander - For surface missions of a few days duration, primary, silver-zinc batteries would supply the electrical energy requirement. As mission duration is extended, a regenerative power source is required. However, a critical parameter limiting extend mission duration is the cycle life capability of the secondary, silver-zinc battery used in conjunction with the regenerative power source. Limited data exists on this parameter so that projections are very uncertain. With a one-cycle-per-day requirement, a cycle life of 90 or more is desirable. Battery cycle life is increased by reducing

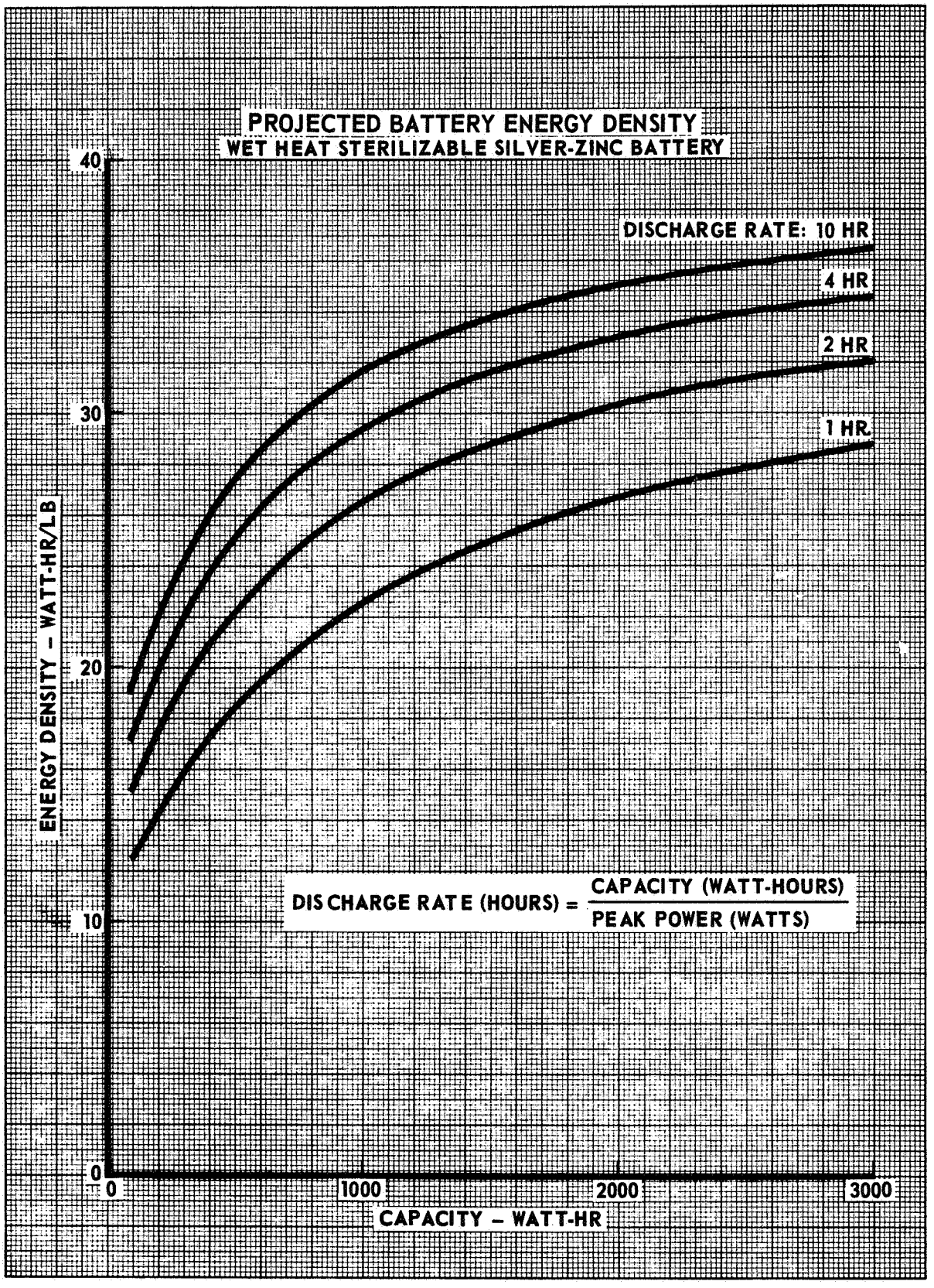
PROJECTED BATTERY ENERGY DENSITY
WET HEAT STERILIZABLE SILVER-ZINC BATTERY
DISCHARGE RATE: 10 HR
4 HR
2 HR
1 HR
ENERGY DENSITY – WATT-HR/LB
40
30
20
10
0
0
1000
2000
3000
CAPACITY – WATT-HR
DISCHARGE RATE (HOURS) = CAPACITY (WATT-HOURS) / PEAK POWER (WATTS)

FIGURE 3.2.3–7

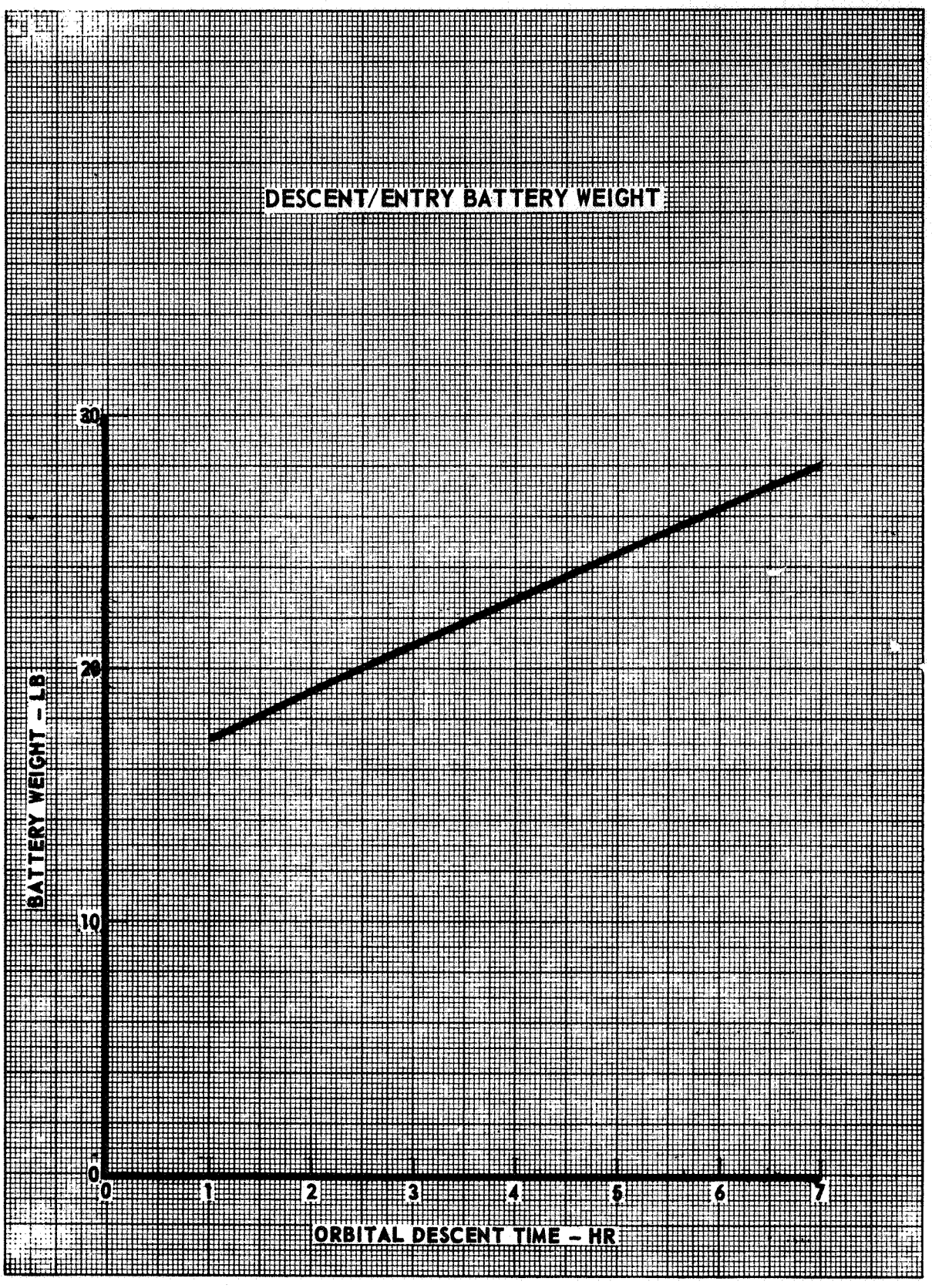
DESCENT/ENTRY BATTERY WEIGHT
BATTERY WEIGHT – LB
30
20
10
0
0
1
2
3
4
5
6
7
ORBITAL DESCENT TIME – HR

FIGURE 3.2.3–8

the depth of discharge. Thus, actual installed battery capacity should be significantly greater than that utilized on each discharge cycle to provide extended cycle life. Wet-sterilizable batteries with inorganic or organic separators are projected to have the cycle life as shown in Figure 3.2.3-9. Silver-zinc batteries, using an inorganic separator design, have produced an extraordinary cycle life exceeding 2500 cycles, using a 30-minute discharge/ 60-minute charge cycle. This type of separator material represents a solution to the requirement for more than 700 cycles of a two-year mission using an RTG power source.

To maximize the confidence in the return of an acceptable quantity of data from a lander, a conservative power system design should provide sufficient battery capacity for lander operation of one diurnal cycle without a contribution from the regenerative power source. With this capacity, the battery will be subjected to a depth of discharge on only 50 to 60 percent assuming proper operation of the regenerative power source. This will insure in a minimum lander life of 90 days (battery cycle life of 90).

Solar Cells - Solar cells are dependent upon the amount of incident Sun illumination for energy conversion. Consequently, performance is affected by an unusually wide variety of parameters such as attitude, array, environment, and cell characteristics.

The analysis of solar array performance includes these common characteristics:

a) Solar cell conversion efficiency at 28°C = 10.5%

b) Solar cell packaging density = 85%

c) Cover glass and coating transmission loss = 6%

d) Wiring and diode loss = 3%

e) Solar cell mismatch loss = 5%

The effective solar array conversion efficiency is the product of these factors which gives an overall efficiency of 7.7 percent (10 WH per sq ft at 1 AU, AMO, and 28°C). This is considered to be attainable for a solar array of small panel area as projected for a Martian lander. Any change in this value

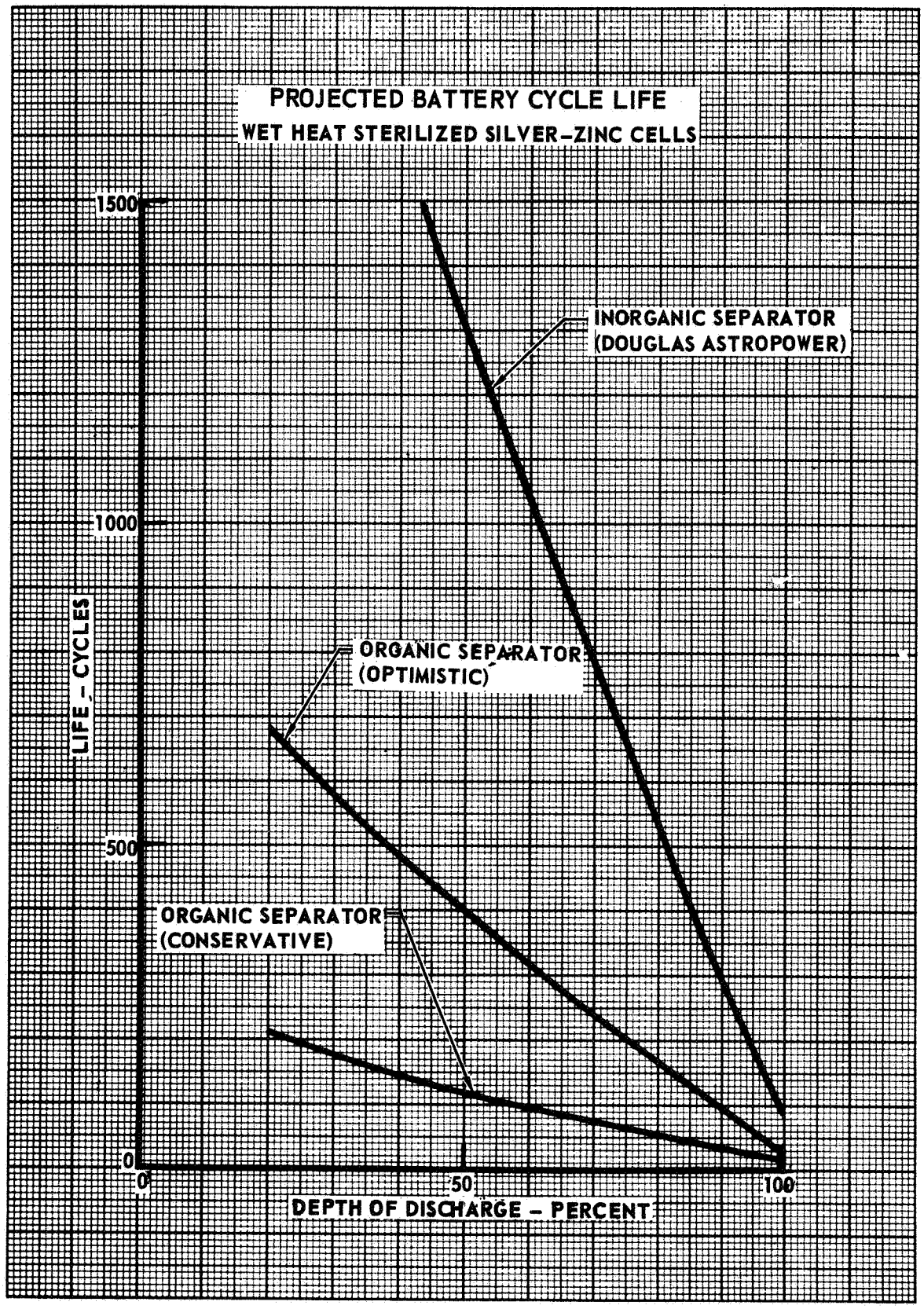
PROJECTED BATTERY CYCLE LIFE
WET HEAT STERILIZED SILVER-ZINC CELLS
1500
1000
500
0
LIFE - CYCLES
INORGANIC SEPARATOR
(DOUGLAS ASTROPOWER)
ORGANIC SEPARATOR
(OPTIMISTIC)
ORGANIC SEPARATOR
(CONSERVATIVE)
0
50
100
DEPTH OF DISCHARGE - PERCENT

FIGURE 3.2.3-9

directly affects the power and energy output. For example, a 1% improvement in the total conversion efficiency (regardless of the source) produces a 1% increase in power and energy output of all solar arrays. However, changes in this value do not affect the relationships of the comparisons made.

o Angle of Incidence - A source of error in all the solar cell array calculations of power output is the assumption that the power output of solar cells is directly proportional to the cosine of the incident angle of illumination. Figure 3.2.3-10 compares the cosine function and the actual measured output of solar cells. From 0° to 55° angles of incidence the agreement is very close -- less than 1% error in power output -- but from 55° to 90° the error increases significantly. However, an offsetting factor is that these large angles of incidence occur for only brief periods at sunrise and sunset, and have a small effect on total energy output over a full day. At large angles of incidence, occurring near sunrise and sunset and at high latitudes, local topographical features may shade the solar panel. No account of the effect of such a shadow is included in the calculation or solar array performance.

o Atmospheric Transmission - A carbon dioxide atmosphere is largely transparent to solar irradiation, as reported in Reference 2, provided the quantity of water vapor is negligible. However, atmospheric scattering would reduce the intensity of direct solar radiation by approximately ten percent. With at least half of this atmospheric scattering directed toward the Martian surface, the expected total atmospheric transmission is 95 percent. This value is used in all the solar array performance calculations. Any change in this value directly affects the power and energy output performance of all solar arrays, but not the relationship of the comparisons.

There is generally a further reduction of solar irradiation as a result of the angle between the local vertical and the position of the sun. However, the effect on atmospheric transmission due to the variation in atmospheric mass effect is considered to be negligible, even at sunrise and sunset.

o Array Configuration - The output of cylindrical, conical, and flat, fixed array shapes are compared in Figures 3.2.3-11 through 3.2.3-19 for various landing site latitudes and local slopes. For these comparisons, the

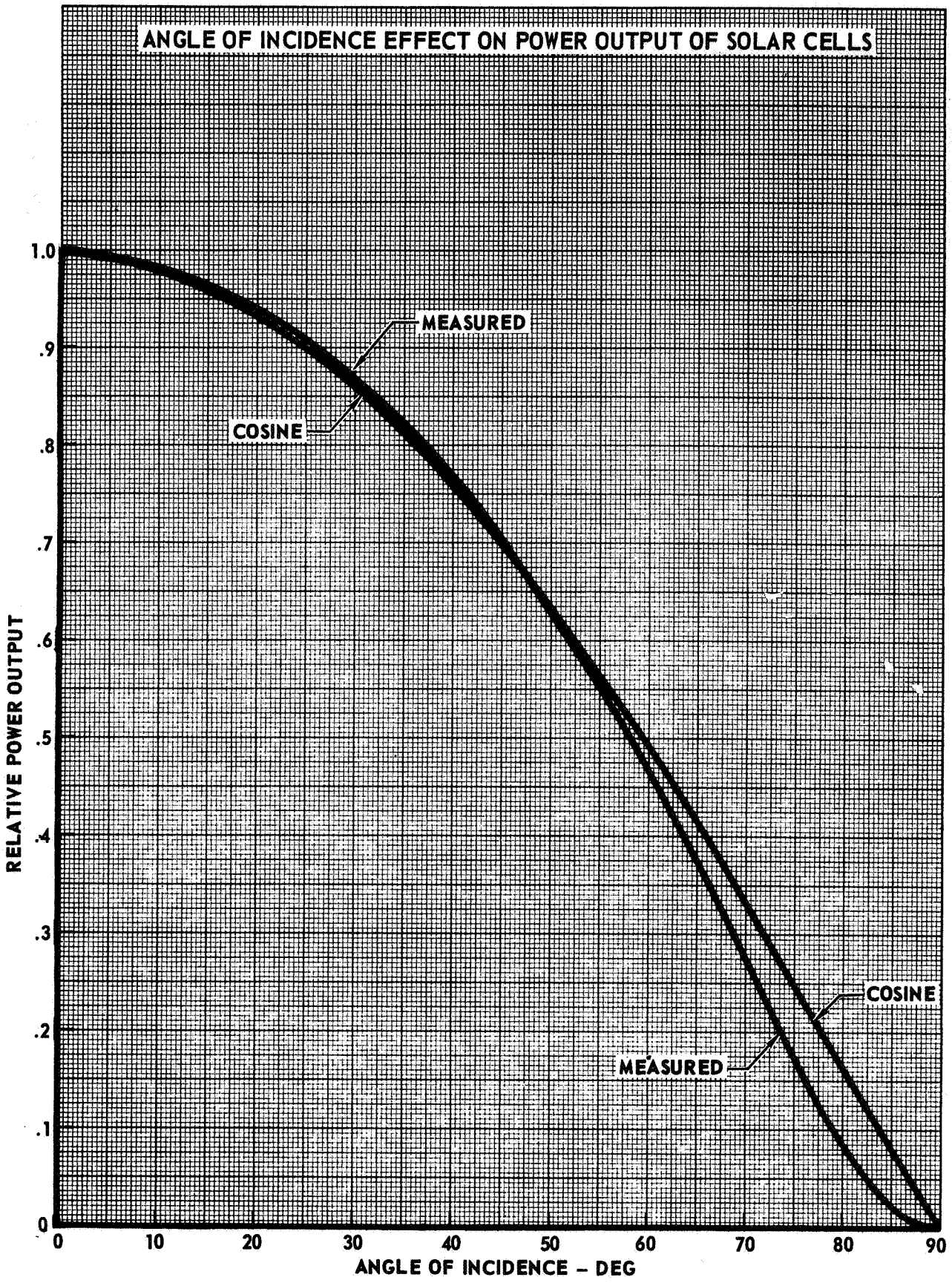

FIGURE 3.2.3–10

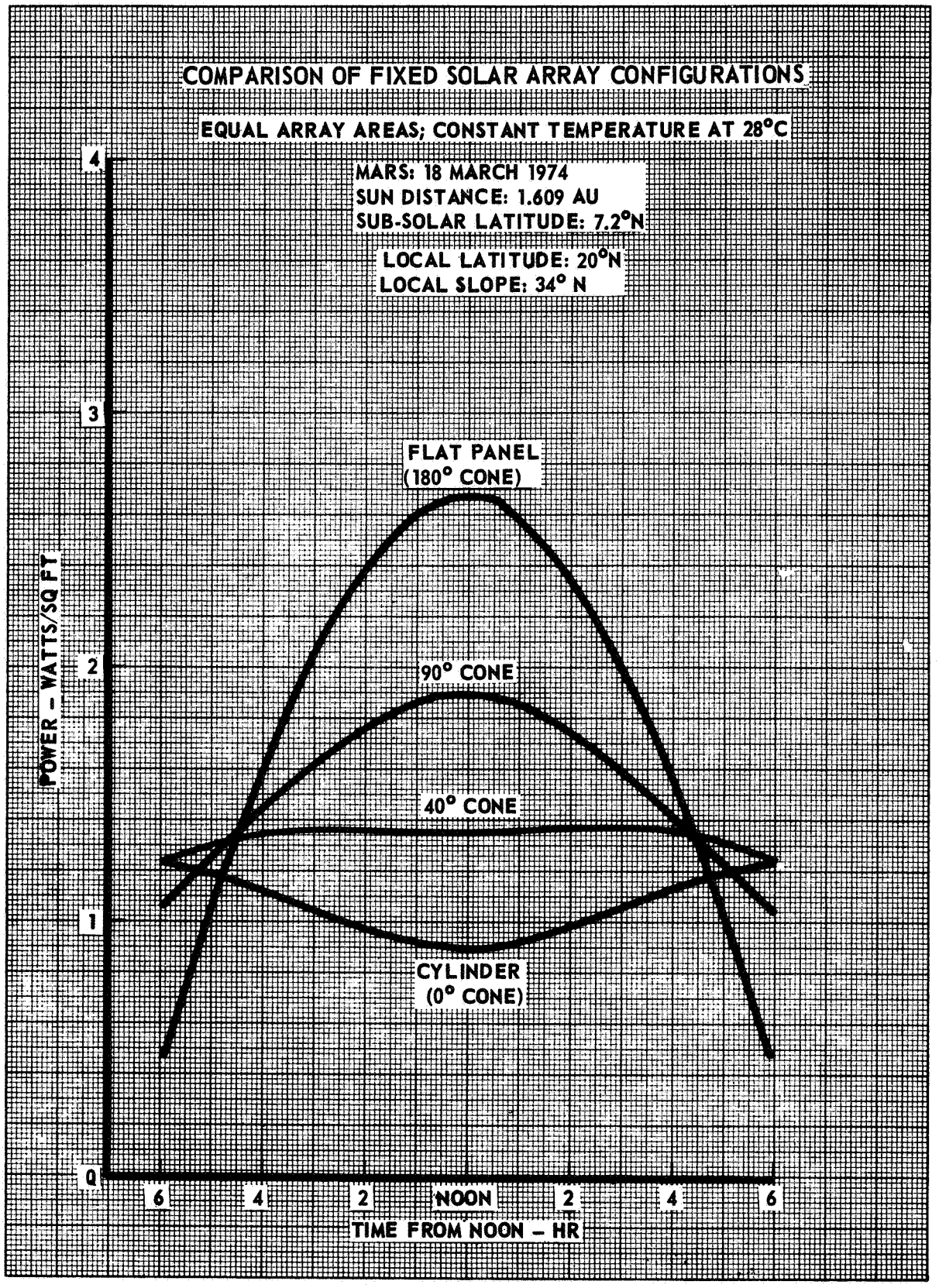

FIGURE 3.2.3-11

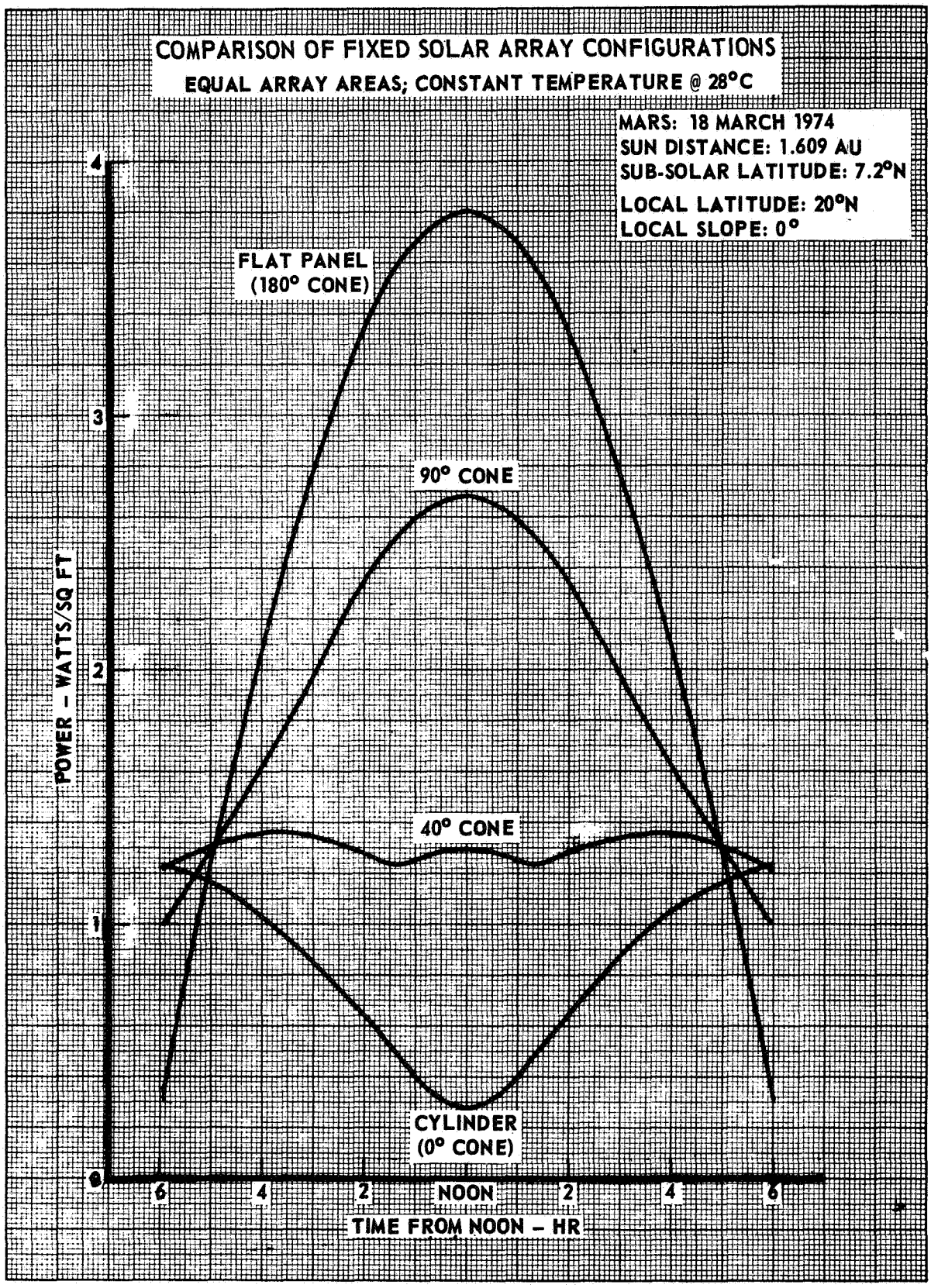

FIGURE 3.2.3–12

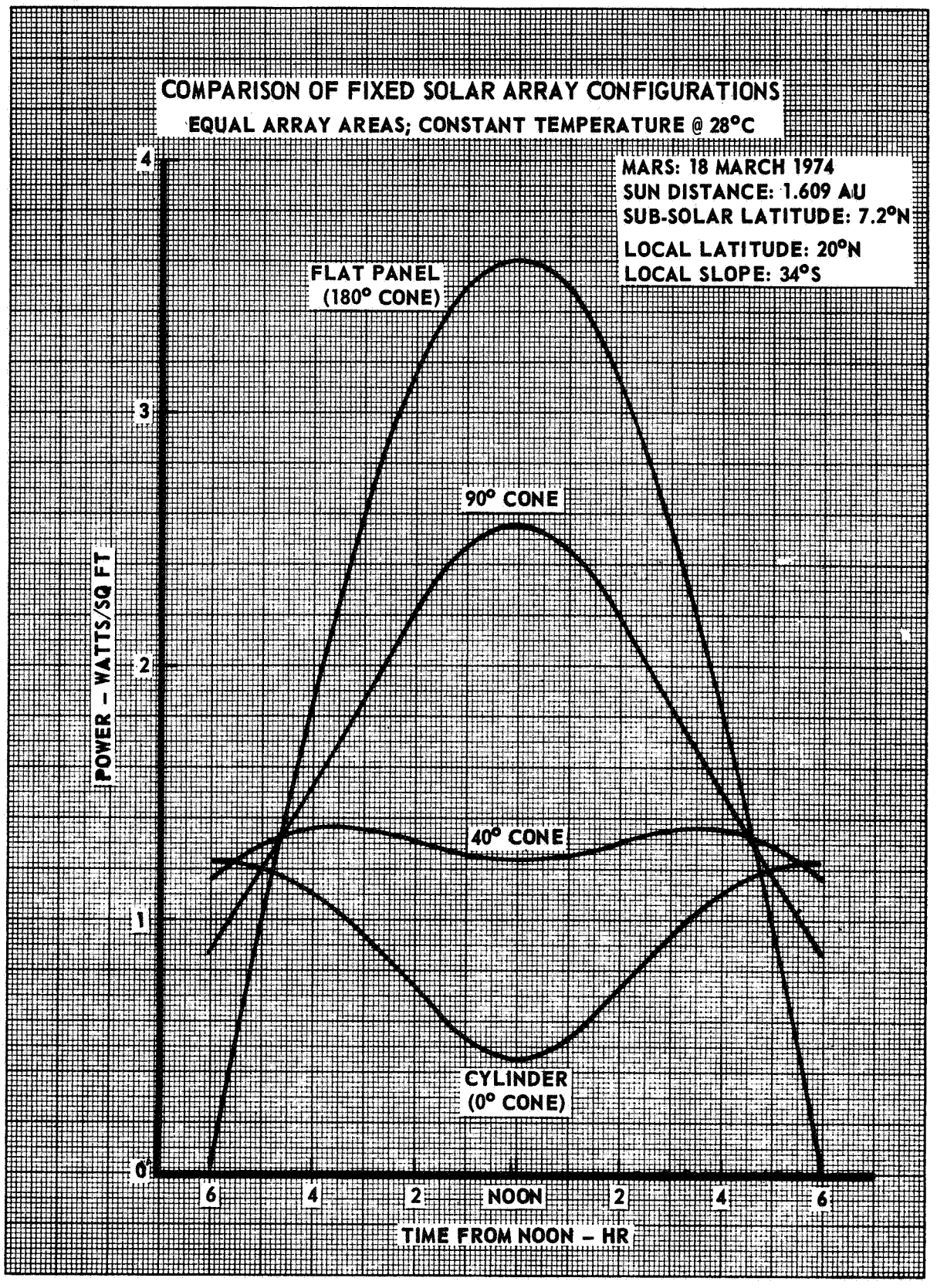

FIGURE 3.2.3–13

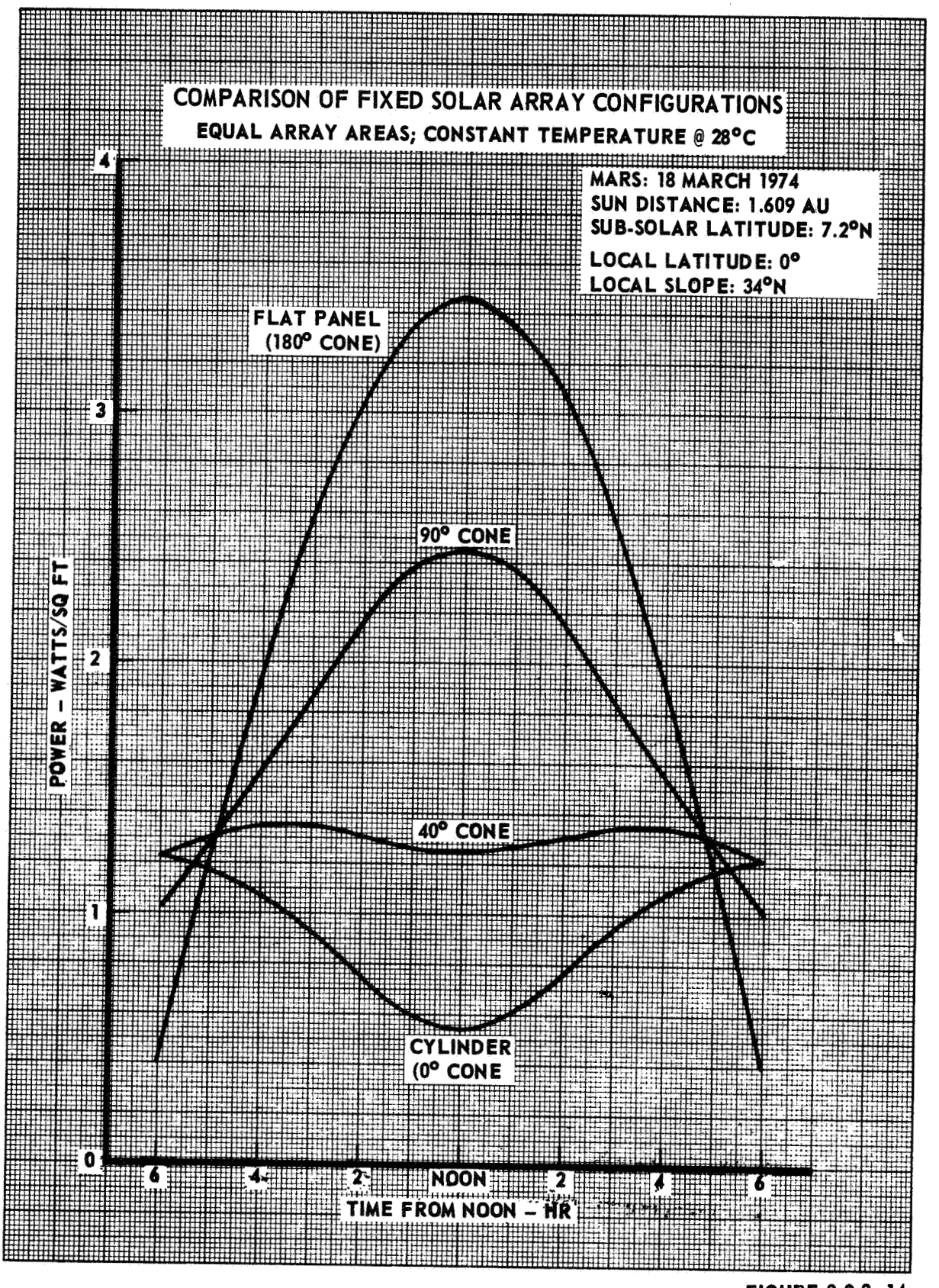

FIGURE 3.2.3–14

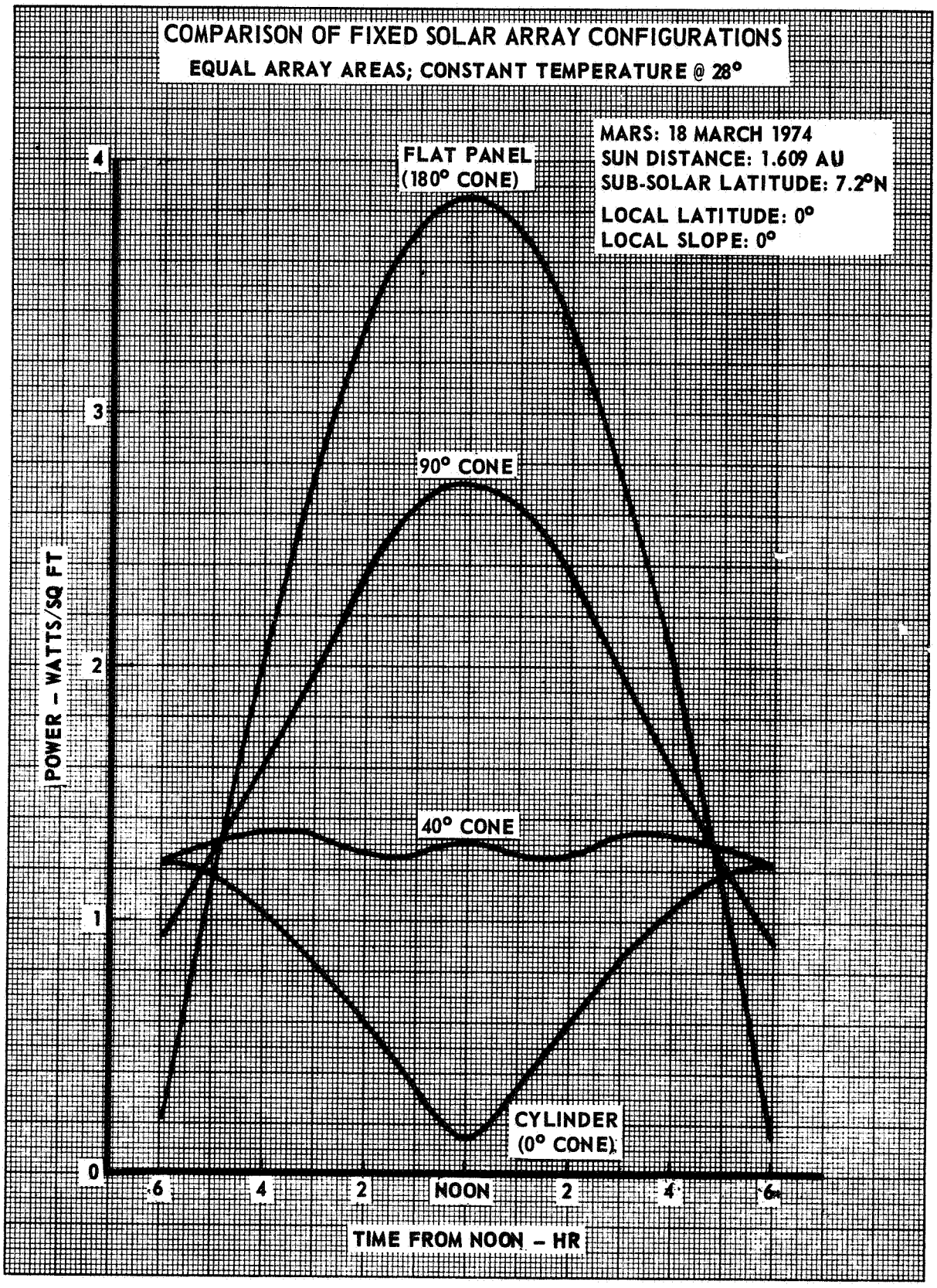

FIGURE 3.2.3–15

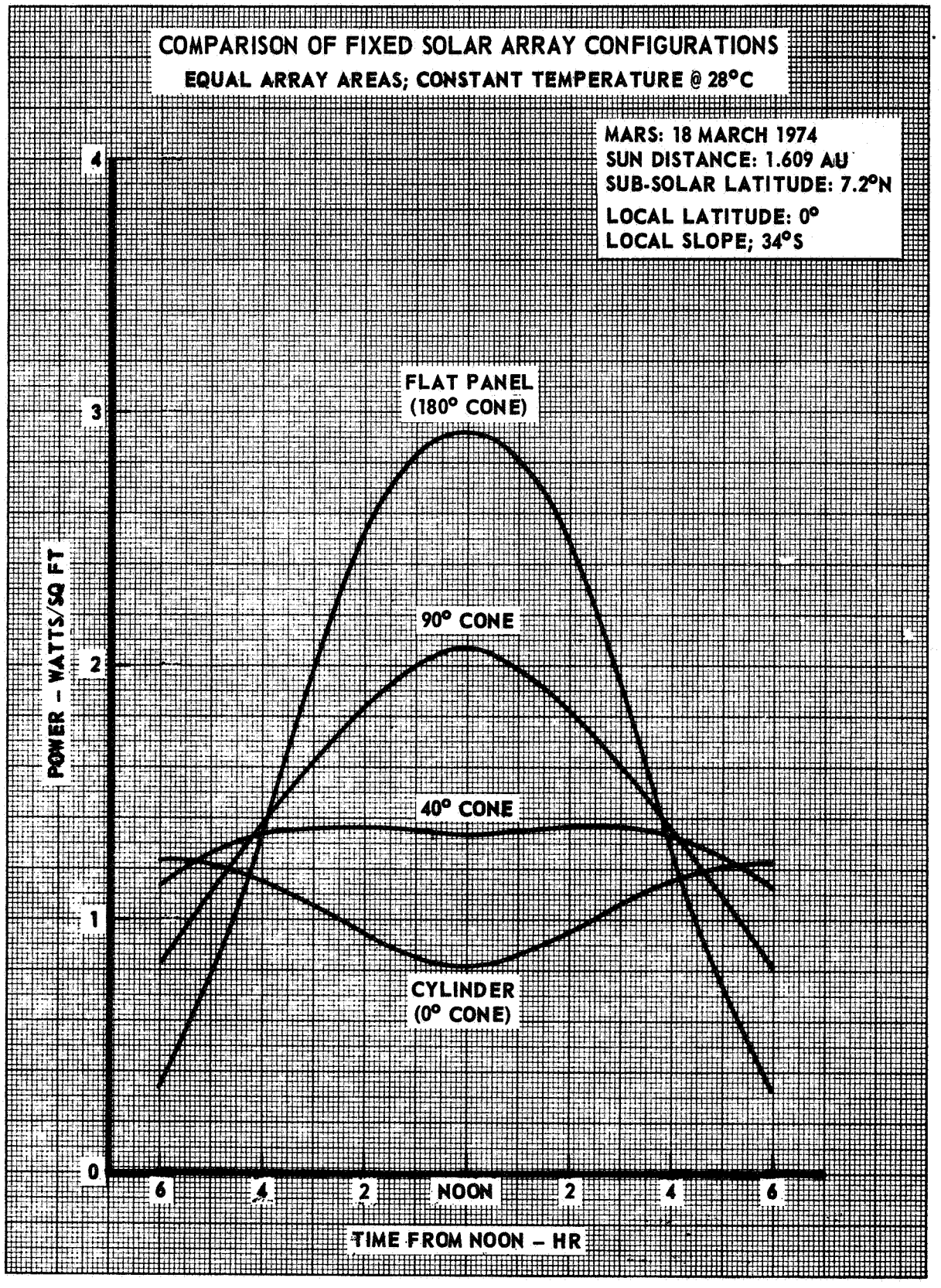

FIGURE 3.2.3–16

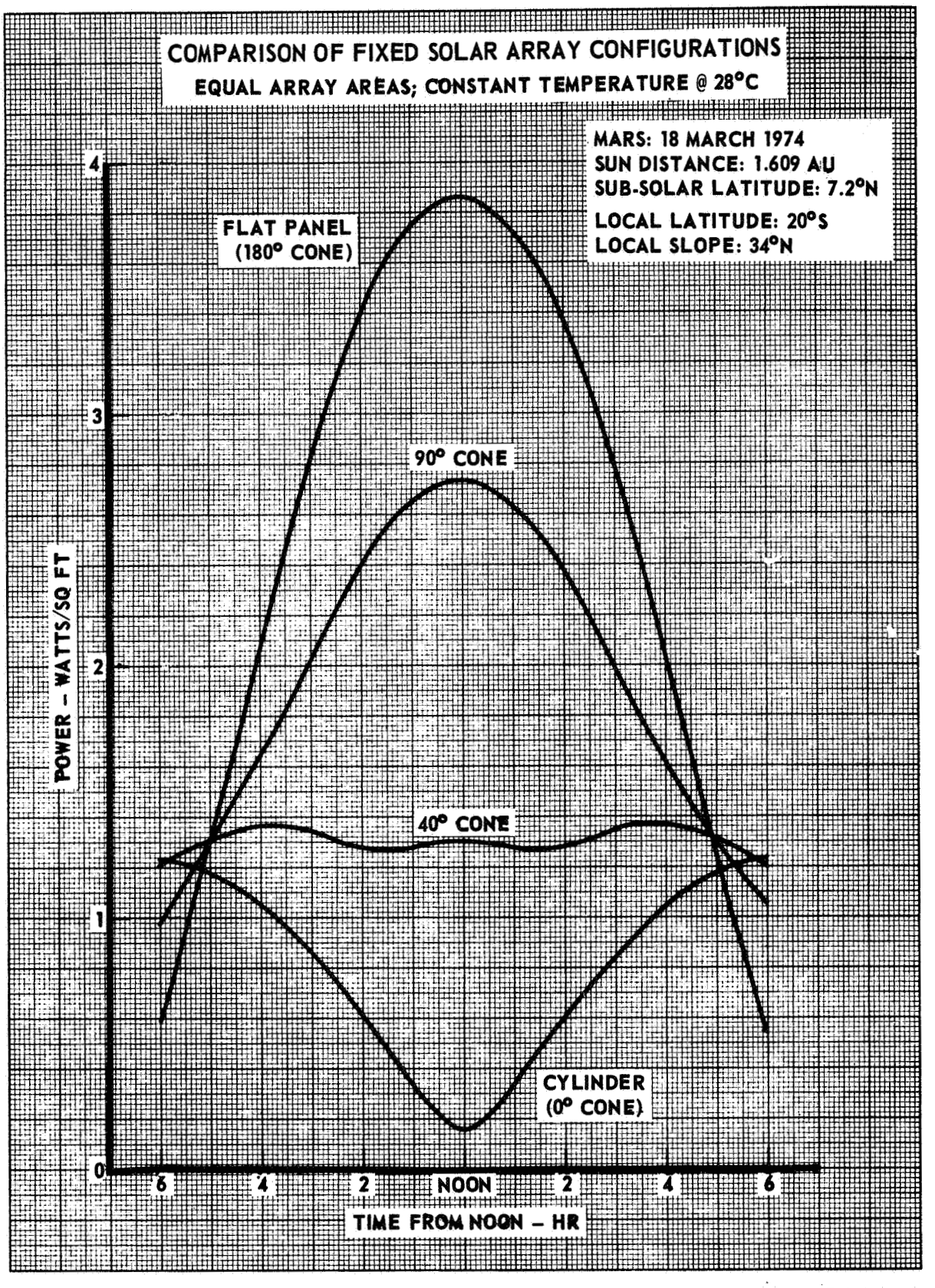

FIGURE 3.2.3–17

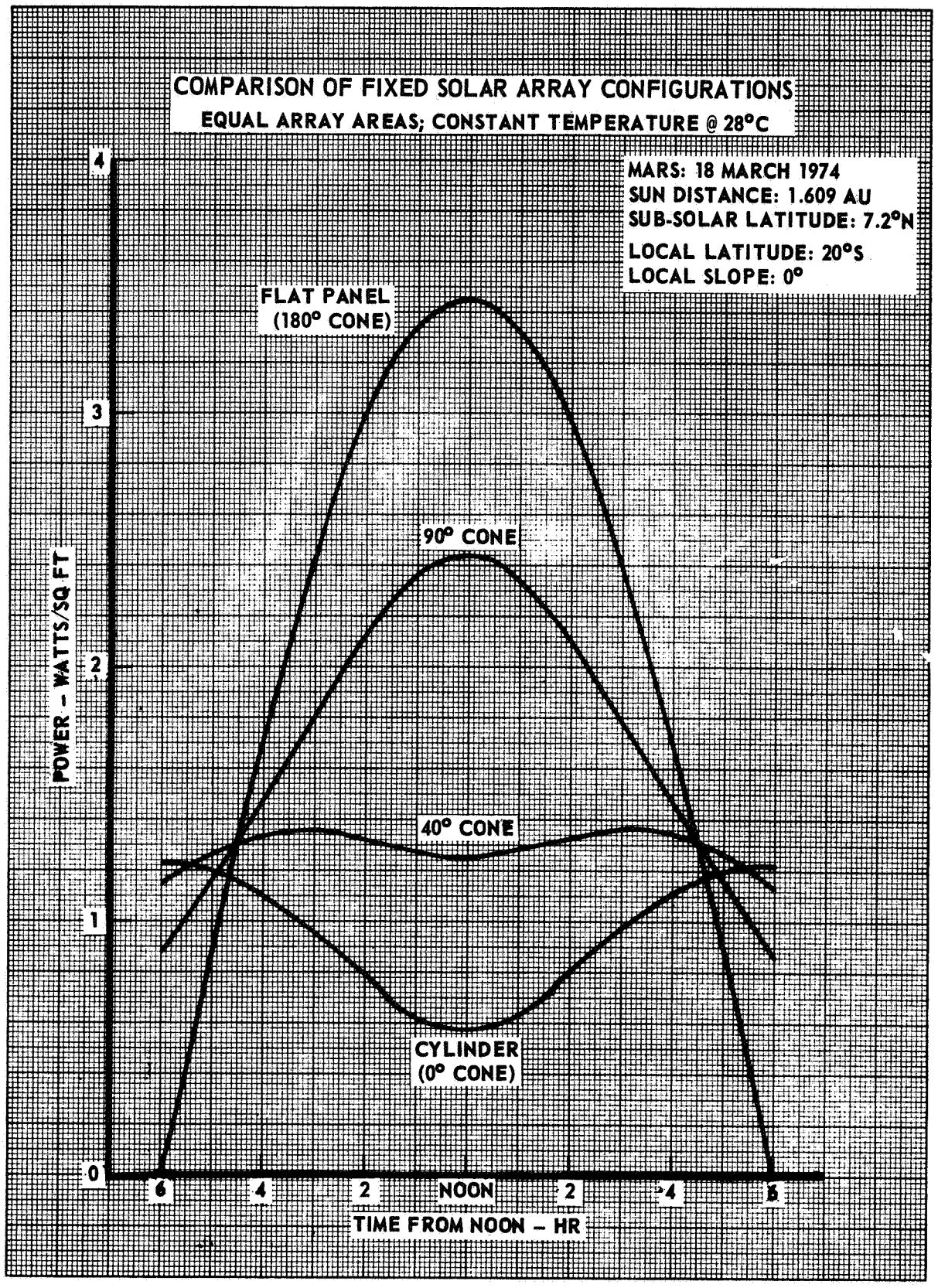

FIGURE 3.2.3–18

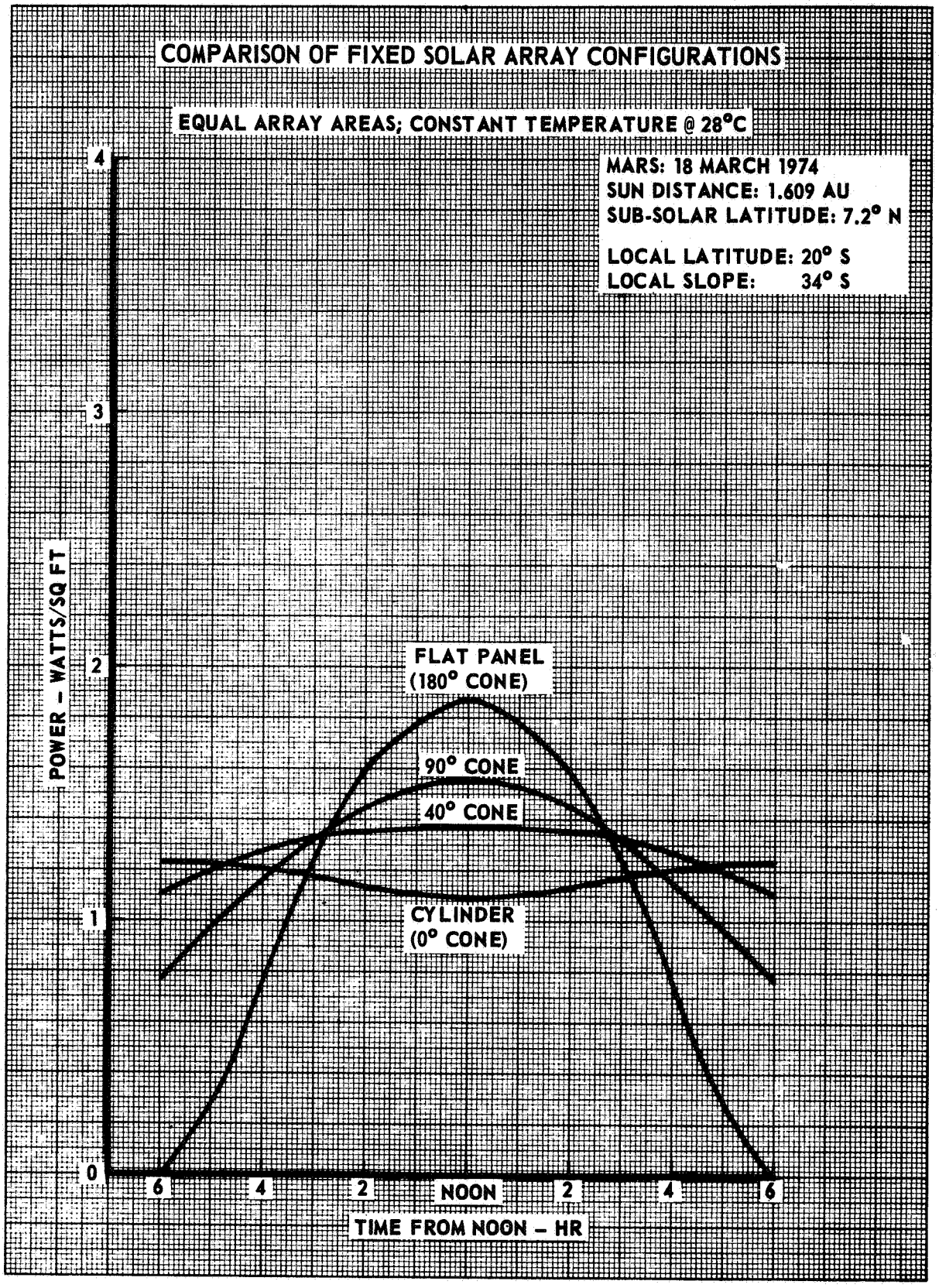

FIGURE 3.2.3–19

axis of the array is considered to be normal to the local surface, and all shapes have equal unit area of active surface and are at a constant 28°C temperature.

Cylindrical shapes are inferior for landing sites near the subsolar latitude. The 40° (total included angle) conical array produces a relatively flat power profile which is preferred for battery charging as compared to the cosine power profile of the flat array. The penalty for this uniform power output profile is reduced energy per day per unit area of array, however, and a consequent increase of about 100% in array area and weight for a given energy output per day. The greatest total energy per day per unit area and given weight is obtained from a flat, fixed array, for landing site latitudes near the equator. Therefore, the flat panel is used to evaluate solar cell array performance characteristics on Mars.

o Temperature - The temperature variation of the solar cells is included in the calculations of power and energy for flat, fixed array performance. The temperature is calculated by the equation:

$$T = [(\alpha/\varepsilon)\ (S\tau/R^2)\ (1-\eta)\ (\cos\theta)/\sigma]^{1/4}$$

where:

T = absolute temperature

S = solar constant at AMO and 1.0 AU

R = Sun-Mars distance

η = solar cell conversion efficiency

θ = angle of incident illumination

σ = Stephan-Boltzman constant

α/ε = panel absorptance/emittance ratio

τ = Martian atmosphere transmission

This equation neglects any heat transfer to the local environment. Considering a flat panel parallel to the local surface, the view factor of the local terrain is negligible, while the atmosphere density makes conductive and convective heat transfer negligible. Therefore, the temperature calculation is considered reasonable and slightly conservative when neglecting these heat transfer modes.

o Absorptance/Emittance Ratio - The absorptance/emittance ratio was chosen as .84, assuming no heat transfer from the back side of the solar cell array which views the equipment package of the landed payload. During daylight periods, this equipment package is expected to be operating at temperatures near that of the solar array so that heat transfer from the backside of the solar array is negligible. In addition, the ratio has only a second order inverse effect on solar array performance, due to the 1/4 power in the temperature equation and the fact that the solar cell array operates at relatively low temperatures on Mars.

o Landing Site Latitude - Figure 3.2.3-20 compares the output of a flat, fixed array parallel with the Martian surface for various landing site latitudes as a function of mission duration. Note that southern latitudes are unfavorable and become progressively so with time due to the relative motion of the sun into the northern hemisphere on these dates. Early arrival dates in 1974 favor 0° to 20°N latitude landing sites, while later arrival dates favor latitudes as high as 40°N.

o Landing Site Slope - Figure 3.2.3-21 shows the output power profiles of a flat, fixed array for 34° slopes in the north, south, east, and west directions. The east or west slopes are the same as the no-slope case but are displaced in time and cut-off by the planet terminator. The north or south slope (depending upon the subsolar latitude) condition represents the worst case performance. Therefore, only north and south slopes are considered in this study.

Figures 3.2.3-22 through 3.2.3-29 compare the solar array output of flat, fixed panels at specific dates as a function of latitude for north and south slopes up to 34°. These figures show a definite preference for northern landing site latitudes, to provide maximum power generation capability. Figures 3.2.3-30 through 3.2.3-34 compare solar array output of flat, fixed panels at a specific latitude as a function of mission duration for slopes up to 34°. These figures reiterate the unfavorable output of southern latitude landing sites. The most favorable sites appear to be near 20°N for maximum, long term, power generation from a solar array.

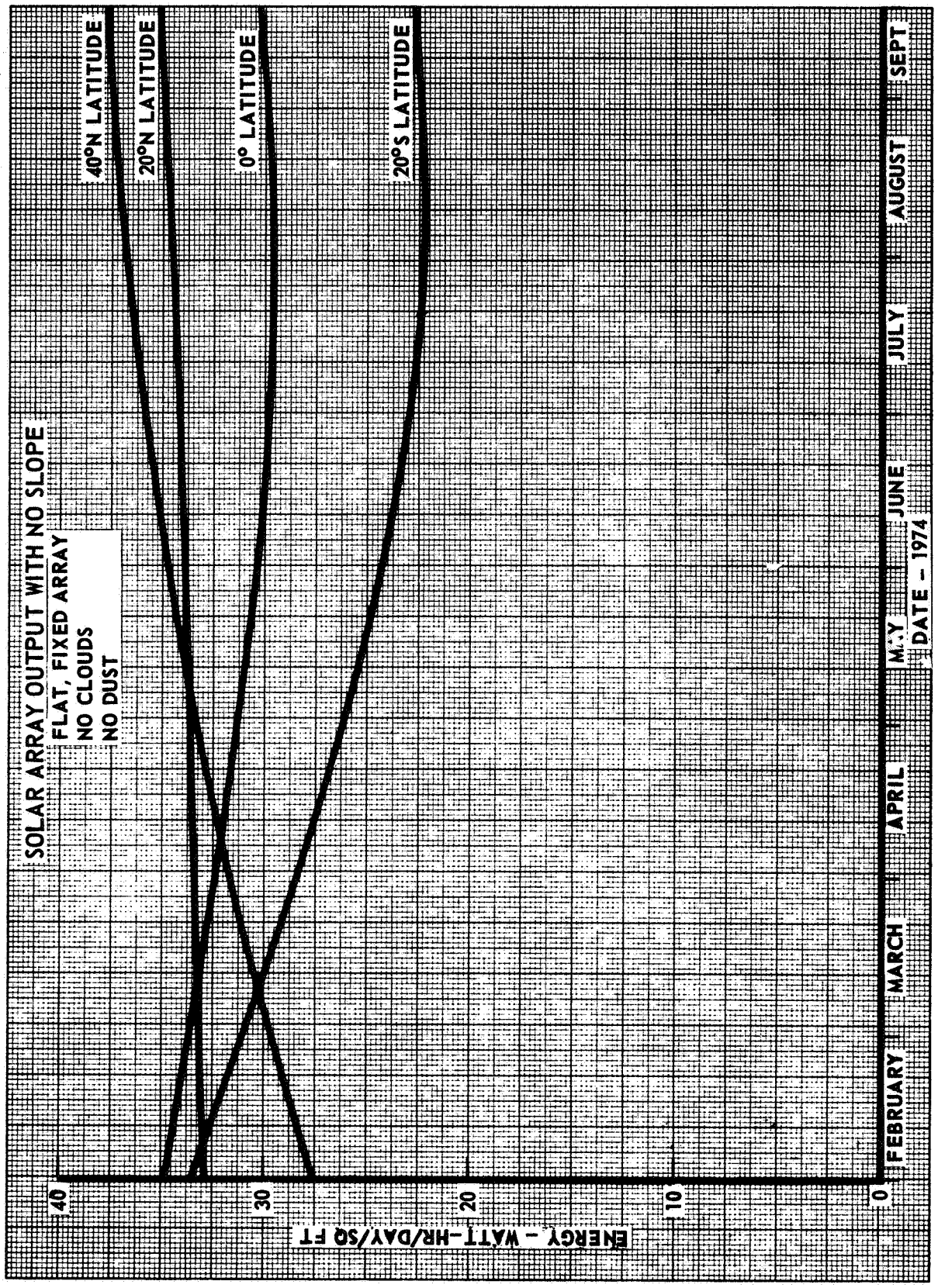

FIGURE 3.2.3–20

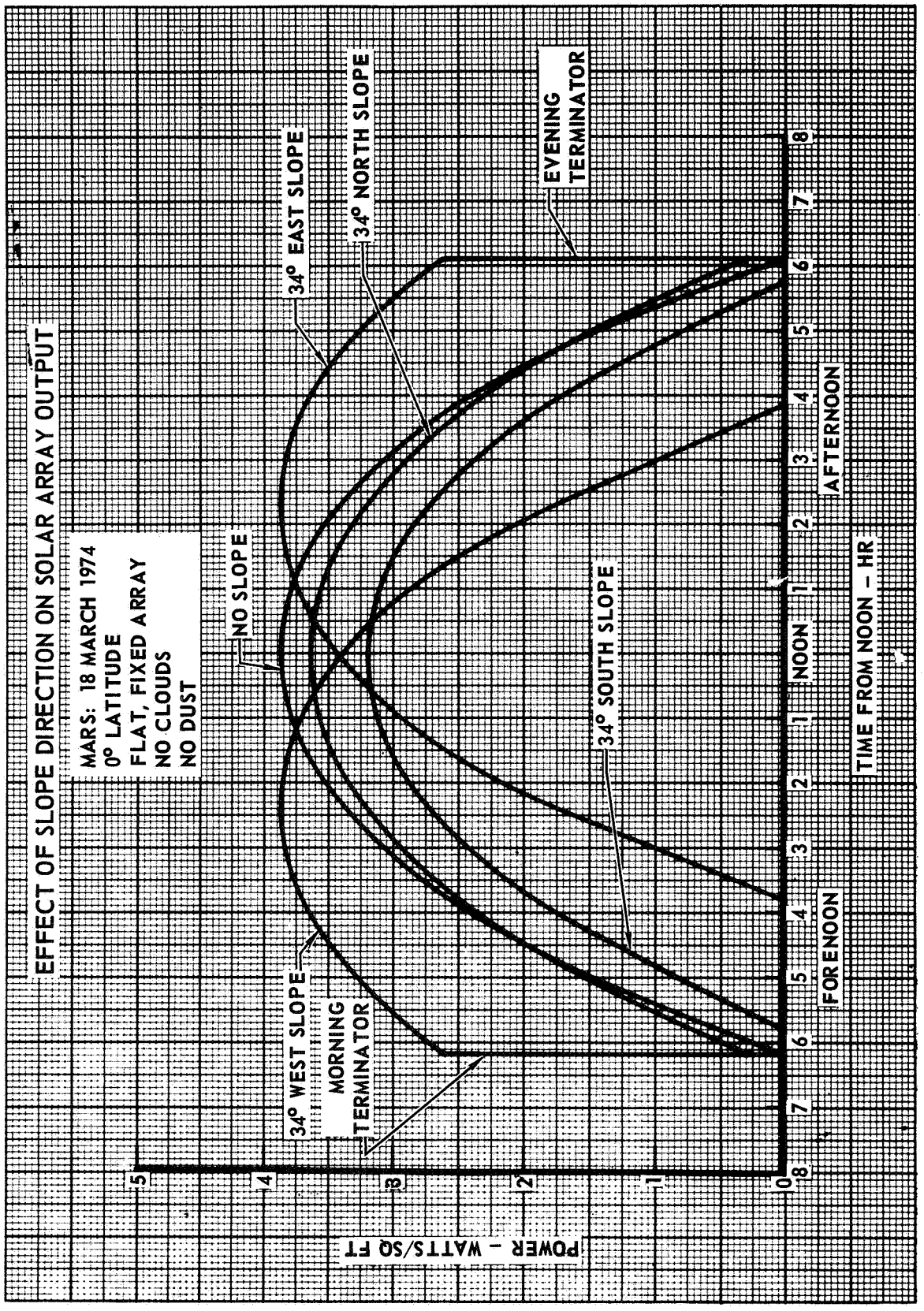

FIGURE 3.2.3–21

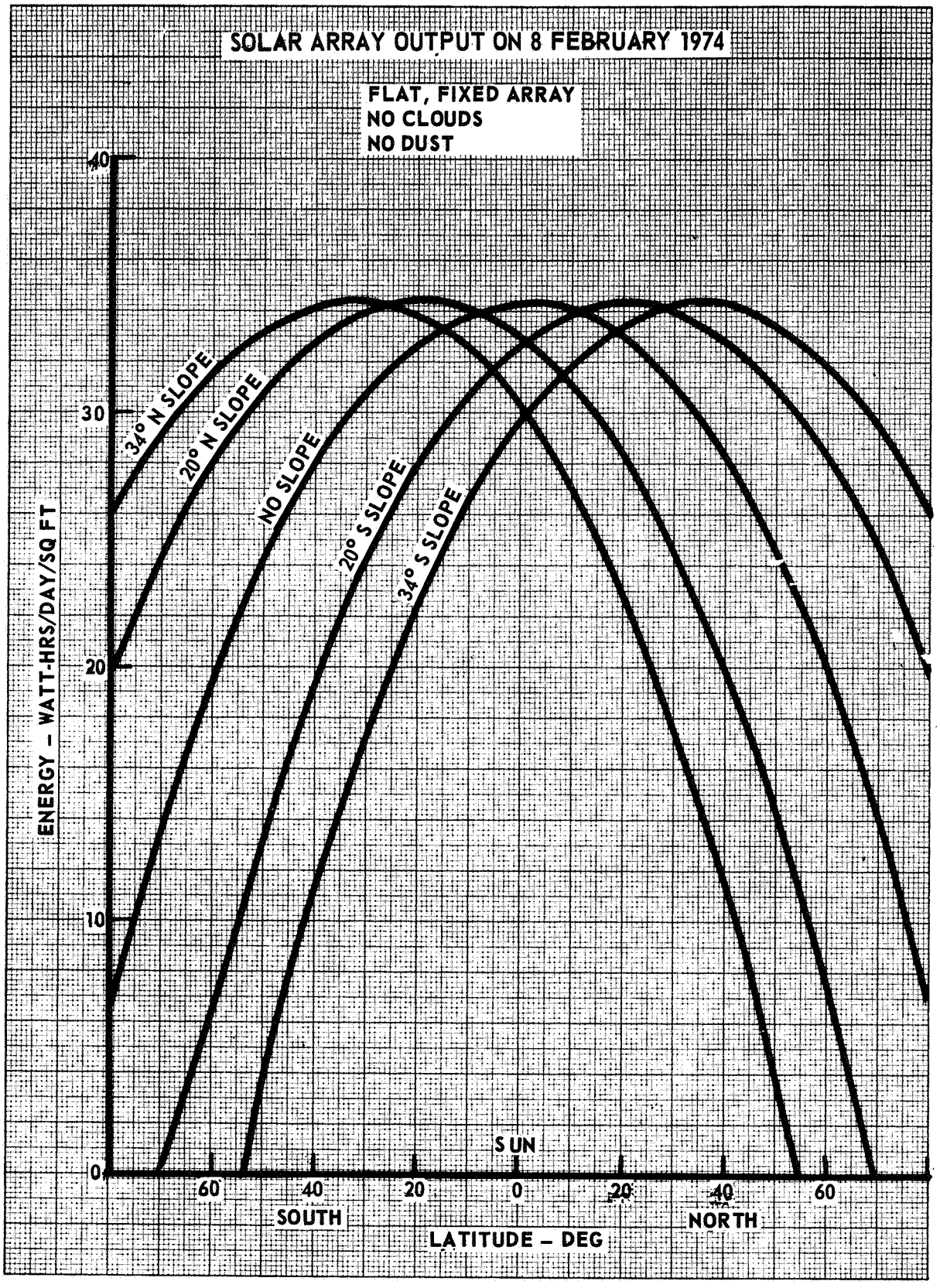

FIGURE 3.2.3–22

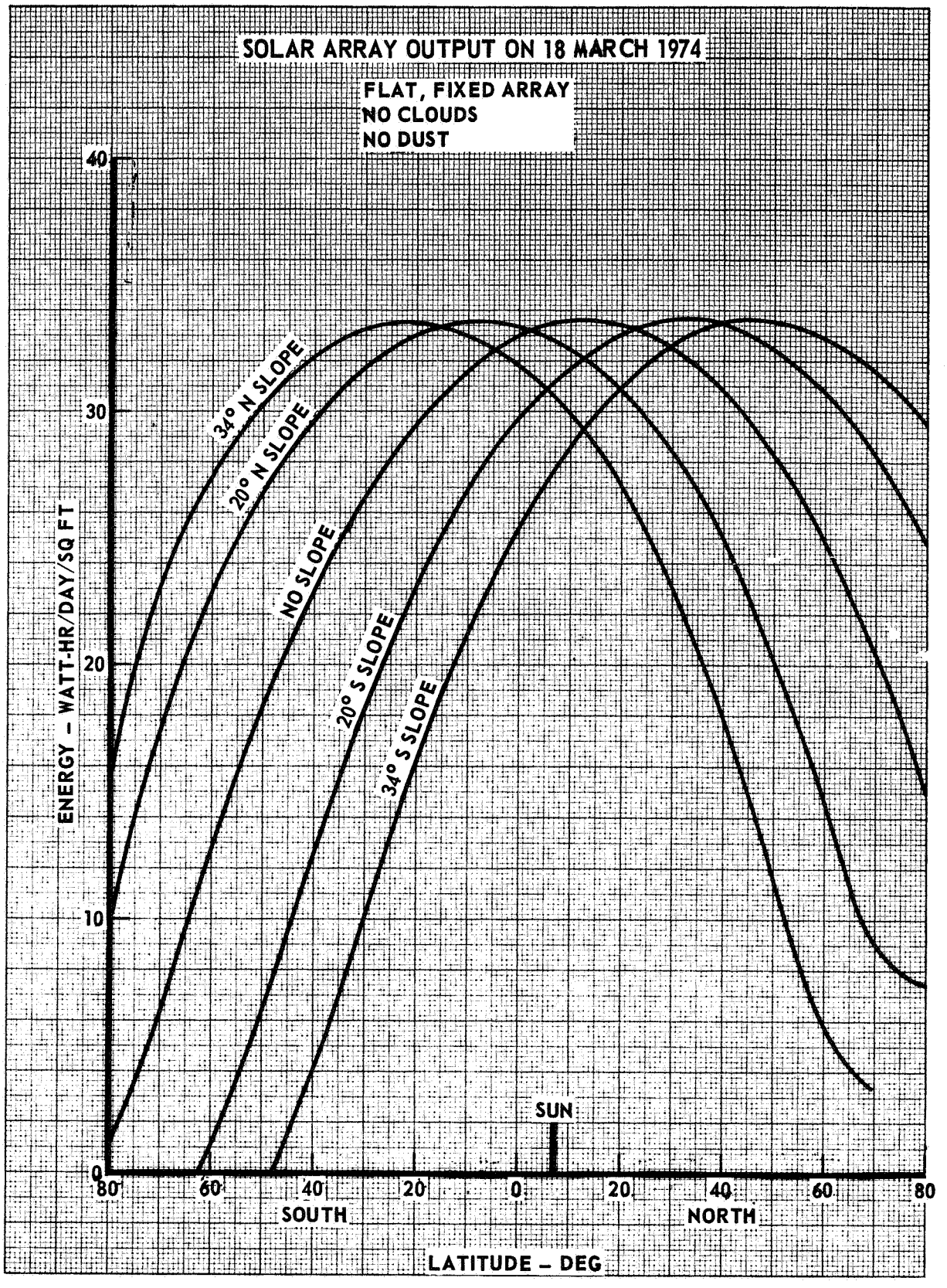

FIGURE 3.2.3–23

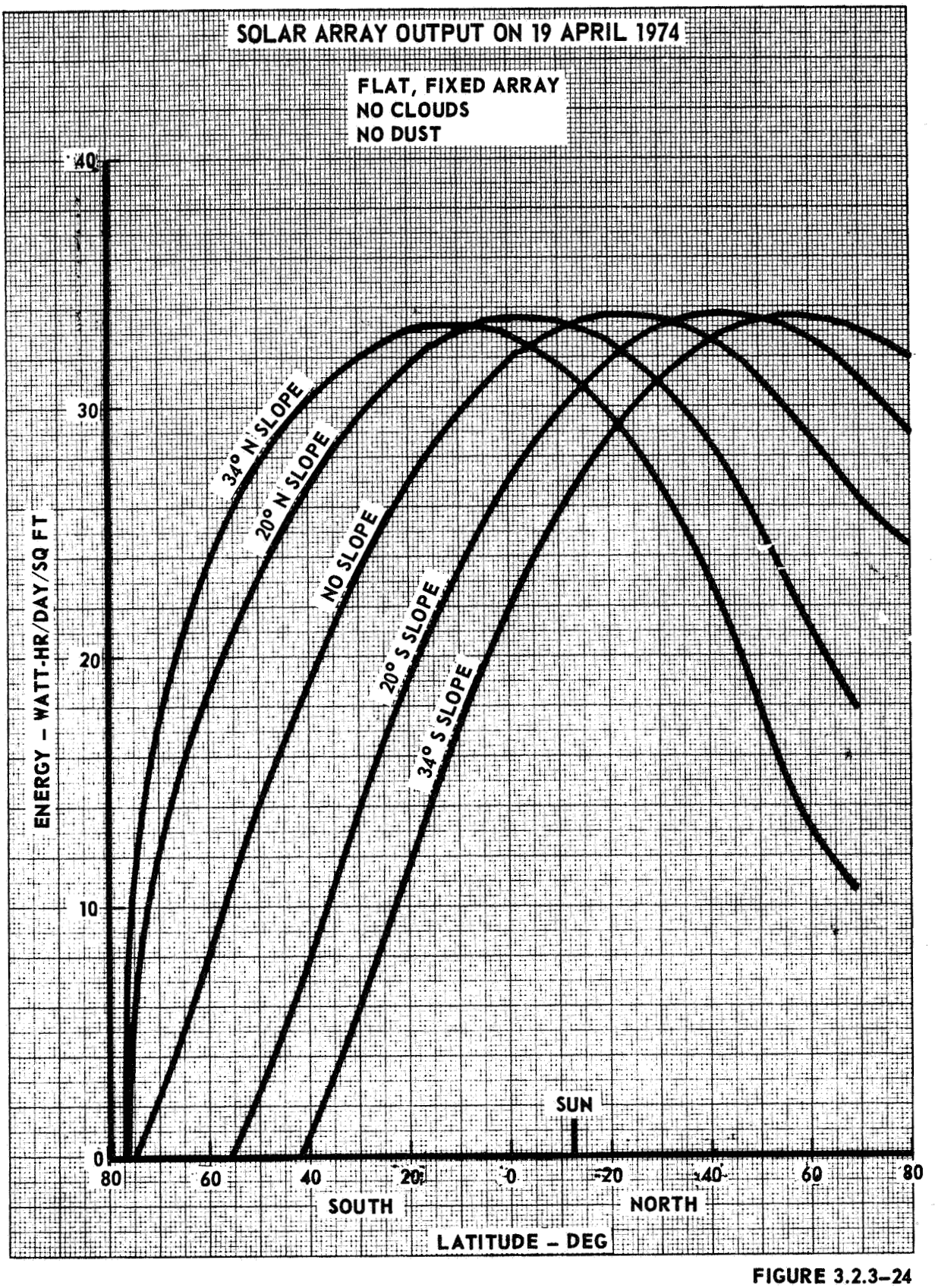

FIGURE 3.2.3–24

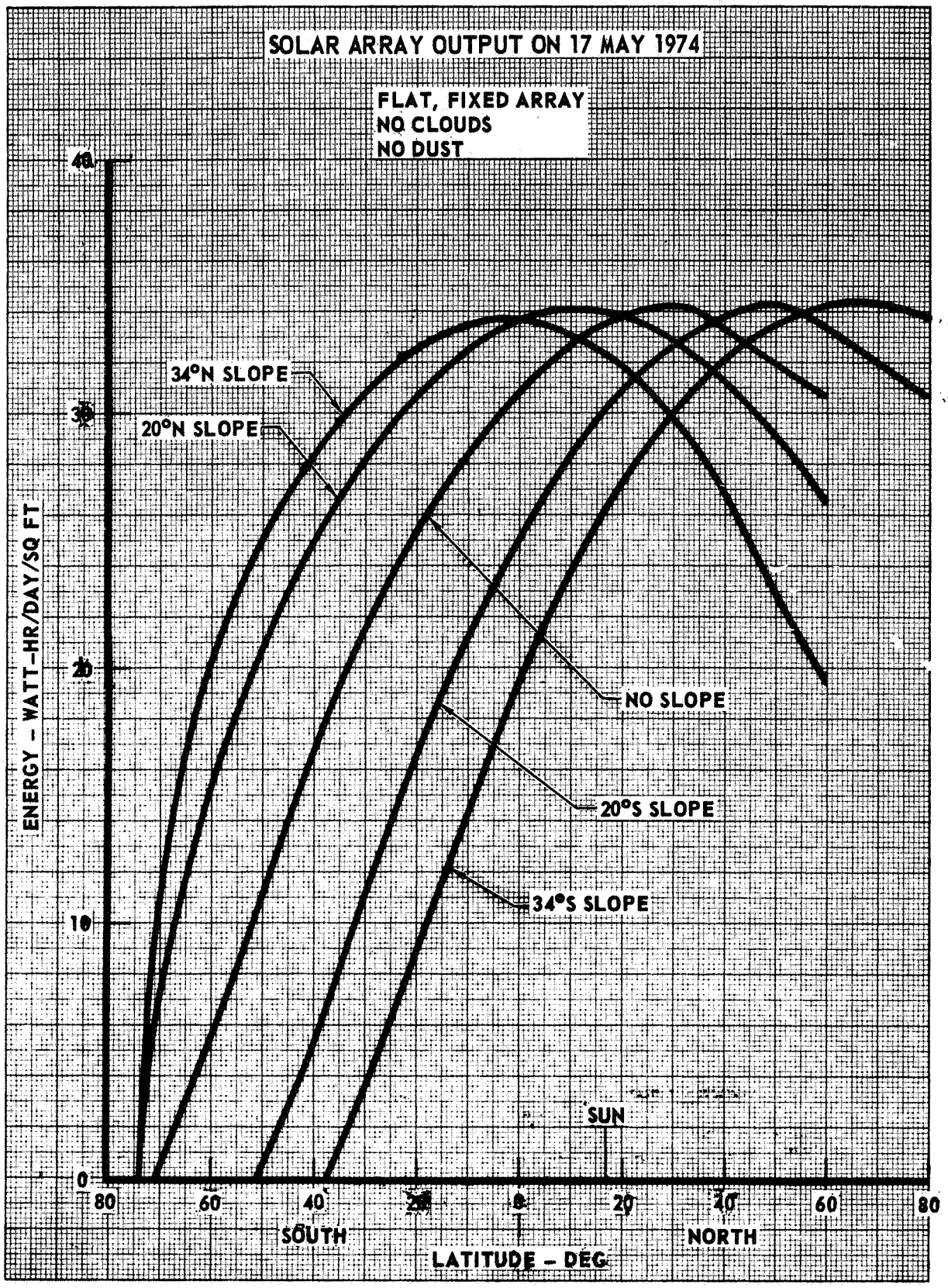

FIGURE 3.2.3–25

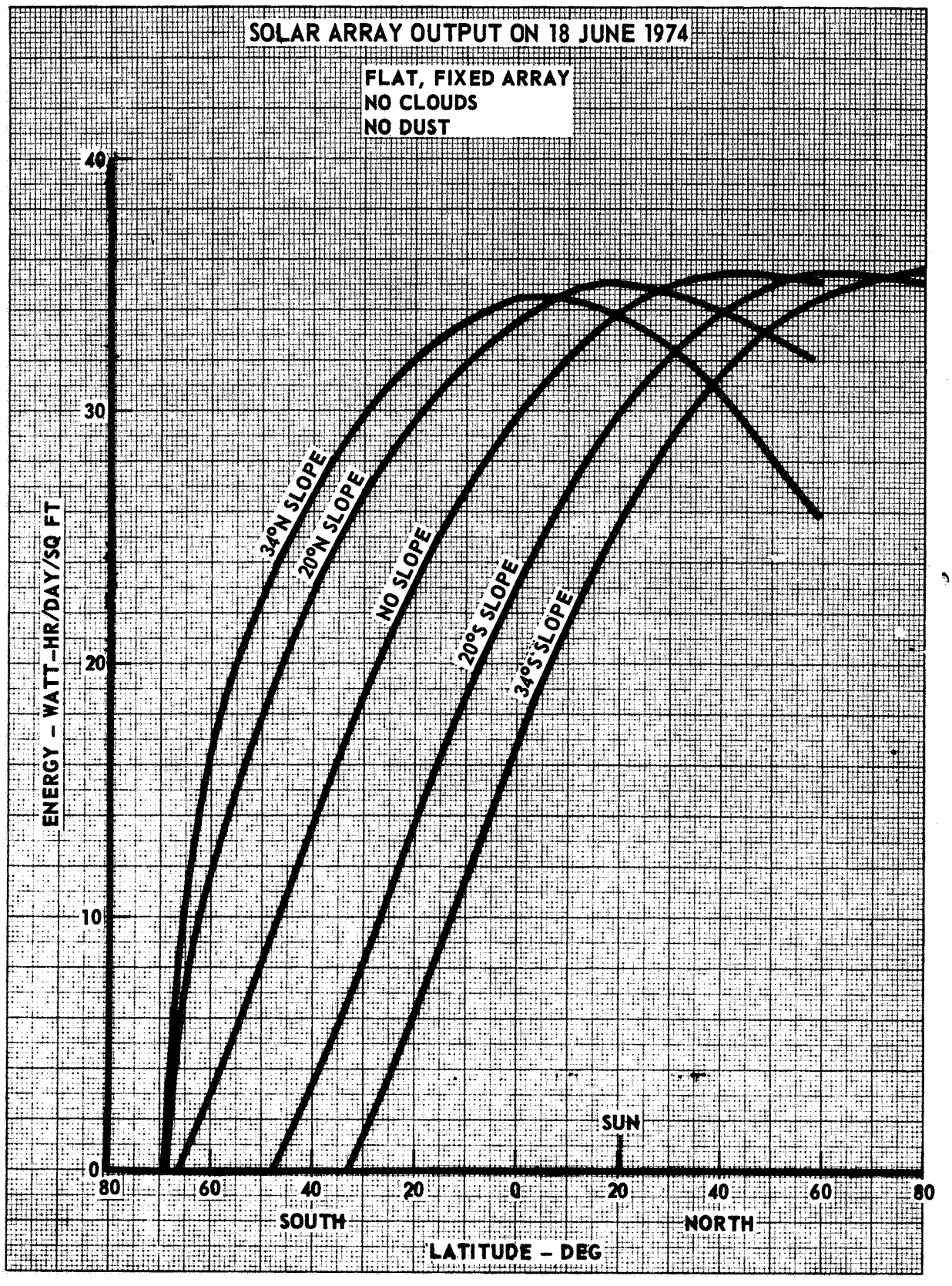

FIGURE 3.2.3–26

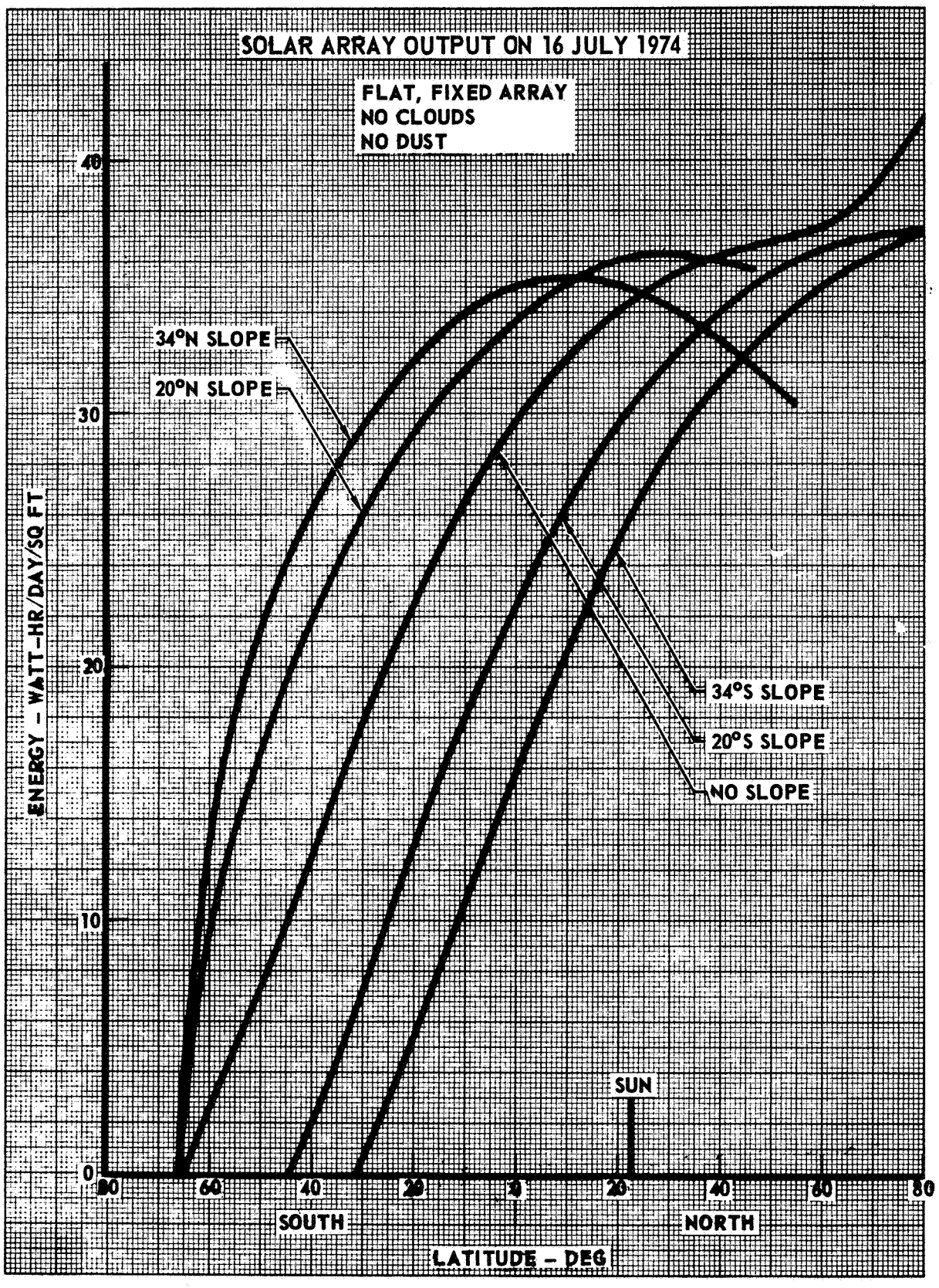

FIGURE 3.2.3–27

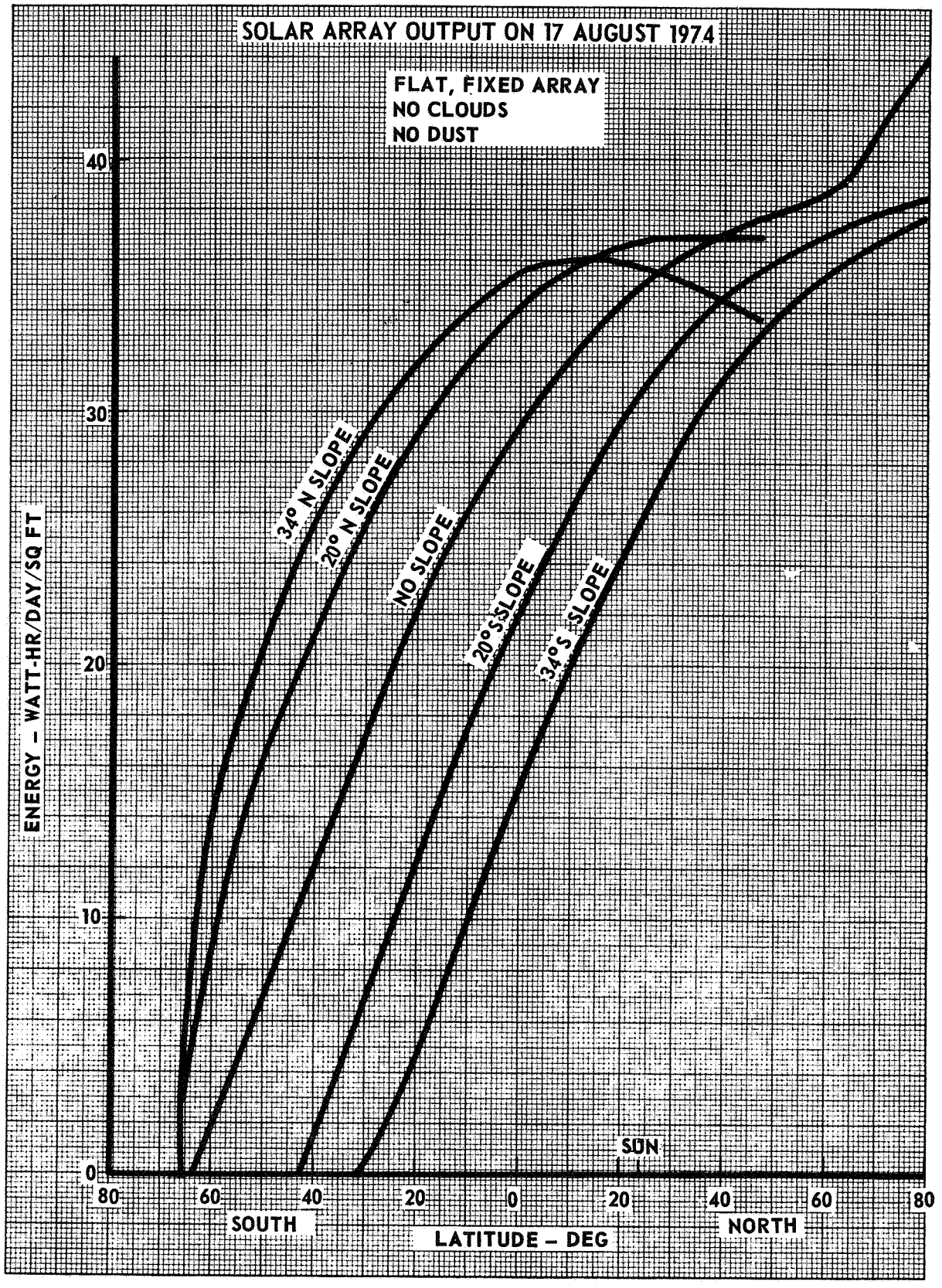

FIGURE 3.2.3–28

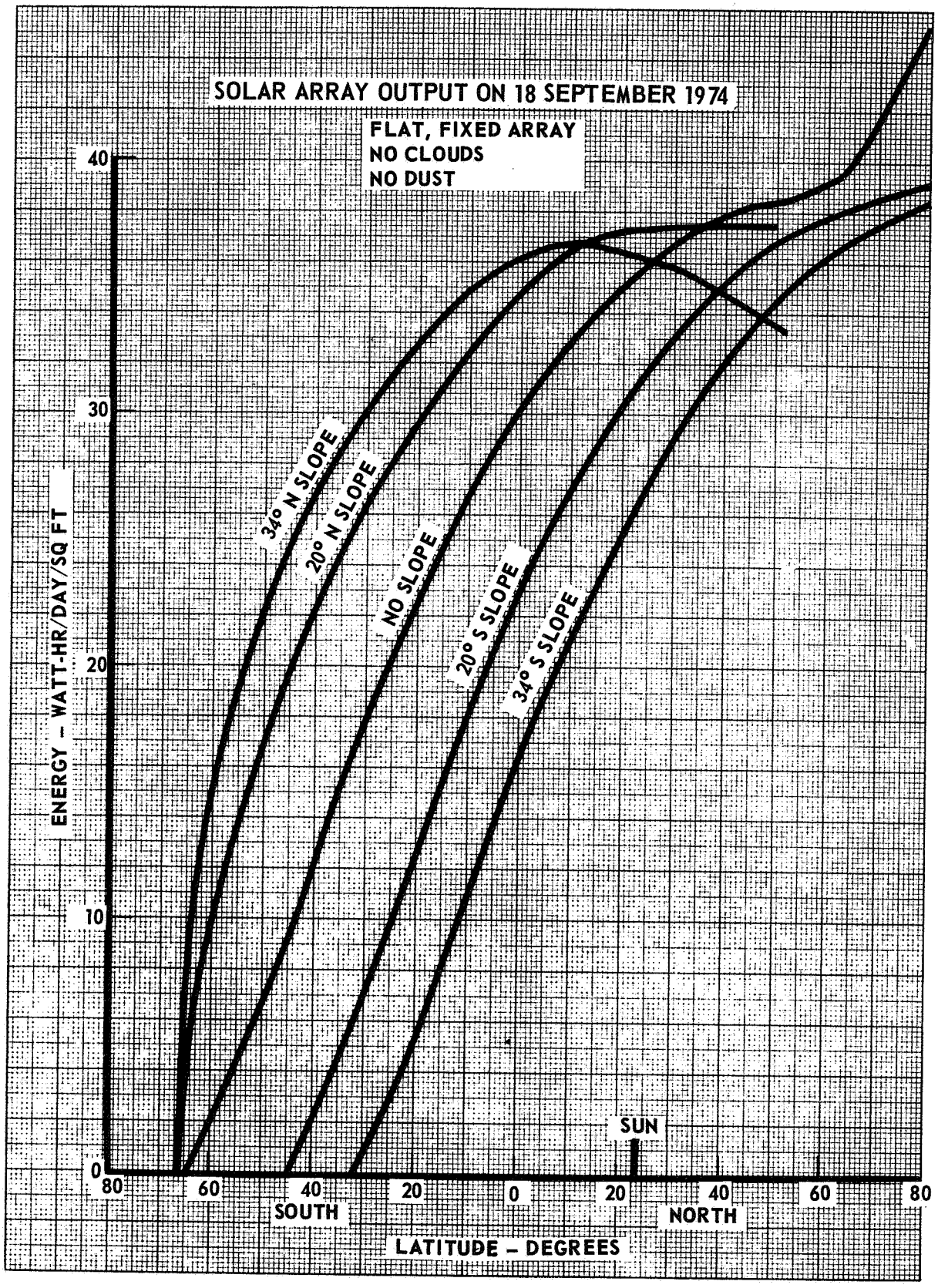

FIGURE 3.2.3–29

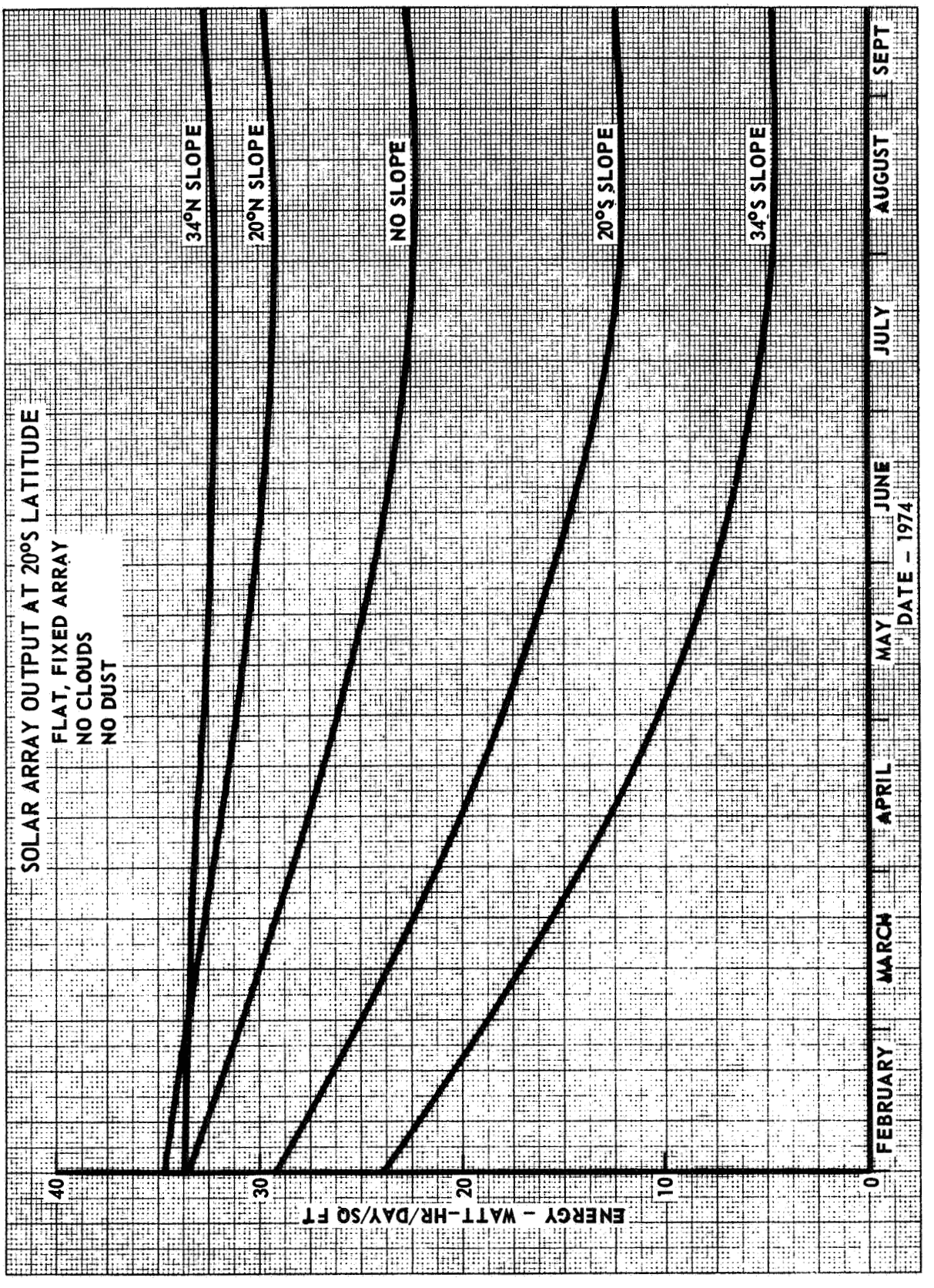

FIGURE 3.2.3–30

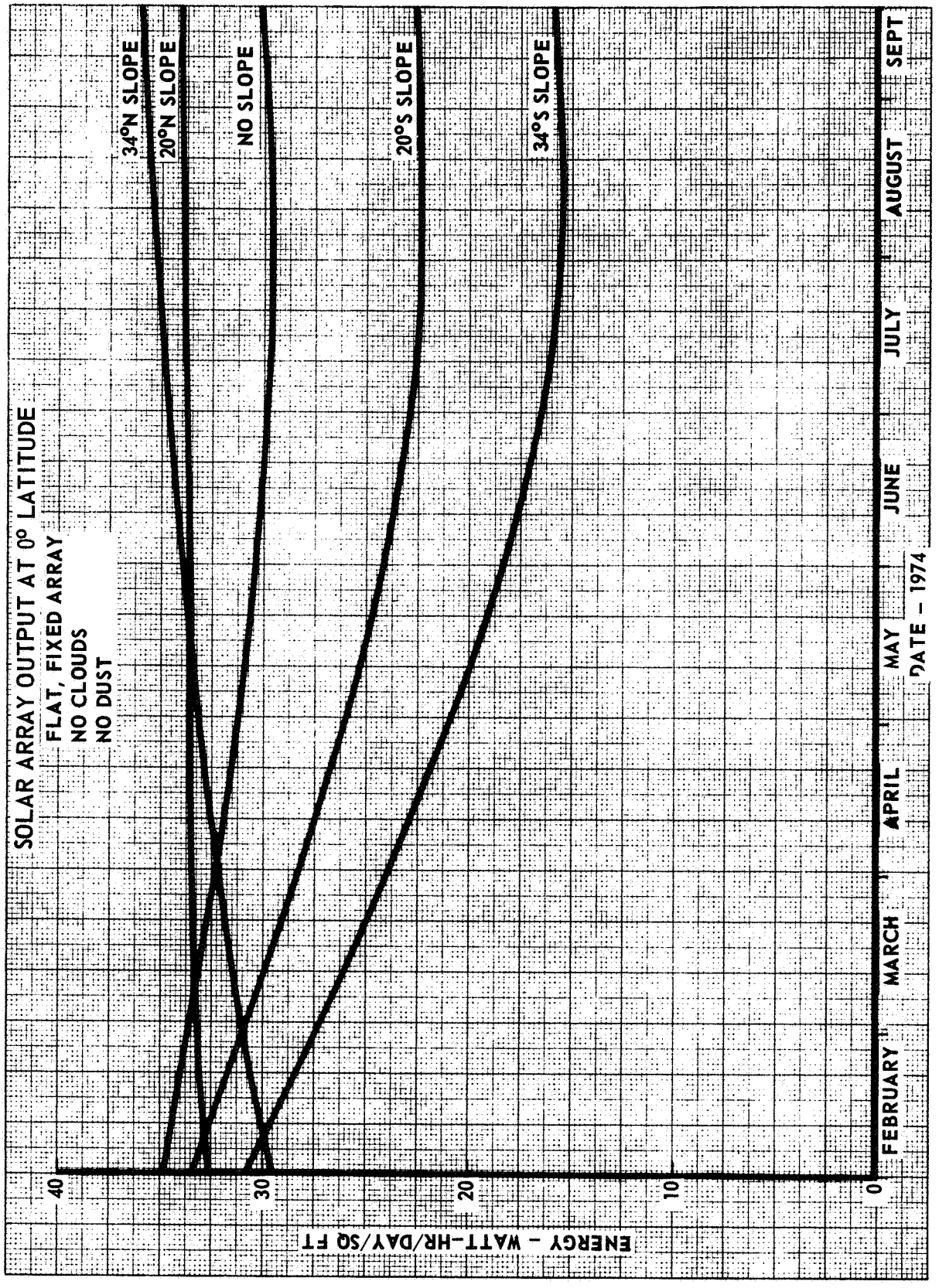

FIGURE 3.2.3-31

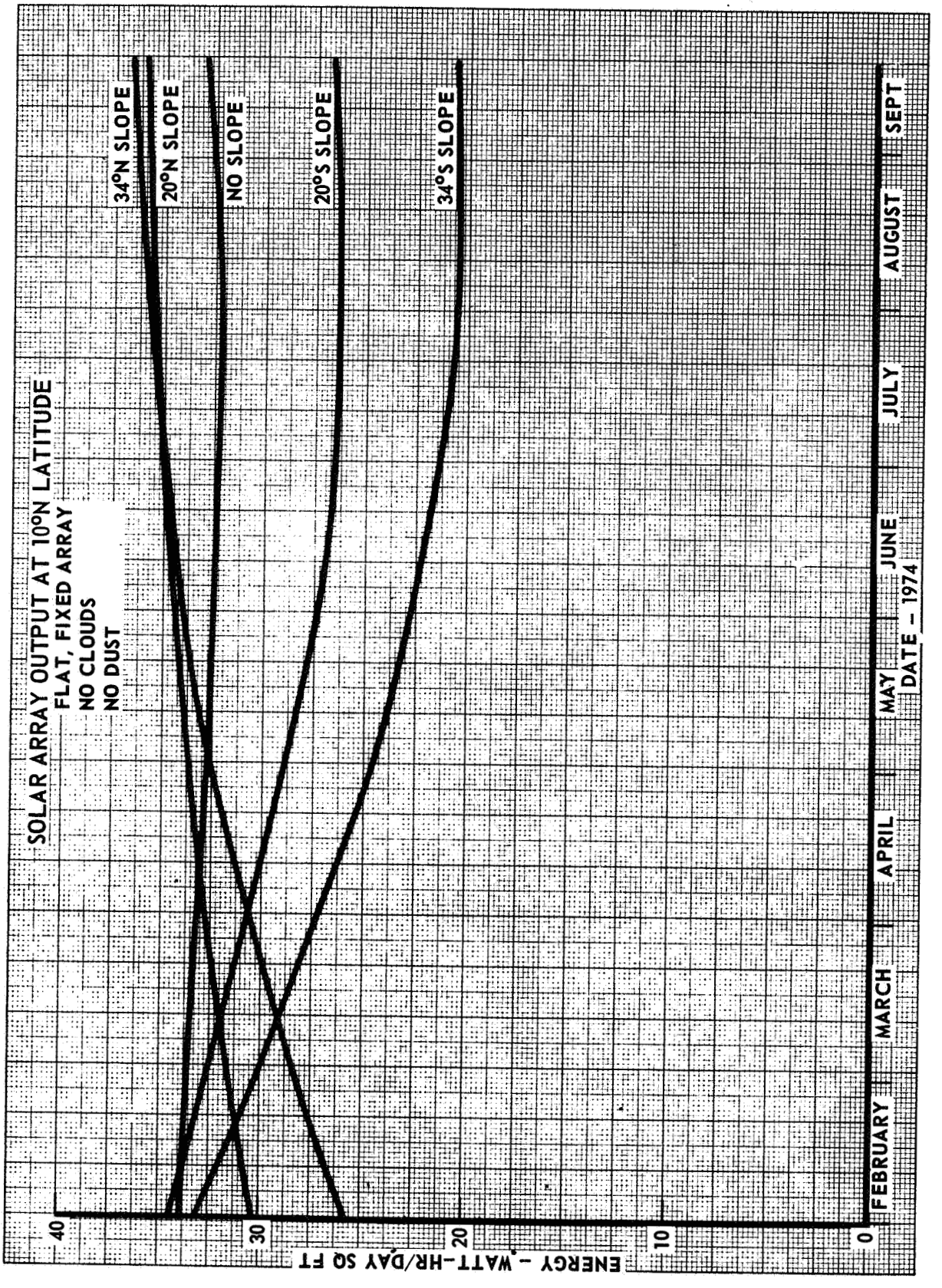

FIGURE 3.2.3–32

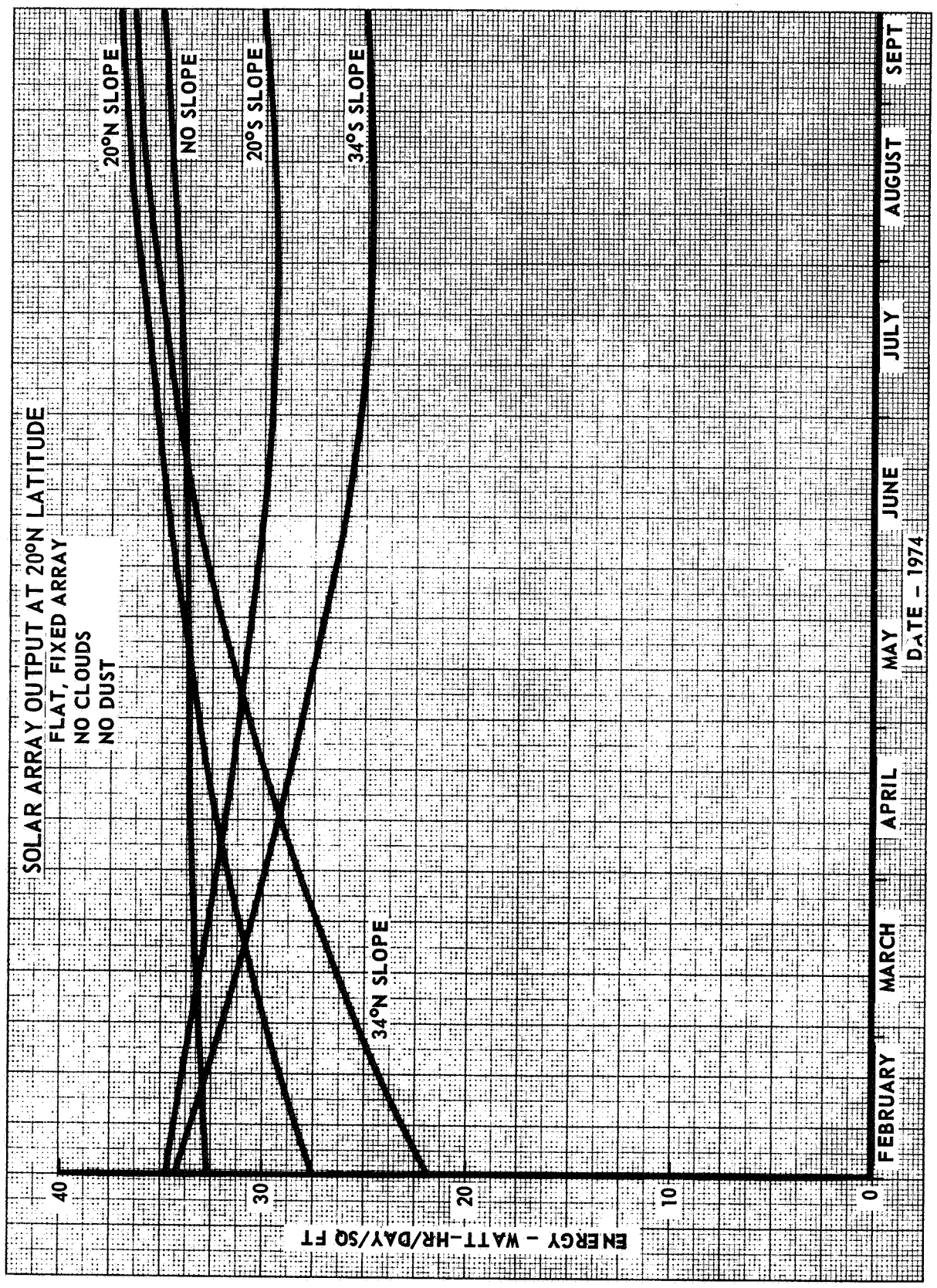

FIGURE 3.2.3-33

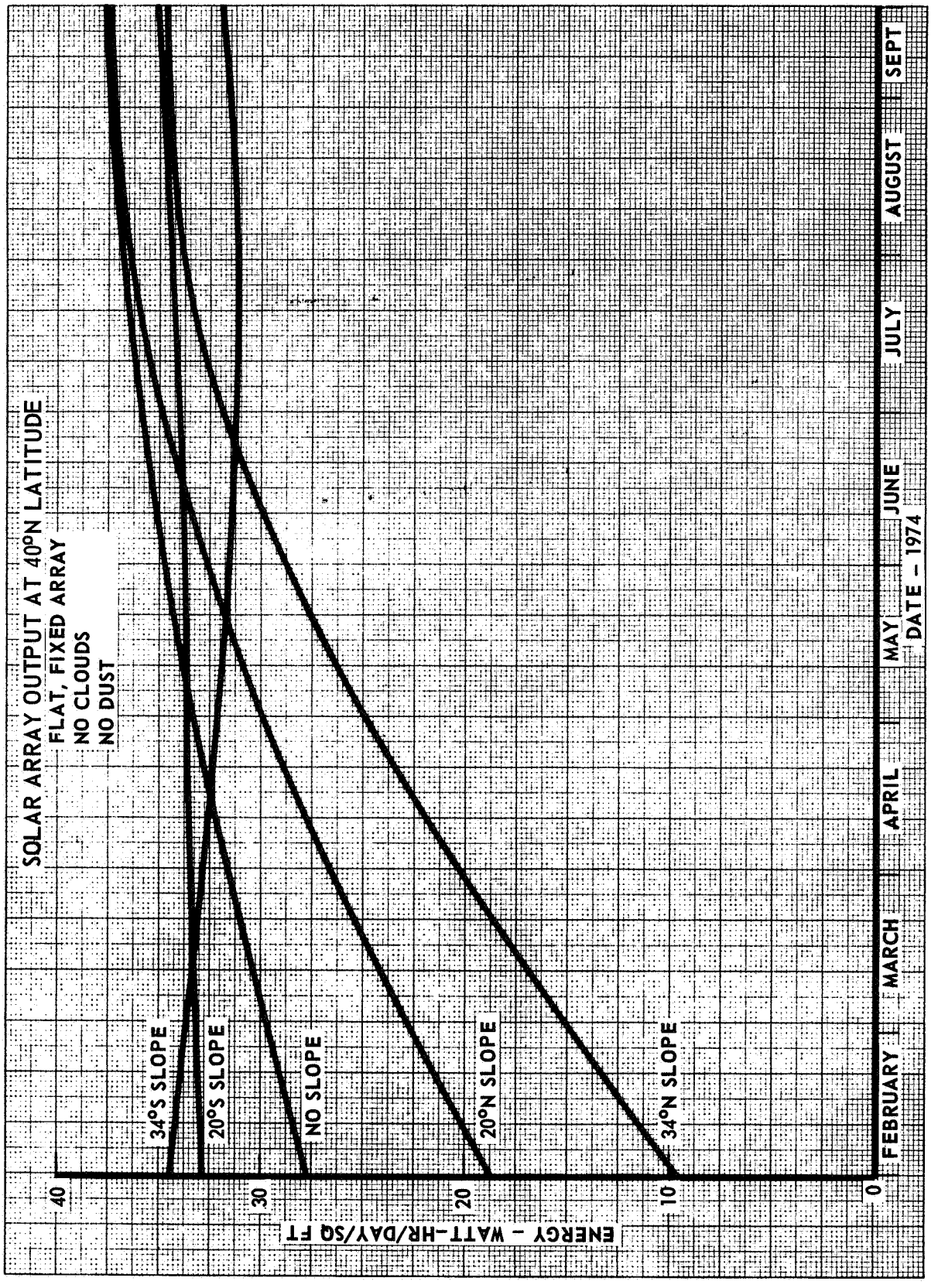

FIGURE 3.2.3–34

o Sand and Dust - Wind blown sand and dust will degrade solar cell performance due to abrasion and erosion of solar cell cover glass material and deposition of material on the solar cells. Insufficient data exists on the actual degree of these effects. Tests conducted by McDonnell Douglas indicate that exposure to wind blown sand is minimized if the exposed array is more than several inches above the surface of the local terrain. However, dust adhesion to the cover glass may be severe. The glass samples tested were repeatedly washed before the transmissibility measurements shown in Figure 3.2.3-35. More investigation of the magnitude of the effects of sand and dust in the Martian atmosphere on solar cell performance is needed, since a very thin layer of dust accumulation adversely effects solar cell output. No account of these effects is included in any of the solar array performance calculations presented herein.

Radioisotope Thermoelectric Generator - An RTG is not significantly influenced by the Martian surface environment or landing site. The lifetime and power output of an RTG are readily predicted, independent of the Martian environmental uncertainties. Therefore, an RTG-battery power system is directly derived from the power profile requirements and is not sensitive to when power peaks occur.

The calculations of RTG system performance assume 1.09 watts per pound for a lead-telluride, plutonium-238 fueled RTG, 29 watt-hours per pound for silver-zinc batteries, and six pounds of fixed weight for a converter-regulator and battery charger. The trends and relationships are not particularly sensitive to these values. However, the actual system and component weight are directly related to the values of these parameters.

RTG power, battery capacity, and system weight are the predominant parameters directly determined from analysis of the power profile requirements. The variations of these parameters as functions of the power profile variables for direct communications (Figure 3.2.3-2), are shown in Figures 3.2.3-36 through 3.2.3-39. The RTG output power is directly related to transmission time, transmission power level, and night power level - the power level without transmitter operation. Battery capacity is also a direct

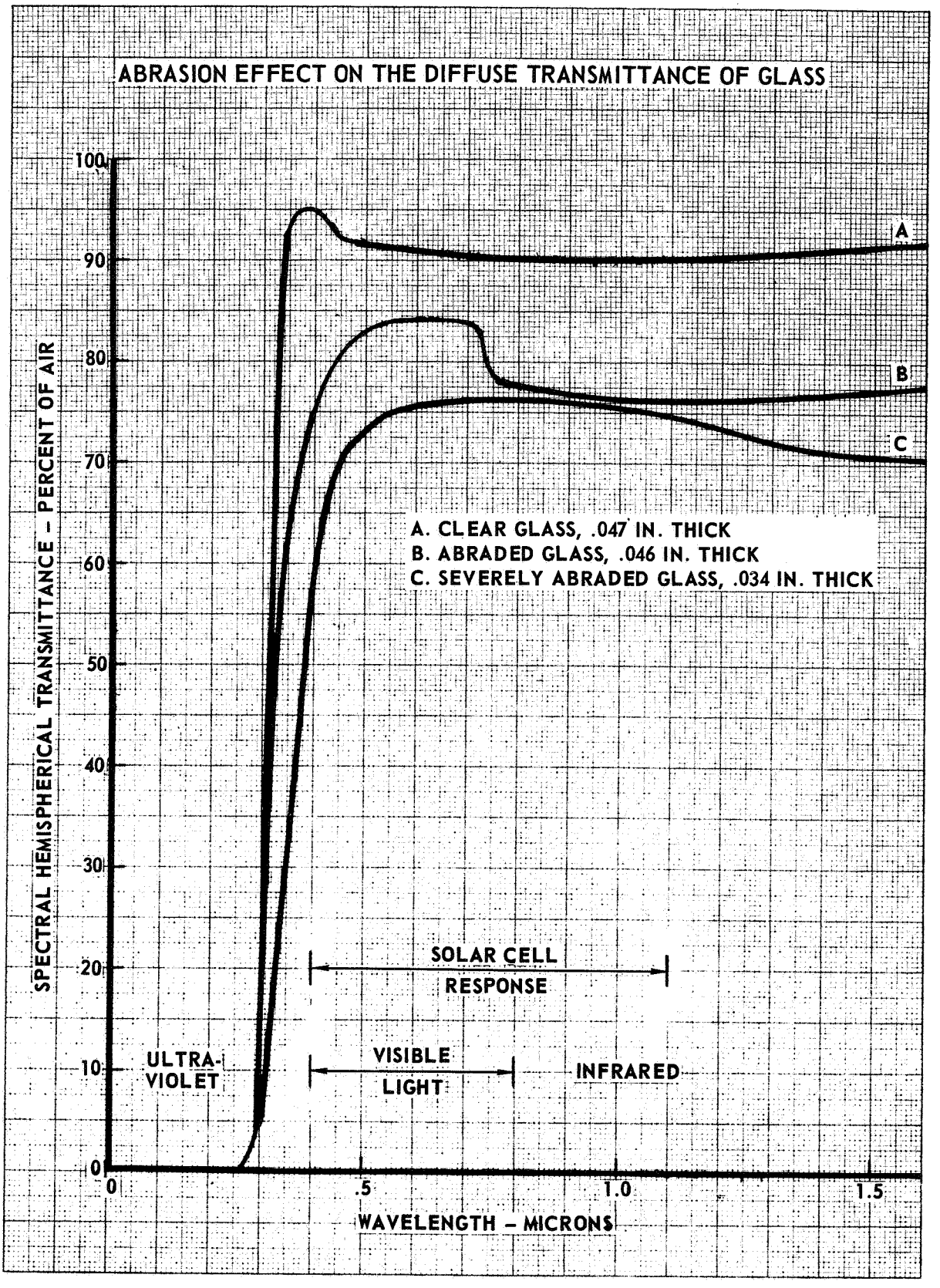

FIGURE 3.2.3–35

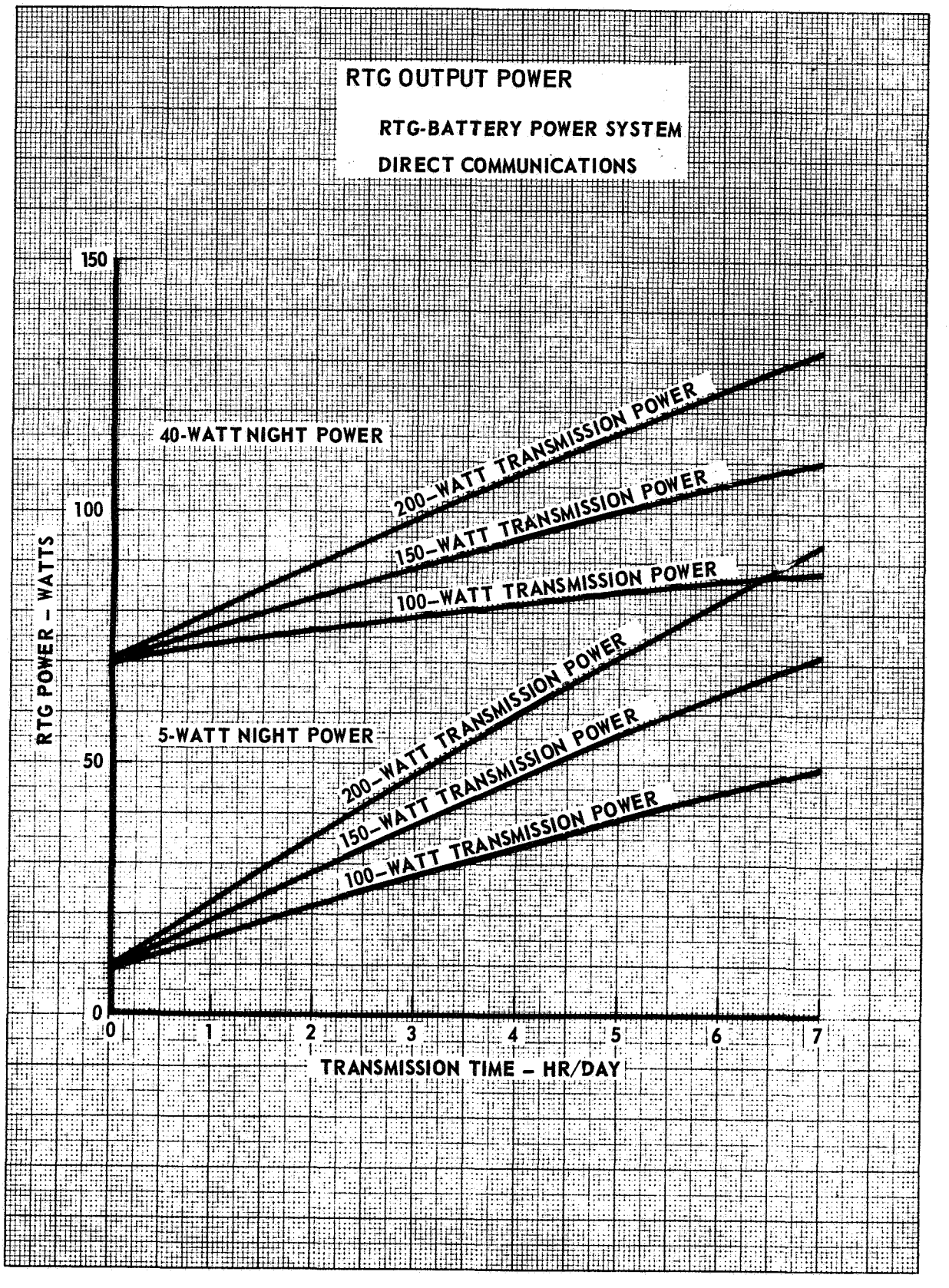

FIGURE 3.2.3–36

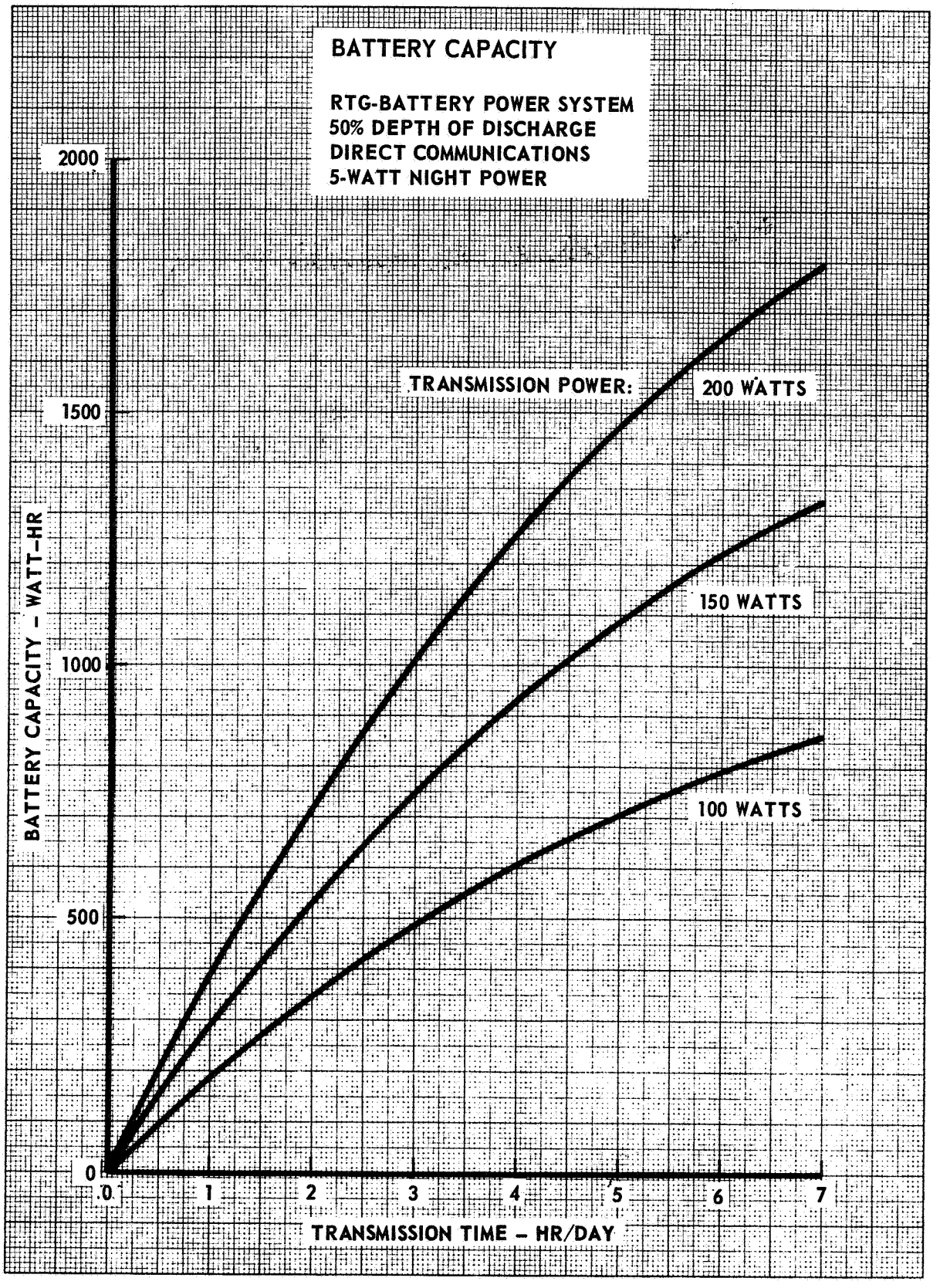

FIGURE 3.2.3–37

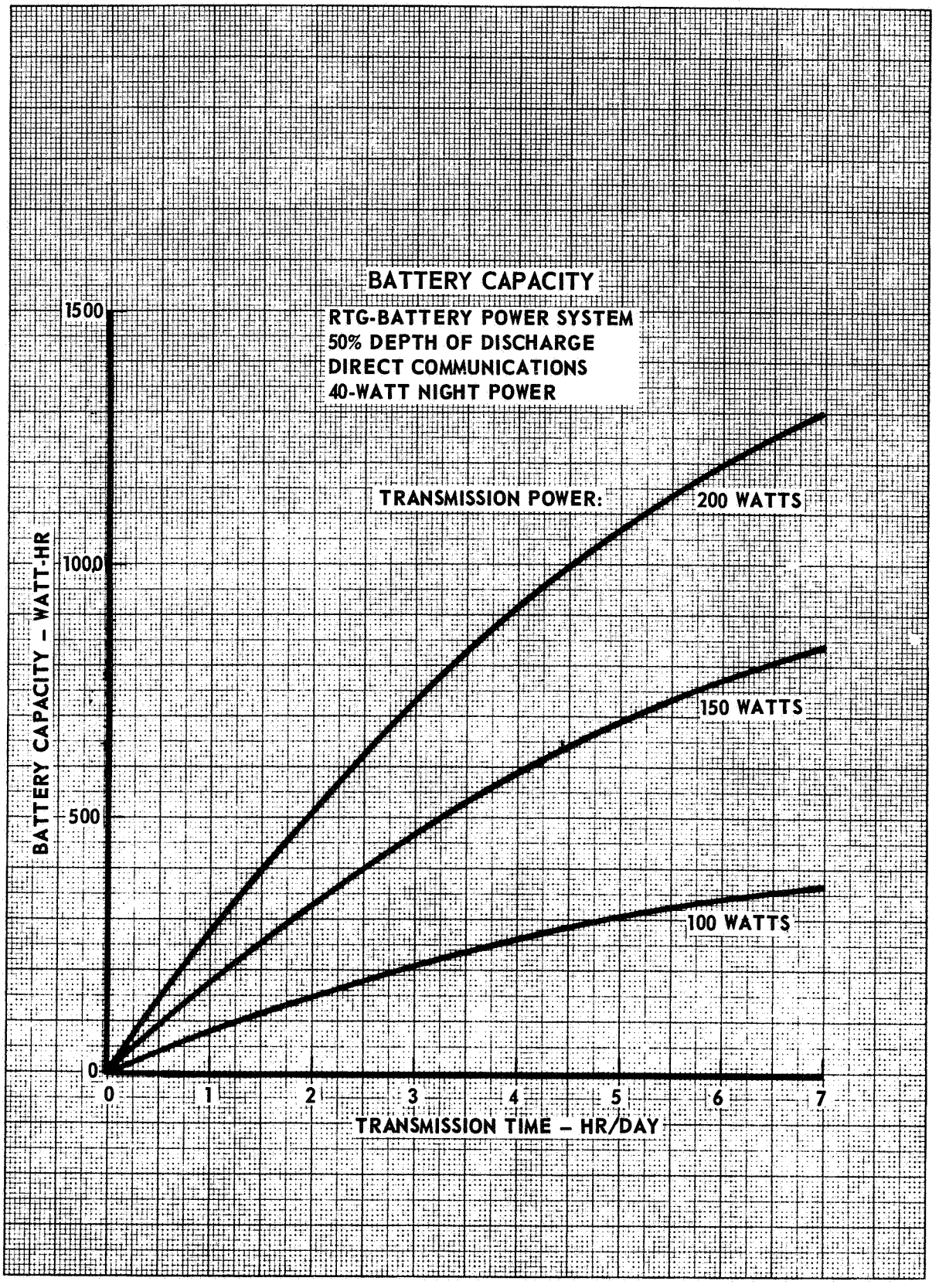

FIGURE 3.2.3–38

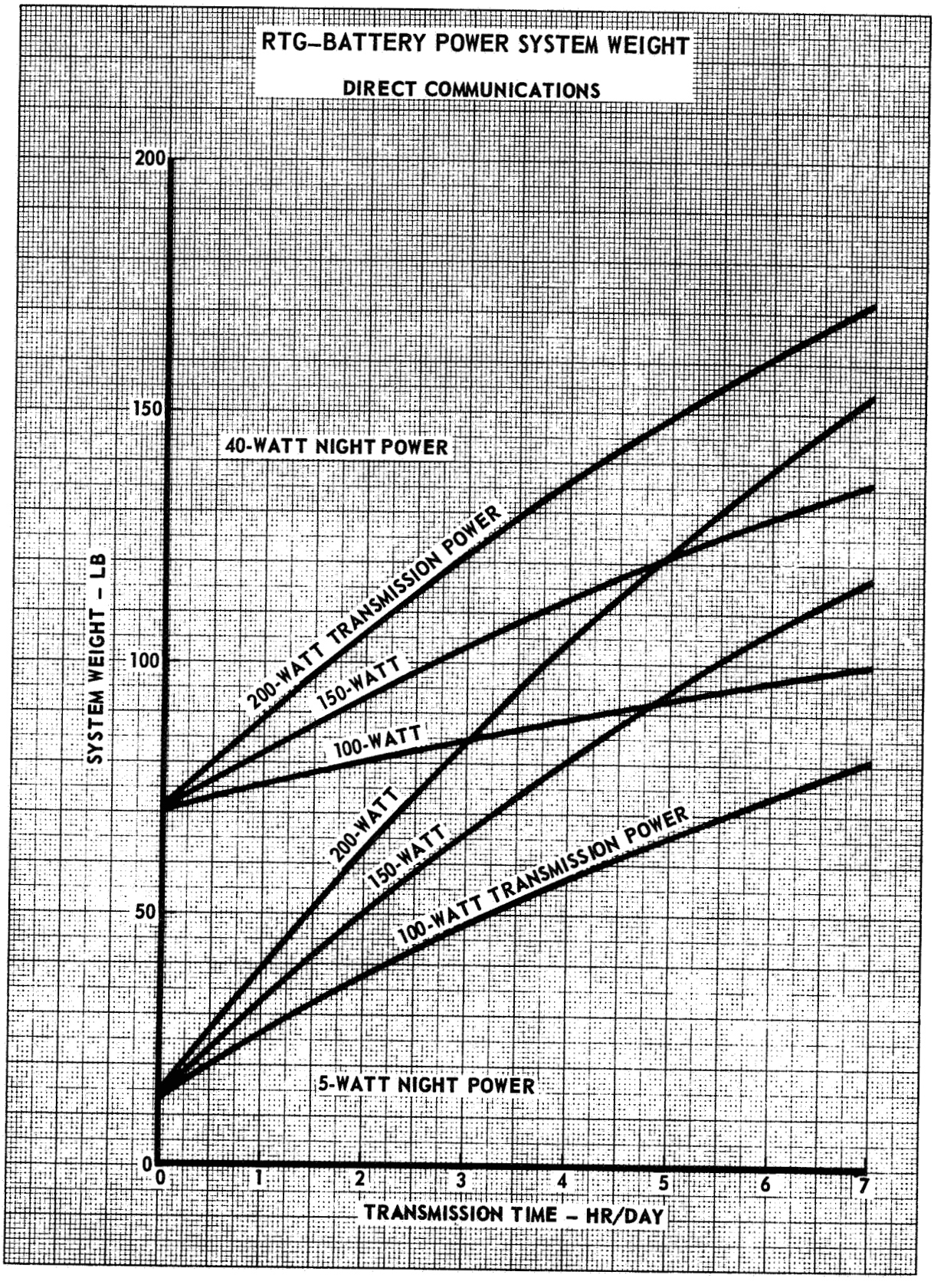

FIGURE 3.2.3–39

function of the night power. Power system weight (the sum of RTG weight, battery weight, and the converter-regulator and battery charger weights) is strongly dependent on night power and transmission duration for short transmission times, but not on transmission power. For long transmission times, the reverse is true: the weight is more dependent on transmission power than transmission time or night power.

The variations of RTG power, battery capacity, and system weight as functions of the transmission power level and night power level of the power profile (Figure 3.2.3-3) for relay communications at periapse are shown in Figures 3.2.3-40 through 3.2.3-42. The required RTG power level is relatively low, is directly sensitive to night power level, but is insensitive to transmission power level. Conversely, battery capacity, though also low (note scale), is a direct function of transmission power level, but is only slightly and inversely affected by the night power level. Consequently, total system weight is primarily a function of the RTG weight, is a direct function of night power but is insensitive to transmission power.

The variations of the parameters of an RTG-battery power system as a function of the transmission power level and night power level of the power profile (Figure 3.2.3-4) for relay communications at apoapse are shown in Figures 3.2.3-43 through 3.2.3-45. The required RTG power level is directly related to both the night power and transmission power levels. Battery capacity is also directly related to transmission power but inversely related to night power. Because of the somewhat offsetting effects of night power on battery capacity and RTG power, system weight is insensitive to night power, but is a strong function of transmission power.

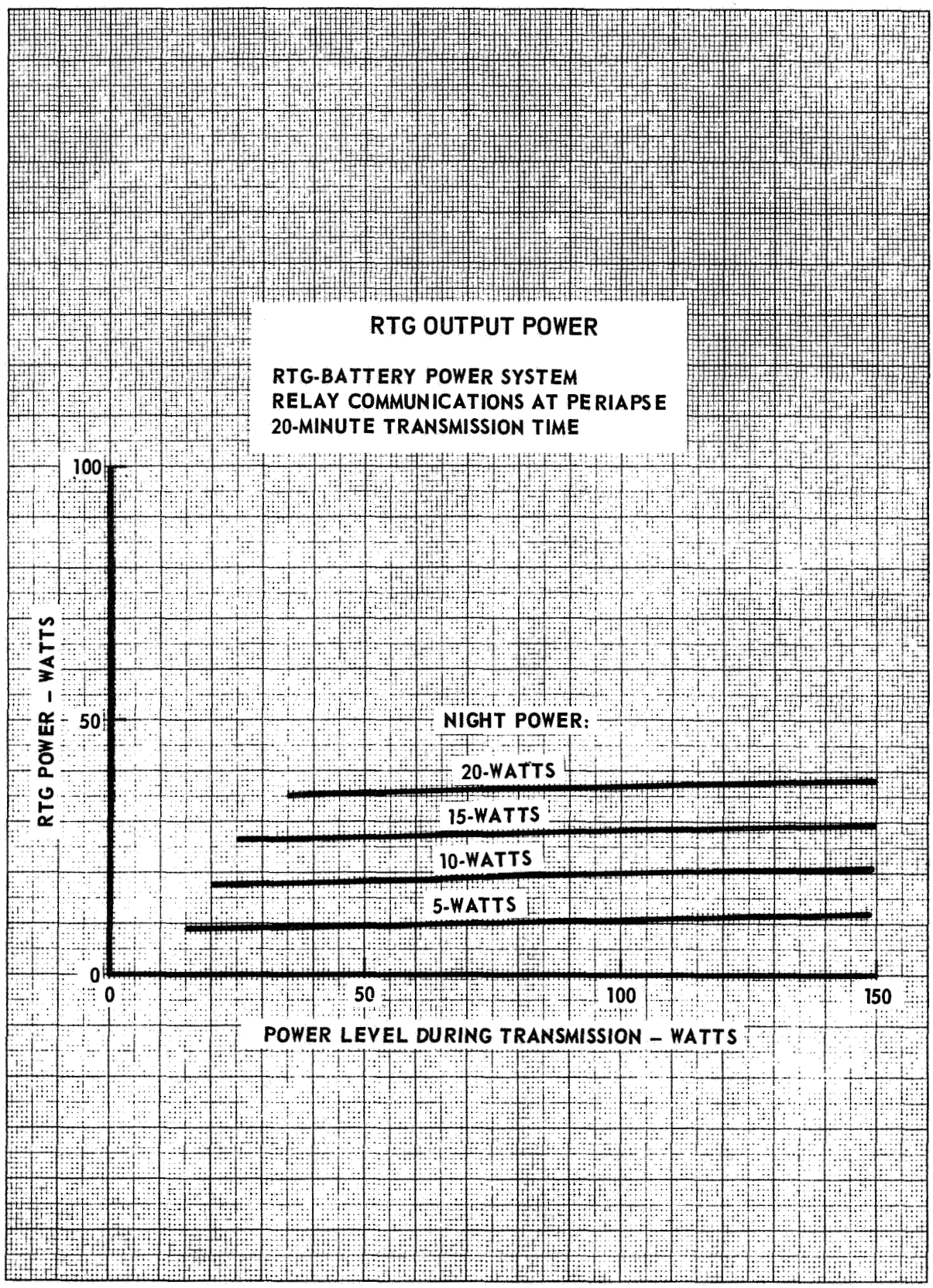

FIGURE 3.2.3–40

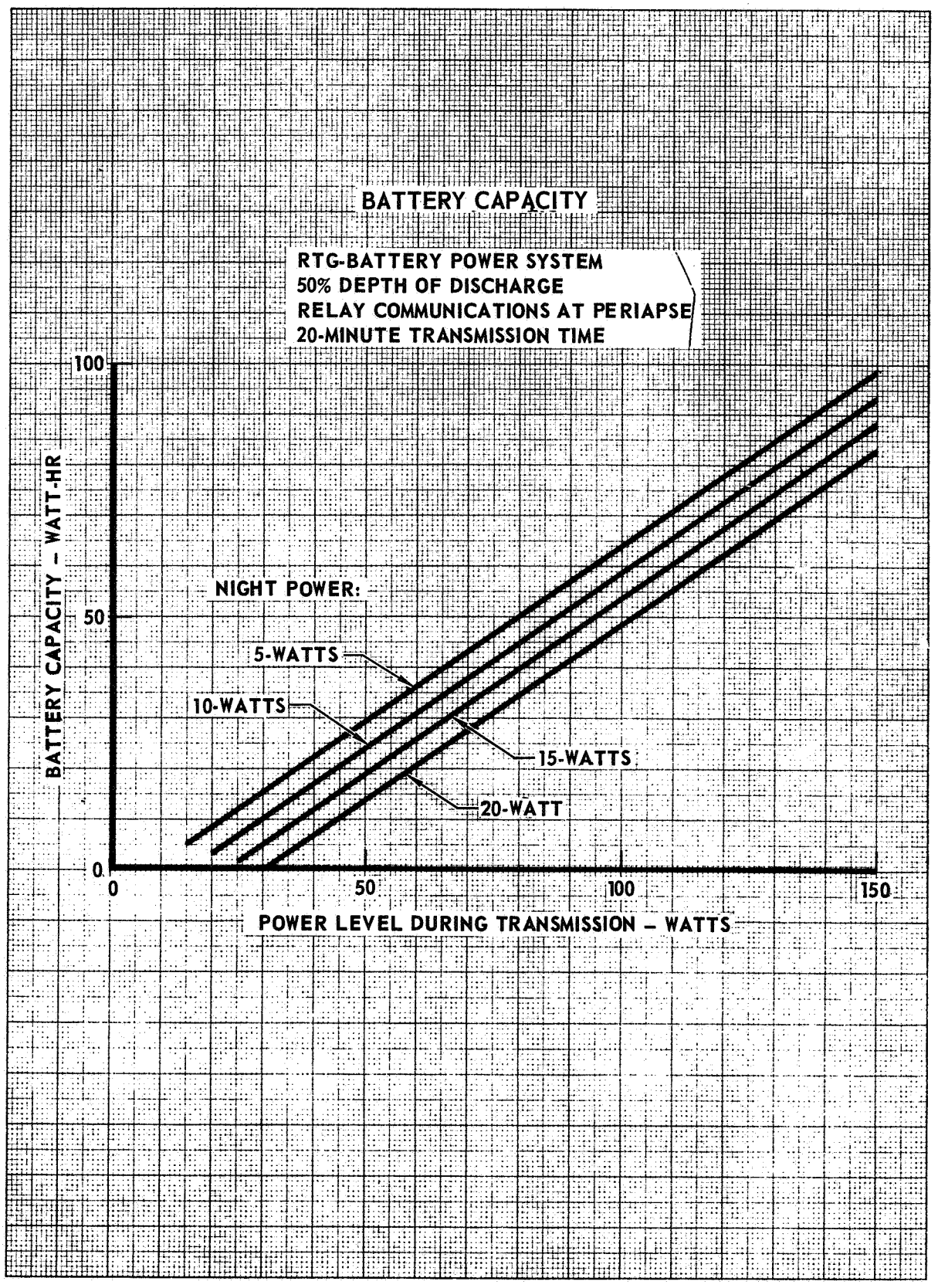

FIGURE 3.2.3–41

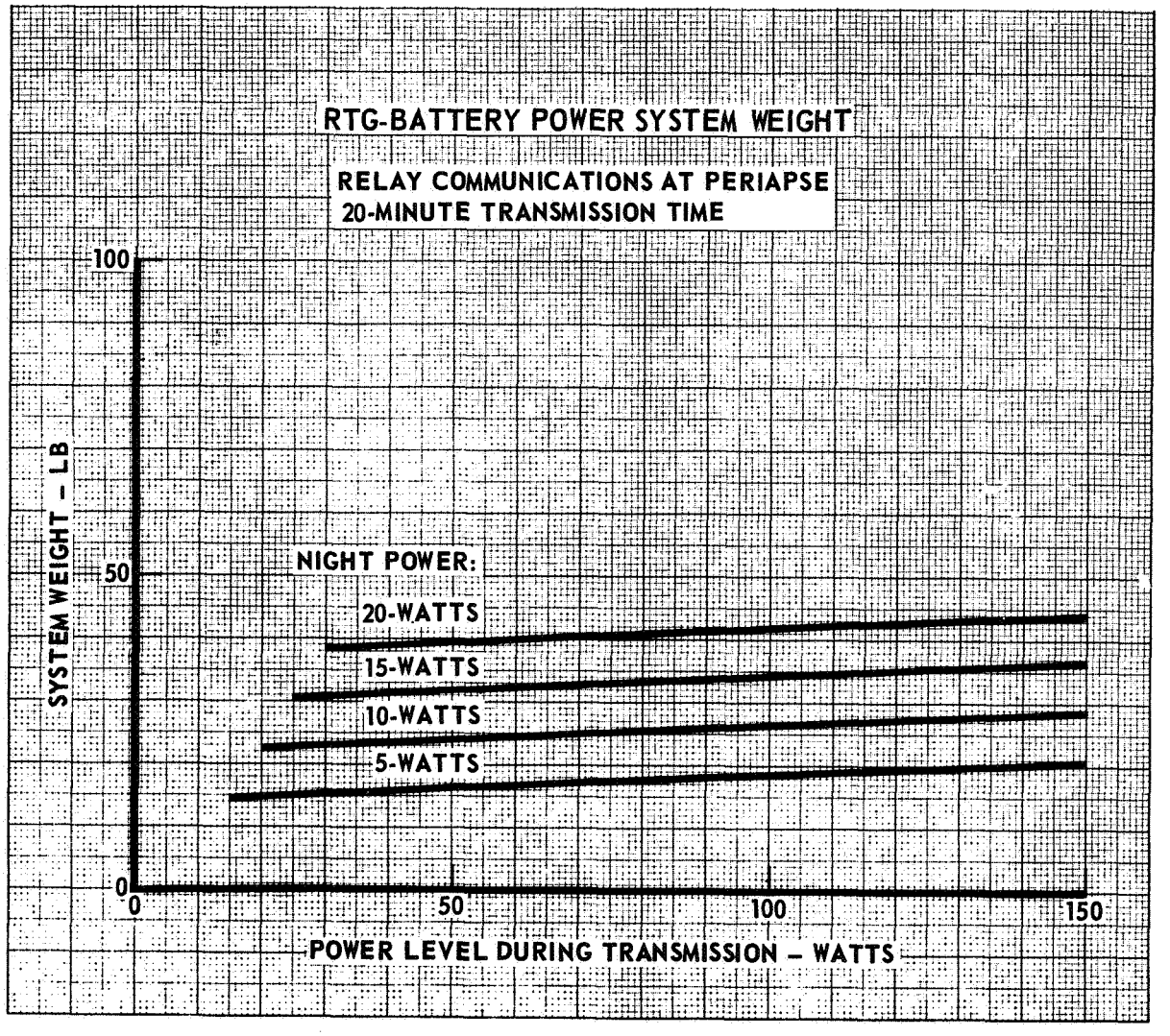

FIGURE 3.2.3–42

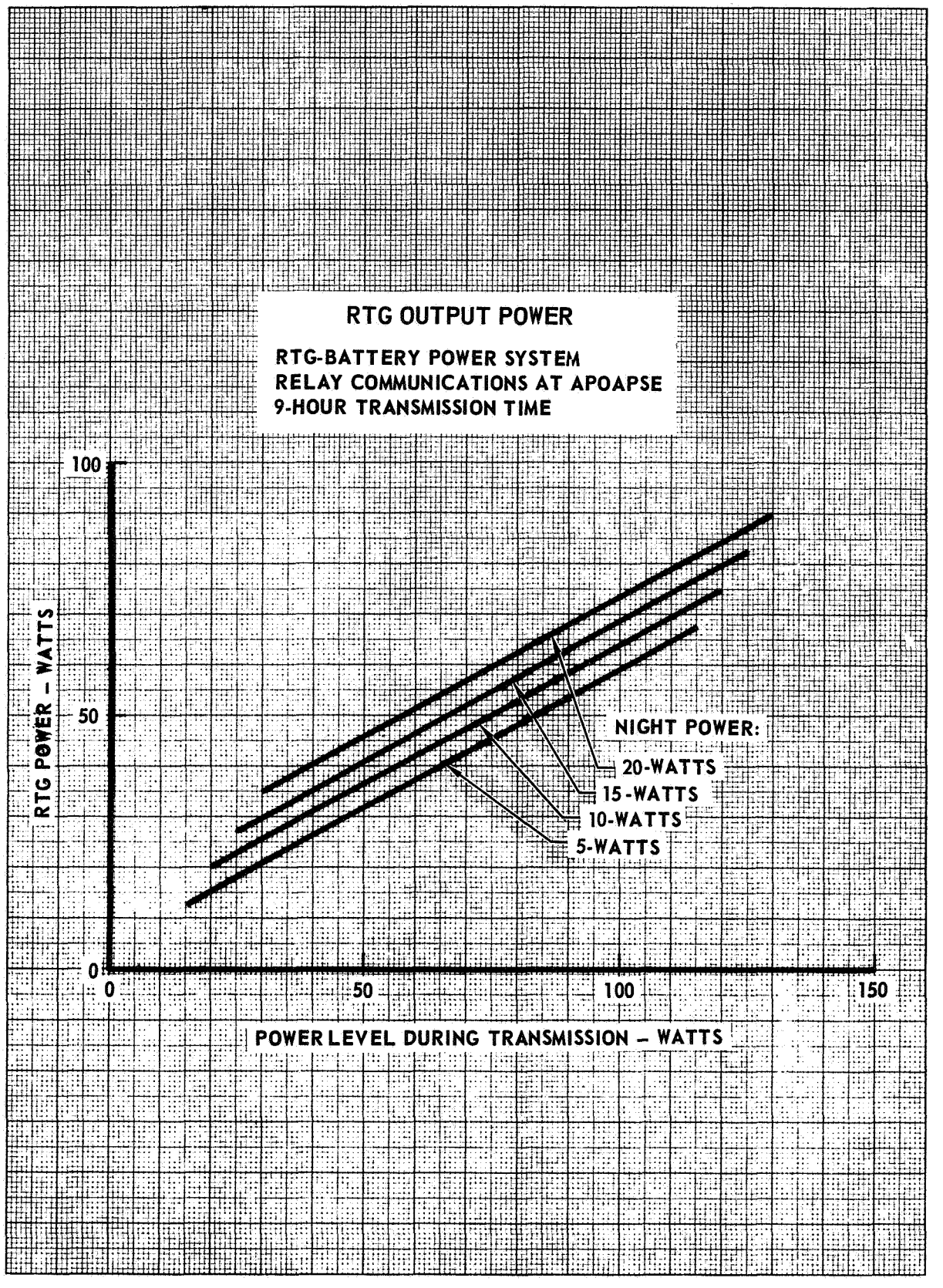

FIGURE 3.2.3–43

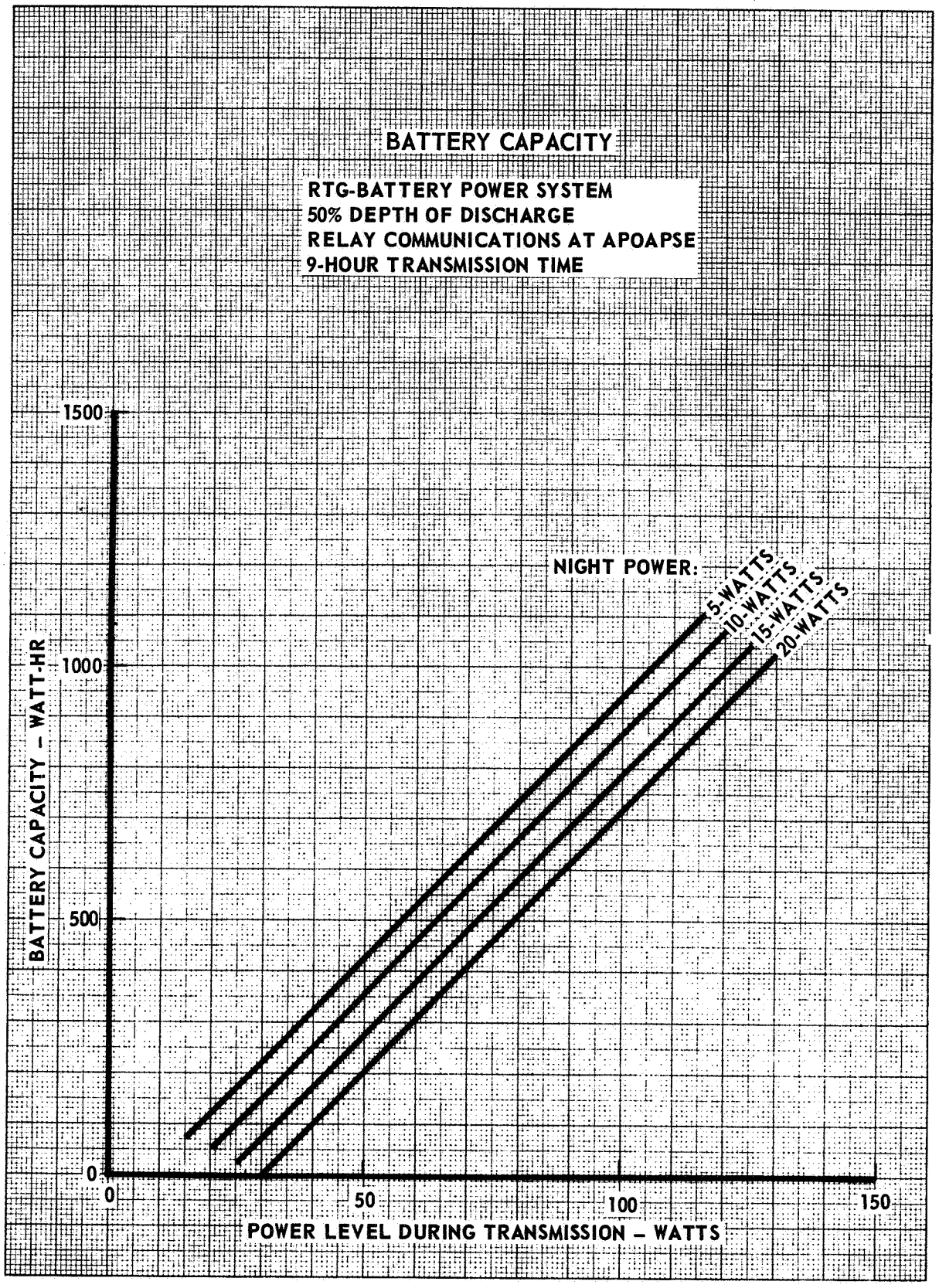

FIGURE 3.2.3–44

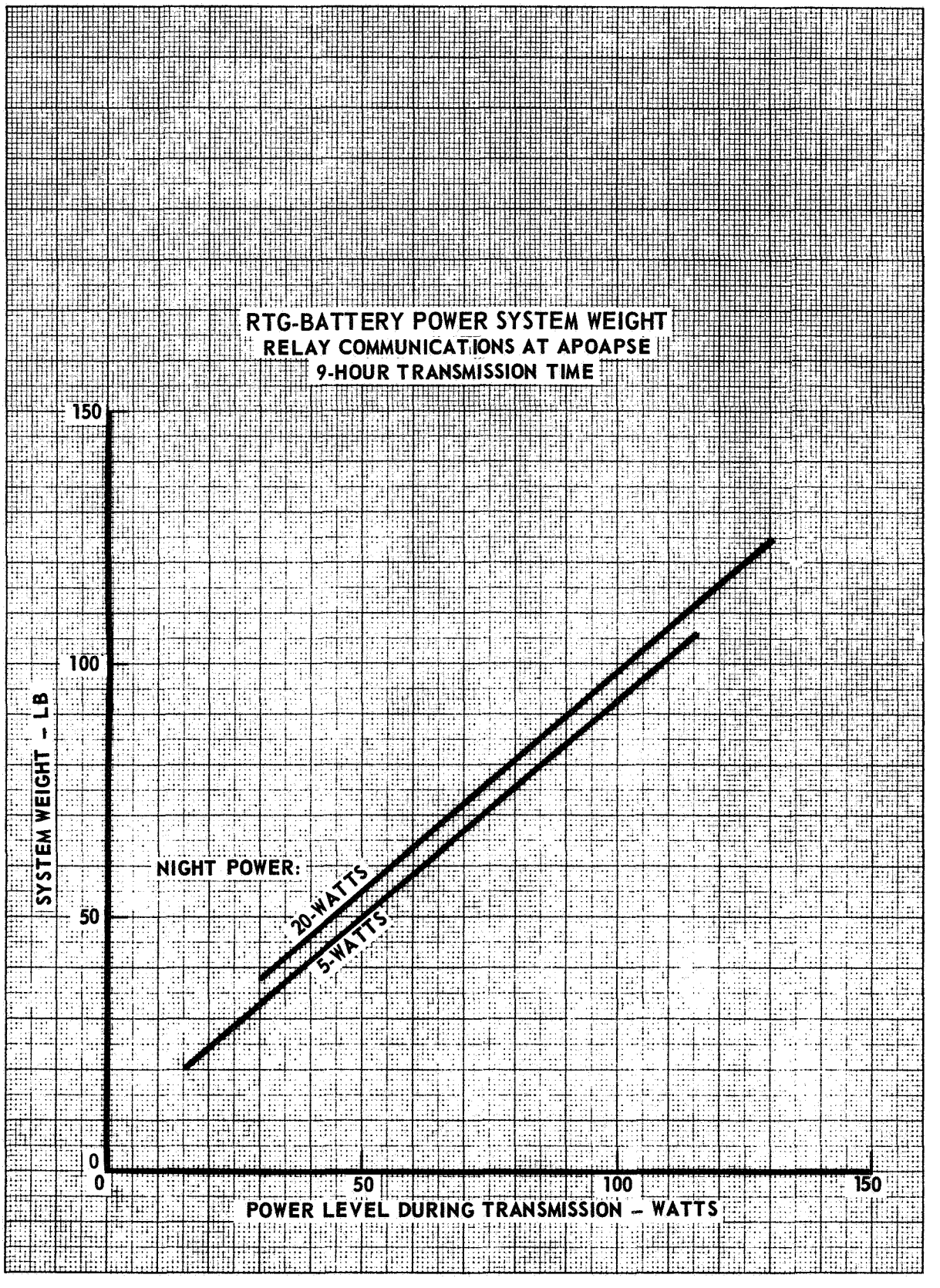

FIGURE 3.2.3–45

Reference 1:

"Particulate and Biological Matter Challenge System for Validation of Sterility Within a Sterile Assembly System," Bi-monthly Report Number 5 15 April 1968, Contract Number NAS 8-21114, McDonnell Douglas Corporation.

Reference 2:

"Thermology of the Martian Surface," by Victor Kachur, AIAA Paper Number 66-436.

3.2.4 GUIDANCE AND CONTROL SYSTEM - The guidance and control system includes the equipment required to sense and control vehicle attitude, attitude rate, acceleration, range, and velocity from capsule separation to Martian surface touchdown. Figure 3.2.4-1 presents the major guidance and control phases and events to be accomplished in a typical soft landing sequence. Comparative and parametric analyses have been performed on a spectrum of candidate system configurations and operational modes to accomplish these events. These parametric results establish the approaches that minimize vehicle weight and maximize control accuracy. The guidance and control system includes the attitude and deorbit velocity control electronics, the landing radar, and the radar altimeter.

3.2.4.1 Attitude/Deorbit Velocity Control Electronics. - Control law and sequence formulations, as well as hardware implementations, have been considered in evaluating the control electronics system alternatives.

3.2.4.1.1 Control Sensor Alternatives: Candidates for attitude reference and deorbit velocity control equipment include strapped-down or gimballed Inertial Measurement Unit (IMU) packages with either digital or analog flight control electronics. Table 3.2.4-1 summarizes the parametric and comparative analyses of these alternative hardware schemes for the control sequence of Figure 3.2.4-1. A detailed presentation of these analyses is included in the Reference 3.2.4-1. A strapped down IMU/digital electronics implementation provides a minimum weight and risk system together with maximum performance and flexibility.

The hardware parametric was extended beyond the type selection analyses to include different technologies and the number of control sensors. For example, the deorbit velocity increment control accuracy is only $\pm 5.9\%$ (3σ) if a simple timed on/off thrust scheme is used. The use of a single roll axis mounted accelerometer with integrated output and velocity comparison improves the control accuracy to $\pm 0.5\%$ (3σ). Lateral velocity dispersions caused by deorbit motor misalignments are not large enough to warrant the use of lateral accelerometers for correction.

MAJOR GUIDANCE AND CONTROL PHASES AND EVENTS

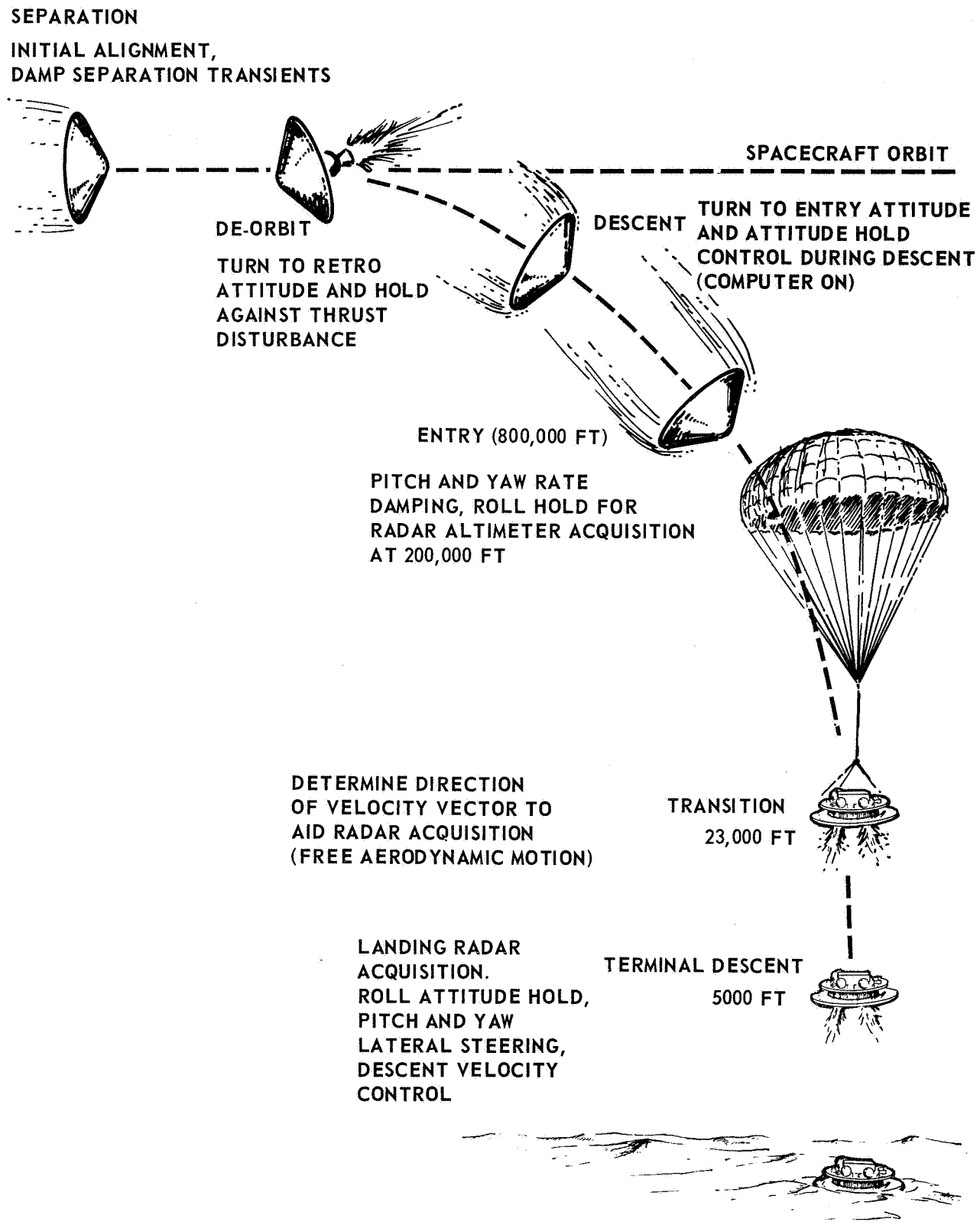

FIGURE 3.2.4–1

TABLE 3.2.4–1

CANDIDATE SYSTEMS COMPARISON MATRIX

COMPARISON/ PARAMETRIC FACTORS	(I) STRAPPED-DOWN IMU DIGITAL ELECTRONICS	(II) STRAPPED-DOWN IMU ANALOG ELECTRONICS	(III) GIMBALLED IMU DIGITAL ELECTRONICS	(IV) GIMBALLED IMU ANALOG ELECTRONICS
EQUIPMENT REQUIREMENT	• 3 RATE INTEGRATING GYROS • 1 PENDULOUS ACCELEROMETER • SMALL DIGITAL COMPUTER • POWER SUPPLIES	• 3 RATE INTEGRATING GYROS • 1 PENDULOUS ACCELEROMETER • SMALL ANALOG COMPUTER • POWER SUPPLIES	• 3 RATE INTEGRATING GYROS • 3 RATE GYROS • 1 PENDULOUS ACCELEROMETER • GIMBAL ASSEMBLY • SMALL DIGITAL COMPUTER • POWER SUPPLIES	• 3 RATE INTEGRATING GYROS • 3 RATE GYROS • 1 PENDULOUS ACCELEROMETER • GIMBAL ASSEMBLY • SMALL ANALOG COMPUTER • POWER SUPPLIES
SIZE WEIGHT POWER	790 IN^3 31.5 LB 70 WATTS	APPROX SAME	25% LARGER 25% MORE WEIGHT 20% MORE POWER	30% LARGER 25% MORE WEIGHT 25% MORE POWER
DE-ORBIT THRUST POINTING ERROR	$\pm 0.81°$ (3σ)	$\pm 0.88°$ (3σ) *INCLUDES ANALOG INTEGRATOR DRIFT	$\pm 0.81°$ (3σ)	$\pm 0.81°$ (3σ)
RELIABILITY (ESTIMATED MTBF RANGE)	2,500–4,800 HOURS	APPROX SAME AS (I)	400–1,000 HOURS	APPROX SAME AS (III)
STERILIZATION & DEVELOPMENT STATUS	STERILIZABLE STRAPPED DOWN SENSORS(GYROS, ACCELEROMETERS) AND DIGITAL COMPUTER CIRCUITRY HAVE BEEN DEVELOPED	SAME AS (I): PARAMETER SHIFTS OF ANALOG CIRCUITS UNDER STERILIZATION IS POTENTIAL PROBLEM–DIGITAL LOGIC ENHANCES STERILIZATION QUALIFICATION	NO STERILIZABLE INERTIAL PLATFORM IN DEVELOPMENT. POTENTIAL PROBLEMS WITH PLATFORM GIMBAL LUBRICANTS, BEARINGS, AND SLIP RINGS UNDER STERILIZATION ENVIRONMENT.	SAME AS (III) PLUS POTENTIAL ANALOG CIRCUITRY STERILIZATION PROBLEM – DIGITAL LOGIC ALLOWS WIDER CIRCUIT TOLERANCES.
FLEXIBILITY	VERY FLEXIBLE–ONLY COMPUTER MEMORY UPDATES NECESSARY FOR MISSION PROFILE CHANGES. SEQUENCING AND TIMING FUNCTION CAN ALSO BE ACCOMPLISHED WITHOUT ADDITIONAL HARDWARE.	INHERENTLY INFLEXIBLE–A CHANGE IN MISSION PROFILE CAN REQUIRE ELECTRONICS CHANGE AT FACTORY AND POSSIBLE REQUALIFICATION.	SAME AS (I)	(SAME AS (II)

Both magnetic core and plated wire memory technologies were studied for the digital computer mechanization. This evaluation for units of the same capacity and operational speeds is summarized in Table 3.2.4-2. The power consumption advantage of the plated wire memory system is not significant for these short missions due to its heavier weight. Moreover, each unit can be programmed to idle all unnecessary logic during the descent phase (the longest duration). This further reduces the effective power consumption advantage of the plated wire technique. The magnetic core memory system is preferred on the basis of development status.

The computer capacity and speed characteristics are based on a recent refinement to the prototype program analyses, word length studies, and growth capability considerations of Reference 3.2.4-2. The prototype program analyses indicate a requirement for 1678 permanent memory words and 286 variable data words. This allows a 46% and 53% growth capability on the permanent and variable word capacities, respectively, assuming the 4096 word (512 variable) unit. This growth capability is sufficient to permit inclusion of the capsule sequencing and checkout testing functions. Also, capacity is available for future mission growth to a full attitude control technique. The prototype program analyses of equation complexity, program control routines, and maximum iteration speeds allow a serial arithmetic processor with an add time of 14 μ sec and a multiply time of 154 μ sec. The 20 bit word of 19 bits data plus 1 sign bit is required to satisfactorily limit the round off error in the inertial attitude equation calculations.

3.2.4.1.2 Attitude Control Concept Alternatives: Alternative attitude stabilization techniques and modes have been studied for the mission phases prior to atmospheric entry. These alternates were studied to evaluate possible system and overall mission weight reductions. All concepts are assumed to follow the same atmospheric entry and soft landing control sequence.

Table 3.2.4-3 describes the control sensors, control sequences, deorbit ΔV pointing accuracies, and mission interaction considerations for three pre-entry attitude control concepts. Figure 3.2.4-2 presents only the control electronics system and power consumption requirement weights for each of the

TABLE 3.2.4–2

GUIDANCE & CONTROL DIGITAL COMPUTER MECHANIZATION COMPARISON

CHARACTERISTIC	MAGNETIC CORE TECHNOLOGY	PLATED WIRE TECHNOLOGY
TYPE, CAPACITY, SPEED	TYPE: SERIAL OPERATION CAPACITY: 4096 WORDS AT 20 BITS/WORD, OF WHICH 512 ARE ELECTRICALLY ALTERABLE SPEED: ADD TIME = 14 μ SEC MULT TIME = 154 μ SEC	
SIZE	338 IN.^{3}	375 IN.^{3}
WEIGHT	14.6 LB	16.0 LB
POWER	30.0 WATTS MAX INCLUDES POWER SUPPLY	20.0 WATTS MAX INCLUDES POWER SUPPLY
STATE OF DEVELOPMENT	MOST COMMON SPACE QUALIFIED MEMORY	LIMITED PREVIOUS APPLICATIONS
VOLATILITY	DRO	NDRO

TABLE 3.2.4–3

PRE-ENTRY ATTITUDE CONTROL CONCEPT COMPARISONS

CHARACTERISTIC OR PHASE	FULLY ACTIVE	ACTIVE/SPIN	SPIN
• CONTROL SYSTEM	RATE INTEGRATING GYROS, VELOCITY METER, COLD GAS JETS	RATE INTEGRATING GYROS, VELOCITY METER, COLD GAS JETS	RATE INTEGRATING GYROS, VELOCITY METER, 2 SOLID SPIN ROCKETS, COLD GAS JETS
• SEPARATION	CAPSULE REACTION JETS	CAPSULE REACTION JETS	MANEUVER SUPPORT SPACECRAFT, SPRING EJECTION
• SEPARATION THROUGH ΔV BURN	MANEUVER CAPSULE, ACTIVE HOLD TO $\pm 0.25^\circ$ DEADBAND, COMPUTED INERTIAL ATTITUDE	MANEUVER CAPSULE, ACTIVE HOLD TO $\pm 0.25^\circ$ DEADBAND, COMPUTED INERTIAL ATTITUDE	SPIN STABILIZED AT 46.5 RPM
• ΔV POINTING ERROR, $\Delta\beta$	$\pm 0.81^\circ$ (3σ)	$\pm 0.81^\circ$ (3σ)	$\pm 1.10^\circ$ (3σ)
• POST ΔV BURN TO ENTRY	MANEUVER FOR ENTRY ALIGNMENT, ACTIVE HOLD TO $\pm 3.0^\circ$ DEADBAND	MANEUVER FOR ENTRY ALIGNMENT, SPIN TO 8.6 RPM, DE-ACTIVATE SYSTEM	SPIN STABILIZED
• ENTRY ENCOUNTER	SWITCH TO ENTRY MODE AT 0.05 g's	ACTIVATE SYSTEM, DESPIN BY COLD GAS AT 0.05 g AND SWITCH TO ENTRY MODE	DESPIN BV COLD GAS AT 0.05 g AND SWITCH TO ENTRY MODE
• MISSION CONSIDERATIONS	• PROVIDES PREFERRED ROLL REFERENCE FOR RADAR ALTIMETER • ALLOWS COMPUTER TO ALSO PERFORM SEQUENCING FUNCTION • ALLOWS GYRO DRIFT COMPENSATION	• DOES NOT PROVIDE A ROLL REFERENCE AT ENTRY • REQUIRES SEPARATE SEQUENCER & TIMER	• REQUIRES ORBITER MANEUVER TO EJECT LANDER • DOES NOT PROVIDE ROLL REFERENCE AT ENTRY • REQUIRES SEPARATE SEQUENCER & TIMER

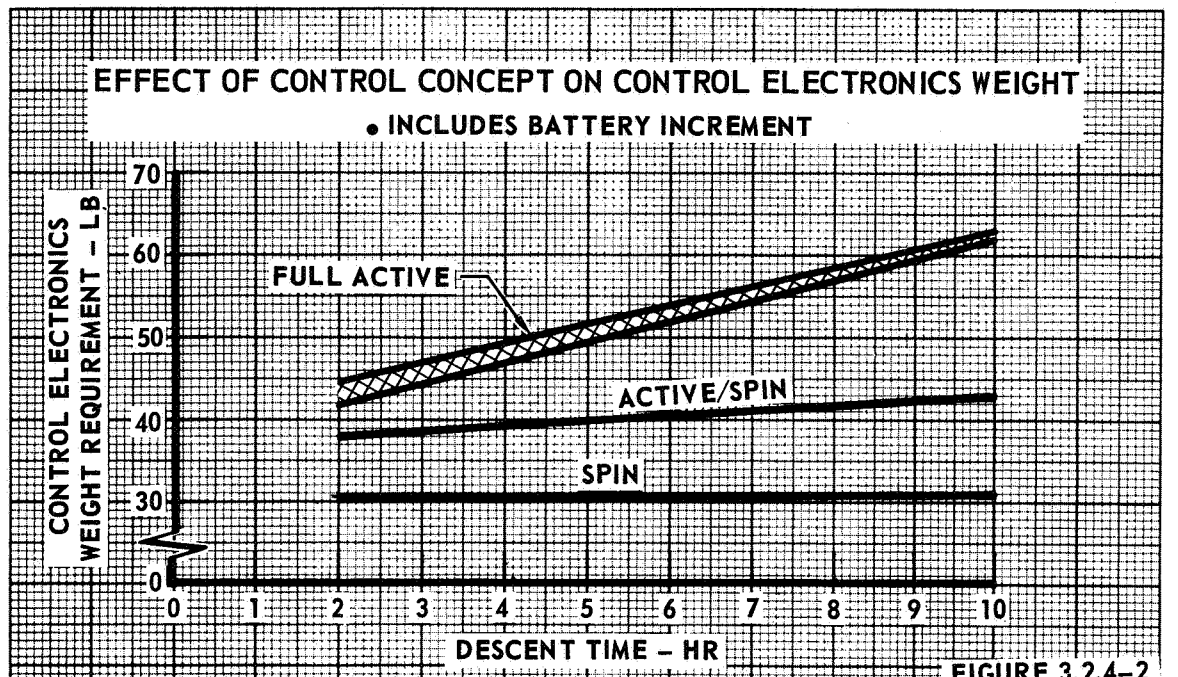

FIGURE 3.2.4–2

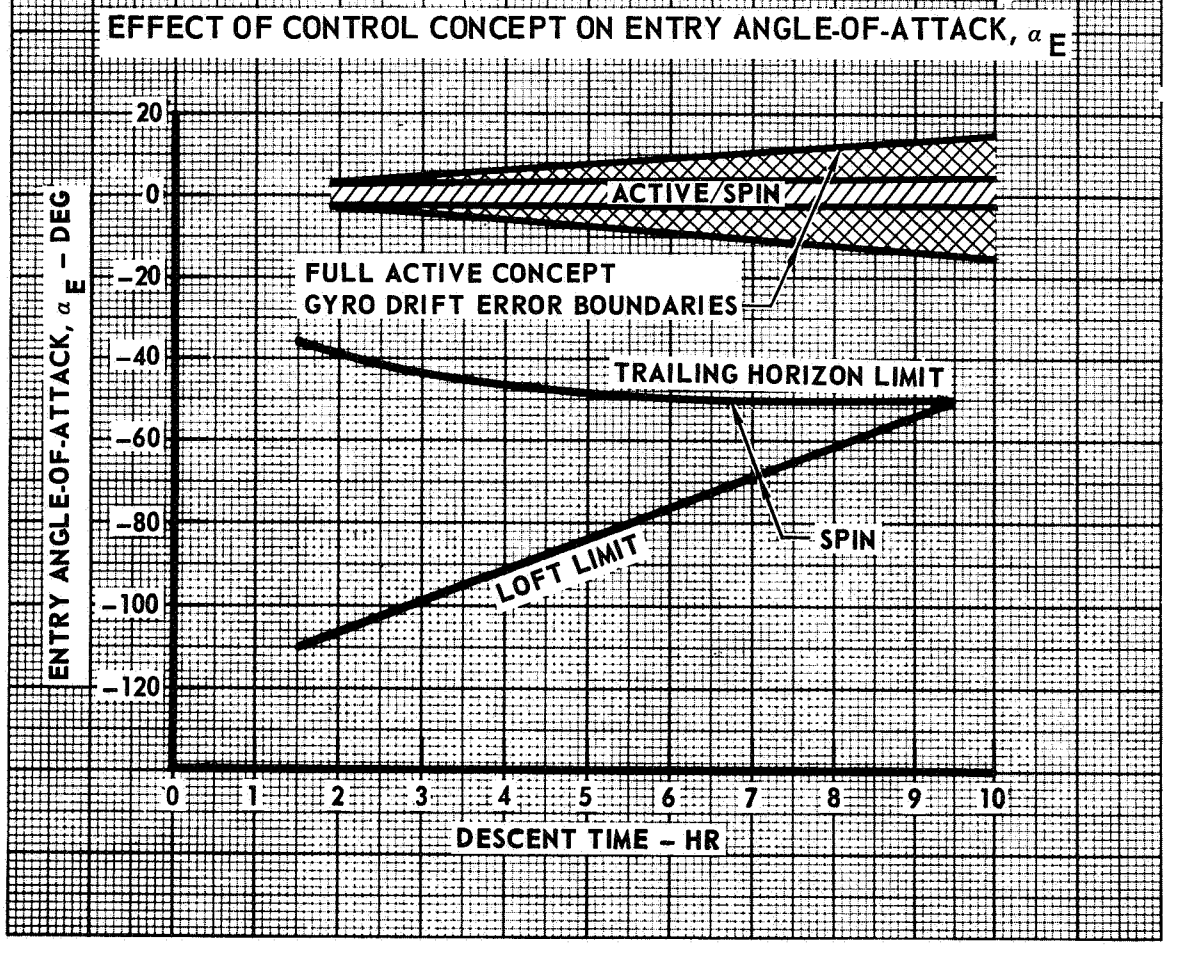

FIGURE 3.2.4–3

three concepts over the entire spectrum of descent times. Figure 3.2.4-3 shows the entry angle-of-attack (α_e) control accuracy associated with each concept. A zero angle-of-attack condition is preferred for stable entry dynamics. The high entry angles-of-attack associated with the spin stabilization concept render it an unacceptable technique.

The range of weights for the full active system, as shown in Figure 3.2.4-2, includes both the use of magnetic core and plated wire computers, and the use of computed or "derived" rate during the descent phase. For the "derived" rate technique the computer is turned off and replaced by pulse ratio modulation circuits. For the computer calculated inertial attitude technique the computer logic is idled when possible; this technique permits almost a 50% reduction in computer power during this low disturbance phase. For the small weight differences (within this concept), the use of the computer to calculate inertial attitude has the advantage of minimizing coning errors.

The Figure 3.2.4-4 provides an overall vehicle weight assessment for each of the pre-entry control concepts. These integrated systems data provide the primary bases for selection of a preferred control concept. The weight data of Figure 3.2.4-4 is based on a design study for a 2,000 lb vehicle. Although the spin concept results in unacceptable entry angle-of-attack conditions, its integrated vehicle weight budget is presented in Figure 3.2.4-4. This data shows the concept is also unacceptable on an overall vehicle weight requirement basis.

The full active concept requires less net vehicle weight than the active/spin technique for descent times less than 5.5 hours. A full active approach is preferred because other mission and system parametrics show a preference for descent times of approximately 3.5 hours (equivalent to de-orbit anomaly of 215 deg.). The full active system is also most attractive for its high degree of systems integration and preferred roll attitude capability. The incorporation of the pre-landing sequencing functional capability into the guidance computer eliminates the weight, development, and integration of two other digital memory units (see section 3.2.5). The preferred roll capability at entry provides favorable conditions for operation of the radar altimeter. The entry angle-of-attack (α_e) control capability of this concept is limited

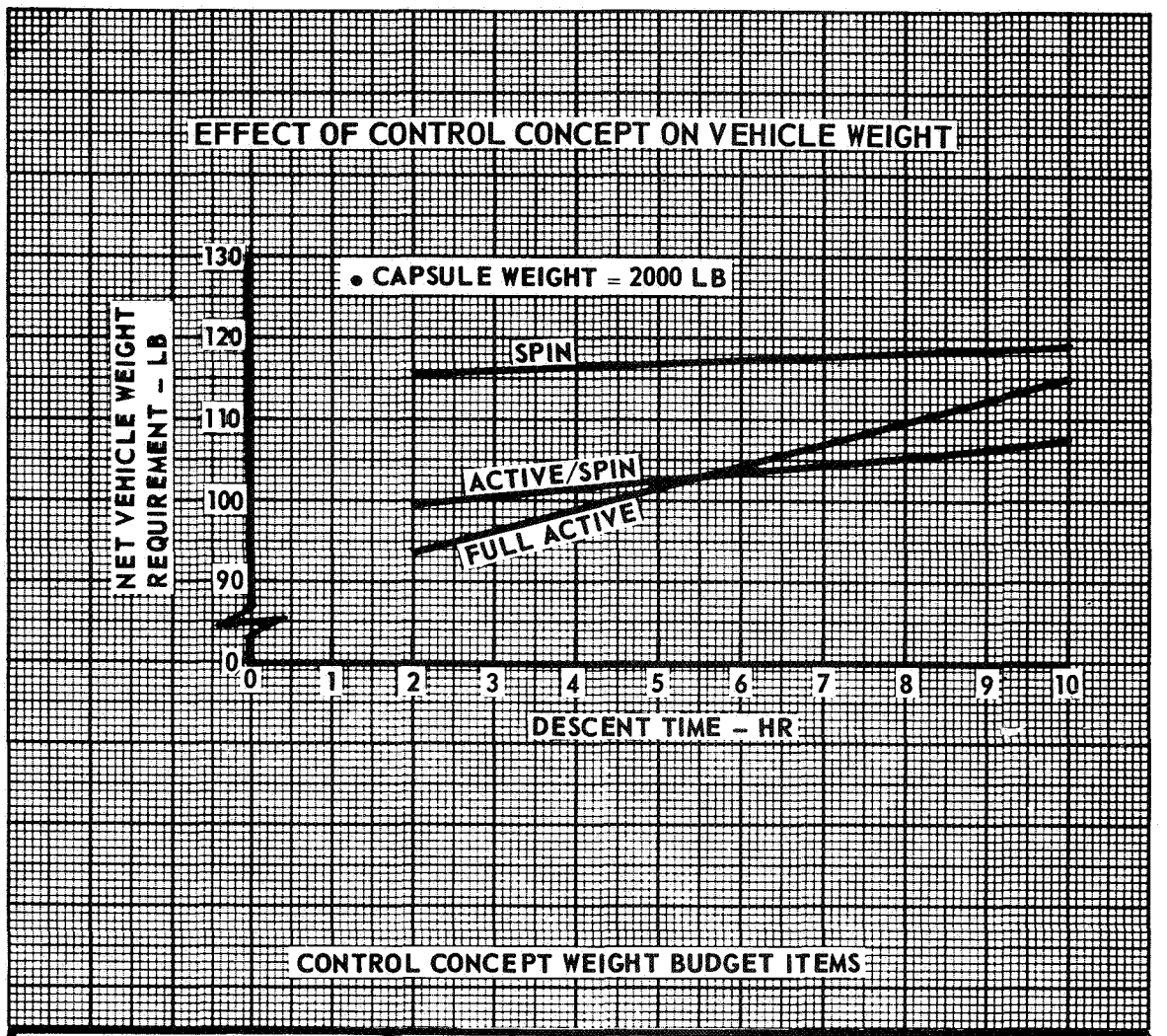

CONTROL CONCEPT WEIGHT BUDGET ITEMS

ACTIVE	SPIN/ACTIVE	SPIN
• CONTROL ELECTRONICS AND BATTERY INCREMENT	• CONTROL ELECTRONICS AND BATTERY INCREMENT	• CONTROL ELECTRONICS AND BATTERY INCREMENT
• REACTION CONTROL JET HARDWARE & FUEL	• REACTION CONTROL JET HARDWARE & FUEL	• REACTION CONTROL JET HARDWARE & FUEL, SPRING EJECTION ASSEMBLY, SOLID SPIN ROCKETS
• COMPUTER PERFORMS SEQUENCING & TIMING	• SEPARATE SEQUENCER AND TIMER MODULE	• SEPARATE SEQUENCER AND TIMER MODULE
• SHAPED(FAN) BEAM RADAR ALTIMETER	• OMNI-DIRECTIONAL RADAR ALTIMETER	• OMNI-DIRECTIONAL RADAR ALTIMETER
		• AEROSHELL HEAT SHIELD WEIGHT INCREMENT FOR LARGE α_e

FIGURE 3.2.4–4

by the gyro drift limits, assumed as ± 1 deg/hr (3σ) in Figure 3.2.4-3. The entry angle-of-attack control accuracy for this concept can be improved to ± 3.1 deg (3σ) by a gyro drift test prior to separation and updating the gyro compensation terms in the computer routines.

3.2.4.2 Landing Radar Systems. - A landing radar system is required to measure the Martian surface referenced velocity vector, and to measure slant range along the lander roll axis. For the landing concepts considered here, landing radar operation is not required before aeroshell separation.

3.2.4.2.1 Requirements and Constraints: The most significant requirements for the landing radar design are listed below.

a) Provide continuous roll axis slant range measurement and 3-axis velocity vector measurement from parachute release to engine cut-off.

b) Provide terminal phase measurement errors (3σ) less than ±1.4% ±5 ft. for range and ±1.5% ±1.5 fps for resolved velocity components.

c) Provide the capability for checkout of the radar after canister enclosure and during flight.

Additional requirements and constraints result from consideration of the following factors: exhaust plumes, reflected signals, vibrations, acoustical noise, the range of dynamic variations in the vehicle attitude and position, uncertainties in the surface slope and radar backscatter model, sterilization, and long in-flight storage.

3.2.4.2.2 Candidate Systems: Using the above described constraints and requirements, representative baseline landing radar systems have been configured with characteristics shown in Table 3.2.4-4. The specific modulation combinations considered are CW-FM/CW with continuous wave modulation for velocity sensing and continuous wave frequency modulation for ranging, and Bessel sideband FM/CW with sinusoidal frequency modulation for both range and velocity sensing.

The accuracy estimates of Table 3.2.4-4 are based on computer simulations of the CW-FM/CW system as described in Reference 3.2.4-1. These range and velocity (resolved orthogonal components) errors are indicative of the terminal landing phase performance, and are considered representative of each system type for equivalent beamwidth, beam configuration, smoothing time, etc.

TABLE 3.2.4–4

LANDING RADAR ALTERNATIVES

	LM RADAR MINIMUM CHANGE	FIVE BEAM LM RADAR	LM RADAR MINIMUM WEIGHT	BESSELL SIDEBAND RADAR
DESCRIPTION	THREE CW VELOCITY BEAMS. ONE LINEAR FM RANGE BEAM.	FOUR CW VELOCITY BEAMS. ONE LINEAR FM RANGE BEAM.	THREE CW VELOCITY BEAMS. ONE LINEAR FM RANGE BEAM.	FIVE SINUSOIDAL FM RANGE AND VELOCITY BEAMS
MAXIMUM ALTITUDE	66,000 FT	66,000 FT	> 66,000 FT	8000 FT
RANGE ACCURACY (3σ)	± 1.4% ± 5 FT	± 1.4% ± 5 FT	± 1.4% ± 5 FT	± 1.4% ± 5 FT
VELOCITY ACCURACY (3σ)	± 1.5% ± 1.5 FPS	± 1.5% ± 1.5 FPS	± 1.5% ± 1.5 FPS	± 1.5% ± 1.5 FPS
ANTENNA	WAVEGUIDE ARRAY 3.6 SQ FT	WAVEGUIDE ARRAY 6.2 SQ FT	WAVEGUIDE ARRAY 3.6 SQ FT	WAVEGUIDE ARRAY 3.7 SQ FT
TOTAL WEIGHT	37 LB	41 LB	30 LB	30 LB
PRIMARY POWER	137 WATTS	145 WATTS	65 WATTS	50 WATTS
STATUS	CURRENTLY IN FLIGHT TEST. AVAILABLE FOR 1973.	MODIFICATIONS NOT READILY AVAILABLE FOR 1973	MODIFICATIONS NOT READILY AVAILABLE FOR 1973	BREADBOARD EXISTS. FLIGHT TESTS PLANNED. NOT AVAILABLE FOR 1973.

The physical characteristics of Table 3.2.4-4 represent the basic systems, and do not include such possible additions as redundant components. A minimum self-test capability, consisting of IF pilot signal injection, is included. It is estimated that more extensive self-test capability (e.g., including RF signal injection) would increase system weight by 1 to 3 lb and power consumption by 3 to 6 watts. In addition, approximately 2 lb of microwave absorbing material is required on the aeroshell interior for checkout after canister enclosure.

A Lambert law radar backscatter model is assumed for the data of this section. The Lambert model vertical incidence radar backscatter coefficient, σ_o, used is -17 dB. Studies indicate that the best Muhleman model fit to the average Mars spectrogram yields a vertical incidence backscatter coefficient equal to + 13.8 dB with the Muhleman slope parameter, α, equal to 0.066. The more conservative (with regard to signal level) Lambert law model is used to allow for observed variations in the Martian average data and for local surface anomalies.

The salient features of these baseline landing radar systems are discussed below. The applicability of the CW-FW/CW system is examined in greater detail because of its advanced development status and the availability of performance data.

Minimum Change LM Radar - This landing radar configuration represents a minimum modification to the existing Lunar Module (LM) landing radar. Three velocity beams employing continuous wave modulation and one range beam employing sawtooth frequency modulation are generated from a single planar array. Range beam velocity compensation is required. The range beam is positioned at the beam group centerline along the roll axis and between the two external velocity beams. The velocity beams are positioned at clock angles of 0, 110, and 180 degrees with half cone angles equal to 25 degrees. This beam configuration corresponds to that originally planned for LM, for which an engineering antenna model has been fabricated and tested.

The performance of the LM type landing radar in a Martian landing situation has been examined in Reference 3.2.4-1, and found to be generally acceptable when properly integrated with the total landing concept. Specific performance

limitations that result in total system constraints include near zero doppler operation, excessive attitude rates, and post-separation aeroshell interference.

The near-zero doppler problem results from the effective increase in radar receiver noise figure at low doppler frequencies due to vibration, acoustical noise, reflected signals, etc. The velocity beam doppler shift is proportional to the beam projected component of the total Martian referenced velocity vector (aerodynamic plus steady state wind). Representative 5,000 ft. altitude radar acquisition cases for three Martian atmospheric models are shown in Figure 3.2.4-5. (The actual acquisition conditions vary with parachute deployment altitude, parachute diameter, radar acquisition altitude, etc.) In the figure, the signal-to-noise ratio of the minimum doppler beam as a function of the angle between the beam and the aerodynamic velocity vector is shown. For the worst case roll position considered, this angle is the sum of the beam configuration half cone angle, α, and the lander pitch attitude deviation, β, from the nominal aerodynamic velocity vector alignment condition. The angle, β, may be considered to represent either the wind gust induced attitude perturbation during the parachute descent phase, or the attitude hold error after parachute release. The figure indicates that for $\alpha = 25$ degrees the maximum allowable value of β is about 10 degrees. This immediately eliminates continuous landing radar operation during the parachute descent phase, because wind gust responses far in excess of 10 degrees are possible. For landing radar acquisition during a post-parachute release, attitude hold mode, a minimum pitch attitude hold error is required.

In the event of excessive attitude hold errors resulting in near-zero doppler conditions, the conditional Reliable Operate (CRO) mode may be employed, where the normal velocity vector alignment maneuver is initiated on the basis of a conditional zero doppler indication from the beam that fails to acquire. If the acquisition failure is due to the low frequency, high noise figure problem, the maneuver yields a positive doppler, and acquisition occurs. The CRO mode was incorporated on the Surveyor radar.

Figure 3.2.4-6 presents the range beam pitch attitude rate tracking limits as a function of beam incidence angle for altitudes equal to 5000, 10 000 and 15 000 ft. Estimated parachute gust response data (Reference 3.2.4-3) are

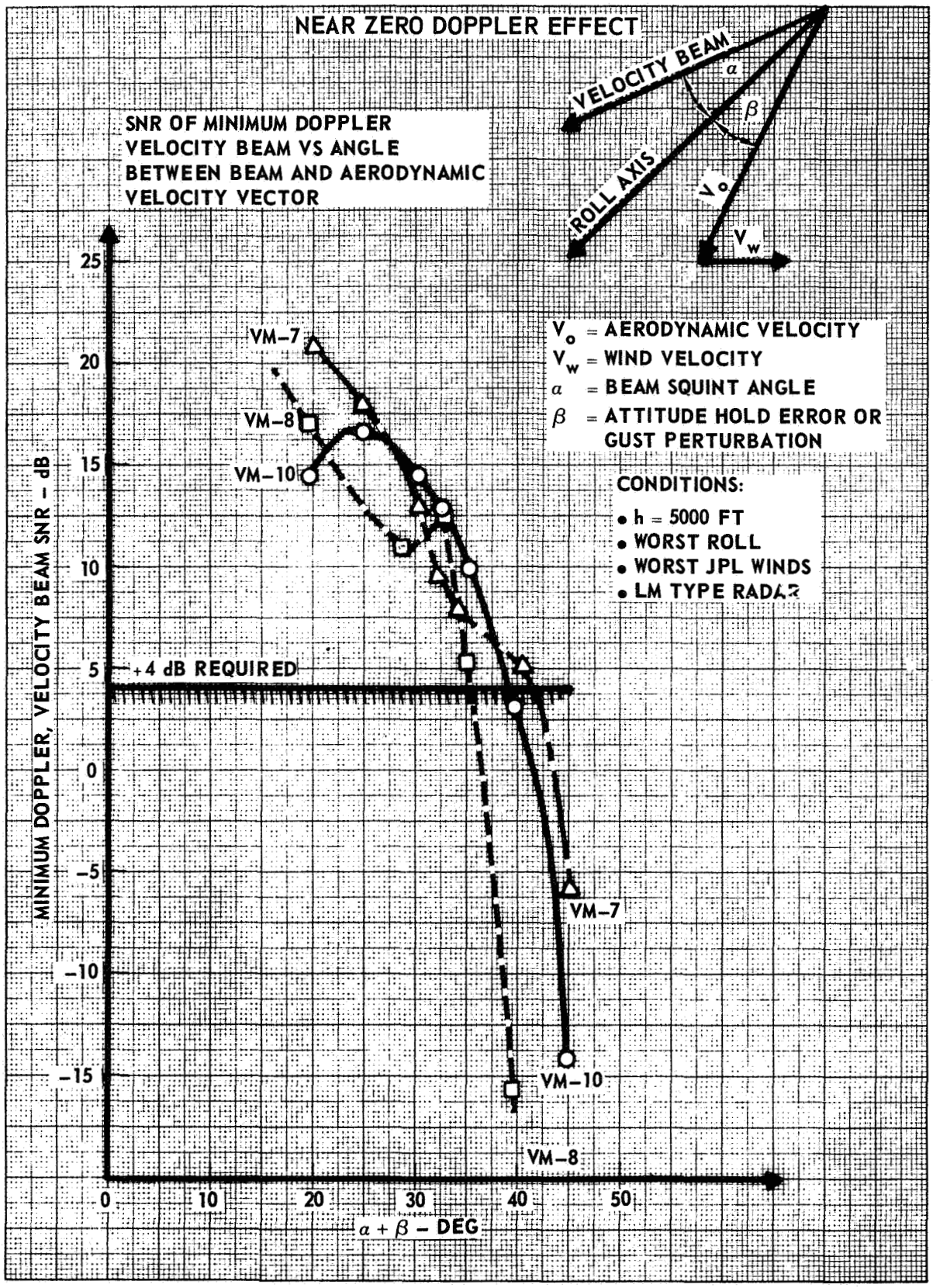
NEAR ZERO DOPPLER EFFECT
SNR OF MINIMUM DOPPLER VELOCITY BEAM VS ANGLE BETWEEN BEAM AND AERODYNAMIC VELOCITY VECTOR
VELOCITY BEAM
ROLL AXIS
α
β
V o
V w
V o = AERODYNAMIC VELOCITY
V w = WIND VELOCITY
α = BEAM SQUINT ANGLE
β = ATTITUDE HOLD ERROR OR GUST PERTURBATION
CONDITIONS:
• h = 5000 FT
• WORST ROLL
• WORST JPL WINDS
• LM TYPE RADAR
+4 dB REQUIRED
VM-7
VM-8
VM-10
MINIMUM DOPPLER, VELOCITY BEAM SNR – dB
25
20
15
10
5
0
-5
-10
-15
0
10
20
30
40
50
α + β – DEG

FIGURE 3.2.4–5

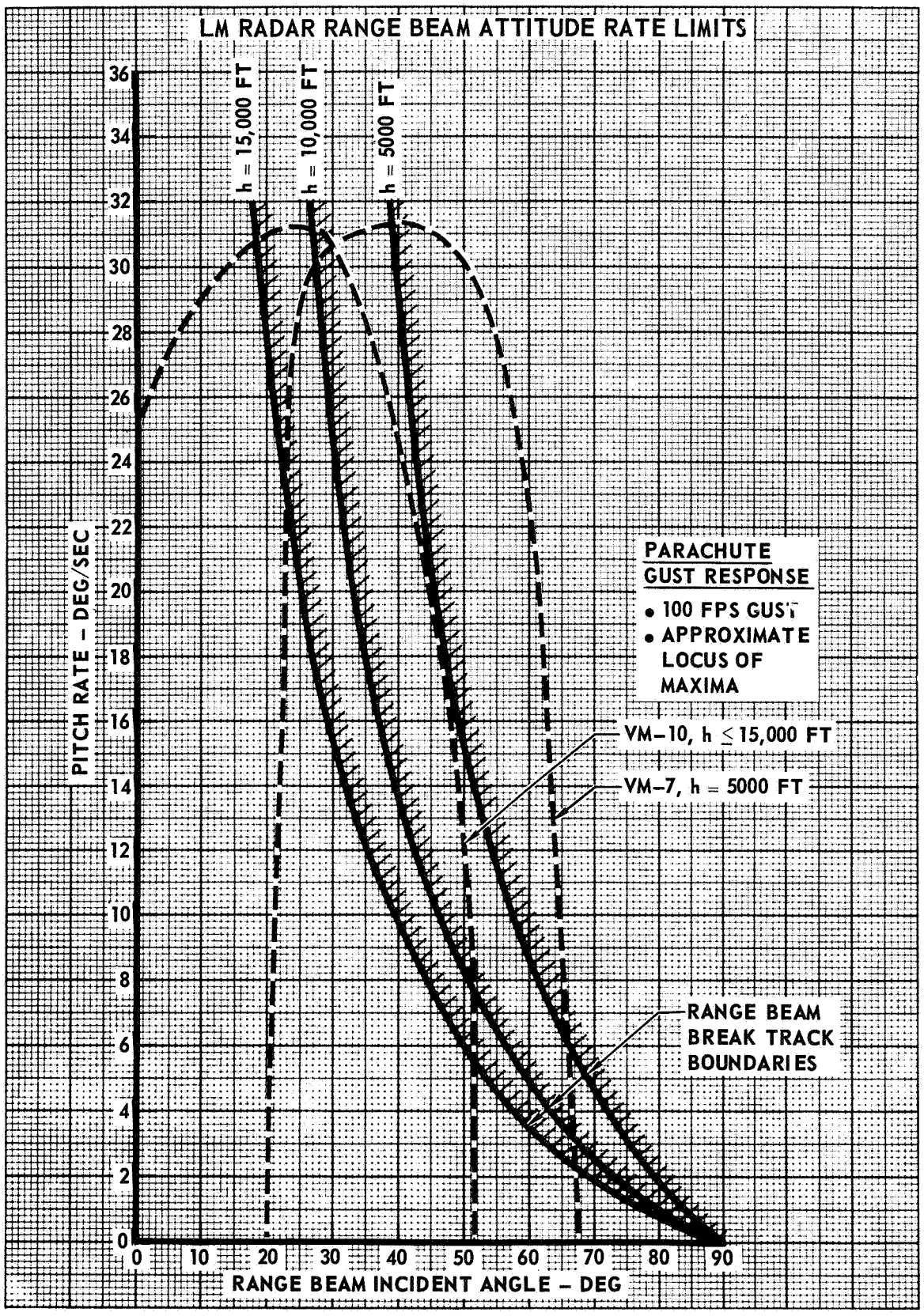
LM RADAR RANGE BEAM ATTITUDE RATE LIMITS
h = 15,000 FT
h = 10,000 FT
h = 5000 FT
PITCH RATE – DEG/SEC
0
2
4
6
8
10
12
14
16
18
20
22
24
26
28
30
32
34
36
0
10
20
30
40
50
60
70
80
90
RANGE BEAM INCIDENT ANGLE – DEG
PARACHUTE GUST RESPONSE
• 100 FPS GUST
• APPROXIMATE LOCUS OF MAXIMA
VM–10, h ≤ 15,000 FT
VM–7, h = 5000 FT
RANGE BEAM BREAK TRACK BOUNDARIES

FIGURE 3.2.4–6

superimposed. As the figure indicates, continuous operation of the range beam during parachute descent is not generally possible.

The problem of operating the landing radar in the presence of an airborne aeroshell (after separation from the lander), results from the large radar cross section of the aeroshell (e.g., up to 4000 sq. ft., Reference 3.2.4-1). The signal returned from the aeroshell can interfere with the minimum change LM radar operation by either (1) inhibiting acquisition and continuous tracking of the desired signal on a particular radar beam, or (2) being mistakenly acquired and tracked as the desired signal.

The aeroshell signal can inhibit acquisition and continuous tracking of the desired signal in either of two ways. First, if the aeroshell negative doppler frequency is equal in magnitude to the desired signal positive doppler frequency, direct signal competition will result. This is due to the LM radar double sideband rejection logic, wherein the detection decision is based upon comparing the power at the tracking frequency with that at the image frequency. Calculations indicate that this mechanism can impair proper radar operation for aeroshell to lander ranges as great as 1500 and 27 000 feet for the aeroshell echo in the landing radar sidelobes and main lobe respectively. Secondly, an aeroshell echo of sufficient level can effectively desensitize the radar receiver by causing a discrete AGC gain state switch. Calculations indicate that this can occur for aeroshell to lander ranges as great as 150 and 2 700 feet for the aeroshell echo in the landing radar sidelobes and main lobe respectively.

In addition, the aeroshell echo strength is sufficient to result in erroneous acquisition for lander to aeroshell ranges as great as 1 500 and 27 000 feet in the radar sidelobes and main lobe respectively. Whether or not acquisition actually occurs depends upon aeroshell lander relative velocity, lander attitude, and the frequency search limits of the radar tracking filters.

No redundant range or velocity beams are provided in the minimum modification LM landing radar described here. Consequently, aeroshell echo signal interference in any single beam will result in a loss of either range or velocity information. Possible LM type radar modifications to minimize this problem are discussed below; however, none of these are considered consistent with a minimum change LM type landing radar. This consideration then requires

that the terminal descent concept be configured to provide sufficient spatial isolation between the landing radar and aeroshell. This requirement can be satisfied by appropriate design of other terminal descent system, (e.g., the Voyager terminal descent concept was configured to provide aeroshell surface impact before landing radar operation).

On the basis of the above considerations the recommended operation of a minimum change LM landing radar is summarized below.

a) Enable radar during parachute descent. Proper operation of the radar can be verified although continuous signal tracking is not generally possible.

b) Employ a wide beamwidth radar altimeter to generate the parachute release mark.

c) Select a terminal descent technique that minimizes potential aeroshell interference.

d) Employ a minimum pitch error attitude hold mode after parachute release, to allow landing radar acquisition under favorable doppler and beam incidence angle conditions.

e) Incorporate the CRO mode as a backup function for potential near zero doppler conditions.

Possible modifications and additions to the minimum change LM landing radar include addition of a fourth velocity beam, and/or range beam modulation switching. A four velocity beam LM type radar is described in Reference 3.4.2-1, and the characteristics are given in Table 3.4.2-4. Current estimates indicate that weight and power requirements would be increased by 4 lb and 8 w relative to the minimum change LM system. Addition of the fourth velocity beam increases the success probability of the landing radar alone from 0.9781 to 0.9865. In addition, with four beams operating, the attitude capability is significantly improved.

Effective velocity beam redundancy can be provided with a three velocity beam configuration by adding an on/off modulation switching mode to the range beam. In the event of a velocity beam failure, alternate periods of CW modulation for velocity measurement and FM/CW for range measurement would be trans-

mitted. This mode of operation would result in degraded parameter measurement accuracy due to increased time lag errors, decreased data smoothing times, etc. This mode can be implemented by modifying the range beam tracker (a second tracker is not required) and data converters for a small increase in power and weight requirements. The modulation switching could also be used to discriminate against the aeroshell interfering signal.

Further extensions and modifications beyond the minimum change LM landing radar have been considered to improve performance in the presence of the airborne aeroshell. As an example, one possible approach is described below. A five beam configuration similar to that of Table 3.2.4-4 and Reference 3.2.4-1 is used. Four beams are positioned symmetrically about the roll axis, and the fifth beam is positioned along the roll axis. CW modulation velocity measurement capability is provided on three of the four symmetrical beams. Range and velocity measurement capability is provided on the roll axis beam and the remaining external beam. The measurement of both range and velocity on a single beam can be accomplished by using either triangular FM/CW periods of pure CW modulation. The velocity measurement capability along five beams allows comparison among sets of three to identify which beam yields inconsistent data, (e.g., due to the aeroshell tracking). Thus, the best three beam set is used for the velocity vector measurement. The roll axis beam is normally used for the range measurement. However, if the velocity beam comparison data indicates a failure in this beam, range information from the external ranging beam is used. This logic effectively combats the problem of false acquisition of the aeroshell by any single beam.

The redundant beams will also minimize the problem of degradation of receiver sensitivity due to aeroshell signal interference (i.e., AGE gain state switching and/or signal masking via the double sideband image filter). These modifications eliminate the problem of aeroshell interference in a beam main lobe and allow operation for aeroshell-to-lander ranges greater than 1500 feet. At 1500 feet, simultaneous multi-beam sidelobe interference becomes a potential problem. Range and velocity measurement closer than 1500 feet is possible provided that sidelobe jamming does not occur in more than one beam simultaneously. If additional individual beam discrimination logic based on range and velocity measurements is incorporated, the capability can be extended further to allow

potential false lock interference in two velocity beams simultaneously. The minimum tolerable aeroshell-to-lander range will occur at about 150 feet where gain state switching in the sidelobes of more than two velocity beams or more than one range beam can render the system insensitive to the desired signal. This radar configuration represents a redesign using established LM techniques as a basis, and is not considered readily available for a 1973 mission.

Minimum Weight LM Radar - This system is functionally equivalent to the minimum change LM radar configuration. However, the size, weight, and primary power estimates are based on using step recovery diode frequency multipliers in place of the varactor multipliers in the transmitters, greater use of integrated circuits, and associated repackaging. These modifications are not considered readily available for a 1973 mission.

Bessel Sideband Radar - The specific configuration considered here employs five sinusoidally frequency modulated beams. Four of the beams are located at half cone angles of 15 degrees and at clock angles of 0, 90, 180, and 270 degrees respectively. The fifth beam is at the beam group centerline and directed along the vehicle roll axis. Velocity is determined on each beam via measurement of the doppler frequency shift on the second order (J_2) Bessel function sideband. Range is determined via measurement of the phase shift on the J_2 sideband. Information from any three of the five beams can be used.

The J_2 processing technique, while more complex than the CW-linear FM/CW method, offers theoretical advantages with regard to discrimination against near zone signals which contribute to the previously mentioned near zero doppler problem. Consequently, antenna space duplexing may not be required. Processing only the J_2 sideband results in a signal power loss greater than 6 dB, increasing with range closure. The high altitude performance of this system is limited by leakage noise and/or range/velocity ambiguities. The optimum modulating frequency varies with altitude. Thus, two or more modulation frequencies are normally employed with mode switching as a function of altitude. The attitude rate capability of this system will be limited at high induced beam range rates as in the case of the LM type radar. Possible Martian wind gust induced attitudes and attitude rates prevent continuous radar operation during parachute descent.

On a per beam basis, the Bessel sideband radar is susceptible to similar aeroshell interference mechanisms (expecting the double sideband signal rejection mechanism) previously described for the minimum change LM landing radar. However, the fact that five range and velocity measuring beams are available in the assumed configuration, allows a performance improvement similar to that previously described for the five beam LM type radar. In addition, with proper design the inherent range as well as velocity discrimination capability can be used to provide additional per beam target resolution capability.

Antenna types considered for this radar configuration include the Luneburg lens, constant K lens, and the planar array. The planar array is generally preferred because the smaller depth dimension. The Luneburg and constant K lenses can be implemented to provide electronic beam tilting to improve incident angles when used with a preferred roll position vehicle. However, problems associated with the Luneburg lens include heat sterilization and development status.

Range and velocity ambiguities limit the maximum altitude of this system. For example, if the maximum doppler frequency is 20 000 Hz, then the maximum beam slant range is limited to about 6300 feet. Consequently, for high range and doppler situations, it has been suggested that interrupted continuous wave (ICW) modulation be used at the higher altitudes. This would increase size, weight, and power requirements.

A breadboard of this type of landing radar has undergone laboratory testing, and a flight test program is planned. FM/CW radars have been used for velocity only measurement for a number of years, but combined range and velocity sensing techniques are less well developed. It is not considered probable that this type of landing radar could be made available for a 1973 mission.

3.2.4.3 Radar Altimeter. - A radar altimeter is required in order to provide continuous altitude information for entry science data correlation, and to provide discrete altitude marks for event sequencing. Discrete altitude marks are required for such functions as parachute deployment, aeroshell release, parachute release, sequencer-timer update, etc.

Previous studies (Reference 3.2.4-2) indicate that the preferred planetary altimetry technique employs non-coherent pulse modulation, leading edge tracking, and a carrier frequency near 1 GHz. Non-coherent pulse modulation is most

commonly used for high altitude measurements because of simplicity, minimum doppler shift effect, and elimination of receiver isolation problems. Leading edge tracking in its various forms is the most common and highly developed pulse altimeter tracking technique. An operating frequency near 1 GHz represents a compromise between operation near 500 MHz to maximize signal-to-noise ratio and higher frequency operation to reduce antenna system size and weight.

3.2.4.3.1 Requirements and Constraints: The primary constraints and requirements affecting the altimeter design are listed below.

a) Provide continuous altitude information, together with discrete altitude marks, from 200 000 ft altitude to landing radar acquisition.

b) Provide maximum accuracy consistent with the maximum operational altitude requirement.

c) Provide the capability for radar checkout after sterilization canister enclosure.

Additional requirements and constraints include electrical breakdown, operation through the aeroshell, reflected signals from the aeroshell after separation, uncertainties in the radar backscatter model and the range of dynamic variations in vehicle attitude and position.

3.2.4.3.2 Radar Altimeter Alternatives: Representative altimeter configurations are listed in Table 3.2.4-5. The primary design variables shown are the antenna system and transmitter. These systems are configured for operation during the aeroshell descent phase. Modifications, as required in some point designs, for post-aeroshell operation to provide a parachute release mark is discussed later.

The three antenna systems considered are a single element T-fed slot for fan beam generation with a preferred roll position vehicle, a three element T-fed slot array for hemispherical coverage, and a nose mounted conical monopole providing hemispherical coverage. Both triode cavity and solid state transmitters are considered.

In order to demonstrate sensitivity to the primary variables in Table 3.2.4-5, specific parameters have been held constant. These include pulse width (5μs), tracker time constant (16 pulse averaging assumed), noise figure

TABLE 3.2.4–5

RADAR ALTIMETER ALTERNATIVES

AEROSHELL DESCENT PHASE

SYSTEM	I	II	III	IV
ANTENNA	NOSE MONOPOLE	THREE AEROSHELL MOUNTED SLOTS	SINGLE SLOT	SINGLE SLOT
PATTERN	HEMISPHERICAL WITH ROLL AXIS NULL	MULTI-LOBED HEMISPHERICAL	90° ROLL x 160° PITCH	90° ROLL x 160° PITCH
TRANSMITTER	TRIODE CAVITY	TRIODE CAVITY	TRIODE CAVITY	SOLID STATE
PEAK POWER	500 WATTS	500 WATTS	500 WATTS	5 WATTS
PULSE WIDTH	5 μ SEC	5 μ SEC	5 μ SEC	5 μ SEC
PRF	500 Hz	500 Hz	500 Hz	500 Hz
FREQUENCY	1 GHz	2 GHz	1 GHz	1 GHz
MAXIMUM ALTITUDE	210 KFT	40 KFT	210 KFT	46 KFT
ACCURACY (3σ)	± 0.16% ± 630 FT	± 3% ± 630 FT	± 0.16% ± 630 FT	± 0.4% ± 630 FT
WEIGHT				
ELEC-TRONICS	13.3 LB	14.0 LB	13.3 LB	10.3 LB
ANTENNA	10.0 LB	3.5 LB	2.2 LB	2.2 LB
PRIMARY POWER	28 WATTS	36 WATTS	28 WATTS	20 WATTS

(5 dB), and two way loss (9 dB). A 5μs pulse was selected to allow operation down to the parachute release altitude with acceptable accuracy, and yet provide sufficient energy for high altitude operation. The 9 dB two way loss accounts for the isolator, circulator, RF switch (for self test), power dividers (for the multi-antenna system), diode gate, and RF window. In addition, peak power has been limited to 500 w to minimize the possibility of electrical breakdown.

In Table 3.2.4-5 the estimated accuracy values assume compensation for bias errors due to altitude change and uncertainty in the surface backscatter model. For purposes of bounding the unknown backscatter model, a range of Muhleman backscatter models (Reference 3.2.4-4) is assumed with the surface slope parameter, α, between 0.01 and 0.10. (A -10dB backscatter coefficient is used for signal strength calculation.) The resultant variation about the mean in the 50% power point on the return pulse is treated as a one sigma error source. Other error sources considered are: bias errors due to tracker bias, receiver delay, and altitude change/antenna pattern effects; flucuating errors due to timing circuit jitter, surface roughness, and thermal noise; and dynamic errors. The one sigma surface roughness error was taken to be 30% of the pulse width based on the 50% power point statistics from the McDonnell Douglas pulse return computer program.

The salient features of the four altimeter systems of Table 3.2.4-5 are described below.

System I - This radar employs a conical monopole antenna located in the nose cap, integrated with the entry science instrumentation similar to that of Reference 3.2.4-2. This integrated science instrumentation/antenna configuration is applicable only to relatively large aeroshells where the radiating element with ground plane may be placed at the nose cap. The resultant pattern provides near hemispherical coverage except for a roll axis null. Advantages of this antenna system include near-hemispherical coverage (as required without a preferred roll position) without the low effective gain regions and multilobed pattern obtained with a multielement system. Primary disadvantages are size and weight.

Primary measurement error contributors are altitude and surface state bias errors, surface roughness, and thermal noise at high altitudes. An additional error not indicated in the Table 3.2.4-5 value results from the roll axis null. This null error is significant only at low altitudes in dense atmospheres and is less than 2%.

The transmitter is a grid pulsed, triode cavity oscillator with 500 w peak power. This combined with the minimum effective gain (0 dB) of the conical monopole antenna allows operation to 210 000 feet.

System II - This configuration is similar to System I with the exception of the antenna system and the operating frequency. The antenna system is a three element, T-fed, slot array. The three slots are located at 120 degree increments around the aeroshell for near hemispherical coverage. An operating frequency of 2 Hz reduces total antenna system weight to 3.5 lb, including power divider and coax. The three element array provides multi-lobed coverage in the forward hemisphere with effective one way gain varying between +3 and -8 dB.

The change in antenna system and frequency combine to reduce the performance of the system relative to System I. The multi-lobed antenna pattern results in altitude measurement errors estimated to be 3% (3σ). The increased λ^2 loss together with the minimum effective gain of -8 dB reduce the maximum operational altitude to about 40 000 ft. The primary power and electronic assembly weight requirements increase due to the frequency increase.

The primary advantage of this system is the hemispherical coverage provided for operation in a random roll position using an antenna system that can be implemented on a small aeroshell. The primary disadvantages are the lower maximum altitude and decreased accuracy.

System III - This radar is identical to System I except that the nose located conical monopole antenna is replaced by a single slot antenna to provide 90 x 160 degree coverage. The wide beamwidth is in the pitch plane, and a preferred roll position is required. With a preferred roll position, the maximum altitude capability and altitude measurement accuracy are similar to System I. The antenna is about 7 lb lighter.

System IV - This configuration is identical to System III except that the 500 w triode cavity transmitter is replaced by a 5 w solid state transmitter. This decrease in peak power reduces the maximum altitude capability to 46 000 feet, and increases the measurement error due to increased thermal noise. Note that identical performance could be obtained without a preferred roll position if the heavier nose mounted conical monopole antenna of System I were used.

This solid state, preferred roll altimeter system represents an attempt to reduce size, weight and power requirements without sacrificing signal processing efficiency. The 5 w peak power at 1 GHz is currently within the state-of-the-art, and greater peak powers will be available for later missions. Larger peak powers are also available at lower frequencies, at the expense of increased antenna weight. For a given transmitter power, the most significant power savings results from the deletion of filament power. The reduced power supply requirements, in turn, reduce the electronics assembly weight. These effects are reflected in Table 3.4.2-5.

3.2.4.3.3 Baseline Alternatives: Possible modifications to the previously described baseline configurations are described below.

Self-Test - The baseline systems include a switch and dummy load for post-sterilization testing. A minimum automatic in-flight checkout capability is provided assuming that the equipment will be exercised in post-sterilization ground testing via external cable from OSE. In-flight checkout then consists of passive monitoring of selected parameters during activation prior to deorbit. A more extensive and automated in-flight test program, similar to that of Reference 3.2.4-2 can be provided by increasing system weight by about 0.75 lb and power by about 3 w.

Redundancy - The baseline configurations include no redundancy features, resulting in an estimated probability of success for the triode cavity systems of 0.9912. (The success probability for the solid state systems would be somewhat greater.) Based on Reference 3.2.4-2, inclusion of redundancy for all altimeter sections but the power supplies and antenna increases the total success probability to 0.9973 with a weight increase of 5 lb and a primary power increase of about 12 w.

Post-Aeroshell Release Operation - Capability is not included in the baseline configuration for operation after aeroshell separation. If a reliable parachute release mark can not be provided by the landing radar (due to excessive attitude rates), radar altimeter operation during parachute descent is required. Such operation requires an additional RF switch mode and a lander located secondary antenna, together with post separation near return receiver banking to minimize aeroshell interference. A linearily polarized cavity backed crossed slot antenna at 1 GHz provides 120 x 120 degrees coverage, and weighs about 3 lb.

Pulse Width Switching - Very low altitude operation requires that a smaller pulse width be used. Addition of a short pulse (e.g., 0.1 us) mode increases system weight by 2.0 lb. and primary power by 8 w, and allows operation to approximately 100 feet. Lower altitude operation requires separate antennas.

SECTION 3.2.4 REFERENCES

3.2.4-1 NASA-CR-89678; Voyager Capsule Phase B Report; Alternatives, Analyses,Selection; Volume II; Part B4; McDonnell Douglas Corp.

3.2.4-2 NASA-CR-89688, Voyager Capsule Phase B Report, Functional Descriptions; Volume II; Part C2; McDonnell Douglas Corp.

3.2.4-3 NASA-CR-89686; Voyager Capsule Phase B Report; Alternatives, Analyses, Selection; Volume II; Part B5; McDonnell Douglas Corp.

3.2.4-4 Muhleman, D.O.; Radar Scattering from Venus and the Moon, Astronomical Journal, Volume 69, No. 1, February 1964, pp. 34-41

3.2.5 SEQUENCER SYSTEM - The sequencer system provides the means for accomplishing, independent of Earth command, the sequential time-based events for:

- o Equipment flight readiness checkout prior to mission commitment.
- o Separation, de-orbit, entry, and landing systems control.
- o Surface mission equipment control.

A ground command update capability is required to permit the updating of critical mission functions such as changing de-orbit maneuver angles and updating time to initiate communications. This update capability is available only in "memory oriented" digital devices.

3.2.5.1 System Configuration Alternatives. - A study was conducted to compare the use of separate devices for each mission phase with the use of an integrated sequences and equipment approach. The choice directly influences entry weight, total system weight, and system complexity. Figure 3.2.5-1 presents three potential systems integration options to perform the three main mission sequences (preseparation checkout, de-orbit and landing flight sequencing, and surface operations control). The surface operations sequencer is always considered separately due to the stringent system internal power and thermoregulation power limitations required to minimize landed payload weight.

The elements of the de-centralization Concept A are the G & C system computer described in Section 3.2.4, and special purpose digital memory devices for the Capsule Sequencer & Timer (CS&T), Test Programmer (TP), and Surface Sequencer & Timer (SS&T). Functional block diagrams and Logic operation of the Capsule Sequencer & Timer, Test Programmer, and Decoder/Drivers are presented in NASA CR 89688 (VOYAGER Capsule Phase B Report, Functional Descriptions; Volume II; Part C2; McDonnell Douglas Corporation.) The Surface Sequencer & Timer is common to all concepts and is similar in design to the Capsule Sequencer & Timer. Table 3.2.5-1 summarizes the analysis of the sequencer element output requirements and growth capabilities for each of the one day and 90 day mission concepts studied. The weight of each of these devices is based on the assumed output circuit capability. The weight differences from those of Reference 3.2.5-1 result from modified mission requirements and more recent vendor equipment design data. The Guidance &

SEQUENCE/HARDWARE INTEGRATION ALTERNATIVES

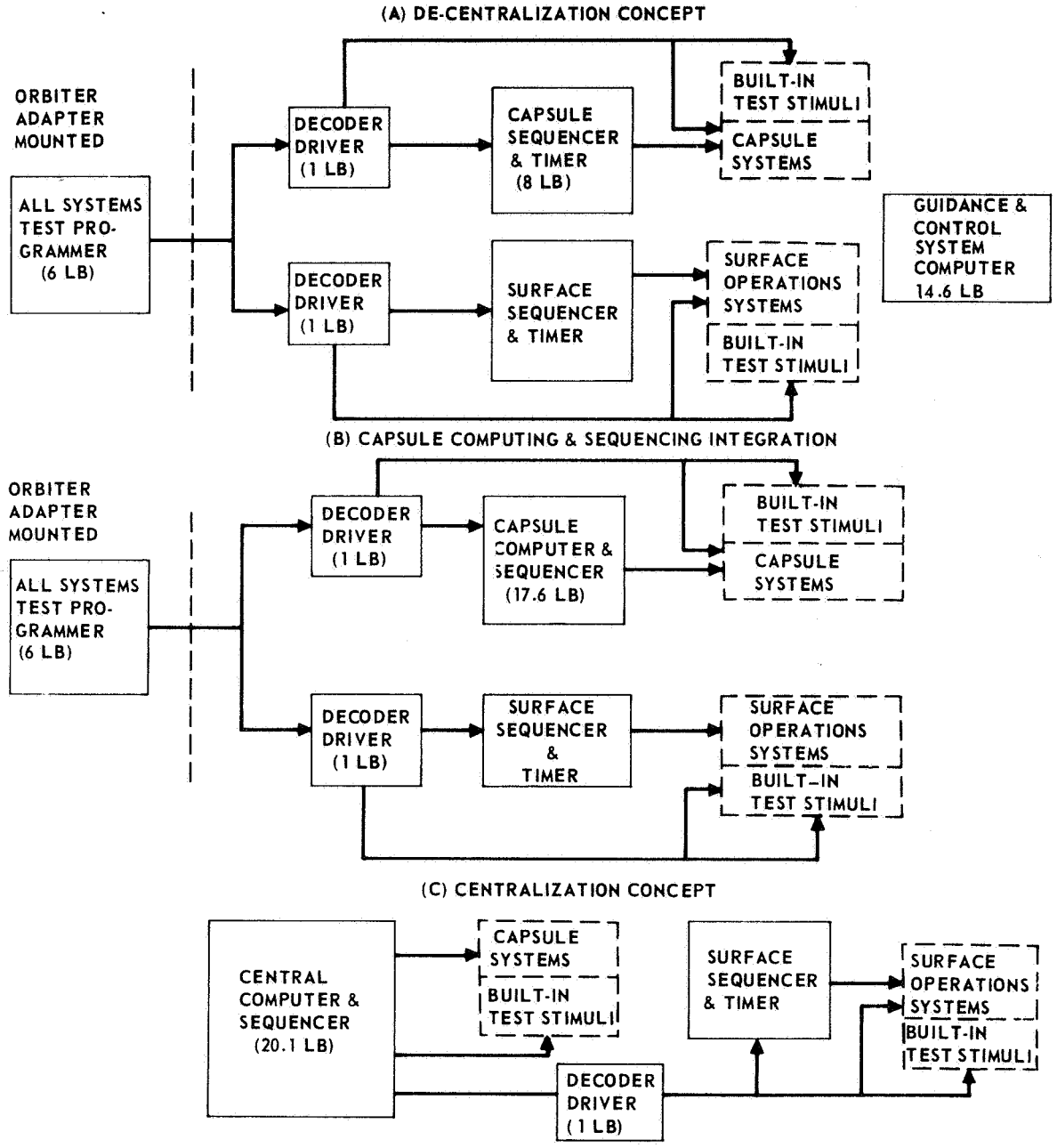

FIGURE 3.2.5.–1

TABLE 3.2.5-1
SEQUENCER SUBSYSTEM OUTPUT SUMMARY

RECEIVING SYSTEM	CS&T OUTPUTS	TP OUTPUTS		SS&T OUTPUTS	
	1 DAY & 90 DAY MISSIONS	1 DAY MISSIONS	90 DAY MISSIONS	1 DAY MISSIONS	90 DAY MISSIONS
TELECOMMUNICATIONS					
• CAPSULE	5	13	13		
• LANDER		9	19	8	22
GUIDANCE & CONTROL					
• CAPSULE	33	29	29		
SEQUENCER & TIMER					
• CAPSULE		10	10		
• LANDER		3	3		
PROPULSION					
• CAPSULE	17	4	4		
ELECTRICAL POWER					
• CAPSULE	3				
• LANDER				1	7
DEPLOY/ERECT MECHANISM/ PYRO					
• CAPSULE	14				
• LANDER				10	13
ENG INSTRUMENTATION					
• CAPSULE	2	2	2		
• LANDER		2	2	4	4
SCIENCE INSTRUMENTS					
• CAPSULE (ENTRY)	4	3	3		
• LANDER (SURFACE)		14	14	26	26
UNASSIGNED OUTPUTS	50	39	29	15	56
TOTAL OUTPUTS	128	128	128	64	128

Control system computer characteristics are derived in Section 3.2.4. A brief study between magnetic core and plated wire techniques for all the digital devices showed a preference for the more common magnetic core technology.

In Concept B the 128 capsule sequence control circuit output drivers are integrated into the guidance computer input/output section. Approximately 228 computer memory words are required for this inclusion; 128 words are needed to store the possible 128 event time words and 100 for additional executive program control. This design integration approach eliminates the duplication of a clock, control and gating circuitry, and a power supply for the Capsule Sequencer & Timer memory words.

In Concept C the 128 Test Programmer event time words are also placed in the computer memory with 228 computer word allocations. This integration approach eliminates the duplication of a clock, control and gating circuitry, a power supply, and one Decoder/Driver for the Test Programmer.

Either Concept B or C can be accomplished without a memory capacity change in the original G&C system computer, since its 4096 word memory provided for a 54 percent growth capability.

3.2.5.2 System Configuration Comparison. - If a guidance scheme other than the fully active concept (of Section 3.2.4) is employed, the guidance computer is not available for continuous flight sequencing. The de-centralized sequencer system hardware Concept A, is then required. The test programmer unit is mounted on the orbiter adapter to minimize capsule entry weight.

If a full active guidance scheme is employed, the computer is continuously available for flight sequencing as shown in the Concept B configuration. This design approach reduces the total system and entry weight relative to Concept A by 5 lb.

The maximum computer utilization is provided by Concept C, where the checkout test programming function is also performed by the guidance computer. This approach provides a total sequencer system weight reduction of 4.5 lb over that of Concept B. The Concept C, however, yields a 1.5 lb heavier entry weight than Concept B, since the test programmer function weight is now moved onto the flight capsule. The centralization Concept C is favored for overall minimum

sequencer system weight and interface simplicity. However, the weight advantages derived by this approach are obtained at the expense of some added complexity in the computer program.

"The aeronautical and space activities of the United States shall be conducted so as to contribute . . . to the expansion of human knowledge of phenomena in the atmosphere and space. The Administration shall provide for the widest practicable and appropriate dissemination of information concerning its activities and the results thereof."

—NATIONAL AERONAUTICS AND SPACE ACT OF 1958

NASA SCIENTIFIC AND TECHNICAL PUBLICATIONS

TECHNICAL REPORTS: Scientific and technical information considered important, complete, and a lasting contribution to existing knowledge.

TECHNICAL NOTES: Information less broad in scope but nevertheless of importance as a contribution to existing knowledge.

TECHNICAL MEMORANDUMS: Information receiving limited distribution because of preliminary data, security classification, or other reasons.

CONTRACTOR REPORTS: Scientific and technical information generated under a NASA contract or grant and considered an important contribution to existing knowledge.

TECHNICAL TRANSLATIONS: Information published in a foreign language considered to merit NASA distribution in English.

SPECIAL PUBLICATIONS: Information derived from or of value to NASA activities. Publications include conference proceedings, monographs, data compilations, handbooks, sourcebooks, and special bibliographies.

TECHNOLOGY UTILIZATION PUBLICATIONS: Information on technology used by NASA that may be of particular interest in commercial and other non-aerospace applications. Publications include Tech Briefs, Technology Utilization Reports and Notes and Technology Surveys.

Details on the availability of these publications may be obtained from:

SCIENTIFIC AND TECHNICAL INFORMATION DIVISION

NATIONAL AERONAUTICS AND SPACE ADMINISTRATION

Washington, D.C. 20546